UNIVERSITY OF LONDON THESIS

Degree PhD Year 2008 Name of Author CHALIDAPONGSA, PRASAI

Steady-state and Dynamic Behaviour of Plate-Fin-Tube Direct Expansion Evaporators when using a Zeotropic Refrigerant Mixture

Prasai Chalidapongse

Department of Mechanical Engineering

University College London

April 2008

Submitted in partial fulfilment of the requirements for the Degree of Doctor of Philosophy

ProQuest LLC
789 East Eisenhower Parkway
P.O. Box 1346
Ann Arbor, MI 48106-1346

Abstract

Both steady-state and dynamic simulations of the operation of plate-fin-tube air coolers, under dry and wet conditions, and also of themostatic expansion valve (TEV) controlled coils under dry condition, were carried out. The investigation aimed at improving our understanding as how the operation behaviour of the cooler coils, under various coil conditions, was influenced by the use of a ternary refrigerant mixture (R407C) when compared to a pure refrigerant (R134a). Based on practical coil configurations, a distributive computer model was implemented, with governing equations for air and refrigerant sides and for tube walls set up for individual coil elements. For the TEV, equipped with an external equalizer, energy and force equations were set up. To compare the two refrigerants, a reference scheme, obtained based on the steady state simulation, was set up: the same air coil-inlet conditions, the same refrigerant mass flow rates and vapour qualities at the coil inlets, and the same refrigerant temperatures at the coil outlet. The dynamic simulation was based on having a step change in the coil inlet dry-bulb (DB) temperature.

The analysis and discussion focussed on the temperature gliding and many other inter-related parameters/factors, e.g. the heat transfer coefficient (HTC), the coil arrangement, the refrigerant superheat and the refrigerant type. It was obsereved that for steady-state, the temperature gliding affected the spatial gradient of the temperature and humidity ratio of the tube-wall, the outlet dry-bulb temperature of the coil-face row, and the row outlet humidity ratio (HR). The temperature glide, when combined with the refrigerant HTC and the coil arrangement, had a strong influence on the sensible and latent heat fluxes, i.e. suppressing the influence of other parameters such as the effective air-side heat transfer and mass transfer coefficients.

For the coil dynamics, the refrigerant temperature gliding influenced the gradients of the time profiles of the DB temperature and HR at the coil-outlet tubes that were unaffected by the superheat. For the TEV-controlled coils, only the temperature gliding-up of R407C, not the temperature drop associated with R134a, was shown to have an impact upon the rate of change of the superheat-initiation location. The combined effect of the temperature gliding and the HTC influenced the transit times between steady states of both the superheat-initiation location and external-equalizer pressure.

Declaration

I hereby declare that the work presented in this thesis is solely my own work and that to my best knowledge the work is original except where otherwise indicated by reference to other authors. No part of this work has been submitted for any other degree or diploma.

(Prasai Chalidapongse)

April 2008

Contents

Nomenclature

Symbols

A	Channel cross-sectional area [m^2]
A_d	Diaphragm area of TEV [m^2]
A_F	Coil face area [m^2]
A_{fin}	Surface area of fin [m^2] or fin surface area per unit length of tube [m^2/m]
$A_{fin,wet}$	Surface area of condensate on fin [m^2] or condensate-on-fin surface area per unit length of tube [m^2/m]
$A_{flow,min}$	Opening flow area at orifice of TEV [m^2]
A_k	Cross-section area of tube occupied by phase-k fluid [m^2]
A_l	Cross-section area of tube occupied by liquid [m^2]
A_{mf}	Minimum flow area [m^2]
$A_{mf,total}$	Total minimum flow area [m^2]
$A_{o,total}$	Total air side surface area [m^2] or total air side surface area per unit length of tube [m^2/m]
$A_{o,total,wet}$	Total air side surface area of condensate [m^2] or total air-side condensate surface area per unit length of tube [m^2/m]
A_p	Primary surface area of tube wall [m^2] or primary surface area of tube wall per unit length of tube [m^2/m]
A_{tube}	Inside cross-section area of tube [m^2]
$A_{tube,l}$	Inside cross-section area of tube occupied by liquid [m^2]
$A_{tube,v}$	Inside cross-section area of tube occupied by vapour [m^2]

$A_{wall,e}$	Sensor-bulb outside surface area exposing to environment per unit length of tube [m^2/m]
$A_{wall,i}$	Inside surface area of tube wall [m^2] or inside tube-wall surface area per unit length of tube [m^2/m]
$A_{wall,o}$	Outside tube-wall surface area between fins [m^2] or outside tube-wall surface area between fins per unit length of tube [m^2/m]
$A_{wall,o,p}$	Primary surface area of tube wall [m^2] or primary surface area of tube wall per unit length of tube [m^2/m]
$A_{wall,o,wet}$	Surface area of condensate on outside tube-wall surface area between fins [m^2], or condensate surface area per unit length of tube for condensate on outside tube-wall surface area between fins [m^2/m]
$A_{wall,tube}$	Tube-and-sensor-bulb contact surface area per unit length of tube [m^2/m]
b_2	Correlation coefficient
b_3	Correlation coefficient
b_4	Correlation coefficient
b_5	Correlation coefficient
Bo	Boiling number
DB	Dry-bulb
bd	Equilibrium break-off-diameter [m]
C_d	Discharge coefficient of orifice of TEV
C_H	Coil height [m]
C_{me}	Correction parameter, considered a mixture effect about mass transfer resistance in two-phase forced convection boiling region
C_{UN}	Correction parameter, considered mixture effects in nucleate boiling region, and developed by Unal
C_W	Coil width [m]
c_p	Specific heat at constant pressure [J/(kg·K)]
$c_{p,a}$	Air specific heat at constant pressure [J/(kg_{dryair}·K)]
$c_{p,bulb}$	Equivalent sensor-bulb specific heat at constant pressure [J/(kg·K)]
$c_{p,c,l}$	Charged-liquid-in-sensor-bulb specific heat at constant pressure

	[J/(kg·K)]
$c_{p,l}$	Liquid specific heat at constant pressure [J/(kg·K)]
D	Diameter [m], tube diameter [m] or mass diffusivity [m^2/s]
D_{fin}	Fin diameter [m]
$D_{fin,eq}$	Equivalent fin diameter [m]
D_h	Coil hydraulic diameter [m]
$D_{ID,tube}$	Tube inner diameter [m]
$D_{OD,tube}$	Tube outer diameter [m]
D_{wa}	Mass diffusivity of water vapour through air [m^2/s]
EEEP	Equivalent external equalizer pressure [Pa]
EEP	External equalizer pressure [Pa]
ESBP	Equivalent sensor-bulb pressure [Pa]
F	Force exerted to overcome friction [N] or dimensionless parameter accounting for increasing in turbulence because of two-phase flow
F_{bulb}	Sensor-bulb force [N]
F_o	Initial spring force [N]
F_{obs}	Fin obstruction factor
F_p	Dimensionless parameter obtained from revising F dimensionless parameter
F_s	Spring force [N]
f_{Darcy}	Darcy friction factor
f_{Fan}	Fanning friction factor
G	Mass flux [kg/(m^2·s)]
G_a	Air mass flux [kg/(m^2·s)]
$G_{a,in}$	Inlet air mass flux [kg/(s·m^2)]
$G_{a,mf}$	Air mass flux at minimum flow area [kg/(s·m^2)]
g	Acceleration due to gravity [m/s^2]
H	Heat transfer coefficient [W/(m^2·K)]
h	Heat transfer coefficient [W/(m^2·K)]
h_{UN}	Heat transfer coefficient, considered mixture effects in nucleate boiling region, and developed by Unal [W/(m^2·K)]
HTC	Heat transfer coefficient [W/(m^2·K)]

i_{fg}	Latent heat of condensation, i.e. the difference between specific enthalpies of saturated vapour and saturated liquid [J/kg]
$i_{fg,water}$	Latent heat of water condensation, i.e. the difference between specific enthalpies of saturated water vapour and saturated liquid water [J/kg]
i_{wa}	Moist-air specific enthalpy [J/kg_{dryair}]
$j_{air,dry}$	Colburn transfer factor for between air and dry surface
$j_{air,wet}$	Colburn transfer factor for between air and condensate-on-tube-wall surface area
$K_{Amin,z}$	Constant coefficient [m]
K_s	Spring coefficient [N/m]
K_v	Valve gain [m·s]
k	Thermal conductivity [W/(m·K)]
k_a	Air thermal conductivity [W/(m·K)]
k_{bulb}	Equivalent thermal conductivity of sensor bulb [W/(m·K)]
$k_{c,l}$	Thermal conductivity of charged liquid in sensor bulb [W/(m·K)]
k_{fin}	Fin thermal conductivity [W/(m·K)]
k_{tube}	Thermal conductivity of tube-wall [W/(m·K)]
L	Length [m]
L_d	Coil depth [m]
Le	Lewis number
M	Molecular weight [gm/gmole]
m	Mass per unit length [kg/m]
$\dot{m}$	Mass flow rate [kg/s]
$\dot{m}_{lv}$	Rate of mass evaporation per unit length [kg/(s·m)]
m_{bulb}	Equivalent sensor-bulb mass per unit length [kg/m]
$m_{c,l}$	Charged-liquid-in-sensor-bulb mass per unit length [kg/m]
N	Parameter due to nucleate boiling
N_R	number of row
N_{TR}	Number of tube per row
Nu	Nusselt number
ONB	Onset of nucleate boiling
P	Wetted perimeter [m]

P_s	Fin density [fin/m]
p	Pressure [Pa] or [N/m^2]
p_{bulb}	Sensor-bulb pressure [Pa] or [N/m^2]
p_r	Bulb pressure [Pa] or [N/m^2]
p_{ss}	Superheat-setting pressure [Pa] or [N/m^2]
p_v	Vapour pressure [Pa] or [N/m^2]
p_w	Partial pressure of water vapour in moist air [Pa] or [N/m^2]
p_{wa}	Total pressure of moist air [Pa] or [N/m^2]
p_{ws}	Pure-water saturation vapour pressure [Pa] or [N/m^2]
Pr	Prandtl number
Pr_a	Air Prandtl number
$\frac{\partial p}{\partial z}$	Total pressure drop of refrigerant or fluid in z-direction [$(N/m^2)/m$]
$\left(\frac{dp}{dz}\right)$	Total pressure drop of refrigerant or fluid in z-direction [$(N/m^2)/m$]
$\left(\frac{dp}{dz}a\right)$	Pressure drop of refrigerant or fluid in z-direction due to acceleration [$(N/m^2)/m$]
$\left(\frac{dp}{dz}F\right)$	Pressure drop of refrigerant or fluid in z-direction due to friction [$(N/m^2)/m$]
$\left(\frac{dp}{dz}z\right)$	Pressure drop of refrigerant or fluid in z-direction due to elevation [$(N/m^2)/m$]
q	Heat flux [W/m^2]
q''	Heat flux at surface [W/m^2]
$q_{bulb,e}$	Heat flux transferred from sensor bulb to environment [W/m^2]
R	Radius [m]
R_h	Moist-air relative humidity [mole fraction/mole fraction)]
R_w	Ideal gas constant for water vapour [J/(kg·K)]
r	Radius [m]
R11	CFC 11, Trichlorofluoromethane, CCl_3F, being a pure refrigerant
R114	CFC 14, Dichlorotetrafluoroethane, $C_2Cl_2F_4$, being a pure refrigerant
R12	CFC 12, Dichlorodifluoromethane, CCl_2F_2, being a pure refrigerant

R123	HCFC-123, Dichlorotrifluoromethylmethane, $C_2HCl_2F_3$, being a pure refrigerant
R125	HFC 125, Pentafluoroethane, C_2HF_5, being a pure refrigerant
R13	CFC 13, Chlorotrifluoromethane, $CClF_3$, being a pure refrigerant
R134a	HFC 134a, Tetrafluoroethane, $C_2H_2F_4$, being a pure refrigerant
R152a	HFC 152a, Difluoroethane, $C_2H_4F_2$, being a pure refrigerant
R22	HCFC 22, Chlorodifluoromethane, $CHClF_2$, being a pure refrigerant
R23	HFC 23, Trifluoromethane, CHF_3, being a pure refrigerant
R32	HFC 32, Difluoromethane, CH_2F_2, being a pure refrigerant
R407C	Refrigerant mixture (R32/R125/ R134a: 0.23/0.25/0.52 by weight)
R500	Refrigerant mixture (R12/R152a: 0.738/0.262 by weight)
Re	Reynold number
Re_a	Air Reynold number
Re_D	Reynold number in channel
S	Suppression parameter, slip factor or force exerted on other phases at interface [N]
S_D	Tube diagonal spacing [m]
S_L	Tube longitudinal spacing [m]
S_T	Tube transverse spacing [m]
s_{fin}	Fin spacing [m]
SBP	Sensor-bulb pressure [Pa]
Sc_a	Air Schmidt number
T	Temperature [K]
T_{bulb}	Sensor-bulb temperature [K]
$T_{cond,fin}$	Temperature of condensate on fin [K]
$T_{cond,wall}$	Temperature of condensate on tube wall [K]
T_{db}	Dry-bulb air temperature [K]
$T_{db,in}$	Inlet dry-bulb air temperature [K]
$T_{db,out,1}$	Outlet dry-bulb air temperature from an above front tube [K]
$T_{db,out,2}$	Outlet dry-bulb air temperature from a below front tube [K]
T_{dp}	Dew-point temperature of moist air [K]

$T_{fin,ave}$	Average fin temperature [K]
$T_{wall,ave}$	Average wall temperature [K]
$T_{wall,coil\text{-}outlet}$	Coil-outlet wall temperature [K]
T_{wb}	Wet-bulb air temperature [K]
t	Time [s]
TEV	Thermostatic expansion valve
TG	Temperature glide [K]
U_{dry}	Heat transfer coefficient between air and dry tube-wall surface area [W/(m^2·K)]
$U_{eff,dry}$	Effective heat transfer coefficient between air and dry tube-wall surface area [W/(m^2·K)]
$U_{eff,wet}$	Effective heat transfer coefficient between air and condensate-on-tube-wall surface area [W/(m^2·K)]
$U_{eff,wet,latent}$	Effective latent heat transfer coefficient between air and condensate-on-tube-wall surface area [W/(m^2·K)]
$U_{eff,wet,sen}$	Effective sensible heat transfer coefficient between air and condensate-on-tube-wall surface area [W/(m^2·K)]
$U_{m,eff,wet}$	Effective mass transfer coefficient between air and condensate-on-tube-wall surface area [kg of dry air/(m^2·s)]
$U_{m,wet}$	Mass transfer coefficient between air and condensate-on-tube-wall surface area [kg of dry air/(m^2·s)]
U_{wet}	Heat transfer coefficient between air and condensate-on-tube-wall surface area [W/(m^2·K)]
$U_{wet,latent}$	Latent heat transfer coefficient between air and condensate-on-tube-wall surface area [W/(m^2·K)]
$U_{wet,sen}$	Sensible heat transfer coefficient between air and condensate-on-tube-wall surface area [W/(m^2·K)]
u	Velocity [m/s]
v	Specific volume [m^3/kg]
v_{fg}	Difference between specific volumes of saturated vapour and saturated liquid [m^3/kg]
W	Moist-air humidity ratio [kg of water/kg of dry air]
$W_{cond,fin}$	Moist-air humidity ratio at saturation at temperature of condensate

	on fin [kg of water/kg of dry air]
$W_{cond,wall}$	Moist-air humidity ratio at saturation at temperature of condensate on tube wall [kg of water/kg of dry air]
W_{in}	Inlet moist-air humidity ratio [kg of water/kg of dry air]
$W_{out,1}$	Outlet moist-air humidity ratio from an above front tube [kg of water/kg of dry air]
$W_{out,2}$	Outlet moist-air humidity ratio from an below front tube [kg of water/kg of dry air]
W_s	Moist-air humidity ratio at saturation [kg of water/kg of dry air]
$W_{s,T_{wb}}$	Moist-air humidity ratio at saturation at wet-bulb air temperature [kg of water/kg of dry air]
w_{bulb}	Equivalent sensor-bulb thickness [m]
$w_{c,l}$	Thickness of charged liquid in sensor bulb[m]
w_{fin}	Fin thickness [m]
X	Mole fraction of more volatile component in liquid phase
X_i	Mole fraction of component i in liquid phase
X_{tt}	Martinelli parameter
x	Co-ordinate in x-direction [m] or quality or mole fraction of more volatile component in liquid phase
Y	Mole fraction of more volatile component in vapour phase
y	Distance from the wall, co-ordinate in y-direction [m] or mole fraction of more volatile component in vapour phase
z	Spring-movement distance or co-ordinate in z-direction [m]

Greek letters

α	Thermal diffusivity [m^2/s], or void fraction
β	Contact angle, plane angle [degree]
Γ_k	Mass transfer rate to phase k [kg/(m·s)]
Γ_l	Mass transfer rate to liquid phase [kg/(m·s)]
Γ_v	Mass transfer rate to vapour phase [kg/(m·s)]
Δ	Difference
δ	Thermal boundary layer thickness or differential distance [m]

$\eta_{fin,dry}$	Dry-coil fin efficiency
$\eta_{fin,wet}$	Wet-coil fin efficiency
$\eta_{W,fin,wet}$	Wet-coil humidity-ratio fin efficiency
Θ	Mass fraction
θ	Angle to horizontal plane [degree]
μ	Dynamic viscosity [N·s/m^2] or [kg/(m·s)]
μ_a	Air dynamic viscosity [N·s/m^2] or [kg_{dryair}/(m·s)]
ν_a	Air kinematic viscosity [m^2/s]
π	Pi (= 22/7)
ρ	Density [kg/m^3]
ρ_a	Air density [kg_{dryair}/m^3]
σ	Surface tension [N/m] or [J/m^2]
τ	Shear stress [N/m^2]
Φ	Surface heat flux [W/m^2] or two-phase frictional multiplier
ϕ	Surface heat flux [W/m^2]
ψ	Geometrical factor for calculating fin efficiency [m]

Subscripts

1	Phase 1, or above element in the front row
2	Phase 2, or below element in the front row
accu	Accumulated
bp	Boiling point
bub	Bubble
bubble	Bubble point
c	Critical or convective boiling
cec	Convective evaporation contribution
charge	At charge condition
dew	Dew point
dynamic	Dynamic state
e	Excess
eff	Effective

FZ	Forster-Zuber equation
fin	Fin
fo	Total flow assumed liquid
i	Component i, ideal, inside, in between times or at Δt_i
ID	Inner diameter
ideal	Ideal
in	Inlet
k	Phase k
kn	Between phase k and n
knz	Between phase k and n in z direction
kw	Between phase k and wall
l	Liquid
lo	Liquid alone flow
lv	Between liquid and vapour
lw	Between liquid and wall
m	Mixture or mean
max	Maximum
min	Minimum
mvc	More volatile component
n	Phase n
nbc	Nucleate boiling contribution
nbp	Normal boiling point
ONB	Onset of nucleate boiling
out	Outlet, or evaporator outlet
p	Pure component or at constant pressure
pseudo	Pseudo
R125	R125 refrigerant
R134a	R134a refrigerant
R32	R32 refrigerant
R407C	R407C refrigerant
ref	Refrigerant
refw	Between refrigerant and wall
s	Surface

SA	Stephan and Abdelsalam
SNB	Suppression of nucleate boiling
sat	Saturated
steady	Steady state
TEV	Thermostatic expansion valve
to	Two-phase total flow
tp	Two-phase flow
v	Vapour
vl	Between vapour and liquid
vo	Vapour alone flow
vw	Between vapour and wall
w	Wall
wall	Wall
wf	Between wall and fluid
x	At constant vapour quality
z	In the z direction

Superscript

t	at time t
t-1	at time t-1
–	denotes average property

List of Tables

List of Figures

state, "TRS" =Time to Reaching Steady-state, "PRC" =Pattern of Rate of Change with time. The disturbance was a step increase of the coil-inlet DB temperature.

Chapter 1 Introduction

Background

Nowadays, more and more air-conditioning and refrigeration systems are using mixture refrigerants. Currently the most common and well-known commercial refrigerants on the market are: R134a, R404A, R410A, and R407C. It can be seen that majorities of these are in fact mixture refrigerants. Since the discovery of the ozone depletion problem via a field study in 1985 [NAS Systems Division Office 2001], a great deal of research and development efforts have been made to identify suitable replacements to CFC and HCFC refrigerants. However, it has been acknowledged that it is practically difficult to obtain single-component/pure refrigerants that have similar or identical thermo-physical properties as those they are replacing. Therefore it is quite a common practice to mix different refrigerants in order to acquire the desirable ranges of properties [Braven & Troxel 1990] [Biven 1995] [Hwang et al. 1997] [Calm & Didion 1998] [E.I.du Pont de Nemours and Company 2002].

There are 3 types of mixtures: zeotropic, near-azeotropic and azeotropic. During a phase change (boiling in the evaporator or condensation in the condenser) at a constant pressure, the first two experience a temperature glide, whereas the temperature of an azeotrope remains unchanged, behaving just like a pure substance. It appears that it is difficult to develop suitable azeotropes in which, at equilibrium, the vapour and liquid phase will have the same composition. Hence, both zeotropic and near-azeotropic mixtures are used and studied extensively [Chen 1992]. They are referred as "refrigerant mixtures" from this point onward.

1.1 Unique characteristics of zeotropic and near-azeotropic refrigerants

When two or more pure refrigerants, with different molecular sizes/masses, are mixed to form a mixture, different intermolecular forces are experienced by individual components within the mixture. When comparing to pure fluids, refrigerant mixtures process the following unique characteristics.

Higher degrees of freedom: Based on the phase rule, a refrigerant mixture has more degrees of freedom, i.e. more numbers of variables in specifying an intensive equilibrium state. For instance, for vapour-liquid, liquid and vapour equilibrium states, a binary (or 2-component) mixture has respectively 2, 3 and 3 degrees of freedom, whereas the corresponding values for a pure substance are 1, 2 and 2. [Smith 1987] .

As a result, problems associated with mixtures are more complex, but it also means there are relatively larger number of possible ways (i.e. a better chance) in reaching a solution of a problem. For an example, at the inlet of a compressor in a refrigeration system, generally the pressure and temperature (superheat) can not be varied much, as constrained by the external/environmental conditions. A binary mixture, having three degrees of freedom of its 2-phase, can have the composition of the liquid feeding the evaporator manipulated to meet the targeted pressure and temperature [Radermacher 1984] [Smith 1987] [Lee 2003] [Greco 2005].

Equations of state with mixing rules: Calculations for refrigerant-mixture equilibrium (or thermodynamic) properties can be done by using an equation of state with mixing rules, and using equilibrium-condition equations [Morrison & McLinden 1985].

For pure fluids, due to the effects of intermolecular attractions and molecular hard cores [Morrison & McLinden 1985], the equation of state usually contains empirical parameters. Within a mixture, the molecules can have at least two kinds of interactions: with like and unlike species. To account for the mixture effect, mixing rules (developed based on experiments), together with additional empirical parameters, are applied to those parameters of the pure components. [Morrison & McLinden 1985]

In the development of heat transfer coefficient correlations of mixed refrigerants, some researchers modified those established for pure refrigerants, by

recognizing the mixture effect in a similar manner to the development of equations of state.

Temperature glide-up: For a mixture refrigerant undergoing a phase change under a given pressure in an evaporator, the more volatile components evaporate faster than the less volatile ones. In other words, the concentrations of the vapour- and the liquid- phases are different and keep changing along the evaporator. The boiling temperature is therefore increasing as the remaining liquid will contain more and more of the high boiling point components, and this increase in temperature is usually called the temperature glide [Jung & Radermacher 1993]. In contrast, for a pure refrigerant, the 2-phase temperature remains constant, assuming no pressure drop, during the phase change.

Taking into consideration of pressure drop during boiling heat transfer, the magnitude of the temperature glide of the mixture refrigerant will be smaller than that for the constant pressure case. On the other hand, for a pure refrigerant, there is a reduction in temperature associated with the pressure drop.

The temperature glide can help improve efficiency by adopting a counter-flow type heat exchanger, matching the temperature profiles between the refrigerant mixture and the heat transfer fluid. The system irreversibility will be reduced relative to pure refrigerant case, i.e. achieving a higher coefficient of performance (COP) [Braven & Troxel 1990] [Kondepudi 1992].

1.2 Understanding the behaviour of an evaporator in a RAC system

The evaporator is one of the main components in a RAC system. It interacts directly with the climate-controlled environments, and, for a given design, its behaviour in turn is governed by the properties of the refrigerant, demanding a thorough understanding of the heat and momentum transfer of both 2-phase and single phase flows. Research in these areas often involves complex modelling, for accurate prediction and analysis of its performance, leading to more reliable designs of such components.

Heat and momentum transfer processes in evaporators significantly affect system performance [Domanski et al. 2005], and it was found that, for an evaporator, a significant proportion deterioration of the coefficient of performance from a Carnot cycle was caused by the pressure and temperature drops of refrigerant [Atwood 1990].

For direct expansion air coolers, complicated momentum, heat and mass transfers occur on both refrigerant- and air- sides, involving two-phase flow boiling, and wet- and frosted- coil conditions, respectively. The operation of the air cooler is often transient in nature, associated with the change in climatic conditions and the regulation of refrigerant mass flow by the Thermostatic Expansion Valve, i.e. a TEV controlled-evaporator.

1.3 Thesis objectives

Based on the backgrounds, the main objective of this work was identified as to investigate the dynamic behaviour of plate-fin-tube evaporators when using a zeotropic refrigerant mixture, relating the unique characteristics of the mixture to the operation of a DX plate-fin-tube evaporator. The performances of cross-counter-flow evaporators under the dry or wet conditions were studied as well as a TEV-controlled evaporator. For comparison purpose, a pure refrigerant was also studied along with the refrigerant mixture. The work started with a steady-state study in order to gain a better understanding of the fundamental differences between the two refrigerants. The investigation adopted a modelling and simulation approach.

1.4 Scopes of Research

Specific details for the tasks involved and their rationales were given as follow.

Plate-fin-tube DX air cooling coils have been chosen as the studied evaporator type as they are the most widely used evaporators in industry [Rich 1973] [Bensafi et al. 1997]. For a refrigerant mixture, the cross-counter flow is known to create less irreversibility [Braven & Troxel 1990], and hence this flow configuration was chosen for this work.

Operating conditions of the air cooler can be dry, wet or frosted; this research focussed on the first two conditions. The work for the dry coils is appropriate for refrigerant comparison, the validation purposes and the examination of the behaviour of a TEV-controlled evaporator, as it involves relative smaller numbers of parameters. On the other hand, wet coils are commonly encountered in air-conditioning application. Under both coil conditions, it was anticipated that the temperature-glide of a zeotrope would affect the coil performances differently when compared to a pure refrigerant.

Steady-state analysis has been usually carried for component design and matching, and many researches have been conducted using both pure and mixed refrigerants. For the pure refrigerants, the model types, such as non-finite-element [Admiraal & Bullard 1995], finite-element [Oskarsson et al. 1990b] and distributive models [MacArthur 1984], had been applied using different available concepts, such as UA [Hewitt et al. 1994] and LMTD [Incropera & Witt 1990], and various different assumptions, under dry- and/or wet-coil conditons. It was found that taking into consideration of the superheat region and the variation in refrigerant HTC gave good results. For mixed refrigerants, many researchers studied the temperature-glide effect upon the air-and-refrigerant-temperature-profile matching through the composition manipulation, the pinch-point concept, and the different flow and circuiting patterns.

In this thesis, the main focus would be on the influences of the temperature-glide and its interaction/combination with other parameters (e.g. the refrigerant heat transfer coefficient and the coil arrangement) upon the heat transfer and condensate rates, the temperature of the tube wall, the dry-bulb temperature and humidity ratio of air. Two well known refrigerants, on pure and one mixture refrigerant, i.e R134a and R407C respectively, are typical for mixed were then selected for the study. Though they have higher GWPs and may be phased out in future, the objectives (i.e. to identify the differences between the two types of fluids) of this study would not be affected as the approach to be developed is believed equally applicable to other mixtures such as HCs. In addition, individual effects of the coil arrangement, the superheat and the refrigerant type on steady state behaviour were also examined.

The published dynamic studies only involved pure refrigerants. There are 2 main categories of dynamics: short and long transient responses. For the former, for example, when there was a step increase or decrease of the refrigerant mass flow rate, the variation of the coil-outlet dry-bulb temperature was studied [Jia et al. 1995, 1999]. For the long transient response, such as during start-up or shut-down, the refrigerant mass flow rate, and the air, wall and refrigerant temperatures were investigated by using a distributive model [MacArthur 1984] [Wang & Touber 1991]. So far no related work on mixed refrigerants has been identified.

For this thesis, due to the gap identified above, the dynamic-behaviour associated with the use of mixed refrigerants in a DX air cooler was the key task of the investigation. A short transient response analysis [Jia et al. 1995, 1999] was chosen, because the long one involves a whole-system dynamics which was beyond the scope of

this research. For a step change of the coil-inlet dry-bulb temperature which was chosen as the input disturbance, the study emphasized mainly on the individual effects of temperature glide, 2-phase pressure-drop, superheat, wet-coil and refrigerant-type upon dynamics of various coil parameters, including the DB temperature and HR at the coil-outlet, the refrigerant coil-outlet pressure, the local 2-phase temperature, etc. In addition, the study was extended to analysing a coil controlled by a thermostatic expansion valve (TEV) that regulates the mass flow rate.

Regarding TEV-controlled evaporators, it seems once again researchers have concerned with only the single component refrigerants. In previous studies, the TEV model, for the needle and the valve seat, and the sensor bulb, and the experiments were carried mainly to investigate the hunting (instability) behaviour [James & James 1987].

For this thesis, a simplified TEV model with a one-row evaporator under dry-coil operation was constructed. With reduced complexity, this will help understanding the evaporator performance that was affected by the temperature-glide, the heat transfer coefficient, the TEV-related parameters (i.e. the sensor bulb and external equalizer pressures), and the refrigerant-type (e.g. the superheat-initiation location and the sensitivity of the pressure-drop profile shifting to change of the coil-inlet DB temperature).

Since it was the intention of this research to provide in-depth dynamic details by using simulation, a deductive-and-distributed type mathematical model, instead of a inductive one was used [Touber 1984] [Jia et al. 1995] [Wang et al. 2007]. The model, represented by a set of governing equations with appropriate assumptions, was suitable for both the steady-state and dynamic mode operation of the evaporator. For the refrigerant side, the continuity, the momentum, and the energy equations were established. The heat transfer coefficients and pressure drop correlations for the mixed refrigerants were carefully selected from published literatures. For the fin and tube walls, the energy balance was applied. Finally, for the air side, the energy and the mass balances were set up.

1.5 Outline of the thesis and originalities of the research

The thesis consisted of 6 chapters: Introduction, Literature review, Applications of theories, Modelling and simulation, Results and discussion, and Conclusions. The Introduction was started off with issues of mixed-refrigerants: the

background introduces the main influential characteristic - the temperature glide. The relevant aspects of evaporators, such as heat transfer and pressure characteristics, were then stated. Later, the objectives and the scopes of the study were highlighted: an investigation into the steady-state and dynamic behaviour the plate-fin-tube evaporators, when using a mixed refrigerant. A comparison to a pure refrigerant was carried out, paying particular attention to the effect of temperature glide and various significant parameters associated with, say, refrigerant HTC and pressure drop.

Chapter 2 had two main parts: review and analysis. The review looked at HTCs and pressure drops of both pure and mixed refrigerants, and the air-side HTCs of both dry- and wet- coils. Different types of evaporator models were surveyed, followed by the steady-state and dynamic studies of evaporators for both pure and mixed refrigerants, including TEV-controlled coils. In the analysis, the relevant details were filtered to be used for the thesis, and the originalities of the work were stated.

The Applications of theories (Chapter 3) covered those related to the heat and mass transfer coefficients for the air side, the fundamentals concerning the internal forced convection boiling, i.e. mainly the HTCs and pressure drops, and the TEV controls. In Chapter 4, Modelling and simulation, the configurations of coils were selected. The model was set up for the air and the finned-tube for both dry- and wet-coil conditions, the refrigerant side for both 2-phase and superheat regions, and the TEV-controlled coil. The details of programming, the software and the program structure, including the discretization of the governing equations, and the simulation were given. In addition, any difficulties encountered were explained thoroughly.

In the Chapter 5, the validations of the program covers both steady-state and dynamics, and pure and mixed-refrigerant HTCs. The results of the dry coils, the wet coils and the TEV-controlled coils were fully discussed and analysed. The Conclusions provides a summary, followed by the main observations and findings, and the remarks and future work.

As for the originalities, apart from the fact that all the programs were created originally by the author, the evaporator model included mass balance of the moist air, which was not usually considered by other researchers when setting up the distributive model. A tube-dividing scheme with both elements and sub-elements to suit the two-phase and superheated region calculation, respectively, was devised to reduce simulation time.

The work adopted practical coil configurations, and used a novel refrigerant comparison scheme, i.e. with the same air coil-inlet conditions, and the same steady-state values of the mass flow rates and vapour qualities at the refrigerant coil inlets and of the temperature at the refrigerant coil outlets. The use of the same coil-outlet refrigerant temperatures as the basis for comparison would allow isolation of the evaporator analysis from other components when using different replacement refrigerants, and at the same time introducing minimum changes in the rest of the system, should the evaporator be contacted to other components in the future. Hence, the results and discussion were original, providing the first coverage for the dynamic and TEV-controlled studies of plate-fin-tube coils, when using a mixture. In addition, this methodology developed could be equally applicable for other pure or mixed refrigerants. Also, the transient process of the evaporators was hypothesised and validated.

Chapter 2 Literature review

Chapter one provides the background information of the work, and highlights the aims and the scope of the present investigation. This chapter reviews extensively previous experimental and simulation research in the performance and the behaviour of direct expansion air coolers or evaporators, when using pure, zeotropic or other mixture refrigerants. The review, arranged mainly chronologically, covers all the relevant topics such as refrigerant and air side heat transfer coefficients, two-phase pressure drops, evaporator modelling, TEV controls, and steady and dynamic behaviour of the evaporators. The review closes with an analysis of the related issues and a list of all the major observations. The analysis demonstrates how the collated information helps identifying areas that need further investigation in this research programme, and the planning and the execution of the work programme.

For the air side heat and mass transfer, the relevant correlations and prediction methods are reviewed for both dry and wet operating conditions.

2.1 Refrigerant heat transfer coefficient and pressure drop

This Section reviews heat transfer coefficients (HTCs) and pressure drop of pure and mixed refrigerants for two-phase saturated flow boiling which is the main mode of heat transfer mechanism in DX coils. The survey includes pure refrigerants because the present investigation compares the heat exchanger performance of both mixed and pure refrigerants. More importantly, the development of heat-transfer and the pressure-drop correlations for mixed refrigerants appears to be mainly based on that of the pure refrigerants.

2.1.1 Pure-refrigerant heat transfer coefficient

Preliminary observation shows that prediction of pure-refrigerant HTC in saturated flow boiling were primarily developed from that of other pure substances (e.g. water) in both vertical and horizontal flows. The flow boiling was usually classified into two regions: nucleate-flow-boiling and two-phase-forced-convective-flow-boiling. With experimental data, many empirical and semi-empirical correlations were formulated for each region by recognizing the influencing variables, for instance, the heat flux. As more and more of the experimental data are becoming available, better-fit-to-data correlations for horizontal flow boiling are being established.

Chen [1963] studied saturated flow boiling heat transfer of pure fluids in vertical annular/annular-mist flow patterns. For the correlation development, it was postulated that total heat transfer was comprised of contributions from micro- and macro- convective mechanisms. The micro-convective contribution was derived from Forster and Zuber's pool boiling correlation [1955]. The macro-convective contribution was taken from the modified Dittus-Boelter's two-phase convective flow boiling correlation. He introduced two dimensionless factors, S and F, in his derivation of HTC correlation. The former accounted for the suppression of saturated-nucleate-flow-boiling by the two-phase forced convection flow boiling. Based on the experimental data, the S factor was represented as a function of the two-phase Reynolds number. The F factor, which was a function of the Martinelli parameter [Lockhart & Martinelli 1949], accounted for the increase in turbulence resulting from the two-phase flow. It was found that the predicted HTCs had an average deviation of about 11% when compared with the experimental data.

Shah [1976] studied experimentally the saturated flow boiling for many common refrigerants, using different pipe materials, and under a wide range of heat and mass flux conditions. Based on the work, he proposed a correlated chart for estimating HTCs. The chart was applicable to four boiling regions: the nucleate-boiling-dominated region, the bubble-suppression region, the convective-dominated region with the fully wet surface and the convective-dominated region with the partly dry surface. Later, Shah [1982] developed a saturated-flow-boiling correlation to represent his earlier chart [Shah 1976]. It was found that the calculated results were in good agreement with the experimental data.

Bjorge et al. [1982] applied superposition principle to obtain semi-empirical heat flux equations for saturated flow boiling of water. There were two superposed heat flux equations: one for the low vapour quality region, and the other for the high-quality region. Each equation consisted of pool boiling contribution, incipient-boiling criterion, and forced convection contribution. When comparing the predicted results with the experimental results, their correlations gave better accuracy than Chen's correlation.

Gungor & Winterton [1986] developed a general correlation for saturated flow boiling of pure fluids by modifying Chen's correlation. They created a large data bank under a wide range of conditions for water, refrigerants and ethylene glycol. They used it to obtain new expressions for the suppression and enhancement factors, i.e. S and E factors. The S factor was a function of the Reynolds number and the E factor. The E factor was a function of the boiling number and the Martinelli parameter. In their correlation, the Cooper's and the Dittus-Boelter's correlations were used in the nucleate and the convective boiling contributions, respectively. When comparing their calculated HTCs with other researchers' correlations, it was found that their correlation gave a more reasonable accuracy.

However, later Liu & Winterton [1991] developed general correlations for saturated flow boiling in tubes and annuli of pure fluids. They used Kutateladze's suggestion [1961] in combining the nucleate and the convective boiling contributions to form their correlations. This caused the nucleate boiling contribution suppression occur at a higher vapour quality than Chen's correlation did at the same flow condition. The suppression factor, S, was a function of the Reynolds number and the F factor was a function only the Martinelli parameter, without the boiling number. By comparing the calculated results with the data from the data bank and other correlations, it was found that their correlation gave a better fit with the data.

Klimenko [1988] proposed that prediction of the HTC for the saturated flow boiling could be done by using the Nusselt numbers [Klimenko 1984] for the nucleate flow boiling and the two-phase-forced-convection-flow-boiling regions. Later, Klimenko [1990] improved his previous correlation [1988] and the focus was on the wall and liquid thermal conductivity ratio, which accounted for the heat transfer intensity effect. With his data bank, it was found that the improved correlation predicted a weaker dependence of the HTC on wall material than the previous one. In his improved correlation, there were no added parameters, for example channel inner wall

roughness, wet-ability, and individual properties of substances. There were two reasons for this. First, the influence of such parameters was rather weak when compared with the influence of the heat flux or the pressure. Second, there was a shortage of the information of such parameters. Predictions from his improved correlation agreed well with experimental data.

Ross et al. [1987] did experiments on saturated flow boiling in a horizontal tube with R152a and R13B1 and validated existing correlations in nucleate flow boiling and two-phase convective flow boiling regimes. In order to compare the HTCs of the tested refrigerants, the pressure at the outlet of the test tube was controlled at a fixed level. In the nucleate-flow-boiling region, they validated Stephan & Abdelsalam's HTC correlation [1980]. It was shown that the correlation predicted the results well. For the prediction of the quality at which the fully suppression of the nucleate flow boiling occurred, Hsu & Graham's model [1976] and Collier et al.'s suppression criterion [1964] were validated. In the two-phase-convective-flow-boiling region, they validated Chen's correlation [1963]. It was found that Chen's correlation without the nucleate boiling term predicted the experimental data well. However, the Prandtl number correction, suggested by Bennett & Chen [1980], was needed when nucleation occurred.

Jung et al. [1989a] carried out experiments on saturated flow boiling in a horizontal tube with R22 and R114. Their test section was made up of two 4-metre long by 0.9 cm i.d. stainless steel tubes connected by a 180 degree U bend. The ranges of heat flux and mass flow rate were 10, 17, 26, 36 and 45 kW/m^2, and 16, 23, 33 and 46 gm/s respectively. To avoid a complete dry-out, the vapour quality was controlled to be between 85-90% at the heat exchanger outlet. In order to compare the results on the same basis, the outlet pressure was set at a fixed reduced pressure.

From their experiments (see Fig. 2.1), for a given mass flow rate (32.8 g/s), it was shown that in the partial boiling regime, up to the quality 20-30%, the HTCs were a function of the heat flux. This suggested the existence of the nucleate flow boiling in that regime. Later, the gradual suppression of the nucleate flow boiling led to a fall of the HTCs with increasing quality. The transition point to enter the two-phase convective flow boiling regime was a function of the heat flux such that it moved to a higher quality as heat flux increased. Beyond this transition quality, the lines for the various heat fluxes merged into a single line indicating that the nucleate flow boiling was suppressed. They explained this finding in terms of various dimensionless

parameters (see Fig. 2.2, plotted **between** the ratio of the two-phase HTC and the single-phase liquid convective HTC (based on the mass flow rate of liquid in the 2-phase flow) **and** the inverse of the Martinelli parameter). In the partial boiling regime (where the inverse of the Martinelli parameter was about between 0.2 to 3), the HTCs were a function of the boiling number. For the small boiling number (the high mass flow rate and the low heat flux), the heat flux dependence of the HTC quickly disappeared at the very low qualities. For the large boiling number (the low mass flow rate and the high heat flux), the opposite happened. In the two-phase convective flow boiling regime, the HTC was found to be depended on the quality or the Martinelli parameter.

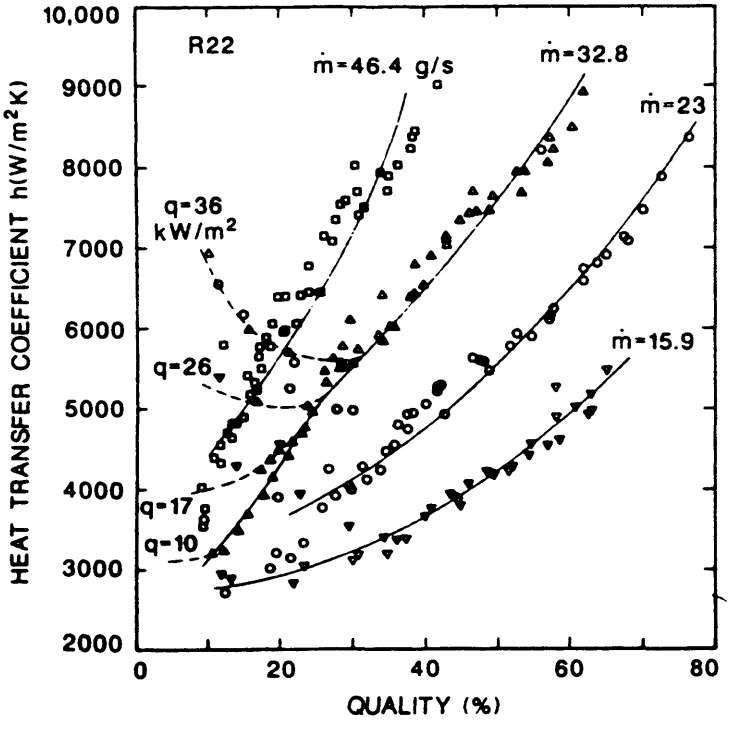

Figure 2.1 Flow boiling heat transfer results for pure R22 at 0.80 reduced pressure as a function of quality for various mass flow rates (Heat flux dependence at low qualities was shown only for 32.8 gm-per-second mass flow rate as an example.)[Jung et al. 1989a]

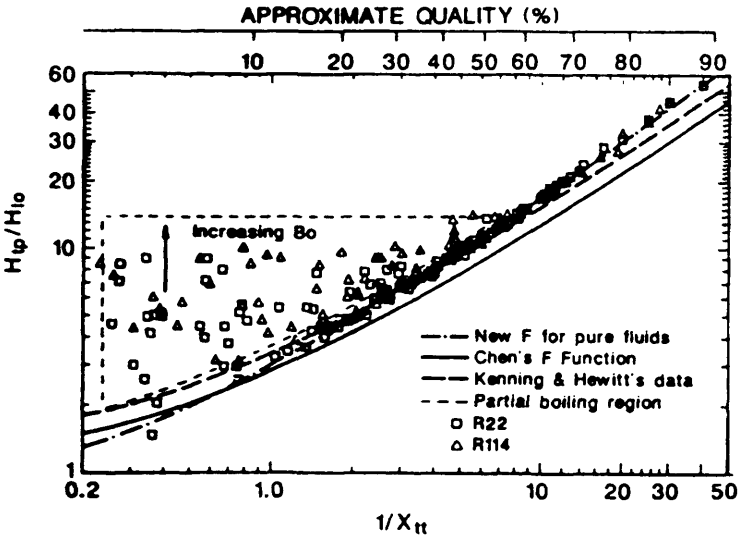

Figure 2.2 Flow boiling heat transfer results for pure R22 and R114 at 0.08 reduced pressure using dimensionless parameters [Jung et al. 1989a]

Jung et al. [1989b] studied experimentally saturated flow boiling in a horizontal tube with R12 and R152a to develop a semi-empirical correlation to predict HTCs. The apparatus and the experimental conditions were the same as their previous study [Jung et al. 1989a], except that the vapour quality was 95% at the heat exchanger outlet. With the experimental data from their work (for R12, and R152a), their previous work, and some other existing works (for R22, R114, and steam-water), the correlation was developed based on Chen's correlation [1963], with two main modifications. First, the F factor value was revised with the experimental data. Second, the micro-convective contribution of Chen's correlation [1963], being the product of Forster & Zuber's correlation [1955] and the S dimensionless factor, was replaced by the product of Stephan and Abdelsalam's correlation [1980] and a newly introduced N dimensionless factor being a function of the Martinelli parameter and the boiling number. When comparing their calculated results with the experimental data, the correlation gave a mean deviation of 7.2%.

Later, Jung & Radermacher [1991] validated Jung et al.'s correlation [1989b]. For R11, the mean deviation between the data and the correlation was 6.3%. For R134a and R12, they used the data from Eckels & Pate's experiments [1991] and the mean deviations between the data and the correlation were 7% and 8% for R134a and R12 respectively.

In addition, Jung & Radermacher [1991] performed cycle simulations when using various refrigerants, including R134a, R32, and R123, to demonstrate the

applicability of Jung et al.'s correlation [1989b]. For the comparison purpose, the cooling capacity and the condenser temperature were fixed for each refrigerant. For the 20-kW/m^2 heat flux, it was noted that the fully suppression of the saturated nucleate boiling happened even at 10% quality for all test refrigerants, except R143 and R32 for which it happened at the greater than the 20% quality.

Murata & Hashizume [1993] experimented on saturated flow boiling in a horizontal tube with R123. They then proposed a semi-empirical correlation to predict the HTC, developed by modifying Chen's correlations [1963]. There were two main modifications. First, the F factor was revised by the regression analysis with their experimental data. Second, for the micro-convection contribution as mentioned in Chen's work [1963], they used Nishikawa et al.'s correlation [1982] with Bennett et al.'s S dimensionless factor [1980] to replace Forster & Zuber's correlation [1955]. It should be mentioned that Chen [1963] arranged Forster & Zuber's correlation [1955] to be in the form which used the same wall superheat as that of the two-phase convective flow boiling, which used the S dimensionless factor. Nishikawa et al's correlation [1982] was used to predict the pool boiling HTC at the same wall superheat as for the two-phase convective flow boiling. In their work, they emphasised that the nucleate-flow-boiling contribution was evaluated from the nucleate-flow-boiling heat flux rather than from the total heat flux. The correlation predicted the HTC to within ±20% of the experimental data, with a mean deviation was 8.5%.

2.1.2 Pure-refrigerant pressure drop

Earlier work on the determination of 2-phase pressure-drop was mainly based on experimental research on water-steam or oil-gas fluids, producing charts and maps for saturated-flow-boiling in tubes. Some correlations were further developed and modified for saturated flow boiling of pure refrigerants in horizontal tubes. Furthermore, all the work on correlation development appeared to be based on single-phase-flow knowledge. A review of the relevant research is given as follows.

Martinelli & Nelson [1948] developed semi-empirical and empirical correlations for predicting pressure drop during forced-circulation boiling of water in tubes. Three main concepts, all based on turbulent vapour and liquid flows, were employed to develop their charts. First, the pressure drop was made up of two parts: the frictional pressure drop and the pressure drop due to the acceleration. Second, the frictional pressure drop was a function of both the only-a-single-phase-flow frictional

pressure drop and the two-phase frictional multiplier also assuming only a single-phase flow. (The ratio of the liquid to the vapour flow-alone two-phase frictional multipliers was defined as the well known Martinelli parameter, shown in Section 3.4.1.). Third, for the pressure drop due to the acceleration, when the pressure drop across the tube was small compared to the absolute pressure, the flow was considered effectively incompressible. To validate the developed charts, predicted results were compared with some experimental data of others, and it was found that the predicted results were within ±30% accuracy.

Lockhart & Martinelli [1949] developed further Martinelli et al.'s correlations [1944, 1946]. They collected the experimental data from four investigators for the simultaneous two-phase flows in which the gas phase was air and the liquid phase was benzene, kerosene, water, or various oils, in tubes of different diameters. They used the experimental data to correlate for the exponent and constant values used in the Martinelli-parameter correlations for various flow types. It was mentioned that more data were needed to establish definitely the validity of the suggested Martinelli-parameter correlations, particularly at the very high and very low values of the Martinelli parameter and at near the critical point.

Baker [1954] studied flow pattern effects on pressure drop prediction for two-phase flow of oil-and-gas fluids inside tubes. He plotted the Baker map, which showed the boundaries of the various flow patterns as functions of the generalised gas-phase mass velocity and the generalised ratio of the liquid to gas phase mass velocities. By using some available experimental data, he used Lockhart & Martinelli's correlations [1949], being regardless of the flow pattern, to calculate the two-phase-frictional-multipliers, based on the pressure gradient for the gas alone flow, for many flow regions. It was found that Lockhart & Martinelli's correlations could not give satisfactory results in some flow regions, especially in the wavy and stratified flows. Baker further developed the two-phase-frictional-multiplier correlations for various flow regions. However, his correlations had more terms than the Lockhart & Martinelli's correlations. For example, in slug flow, the liquid-phase-mass-flux term was added into his correlation. From the investigation, it seemed that the type of the flow pattern was necessary to be taken into account when estimating the two-phase flow pressure drop.

Pierre [1957] developed a semi-empirical correlation for the prediction of a dimensionless turbulent friction factor for boiling of refrigerants in a straight horizontal tube. He used three main assumptions in his derivation. First, the velocities of the vapour and the liquid were identical, so that the flowing fluid could be considered homogeneous. Second, the flow resistance due to friction was generated from the shear force on the wet tube wall. Finally, the flow resistance was a function of the square of the two-phase velocity. His experimental work used R12 and R22 and the inlet quality ranged from 0.10 to 0.20. It was found that the friction varied in a similar way to that for a single-phase flow, i.e. as a function of the square of the two-phase velocity. In addition, it was shown that the factor was a function of the Reynolds number and the boiling number. The basic difference between this correlation and that for turbulent single-phase flow was the added boiling number.

Altman et al. [1960] performed experiments on pressure drop of R22 evaporating in horizontal tubes. The inlet qualities ranged from 0.20 to 0.99. Martinelli & Nelson's [1948] method for calculating two-phase pressure drop inside tubes was extended to use with R22. 80% of the experimental data on the local pressure drop correlated between +5 % and -20 % of those calculated. Anderson et al. [1961] measured pressure drop of boiling R22 in a horizontal tube for inlet-qualities ranged between 0.19 and 0.82. The measured values fell between those predicted by Martinelli & Nelson's [1948] and Pierre's [1957] correlations.

Singal et al. [1983] measured pressure drops for R12 boiling in a tube and then developed correlations for predicting total and frictional pressure drops. (It is needed to remind that their work was also done for R12/R13 mixtures.) They found that Martinelli & Nelson's [1948] correlation mostly over-predicted the pressure drop data. They developed their two pressure-drop correlations as a function of the Martinelli & Nelson's pressure-drops and the concentration of R13. When they used the correlations with pure R12, i.e. by setting the concentration of R13 to zero, it was found that the predicted results were within an accuracy of ±30% of the experimental data.

Jung & Radermacher [1989] developed correlations for horizontal-annular-flow-boiling pressure drop in a tube with R22, R114, R12, and R152a. The test section, the ranges of heat flux and the mass flow rate were the same as that in Jung et al.'s work [1989a]. The quality at the heat exchanger outlet was up to 95%. The pressure at the outlet was kept at 0.08 - 0.16 reduced pressures.

When comparing the experimental data with the predictions, it was found that Pierre's correlation gave the mean deviation of 12%, but the correlation application range did not cover half of their test data. This was because the values of Reynolds number-to-boiling-number-ratio from the half of the experimental data were out of the applicable range in the Pierre's correlation. On the other hand, the Martinelli & Nelson's correlation over-predicted the experimental data by 20%. So, Jung & Radermacher selected the Martinelli & Nelson's correlation to be modified by using three concepts. First, the accelerating pressure drop was negligible when the ratio of the tube length and diameter was in the range of 500 – 1000. Second, they defined the two-phase frictional multiplier as a function of two factors: the frictional pressure drop, occurring if only the liquid-phase flew in the tube, and the total two-phase pressure drop. Finally, the two-phase frictional multiplier was correlated with the experimental data to be a function of the Martinelli parameter. With these concepts, the two-phase frictional multiplier, assuming the total flow to be liquid, was shown to be a function of the Martinelli parameter and the vapour quality. This multiplier would then be used in the integration term of the total-pressure-drop correlation. It was found that the predicted results were within the accuracy of ±10% with the experimental data, and had the mean deviation of 8.4%.

2.1.3 Refrigerant-mixture heat transfer coefficient

In the studies of refrigerant-mixture heat transfer coefficient for saturated flow boiling, many correlations were proposed for the nucleate- and the two-phase-convective- flow-boiling regions. Researchers have been trying to identify mixture effects and incorporate them in the correlations. The development of the correlations was either using the semi-empirical or theoretical approach with or without phase-equilibrium concepts [Smith & Ness 1987]. In addition, the nucleate-flow-boiling suppression was investigated on how it was influenced by mixture effects.

Ross et al. [1987] did experiments and validated other researchers' correlations with boiling of R152a/R13B1 mixtures in a horizontal tube. In the nucleate-flow-boiling region, they validated Thome's pool boiling correlation [1983]. Comparing with the experimental data, this correlation predicted the results well. Although they could not carry out any experiments related to the initiation of the fully nucleate-flow boiling suppression, their correlative variables suggested that the suppression would be easier to achieve with refrigerant mixtures than the pure refrigerants. In the two-phase-

convective-flow-boiling region, they verified Chen's correlation [1963] but without using the nucleate boiling term. It was found that the predicted results agreed well with the data, particularly at the high vapour qualities.

Jung et al. [1989a] experimented on saturated horizontal-flow boiling of R22/R114 zeotropic mixtures. It was shown that, when compared with or based on the pure refrigerants (Figs. 2.1 and 2.2), the nucleate-flow-boiling suppression could be described in the same way, but happened at a lower quality (Figs. 2.3 and 2.4, respectively). (The component-volatility difference caused mass-transfer-resistance and loss-of-wall-superheat effects, seen in Fig. 2.5, which created the slower-growing bubbles and smaller bubble departure sizes.) For the two-phase convective flow boiling region (Fig. 2.6), it was shown that the experimental HTCs of the mixture were lower than that of the ideal value. (The ideal coefficients were based on the mole fraction of the mixture components only.) For instance, at the 65% quality for the 0.47/0.53 mixture by mass, the experimental value was as much as 36% lower than the ideal one. The calculated values, using the phase-equilibrium concept in Chen's correlations [1963], also showed the same trend but gave values in between the ideal and the experimental ones.

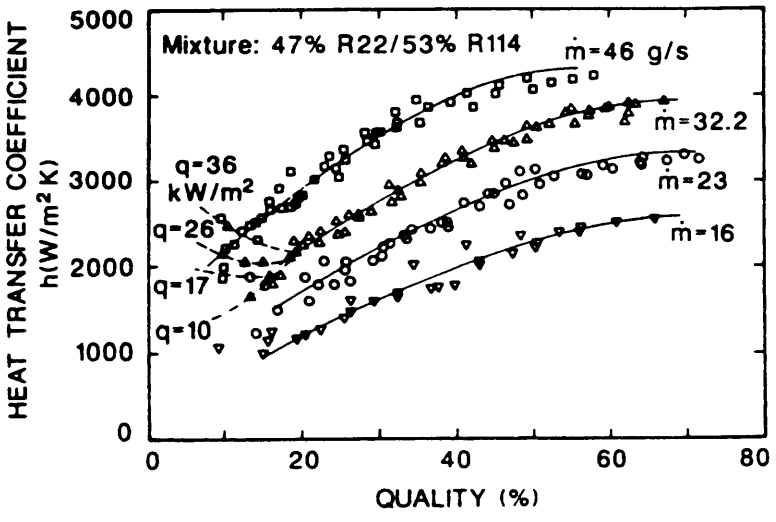

Figure 2.3 Flow boiling heat transfer results for 47% R22 / 53% R114 at 0.08 reduced pressure as a function of quality for various mass flow rate (Heat flux dependence at low qualities was shown only for 32.8 gm-per-second mass flow rate as an example.) [Jung et al. 1989a]

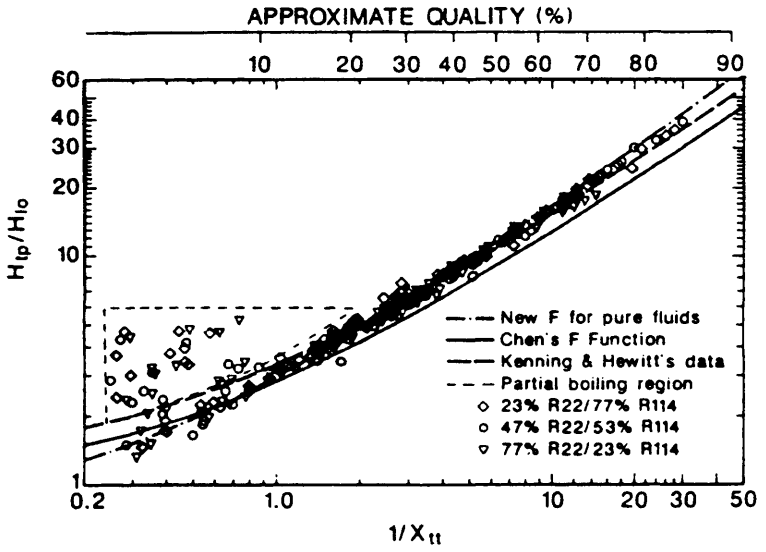

Figure 2.4 Flow boiling heat transfer results for R22 / R114 mixtures at 0.08 reduced pressure using dimensionless parameters [Jung et al. 1989b]

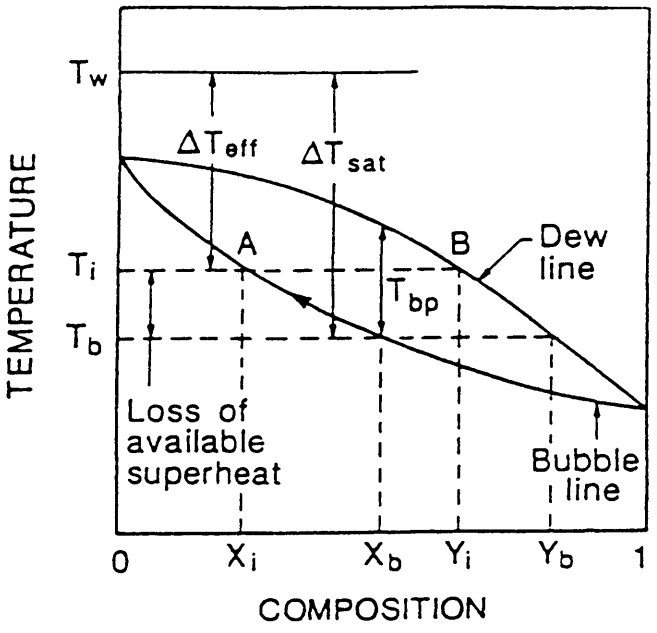

Figure 2.5 Bubble growth process of a binary mixture illustrated on a phase equilibrium diagram [Jung & Radermacher 1993]

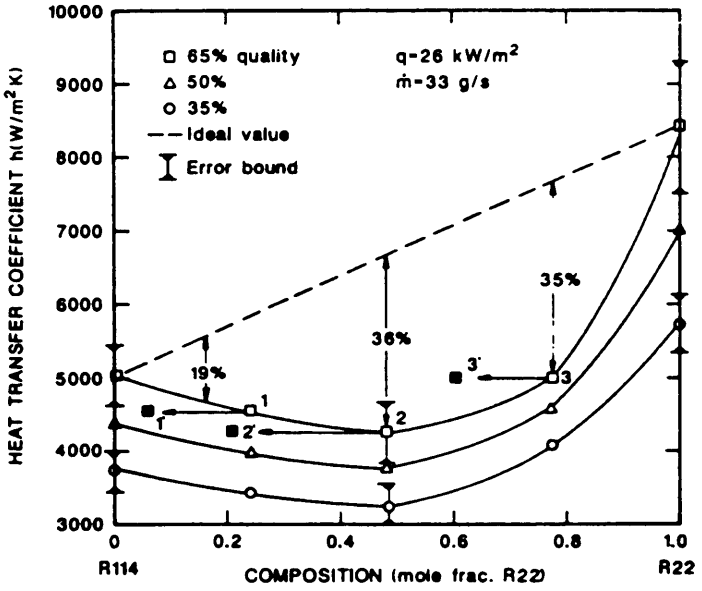

Figure 2.6 Heat transfer coefficients of pure and mixed refrigerants of R22 and R114 in convective evaporation region as functions of composition and quality at 0.08 reduced pressure [Jung et al. 1989a]

The degradation of the calculated values from the ideal values was caused by physical mixture-property variations (three causes). These (first two causes) included the equilibrium temperature variation, due to mixing, and the changes in liquid phase composition at higher qualities; the latter could not be avoided for any mixtures, except at azeotropes. The third cause was due to the non-ideal mixture-property variation, which would be absent if the properties varied ideally. Jung et al. found that the effect of equilibrium temperature variation and the composition change was two to three times larger than the non ideal effect.

Therefore Jung et al. concluded that the degradation for the calculated values equalled to about 80% of that from the experiments. The remaining 20% of the experimental degradation, which was less than 10% of the experimental HTC, was due to the mass-transfer-resistance effect in the evaporation of the mixtures.

Jung et al. [1989b] were experimenting with both zeotropic and azeotropic refrigerant mixtures, i.e. R22/R114 and R12/R152a respectively, to develop semi-empirical correlation. Based on their pure-refrigerant correlation [Jung et al. 1989a] and the mixture-phase-equilibrium concept, three main modifications were carried out. First, the revised F factor was multiplied by the correction factor, C_{me}, which considered the mass-transfer-resistance effect from the two-phase convective flow boiling. Second, for the nucleate pool boiling heat transfer, Unal's correlation

[1986], developed to account for the mixture effect in the saturated nucleate flow boiling, was used instead of Stephan and Abdelsalam's correlation [1980]. However, the nucleate pool boiling HTC of pure components in the mixtures was still calculated by using the Stephan and Abdelsalam's correlation. Finally, the N factor was divided by the correction factor, C_{UN}, originally developed by Unal [1986], again to reflect the mixture effect in the saturated nucleate flow boiling. Jung et al.'s correlation gave the mean deviation of 9.6% with the data.

Jung & Radermacher [1993] performed cycle simulations under the same conditions as that in their previous work [Jung & Radermacher 1991] for pure refrigerants and zeotropic refrigerants, including R32/R142b and R32/R152a. It was found that the saturated-nucleate–boiling suppression occurred at the less than 20% vapour qualities for all the tests, and those qualities for the refrigerant mixtures were lower than that for the pure refrigerants.

Hihara & Saito [1990] developed a theoretical binary-mixture correlation for two-phase forced convective boiling in a horizontal tube, and validated it with their R22/R114 data. It was postulated that the correlation comprised of the nucleate-and the two-phase-convective flow boiling contributions. Each consisted of a heat-transfer-coefficient correlation of the equivalent single-component fluid, and a correction factor for mixtures. For the nucleate-flow-boiling-contribution, they used Calus & Leonidopoulos' [1974], Stephan & Korner's [1969], and Thome's [1983] correlations. It should be mentioned that for the wall superheat calculation used in the calculation of the correction factor, the Stephan & Korner's method [1969] used an estimated value based on an experimentally determined constant factor. For the two-phase-convective-flow-boiling-contribution, the annular flow model, with the phase-equilibrium concept, was formed by the liquid-film and the vapour heat balances, and by the phase-interface and the overall mass balances. Since neither momentum nor heat transfer near a phase interface was understood well, the two-phase pressure drop multiplier was used in estimating the mass transfer coefficient in the liquid film. In addition, the heat- and the mass- transfer coefficients in the vapour were formed by analogy with the interfacial shear stress in the condensing flow of steam. Compared with their experimental data, the HTCs could be predicted with moderate accuracy.

Granryd [1991] developed a theoretical approach to predict HTCs of zeotropic refrigerants in a saturated annulus flow. This approach recognised that vapour and liquid phases were not in the equilibrium due to the heat and mass transfer

resistances. In developing the model, many assumptions were used, and the two crucial ones were: First, the specific heats of the liquid, vapour, and two-phase refrigerant mixtures at the temperature between the liquid and vapour temperatures were constant and equal to each other. Second, the HTC between the vapour and the liquid could be estimated from the multiplication of the Dittus-Boelter equation and a correction factor that took into account the liquid-vapour-interface effects. By comparing the calculated results with other researchers' experimental data, it was found that there was a relatively good agreement.

Zhang et al. [1997] developed Hihara & Saito's model [1990] to be used for a ternary mixture (R32/R125/R134a 0.23/0.25/0.52) under mostly the same postulations and assumptions, except for the nucleate-flow- boiling contribution that Stephan & Korner's [1969] or Thome's [1983] method was used for determining the correction factor in the calculation of the wall superheat. It should be mentioned that, in the Stephan & Korner's method [1969], the estimated value of the experimentally determined constant factor for the binary mixtures was used for the ternary mixture. , The predicted results showed fairly good agreement with their experimental data.

Murata & Hashizume [1993] experimented and proposed a semi-empirical correlation for a zeotropic refrigerant (R123/R134a 0.9/0.1 by mass). The concept was that the heat flux at the tube wall was equal to the sum of the heat flux transferred to the liquid film and the heat flux used in the nucleate flow boiling. The method used to calculate the nucleate-pool-boiling HTC was in the same format as Stephan & Korner's method [1969] for calculating the wall superheat. Comparing with the experimental data, the predicted results were within ±20% with a mean deviation of 16%.

2.1.4 Refrigerant-mixture pressure drop

For refrigerant-mixtures, same observations (Section 2.1.2) could be made for the development of pressure-drop correlations. Researchers first conducted experiments in flow boiling mainly in horizontal tubes. They then investigated influences of the effects of mixture-concentration on the pressure drop. Much of the efforts focused on improving or modifying existing correlations (for pure refrigerants) to obtain the pressure-drop correlations for mixtures.

Singal et al. [1983] did experiments on R13/R12 mixtures and developed pressure-drop correlations through improving the work of Martinelli and Nelson [1949].

It was found that Martinelli & Nelson's correlation under-predicted the pressure drop with 25 to 50% deviations for 5 to 20% by weight of the R13 concentrations. This indicated that pressure drop was a function of the mixture composition. They further developed the total-pressure-drop and frictional-pressure-drop correlations which reflect the influence of compositions. These pressure drop correlations, however, covered only up to 20% by weight of R13. The predicted results were within ±30% of the experimental data, but had a mean deviation of nearly zero%.

Jung & Radermacher [1989] did work on R22/R114 (0.23/0.77, 0.48/0.52, and 0.77/0.23 by weight) and R12/R152a (0.21/0.79, 0.6/0.4, and 0.88/0.12 by weight). From their experiments, they found that Pierre's correlation could not be applied to half of their test data. This was because the values of the Reynolds number-to-boiling number ratio from the half of the experimental data were out of the applicable range of the Pierre's correlation. It was also observed that Martinelli & Nelson's correlation overestimated the data by 20% for all the tested mixtures. This finding was the same for the pure refrigerants, R12 and R13, as mentioned previously. By using the dimensionless analysis, they have shown that the predicted dimensionless pressure drops of both pure and mixed refrigerants were equally well correlated with the experimental dimensionless pressure drop by the Martinelli parameter. It was, therefore, an indication that there was no composition dependence for the pressure drop.

To obtain the pressure drop correlations, they modified Martinelli & Nelson's correlation by using the three concepts described earlier. In the third concept, the two-phase frictional multiplier, when considering the total flow to be both liquid and vapour, was correlated with the experimental data from both pure and mixed refrigerants to be a function of the Martinelli parameter. The developed correlation could predict pressure drops of the mixture refrigerants with a mean deviation of 8.4%. The correlation could be used for pure refrigerants as well.

2.2 Air-side heat transfer coefficient and pressure drop

This Section reviews the development of heat transfer coefficients and pressure drops for the air side of plate-finned-tube evaporators. The review covers conditions including dry and wet operations. Before considering the details, the fundamental links between HTCs and Colburn j-factors, and pressure drops and friction factors need to be introduced. The j-factor analogy [Chilton &Colburn 1934], relating momentum, heat and mass transfers, suggests that the air-side HTCs is a function of or

obtained from the Colburn j-factors. From the Buckingham pi non-dimensional analysis and the Darcy-Weisback equation, the pressure drops are expressed as a function of the friction factors. It means that the pressure drop can be calculated if the friction-factor value is known.

2.2.1 Dry plate-fin-tube evaporator

Colburn-j- and friction- factor correlations for air-side dry plate-fin-tube evaporators involved independent variables which consisted of air properties and coil configurations.

Elmahdy & Biggs [1979] used other researchers' data to develop a Colburn j-factor correlation for finned tube coils. They also performed experiments to verify the correlation. The coil configuration was a multi-row and staggered circular tube arrangement with either the circular or the continuous flat plate fins. Their correlation showed that the Colburn j-factor was a function of the air Reynolds number, the coil hydraulic diameter, the fin spacing and thickness, and the fin height. It was observed that the higher the Reynolds number, the less was the Colburn j-factor. In addition, when the fin-thickness-to-fin-height ratio or the coil-hydraulic-diameter-to-fin-thickness ratio increased, the Colburn j-factor increased. It was shown that the predicted j-factor was a little higher than the experimental one.

McQuiston [1978a] did an experiment on plate-fin-tube heat exchangers with five different fin pitches in order to study behaviour of heat and momentum transport between air- and hot water. Later McQuiston [1978b] developed Colburn j- and friction factor correlations by using his own data [McQuiston 1978a]. He found that the Colburn j-factor was a function of the air Reynolds number and the coil configurations. (i.e. the tube diameter, the tube hydraulic diameter, the tube longitudinal and transverse spacing, the ratio of the minimum free flow area to the frontal area, and the number of tube rows.) The friction factor was found to be a function of the air Reynolds number, the transverse spacing, the tube outside radius, the surface area of bare tubes, the air-side surface area, and the fin spacing and thickness.

Gray & Webb [1986] developed Colburn j- factor correlation without including the tube hydraulic diameter, the ratio of the minimum free flow area to frontal area, and the number of tubes. However for the friction factor, they used the surface area of fins instead of the surface area of bare tubes. When comparing with McQuiston's correlation [1978b], their correlations gave improved results.

Turaga et al. [1988] investigated performance of direct expansion plate-fin-tube coils with a refrigerant flowing inside the tubes. With fixed values of the tube diameter, and the tube longitudinal and transverse spacing, both Colburn j- and friction factors were found to be a function of airflow Reynolds number, the surface area of bare tubes, and the total air-side surface area. When comparing their predicted results and other correlations with their experimental data, their results gave a small mean deviation.

2.2.2 Wet plate-fin-tube evaporator

In developing the Colburn-j- and the friction- factors for air-side of wet coils more independent variables needed to be incorporated than that of dry coils. The review would also demonstrate that it is significant to exercise care in properly applying a correlation for wet coils.

McQuiston [1978a] also performed experiments for wet coils. Two types of the wet conditions: the film-wise condensation and the drop-wise condensation were examined. For wet conditions, McQuiston [1978a and 1978b] found that the Colburn j- and the friction- factors were a function of the fin spacing in addition to those mentioned in their dry-coil studies. It was pointed out that for the fin pitch greater than 12 fins per inch with the face velocities greater than 500 fpm, the Colburn j-factor correlations gave the poorest accuracy. This was thought to be due to the extreme interaction between the condensate and the air stream.

Turaga et al. [1988] also studied film-wise condition. Both Colburn j- and friction- factors were a function of the spacing and the thickness of fins, as well as those for the dry-coil case. Their predicted results had a smaller mean deviation when compared to McQuiston' correlations [1978b].

Chuah et al [1998] used the Elmahdy & Biggs's correlation [1979] and Myers' correlation to obtain the air side HTCs. By comparing the results from experiments (on a 3 row plate-fin-tube coils) and the prediction, it was found that, for the total heat transfer, the predicted results were in the same trends as the experimental ones, but with higher values. For the dehumidification capacity, not only were the resulted over predicted, over-predicting, the trends were different too. They thought that the causes were due to the use the heat-mass-transfer-calculation correlations for evaporators with more than six rows and the inadequacy of the analysis in predicting the dehumidification capacity.

2.3 Types of evaporator models

The survey reveals that there are two main types of mathematical models adopted by researchers: non-distributive and distributive models. The former are mainly used for steady-state studies, while the later are generally employed for dynamic studies.

2.3.1 Non-distributive models

From this review, it can be seen that non-distributive models have wide ranges of application with various degrees of complexity and accuracy. It can be further categorized into non-finite-element models and finite-element models. The former is generally expected to give less accurate results than the latter which is normally chosen for more accurate analysis or design.

a) Non-finite-element models (zone-region-or-tube models)

When using non-finite-element models for plate-finned-tube evaporators, the studies generally are based on the refrigerant side. The evaporator can be arranged into either two-phase or two-phase-and-superheat zones, quality-range regions, or tube-by-tube portions. Many assumptions or concepts are used, for instance, negligible refrigerant pressure drop, UA [Hewitt et al. 1994] and LMTD [Incropera & Witt 1990] concepts, etc.

Oskarsson et al. [1990b] studied the performance of evaporators when using a pure refrigerant under steady states for dry and wet conditions. The evaporator was modelled through a UA two-zone concept with three regions identified by qualities. The three regions consisted of a two-phase region (the quality up to 0.75), a transition region (from .75 to dry-out), and a superheated region. They used the assumption that the air HTC for the wet coil was the same as that for the dry coil. The refrigerant-side HTCs for the two-phase and superheated flows were Pierre's and Hiller's correlations respectively, and the refrigerant-side pressure drop was neglected. In addition, the model did not include dehumidification in the superheat region.

When comparing the predicted heat transfer with the experimental results, the errors were within 2 and 17% for the dry and the wet cases, respectively. For the dehumidification–rate prediction, the errors were within 40% and 10% for the low- and the high- dehumidification-rates, respectively. It was found that the model, in some

cases, predicted dry operation whereas the experimental results showed the occurrence of condensation, especially at the low dehumidification rates.

Domanski & McLinden [1992] used non-finite-element evaporator model in cycle analysis for performance rating of pure refrigerants, R134a and R134. They implemented UA two-zone and LMTD concepts, and isobaric-refrigerant heat transfer with the same U value throughout the evaporator. In addition, the refrigerant at the exit of the evaporator was assumed to be saturated, and the refrigerant temperature at the compressor inlet was fixed at constant values.

Admiraal & Bullard [1995] created a counter-flow evaporator model by using the UA concept with a uniform air distribution, for pure refrigerants, under steady-state operation. The overall air-side HTC was treated as a constant value through out the evaporator for a given volumetric airflow rate. When comparing with the experimental data [Admiraal & Bullard 1993], the model predicted the total heat transfer well.

b) Finite element model

Finite element models are in fact modified non-finite-element models which have more than one element in each tube or zone.

Oskarsson et al. [1990b] also used a finite-element model in their study. When comparing the heat transfer from both non-finite and finite models, the differences were within 2%. However, at low dehumidification-rate operating conditions, the dehumidification-rate error could become very large. Domanski & McLinden's [1992] used the finite-element evaporator model for zeotropic refrigerant mixtures, R22/R123, with the temperature-nonlinearity along the tube of the refrigerant neglected and recognized, respectively.

2.3.2 Distributive models (differential volume models)

Distributive models are essentially based on the finite-element-model. When each element is applied with unsteady-state forms of continuity, momentum and energy equations, and the equations are discretized for numerical solving, the model becomes distributive model. The distributive models are mainly used for more accurate predictions and for dynamic analysis.

MacArthur [1984] studied theoretically the transient behaviour of a heat pump using a pure refrigerant by applying a differential-volume-approach. For the one-

tube evaporator model, the energy and continuity equations were formed for both the air side and the refrigerant side, and the energy equation was also established for the tube wall. In the two-phase region, the homogeneous flow and the vapour-and-liquid-temperature equilibrium were assumed. The air density was treated as a constant value. All the equations were discretized by using the implicit-finite-difference concept.

Wang & Touber [1991] analysed steady and dynamic behaviour of a pure-refrigerant direct-expansion plate-fin-tube evaporator. For the refrigerant, a heterogeneous flow concept with vapour-and-liquid-temperature in equilibrium was implemented. The fundamental equations for the refrigerant, the tube wall, and the air were set up. However, the refrigerant momentum transport was assumed to reach the equilibrium quickly and thus the momentum equation was considered as time-independent. Moreover, because of its small heat capacity, the accumulated energy and mass of the moist air were not considered. All the equations were discretized by using the implicit-finite-difference concept. For the calculation of the refrigerant HTC and pressure drop, they used Lockhart-Martinelli's and Pierre's correlations, respectively. The air-side HTC was calculated from McQuiston's correlation. For the model validation, the simulated and the experimental dry-coil cases were carried out for three sets of condition: the steady-state operations, the capacity-control dynamic operation, and start-up after a long off-period. Results showed that the model simulation could satisfactorily predict the evaporator operation, especially for the start-up period.

Jia et al. [1995] studied both theoretically and experimentally the transient-response of an evaporator when using R134a. The model divided the evaporator into small volumetric elements and formed the continuity, momentum, and/or energy for the refrigerant, the tube wall and the air. The two-phase refrigerant assumption was the same as that in MacArthur's [1984]. The moist-air assumption was similar to that of Wang & Touber's [1991]; the air density was kept as a constant value. The simulation was carried out with a step change of the refrigerant mass flow rate. To validate the model, the experiments were carried out on a commercial container refrigeration system. It was found that the model provided satisfactory prediction of the transient response.

Jia et al. [1999] developed the model further based on their previous work [Jia et al. 1995]. The model took account of the non-homogeneous flow in the two-phase region. Three drift flux flow models, namely, Chisholm [1973], Smith [1970], and CISE [Premoli et al. 1971, Hewitt 1990], were examined. Results from both

the experiment and the simulation showed that all the three drift flux models could satisfactorily predict the evaporator performance. The homogeneous model underestimated the degrees of the superheat and predicted a faster transient response.

Judge & Radermacher [1997] developed a model to study steady-state performance of dry single-tube finned evaporators when using both pure and mixed refrigerants, including R407C. The concepts used in the model were similar to Jia et al.'s concept [1995]. The differences were: the temperature change of the tubes and fins with time was assumed to be the same as that of the refrigerants; and the moist-air accumulated energy was recognized. The flow boiling heat transfer correlations of Gungor & Winterton [1986], Shah [1982], Kandlikar [1991], Chen [1966], and Jung et al. [1989b] were used in the simulations. Only Kandlikar's and Jung et al.'s correlations were developed for both pure and mixed refrigerants. These two correlations were generally applicable to any binary halogenated refrigerant mixtures. When using these correlations with the ternary refrigerant mixture, R407C (R32/R125/R134a 0.23/0.25/0.52), the two of the three compositions with the most similar vapour pressures (R32 and R125) were treated as the one component for the HTC calculations.

When the simulated results were compared to their experimental ones, it was shown that Jung et al.'s correlation was the most satisfactory. The Baker's flow map showed that the large fraction of the energy was transferred in the annular regime and the rest was transferred in the wavy regime. In addition, a strategy of the comparison between the pure refrigerant and the refrigerant mixture was established, basing on the same average refrigerant temperature along the evaporator.

2.4 Steady-state studies when using pure refrigerants

Oskarsson et al. [1990b] modelled and simulated, and experimented on evaporators operating under dry and wet conditions. The engaged parameters were: the coil-inlet refrigerant temperature, vapour quality and mass flow rate, the refrigerant degree of superheat, the heat transfer rate, the dehumidification rate, and the air coil-inlet-and-outlet air temperatures and relative humidity.

Wang & Touber [1991] studied, experimentally and computationally, an evaporator under various dry-coil conditions. The involved parameters were: the coil-inlet-and-outlet refrigerant temperatures and mass flow rates, the degree of superheat, the coil-outlet refrigerant pressure, the refrigerant void fraction, the refrigerant vapour

and liquid velocities, and the interfacial momentum-transport coefficient, the coil-inlet-and-outlet air temperatures, and the air volume flow rate.

Admiraal & Bullard [1995] created program for an evaporator to study the refrigerant HTC variation. It was found that allowing for the variation of HTC along the tubes gave better predicted results than assuming constant HTCs.

Jia et al. [1999] investigated the effect of the refrigerant dry out position upon the air temperature of a DX evaporator under wet-coil conditions. It was found that by controlling the superheat position at the two ends of the coil for a given row, or by decreasing the degree of superheat, the more uniform air temperature distribution of the evaporator could be obtained.

2.5 Dynamic studies when using pure refrigerants

In this Section, research into both the dynamic behaviour of evaporators and thermostatic-expansion-valve (TEV) controlled evaporators are reviewed. The studies looked at the responses of the evaporators due to parameter changes and also included validation of various correlations with experimental data. For the TEV-controlled evaporators, research had been mainly focussing on how to improve stability of the evaporator control.

2.5.1 Evaporator

Research to-date was carried out in many aspects related to the control of system operation parameters.

MacArthur [1984] studied the variations of the total mass flow rate and the liquid mass per unit length along the evaporator during the start-up. In addition the time functions of air, wall, and refrigerant temperatures at various points in the evaporator were examined.

Wang & Touber [1991] found that complex distributive dynamic models were useful only for short-term simulations, such as one hour (rather than days or years). In case of the long-term simulations, the combination of the steady-state refrigerating machine model with the dynamic refrigerated room model was feasible.

Jia et al. [1995 & 1999] looked at the transient response of the degree of superheat to a step change in the refrigerant mass flow rate. It was found that the transient time of the superheat for a step decrease in the flow rate was about 30 seconds shorter than that for a step increase. For the case of the step increase, the heat stored in

the pipe must be removed by evaporation before steady conditions were reached. On the other hand, for the case of the step decrease, there is no heat to be removal. They also validated the homogeneous and non-homogeneous refrigerant flow models. The results were already mentioned in the Section 2.3.2.

2.5.2 Thermostatic Expansion Valve (TEV) controlled evaporator

To control the degree of refrigerant superheat in DX evaporators when changes in the air side parameters/conditions occur, commonly a TEV with a sensor bulb can be used. Stability of the control was the main subject studied by various researchers. They paid attention to the design variables of the TEVs and the characteristics of the sensor bulbs. The following review shows the relevant work when using pure refrigerants.

Najork [1971] investigated theoretically and experimentally an evaporator control loop. He proposed that the possibilities of the loop-stability improvement through increase of the valve spring constant, increase heat conductivity resistance between the bulb and the tube, and changes in coil design (say, by using parallel flow evaporator and more tube rows).

Broersen & van der Jagt [1980] studied hunting behaviour of a TEV-controlled evaporator under dry-coil conditions. They set up a model consisting of an evaporator (having 2-phase and superheat regions) and a TEV, and obtained a single-input, single-output feedback control system. They introduced various methods to improve the stability of the system; such as higher superheat settings, slower/faster bulb dynamics, and an automatic valve without a bulb.

James & James [1987] proposed a TEV model which was consisted of two sub-models, a needle and seat, and a sensor bulb. For the needle-and-seat-model, assumptions were: the direct proportion between the valve opening area and the valve-stem rise; the constant refrigerant-liquid density before and after the valve orifice; and the constant refrigerant pressure drop over the orifice. It was shown that the refrigerant mass flow rate was a function of the bulb pressure, the evaporator-outlet refrigerant pressure, and the static superheat setting. The sensor bulb, charged with a fluid having the vapour-and-liquid coexisting, was modelled with four possible types. First, both the sensor-bulb and the coil-outlet walls were arranged into eight zones. Heat and mass were balanced for each zone and the whole sensor bulb. The second type was made up with only one zone for each wall. The third type was assumed of having a thermal

equilibrium between the wall and the charged fluid of the sensor bulb, and forming only one zone for the coil-outlet wall. The last type was the same as the third type, but having a first-order lag instead of the thermal equilibrium.

They simulated the sensor bulb with all models in dynamical cooling and heating modes. It was found that there were no significant differences between results of the first and the second model type. When comparing with the first model, the third model was able to be used for the cooling but not for the heating. Finally, deviation between the third- and the fourth- model results was not significant except for the cases with large differences between the sensor-bulb and surrounding temperature.

Mithraratne [1992] modelled and simulated a TEV-controlled double-pipe counter-flow water chiller by using a distributive model. For the needle-and-seat-model, it was essentially the same as that of James & James [1987], but presented in a different form. For the sensor-bulb model, he modified James & James' third type model [1987] with three added assumptions. First, there is no change of the liquid level in the bulb for all operating conditions of the evaporator. Second, the charged-vapour-phase pressure was a linear function of the charged-fluid temperature. Third, it was assumed that the bulb and the coil-outlet walls were insulated enough thus no significant heat transfer from the environment to the walls. The simulated results included the variation in the length of the superheated section, the degree of superheat, and the refrigerant mass flow rate versus time when introducing a step change of the chiller-inlet water temperature.

Mithraratne et al. [2000] further modified Mithraratne's [1992] model for parametric studies. They investigated the evaporator behaviour both with and without recognizing the bulb thermal capacitance effect and the thermal resistance effect between the bulb and the coil-outlet-wall. They also looked at the design variables of both the needle-and-seat and the bulb models in relation to above effects. For the two-phase refrigerant flow, the void fraction model accounting for the liquid-vapour slip was applied. From their study, few key observations were made. First, the predictions were in the good agreement with other researchers' experimental data. Second, the TEV valves, which showed the diverging oscillatory behaviour in the response to the change in the water temperature, gave a stable output when recognizing those two mentioned effects. Third, the nature of the response, i.e. stable or otherwise, of the TEV-evaporator system was found to depend on if water temperature was increased or decreased.

Fourth, the parametric study revealed that the stability limits of the system depended on the design variables of the TEV and the bulb.

2.6 Steady-state and dynamic studies when using refrigerant mixtures

The following Section reveals various studies of steady-state behaviour evaporators when using mixture; however, so far no published work on the dynamic analysis involving mixtures has been found.

Braven & Troxel [1990] programmed an evaporator of a heat pump when using varied compositions, R22/R114 and R22/R11. It was found that the composition of the refrigerant mixtures, corresponding to large UA-per-unit-capacity values, showed good matches for the temperature profiles of the refrigerant mixture and the heat transfer fluids, and yielded higher COPs.

Haselden & Chen [1994] investigated performance of evaporators in an air-conditioning system using a zeotropic mixture, R22/R142b, through modelling and simulations. They used the pinch-point concept, being that in an evaporator there would be a pinch point between the air and refrigerant temperature profiles. Their work showed that for a given value of pinch point, when the composition of R22 was varied, the COP also varied and there was a maximum COP. To achieve this, the fin area also needed to be varied too. So this suggested that overall power savings were likely when the refrigerant mixtures were properly applied.

Judge & Radermacher [1997], apart from working on mixed-refrigerant HTC correlations comparison, also simulated the air-conditioning to investigate the R407C temperature glide effect upon the coil-capacity of various evaporator flow geometries. It was found that when based on the cross-flow performance, the parallel flow one was down by 8.3%, while the counter-flow one compared to the cross flow one was up by 4.4%.

2.7 Literature-review analysis

This Section highlights the relevant information and observations, from the review, to be used and/or applied in the present work. First, the author summarised some important issues/points and raised some ideas for further implementation opportunities. Later, the author clarified some ambiguous points which could affect the decision-making stages in the work. Appropriate factors from the review were taken

into consideration when formulating the present research programme; the originalities of the work were highlighted at the end of this analysis.

2.7.1 Heat transfer coefficient for pure refrigerants

Chen's correlation [1963] was only developed for vertical-tubes and should be avoided for horizontal-tube applications. However his postulation about the micro- and macro- convective mechanisms appeared to be practically valid, and had been adopted or modified by many other researchers. The work of Bjorge et al [1982] based on the superposition principle did not give any more accurate results than Chen. Without experimenting on any pure refrigerant, Chen's and Bjorge's correlations may not be entirely appropriate for predicting pure refrigerant behaviour.

The chart developed by Shah [1976], based on experiments with refrigerants, was inconvenient to be employed in computer calculations. It seemed that the correlation could not give accurate results in the liquid-deficient region, i.e. from the 80% vapour quality onwards, since the chart was not originally developed for that region. It appeared that Gungor & Winterton's correlations [1986] are more suitable for refrigerants as their work was based on a large amount of data from many refrigerants.

Klimenko's works [1988, 1990] suggested both the wall thermal conductivity effect and wall material should be considered, but his thinking was not widely adopted by other researchers. Ross et al.'s work [1987] suggested that it was possible to predict the saturated nucleate flow boiling even by using pool boiling correlation without including the mass flux and quality effect terms.

Jung et al.'s work [1989b] seemed to be based on applying the superposition principle and on using the same form of correlation as Chen's which was developed based on the postulation of the contribution of the heat flux. That was why the same heat flux at the tube wall was used, by Jung et al, in the calculations of the nucleate-flow-boiling and the two-phase-convective-flow-boiling terms. It appeared that they gained confidence based on Ross et al.'s validation work [1987]. Their correlation can be used in all three regimes, i.e. the saturated nucleate flow boiling regime, the partial boiling regime, and the two-phase convective flow boiling regime.

Murata & Hashizume's work [1993] on correlation development strictly adhered to Chen's postulation and their modification is for strengthening Chen's correlation to give a more accurate prediction.

From Table 2.1 (Murata & Hashizume, 1993), it can be seen that Murata & Hashizume's correlation gave the least mean deviation when compared to Ross et al.'s and Jung et al.'s correlation. On the other hand in Table 2.2 (Jung et al., 1989b), it is shown that Ross et al.'s correlation gave higher mean deviations than Jung et al.'s.

Table 2.3 shows that, from the correlation-development point of view, Jung et al.'s correlation was obtained based on the data from a larger number of refrigerants than those of Murata & Hashizume's work. Moreover, Jung et al.'s mean deviations were mostly lower than that of Murata & Hashizume's ones. In addition, Jung et al.'s correlation was validated (Table 2.3) with three other experimental-data sources. Murata & Hashizume's correlation had, however, been validated with only R123.

Murata & Hashizume [1993] commented that in Ross et al.'s and Jung et al.'s correlations, the nucleate boiling contribution should have been evaluated from the nucleate boiling heat flux, q_{NB} instead of the total heat flux, q. For the Ross et al.'s correlation [1987], it used the Stephan & Abdelsalam's correlation [1980] to predict HTCs in the nucleate-flow-boiling regime up to the point of the nucleate-boiling full suppression. So Ross et al. should be correct in using the total/wall heat flux in their calculation. For the Jung et al.'s correlation [1989b], their concept as being explained previously was not the same as the Chen's postulation; it appeared that Jung et al. was also correct in using the total/wall heat flux in their calculation.

Based on the above discussion, Jung et al.'s [1989b] correlation was chosen for the HTC prediction of pure refrigerants in this thesis.

Table 2.1 Comparison of mean deviations (%) for HTCs between correlations and experimental data (all correlations used Murata & Hashizume's experimental data) [Murata & Hashizume 1993]

Fluid	Ross et al.'s correlation Mean dev. (%)	Jung et al.'s correlation Mean dev. (%)	Murata & Hashizume's correlation Mean dev. (%)
R123	9.9	12.0	8.5

Table 2.2 Comparison of mean deviations (%) for HTCs between correlations and experimental data (both correlations used Jung et al.'s experimental results) [Jung et al. 1989b]

Fluid	Ross et al.'s correlation Mean dev. (%)	Jung et al.'s correlation Mean dev. (%)
R22	11.8	5.77
R114	22.1	9.3
R12	15.2	7.6
R152a	15.3	7.4
R500	15.5	7.82

Table 2.3 Development and validation of Jung et al.'s [1989b] and Murata & Hashizume's [1993] correlations for HTCs for pure and azeotropic refrigerants

Fluid	Jung et al.'s correlation	Murata & Hashizume's correlation
For correlation development	**R22** (5.77% mean dev.), **R114** (9.3% mean dev.), **R12** (7.6% mean dev.), **R152a** (7.4% mean dev.) and **R500** (7.82% mean dev.)	**R123** (8.5% mean dev.)
For correlation validation	Apart from the correlation- development work, the following fluids were used in the validation: **R11** (6.3% mean dev., Jung & Radermacher's exp. data [1991]), **R134a** (7.0% mean dev., Eckels & Pate's exp. data [1991]), **R12** (8.0% mean dev., Eckels & Pate's exp. data [1991]), and **R22** (-5.0% and 3.8% for max. diff. between simulated and experimented results, Judge & Radermacher's data [1997]).	Apart from the fluid used in the correlation development, there was no any another fluid used in the validation.

2.7.2 Pressure drop for pure refrigerants

Martinelli & Nelson's correlation [1948] have been accepted and further developed by many researchers. Lockhart & Martinelli's work [1949] did not consider the effect of the several flow patterns in their correlations, and their basic assumptions tended to limit to the annulus flow. Baker tried to verify the flow pattern effect and his map of flow-pattern regions is useful for verifying various pressure-drop and heat-transfer-coefficient correlations. Judge & Radermacher [1997] used the Baker's flow map to show that Jung & Radermacher's [1989] correlation could be applied not only to annular flow but to a range of flow patterns.

Jung & Radermacher [1989] showed that their correlation could predict pressure drops with better accuracy and deviation percentage than both the Pierre's

[1957] and the Martinelli & Nelson's [1948] correlations. Between the Jung & Radermacher's [1989] and the Singal et al.'s [1983] correlations, the former one was chosen for the present study for the following considerations, Table 2.4. First, Singal et al.'s results had larger inaccuracies when compared to Jung & Radermacher's results. Second, Jung & Radermacher used many more pure refrigerants than Singal et al.

Table 2.4 Comparison between Jung & Radermacher's [1989] and Singal et al.'s [1983] correlations for total pressure drops of pure refrigerants

Description	Jung & Radermacher's correlation	Singal et al.'s correlation
Accuracy	±10%	±30%
Fluid(s) used in correlation development	R22, R114, R12, R152a and R500	R12

2.7.3 Heat transfer coefficient for mixed refrigerants and for air side

The HTCs for mixed refrigerants and the air side are mentioned here. For the former, in Hihara & Saito's work [1990], many terms used in the equations cannot be obtained and many assumptions cannot verified at the moment due to lack of the information. Zhang et al.'s work [1997] was an extension of Hihara & Saito 's work [1990], therefore facing similar uncertainties. It is the author's opinion that two of Granryd [1991] assumptions may not be valid, because first the specific heat of the liquid phase was significantly less than that of the vapour phase and the two-phase fluid. Another point is that, in the prediction of the HTC between the vapour and the liquid, he used the tube diameter instead of the vapour-phase diameter. This may cause some errors for the partial-boiling regime, where the annulus flow has a thicker liquid layer than that in the two-phase convective flow boiling. In addition, in the comparison of the results from his prediction and the available experimental data, they did not include partial-boiling regime. Ross et al.'s work [1987] did not even recognize the partial boiling regime.

For Jung et al.'s correlation [1989b] which was based on the superposition principle, it appeared that the two of their modifications, i.e. introducing the Unal's correlation [1986] and the C_{UN} correction factor, are acceptable, since both were developed with the concept of using the tube-wall heat flux (see Section 2.7.1).

From the above discussion, it can be seen that either Jung et al.'s [1989b] or Murata & Hashizume's [1993] correlations could be considered applicable for this research. From the Tables 2.5 to 2.7, it was shown that Jung et al.'s correlation gave smaller mean deviations than Murata & Hashizume's correlation. Jung et al.'s correlation also based on more refrigerant mixtures. In addition, Jung et al. used more mixed refrigerants and data sources than Murata & Hashizume for their validations. Based on the same previous argument, Jung et al. was correct in using the total/wall heat flux in their correlation calculation. It can therefore be concluded that Jung et al.'s [1989b] correlation is the most suitable and reliable correlation, and is adopted for this thesis.

Table 2.5 Comparison of mean deviations (%) for HTCs of a refrigerant mixture between correlations and experimental data (Murata & Hashizume's experimental data were used, for all correlations) [Murata & Hashizume 1993]

Fluid	Ross et al.'s correlation Mean dev. (%)	Jung et al.'s correlation Mean dev. (%)	Murata & Hashizume's correlation Mean dev. (%)
R123/R134a (0.9/0.1)	23.1	13.9	16.0

Table 2.6 Comparison of mean deviations (%), for HTCs of zeotropic refrigerant mixtures, between correlations and experimental data (both correlations used the same data from Jung et al.'s experiments) [Jung et al. 1989b]

Fluid	Ross et al.'s correlation Mean dev. (%)	Jung et al.'s correlation Mean dev. (%)
R22/ R114 (0.23/0.77)	13.8	6.8
R22/ R114 (0.48/0.52)	13.0	8.9
R22/ R114 (0.77/0.23)	12.9	9.6
R12/R152a (0.21/0.79)	25.4	9.0
R12/R152a (0.88/0.12)	28.2	13.1

Table 2.7 Development of HTC correlations for zeotropic mixtures for Jung et al.'s [1989b] and Murata & Hashizume's [1993]

Fluid	Jung et al.'s correlation	Murata & Hashizume's correlation
For correlation development	**R22/ R114 (0.23/0.77)** (6.8% mean dev.), **R22/ R114 (0.48/0.52)** (8.9% mean dev.), **R22/ R114 (0.77/0.23)** (9.6% mean dev.), **R12/R152a (0.21/0.79)** (9.0% mean dev.) and **R12/R152a (0.88/0.12)** (13.1% mean dev.)	**R123/R134a (0.9/0.1)** (16.0% mean dev.)
For correlation validation	Apart from the fluids used in the correlation development, the following fluids were used in the validation: **R407C**, **R32/R125/R134a (0.3/0.1/0.6)** and **R23/R32/R134a (0.045/0.215/0.74)**. (These three zeotropic refrigerant mixtures had -5.0% and 3.8% for max. diff. between simulated and experimented results, Judge & Radermacher's data [1997].)	Apart from the fluid used in the correlation development, there was no any another fluid used in the validation.

When reviewing the air side heat transfer and pressure drop of the dry and wet plate-fin-tube evaporators (Sections 2.2.1 and 2.2.2), it appears that the most accurate correlation for the prediction of both Colburn j- and friction factors should be the Turaga et al.'s correlations.

2.7.4 Pressure drop for mixed refrigerants

For choosing an appropriate correlation, from Table 2.8, Jung & Radermacher showed that there was no mixture-composition dependence on the pressure drops, while Singal et al. did not agree. However, Jung & Radermacher used more refrigerant mixtures in the correlation development than Singal et al.. Moreover, Jung & Radermacher's work covered composition range between 20% to 80%, which is much bigger than that of Singal et al.'s. Finally, though Singal et al.'s correlation [1983] gave a smaller mean deviation but had a greater inaccuracy than Jung & Radermacher's correlation [1989]. It can therefore be concluded that Jung & Radermacher's correlation [1989] is a better correlation for the pressure drop prediction for refrigerant mixtures, and was therefore adopted for the thesis.

Table 2.8 Comparison between Jung & Radermacher's [1989] and Singal et al.'s correlations for total pressure drop prediction for mixtures

Description	Jung & Radermacher's work	Singal et al.'s work
Including composition dependence in the correlation	No	Yes
Fluids used in correlation development	R22/ R114 (0.23/0.77), R22/ R114 (0.48/0.52), R22/ R114 (0.77/0.23), R12/R152a (0.21/0.79), R12/R152a (0.6/0.4) and R12/R152a (0.88/0.12)	R13/R12 (0.05/0.95), R13/R12 (0.1/0.9), R13/R12 (0.15/0.85) and R13/R12 (0.2/0.8)
Mean deviation of the correlation	8.4%	Near zero percent
Accuracy of the correlation	±10%	±30%

2.7.5 Evaporator modelling

It is clear that among the three kinds of model; only the distributive model is used for the dynamic study.; it generally gives the highest accuracy too. For the distributive model, having investigated all reviewed works, it was found that their main structures were the same, but there were differences in the assumptions/conditions used. This thesis adopts the distributive model, and selects some of those assumptions/conditions that are applicable and reasonable for the project objective. They are: use of the refrigerant unsteady-state momentum equation, assuming two-phase homogeneous flow with the vapour-and-liquid temperature equilibrium, application of the fin-tube-wall energy equation, and recognition of the moist-air accumulated energy and mass with constant air density. It appears that no previous researchers have applied the unsteady momentum equation for air under dry and wet conditions; the same applied here.

In addition, the zeotropic refrigerant mixture has a temperature glide, whilst pure refrigerants do not have such a characteristic. Then, in this thesis, the comparison strategy for pure and mixed refrigerants is to base on the same refrigerant temperature at the exit of the evaporator [Domanski & McLinden 1992].

2.7.6 Evaporator steady-state and dynamic studies when using pure and mixed refrigerants

For the steady-state studies of mixed-refrigerant, many researchers tried finding ways to utilize the temperature glide. This thesis instead investigated the temperature glide behaviour itself and its effect, and compared any relevant parameters to the pure cases. For the dynamic studies, there were no published work, and other researchers may think that there were no behaviour differences when using either pure or mixed refrigerants.

2.7.7 TEV-controlled evaporator studies for pure and mixed refrigerants

Earlier work with TEVs focussed on the sensor bulbs and the operating conditions, when using pure refrigerants, but not mixed refrigerants. For the pure refrigerants, the most common methods improving stability of a temperature control loop were using the slower bulb dynamics and the higher set point of the superheat. For the refrigerant mixtures, up to now a very limited number of journal papers had been published and none of them dealt with dynamic behaviour of TEV controlled evaporator.

This study employs a mixed refrigerant under dry-coil conditions, and looked at the coil response when there was a step increase of the coil-inlet dry-bulb temperature. For the needle and seat model, James & James' model [1987], which Mithraratne [1992] and Mithraratne et al. [2000] used successfully, is considered to be suitable for this thesis. For the sensor bulb model, based on the work of Mithraratne [1992], there are 5 assumptions introduced: a small size, negligible heat capacitance (also applied for the tube-wall), being clamped very closed to the coil-outlet, using the same fluid for both the charged fluid the refrigerant, and, for R407C, the mole fractions of the liquid phase in the bulb remained unchanged at all times. This confines the scope of the thesis to investigating only the refrigerant-properties effect upon the operation of the TEV-controlled evaporator.

2.7.8 Originalities

By using directly and indirectly the information from the literature, three original investigations for the evaporator when using the zeotropic refrigerant mixture in the thesis were planned and carried out.

First, the evaporator dynamic model comprises of: the continuity, momentum, and energy equations for the refrigerant; the energy equation for the fins

and tube walls; and the mass and the energy balances for the moist air. In addition, each tube in the two-phase region was divided into several elements, each of which was assigned with the same suitable length based on both Jung et al.'s [1989a] and Jung & Radermacher's [1989] works. Moreover, each element in the superheat region was divided into several sub-elements of equal length. Based on the difference between the two-phase and the superheat properties (i.e. the HTC), the sub-element length could be estimated.

Second, the steady-state and dynamic behaviour of the evaporator when using a mixed refrigerant under dry and wet conditions was investigated, and compared to pure refrigerant. For the steady-state behaviour, the complete results are shown and the analysis were carried out particularly for the air temperatures and humidity, the dehumidification rates, and the temperature glide/drop effect. For the dynamic behaviour, the coil-inlet air temperature was changed (increased or decreased) with a step input. The main studied parameters, apart from those in the steady-state cases, were the coil-outlet refrigerant properties, the coil accumulated heat fluxes and their effects, the superheat and its effect, and the refrigerant degree-of-freedom effect.

Third, the TEV controlled evaporator when using a mixed refrigerant under a dry condition is studied. The temperature glide effect upon the TEV-controlled-evaporator behaviour was investigated when there was a step increase of the coil-inlet air temperature.

Chapter 3 Applications of Theories

In this chapter, relevant theories concerning momentum, heat, and mass transfer for both air and refrigerant sides of a plate-fin-tube evaporator were examined, with emphasis on the refrigerant side. For the air side, the two coil conditions, namely: dry and wet, were addressed, with the associated theories. For the refrigerant side, for both pure and mixed refrigerants, boiling processes were examined, followed by details of pressure drop and heat transfer coefficients formulations. Finally, principles of operation of a TEV-controlled evaporator were given.

3.1 Heat and mass transfer for air side

For the heat transfer, the HTC and the fin efficiency needed to be specified under both dry and wet coil conditions. For the mass transfer, the water-vapour mass transfer coefficient had to be applied for the wet condition. In addition, the air pressure drop across the coil for both conditions was assumed negligible, i.e. no momentum transfer.

3.1.1 Heat transfer coefficient for dry coils

Four relevant parameters were involved: the effective HTC, the fin efficiency, the HTC and the Colburn j-factor. The effective HTC of the dry coil is related to the coil surface area by taking into account the fin efficiency, as shown in Hewit et al. [1994], Eq. 3.1, which is to be used in Eqs. 4.1 and 4.9.

$$U_{eff,dry} = \left(\frac{\eta_{fin,dry} A_{fin} + A_{wall,o}}{A_{o,total}} \right) U_{dry} \tag{3.1}$$

Without any fins, it is clear from Eq. 3.1 that the effective HTC is equal to the HTC, i.e. $U_{eff,dry} = U_{dry}$. For the dry-coil fin efficiency, with fins having greater equivalent diameter relative to the tube diameter, it can be shown that [Hewitt et al. 1994], Eq. 3.2:

$$\eta_{fin,dry} = \frac{\tanh\left(\left(\frac{2U_{dry}}{w_{fin}k_{fin}}\right)^{0.5}\psi\right)}{\left(\frac{2U_{dry}}{w_{fin}k_{fin}}\right)^{0.5}\psi} \tag{3.2}$$

where

$$\psi = \frac{D_{OD,tube}}{2}\left(\frac{D_{fin}}{D_{OD,tube}} - 1\right)\left(1 + 0.35\ln\left(\frac{D_{fin}}{D_{OD,tube}}\right)\right) \tag{3.3}$$

Since the fin was a plate-fin type, its diameter can be approximated from the equivalent fin diameter using Rohsenow & Hartnett [1998] equation, Eq. 3.4.

$$D_{fin} \cong D_{fin,eq} = \left(\frac{4S_T S_L}{\pi}\right)^{(1/2)} \tag{3.4}$$

The dry-coil fin efficiency can also be expressed as Eq. 3.5, based on the definition by Domanski [1991]. This equation is to be used for determining the average fin temperature at the time "t" of Eqs. 4.9 and 4.10.

$$\eta_{fin,dry} = \frac{\left(T_{db,in} - T_{fin,ave}\right)}{\left(T_{db,in} - T_{wall,ave}\right)} \tag{3.5}$$

For the dry-coil heat transfer coefficient and the dry-coil Colburn j-factor, as mentioned in Chapter 2, it is calculated from Turaga et al.'s correlation [Turaga et al. 1988a, 1988b]. This correlation is applicable for $300 < Re_a < 1500$ and $20 < (A_{o,total}/A_{wall,o,p}) < 50$. The dry-coil heat transfer coefficient is, Eq. 3.6:

$$U_{dry} = \frac{j_{air,dry}G_{a,mf}c_{p,a}}{Pr_a^{(2/3)}} \tag{3.6}$$

where

$$Pr_a = \frac{c_{p,a}\mu_a}{k_a} \tag{3.7}$$

$$G_{a,mf} = \frac{G_a}{(A_{mf}/A_F)} \tag{3.8}$$

The dry-coil Colburn j-factor is, Eq. 3.9:

$$j_{air,dry} = 0.053\left(\frac{A_{o,total}}{A_{wall,o,p}}\right)^{-0.24} Re_a^{-0.18} \tag{3.9}$$

where

$$Re_a = \frac{G_{a,mf} D_h}{\mu_a} \tag{3.10}$$

$$D_h = \frac{4A_{mf} L_d}{A_{o,total}} \tag{3.11}$$

It should be borne in mind that Turaga et al.'s correlation was obtained from their experiments using the parameters of coil configurations shown in Chapter 4.

3.1.2 Heat and mass transfer coefficients for wet coils

Both heat and mass transfer processes occur simultaneously under a wet condition. For the mass transfer, water vapour in the air condenses onto the coil surface that is at a temperature less than the dew-point temperature of the air but higher than 0 °C.

a) Heat transfer coefficient

Calculation of three effective HTCs (i.e. wet coil, wet-coil sensible and wet coil latent) involved 4 main variables: a wet-coil fin efficiency, wet-coil HTC, wet-coil sensible and latent HTCs. First, the wet-coil effective HTC is given in Eq. 3.12, which is similar to that for the dry-coil case and is to be used in Eqs. 4.3 and 4.11.

$$U_{eff,wet} = \left(\frac{\eta_{fin,wet} A_{fin,wet} + A_{wall,o,wet}}{A_{o,total,wet}}\right) U_{wet} \tag{3.12}$$

The surface areas of the fins and the outside tube walls between fins, and the total area of the coil under wet condition could be approximated using the corresponding dry-coil values. They were given respectively in Eqs. 3.13 to 3.15, to be substituted in Eq. 3.12 .

$$A_{fin,wet} \cong A_{fin} \tag{3.13}$$

$$A_{wall,o,wet} \cong A_{wall,o} \tag{3.14}$$

$$A_{o,total,wet} \cong A_{o,total} \tag{3.15}$$

It was assumed that, on the fins and the outside tube walls between fins, the thermal-resistance values of condensate were negligible [Oskarsson et al. 1990a]. Thus, the temperature values of the condensate were approximately the same as that of the fin and the outside tube wall surfaces.

For the wet-coil fin efficiency, based on Eq. 3.5, it could be shown as Eq. 3.16, which is used for calculating the average fin temperature at the time "t" of Eqs. 4.10 (when using for a wet coil) and 4.11.

$$\eta_{fin,wet} = \frac{(T_{db,in} - T_{cond,fin})}{(T_{db,in} - T_{cond,wall})} \cong \frac{(T_{db,in} - T_{fin,ave})}{(T_{db,in} - T_{wall,ave})} \tag{3.16}$$

There was an alternative way to obtain the wet-coil fin efficiency mentioned by Oskarsson et. al. [1990a] which was based on McQuiston's derivation [1975]. Accounting for the effect due to water-vapour transfer and phase-change, the wet-coil fin efficiency, corresponding to the dry-coil fin efficiency in Eq. 3.2, can be expressed as in Eq. 3.17.

$$\eta_{fin,wet} = \frac{\tanh\left(\left(\frac{2U_{wet}}{w_{fin}k_{fin}}\right)^{0.5}\psi\right)}{\left(\frac{2U_{wet}}{w_{fin}k_{fin}}\right)^{0.5}\psi} \tag{3.17}$$

The wet-coil HTC is in turn formed by combining the HTCs of the sensible and the latent [Oskarsson et. al. 1990a] as shown in Eq. 3.18.

$$U_{wet} = U_{wet,sen} + U_{wet,latent} \tag{3.18}$$

The wet-coil sensible HTC, as discussed in Chapter 2, is calculated using Turaga et al.'s correlation [1988a, 1988b], Eq. 3.19, for $300 < Re_a < 1300$, $20 < (A_{o,total}/A_{wall,o,p}) < 50$, $10 < (s_{fin}/w_{fin}) < 22$:

$$U_{wet,sen} = \frac{j_{air,wet} G_{a,mf} c_{p,a}}{Sc_a^{(2/3)}} \tag{3.19}$$

where

$$Sc_a = \frac{\nu_a}{D_{wa}} \tag{3.20}$$

The wet-coil Colburn j-factor, for a fully-wet surface, is given in Eq. 3.21.

$$j_{air,wet} = 0.04 \left(\frac{A_{o,total}}{A_{wall,o,p}} \right)^{0.23} \left(\frac{s_{fin}}{w_{fin}} \right)^{1.15} Re_a^{-0.75} \tag{3.21}$$

The wet-coil latent HTC is obtained by considering the heat flux due to condensation of water vapour on the coil, Eq. 3.22.

$$U_{wet,latent} = \frac{U_{m,wet} i_{fg,water} (W_{in} - W_{cond,wall})}{(T_{db,in} - T_{wall,ave})} \tag{3.22}$$

The wet-coil effective sensible and latent HTCs can be expressed respectively in the same way as the wet-coil effective HTC, Eqs. 3.23 and 3.24, and they are needed in the result analysis (Sub-section 5.4.1).

$$U_{eff,wet,sen} = \left(\frac{\eta_{fin,wet} A_{fin,wet} + A_{wall,o,wet}}{A_{o,total,wet}} \right) U_{wet,sen} \tag{3.23}$$

$$U_{eff,wet,latent} = \left(\frac{\eta_{fin,wet} A_{fin,wet} + A_{wall,o,wet}}{A_{o,total,wet}} \right) U_{wet,latent} \tag{3.24}$$

b) Mass transfer coefficient (MTC)

Three main variables are involved: a wet-coil effective MTC, a wet-coil MTC, and a wet-coil humidity-ratio fin efficiency. The wet-coil effective MTC, Eq. 3.25, can be written the same way as the wet-coil effective HTC, Eq. 3.12, and is to be used in Eq. 4.8.

$$U_{m,eff,wet} = \left(\frac{\eta_{W,fin,wet} A_{fin,wet} + A_{wall,o,wet}}{A_{o,total,wet}} \right) U_{m,wet} \tag{3.25}$$

In McQuiston & Parker [1994], it was shown that a relation between the wet-coil sensible HTC and the wet-coil MTC exists.

$$\frac{U_{wet,sen}}{U_{m,wet}} = c_{p,a} Le^{2/3} \tag{3.26}$$

The $Le^{2/3}$ value is approximately 1.0 for moist air under general conditions. The wet-coil humidity-ratio fin efficiency can be expressed as in Eq. 3.27.

$$\eta_{W,fin,wet} = \frac{(W_{in} - W_{cond,fin})}{(W_{in} - W_{cond,wall})} \tag{3.27}$$

Furthermore, the wet-coil humidity-ratio fin efficiency approximately equalled to the wet-coil fin efficiency, Oskarsson et al. [1990a], Eq. 3.28.

$$\eta_{W,fin,wet} \cong \eta_{fin,wet} \tag{3.28}$$

3.2 Overview of boiling theory for pure or single-component refrigerant

For pure refrigerants, two types of boiling, pool and forced-convection, needed to be considered. Only the boiling occurring at a solid-liquid interface, where the temperature of the solid surface exceeds the saturation temperature of the liquid (the difference of these two temperatures is usually referred as excess temperature) [Incropera & De Witt 1990], i.e. the heterogeneous boiling, was dealt with in this thesis.

3.2.1 Pool boiling

Pool boiling, Fig. 3.1, taking place in the at-rest liquid with a motion near a solid surface due to free convection and bubble activities, has four developing stages: free convection, nucleate, transition, and film as excess temperature increases, Fig. 3.2 [Incropera & De Witt 1990]. For the *free-convection-boiling mode*, as the excess temperature gets larger, the surface heat flux also increases. At the onset of nucleate boiling, ONB, i.e. at the point A, the bubbles initiate at and depart from the solid surface. For the *nucleate boiling mode*, with 2 regimes: for the *isolated-bubbles* (from A to B), the departure of the bubbles causes fluid mixing, resulting in the large values of HTC. For the *jets-and-columns* (from B to C), the bubbles merge to become vapour slugs, thus causing a deterioration in the HTC; the rate of change of the heat flux with the increasing of the excess temperature decreases until having a maximum heat flux, called the critical heat flux.

For the *transition boiling mode* (from C to D), because of having a vapour blanket formed unstably on the solid surface, the HTC decreases, while the excess temperature increases; the heat transfer is reducing to the minimum heat flux, "Leidenfrost point". Finally, for the *film boiling mode* (from D onwards), the vapour film is stable, the transferring of the heat flux from the surface to the vapour blanket is by conduction and radiation. The more the excess temperature, the more the heat transfers by the radiation contribution.

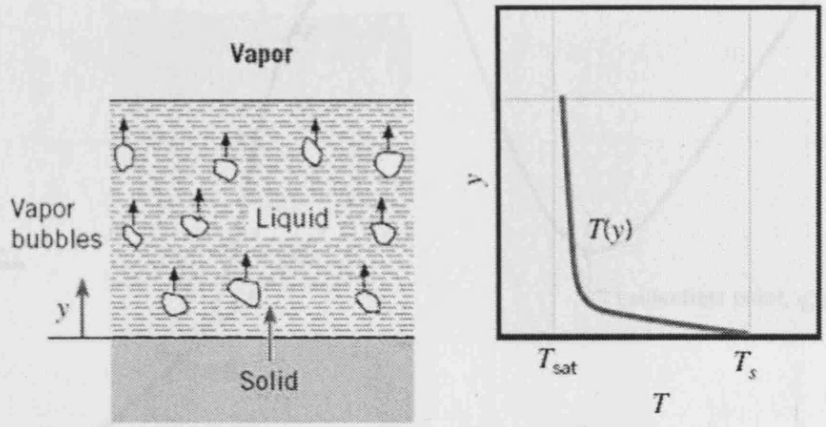

Figure 3.1 Temperature distribution in saturated pool boiling with a liquid vapour interface [Incropera et al. 1990]

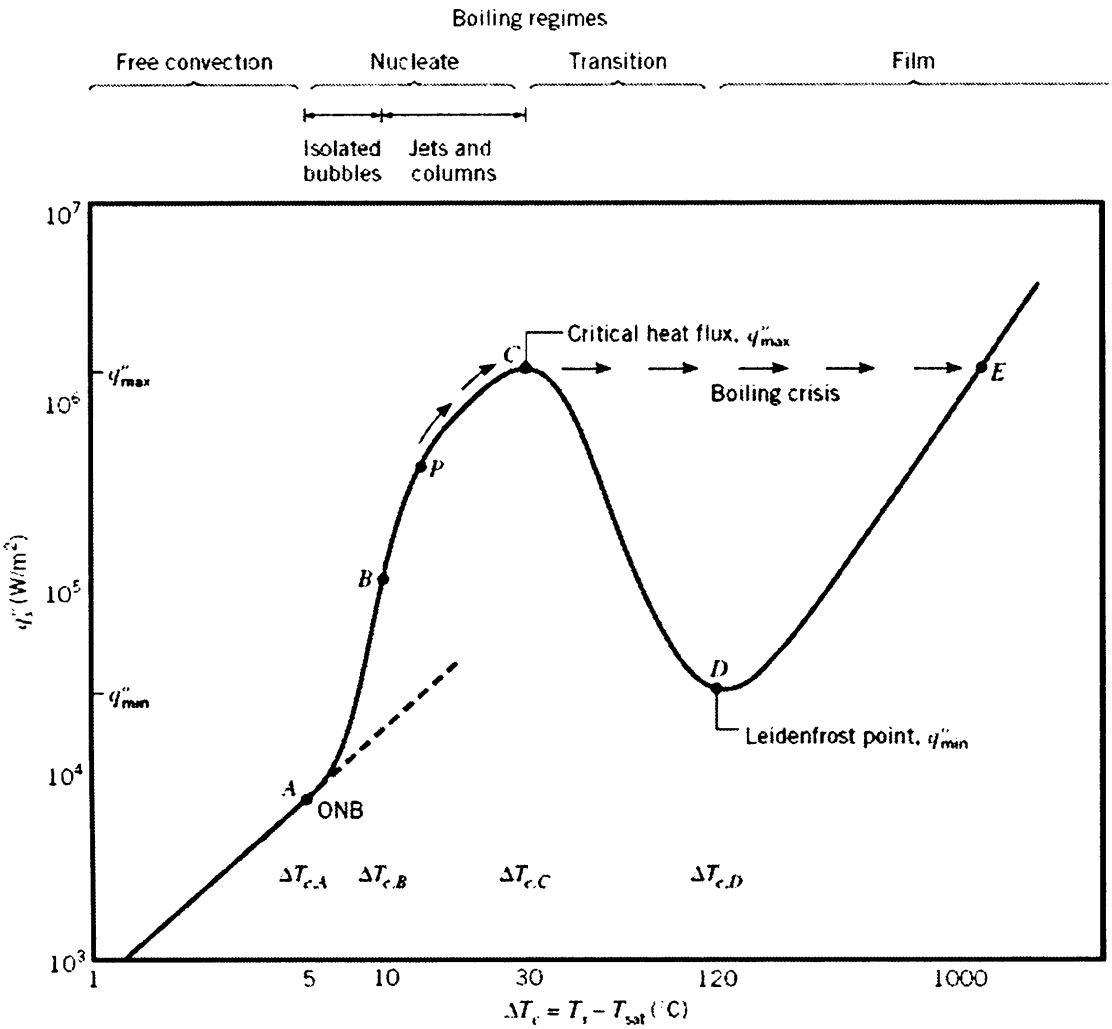

Figure 3.2 Typical boiling curve for water at one atmosphere with a wire heater supplied with a constant electrical power input shows surface heat flux as a function of excess temperature [Incropera et al. 1990]

The bubble-growth behaviour in the nucleate boiling, essential to the understanding the forced convection boiling (see Sections 3.2.2.b, 3.3 and 3.4.3), consists of two mechanisms (Fig. 3.3): the inertia-controlled and thermal-diffusion-controlled. For the former, when a bubble grows up to the mouth of an ideal cavity (Fig. 3.4), it starts to form a curving shape, in which the pressure can be calculated from Eq. 3.29 [Whalley 1990].

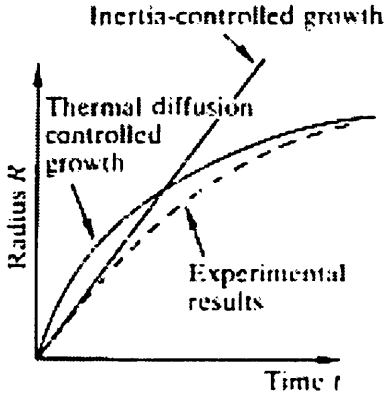

Figure 3.3 Bubble growth as a function of time [Whalley 1990]

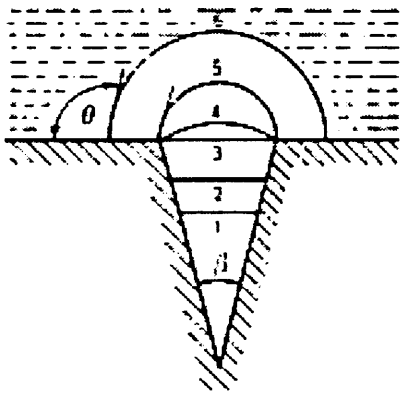

Figure 3.4 Nucleation from a cavity [Collier et al. 1996]

$$p_{bub} = p_l + \frac{2\sigma}{r_{bub}} \tag{3.29}$$

To achieve equilibrium for the bubble, the wall superheat had to approximately satisfy Eq. 3.30.

$$\Delta T_{sat} = T_{wall} - T_{sat} = \frac{dT_l}{dp_l}(p_{bub} - p_l) \tag{3.30}$$

To obtain the function of $\frac{dT_l}{dp_l}$, the Clapeyron equation [Whalley 1990], Eq. 3.31, is used.

$$\frac{dp_l}{dT_l} = \frac{i_{fg}}{(v_v - v_l)T_{sat}} \tag{3.31}$$

If the specific volume of the vapour phase is much more than that of the liquid phase, then, after substituting Eq. 3.31 into Eq. 3.30, the equation for the wall superheat can be written as Eq. 3.32.

$$\Delta T_{sat} = T_{wall} - T_{sat} = \frac{2\sigma}{r_{bub}} \frac{T_{sat}}{i_{fg}\rho_v} \tag{3.32}$$

For the thermal-diffusion controlled mechanism, in the thermal boundary layer of the liquid (Fig. 3.5), there is a gradient of the temperature, with the temperature varies from the wall to the free-stream temperature (which is equal to the saturated temperature). At a distance from the wall, the liquid temperature is determined by Eq. 3.33.

$$T_l = T_{wall} - \frac{qy}{k_l} \tag{3.33}$$

Hsu [1962] postulated that, during the growth of a bubble under equilibrium (Fig. 3.5), the temperature of the liquid surrounding the top of the bubble (Eq. 3.33) should be equal to or larger than the wall temperature that was calculated by Eq. 3.32 and was plotted as the line of the equilibrium bubble criterion in Fig. 3.5 (the dotted line).

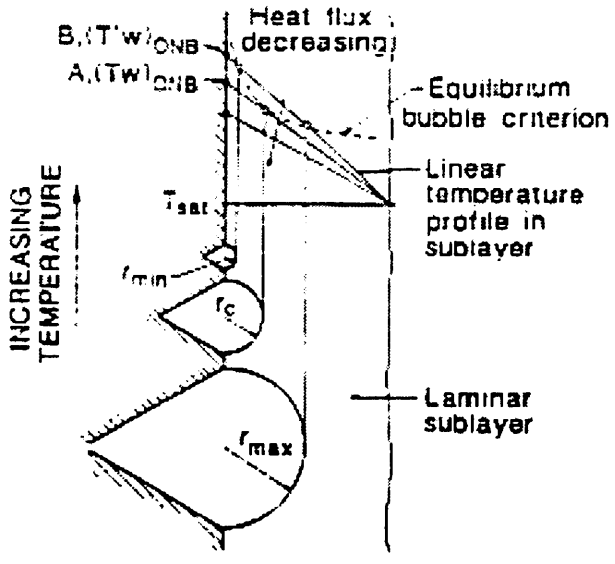

Figure 3.5 Bubble nucleation from a conical cavity [Jung et al. 1989a]

Later Davis & Anderson [1966] studied the following two cases, both of which with increasing wall temperature during bubble growing. First, when there is a wide range of cavity sizes available on the surface, the bubbles that had tangency between their liquid temperature profile and the curve of the equilibrium bubble criterion (looking at "A", Fig. 3.5) would have a quicker development of bubbling, i.e. releasing earlier from their cavities, than others. Second, when available cavity sizes on the surface are limited, hence the bubbles from the maximum-size cavities will be firstly released, and the corresponding wall superheat is given as Eq. 3.34.

$$(T_{wall} - T_{sat})_{ONB} = \frac{2T_{sat}\sigma v_v}{i_{fg} r_{bub,c}} + \frac{q_{ONB} r_{bub,c}}{k_l} \tag{3.34}$$

3.2.2 Internal forced convection boiling

The theoretical overview of internal forced convection boiling covers: fundamental equations, flow-models and HTC for two-phase, and HTC for single-phase vapour. Before going into the details, it was necessary to understand the physical characteristics of the boiling flow patterns and boiling regions, pointing out first that, horizontal flow patterns are different from vertical ones, Figs. 3.6 and 3.7. Only the horizontal wavy and annular flows were considered in the thesis. Boiling is usually classified into 4 regions: single-phase liquid forced convection, sub-cooled boiling, saturated boiling, single-phase vapour forced convection. Due to the use of direct-expansion evaporator in this study, only the last two regions were considered.

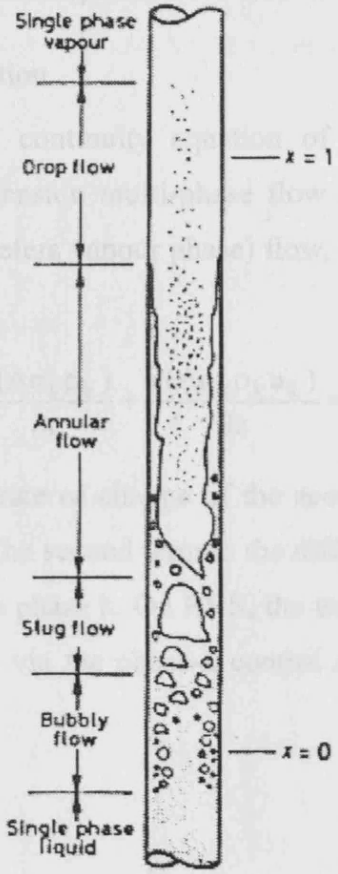

Figure 3.6 Flow patterns in a vertical evaporator tube [Collier et al. 1996]

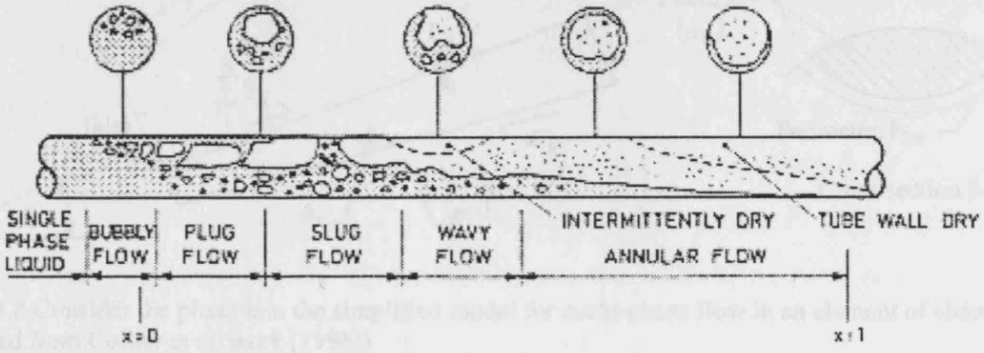

Figure 3.7 Flow patterns in a horizontal evaporator tube [Collier et al. 1996]

a) Fundamental equations and models for two-phase flow

Since there is mass, momentum and heat transfer happening in the flow, essential information of the transfer was given and explained here, except for the energy

equation that was discussed in Chapter 4. Due to the presence of 2-phase flow, frictional multipliers, and homogeneous and separate flow models were also described.

a.1) Continuity equation

To analyse the continuity equation of a two-phase flow, let's first consider a simplified one-dimension multi-phase flow inside a channel element, Fig. 3.8. For a phase-k (e.g. k = v refers vapour phase) flow, its unsteady-state mass balance is shown in Eq. 3.35.

$$\frac{\partial(A\alpha_k\rho_k)}{\partial t}+\frac{\partial(A\alpha_k\rho_k u_k)}{\partial z}=\Gamma_k \tag{3.35}$$

The first term on LHS is the rate of change of the accumulated mass for the phase-k fluid in the channel element. The second term is the difference between the rates of the inlet and the outlet mass of the phase k. On RHS, the term represents the mass-transfer rate of fluids into the phase k via the phase-k control surface, except at the inlet and outlet.

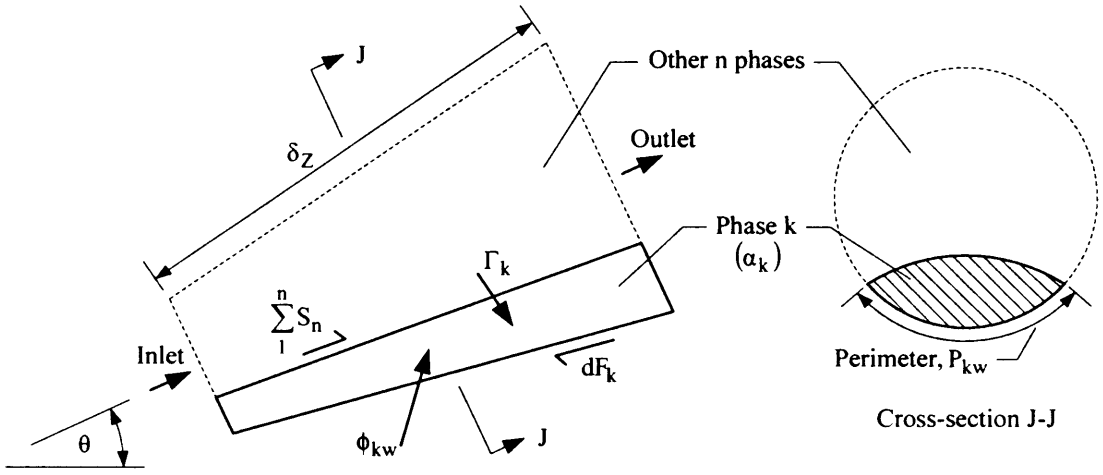

Figure 3.8 Consider the phase k in the simplified model for multi-phase flow in an element of channel (modified from Collier et al. work [1996]).

When dealing with 2-phase flow in a channel, along the control surface, except at the inlet and outlet, the net mass-transfer rate between the vapour and the liquid is zero, as expressed by Eq. 3.36.

$$\Gamma_v=-\Gamma_l \tag{3.36}$$

In addition, if the flow is under a steady-state condition in a channel with a constant cross-section area, then, from Eqs. 3.35 and 3.36, at the inlet and outlet of the element, the net mass flow rate of the vapour phase is the same as that of the liquid phase, as in Eq. 3.37.

$$\frac{d(A_v\rho_v u_v)}{dz} = -\frac{d(A_l\rho_l u_l)}{dz} \tag{3.37}$$

a.2) Momentum equation

Momentum change for a 2-phase flow can be described with the same procedure as the above sub-section, Fig. 3.8; obviously, only a channel with a constant cross-section area is considered. For the phase-k, the unsteady-state momentum balance is shown in Eq. 3.38.

$$\begin{aligned}&\frac{\partial(A_k\rho_k u_k\delta_z)}{\partial t} + \delta_z\frac{\partial(A_k\rho_k u_k^2)}{\partial z} = \\ &-A\alpha_k\delta_z\frac{\partial p}{\partial z} - \tau_{kw}P_{kw}\delta_z + \sum_1^n \tau_{knz}P_{kn}\delta_z - A\alpha_k\rho_k\delta_z g\sin\theta + u_k\Gamma_k\delta_z\end{aligned} \tag{3.38}$$

The two terms on LHS are respectively the rate of change of the accumulated momentum inside the control volume and the net rate of change of the momenta at the inlet and the outlet. For RHS, the first term is the net pressure force of the phase-k upon the control volume at the inlet and outlet. The second term is the wall shear force on the phase-k control surface. The third term is the sum of all shear forces on the phase-k control surface at its contacts with other phases. The fourth term is the gravitational force. The last term is the rate of change of *the momentum* due to the other fluids *entering* the phase-k via the control surface, except at the inlet and outlet.

When applying Eq. 3.38 for steady-state 2-phase flow, the 3rd and 5th terms on RHS become zero, and Eq. 3.39 expresses the momentum balance.

$$\frac{d(A_l\rho_l u_l^2 + A_v\rho_v u_v^2)}{dz} = -A\frac{dp}{dz} - \tau_{vw}P_{vw} - \tau_{lw}P_{lw} - g\sin\theta(A_l\rho_l + A_v\rho_v) \tag{3.39}$$

The term on LHS represents the net rate of change of the liquid and vapour momenta at the inlet and outlet of the element with respect to distance. On the RHS, the first term is the net pressure force on the control volume at the inlet and outlet. The second and third terms are the wall shear forces on the control surfaces of the vapour and the liquid

phases, respectively. The last term is the sum of the gravitational forces of the liquid and vapour phases inside the control volume.

Rearrangement of the above equation shows how the total pressure gradient is formed from the friction, acceleration, and potential heads, Eqs. 3.40 to 3.43:

$$\left(\frac{dp}{dz}\right)=\left(\frac{dp}{dz}F\right)+\left(\frac{dp}{dz}a\right)+\left(\frac{dp}{dz}z\right) \tag{3.40}$$

where

$$-\left(\frac{dp}{dz}F\right)=\frac{\tau_{vw}P_{vw}}{A}+\frac{\tau_{lw}P_{lw}}{A} \tag{3.41}$$

$$-\left(\frac{dp}{dz}a\right)=\frac{d\left(\frac{A_l\rho_l u_l^2+A_v\rho_v u_v^2}{A}\right)}{dz}=G^2\frac{d\left(\frac{x^2v_v}{\alpha}+\frac{(1-x)^2v_l}{(1-\alpha)}\right)}{dz} \tag{3.42}$$

$$-\left(\frac{dp}{dz}z\right)=g\sin\theta\left(\frac{A_v}{A}\rho_v+\frac{A_l}{A}\rho_l\right)=g\sin\theta\left(\alpha\rho_v+(1-\alpha)\rho_l\right) \tag{3.43}$$

a.3) Two-phase frictional multiplier

Two-phase frictional multipliers are necessary when applying single-phase frictional knowledge to determine the 2-phase flow pressure drop. Lockhart & Martinelli [Martinelli et al. 1944, Lockhart & Martinelli 1949] defined three types of multiplier, Eqs 3.44 to 3.46: if-only-liquid-alone-flow, total-flow-assumed-liquid, and vapour-alone-flow, respectively.

$$\Phi_{lo}=\left(\left(\frac{dp}{dz}F\right)\Big/\left(\frac{dp}{dz}F\right)_{lo}\right)^{1/2} \tag{3.44}$$

$$\Phi_{fo}=\left(\left(\frac{dp}{dz}F\right)\Big/\left(\frac{dp}{dz}F\right)_{fo}\right)^{1/2} \tag{3.45}$$

$$\Phi_{vo}=\left(\left(\frac{dp}{dz}F\right)\Big/\left(\frac{dp}{dz}F\right)_{vo}\right)^{1/2} \tag{3.46}$$

With Fanning equation [Welty et al. 1984], the four frictional pressure-drop terms involved in the above three equations are represented in Eqs. 3.47 to 3.50.

$$-\left(\frac{dp}{dz}F\right)=\frac{2f_{Fan,tp}G^2\bar{v}}{D_{ID}} \tag{3.47}$$

$$-\left(\frac{dp}{dz}F\right)_{lo}=\frac{2f_{Fan,lo}G^2(1-x)^2v_l}{D_{ID}} \tag{3.48}$$

$$-\left(\frac{dp}{dz}F\right)_{fo}=\frac{2f_{Fan,fo}G^2v_l}{D_{ID}} \tag{3.49}$$

$$-\left(\frac{dp}{dz}F\right)_{vo}=\frac{2f_{Fan,vo}G^2x^2v_v}{D_{ID}} \tag{3.50}$$

Eqs. 3.48 to 3.50 will be used in the following derivation, e.g. in Eqs. 3.56 and 3.75.

a.4) Homogeneous-flow model for two-phase flow

Equality of vapour and liquid velocities is assumed in the homogeneous model of 2-phase flow. From the continuity equation, Eq. 3.37, the fluid mass flow rate can be expressed as Eq. 3.51.

$$\dot{m}=A\overline{\rho u} \tag{3.51}$$

The momentum equation, Eq. 3.39, can be reduced to Eq. 3.52.

$$\frac{d(\overline{\rho u}^2)}{dz}=-\frac{dp}{dz}-\frac{\tau_w P}{A}-\bar{\rho}g\sin\theta \tag{3.52}$$

Based on Eqs. 3.52 and 3.42 – 3.43, the following three equations are obtained. First, applying the Fanning equation for a circular channel, the friction head can be expressed as Eq. 3.53.

$$-\left(\frac{dp}{dz}F\right)=-\frac{\tau_w P}{A}=\frac{2f_{Fan,tp}G^2\bar{v}}{D_{ID}} \tag{3.53}$$

Second, the acceleration head, Eq. 3.42, can be written as Eq. 3.54.

$$-\left(\frac{dp}{dz}a\right) = G\frac{d\bar{u}}{dz} = G^2\frac{d\bar{v}}{dz} \tag{3.54}$$

Finally, the potential head, Eq. 3.43, is displayed as Eq. 3.55.

$$-\left(\frac{dp}{dz}z\right) = \bar{\rho}g\sin\theta = \frac{g\sin\theta}{\bar{v}} \tag{3.55}$$

To obtain the 2-phase frictional pressure drop, which is a function of the 2-phase Fanning friction factor, $f_{Fan,tp}$, there are two possible approaches, both utilize the normal Fanning friction factor which is defined for single-phase flow. First, the 2-phase Fanning friction factor, $f_{Fan,tp}$, is assumed equal to the Fanning friction factor for the total-flow-assumed-liquid, $f_{Fan,fo}$, [Collier & Thome 1996]. Consequently, the 2-phase frictional pressure drop, based on Eq. 3.53 and Eq. 3.49, is calculated as shown in Eq. 3.56.

$$-\left(\frac{dp}{dz}F\right) = \frac{2f_{Fan,fo}G^2v_l}{D_{ID}}\left(1+x\left(\frac{v_{fg}}{v_l}\right)\right) = -\left(\frac{dp}{dz}F\right)_{fo}\left(1+x\left(\frac{v_{fg}}{v_l}\right)\right) \tag{3.56}$$

In the second approach, from Eq. 3.45, the 2-phase frictional pressure drop can be written as Eq. 3.57.

$$-\left(\frac{dp}{dz}F\right) = -\left(\frac{dp}{dz}F\right)_{fo}\Phi_{fo}^2 \tag{3.57}$$

To obtain the 2-phase frictional multiplier for the total-flow-assumed-liquid case, Φ_{fo}, one has to consider the normal Fanning friction factor as in Eq. 3.58 and the mean value of the 2-phase dynamic viscosity generally written as Eq. 3.59 [Carey 1992].

$$f_{Fan} = 0.079\left(\frac{GD_{ID}}{\mu}\right)^{-1/4} \tag{3.58}$$

$$\frac{1}{\bar{\mu}} = \frac{x}{\mu_v} + \frac{(1-x)}{\mu_l} \tag{3.59}$$

Now, with the above two equations, both the 2-phase Fanning friction factor, $f_{Fan,tp}$, and the total-flow-assumed-liquid Fanning friction factor, $f_{Fan,fo}$, can be shown as functions of the dynamic viscosities of the liquid and the vapour. In other words, both the frictional pressure drop for the 2-phase and total-flow-assumed-liquid can be calculated

(using Eqs. 3.47 and 3.49). Then, the 2-phase frictional multiplier for the total-flow-assumed-liquid can be expressed as Eq. 3.60.

$$\Phi_{fo}^2 = \left(1+\left(\frac{\mu_l}{\mu_v}-1\right)x\right)^{-0.25}\left(1+\left(\frac{\rho_l}{\rho_v}-1\right)x\right) \tag{3.60}$$

a.5) Separate-flow model for two-phase flow

In the separate-flow model, the velocities of the vapour and liquid phases are not necessarily the same. The continuity equation is the same as shown in Eq. 3.37, whereas the momentum equation, Eq. 3.39, is rearranged into a more applicable form by adopting the following simplifications.

From Eq. 3.45, it is seen that the 2-phase frictional pressure drop is a function of two parameters, $\left(\frac{dp}{dz}F\right)_{fo}$ and Φ_{fo}^2, both of which are for the total-flow-assumed-liquid. To represent $\left(\frac{dp}{dz}F\right)_{fo}$ in term of the total-flow-assumed-liquid Fanning friction factor, $f_{Fan,fo}$, Eq. 3.49 is substituted into Eq. 3.45. Based on the resulting formulation and together with Eqs. 3.42 and 3.43, also by neglecting compressibility of the liquid phase, the total pressure drop, Eq. 3.40 becomes Eq. 3.61 [Collier & Thome 1996].

$$-\left(\frac{dp}{dz}\right) = \left[\begin{array}{l} \dfrac{2f_{Fan,fo}G^2v_l}{D_{ID}}\Phi_{fo}^2 + \\ G^2\dfrac{dx}{dz}\left\{\left(\dfrac{2xv_v}{\alpha}-\dfrac{2(1-x)v_l}{(1-\alpha)}\right)+\left(\dfrac{\partial\alpha}{\partial x}\right)_p\left(\dfrac{(1-x)^2v_l}{(1-\alpha)^2}-\dfrac{x^2v_v}{\alpha^2}\right)\right\}+ \\ g\sin\theta(\rho_v\alpha+\rho_l(1-\alpha)) \end{array}\right] \div \left[1+G^2\left\{\frac{x^2}{\alpha}\left(\frac{dv_v}{dp}\right)+\left(\frac{\partial\alpha}{\partial p}\right)_x\left(\frac{(1-x)^2v_l}{(1-\alpha)^2}-\frac{x^2v_v}{\alpha^2}\right)\right\}\right] \tag{3.61}$$

By assuming negligible compressibility for the gaseous phase, and the specific volumes of both phases and the $f_{Fan,fo}$ remain constant over the considered length of the element, when the boiling occurs from saturated liquid (x = 0) with a linear

variation of vapour quality over the length, the total pressure drop (Eq. 3.61) can be shown as Eq. 3.62.

$$\Delta p = \frac{2f_{Fan,fo}G^2 v_l L}{D_{ID}}\left(\frac{1}{x}\int_0^x \Phi_{fo}^2 dx\right) + G^2 v_l\left\{\frac{x^2}{\alpha}\left(\frac{v_v}{v_l}\right) + \frac{(1-x)^2}{(1-\alpha)} - 1\right\} + \frac{Lg\sin\theta}{x}\int_0^x (\rho_v\alpha + \rho_l(1-\alpha))dx \quad (3.62)$$

As an example for applying Eqs. 3.61 and 3.62, Martinelli & Nelson [1948] developed charts for Φ_{fo}^2 (as a function of pressure and vapour quality), $(1/x)\int_0^x \Phi_{fo}^2 dx$ (as a function of absolute pressure and vapour quality), and α (as a function of absolute pressure and vapour quality) for a steam-water system. Based on the water-steam charts, other researchers carried out analysis for other vapour-liquid systems. Later, Jung & Radermacher [1989] modified the equation for refrigerants (as shown in details in Sub-section 3.4.1).

b) Heat transfer coefficient for saturated boiling

Chen's work [1963] on saturated boiling formed one of the fundamental basis of the application of HTC correlation in this thesis. As mentioned in Chapter 2 for the pure fluid, Chen postulated that the heat transfer is comprised of the contributions from the micro- and macro- convective mechanisms; they correspond to the two regions of saturated boiling, namely: saturated-nucleate-boiling and 2-phase-forced-convection, respectively. His correlation for the HTC is shown in Eqs. 3.63 to 3.65:

$$h_{tp} = h_{nbc} + h_{cec} \quad (3.63)$$

where

$$h_{nbc} = S\,h_{FZ} \quad (3.64)$$

$$h_{cec} = F\,h_{lo} \quad (3.65)$$

The h_{FZ} is the corresponding Forster and Zuber's [1995] correlation arranged to reflect the effect of flow boiling, Eq. 3.66.

$$h_{FZ} = \frac{0.00122\left(\Delta T_{sat}^{0.24}\Delta p_{sat}^{0.75} c_{p,l}^{0.45}\rho_l^{0.49}k_l^{0.79}\right)}{\sigma^{0.5}i_{fg}^{0.24}\mu_l^{0.29}\rho_v^{0.24}} \quad (3.66)$$

The h_{lo} is the single-phase liquid convective HTC based on the mass flow rate of liquid in the 2-phase flow. It is calculated from Eq. 3.67 corresponding to the modified Dittus-Boelter equation:

$$Nu_{lo} = 0.023 Re_{lo}^{0.8} Pr_l^{0.4} \tag{3.67}$$

where

$$Nu_{lo} = \frac{h_{lo} D_{ID}}{k_l} \tag{3.68}$$

$$Re_{lo} = \frac{G(1-x)D_{ID}}{\mu_l} \tag{3.69}$$

$$Pr_l = \frac{\mu_l c_{p,l}}{k_l} \tag{3.70}$$

The S dimensionless parameter in Eq. 3.64 accounts for the suppression of the saturated-nucleate-flow boiling by the 2-phase forced convection flow boiling. The F dimensionless parameter in Eq. 3.66 represents the increase in turbulence due to the 2-phase flow. The F parameter can be expressed as a function of a 2-phase Reynolds number, R_{TP}, shown in Eq. 3.71.

$$Re_{tp} = Re_{lo} F^{1.25} \tag{3.71}$$

c) Heat transfer coefficient for single-phase vapour forced convection

For the single-phase vapour forced convection region, there are many correlations for the HTC calculation. For example, the Gnielinski correlation [Incropera & De Witt 1990], Eq. 3.72, being valid for $0.5 < Pr < 2000$ and $2300 < Re_D < 5\times10^6$:

$$Nu = \left(\frac{f_{Darcy}}{8}\right) \frac{(Re - 1000)Pr}{\left(1 + 12.7\left(\frac{f_{Darcy}}{8}\right)^{(1/2)}\left(Pr^{(2/3)} - 1\right)\right)} \tag{3.72}$$

where, for a smooth tube, the f_{Darcy} is calculated from Eq. 3.73.

$$f_{Darcy} = (0.79 \ln Re - 1.64)^{-2} \tag{3.73}$$

3.3 Background for boiling and heat transfer of mixtures under internal forced convection

To understand the flow boiling, saturated boiling, single-phase vapour forced convection and heat transfer of mixtures, it was necessary to provide some relevant background for its thermodynamics.

Equilibrium: For a system isolated from its surroundings, when its properties do not change with time, it is in an equilibrium state. Therefore, for a closed system, a steady state is an equilibrium state, whereas, for an open system, due to interacting with the surrounding, its steady state is strictly speaking not an equilibrium state. However for the present investigation of a DX evaporator operation, the steady state is assumed to be in equilibrium in relation to the use of the refrigerant properties.

Phase rule, degrees of freedom: To specify an equilibrium state for a pure-component or a mixture system with a single or multi phases, the phase rule provides the number of intensive-and-state variable(s), called the degrees of freedom. Based on the practical acquisition of data, these variables are temperature, pressure and mol fractions (as used in Refprop [Huber et al. 1996]), etc.

Equations of state: From P-v-T data, an equation of state, EOS, is the result of a curve fitting. The EOS , as employed in Refprop [Huber et al. 1996], is for calculating pressure, specific volume or temperature of an equilibrium state, and generally contains semi-empirical parameters. For a mixture, parameters of some EOS are obtained from mixing rules operating algebraically on the pure-component parameters, and from curve fitting with the data of the mixture.

Pure components and mixtures: A pure component, either element or compound type, is only regarded as one chemical substance in this thesis. A mixture, homogeneous or heterogeneous, consists of at least two pure components mixed together; only the homogeneous type assumed having constant composition is considered in this thesis.

Temperature glides: Referring to the brief mentioning in Chapter 1, the details are explained as the follow. When heating a binary mixture under a constant pressure, Fig. 3.9, the boiling begins at the bubble-point temperature, R. The vapour phase is rich in the more volatile component, S. During boiling until depleting of the liquid, W, at any time (e.g. U), the concentrations of this component in both phases become less and less, the mixture temperature then increases, i.e. glides up,

correspondingly. The work presented in this thesis will demonstrate here how the unique feature of the temperature gliding-up influences the dynamic behaviour of the DX evaporator.

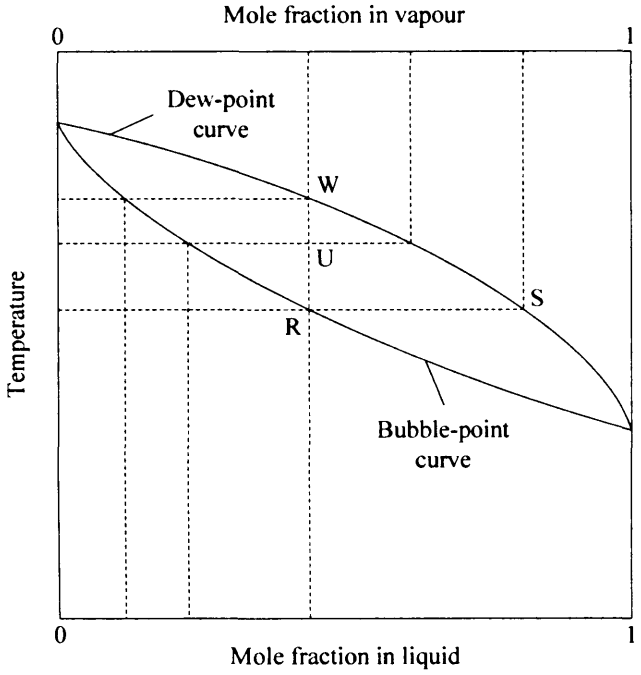

Figure 3.9 Elementary phase equilibrium for a zeotropic mixture [modified from Collier et al. 1996]

Pool boiling: A mixture behaves differently to a pure component in two main aspects [Collier et al. 1996]: onsets of nucleate boiling and HTCs. The onset of nucleate boiling of a mixture occurs at the higher wall superheat value than that of a pure component. This is due to setting up of the temperature gradient in the pool to accommodate the corresponding gradient of liquid compositions. This aspect is included, since both Chen's correlation (Eq. 3.63) and Jung et al.'s correlations (Sub-sections 3.4.2 and 3.4.3), used in calculating the HTCs for the saturated flow boiling, contained the nucleate-pool-boiling HTC correlation.

The HTC of a mixture is generally lower than that of a pure component, because of the following two causes. First, when a bubble is growing, Fig. 3.10, the more volatile component of the surrounding liquid layer evaporated rapidly, the saturated temperature is then increasing. This results in the decreasing of the wall superheat, the heat transfer rate and subsequently the HTC [Whalley 1990]. Furthermore, due to the higher wall superheat value for the onset of nucleate boiling, the

numbers of sites for the bubble initiation are less than that of the pure component [Thome 1983] [Inoue 1994].

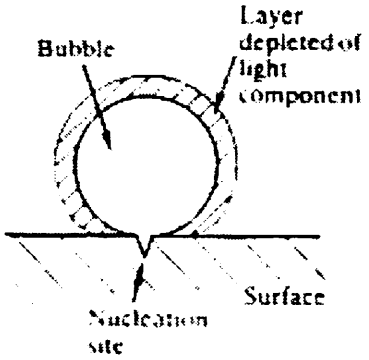

Figure 3.10 Mechanism of the reduction in heat transfer to a bubble in a zeotropic mixture [Whalley 1990]

3.4 Pressure drop and heat transfer coefficient for refrigerant side

For the refrigerant side, the two-phase saturated flow boiling and the single-phase vapour forced convection heat transfer occurred inside a horizontal tube. Theories discussed here deal with both pressure-drop and HTC calculations for both pure and mixed refrigerants.

3.4.1 Pressure drop calculation for pure and mixed refrigerants

For both pure and mixed refrigerants, pressure drop theories of the two- and single- phases were explained.

Two-phase pressure drop: Based on the observation made in Chapter 2, there are no significant effects from a mixture fluid on the 2-phase pressure drop [Jung & Radermacher 1989]. Therefore, pressure-drop correlations discussed here can be applied to both pure and mixed refrigerants. For horizontal tubes having zero values of the potential pressure drop, Eq. 3.62 can be written as Eq. 3.74.

$$\Delta p = \frac{2f_{Fan,fo}G^2 v_l L}{D_{ID}}\left(\frac{1}{x}\int_0^x \Phi_{fo}^2 dx\right) + G^2 v_l\left\{\frac{x^2}{\alpha}\left(\frac{v_v}{v_l}\right) + \frac{(1-x)^2}{(1-\alpha)} - 1\right\} \qquad (3.74)$$

In order to calculate the integration term, the two-phase frictional multiplier for the total-flow-assumed-liquid, Φ_{fo}, is to be presented as a function of vapour quality by implementing the following five steps. **First**, the Martinelli parameter, X_{tt}, as defined by Lockhart & Martinelli [1949], is arranged into a function of the vapour quality, as shown below, Eq. 3.75.

$$X_{tt} = \left(\left(\frac{dp}{dz} F \right)_{lo} \Big/ \left(\frac{dp}{dz} F \right)_{vo} \right) \tag{3.75}$$

From Eqs. 3.48 and 3.50, it is seen that the frictional pressure drops for the liquid-alone-flow, $\left(\frac{dp}{dz} F \right)_{lo}$, and for the vapour-alone-flow, $\left(\frac{dp}{dz} F \right)_{vo}$, are functions of Fanning factors for the liquid-alone-flow, $f_{Fan,lo}$, and for the vapour-alone-flow, $f_{Fan,vo}$, respectively. For a smooth tube, Fanning friction factors in the range of $5{,}000 < Re < 200{,}000$ are given in Eqs. 3.76 to 3.78.

$$f_{Fan,lo} = 0.046 Re_{lo}^{-0.2} \tag{3.76}$$

$$f_{Fan,fo} = 0.046 Re_{fo}^{-0.2} \tag{3.77}$$

$$f_{Fan,vo} = 0.046 Re_{vo}^{-0.2} \tag{3.78}$$

Substituting Eqs. 3.48, 3.50, 3.76 and 3.78 into Eq. 3.75, gives the Martinelli parameter, Eq. 3.79.

$$X_{tt} = \left(\frac{1-x}{x} \right)^{0.9} \left(\frac{\rho_v}{\rho_l} \right)^{0.5} \left(\frac{\mu_l}{\mu_v} \right)^{0.1} \tag{3.79}$$

Second, it is necessary to establish a relation between Φ_{fo} and Φ_{lo}, since the latter needs to be linked to a newly established parameter that can be calculated (seeing the 4th step below). Then, substitute $f_{Fan,lo}$ and $f_{Fan,fo}$ from Eqs. 3.76 and 3.77 into Eqs. 3.48 and 3.49 respectively, which are used for calculating $\left(\frac{dp}{dz} F \right)_{lo}$ and $\left(\frac{dp}{dz} F \right)_{fo}$. Substitute the outcomes into Eqs. 3.44 and 3.45 respectively to obtain Eq. 3.80.

$$\Phi_{fo}^2 = \Phi_{lo}^2 (1-x)^{1.8} \tag{3.80}$$

Third, the 2-phase frictional multiplier for the liquid-alone-flow, Φ_{lo}, is to be related to a newly defined 2-phase multiplier for total-pressure-drop, Φ_{to}. For typical forced convection evaporators with the aspect ratio, L/D, generally in the range of 500-1000, Soumerai [1987] showed that the ratio of the acceleration pressure drop to

the frictional pressure drop will be around 0.025-0.05, and that the total pressure drop approximately equals to the frictional pressure drop, Eq. 3.81.

$$\left(\frac{dp}{dz}\right) \approx \left(\frac{dp}{dz}F\right) \tag{3.81}$$

Jung & Radermacher [1989] defined the 2-phase multiplier for the total-pressure-drop, Φ_{to}, as shown in Eq. 3.82.

$$\Phi_{to} = \left(\left(\frac{dp}{dz}\right) \Big/ \left(\frac{dp}{dz}F\right)_{lo}\right)^{1/2} \tag{3.82}$$

Substitute the total pressure drop from Eq. 3.81 into Eq. 3.82, the 2-phase multiplier for the total-pressure-drop, Φ_{to}, becomes the 2-phase frictional multiplier for the liquid-alone-flow, Φ_{lo}, Eq. 3.83.

$$\Phi_{to} = \left(\left(\frac{dp}{dz}\right) \Big/ \left(\frac{dp}{dz}F\right)_{lo}\right)^{1/2} = \Phi_{lo} = \left(\left(\frac{dp}{dz}F\right) \Big/ \left(\frac{dp}{dz}F\right)_{lo}\right)^{1/2} \tag{3.83}$$

The fourth step is to establish a relationship between the 2-phase multiplier for the total-pressure-drop, Φ_{to}, and the Martinelli parameter, X_{tt}. Jung & Radermacher [1989] referred to Wallis' work [1969] that the void fraction could be correlated by using only X_{tt}, and that the acceleration pressure drop in Eq. 3.74 can be correlated with X_{tt}. With Eq. 3.74 (for calculating the total pressure drop), they applied this reasoning to point out that the 2-phase multiplier for the total-pressure-drop, Φ_{to}, shown in Eq. 3.82, is able to be expressed as a function of X_{tt}. With their experimental data of the pure and mixed refrigerants in the annular flow regime, Jung & Radermacher [1989] obtained the functional dependence of Φ_{to} on X_{tt} as shown in Eq. 3.84.

$$\Phi_{to} = 3.58 X_{tt}^{-0.735} \tag{3.84}$$

As mentioned previously, Jung & Radermacher [1989] found that there is no significant mixture effect on the two-phase pressure drop. Hence Eq. 3.84 is applicable for both pure and mixed refrigerants.

Fifth, based on the 2nd to the 4th steps, substitute Φ_{to} from Eq. 3.84 into Eq. 3.80 for Φ_{lo}, this results in Eq. 3.85.

$$\Phi_{fo}^2 = \Phi_{to}^2 (1-x)^{1.8} = 12.82 X_{tt}^{-1.47} (1-x)^{1.8} \tag{3.85}$$

For pure refrigerants, Eq. 3.85 is modified further as follows. Jung & Radermacher [1989] showed that it is possible to replace the ratios of the densities and the viscosities with a function of the reduced pressure, Eq. 3.86.

$$\left(\frac{\rho_v}{\rho_l}\right)^{0.5}\left(\frac{\mu_l}{\mu_v}\right)^{0.1} = 0.551 p_r^{0.492} \tag{3.86}$$

The above correlation is applicable for the range of $0.06 < p_r < 0.7$ with a maximum deviation of 5%. Substitute Eq. 3.86 into Eq. 3.79, X_{tt} can then be expressed as Eq. 3.87.

$$X_{tt} = 0.551\left(\frac{1-x}{x}\right)^{0.9} p_r^{0.492} \tag{3.87}$$

Substituting X_{tt} from Eq. 3.87 into Eq. 3.85 gives Eq. 3.88.

$$\Phi_{fo}^2 = 30.78 x^{1.323} (1-x)^{0.477} p_r^{-0.7232} \tag{3.88}$$

For the above equation, if x = 0, Φ_{fo}^2 was assigned a value of 1, and if x = 1, $\Phi_{fo}^2 = 3.29 p_r^{-0.984}$ [Jung & Radermacher 1989].

In conclusion, for the 2-phase pressure drop shown in Eq. 3.74, with the approximation in the third step represented by Eq. 3.81, the presure can be given as Eq. 3.89:

$$\Delta p = \frac{2 f_{Fan,fo} G^2 L}{D_{ID} \rho_l}\left(\frac{1}{x}\int_0^x \Phi_{fo}^2 dx\right) \tag{3.89}$$

or as a more general equation, Eq. 3.90.

$$\Delta p = \frac{2 f_{Fan,fo} G^2 L}{D_{ID} \rho_l}\left(\frac{1}{\Delta x}\int_{x_1}^{x_2} \Phi_{fo}^2 dx\right) \tag{3.90}$$

The $f_{Fan,fo}$ is calculated from Eq. 3.77, whereas the Φ_{fo}^2 is obtainable from Eq. 3.85 or Eq. 3.88 (see the fifth step).

Single-phase vapour pressure drop: Because there is no composition change for single-phase flow, equations of the frictional pressure drop calculation can

be used for both pure and mixed refrigerants, such as the Darcy-Weisbach equation [e.g. Welty et al. 1984]. The total pressure drop, when neglecting the acceleration and potential pressure drops, can be given as in Eq. 3.91:

$$\Delta p = \frac{f_{Darcy} G^2 vL}{2D_{ID}} \tag{3.91}$$

where, for a smooth tube, the f_{Darcy} is given in the equation (3.73).

3.4.2 Heat transfer coefficient calculation for pure refrigerants

An adopted HTC correlation for pure refrigerants in the horizontal saturated flow boiling was explained below, whereas the single-phase vapour convection was same as discussed in Sub-section 3.2.2.c. As discussed in Chapter 2, Jung et al.'s correlation [1989b] was selected in this study; it had been pointed out that the correlation was developed by applying the superposition principle to Chen's correlation [1963].

Jung et al. [1989b] first revised the F factor in Eq. 3.66 with their data, resulting in a F value for pure component, F_p, Eq. 3.92.

$$F_p = 2.37\left(0.29 + \frac{1}{X_{tt}}\right)^{0.85} \tag{3.92}$$

F in Eq. 3.65 was replaced with F_p, giving the HTC from the convective evaporation contribution as in Eq. 3.93.

$$h_{cec} = F_p h_{lo} \tag{3.93}$$

For the nucleate boiling contribution, Eq. 3.64, they improved both h_{FZ} and S. The nucleate pool boiling HTC correlation of Forster and Zuber [1955] was replaced by that of Stephan & Abdelsalam [1980], h_{SA}, shown in Eq. 3.94:

$$h_{SA} = 207\frac{k_l}{(bd)}\left(\frac{q(bd)}{k_l T_{sat}}\right)^{0.745}\left(\frac{\rho_v}{\rho_l}\right)^{0.581} Pr_l^{0.533} \tag{3.94}$$

where

$$bd = 0.0146\beta\left(\frac{2\sigma}{g(\rho_l - \rho_v)}\right)^{0.5} \tag{3.95}$$

with $\beta = 35°$.

For improving the S parameter, Jung et al. [1989b] observed that, for a given vapour quality, the h_{nbc} is a strong function of heat flux and mass flow rate. By normalizing it with h_{SA}, a N parameter was defined, Eq. 3.96.

$$N = \frac{h_{nbc}}{h_{SA}} = fn(x, q, \dot{m}) \tag{3.96}$$

They proposed that the functional dependence of N on x, q and $\dot{m}$ can be represented by the Martinelli parameter and the boiling number, Eq. 3.97.:

$$N = fn(X_{tt}, Bo) \tag{3.97}$$

The boiling number is the ratio of the mass flux of vapour generated on the heated surface to the total mass flux parallel to the heated surface, as defined in Eq. 3.98.

$$Bo = \frac{q}{Gi_{fg}} \tag{3.98}$$

With their data from pure and azeotropic refrigerants, they established semi-empirical equations of the N parameter as shown in Eqs. 3.99 and 3.100.

$$N = 4048 X_{tt}^{1.22} Bo^{1.13} \qquad \text{for} \quad X_{tt} < 1 \tag{3.99}$$

$$N = 2.0 - 0.1 X_{tt}^{-0.28} Bo^{-0.33} \qquad \text{for} \quad 1 \le X_{tt} \le 5 \tag{3.100}$$

In conclusion, Jung et al.'s correlation [1989b] for the HTC calculation of pure refrigerants in the horizontal saturated flow boiling can be written as Eq. 3.101.

$$h_{tp} = h_{nbc} + h_{cec} = N h_{SA} + F_p h_{lo} \tag{3.101}$$

It should be borne in mind that both nucleate boiling and convective evaporation contributions are formed with the superposition principle.

3.4.3 Heat transfer coefficient calculation for mixture refrigerants

Jung et al.'s [1989b] developed the correlation by recognizing mixture effects on their saturated flow boiling correlation for horizontal flow for pure refrigerants. For the 2-phase forced convection contribution, from Sub-section 2.1.3 of Chapter 2, Jung et al.[1989a] noticed that the calculated HTCs of the mixture

refrigerants, Eq. 3.93, i.e. $F_p h_{lo}$, are a bit higher than the experimental values. This difference is believed to be attributed to the mass transfer resistance effect. Subsequently, they substituted the F_p parameter with a newly defined F_m parameter as shown in Eq. 3.102.

$$F_m = C_{me} F_p \tag{3.102}$$

The C_{me} parameter, reflecting the mass transfer resistance effect, can be calculated by using a semi-empirical equation, Eq. 3.103, obtained from data with a phase-equilibrium assumption.

$$C_{me} = 1 - 0.35|Y - X|^{1.56} \qquad \text{for} \quad 0.9 < C_{me} < 1 \tag{3.103}$$

By substituting Eq. 3.102 into Eq. 3.93, the HTC correlation for the 2-phase forced convection contribution can be obtained, Eq. 3.104.

$$h_{cec} = C_{me} F_p h_{lo} \tag{3.104}$$

Before looking at the development of the correlation for the nucleate boiling contribution, the following four issues, introducing the mixture effect into the prediction of nucleate-boiling suppression which was originally developed for pure refrigerants, need to be understood (Note: Suppression is the opposite of the bubble growth, explained in Sub-section 3.2.1 and it happens when wall superheat decreases to a value that bubbles cannot be initiated).

First, when considering saturated flow boiling, as the flow pattern becomes annular, the main heat transfer mechanism is the heat conduction across the liquid layer. When the vapour quality increases, the liquid layer is getting thinner; the HTC becomes higher due to less thermal resistance. Thus, the wall superheat in the liquid layer will decrease; when it falls below that required for bubble formation, the nucleate boiling is fully suppressed, and the nucleate boiling contribution is zero. When considering Eq. 3.101 together with Eq. 3.34, being the wall superheat for the ONB, it was shown that, for pure refrigerants, at the suppression of nucleate boiling, the wall superheat and the heat flux can be calculated from Eqs. 3.105 and 3.106, which can be used for obtaining the transition vapour-quality at the suppression.

$$\Delta T_{SNB} = \frac{2T_{sat}\sigma k_l}{i_{fg}\rho_v r_{bub,max}(k_l - F_p h_{lo} r_{bub,max})} \tag{3.105}$$

$$q_{SNB} = F_p h_{lo} \Delta T_{SNB} \tag{3.106}$$

Second, regarding the mixture effect on bubble formation, when referring to Scriven's work [1959], Jung et al. [1989b] showed that a bubble radius of a mixture is a function of that of a pure refrigerant, Eq. 3.107.

$$r_{bub,m} = \frac{r_{bub,p}}{1 - \frac{c_{p,l}}{i_{fg}}\left(\frac{\alpha}{D}\right)_l^{0.5}(Y-X)\left(\frac{dT}{dX}\right)_{bub}} \tag{3.107}$$

They discussed that the denominator of the RHS term is an analytically developed correction factor to consider mixture effects. Knowing that the wall superheat is inversely proportional to the bubble radius, Eq. 3.32, a ratio of wall superheat for a mixture to that for an ideal mixture (without the mixture effects) can be expressed as in Eq. 3.108 [Jung et al. 1989b]:

$$\frac{\Delta T_m}{\Delta T_i} = 1 - \frac{c_{p,l}}{i_{fg}}\left(\frac{\alpha}{D}\right)_l^{0.5}(Y-X)\left(\frac{dT}{dX}\right)_{bub} \tag{3.108}$$

where

$$\Delta T_i = X_1 \Delta T_1 + X_2 \Delta T_2 \tag{3.109}$$

Third, on the other hand, Unal [1986] developed an empirical correlation for the ratio as in Eqs. 3.110 to 3.116.

$$\frac{\Delta T_m}{\Delta T_i} = C_{UN} = (1.0 + (b_2 + b_3)(1.0 + b_4))(1.0 + b_5) \tag{3.110}$$

$$b_2 = (1.0 - X)\ln\left(\frac{1.01 - X}{1.01 - Y}\right) + X\ln\left(\frac{X}{Y}\right) + |Y - X|^{1.5} \tag{3.111}$$

$$b_3 = 0.0 \qquad \text{for} \quad X \geq 0.01 \tag{3.112}$$

$$b_3 = \left(\frac{Y}{X}\right)^{0.1} - 1 \qquad \text{for} \quad X < 0.01 \tag{3.113}$$

$$b_4 = 152\left(\frac{p}{p_{c,mvc}}\right)^{3.9} \tag{3.114}$$

$$b_5 = 0.92(|Y - X|)^{0.001}\left(\frac{p}{p_{c,mvc}}\right)^{0.66} \tag{3.115}$$

$$\frac{X}{Y} = 1 \qquad \text{for} \quad X \text{ or } Y = 0 \tag{3.116}$$

NB The condition of Eq. 3.116 meant that, for calculating the parameters b_2, b_3 and b_5, whenever X or Y was equal to zero, the other would be assigned zero, and their ratio was put as 1, as shown in Eq. 3.116.

Finally, as shown Eq. 3.106 that the heat flux is direct proportional to the wall superheat, the heat flux at the SNB for a mixture refrigerant can be expressed as in Eq. 3.117.

$$q_{SNB,m} = C_{UN} q_{SNB,i} = C_{UN}(F_P h_{lo} \Delta T_{SNB,i}) \tag{3.117}$$

Based on the above derivation and the contribution of mixture effects, for the nucleate boiling contribution, for mixtures, Jung et al. [1989b] proposed using h_{UN} and dividing the N parameter, being the factor due to the nucleate boiling for a pure refrigerant, by the C_{UN}, as shown in Eq. 3.118. In other words, from Eq. 3.101, which is for calculating HTC of pure refrigerants, for the contribution part of the nucleate boiling, it was modified for mixed refrigerants by introducing the C_{UN} term.

$$h_{nbc} = \frac{N}{C_{UN}} h_{UN} \tag{3.118}$$

where

$$\frac{h_{UN}}{h_i} = \frac{1}{C_{UN}} \tag{3.119}$$

$$h_i = \frac{1}{\frac{X_1}{h_1} + \frac{X_2}{h_2}} \tag{3.120}$$

The nucleate pool boiling HTCs of components 1 and 2, h_1 and h_2, are calculated by using Stephan and Abdelsalam's correlation, h_{SA}, shown in Eq. 3.94:

$$h_{SA} = 207\frac{k_l}{(bd)}\left(\frac{q(bd)}{k_l T_{sat}}\right)^{0.745}\left(\frac{\rho_v}{\rho_l}\right)^{0.581} Pr_l^{0.533} \tag{3.94}$$

where

$$bd = 0.0146\beta\left(\frac{2\sigma}{g(\rho_l - \rho_v)}\right)^{0.5} \tag{3.95}$$

with $\beta = 35°$.

In conclusion, Jung et al.'s HTC correlation [1989b], for mixture refrigerants, adopted in this thesis, is given in Eq. 3.121.

$$h_{tp} = \frac{N}{C_{UN}} h_{UN} + C_{me} F_p h_{lo} \tag{3.121}$$

The procedures and a sample calculation of the heat transfer coefficient for mixture were given in Section A.3 of Appendix A and Section D.3 of Appendix D, respectively.

3.5 Dynamics of evaporator

Investigation into dynamics of evaporators generally concerned with three main inter-related areas: development of fundamental/governing equations, understanding the dynamic behaviour and its influences on operations (controls, efficiency, stability, etc.) associated with individual applications [Roetzel & Xuan 1999]. Evaporators are generally operating in dynamic modes associated with system start-up, and variations in pressures, flow rates and temperatures of fluid streams in finite times.

For this study, the correlations and the parameters influenced by the refrigerant properties were first identified and selected for use in establishing the governing equations. The modelling and simulation of both evaporator and TEV was performed to investigate the influence of refrigerant properties on evaporator dynamics. The disturbance chosen was a step change(s) of the coil-inlet DB air temperature. The transient analysis focussed on two areas: fundamental coil-analyses for the dry and

totally wet conditions, and a TEV-controlled-evaporator study. The theoretical details of the latter were explained in the following Sub-section.

3.5.1 TEV-controlled evaporator

A TEV is equipped to an evaporator for controlling the degree of superheat for the refrigerant at the evaporator outlet, Fig. 3.11. It consists of a diaphragm-and-needle valve, arranged together with a sensor bulb and an external equalizer. When cooling load increases, the superheated temperature of the refrigerant vapour at the coil outlet is higher; the feedback pressure from the sensor bulb then increases. After that, there is a force imbalance at the diaphragm; hence, the needle moves downward to allow an increase in the inlet mass flow rate of refrigerant. When cooling load decreases, the reverse happens.

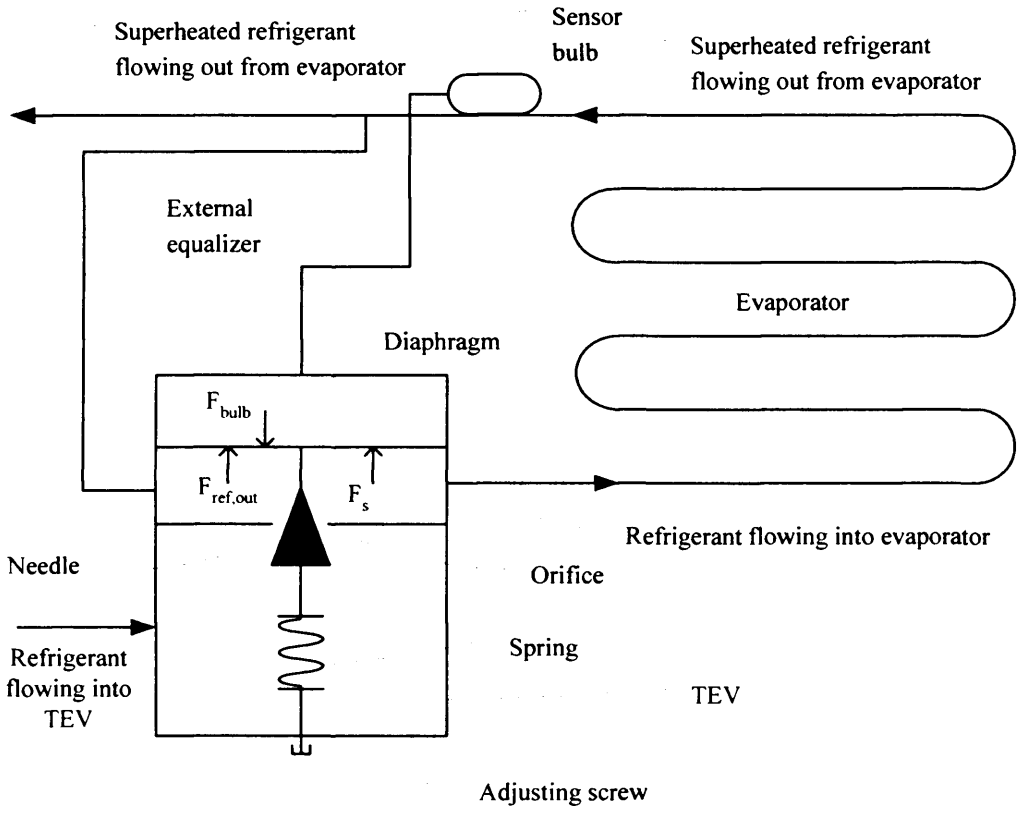

Figure 3.11 Simplified diagram for TEV-controlled evaporator

a) TEV

To obtain an equation for calculating the mass flow rate of refrigerant through the TEV, the force balance on the diaphragm of the TEV is considered, as shown in Eq. 3.122 [James & James 1987] (see Fig. 3.11).

$$(p_{bulb} - p_{ref,out})A_d - F_s = 0 \tag{3.122}$$

On the LHS, the first term is the summation of the two forces from the feedback pressure of the sensor bulb and the external equalizer. The second term is the spring force that consists of 2 components, as shown in Eq. 3.123, derived with 2 assumptions: a constant spring coefficient (K_s) and a negligible spring-hysteresis [James & James 1987].

$$F_s = F_o + K_s z \tag{3.123}$$

The F_o is an initially adjusted spring force to match a preset maximum value of a static superheat before the needle valve begins to open. The second term on the RHS is the force due to the displacement of the spring.

Substituting Eq. 3.123 into Eq. 3.122 gives:

$$z = \left(\frac{A_d}{K_s}\right)(p_{bulb} - p_{ref,out} - p_{ss}) \tag{3.124}$$

where

$$p_{ss} = \frac{F_o}{A_d} \tag{3.125}$$

Eq. 3.126 assumes that the opening flow area at the orifice is directly proportional to the spring displacement, z [James & James 1987].

$$A_{flow,min} = K_{Amin,z} \cdot z \tag{3.126}$$

Putting Eq. 3.126 into Eq. 3.124 results in:

$$A_{flow,min} = \left(\frac{K_{Amin,z} \cdot A_d}{K_s}\right)(p_{bulb} - p_{ref,out} - p_{ss}) \tag{3.127}$$

The refrigerant mass flow rate passing through the flow area can be obtained from Eq. 3.128 [Gosney 1982].

$$\dot{m}_{ref} = C_d \cdot A_{flow,min} \left(\rho_{ref,l,TEV,in} \cdot \left(p_{ref,l,TEV,in} - p_{ref,TEV,out}\right)\right)^{(1/2)} \quad (3.128)$$

Substitute Eq. 3.127 into Eq. 3.128 gives.

$$\dot{m}_{ref} = \left(\frac{C_d \cdot K_{Amin,z} \cdot A_d}{K_s}\right) \cdot \left(\rho_{ref,l,TEV,in} \cdot \left(p_{ref,l,TEV,in} - p_{ref,TEV,out}\right)\right)^{(1/2)} \left(p_{bulb} - p_{ref,out} - p_{ss}\right) \quad (3.129)$$

In addition, the flow through the valve is assumed to be isenthalpic, Eq. 3.130 [Moran 1993].

$$i_{ref,l,TEV,in} = i_{ref,TEV,out} \quad (3.130)$$

b) Sensor bulb

For establishing the governing equations, it is assumed there is sufficient amount of fluid in the sensor bulb to ensure that liquid always coexists with vapour. Apart from the phase-equilibrium assumption, it was also assumed that, when compared to the quantity of vapour within the bulb, there was a lot more liquid; thus the liquid level inside the bulb could be assumed constant for all operating conditions of the evaporator [Omag 1999] (see Fig. 3.12). Therefore, only the bulb and the tube-wall energy balances, not fluid charge mass balances, are needed.

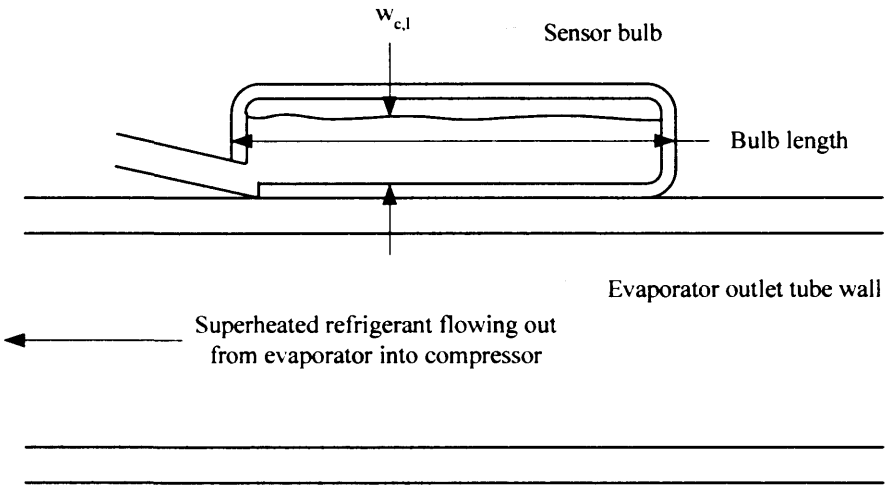

Figure 3.12 Simplified diagram for a sensor bulb attached on an evaporator outlet tube

For the energy balance of the tube-wall, where the sensor bulb is attached, Fig. 3.12, with an assumption that there is a thermal equilibrium between the sensor-bulb wall and the charged fluid (i.e. both having the same temperature), it can be established as Eq. 3.131 [Mithraratne 1992, James & James 1987]:

$$c_{p,wall} m_{wall} \frac{dT_{wall,ave}}{dt} = \frac{A_{wall,tube}\left(T_{bulb} - T_{wall,ave}\right)}{\left(\frac{D_{OD,tube} - D_{ID,tube}}{2k_{tube}} + \frac{w_{bulb}}{k_{bulb}}\right)} - q_{wf} A_{wall,i} \qquad (3.131)$$

where

$$w_{bulb} \cong w_{c,l} \qquad (3.132)$$

$$k_{bulb} \cong k_{c,l} \qquad (3.133)$$

For Eq. 3.131, the term on LHS is the rate of change of the accumulated heat in the tube wall. On RHS, the first and the second terms are the rates of the heat transfer from the sensor bulb to the tube-wall and from this tube-wall to the refrigerant, respectively. Eqs. 3.132 and 3.133 [Mithraratne 1992] suggest that the thickness and the thermal conductivity of the sensor bulb and of the charged liquid are approximately the same, equivalent to having very thin sensor-bulb walls.

Eq. 3.134 shows the energy balance of the sensor bulb, Fig. 3.12 [Mithraratne 1992, James & James 1987]:

$$c_{p,bulb} m_{bulb} \frac{dT_{bulb}}{dt} = q_{bulb,e} A_{wall,e} - \frac{A_{wall,tube}\left(T_{bulb} - T_{wall,ave}\right)}{\left(\frac{D_{OD,tube} - D_{ID,tube}}{2k_{tube}} + \frac{w_{bulb}}{k_{bulb}}\right)} \qquad (3.134)$$

where

$$m_{bulb} \cong m_{c,l} \qquad (3.135)$$

$$c_{p,bulb} \cong c_{p,c,l} \qquad (3.136)$$

In Eq. 3.134, the term on LHS is the rate of change of the accumulated heat in the sensor bulb. The first and the second terms on RHS are the rates of the heat transfer from the surroundings to the bulb and from the bulb to the tube-wall, respectively. The mass and the specific heat at constant pressure of the sensor bulb are assumed to be approximately equal to that of the charged liquid, Eqs. 3.135 and 3.136.

Chapter 4 Modelling and simulation

Applying the relevant theories described previously, a mathematical model was constructed to simulate the dynamics of a DX evaporator. Regarding the evaporator configurations, selection of the physical parameters involved and the dividing scheme for the element-based approach were first described. The establishment of the governing equations, representing the associated physical processes, was then explained. Air-side and finned-tube modelling comprised of two coil conditions: dry and wet. Refrigerant-side modelling dealt with both single- and two- phase flows, as well as a TEV-controlled evaporator. The programming and simulation sections presented details on how the codes were developed, written and run. In addition, the differences between pure and mixed refrigerants with respect to the temperature gliding and the degrees of freedom, and the associated experiences/difficulties encountered in the programming and the simulation were explained. Assumptions and constraints were stated wherever appropriate.

4.1 Evaporator configurations

The studied plate-fin-tube evaporators were counter-cross flow direct expansion air coolers, an example of which was shown in Figs. 4.1 and 4.2. At the coil inlet on the right, the refrigerant entered as a two phase fluid and became superheated vapour near the end of the coil outlet on the left hand side. It is useful to point out that in practice the inlet and the outlet refrigerant are on the same side of the coil. For simplicity, all the connecting U-bends were ignored in the analysis. The physical parameters of the evaporator were mainly configured based on the work of Turaga et al. [1988a and 1988b]. The fixed parameters, such as the coil width and the tube diameter, were given in Table 4.1. The variables used in the present study, e.g. the fin spacing to

thickness ratio, were presented in Chapter 5 for individual coil condition and TEV-controlled cases.

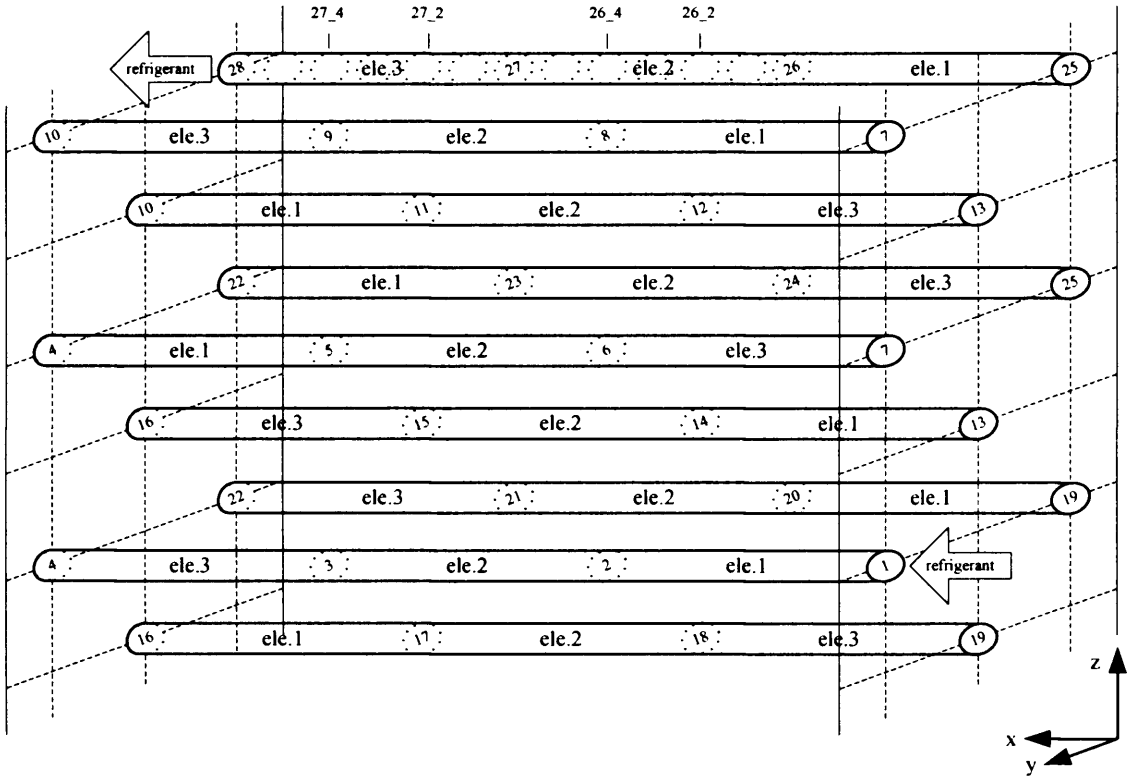

Figure 4.1 An example of an arrangement in a plate-fin-tube evaporator had the nodes of Elements numbered from the refrigerant inlet to the refrigerant outlet (1 – 28). For each Tube, the Elements were numbered from the refrigerant inflow end (element 1 – 3). In the last Tube of the coil, each Element contained Sub-elements, (e.g. Sub-element 2 having the inlet and outlet at the nodes 26_1 and 26_2, respectively).

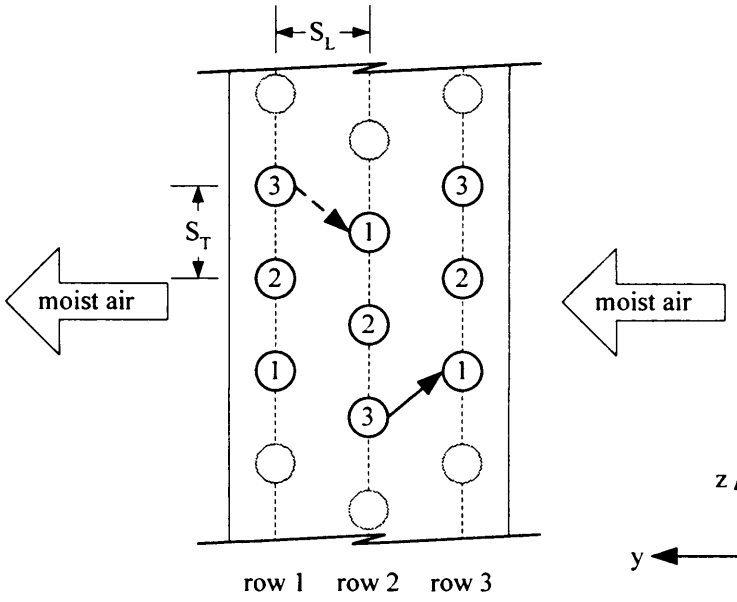

Figure 4.2 A side view of the tube arrangement in the plate-fin-tube evaporator showed the first tube in Row 1 being the refrigerant coil-inlet. For each row, the refrigerant flows from tube 1 to 2 to 3.

The height and the width of the coil are 0.559 m and 1.219 m, respectively. The outside and inside diameters of the smooth copper tube are 0.0134 m and 0.0126 m, respectively. The tube arrangement is a staggered type with the same longitudinal and transverse spacing, S = 0.0381 m. The flat-plate aluminium fin thickness is 0.00016 m. As an example, for Coil No. 3, Table 4.2, the number of row per evaporator is 3, and the ratio of the fin spacing to the fin thickness is 12.3; the rest of the coil configurations can be obtained with the physical-relation equations given in Table A.2 of Appendix A.

Table 4.1 Fixed parameters of the coil used in the work of Turaga et al. [1988a and 1988b] and adopted in this thesis

C_H = 0.559 m	C_w = 1.219 m
$S_T = S_L$ = 0.0381 m	w_{fin} = 0.00016 m
$D_{OD,tube}$ = 0.0134 m	$D_{ID,tube}$ = 0.0126 m
fin type: flat plate fin	fin material: aluminium

Table 4.2 Variable parameters of the coil used in the work of Turaga et al. [1988a and 1988b]

coil no.	N_R	P_s [fin/m]	D_h [m]	A_{mf}/A_F	N_{TR}	L_d [m]	$A_{o,total}/A_p$	$A_{o,total}/A_{wall,i}$	s_{fin}/w_{fin}
1	3	390	0.0032	0.58	15	0.114	26.5	27.0	17.2
2	3	470	0.0027	0.57	15	0.114	31.8	32.2	14.4
3	3	550	0.0022	0.56	15	0.114	37.2	37.4	12.3
4	4	550	0.0022	0.56	15	0.152	37.2	37.4	12.3
5	6	310	0.0040	0.60	15	0.229	21.2	21.8	21.6
6	6	390	0.0032	0.58	15	0.229	26.5	27.0	17.2
7	6	470	0.0027	0.57	15	0.229	31.8	32.2	14.4
8	8	310	0.0040	0.60	15	0.305	21.2	37.4	12.3
9	8	390	0.0032	0.58	15	0.305	26.5	27.0	17.2
10	8	550	0.0022	0.56	15	0.305	37.2	37.4	12.3

With the distributive model, the coil was divided into a number of elements/sub-elements, each of which was set up with the continuity, momentum and/or energy equations. The length of the element, specifically in the two-phase section, was chosen not to exceed the distance between the two locations for the data collection (temperature and pressure) in Jung et al.'s [1989a] and Jung & Radermacher's [1989] work. In addition, each element in the superheat region is further sub-divided into sub-

elements to facilitate the calculation of the superheat flow. This was due to the lower HTCs, reduced heat flux and larger magnitudes of the change in refrigerant temperature encountered in the superheat region.

4.2 Air-side modelling

Air-side modelling for a differential control volume dealt with heat and mass transfers from moist air to coil surfaces directly or indirectly (through water-condensate). At the coil face, the distribution/profile of the air velocity, the temperature and the humidity ratio was assumed to be uniform. Through the coil, it was assumed that the air was incompressible, and the air density changed insignificantly. At each element or sub-element, the inlet air mass flux was assumed to be equal; otherwise, enormous amount of calculation time will be consumed by using the trial-and-error calculation scheme.

4.2.1 Dry-coil condition

For the dry coil, only an energy balance of the moist air was required because the air pressure drop along the coil was assumed to be negligible, MacArthur [1984] and Wang & Touber [1991]. When considering a differential control volume of a dry-coil element, Figure 4.3, the energy balance equation, Eq. 4.1, can be written.

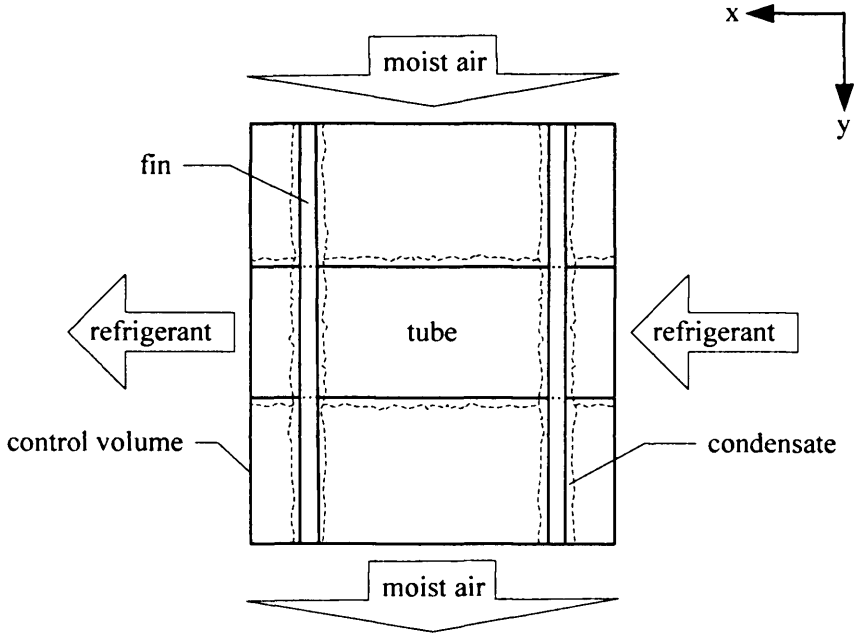

Figure 4.3 A differential control volume for a fin-tube element under a wet-coil condition, when having no condensate, the element being under a dry-coil condition

$$\rho_a \frac{\partial i_{wa}}{\partial t} + G_a \frac{\partial i_{wa}}{\partial y} = -\frac{U_{eff,dry} A_{o,total} (T_{db,in} - T_{wall,ave})}{dydz} \quad (4.1)$$

In Eq. 4.1, the first term is the rate of change of accumulated energy in the control volume. This term was not adopted in some previous research works such as Wang & Touber's work [1991] who neglected the accumulated energy in their model. The second term is the net rate of the energy-flow due to the inlet and outlet air flows. The term on the right hand side is the rate of the heat transfer from the air to the finned tube. The inlet dry-bulb air temperature (see Figs. 4.1 and 4.2) can be calculated from Eq. 4.2 based on the outlet DB temperatures of the corresponding tube elements in the preceding row. For instance, Fig. 4.2, the inlet air flow for the 2nd tube of the 2nd row came from both outlet air flows from the 2nd and the 1st tubes of the 1st row.

$$T_{db,in} = \frac{(T_{db,out,1} + T_{db,out,2})}{2} \quad (4.2)$$

4.2.2 Wet-coil condition

The model consists of an energy balance of moist air and a mass balance for water content. The same assumption of pressure drop as for the dry coil; Jia et al. [1995 &1999] also used this assumption in their model. The energy balance of the moist air for the control volume, Fig. 4.3, is given as Eq. 4.3.

$$\rho_a \frac{\partial i_{wa}}{\partial t} + G_a \frac{\partial i_{wa}}{\partial y} = -\frac{U_{eff,wet} A_{o,total,wet} (T_{db,in} - T_{cond,wall})}{dydz} \quad (4.3)$$

The two terms on the LHS are the same as the ones used for the dry coil. However, Jia et al. [1995 &1999] did not apply the first term in their model without giving any reason. On the right hand side, it is the rate of heat transfer from the air to the condensate. Referring to the HTC calculations in Chapter 3 and substituting Eqs. 3.18, 3.23 and 3.24 into Eq. 3.12, the heat-transfer rate term on the RHS in Eq. 4.3 can then be expressed as a summation of the sensible and the latent heat-transfer rates, Eq. 4.4:

$$U_{eff,wet} = \left(\frac{\eta_{fin,wet} A_{fin,wet} + A_{wall,o,wet}}{A_{o,total,wet}} \right) U_{wet} \quad (3.12)$$

$$U_{wet} = U_{wet,sen} + U_{wet,latent} \quad (3.18)$$

$$U_{eff,wet,sen} = \left(\frac{\eta_{fin,wet} A_{fin,wet} + A_{wall,o,wet}}{A_{o,total,wet}} \right) U_{wet,sen} \tag{3.23}$$

$$U_{eff,wet,latent} = \left(\frac{\eta_{fin,wet} A_{fin,wet} + A_{wall,o,wet}}{A_{o,total,wet}} \right) U_{wet,latent} \tag{3.24}$$

$$\begin{aligned} &\frac{U_{eff,wet} A_{o,total,wet} \left(T_{db,in} - T_{cond,wall}\right)}{dydz} = \\ &\frac{U_{eff,wet,sen} A_{o,total,wet} \left(T_{db,in} - T_{cond,wall}\right)}{dydz} + \\ &\frac{U_{eff,wet,latent} A_{o,total,wet} \left(T_{db,in} - T_{cond,wall}\right)}{dydz} \end{aligned} \tag{4.4}$$

where $U_{eff,wet,latent}$ is the effective latent HTC between air and condensate.

On the right hand side, the first term is the sensible heat transfer rate, defined based on the temperature change in the moist air, and represented by the difference between the inlet DB temperature and the surface temperature of the condensate on the tube wall. The last term is the latent heat transfer rate, based on the rate of water condensation, Eq. 3.22. The inlet DB temperature, $T_{db,in}$, and the inlet moist-air humidity ratio, W_{in} are obtained from Eqs. 4.5 and 4.6, respectively:

$$U_{wet,latent} = \frac{U_{m,wet} i_{fg,water} \left(W_{in} - W_{cond,wall}\right)}{\left(T_{db,in} - T_{wall,ave}\right)} \tag{3.22}$$

$$T_{db,in} = 273.15 + \frac{\left(\frac{i_{wa,in}}{1000} - 2501 W_{in} \right)}{\left(1.006 + 1.805 W_{in}\right)} \tag{4.5}$$

$$W_{in} = \frac{\left(W_{out,1} + W_{out,2}\right)}{2} \tag{4.6}$$

where

$$i_{wa,in} = \frac{i_{wa,out,1} + i_{wa,out,2}}{2} \tag{4.7}$$

The mass balance of the water content for the control volume can be expressed as in Eq. 4.8.

$$\rho_a \frac{\partial W}{\partial t} + G_a \frac{\partial W}{\partial y} = -\frac{U_{m,eff,wet} A_{o,total,wet} \left(W_{in} - W_{cond,wall}\right)}{dydz} \tag{4.8}$$

As analogy with the energy balance, the first term is the rate of change of accumulated water vapour in the control volume. The second term is the net rate of change of water vapour in the moist air flows between the inlet and the outlet. The last term is the rate of the water condensation from the moist air onto the finned tube.

4.3 Finned-tube modelling

For both coil conditions, the model consists of a heat balance of the finned tube that is similar in details for each condition. It was assumed that, for both conditions, the fin, the fin-contact and the tube-wall thermal resistances were negligible. In other words, the heat transfer rate from the flowing air to the tube wall was regarded as primarily air-side controlled.

4.3.1 Dry-coil condition

Considering the differential control volume shown in Fig. 4.3, the energy balance of the finned tube is, Eq. 4.9:

$$c_{p,wall} m_{wall} \frac{dT_{wall,ave}}{dt} + c_{p,fin} m_{fin} \frac{dT_{fin,ave}}{dt} = U_{eff,dry} A_{o,total} \left(T_{db,in} - T_{wall,ave}\right) - q_{wf} A_{wall,i} \tag{4.9}$$

where the average fin temperature is calculated using Eq. 3.5.

The first and second terms are the rates of changes of the accumulated heat in the tube wall and in the plate fins, respectively. For the RHS, the first term is the rate of the heat transferring from the moist air to the finned tube (including the fins), based on the tube-wall temperature. The last term is the heat-transfer rate from the tube wall to the refrigerant. When relating to the first and second terms on the LHS, the accumulated-heat rate in the finned tube per unit surface area of the inner tube wall (i.e. in a term of heat flux) can be expressed as Eq. 4.10.

$$q_{wall,accu} = \frac{\left(c_{p,wall} m_{wall} \frac{dT_{wall,ave}}{dt} + c_{p,fin} m_{fin} \frac{dT_{fin,ave}}{dt} \right)}{A_{wall,i}} \tag{4.10}$$

4.3.2 Wet-coil condition

From Fig. 4.3, the energy balance of the finned tube under wet condition is, Eq. 4.11.

$$c_{p,wall} m_{wall} \frac{dT_{wall,ave}}{dt} + c_{p,fin} m_{fin} \frac{dT_{fin,ave}}{dt} = U_{eff,wet} A_{o,total,wet} \left(T_{db,in} - T_{cond,wall} \right) - q_{wf} A_{wall,i} \tag{4.11}$$

The construction of the equation is similar to that of the dry coil except that for the first term on the RHS, the heat-transfer rate from the moist air to the condensate is based on the surface temperature of the condensate on the tube wall, whereas for the dry coil, it was based on the tube-wall surface temperature. However, in this study, both temperatures were assumed to be of the same value. The accumulated heat rate in the finned tube per unit surface area can be obtained by using the equation (4.10), whereas the average fin temperature is obtainable by Eq. 3.16 that is similar to Eq. 3.5.

$$\eta_{fin,wet} = \frac{\left(T_{db,in} - T_{cond,fin} \right)}{\left(T_{db,in} - T_{cond,wall} \right)} \cong \frac{\left(T_{db,in} - T_{fin,ave} \right)}{\left(T_{db,in} - T_{wall,ave} \right)} \tag{3.16}$$

4.4 Refrigerant-side modelling

Modelling is performed by considering the momentum, energy and mass transfer of the refrigerant flow. As discussed earlier, the refrigerant is mainly under the saturated boiling stage of the force convection flow, except near the coil outlet where the refrigerant is superheated. In the two-phase model, a void fraction variable, representing a fraction showing the proportion of the total cross-sectional area of the tube occupied by the vapour, will be appropriately incorporated.

The significance and application of the governing equations can be explained as followings. The continuity equation enabled calculating the refrigerant velocities, which were used in the momentum and the energy equations. The momentum equation was used to establish the pressure drop, which allowed investigating the refrigerant pressure behaviour in the control volume. Finally, the

energy equation was mainly for determining the refrigerant temperature. Both pressure and temperature are needed for determining a refrigerant state.

The two-phase model was developed based on Jia et al.'s works [1995 &1999]; many other researches, such as Judge & Radermacher [1997], also adopted the same approach. The model is considered suitable for the dynamic investigation, since the momentum equation includes the accumulated momentum in the control volume. Moreover, it is generally acknowledged that the distributive model can be used for either pure or mixed refrigerants.

At this stage, it is useful to acknowledge several unique features of mixture refrigerants modelling. To use the HTC correlation for R407C which is a 3-component mixture, this study adopted Judge & Radermacher's implementation [1997]. R32 and R125 were first grouped to form a "single" component, and R134a was the other component; so that the mixture could be treated as a binary mixture. This is justified because R32 and R125 exhibit very similar vapour pressure under a saturated boiling regime. In addition, due to being a near azeotrope of these two refrigerants, the relative concentrations of R32 and R125 remain nearly constant in both the liquid and the vapour during the phase change. Detailed procedures and a sample calculation of the heat transfer coefficient for mixture were given in Section A.3 of Appendix A and Section D.3 of Appendix D, respectively. Furthermore, as applied in Domanski & McLinden's [1992] work (Section 2.3.1), using the element-by-element approach, the tube was divided to reflect the glide effect of the mixture refrigerant.

As discussed in Chapter 2, the pressure-drop and HTC of R134a was calculated with Jung & Radermacher's correlation [1989] and the Jung et al.'s correlation [1989b], respectively. The pressure drop of R407C was also obtained from Jung & Radermacher's correlation [1989]; however, the HTC was predicted from Jung et al.'s correlation [1989b], being generally more applicable for binary refrigerant mixtures.

4.4.1 Two-phase flow

a) Continuity equation

Eqs. 4.12 and 4.13 represent the conservation of refrigerant mass for a differential control volume, Fig. 4.4 for the vapour and the liquid phases, respectively.

$$\frac{\alpha\rho_{ref,v}A_{tube}\Delta x}{\Delta t} = \left[\alpha\rho_{ref,v}u_{ref,v}A_{tube}\right]_{in} - \left[\alpha\rho_{ref,v}u_{ref,v}A_{tube}\right]_{out} + \dot{m}_{lv}\Delta x \tag{4.12}$$

$$\frac{(1-\alpha)\rho_{ref,l}A_{tube}\Delta x}{\Delta t} = \left[(1-\alpha)\rho_{ref,l}u_{ref,l}A_{tube}\right]_{in} - \left[(1-\alpha)\rho_{ref,l}u_{ref,l}A_{tube}\right]_{out} - \dot{m}_{lv}\Delta x \tag{4.13}$$

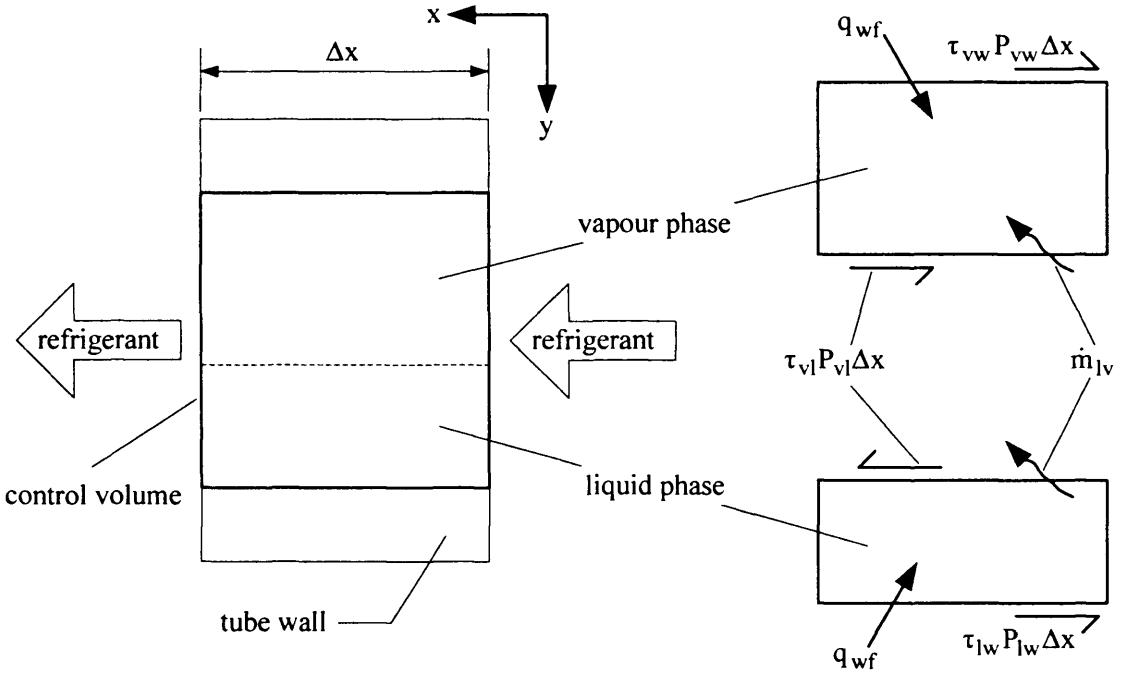

Figure 4.4 A simplified differential control volume for two-phase refrigerant modelling

For the vapour phase, Eq. 4.12, the LHS term is the rate of change of the accumulated mass in the control volume. On the RHS, the first and the second terms are the rates of the inlet and the outlet mass, respectively, and the last term is the evaporation rate per unit tube length. For the liquid phase, Eq. 4.13, the same explanation applied.

By dividing Eqs. 4.12 and 4.13 by ($A_{tube}\Delta x$) and then taking limits as $\Delta t \to 0$ and $\Delta x \to 0$, they become:

$$\frac{\partial(\alpha\rho_{ref,v})}{\partial t} + \frac{\partial(\alpha\rho_{ref,v}u_{ref,v})}{\partial x} = \frac{\dot{m}_{lv}}{A_{tube}} \tag{4.14}$$

$$\frac{\partial\left((1-\alpha)\rho_{ref,l}\right)}{\partial t}+\frac{\partial\left((1-\alpha)\rho_{ref,l}u_{ref,l}\right)}{\partial x}=-\frac{\dot{m}_{lv}}{A_{tube}} \tag{4.15}$$

The equations (4.14) and (4.15) are combined together to form the continuity equation of the control volume, Eq. 4.16.

$$\frac{\partial\left(\alpha\rho_{ref,v}+(1-\alpha)\rho_{ref,l}\right)}{\partial t}+\frac{\partial\left(\alpha\rho_{ref,v}u_{ref,v}+(1-\alpha)\rho_{ref,l}u_{ref,l}\right)}{\partial x}=0 \tag{4.16}$$

The first term is the rate of change of the accumulated mass, while the second term is the net rate of the outlet mass flow. In addition, the void fraction, used in Eq. 4.16, can be obtained from Eq. 4.17.

$$\alpha=\frac{A_{tube,v}}{A_{tube}}=\frac{1}{1+S\left(\frac{\rho_{ref,v}}{\rho_{ref,l}}\right)\left(\frac{1-x}{x}\right)} \tag{4.17}$$

where the slip factor, S, [Collier & Thome] is given in Eq. 4.18.

$$S=\frac{u_v}{u_l}=\left(\frac{x}{1-x}\right)\left(\frac{\rho_{ref,l}}{\rho_{ref,v}}\right)\left(\frac{1-\alpha}{\alpha}\right) \tag{4.18}$$

In this study, for simplicity, the value of the slip factor, S, was assigned to be one, meaning both the vapour and the liquid phases travel at the same velocity. This assumption was applied by many researchers dealing with pure refrigerants, such as Mac Arthur's work [1984] and Jia et al.'s works [1995 & 1999]. However, up to the present, it has not been adopted in any research using a mixed refrigerant.

To justify its adoption in this study, three issues need to be considered. ***First***, when considering Eq. 4.17, as it can be seen that *the void fraction* is a function of the slip factor, the vapour quality, and the vapour and liquid densities. As seen in Eq. 4.18, for a range of the vapour qualities from 0.2 to around 1, *the relationship between the vapour and the liquid densities is the only factor influencing the slip factor.* The smaller the density difference, the S value will approach unity.

Second, a preliminary investigation of the variation of vapour and liquid densities along the flow for the dry coil was performed, Figs. 4.5 – 4.9. At a vapour quality of around 0.2, for R134a, the liquid-to-vapour density ratio was about 75, whereas, for R407C, it was around 54 (Figs. 4.5 and 4.6). This means that, at that vapour quality, it was justified to apply the assumption to R407C.

Third, from 0.2 vapour quality up to around 1.0, the liquid densities of R134a increased with a magnitude of 3.8 kg/m^3, whereas the vapour densities decreased by 1.6 kg/m^3 (Fig. 4.5). However, for R407C, the liquid densities increased and then decreased with a maximum-to-minimum difference of around 0.8 kg/m^3, whereas its vapour densities increased with 0.75 times of the difference (Fig. 4.6). Furthermore, when examining the variations of the liquid-to-vapour density ratios, the increase in R134a was about 2.27 times larger than the decrease in R407C (Fig. 4.7). In other words, the variations in the value of the liquid-to-vapour density ratio of R134a were more than that of R407C. Therefore, this further strengthened the validity of assumption for its application to R407C.

In addition to the above consideration of density behaviour, it must be recognised that the refrigerant-type also influences the variations in densities. For the 2-phase region, R134a has 1 degree of freedom: pressure (i.e. pressure drop), whilst R407C has 3: pressure (i.e. pressure drop), temperature (i.e. heat flux) and a component composition (i.e. composition evaporation). Hence, for R407C (R32/R125/R134a), either liquid or vapour density is affected by its component densities (i.e. the gradients of the densities vs. nodes along the coil) (Figs. 4.8 and 4.9).

Figure 4.5 Liquid and vapour densities of R134a vs nodes for a dry coil

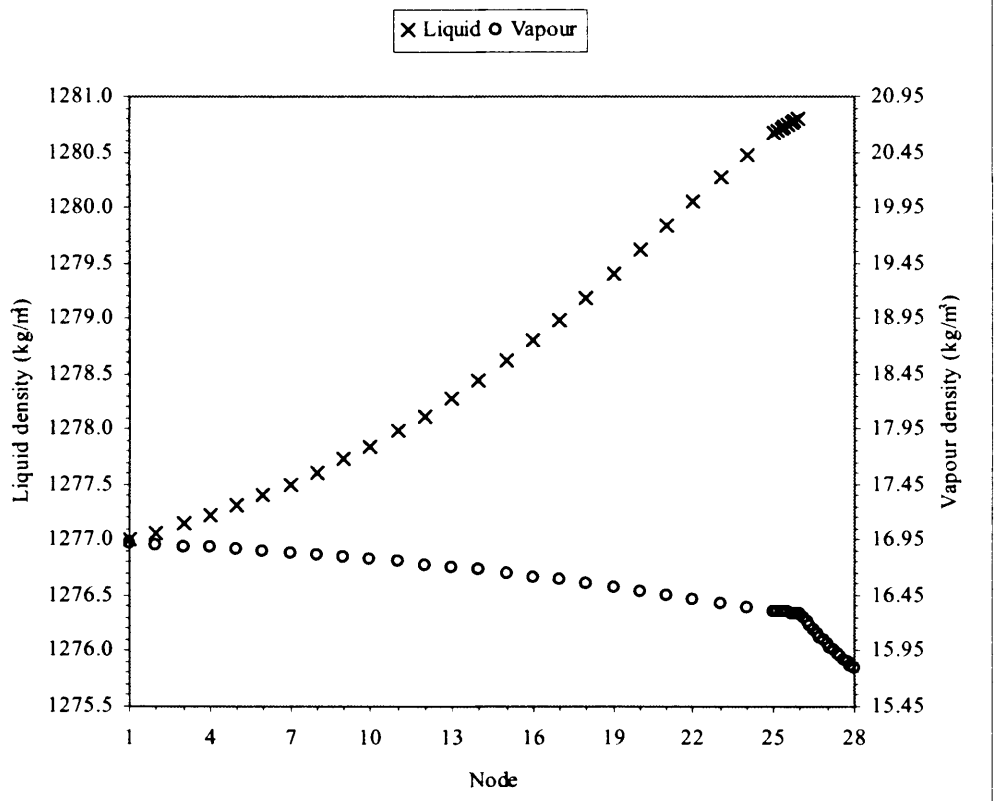

Figure 4.6 Liquid and vapour densities of R407C vs nodes for a dry coil

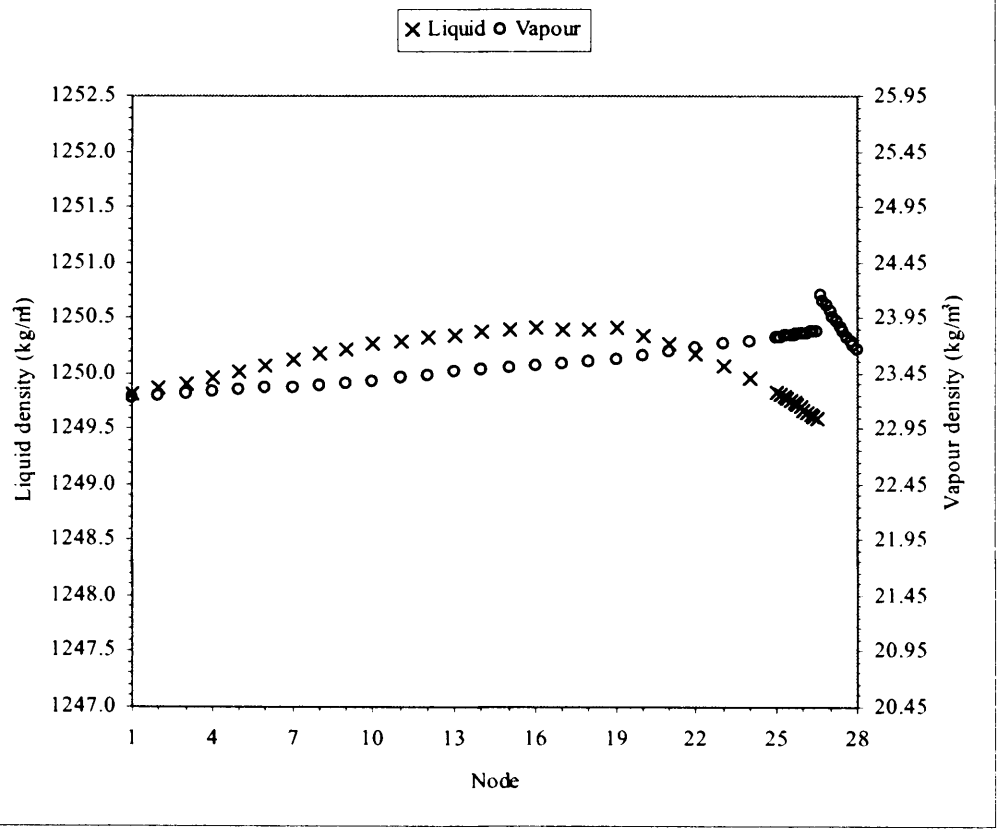

Figure 4.7 Ratios of liquid to vapour densities vs nodes for a dry coil

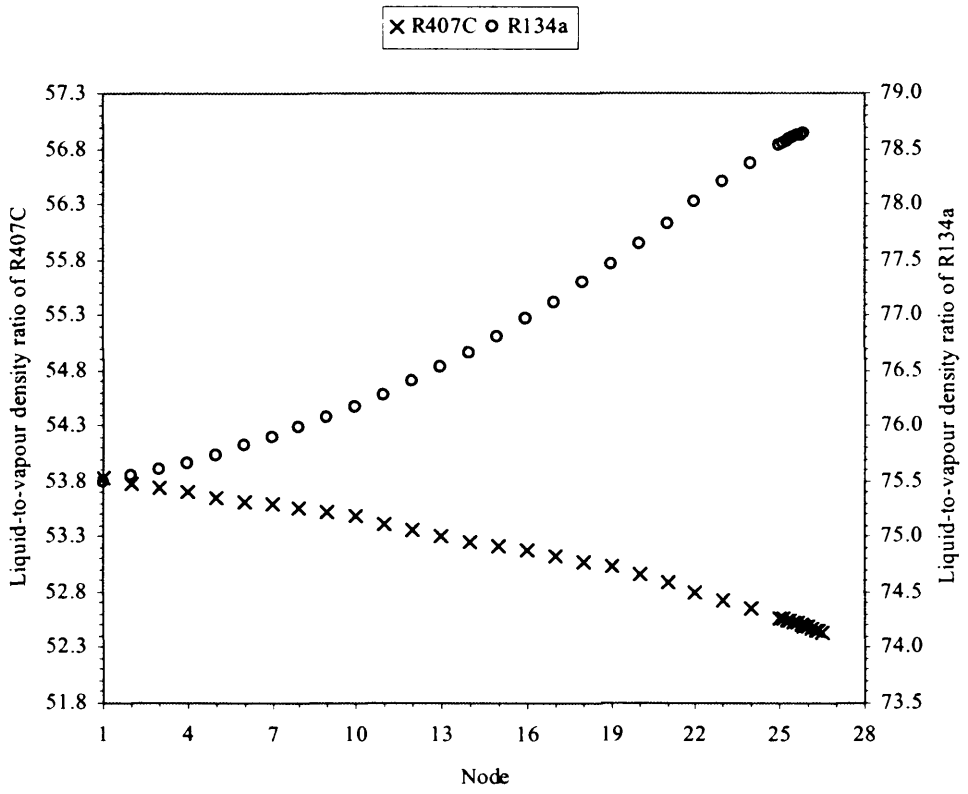

Figure 4.8 Liquid-component densities of R407C vs nodes for a dry coil

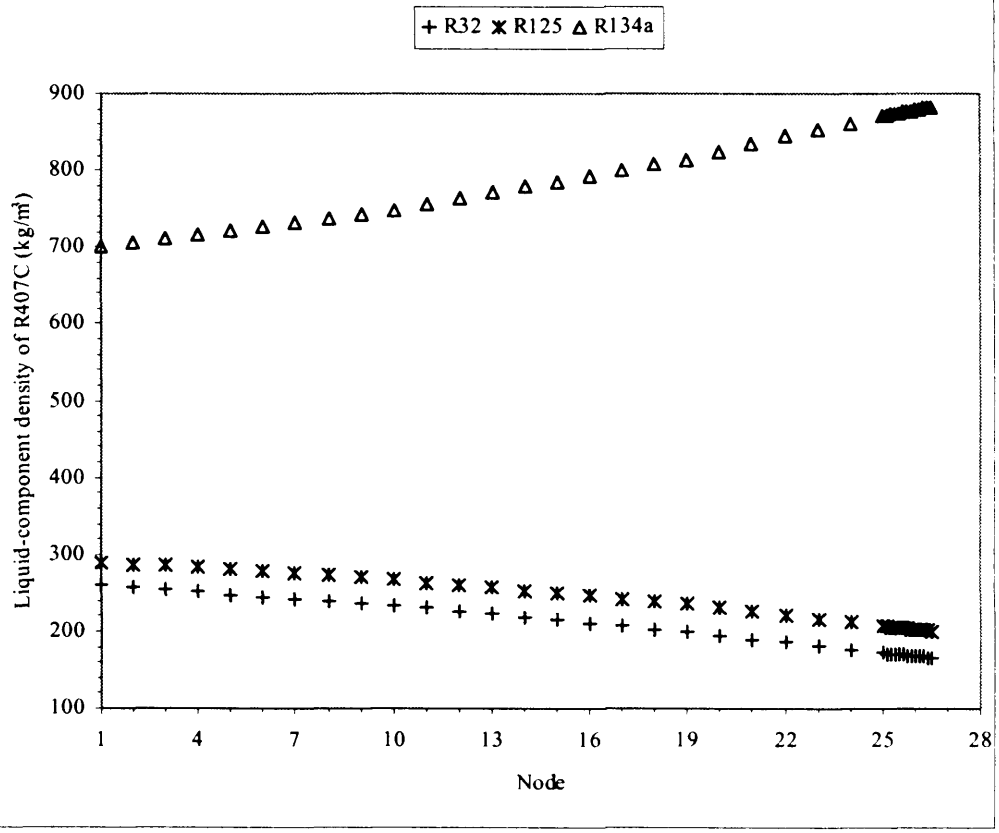

Figure 4.9 Vapour-component densities of R407C vs nodes for a dry coil

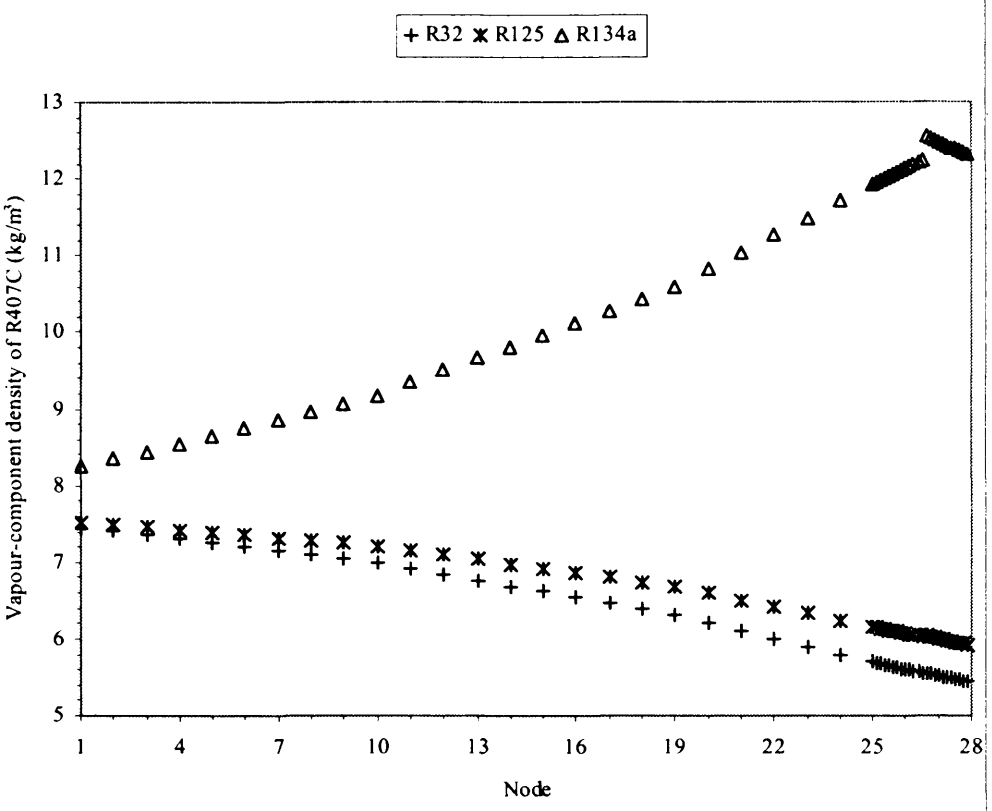

b) Momentum equation

Momentum equations of the refrigerant vapour and liquid, Fig. 4.4, were set up respectively as Eqs. 4.19 and 4.20.

$$\frac{(\alpha\rho_{ref,v}A_{tube}\Delta x)u_{ref,v}}{\Delta t} = [(\alpha\rho_{ref,v}A_{tube}u_{ref,v})u_{ref,v}]_{in} - [(\alpha\rho_{ref,v}A_{tube}u_{ref,v})u_{ref,v}]_{out} - ([\alpha A_{tube}p]_{out} - [\alpha A_{tube}p]_{in}) - \tau_{vw}P_{vw}\Delta x - \tau_{vl}P_{vl}\Delta x \quad (4.19)$$

$$\frac{((1-\alpha)\rho_{ref,l}A_{tube}\Delta x)u_{ref,l}}{\Delta t} = [((1-\alpha)\rho_{ref,l}A_{tube}u_{ref,l})u_{ref,l}]_{in} - [((1-\alpha)\rho_{ref,l}A_{tube}u_{ref,l})u_{ref,l}]_{out} - ([(1-\alpha)A_{tube}p]_{out} - [(1-\alpha)A_{tube}p]_{in}) - \tau_{lw}P_{lw}\Delta x + \tau_{vl}P_{vl}\Delta x \quad (4.20)$$

For the vapour phase, Eq. 4.19, the first term is the rate of change of the accumulated vapour momentum in the control volume. On the RHS, the first and the second terms are the rates of the inlet and the outlet vapour momenta, respectively. The third term is

the difference of the vapour pressure forces at the outlet and the inlet of the control volume. The fourth term is the shear force due to the shear stress between the vapour and the inside tube wall, whereas the last term is the shear force owing to a shear stress between the vapour and the liquid. For the liquid phase, Eq. 4.20, the same logic of formulation was applied.

Dividing Eqs. 4.19 and 4.20 by ($A_{tube}\Delta x$) and taking the limits as $\Delta t \to 0$ and $\Delta x \to 0$ gives Eqs. 4.21 and 4.22.

$$\frac{\partial(\alpha\rho_{ref,v}u_{ref,v})}{\partial t}+\frac{\partial(\alpha\rho_{ref,v}u_{ref,v}^2)}{\partial x}+\frac{\tau_{vw}P_{vw}}{A_{tube}}+\frac{\tau_{vl}P_{vl}}{A_{tube}}=-\frac{\partial(\alpha p)}{\partial x} \tag{4.21}$$

$$\frac{\partial((1-\alpha)\rho_{ref,l}u_{ref,l})}{\partial t}+\frac{\partial((1-\alpha)\rho_{ref,l}u_{ref,l}^2)}{\partial x}+\frac{\tau_{lw}P_{lw}}{A_{tube}}-\frac{\tau_{vl}P_{vl}}{A_{tube}}=-\frac{\partial((1-\alpha)p)}{\partial x} \tag{4.22}$$

Eqs. 4.21 and 4.22 are combined together to form the momentum equation of the saturated-boiling refrigerant, Eq. 4.23.

$$\begin{aligned}&\frac{\partial(\alpha\rho_{ref,v}u_{ref,v}+(1-\alpha)\rho_{ref,l}u_{ref,l})}{\partial t}+\\&\frac{\partial(\alpha\rho_{ref,v}u_{ref,v}^2+(1-\alpha)\rho_{ref,l}u_{ref,l}^2)}{\partial x}+\frac{\tau_{vw}P_{vw}}{A_{tube}}+\frac{\tau_{lw}P_{lw}}{A_{tube}}=-\frac{\partial p}{\partial x}\end{aligned} \tag{4.23}$$

Finally, the momentum equation was re-arranged to give Eq. 4.24.

$$\frac{\partial(\alpha\rho_{ref,v}u_{ref,v}+(1-\alpha)\rho_{ref,l}u_{ref,l})}{\partial t}-\left(\frac{\partial p}{\partial x}a\right)-\left(\frac{\partial p}{\partial x}F\right)=-\frac{\partial p}{\partial x} \tag{4.24}$$

Eq. 4.24 essentially states that the total pressure drop equals to the summation of the rate of change of the accumulated momentum in the control volume, the accelerating pressure drop and the frictional pressure drop.

c) Energy equation

The energy balance equation of the saturated-boiling refrigerant for the differential control volume, Fig. 4.4, can be established, Eq.4.25.

$$\frac{\left(\alpha\rho_{ref,v}A_{tube}\Delta xi_{ref,v}+(1-\alpha)\rho_{l}A_{tube}\Delta xi_{ref,l}\right)}{\Delta t}=$$
$$\left[\alpha\rho_{ref,v}A_{tube}u_{ref,v}i_{ref,v}+(1-\alpha)\rho_{ref,l}A_{tube}u_{ref,l}i_{ref,l}\right]_{in}-$$
$$\left[\alpha\rho_{ref,v}A_{tube}u_{ref,v}i_{ref,v}+(1-\alpha)\rho_{ref,l}A_{tube}u_{ref,l}i_{ref,l}\right]_{out}+$$
$$A_{wall,i}\Delta xq_{wf} \tag{4.25}$$

The LHS represents the rate of change of the accumulated energy in the control volume. On the RHS, the first and the second terms are the rates of the refrigerant inflow and outflow energy, respectively. The last term is the rate of the heat transfer from the tube wall to the refrigerant flowing inside the tube.

By dividing equation 4.25 by $(A_{tube}\Delta x)$ and taking the limit as $\Delta t\rightarrow 0$ and $\Delta x\rightarrow 0$, Eq. 4.26 was formed. It shows that the heat transfer rate from the tube wall to the refrigerant represents the summation of the net rate of the outflow energy and the rate of change of the accumulated energy:

$$\frac{\partial\left(\alpha\rho_{ref,v}i_{ref,v}+(1-\alpha)\rho_{ref,l}i_{ref,l}\right)}{\partial t}+$$
$$\frac{\partial\left(\alpha\rho_{ref,v}u_{ref,v}i_{ref,v}+(1-\alpha)\rho_{ref,l}u_{ref,l}i_{ref,l}\right)}{\partial x}=\frac{A_{wall,i}}{A_{tube}}q_{wf} \tag{4.26}$$

where

$$q_{wf}=h_{ref}\left(T_{wall}-T_{ref}\right) \tag{4.27}$$

4.4.2 Single-phase flow

For the single-phase flow, Fig. 4.10, i.e. the superheated refrigerant, the governing equations were the same as that for the two-phase flow when the void fraction, α, equalled to one. Based on Eq. 4.16, the continuity equation becomes Eq. 4.28.

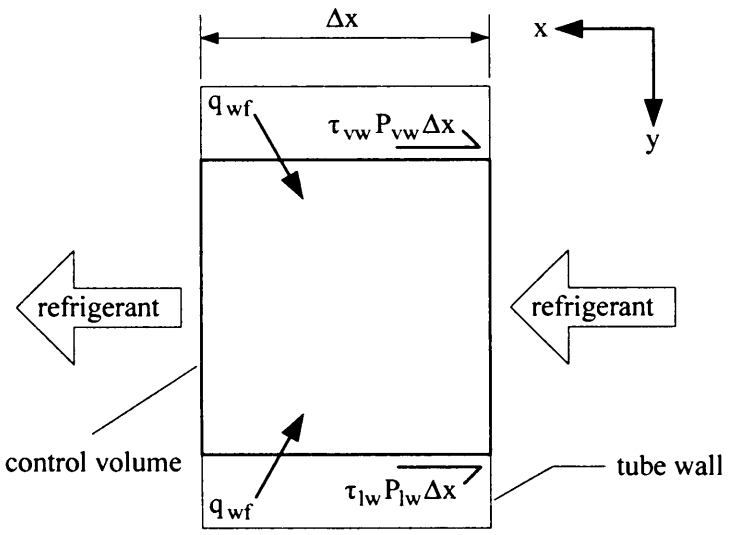

Figure 4.10 A simplified differential control volume for superheated refrigerant modelling

$$\frac{\partial \rho_{ref}}{\partial t} + \frac{\partial (\rho_{ref} u_{ref})}{\partial x} = 0 \tag{4.28}$$

Accordingly, the momentum equation becomes Eq. 4.29:

$$\frac{\partial (\rho_{ref} u_{ref})}{\partial t} - \left(\frac{\partial p}{\partial x} a\right) - \left(\frac{\partial p}{\partial x} F\right) = -\frac{\partial p}{\partial x} \tag{4.29}$$

where the pressure drop due to acceleration, $\left(\frac{\partial p}{\partial x} a\right)$ and the frictional pressure drop, $\left(\frac{\partial p}{\partial x} F\right)$ are expressed as in Eqs. 4.30 and 4.31, respectively.

$$\left(\frac{\partial p}{\partial x} a\right) = -\frac{\partial \left(\rho_{ref} u_{ref}^2\right)}{\partial x} \tag{4.30}$$

$$\left(\frac{\partial p}{\partial x} F\right) = -\frac{\tau_{refw} P_{refw}}{A_{tube}} \tag{4.31}$$

Finally, based on Eq. 4.26, the energy equation can be written as Eq. 4.32.

$$\frac{\partial (\rho_{ref} i_{ref})}{\partial t} + \frac{\partial (\rho_{ref} u_{ref} i_{ref})}{\partial x} = \frac{A_{wall,i}}{A_{tube}} q_{wf} \tag{4.32}$$

4.4.3 TEV-controlled evaporator model

Fig. 4.11 shows a control loop representing a TEV-controlled evaporator assembled with a sensor bulb and an external equalizer. The figure also highlights the two important parameters, namely the superheat pressure and the superheat temperature, that are closely related to refrigerant properties. Corresponding to Fig. 3.11, the equations presented in Sub-section 3.5.1 for both the TEV and the sensor bulb are rearranged to be used in the simulation. For the needle valve, its derived equation of the refrigerant mass flow rate is given by Eq. 3.129.

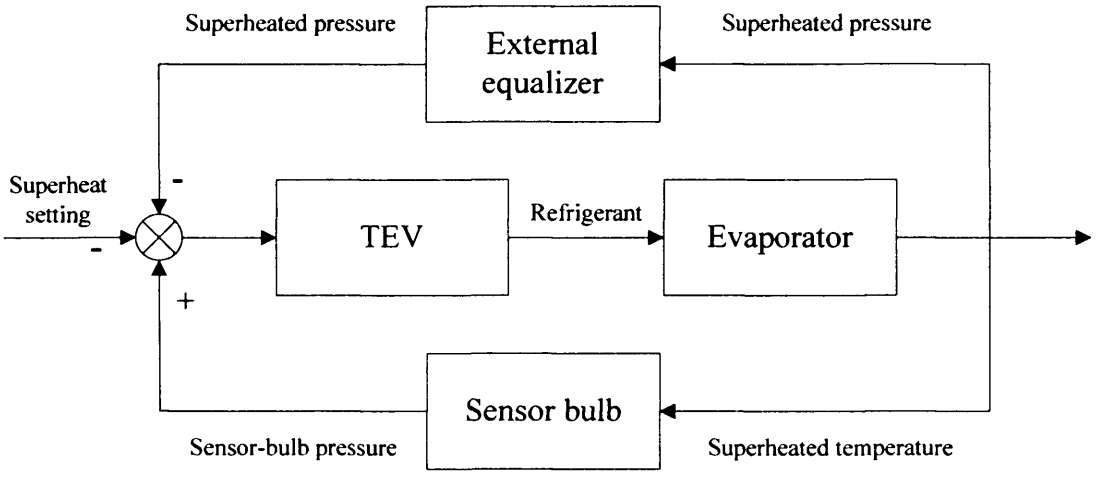

Figure 4.11 A simplified block diagram for a TEV-controlled evaporator control loop

$$\dot{m}_{ref} = \left(\frac{C_d \cdot K_{Amin,z} \cdot A_d}{K_s}\right) \cdot \left(\rho_{ref,l,TEV,in} \cdot \left(p_{ref,l,TEV,in} - p_{ref,TEV,out}\right)\right)^{(1/2)} \left(p_{bulb} - p_{ref,out} - p_{ss}\right) \tag{3.129}$$

It can be written as Eq. 4.33, containing the K_v parameter given by Eq. 4.34.

$$\dot{m}_{ref} = K_v \left(p_{bulb} - p_{ref,out} - p_{ss}\right) \tag{4.33}$$

$$K_v = \left(\frac{C_d \cdot K_{Amin,z} \cdot A_d}{K_s}\right) \left(\rho_{ref,l,TEV,in} \cdot \left(p_{ref,l,TEV,in} - p_{ref,TEV,out}\right)\right)^{(1/2)} \tag{4.34}$$

For both refrigerants, the values of p_{ss} are treated as constants. For the K_v, because only the TEV-controlled evaporator of the cycle/system was studied, the liquid density at the TEV-inlet and the pressure drop across the TEV for any instance of time are therefore assumed to remain unchanged. In addition, the above two equations imply that

the TEV design, the valve operation and setting, and the hunting are all influenced by the refrigerant properties.

For the sensor bulb, three assumptions are employed: a rather small size, negligible heat capacitance (also applied for the tube-wall, where it is attached), and being clamped very closed to the coil-outlet. When introducing the first two assumptions to the energy balance of the bulb, i.e. Eq. 3.134, it can then be said that the rate of the heat transfer from the surroundings to the bulb is near zero (Eq. 4.35), and that the temperature of the bulb is approximately equal to that of the tube-wall (Eq. 4.36).

$$c_{p,bulb}m_{bulb}\frac{dT_{bulb}}{dt} = q_{be}A_{wall,e} - \frac{A_{wall,tube}\left(T_{bulb} - T_{wall,ave}\right)}{\left(\frac{D_{OD,tube} - D_{ID,tube}}{2k_{tube}} + \frac{w_{bulb}}{k_{bulb}}\right)} \tag{3.134}$$

$$q_{bulb,e}A_{wall,e} \cong 0 \tag{4.35}$$

$$T_{bulb} \cong T_{wall,ave} \tag{4.36}$$

Furthermore, applying Eq. 4.36 and the second assumption to the energy equation of the tube-wall (Eq. 3.131), it can be seen that the rate of heat transfer from the tube-wall to the refrigerant becomes negligible (Eq. 4.37).

$$c_{p,wall}m_{wall}\frac{dT_{wall,ave}}{dt} = \frac{A_{wall,tube}\left(T_{bulb} - T_{wall,ave}\right)}{\left(\frac{D_{OD,tube} - D_{ID,tube}}{2k_{tube}} + \frac{w_{bulb}}{k_{bulb}}\right)} - q_{wf}A_{wall,i} \tag{3.131}$$

$$q_{wf}A_{wall,i} \cong 0 \tag{4.37}$$

With all three assumptions, the temperature of the bulb is considered equal to that of the tube-wall at the coil-outlet, Eq. 4.38.

$$T_{bulb} \cong T_{wall,coil\text{-}outlet} \tag{4.38}$$

In addition, two more assumptions were made for the model. First, the charged fluid was the same fluid as the refrigerant used in the evaporator. Second, under the saturated state, for R407C, the mole fractions of the liquid phase in the bulb remained unchanged at all times.

4.5 Programming

There were three areas to be addressed in this section. These are: integration of several software packages in the programming stage, development of program code at two levels (coil and element) in relation to discretization of the governing equations, and main difficulties encountered.

4.5.1 Utilization of software

Microsoft Excel, Digital-Visual-Fortran-Professional (DVF) and REFPROP [Huber et al., 1996] were used together to create the necessary simulation programs and the associated sub-routines. Almost all of the program modules were written within MS Excel environment, through a built-in tool - Visual-Basic-for-Application language (VBA). As for obtaining the thermal-physical properties of the refrigerants from REFPROP (being written with the FORTRAN-77), the modules were written in MS Excel with VBA and DVF with FORTRAN-90. For creating this type of modules, a unique way of a mixed-language programming method [Microsoft Company 1998] was implemented. Whenever the refrigerant properties are needed, the modules in MS Excel will call the modules in DVF, which contains the sub-routines of REFPROP. This calling scheme is very convenient and reliable, as it is not only useful for R134a and R407C but also for many other pure and mixed refrigerants, offered in REFPROP.

4.5.2. Structure

All programs concerning the steady-state and the dynamic simulations were written and structured into two levels: the coil and the element/sub-element levels. In either level, the governing equations were discretized before they were solved numerically via the programs. In addition, it is useful to point out a difference between mixed and pure refrigerants in relation to the degrees of freedom that, for R407C, the condition of the refrigerant coil-inlet was specified by its temperature, pressure and feed compositions (i.e. the charge compositions); for R134a, it was temperature and vapour quality.

a) **Coil level**

The coil-level programming (only the dry-coil condition being explained as an example, Fig. 4.12), shown as the bold frame-line blocks, was to perform the air-

side calculation; its modules can be arranged into two groups: ***the first group*** was for configuring the physical feature of the coil.

In ***the second group***, there were modules for assigning the conditions of the air at the coil face and of the refrigerant at the refrigerant coil-inlet. The inlet air condition for each element and sub-element for *the initial iteration* was guessed. After that, the program advanced the calculation element-by-element until the last element/sub-element. Then, returning to the coil-level, a check for termination of the iteration loops was performed, (Table 5.8) examining the resolutions of the difference between the inlet and the outlet temperature for each element in the coil, and the difference between the consecutive-loop values of the outlet DB temperatures was checked. For this module group, if the checking condition to terminate the overall-coil loop calculation had not been satisfied, the inlet DB temperature and relative humidity for each element/sub-element were assigned. Furthermore, in the dynamic simulation, there was a checking whether the time step was the last one or not.

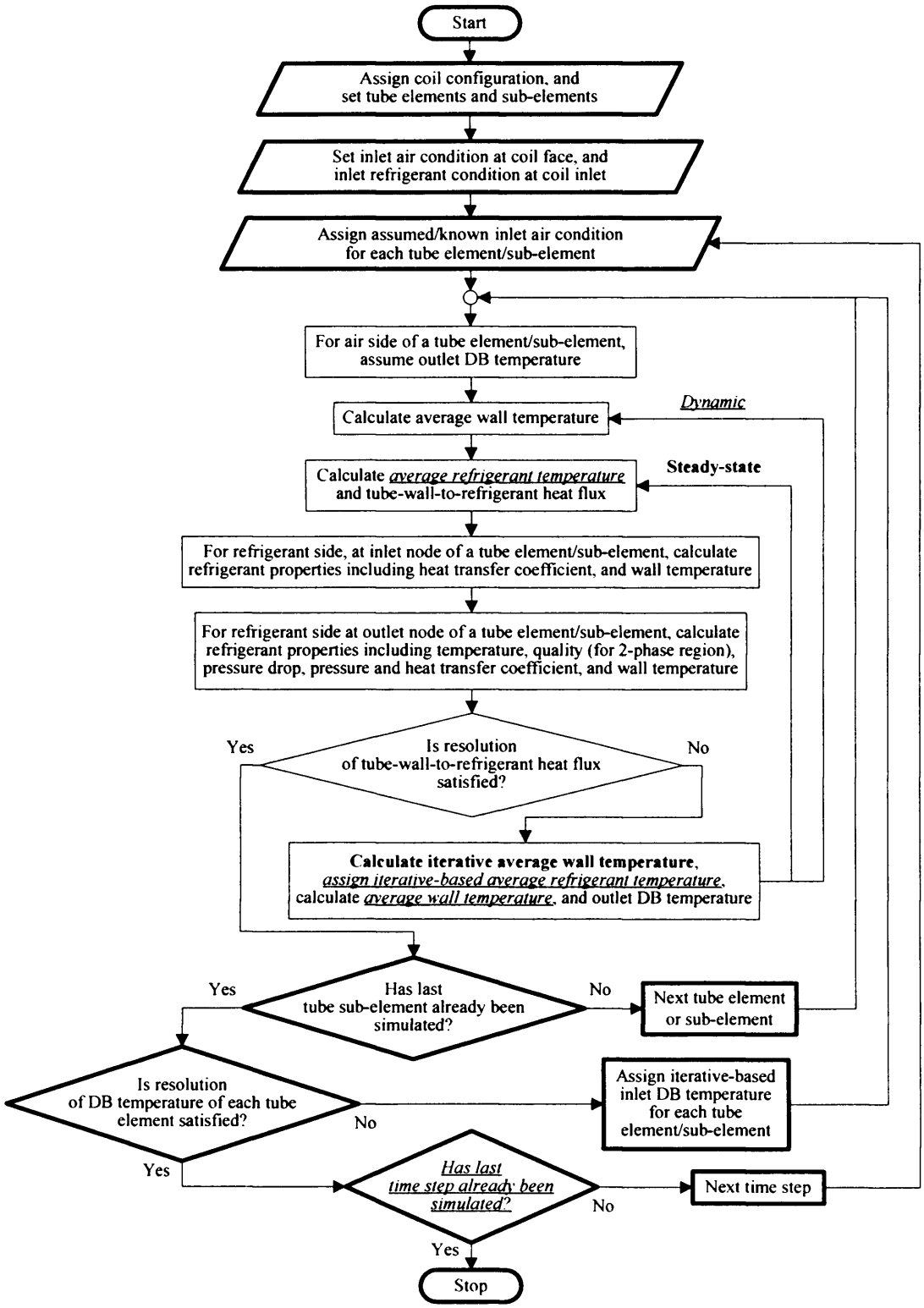

Figure 4.12 A computer flow chart showed a **dry-coil** simulation under steady and dynamic (a step change of coil-inlet DB temperature) states , when using a pure or zeotropic refrigerant. (Remark: The bold frame-line blocks are for the coil level, whereas the thin ones are for the element/sub-element level. The bold letters are for steady-state, whereas the italic-underlined letters are for dynamic.) Via this calculation routine, various parameters, such as refrigerant and air temperatures were calculated.

b) **Element level**

Aiming at providing the outlet values of both the air and refrigerant for each element/sub-element, the element-level programming consisted of many more modules than that of the coil-level, and could be arranged in to six main programming parts, Fig. 4.12. First, the outlet air condition was assigned using assumed values. Second, the tube-wall to refrigerant heat flux was calculated. Third, at the inlet of the element/sub-element, the relevant refrigerant properties, such as the HTC, were determined. Fourth, all the outlet refrigerant properties were then calculated. Fifth, having obtained details of the inlet and the outlet refrigerant conditions, the tube-wall to refrigerant heat flux was revised until the iteration-stopping criterion (seeing Table 5.8) for an element was satisfied. Finally, if the looping was to be continued, the iterative outlet condition of the air would be calculated. It should be noted that a main difference between the steady-state and the dynamic calculation procedures was that the calculation relied on the average temperatures of the wall for the former and of the refrigerant for the latter, Fig. 4.12.

c) Discretization

To solve numerically the governing equations, it was necessary to have the partial-differential and the differential forms discretized by using the implicit method with the forward finite-divided difference scheme and the general forward finite-divided difference scheme, respectively. From Eqs. 4.1 and 4.3, which were the energy balances of the moist air for the dry- and wet- coil conditions, respectively, their discretized forms are:

$$\rho_a \frac{\left(i_{wa}\big|_{out}^{t} - i_{wa}\big|_{out}^{t-1}\right)}{\Delta t} + G_a \frac{\left(i_{wa}\big|_{out}^{t} - i_{wa}\big|_{in}^{t}\right)}{\Delta y} = -\left(\frac{U_{eff,dry} A_{o,total}\left(T_{db,in} - T_{wall,ave}\right)}{\Delta y \Delta z}\right)\Bigg|^{t} \tag{4.39}$$

$$\rho_a \frac{\left(i_{wa}\big|_{out}^{t} - i_{wa}\big|_{out}^{t-1}\right)}{\Delta t} + G_a \frac{\left(i_{wa}\big|_{out}^{t} - i_{wa}\big|_{in}^{t}\right)}{\Delta y} = -\left(\frac{U_{eff,wet} A_{o,total,wet}\left(T_{db,in} - T_{cond,wall}\right)}{\Delta y \Delta z}\right)\Bigg|^{t} \tag{4.40}$$

For the mass balance of the water vapour for the wet- coil condition, i.e. Eq. 4.8, its discretized form is shown below.

$$\rho_a \frac{\left(W\big|_{out}^{t} - W\big|_{out}^{t-1}\right)}{\Delta t} + G_a \frac{\left(W\big|_{out}^{t} - W\big|_{in}^{t}\right)}{\Delta y} = -\left(\frac{U_{m,eff,wet} A_{o,total,wet} \left(W_{in} - W_{cond,wall}\right)}{\Delta y \Delta z}\right)\Bigg|^{t} \tag{4.41}$$

Eqs. 4.9 and 4.11, representing the energy balance of the finned tube for the dry- and the wet- coil conditions, respectively, were discretized to become Eqs. 4.42 and 4.43.

$$c_{p,wall} m_{wall} \frac{\left(T_{wall,ave}\big|^{t} - T_{wall,ave}\big|^{t-1}\right)}{\Delta t} + c_{p,fin} m_{fin} \frac{\left(T_{fin,ave}\big|^{t} - T_{fin,ave}\big|^{t-1}\right)}{\Delta t} = \left(U_{eff,dry} A_{o,total} \left(T_{db,in} - T_{wall,ave}\right) - q_{wf} A_{wall,i}\right)\Big|^{t} \tag{4.42}$$

$$c_{p,wall} m_{wall} \frac{\left(T_{wall,ave}\big|^{t} - T_{wall,ave}\big|^{t-1}\right)}{\Delta t} + c_{p,fin} m_{fin} \frac{\left(T_{fin,ave}\big|^{t} - T_{fin,ave}\big|^{t-1}\right)}{\Delta t} = \left(U_{eff,wet} A_{o,total,wet} \left(T_{db,in} - T_{cond,wall}\right) - q_{wf} A_{wall,i}\right)\Big|^{t} \tag{4.43}$$

Discretization of Eq. 4.10, representing the accumulated heat rate in the finned tube per unit surface area of the inner tube wall for both the dry- and the wet- coil conditions, gave Eq. 4.44.

$$q_{wall,accu}\big|^{t} = \frac{\left(c_{p,wall} m_{wall} \frac{\left(T_{wall,ave}\big|^{t} - T_{wall,ave}\big|^{t-1}\right)}{\Delta t} + c_{p,fin} m_{fin} \frac{\left(T_{fin,ave}\big|^{t} - T_{fin,ave}\big|^{t-1}\right)}{\Delta t}\right)}{A_{wall,i}} \tag{4.44}$$

The discretized forms of Eqs. 4.16, 4.24 and 4.26, representing the continuity, the momentum and the energy equations of the two-phase refrigerant, respectively, are as follow.

$$\frac{\begin{bmatrix}\left(\alpha\rho_{ref,v}+(1-\alpha)\rho_{ref,l}\right)_{out}^{t}-\\ \left(\alpha\rho_{ref,v}+(1-\alpha)\rho_{ref,l}\right)_{out}^{t-1}\end{bmatrix}}{\Delta t}+\frac{\begin{bmatrix}\left(\alpha\rho_{ref,v}u_{ref,v}+(1-\alpha)\rho_{ref,l}u_{ref,l}\right)_{out}^{t}-\\ \left(\alpha\rho_{ref,v}u_{ref,v}+(1-\alpha)\rho_{ref,l}u_{ref,l}\right)_{in}^{t}\end{bmatrix}}{\Delta x}=0 \qquad (4.45)$$

$$\frac{\begin{bmatrix}\left(\alpha\rho_{ref,v}u_{ref,v}+(1-\alpha)\rho_{ref,l}u_{ref,l}\right)_{out}^{t}-\\ \left(\alpha\rho_{ref,v}u_{ref,v}+(1-\alpha)\rho_{ref,l}u_{ref,l}\right)_{out}^{t-1}\end{bmatrix}}{\Delta t}+(\Delta p)_{steady}\Big|^{t}=(\Delta p)_{dynamic}\Big|^{t} \qquad (4.46)$$

$$\frac{\begin{bmatrix}\left(\alpha\rho_{ref,v}i_{ref,v}+(1-\alpha)\rho_{ref,l}i_{ref,l}\right)_{out}^{t}-\\ \left(\alpha\rho_{ref,v}i_{ref,v}+(1-\alpha)\rho_{ref,l}i_{ref,l}\right)_{out}^{t-1}\end{bmatrix}}{\Delta t}+$$

$$\frac{\begin{bmatrix}\left(\alpha\rho_{ref,v}u_{ref,v}i_{ref,v}+(1-\alpha)\rho_{ref,l}u_{ref,l}i_{ref,l}\right)_{out}^{t}-\\ \left(\alpha\rho_{ref,v}u_{ref,v}i_{ref,v}+(1-\alpha)\rho_{ref,l}u_{ref,l}i_{ref,l}\right)_{in}^{t}\end{bmatrix}}{\Delta x}= \qquad (4.47)$$

$$\left(\frac{A_{wall,i}}{A_{tube}}q_{wf}\right)\Big|^{t}$$

The $(\Delta p)_{steady}$, appearing in the momentum equation (Eq. 4.46), is obtained by using Eq. 3.90.

For single-phase refrigerants, Eqs. 4.28 – 4.32, the discretized equations for the continuity, the momentum and the energy were Eqs. 4.48 – 4.50, respectively.

$$\frac{\left(\rho_{ref}\big|_{out}^{t}-\rho_{ref}\big|_{out}^{t-1}\right)}{\Delta t}+\frac{\left(\left(\rho_{ref}u_{ref}\right)_{out}^{t}-\left(\rho_{ref}u_{ref}\right)_{in}^{t}\right)}{\Delta x}=0 \qquad (4.48)$$

$$\frac{\left(\left(\rho_{ref}u_{ref}\right)_{out}^{t}-\left(\rho_{ref}u_{ref}\right)_{out}^{t-1}\right)}{\Delta t}+(\Delta p)_{steady}\Big|^{t}=(\Delta p)_{dynamic}\Big|^{t} \qquad (4.49)$$

$$\frac{\left(\left(\rho_{ref} i_{ref}\right)_{out}^{t} - \left(\rho_{ref} i_{ref}\right)_{out}^{t-1}\right)}{\Delta t} + \frac{\left(\left(\rho_{ref} u_{ref} i_{ref}\right)_{out}^{t} - \left(\rho_{ref} u_{ref} i_{ref}\right)_{in}^{t}\right)}{\Delta x} = \left(\frac{A_{wall,i}}{A_{tube}} q_{wf}\right)\Bigg|^{t} \tag{4.50}$$

The single phase $(\Delta p)_{steady}$, which is present in the momentum equation, (4.49), is calculated by using Eq. 3.91.

4.5.3 Difficulties in programming

Apart from some general difficulties encountered in various programming stages, specific problems were also experienced in programming at coil level and element/sub-element level, and in wet-coil. In addition, for both the dry and wet coils and the TEV case, a minor difficulty was experienced which concerned with the changeable configuration of the studied coils, such as numbers of row per evaporator, requiring continuous update through out the program according to the study.

Generally speaking: It was very time consuming to debug the program caused by hidden constraints in the software. For instance, the VBA module cannot be programmed with more than 2500 lines. If so, the module will be bypassed; this problem was noted and solved accidentally by acquiring the information on the internet. Debugging the program also required considerable amount of effort and time, since the program could contain many forms of error, e.g. misunderstanding or misinterpreting of the governing equations. Whenever corrections and modifications were made to a module(s) of a particular coil condition, the rest of the programs for other conditions would require the corresponding modifications; once again it was a time consuming task especially when changes in program structure were involved. Finally, for managing the data, creating and maintaining/correcting modules became a rather tedious task. It was because the data management involved writing a data file after each converged time-step simulation, reading a data file to restore the previous time-step simulation (for any causes or reasons) and routine verification of individual variables in both coil- and element/sub-element- level modules. Moreover, arrangement for data presentation in the Excel worksheet, as required for both visual-aided simulation and the graphical plotting, involved multi-writing statements in many locations or sub-procedures.

Coil level: Two issues had to be carefully thought through for programming at this level. First, due to the use of the realistic coil configurations under

many different coil conditions, and the need to run the program for validation purposes, a great deal of care was needed to develop and write a versatile and flexible program. For instance, when dealing with a coil with the numbers of row other than 3, it was necessary to take great care in assigning the inlet air condition for each element/sub-element, because it involved modifications of the coil configuration in several parts of the program at the same time.

It was also a rather complex task to write modules for sub-element calculations, which included managing the calculated outputs of both the element and sub-element, since all the related physical coil features and the air- and refrigerant side flow patterns were involved.

Element/sub-element level: For the 2-phase region, for both steady-state and dynamic calculations, the main difficulty concerned with how to assume appropriate outlet DB temperature and the outlet vapour quality for an element/sub-element, especially, for the first element of the refrigerant coil inlet. In the superheat region, assuming an appropriate outlet DB temperature of an element/sub-element also needed attention because when compared to the 2-phase region, the air temperature changed very little, whilst the refrigerant temperature changed a lot resulting in convergence problems in the numerical scheme. In addition, assigning suitable iterative average temperatures of the wall and the refrigerant for the steady-state and the dynamic (respectively) was not an easy task too, usually involved a trial and error approach. Finally, to obtain physical properties of the refrigerants, by using the software and the scheme mentioned in Section 4.5.1, required careful and precise defining of variables.

Wet-coil: The wet-coil study, using the distributive model, was initially tried on a partially wet-coil condition; however there was instability of the convergence during the iteration. It was attributed to two causes: an "ambiguous" element/sub-element to be assigned as dry or wet, and a large difference between the air-side HTCs for the dry-coil and the wet-coil conditions. For instance, when operating a partially-wet coil near to a totally wet or a dry region, the air-side HTC of an ambiguous element/sub-element would be valued as under wet or dry condition, respectively. However, in the next iteration, the ambiguous element might change into the other coil condition, thus getting diverged. Under this circumstance, even if the HTCs for the coil conditions were of similar values, the simulation would be unstable already. The simulation would

certainly be unstable, since the HTC of the wet-coil is about two times larger than that of the dry-coil. For this reason, partially wet coil was excluded in this project.

Resolving difficulties: The ways as how some of the raised difficulties were managed were explained here. The program was regularly debugged by utilizing the debug tools provided in the Visual Basic Editor (VBE), especially the Auto Syntax Check option and the Watch window. In addition, debugging was also conducted by checking the governing equations in all forms, i.e. differential, discretized and programming forms, and by examining the assigned/transferred values between variables. The corrections and modifications of the programs were facilitated; for instance, by using Log book, utilizing Find option in the Edit menu of the VBE, and writing Remarked sentences in the programs.

For the element-or-sub-element- level programming, the results from the trial-and-error approach and from the previous element or sub-element calculations were used as a source of data to assume the outlet DB temperature in both the 2-phase and superheat regions. For instance, for steady state, regarding the first element of the refrigerant coil inlet, firstly, the wall temperature was guessed to be equal to the summation of the inlet refrigerant temperature and the modified value (by multiplying a constant to the difference between the inlet temperatures of the refrigerant and the air). Then the outlet DB temperature was estimated, and assigned to be the assumed value for the further simulation.

4.6 Simulation

Simulations were performed for dry- and wet- coil conditions, and for the dry coils the study was extended to include the TEV control. For all the coil conditions, the simulation was initiated with the steady state scheme. In other words, any dynamic simulation was established on a steady-state simulation as the starting point. The air state conditions at the coil face for all the simulations were always assigned. The refrigerant conditions at the coil inlet in the simulations were always fixed, except for the refrigerant mass flow rates for the TEV-controlled case. Generally, for a PC with 2.8 GHz CPU, the dry-coil or wet-coil simulation would take about 6 hours to run, whereas the TEV-controlled-coil simulation would take 3 times more.

The differences between pure and mixed refrigerants in the simulation procedure would be only discussed in Section 4.6.1 for the dry-coil simulation, unless otherwise stated, since in general the same differences also applied to the wet

conditions. It was noted that constraints related to the actual coil configuration and the comparison scheme for the two refrigerants (i.e. having the same values of the coil-outlet temperature and the coil-inlet mass flow rate) caused various difficulties in the development and implementation of the simulation scheme (e.g. in choosing the number of rows, tubes, elements and sub-elements, and assigning the coil-inlet refrigerant conditions).

4.6.1 Dry-coil simulation

a) General

Details of the simulation with no dehumidification, as shown in Fig. 4.12, applicable to both steady-state and dynamic simulations unless otherwise specified, were explained below. **First**, basic/fixed parameters of the coil configuration, e.g. rows per evaporator, tubes per row, elements per tube, sub-elements per element, tube inside diameter, were assigned. It should be stated that a three-row evaporator was chosen because it represents the minimum number of rows that is able to characterise the air and the refrigerant flows at both the inlets and outlets of the coil as well as the conditions inside the coil. More-than 3 rows could also be used but it would require a lot more computational time and computer memories. The coil block was designed to have 15 tubes per row and a five-refrigerant-circuit arrangement was chosen. This resulted in a three tube per row for each circuit, which allowed the air and the refrigerant behaviour in three separate regions (upper, "in-between" and lower regions) to be studied. For instance, referring to Fig. 4.2, the tube numbers 3, 1 and 3 of the row numbers 1, 2 and 3 represented the upper region, whereas all of the tube number 2 was recognised as in the in-between region.

For a dynamic simulation, the time duration, the number of the time step and the time interval of each time step would be specified. Other parameters associated with the coil configuration were then calculated, e.g. a fin density, a total finned-tube surface area per unit length, etc. At the coil face, the conditions of the air were specified based on the guideline of Grimm & Rosaler [Grimm & Rosaler 1990]. For the dynamic studies, the change of the condition was arranged to aid the study. For instance, the inlet DB temperature changed by 0.5 °C so that the movement of the superheat initiation position was confined to within the last tube of the last row.

For assigning the refrigerant condition at the coil inlet, there were two constraints. The first one was the same amount of the mass flow rate (or mass flux) for both pure and mixture refrigerants, for both steady-state and dynamic simulations. This was to aim at acquiring approximately the same coil-outlet refrigerant temperature for the steady-state. In addition, a 4 °C of the degree of superheat was set for R407C as the reference under the steady state condition, accepting that for R134A a different degree of superheat would result.

Second, for all elements/sub-elements, except those at the coil face, the inlet DB temperatures were guessed. Third, for each element/sub-element, the outlet DB temperature was guessed based on the assumed inlet temperature. The average wall temperature (for the steady-state) and the average values of both wall and refrigerant temperatures (for the dynamic) were calculated (seeing Fig. 4.12). The heat flux transferring from the tube wall to the refrigerant could then be determined. (NB This heat flux would be used in the 5^{th} step below. For the iteration-loop termination, Step 5, for the first iteration, this heat flux value would be checked against a zero value instead of a previous value.) Forth, for the refrigerant side, at both inlet and outlet, various properties and variables were then calculated, e.g. the HTCs, the wall temperatures (for the steady-state), the outlet vapour quality (for the two-phase region) and the outlet temperature (seeing Fig. 4.12). In addition, the pressure drop was also determined at this stage.

Fifth, the refrigerant-side iteration loop was stopped by checking the tube-wall-to-refrigerant heat fluxes against the resolution (seeing Table 5.8) for convergence. If not satisfying, the iterative average wall temperature (for the steady-state) was calculated or for the dynamic simulation the iterative average refrigerant temperature for obtaining the average wall temperature was assigned. The outlet DB temperature could then be determined, and the iterative loop would begin with the third step (as described above) for calculating the average wall temperature. However if the convergence was satisfied, the simulation would continue for the next element/sub-element from the beginning of the third step again. The simulation was carried out like this until all elements/sub-elements were completed.

Sixth, the simulation was terminated by using the scheme mentioned in Section 4.5.2.a. If the convergence was not achieved, all the elements/sub-elements were assigned with the iterative inlet DB temperatures so that the calculation would be

looped from the beginning of the third step. On the other hand, if converging, for the steady-state, the simulation was terminated. For the dynamic simulation, the next time step was carried out by looping at the second step (discussed above).

b) Differences between pure and mixed refrigerants

For the objective of this work it was decided to perform the simulation for R407C first followed by that of the R134a in both steady-state and dynamic conditions, and hence the main simulation/reference constraints were considered based on R407C; for instance, the setting of the degree of superheat at the steady-state and the moving distance of the superheat initiation position.

Due to the difference in the degree of freedom in 2-phase between R407C and R134a, it was assumed no shift in the feed composition for R407C, and the coil inlet condition was specified with the temperature and the pressure. For R134a, the temperature and the vapour quality were assigned.

For the two-phase region, in relation to the degree-of-freedom, there were in general more properties or parameters for R407C to be determined or handled, e.g. the vapour quality and mole fractions of each component in both liquid and vapour phases. Because of this difference, when using the bi-section method in solving the refrigerant properties at the element/sub-element outlet, the key parameters assumed in the iterative calculation were the temperature for R407C and the vapour quality for R134a respectively.

c) Difficulties in simulation

The main difficulty encountered concerned with the "trial-and-error" schemes, involving three situations. The first referred to both steady-state and dynamic simulations. What should be the assumed value of the outlet DB temperature of an element/sub-element, especially for the element at the refrigerant coil-inlet? For the two-phase region of R407C, how the limits of the lower and the upper refrigerant temperatures for the bi-section method should be assigned. For R134a, how the lower and the upper refrigerant vapour qualities should be assumed. In superheat region of both refrigerants, for the steady-state and the dynamic simulations, what average temperatures of the tube-wall and the refrigerant, respectively, should be assigned.

The second applied to the steady-state simulation. For R407C at the coil inlet, what the temperature, the pressure and the mass flow rate should be. For R134a

with the same mass flow rate as that of R407C, what the temperature and the vapour quality should be in order to obtain approximately the same refrigerant temperature at the coil outlet. Finally, regarding the dynamic simulations, what the number of time steps should be. How long should the time step be? What should be the magnitude of the step change in the air temperature at the coil face?

4.6.2 Wet-coil simulation

For the formulation of the wet-coil simulation, via the "trial-and-error", there are 2 main issues to consider. **First**, as explained previously the simulation in this thesis was limited to run in a totally-wet coil condition. It should be noticed that, for both steady-state and dynamic runs of each refrigerant, the whole coil including the superheat region was under the wet conditions.

Second, for a DX-coil, the more rows an evaporator has, the more reduction in the humidity ratio and air temperature results. When considering the scheme for the comparison of the refrigerants (i.e. the same values of the coil-inlet mass flow rate and the coil-out temperature for the refrigerants), the suitable coils are the ones with less rows per evaporator. Otherwise, the "apparent" relative humidity of more 100% (i.e. having water droplets in the air stream) in the later rows (because of the lower air temperature than the dew-point temperature) and/or a large refrigerant pressure drop in the coil would result.

a) General

The algorithm shown in Fig. 4.13 was for both steady- and dynamic-state unless otherwise specified. In general, the procedure was similar to that of the dry-coil simulation. **First**, however, at the coil face, the DB temperature and the humidity ratio were specified with values recommended in the British Standard [BS 5720:1979]. **Second**, both DB temperature and relative humidity at the inlet of each element/sub-element, except the ones at the coil face, were assumed.

Third, based on the assumed/known inlet air conditions for each element/sub-element, for the steady state, a dry-coil condition was assumed, and the DB temperature at the outlet was guessed. For the dynamic simulation, either a dry or a wet coil could occur, and correspondingly only the DB temperature or both DB temperature and relative humidity at the outlet was guessed. The average temperatures of the wall and the refrigerant were calculated the same way as that in the dry-coil simulation. The

next step, only for the steady state, was to check whether the element/sub-element is under a wet-coil state or not. If it was wet, then the relative humidity and the DB temperature at the outlet were calculated. The next step was then to calculate the heat flux transferring from the tube wall to the refrigerant.

The last three steps of Fig. 4.13 were mostly the same as that for the dry-coil simulation. An additional step was that, when the resolution of the tube-wall-to-refrigerant heat flux was not satisfied, and before the calculation of the outlet DB temperature, there was a checking for the wet coil status. If the coil was wet, the outlet humidity ratio was calculated.

b) Difficulties in simulation

Difficulties in simulation were similar to that of the dry-coil simulation, except it also needs to be recognised that the dew-point temperature was an additional constrain, concerning with the assuming of the values of the outlet DB temperature for an element/sub-element.

Despite the totally-wet condition, the divergence of the iteration mentioned earlier could still occur in two situations. The first situation was that, for both pure and mixed refrigerants, due to the trial-and-error scheme in the simulation, some iteration calculations with unsuitable assumed/assigned values would result in a divergence. The second situation of the divergence only concerned with R134a. Due to the fact that the refrigerant coil-inlet condition was referenced to the coil operating condition of R407C and to the same coil-outlet refrigerant temperature, one (or few) element(s) in the first row was under the dry-coil. To understand more about this divergence and the associated solution strategy, let's consider the following. In some occasions, when the element/sub-element was wet, but the iterative average wall temperature was higher than the dew-point temperature, suggesting, on the contrary, the coil was indeed dry. The reverse could also happen when the element/sub-element was dry. The adopted solution was that the HTC of the dry coil was assigned with an sensible HTC. One should bear in mind that, because only one or few elements were under the second situation, then the rectification performed for a dry-coil element was expected to cause a negligible influence upon the coil performance.

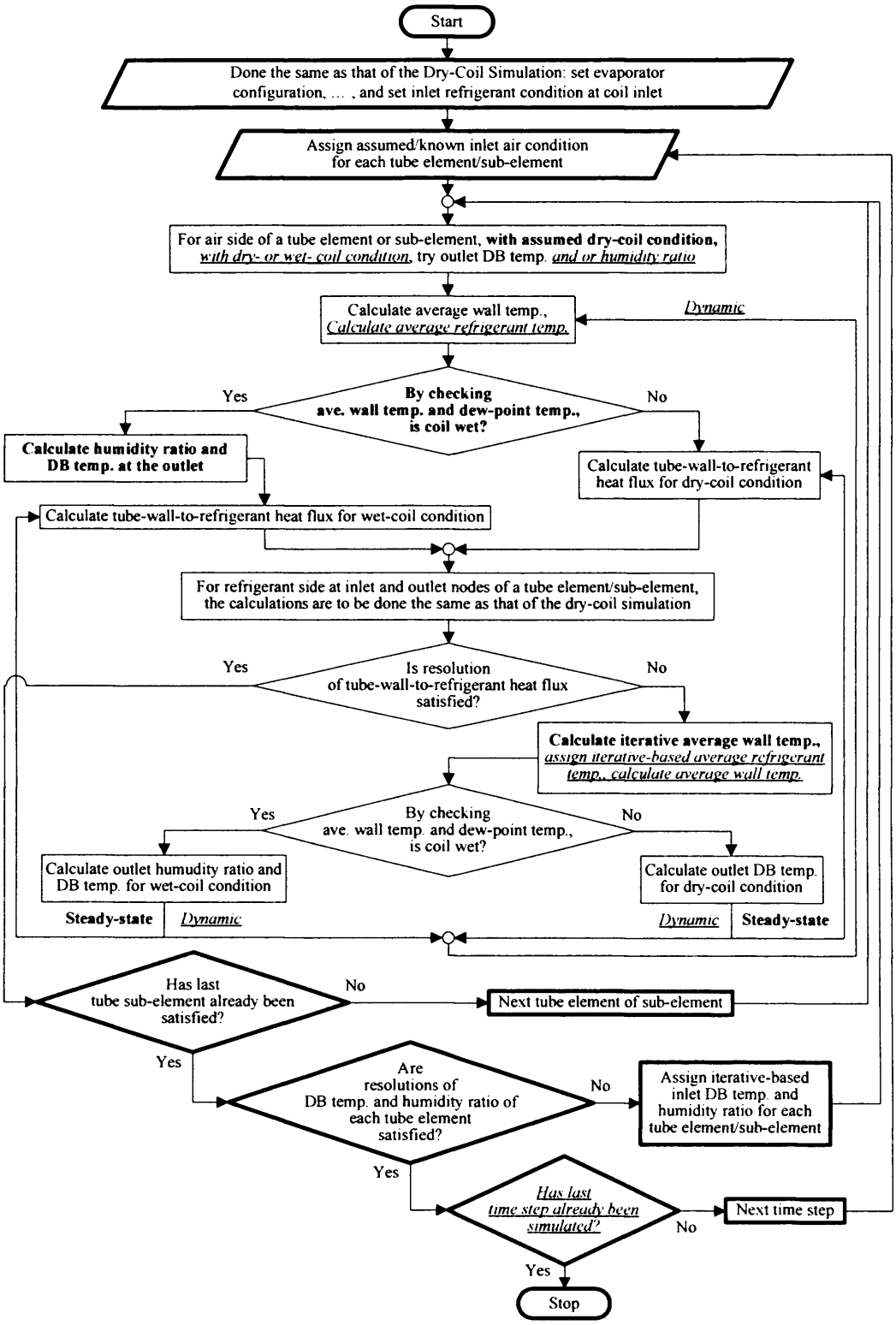

Figure 4.13 A computer flow chart for a **totally-wet-coil** simulation under steady and dynamic (a step change of coil-inlet DB temperature) states, when using pure or zeotropic mixed refrigerants (Remark: The bold frame-line blocks are for the coil level, whereas the thin ones are for the element/sub-element level. The bold letters are for steady-state, whereas the italic-underline letters are for dynamic.)

4.6.3 TEV-controlled evaporator simulation

For both refrigerants, the simulation (involving selecting a coil configuration for dry-coil operations, and providing properly sized TEVs at design conditions) was performed to investigate the effect of refrigerant type/properties on the TEV controlled operation. The disturbance was a 0.5 °C step increase of the coil-inlet DB temperature.

The simulation involved 4 aspects: refrigerant circuit patterns, coil configuration, assigning a TEV for a coil, and procedures/implementation of the simulation. For *the refrigerant-circuit patterns*, there were 3 possibilities: more than 1-row per evaporator with more than 1-tube per row, more than 1-row per evaporator but with only 1-tube per row, and only 1-row per evaporator with more than 1-tube per row. The first two patterns are useful in studying the effects of the superheat and the number of row upon the TEV operation, whlist, for the last pattern, the 2-phase refrigerant properties including the temperature glide/drop could be examined independently and explicitly, i.e. without any influences from the superheat and row effects. This pattern was selected for the TEV study, though it must be emphased that this pattern is different from real circuit arrangement in practical cases.

For *the coil configuration*, 3 alternatives were considered. ***The first type***, having 1-row per evaporator with 7-tubes per row, was considered. The degree of superheat was about 3.78 °C. ***The second type*** was created by modifying the first type to gain more degrees of superheat in the last tube. The coil has a smaller number of tube per row but longer length per tube. ***The third type*** was formed by modifying the first type but having the last 2 tubes with sub-elements, instead of having the sub-elements only in the last tube, in order to obtain both a large degree of superheat and a larger distance for the movement of the superheat initiation point. Having tried all these alternatives, the second type was selected as a compromise in getting acceptable degree of superheat and sufficient length for the movement. It also used less simulation time than the third type.

For *assigning a TEV to a refrigerant circuit*, 2 values were needed (referring to Eq. 4.33): K_v and p_{ss}. By running the coil under steady-state for 2 conditions: design and fully-open TEV (~1.25 times of the design load), the 2 unknowns can be obtained. To operate at ***the design condition***, a coil-inlet air condition that was the same for both the pure and mixed refrigerants was selected first. Then, use

trial-and-error to establish the coil-inlet refrigerant condition (being different for each refrigerant) under 2 constraints that were introduced for the purpose of performing the comparison between 2 refrigerants, i.e. having about the same values of the coil-outlet refrigerant temperature and the coil-inlet refrigerant mass flow rate. To run ***the fully-open TEV condition***, for each refrigerant, 3 constraints were applied. First, changing from the design operation to the fully-open TEV was implemented by increasing both the coil-inlet DB temperature and the coil-inlet refrigerant mass flow rate. Second and third, respectively the heat load was varied (by adjusting the coil inlet air temperature and refrigerant mass flow rate) to about 1.3 times larger than that of the designed-operating condition, and values of the degrees of superheat were maintained to be around the same as the design condition.

For the *procedures of the simulation*, according to Figs. 4.12 and 4.14, under a dry-coil condition, it started off with a steady state operation (at the design condition) followed by a 0.5 °C step increase of the coil-inlet DB temperature. The TEV, with the assigned valve gain and the chosen superheat-setting pressure, attempted to restore to an approximately constant degree of superheat by providing the coil-inlet refrigerant mass flow rate as calculated from Eq. 4.33 with the parameter values at the previous time step. Later, having the TEV (including the sensor-bulb and the external equalizer) removed, the coil was simulated with the same step change (discussed in Chapter 5). Due to the 3 constraints applied in establishing the fully-open-TEV condition, many trial-and-error runs were needed.

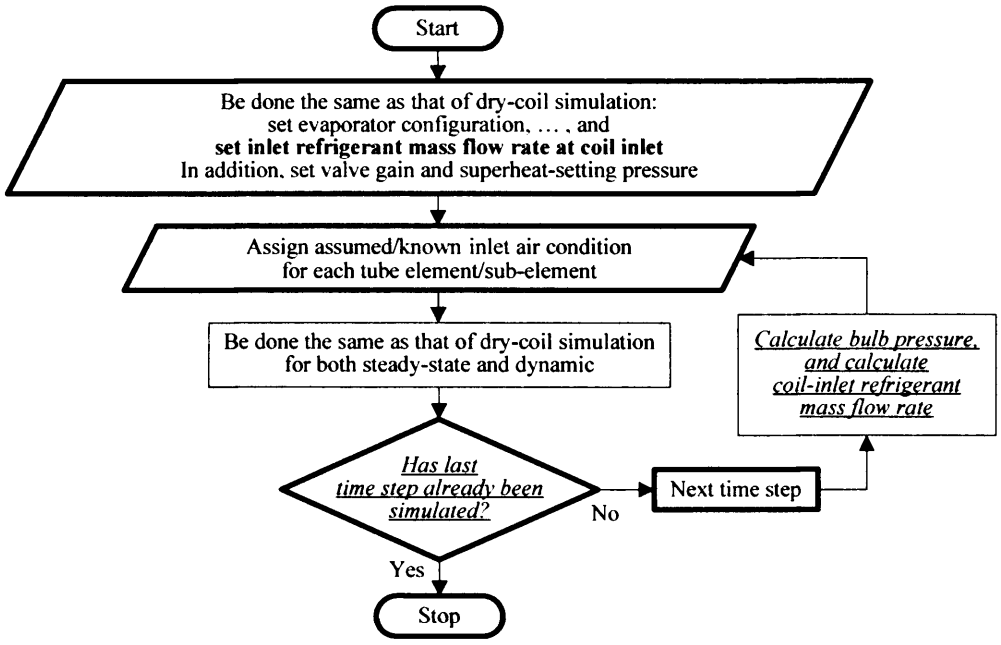

Figure 4.14 A computer flow chart for **TEV-controlled** plate-fin-tube evaporator, when using pure or zeotropic mixed refrigerant under a dry-coil condition (Remark: The bold letters are for steady-state, whereas the italic-underlined letters are for dynamic.)

Chapter 5 Results and discussion

This Chapter consisted of three main parts: computer model validations, results and discussion. A validation exercise was carried out to ensure the correctness of the model formulation and logics of the program codes. The results show how the R407C and the R134a evaporators performed and behaved differently.

5.1 Computer-program validations

Validations of the simulations for both steady and dynamic state data, as well as for the refrigerant HTC calculations, were mainly based on results from published literatures.

5.1.1 Steady-state validation

The models for steady-state-behaviour were "validated" for both R22 and R407C by using Ebisu & Torikoshi's experimental data [1995]. However, the exercise was not aiming at matching quantitatively the simulated results with the experimental data, but to show that the predictions provide the same behavioural trends between the two refrigerants as in Ebisu & Torikoshi's work. In any case, it was not possible to set the simulation parameters (both physical and operational) to be exactly identical to their experimental conditions (see the Table 5.1), due to various reasons. For instance, flat fins were used in this study in stead of louvered fins, hence, the air-side heat transfer coefficients of the flat-plate-fin type were modified to be that of a louvered one by using the 2.0-value enhancement factor (as in Bensafi et al.'s [1997]). This was necessary due to the restrictions applied when adopting the air side HTC correlations developed by Turaga et al. [1988] in this study; a similar argument applied when a different air velocity was used. In addition, smooth tubes instead of grooved types were used to

allow Jung et al.'s [1989b] correlations to be employed in the current study; no information on the grooved tube was given by Ebisu & Torikoshi. Although only dry coil was simulated as opposed to their wet conditions, Fig. 5.1, the trends agreed well showing very little differences between the two studies. NB For both refrigerants, due to the need of maintaining a constant average refrigerant temperature of 5 °C over the entire range of the mass flow rates, the temperature profiles along the coil then needed to have a pivoting location at around the mid point of the coil. Accordingly, the coil inlet air velocity, the inlet coil face DB and WB temperatures used by the author were set as given in Table 5.1. For the same reason, the gradients of the coil cooling-load vs. the mass flow rate were also relatively flat for the author's case. On the other hand, Ebisu and Torikoshi had steeper gradients over the first parts of mass flow rates; this was thought to be caused by the use of enhanced surface and hence a much higher HTC.

Table 5.1 Input values/parameters in Ebisu and Torikoshi's experimental work [1995] and in the current simulation for both R22 and R407C cases

Description	Ebisu and Torikoshi [1995]	Author's model's input or specifications
Flow pattern	Counter cross flow	Counter cross flow
Coil width (mm)	650	650
Coil height (mm)	296	296
Coil depth (mm)	24	24
Number of circuits per coil	2	2
Number of rows per coil	2	2
Number of tubes per row	7	7
Fin thickness (mm)	Not available	0.00011
Fin spacing (mm)	1.4	1.4
Type of fin	Louvered fins	Flat-plate fins
Tube surface	Inner grooved copper tube	Smooth copper tube
Tube outside diameter (mm)	7.0 (before expansion)	10.08 (with 0.35-mm-thick wall)
Average refrigerant temp. (°C)	5	5
Refrigerant inlet vapour quality	0.2	0.2
Refrigerant inlet vapour quality	0.2	0.2
Refrigerant mass flow rate (kg/hr)	55, 60, 65, 70, 75 and 80 (over two refrigerant circuits)	55, 60, 65, 70, 75 and 80 (for one refrigerant circuit)
Coil-inlet air velocity (m/s)	0.7	1.9
Dry-bulb temperature of inlet air at coil face (°C)	27	20.5
Wet-bulb temperature of inlet air at coil face (°C)	19	9.5

Figure 5.1 Evaporator cooling loads vs refrigerant mass flow rates from Ebisu & Torikoshi's [1995] experiment and author's simulation.

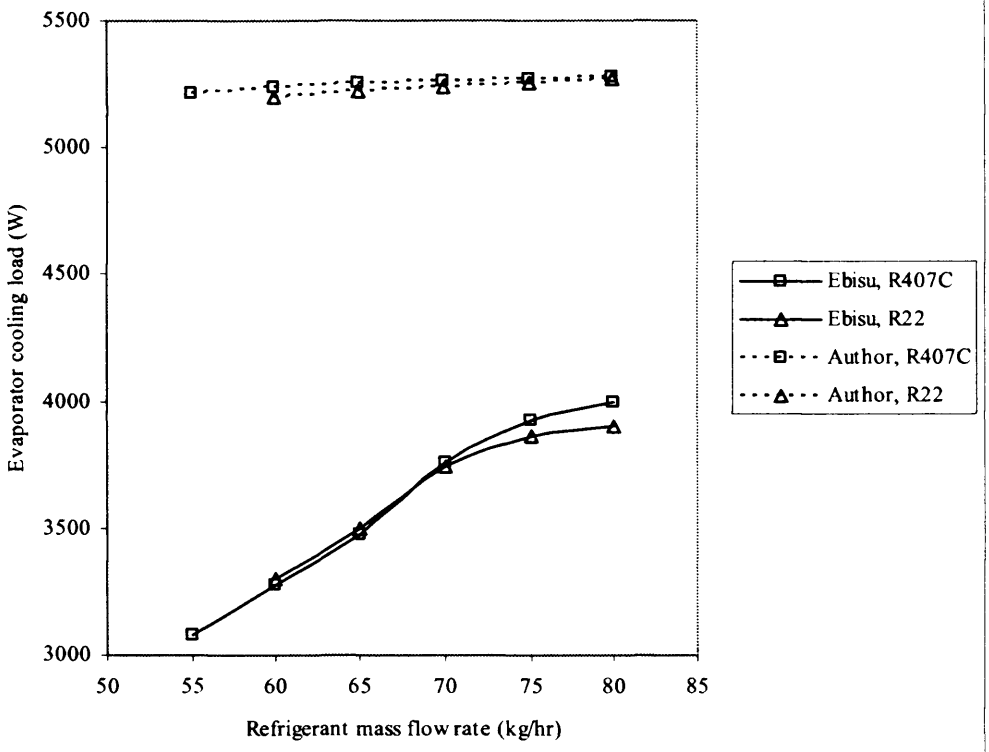

5.1.2 Dynamic validation

Validation for the dynamic simulation was performed for the R134a by using Jia et al's data [1995, 1999]. They experimented and simulated a commercial refrigerated container, in which the refrigerant mass flow rate was controlled by an electronic expansion valve. When comparing with the experiment, with *a step increase in the coil-inlet refrigerant mass flow rate*, their homogeneous-flow model gave an underestimated and a faster response for the degree of superheat, and a faster response for the air-off temperature (Figs. 5.2 and 5.3). Once again, not all the current simulation parameters could be set to the same values as Jia et al (see the Table 5.2). For example, Jia et al. did not specify the wet-bulb temperature though they said that the evaporator was operated under a wet condition; inlet vapour quality was not specified either. The present simulation (Figs. 5.2 and 5.3) therefore again aims at getting the similar trends rather than the exact values. A dry-coil run was carried out with the same air-on temperature and air mass flow rate as Jia et al. The step increases of the temperature, pressure and mass flow rate of the refrigerant at the coil-inlet were set to give similar changes in the degree of superheat as Jia et al.

Figure 5.2 R134a degrees of superheat vs times from Jia et al.'s work [1995, 1999] and author's work

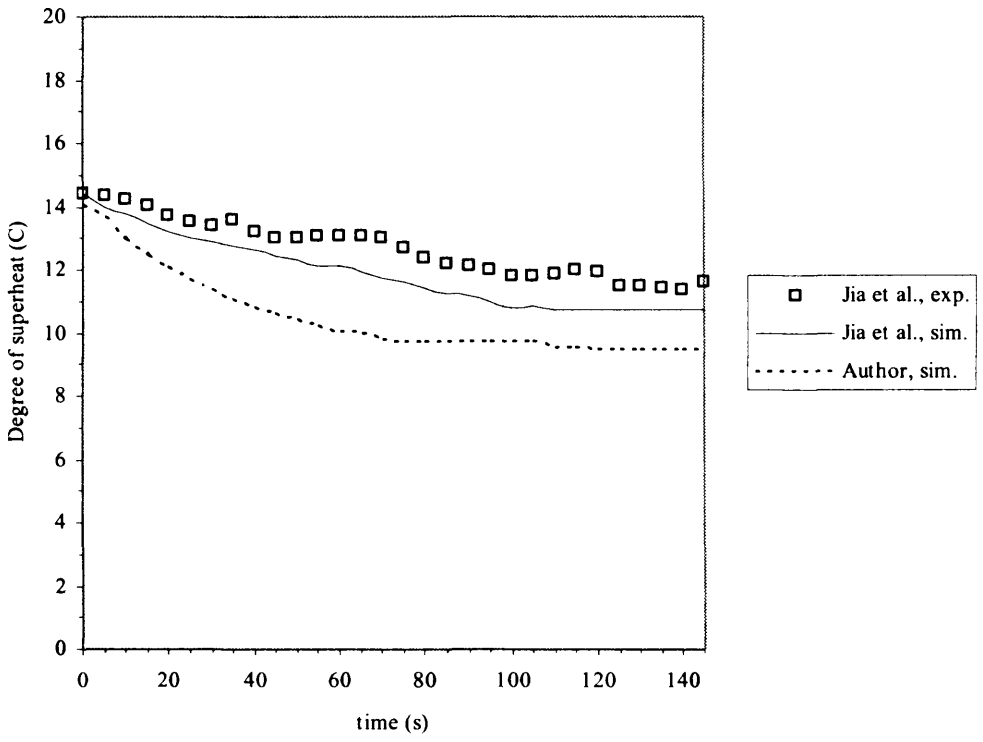

Figure 5.3 Coil-outlet dry-bulb temperatures at an end-side of coil vs times from Jia et al.'s work [1995, 1999] and author's work.

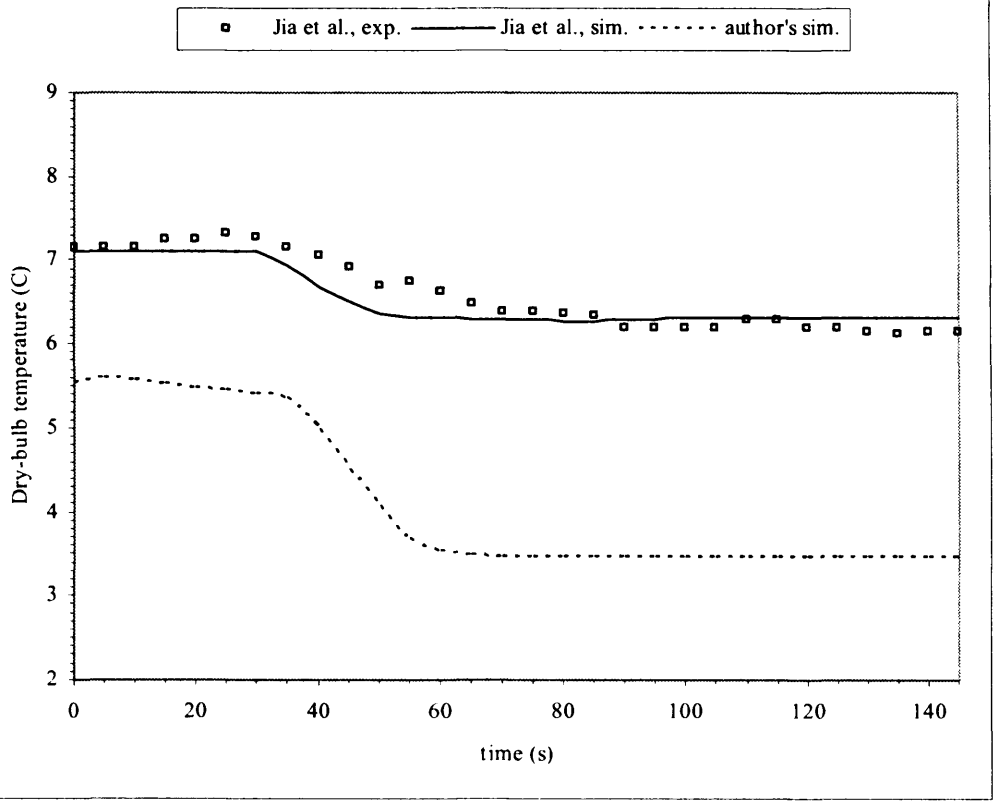

From the Figs. 5.2 and 5.3, it can be concluded that the dynamic program gave the expected results that were in general agreement with Jia et al's data.

Table 5.2 Input values/parameters of Jia et al.'s experimental and simulating work [Jia et al. 1995, 1999] and current simulation for the R134a.

Description	Jia et al. [1995, 1999]	Author's model
Coil width (mm)	1632	1632
Coil height (mm)	286	286
Coil depth (mm)	165	165
Number of circuits per coil	9	9
Number of rows per coil	6	6
Number of tube per row	1	1
Fin type	Flat-plate fins	Flat-plate fins
Number of aluminium fins	514	514
Tube outside diameter (mm)	12.7 (0.432-mm-thick wall)	12.7 (0.432-mm-thick wall)
Total air-side surface area (m^2)	44.8	44.8
Scheme for flow between air and refrigerant	Counter cross flow	Counter cross flow
Coil-inlet dry-bulb temperature (°C)	14.5	14.5
Coil-inlet wet-bulb temperature (°C)	(Not mentioned)	6.8
Coil-inlet air mass flow rate (kg/s)	1.14	1.14
Coil-inlet refrigerant temperature when steady state (°C)	-1.96	-1.17
Coil-inlet refrigerant temperature when dynamic (°C)	-0.02	-0.79
Coil-inlet refrigerant pressure when steady state (kPa)	272.0	280.0
Coil-inlet refrigerant pressure when dynamic (kPa)	gradually increase to 292.0	a step increase to 284.0
Coil-inlet refrigerant inlet vapour quality	(Not mentioned)	0.2
Coil-inlet refrigerant inlet mass flow rate when steady state (g/s)	8.11	7.0
Coil-inlet refrigerant inlet mass flow rate when dynamic (g/s)	8.89	8.0

Table 5.2 Input values/parameters of Jia et al.'s experimental and simulating work [Jia et al. 1995, 1999] and current simulation for the R134a.

Description	Jia et al. [1995, 1999]	Author's model
Tube-dividing scheme or schemes for cell-wise simulation	30-elements-per-tube for all tubes in coil	5-elements-per-tube, with 6 sub-elements per element for the tubes in last two rows (The author had also tried 15 elements per tube, with 2 sub-elements per element for tubes in last two rows. It did not give any noticeable differences in the values of coil-outlet refrigerant temperatures.)

5.1.3 Pure-refrigerant HTC validation

To ensure that the correlations obtained from the literature were applied correctly, the calculation for R22 HTC was checked based on Jung et al.'s work [1989a] on saturated-flow-boiling inside a horizontal tube (see the Table 5.3). From their experimental results, Fig. 5.4, they concluded that, for the partial flow boiling regimes, the heat transfer coefficients strongly depended on the heat flux, and the heat flux has no influence on the two-phase convective flow boiling.

Table 5.3 Parameters of Jung et al.'s experimental work [1989a] for determining R22 heat transfer coefficients

Tube inner diameter (mm)	9
Tube surface	Smooth
Tube length (m)	Two 4m-long tubes
Tube heating	Direct heaters with DC current were fixed at many points along tubes so the tubes could be arranged for partly or fully controlled heating
Heat flux (kW/m^2)	10, 17, 26, and 36
Refrigerant outlet pressure (kPa)	400
Refrigerant mass flow rate (g/s)	32.8

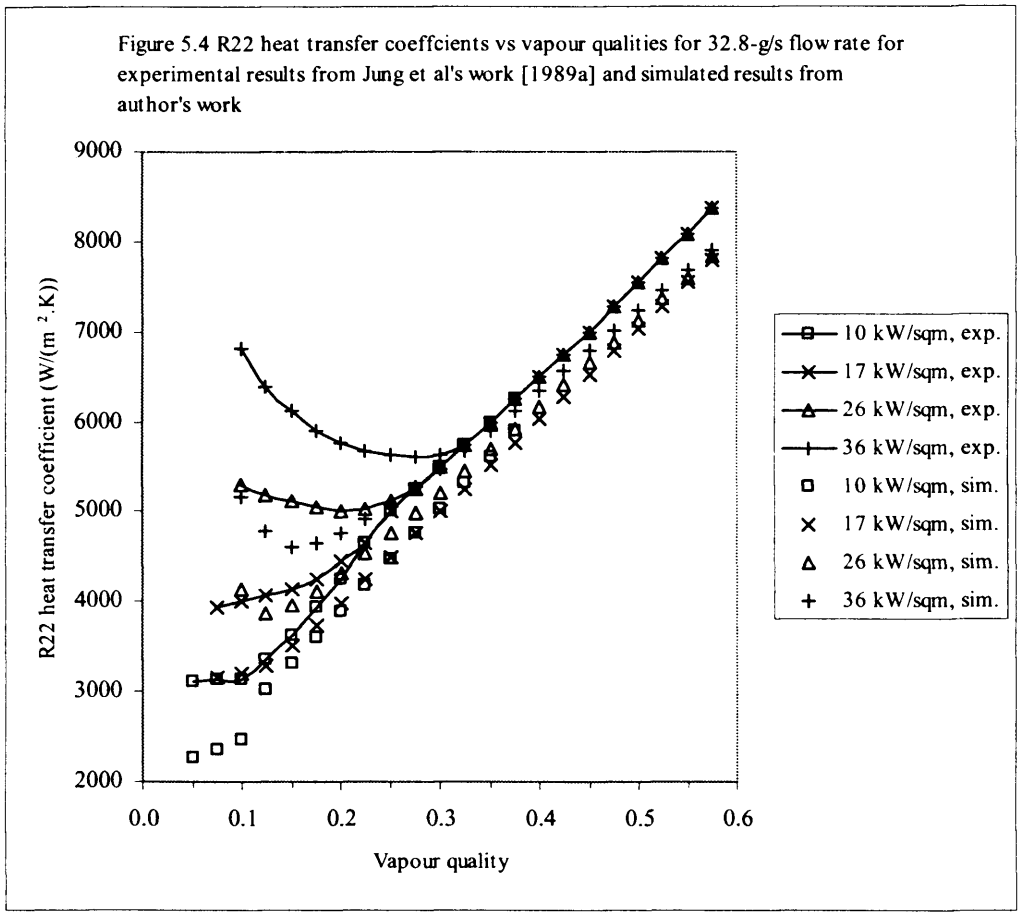

Figure 5.4 R22 heat transfer coeffcients vs vapour qualities for 32.8-g/s flow rate for experimental results from Jung et al's work [1989a] and simulated results from author's work

The program calculates the HTC, Fig. 5.4, based on the same parameters given in the Table 5.3. It was noted that the calculated HTCs in the partial-boiling regime were not so accurate (up to the quality 20-30%), while those in the two-phase-convective-flow-boiling regime were acceptable (see Figs. 2.1 and 2.3). However, this study mainly deals with the two-phase convective flow-boiling regime, and it can be said that the program performed as expected with satisfactory results.

5.1.4 Refrigerant mixture HTC validation

Similarly to check the calculation procedure for the mixed-refrigerant heat-transfer-coefficient, simulated results (Fig. 5.5) obtained using Jung et al.'s correlation [1989b], were compared with Judge & Radermacher's results [1997] which were calculated using the same correlations.

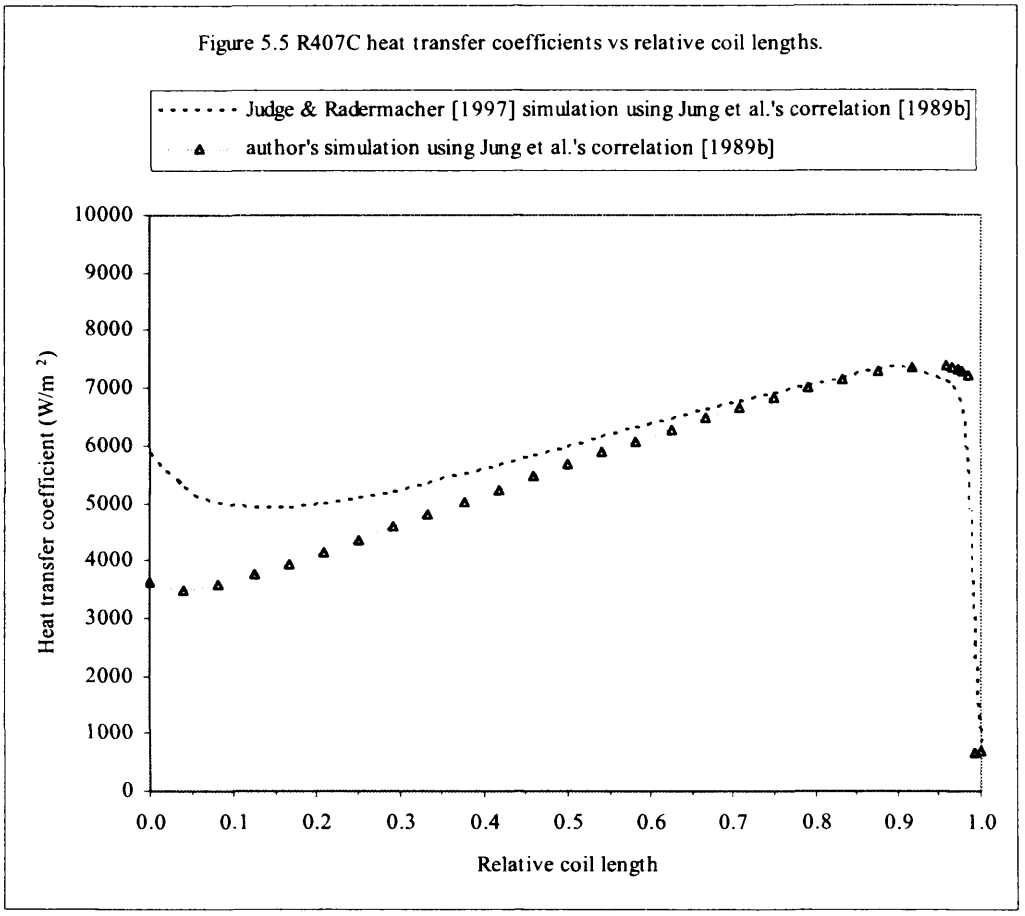

Figure 5.5 R407C heat transfer coefficients vs relative coil lengths.

Since Judge & Radermacher [1997] provided only limited information on their operating conditions (Table 5.4) to allow for a comparable parametric setting, the author's calculations were performed for the saturated flow boiling in a horizontal tube with *the uniform heat flux* and based on some deduced parameters, Table 5.5. Based on the observation that the HTCs in the convective flow boiling (nominal/relative coil length from 0.3 to 0.98) do not depend on the heat flux, the author was able to match the HTCs in this regime satisfactory with that from the Judge & Radermacher's work, by varying the refrigerant mass flow rates.

However discrepancies between the calculations in the partial boiling regime (nominal coil length less than 0.3) were noted, Fig. 5.5. In this region, for a constant refrigerant mass flow rate, the heat transfer coefficient is a function of the heat flux. Judge & Radermacher [1997] did not provide any information on the tube arrangement. If it were the one-tube model as in Judge et al.'s work [1996], the refrigerant heat flux in this region would be higher than that in the convective flow boiling regime, because of the temperature-glide effect, though the later would have higher HTCs. Then, their calculated HTCs in the partial boiling regime would be higher

than that of author's who was using a constant and a lower heat flux. At this stage, it was evident that the R407C HTC calculation was implemented correctly.

Table 5.4 Parameters of Judge & Radermacher's work [1997] for studying steady state behaviour of a R407C.evaporator

Fin type	Wavy fins
Dry-bulb temperature of inlet air at coil face (°C)	26.7
Wet-bulb temperature of inlet air at coil face (°C)	Less than 13.9
Tube-dividing scheme or scheme for cell-wise simulation	(Mentioned only quantities of nodes, 100)

Table 5.5 Deduced (from Judge & Radermacher's work, 1997) parameters used in the computer program for evaluating the R407C.heat transfer coefficients

Tube inner diameter (mm)	9
Tube surface	Smooth
Tube length (m)	3
Heat flux type	Uniform heat flux
Heat flux from tube wall to refrigerant (W/m^2)	28500
Refrigerant inlet temperature (°C)	6.85
Refrigerant inlet vapour quality	0.12
Refrigerant mass flow rate (g/s)	26

5.2 Dry-coil Results

For both the R407C and the R134a, the results, both steady-state and dynamic, were simulated for the dry coil conditions. Both refrigerants adopted the same coil configurations as detailed in Table 5.6. A 3-row evaporator was chosen based on the reasons given in Sub-section 4.6.1.

Table 5.6 Coil configuration for dry-coil conditions when using R407C and R134a

Coil width (cm)	121.9
Numbers of rows	3
Numbers of tubes in a row	15
Numbers of refrigerant circuits	5

Table 5.6 Coil configuration for dry-coil conditions when using R407C and R134a

Tube material	Copper
Inside/outside tube diameters (mm)	12.6/13.4
Tube arrangement	Staggered
Tube transverse/longitudinal spacing (mm)	38.1/38.1 (Then, each refrigerant circuit height was 11.43 cm.)
Fin type	Flat plate
Fin material	Aluminium
Fin thickness (mm)	0.16
Fin spacing to thickness ratio	12.3

The simulated results were presented for only one of the refrigerant circuits (as shown in Figs. 5.6 and 5.7). Each row consisted of 3 tubes, each of which was divided into 3 control volumes, called elements. For the last tube in the last row, each element was further divided into 8 sub-elements. The refrigerant inlet and outlet of the coil were at the node 1 and 28, respectively. The air flew into and out from the coil at the last and the first rows, respectively.

The operating conditions for the dry coil were shown in the Table 5.7. The coils were initially operating in the steady state, then subject to a step change (±) in the air-side dry bulb temperature in the dynamic simulations. In the steady-state analysis, for both refrigerants, the coil-inlet air conditions and the coil-outlet refrigerant temperatures were the same, and in the dynamic studies, same step changes in air temperature were applied. Both steady and dynamic studies also used the same refrigerant conditions at the coil inlet. The main iteration resolutions for the refrigerant heat fluxes and the element-inlet and coil-outlet dry-bulb temperatures were shown in the Table 5.8.

Though the simulations involved usually small values of changes in various parameters, they were considered sufficient to provide the information/details needed for the analysis and discussion. This was because only the relative comparison of the 2 refrigerants was required. In addtion, most of the iterative calculations only involved one or two governing equations, allowing convergence and giving little chances of generating large numerical errors.

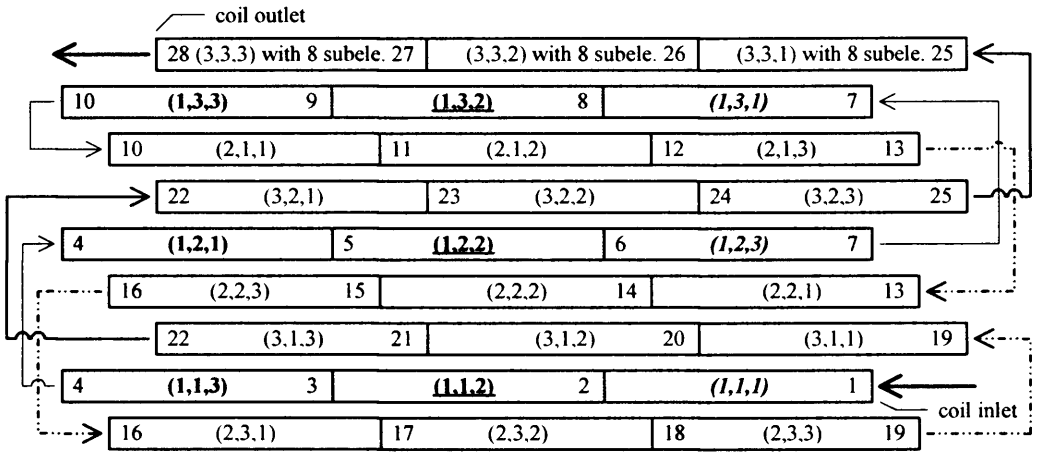

Figure 5.6 For Element and Sub-element arrangements in the refrigerant circuit following the flow of the refrigerant, an Element was labelled with either a ***node numbers*** or a ***bracketed code***. The former started from the coil-inlet to the coil-outlet, whilst the latter represented the row, tube, and element numbers, respectively. For instance, the Element 2 of the tube 1 in the row 1 had the inlet and outlet nodes 2 and 3, and was represented by a (1,1,2), i.e. (row 1, tube 1, element 2), respectively. For the last tube, each element was divided into 8 sub-elements and hence each sub-element took up $1/8^{th}$ (or 0.125) of the length of the element. Therefore, as an example, the second Sub-element of (3,3,1) was labelled as having its inlet and outlet nodes as 25.125 and 25.25, respectively. The highlighted tubes corresponded to the tubes in row 1 of Fig. 5.7.

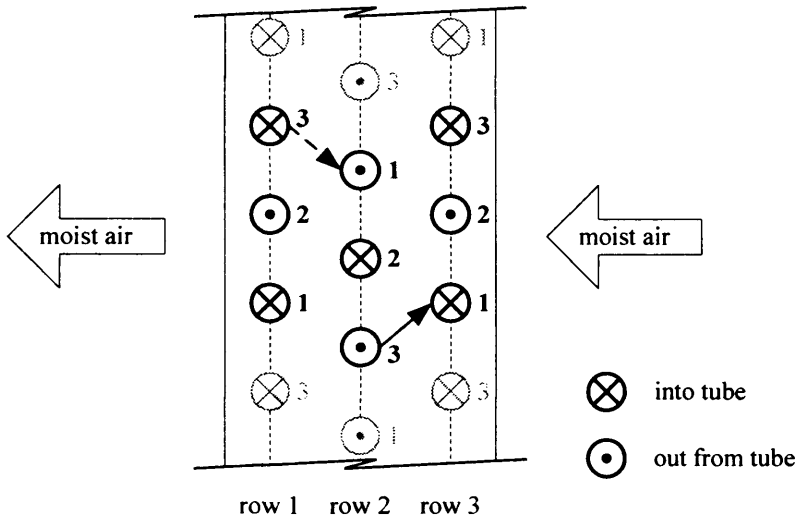

Figure 5.7 Side view of the coil by looking from the coil end with the refrigerant coil-inlet

Table 5.7 Operating conditions for the dry-coil (The same values were used in both the steady-state and the dynamic modes, unless otherwise stated.)

Description	R407C	R134a
Coil-inlet dry-bulb temperature (°C)	21.0, step changed to either 21.5 or to 20.5 in the dynamic study	21.0, step changed to either 21.5 or to 20.5 in the dynamic study
Inlet air mass flux for the coil	2.21	2.21

Table 5.7 Operating conditions for the dry-coil (The same values were used in both the steady-state and the dynamic modes, unless otherwise stated.)

Description	R407C	R134a
(kg/(s.m^2))		
Refrigerant-inlet conditions	2.0 °C and 583488 Pa Mass flow rate = 0.0221 kg/s	5.05 °C and vapour quality = 0.2 Mass flow rate = 0.0221 kg/s

Table 5.8 Simulation resolutions for both the R407C and the R134a under dry-coil conditions

Description	Resolutions
Absolute values of the refrigerant-heat-flux differences between the consecutive iterations in the two-phase regions (W/m^2)	Less than 0.5
Absolute values of the refrigerant-heat-flux differences between the consecutive iterations in the superheat regions (W/m^2)	Less than 0.05
Absolute values of the inlet-dry-bulb-temperature differences between the consecutive iterations (K)	Less than 0.005
Absolute values of the coil-outlet-dry-bulb-temperature differences between the consecutive iterations (K)	Less than 0.005
Absolute values of the inlet-dry-humidity-ratio differences between the consecutive iterations (kg of water/kg of dry air)	Less than 0.000005
Absolute values of the coil-outlet-humidity-ratio differences between the consecutive iterations (kg of water/kg of dry air)	Less than 0.000005

5.2.1 Dry-coil steady-state behaviour

This section is arranged in two parts, (a): refrigerant side behaviour and (b) the air-side behaviour. Many parameters were investigated and their associations to coil performance/behaviour, energy transfer/loss, compressor performance/operation, refrigerant influences, etc. were shown in Table 5.9.

Table 5.9 Importance of the studied parameters

Coil-outlet refrigerant pressure	Influence on compressor performance
Coil refrigerant pressure drop	Estimation of energy loss; analyzing refrigerant behaviour
Coil-outlet refrigerant temperature	Influence on compressor performance
Coil two-phase refrigerant temperature change	Understanding heat transfer potential
Superheat initiation position	Understanding/analyzing the superheat effect

Table 5.9 Importance of the studied parameters

Degree of superheat	Understanding/analyzing the superheat effect
Profile of two-phase refrigerant temperature changes per length	Analyzing the refrigerant behaviour
Two-phase refrigerant heat transfer coefficients	Analyzing the refrigerant behaviour
Coil-outlet refrigerant specific volume	Influence on compressor performance
Refrigerant specific volumes along the coil	Quantification of refrigerant mass
Refrigerant densities along the coil	Quantification of refrigerant mass
Refrigerant velocities along the coil	Estimation of refrigerant mass flow rate
Refrigerant vapour qualities	Supportive information for analyzing refrigerant/coil behaviour
Two-phase refrigerant heat fluxes	Understanding heat transfer potential and refrigerant behaviour; supportive information for analyzing refrigerant/coil behaviour
Refrigerant heat loads (For the first, the second, and the last rows, and for the coil, respectively)	Understanding heat transfer potential; supportive information for analyzing refrigerant/coil behaviour
Two-phase wall temperatures	Supportive information for analyzing refrigerant/coil behaviour
Total heat fluxes	Understanding heat transfer potential and refrigerant behaviour; supportive information for analyzing refrigerant/coil behaviour
Total heat loads	Understanding heat transfer potential and refrigerant behaviour; supportive information for analyzing refrigerant/coil behaviour
Coil-outlet dry-bulb temperatures	Specification of air-off temperature for a given application

a) Refrigerant-side performance

Refrigerant pressures and related parameters: As shown in Fig. 5.8, the inlet and the outlet pressures for R407C were 583.5 and 571.2 respectively, resulting in an overall pressure drop of the coil 12.3 kPa. The corresponding values for R134a were 347.9, 335.2 and 14.5 kPa. Fig. 5.9 showed that for both refrigerants, the two-phase pressure drops (outlet pressure of an element/sub-element minus the inlet pressure of that element/sub-element) increased along the coil reaching their peak values at node 22 in the second tube of the last row (the corresponding vapour qualities were around 0.72, Fig. 5.10); this position also corresponded to the maximum difference between the two refrigerants. Within the first two rows, the differences were relatively small. The

pressure then decreased sharply from node 22 to around node 26 as a result of changing from annular flow pattern to mist flow pattern. The superheat started slightly earlier for R134a, Fig. 5.11, than that for R407C, and the pressure drop in the region was only marginally higher for R134a.

Refrigerant temperatures and related parameters: It was shown in Fig. 5.12, the two-phase temperature glide-up was 4.24 °C for R407C and in contrast, R134a has a two-phase temperature drop of 1.13 °C. For the comparison scheme adopted, the coil-inlet temperatures for R407C and R134a were 2.0 °C and 5.05 °C, respectively. The degree of superheat for the R407C, 3.61 °C, was smaller than that for R134a, 5.84 °C. The simulated results showed that for R407C the superheat initiation position was at a 5 sub-element distance (25.4 cm) after that of R134a.

Concerning the local the temperature gliding, the temperature changes per unit length (vs node point) for the two-phase regions along the coil were shown in Fig. 5.13. For R407C, three patterns, essentially corresponding to the 1st, 2nd and the 3rd row of the coils, can be identified. The average temperature change/unit length is the highest in the 3rd row (air inlet side), whereas the 1st row (air outlet side) had the lowest average; there were little variations in these two rows. However, two peaks were observed in the 2nd row, this was caused by high temperatures of inlet air that had passed superheated elements containing the two peaks. (The peak temperatures occurred in Elements (2,1,1) and (2,3,1) that were influenced by Elements (3,3,3) of the same and the lower refrigerant circuits, respectively, see Figs. 5.6 and 5.7.) In contrast, for the R134a, the temperature change per unit length gradually decreased until within the last two tubes of the third row. For the superheat regions, both refrigerants had the maximum and the minimum temperature changes per unit length at the superheat-initiation points and the coil outlets, respectively, with a rather linear and sharp decrease.

Refrigerant heat transfer coefficients: Both the R407C and the R134a two-phase heat transfer coefficients increased along the coil, Fig. 5.14. They had very similar values in the first two rows, with R407C having slightly lower values in the last row.

Refrigerant specific volume and velocities: Along the evaporators, the 2-phase specific volumes of R407C were always smaller than that of the R134a, Fig. 5.15, and their differences gradually increased from the inlet to the outlet of the coil. The coil-outlet specific volumes of the superheated vapour for R407C and R134a were 0.04228

m^3/kg and 0.06332 m^3/kg respectively. The variations of refrigerant velocities along the coil shared the same pattern, Fig. 5.16, as that of the specific volumes. It can be seen in Fig. 5.17, that both profiles of the changes in specific-volume per unit length were similar. This implies that the specific volumes of both refrigerants were probably influenced by the same parameter(s).

Refrigerant vapour qualities: Fig. 5.10 showed that both refrigerants had almost the same values of vapour qualities along the coil. It was interesting to point out that for the changes of vapour quality per unit length along the coil, Fig. 5.18, two refrigerants had similar values in the 2nd row, whereas for the 1st row, R407C had the higher values, and for the last row, R134a had the higher values (to be discussed later).

Refrigerant heat fluxes and loads: As shown in Fig. 5.19, R407C the two-phase heat fluxes for R407C were higher than that of the R134a, except in the last row. The calculated total heat loads for R407C and R134a were respectively 3758 Watts and 3476 Watts, i.e. the ratio of R407C to R134a total heat loads was 1.08. In addition, the corresponding splits between the three rows were 890, 1298 and 1571 for R407C, and 666, 1194 and 1616 for R134a respectively.

Figure 5.8 Refrigerant pressures vs nodes for dry coils

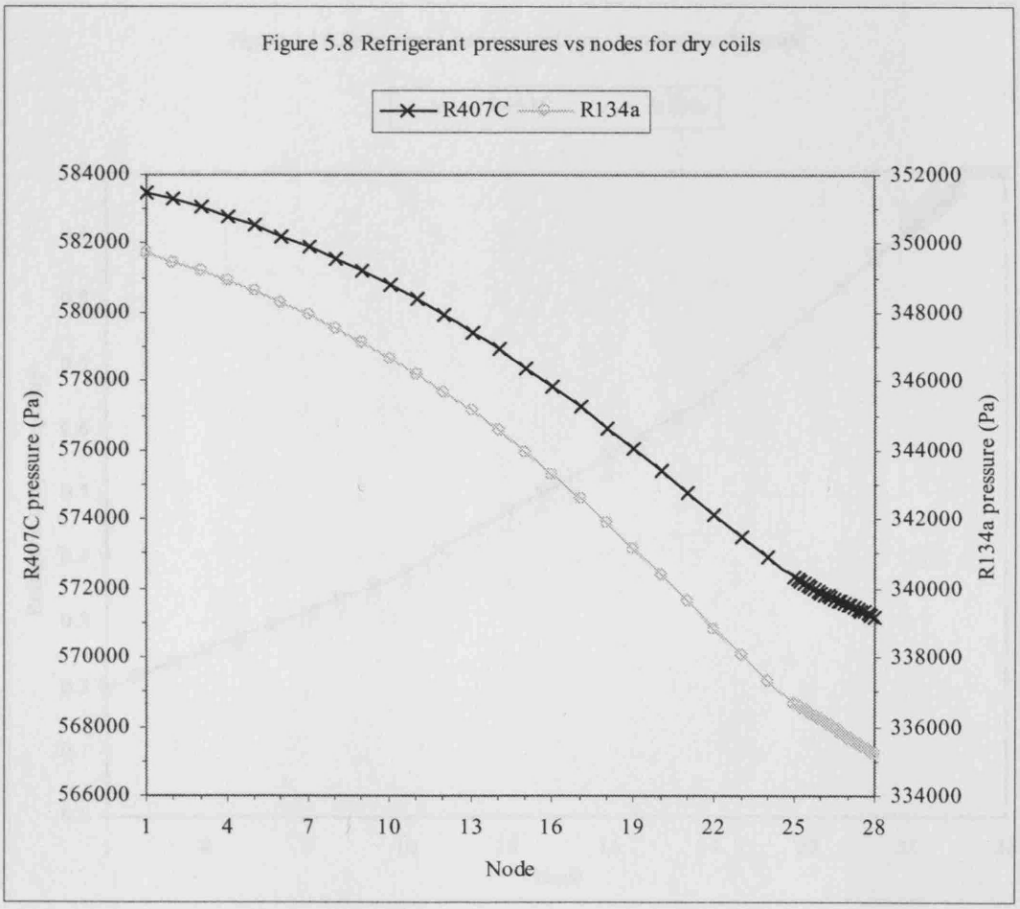

Figure 5.9 Refrigerant pressure drops vs nodes for dry coils

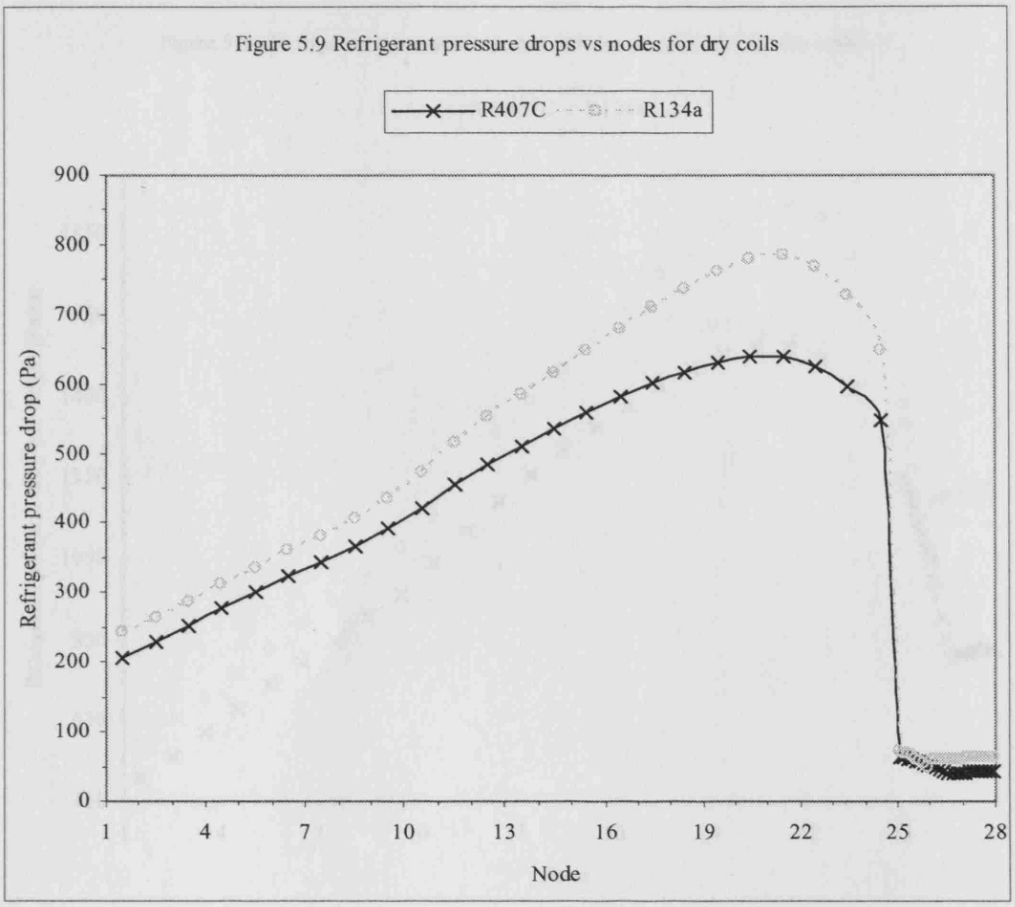

Figure 5.10 Refrigerant vapour qualities vs nodes for dry coils

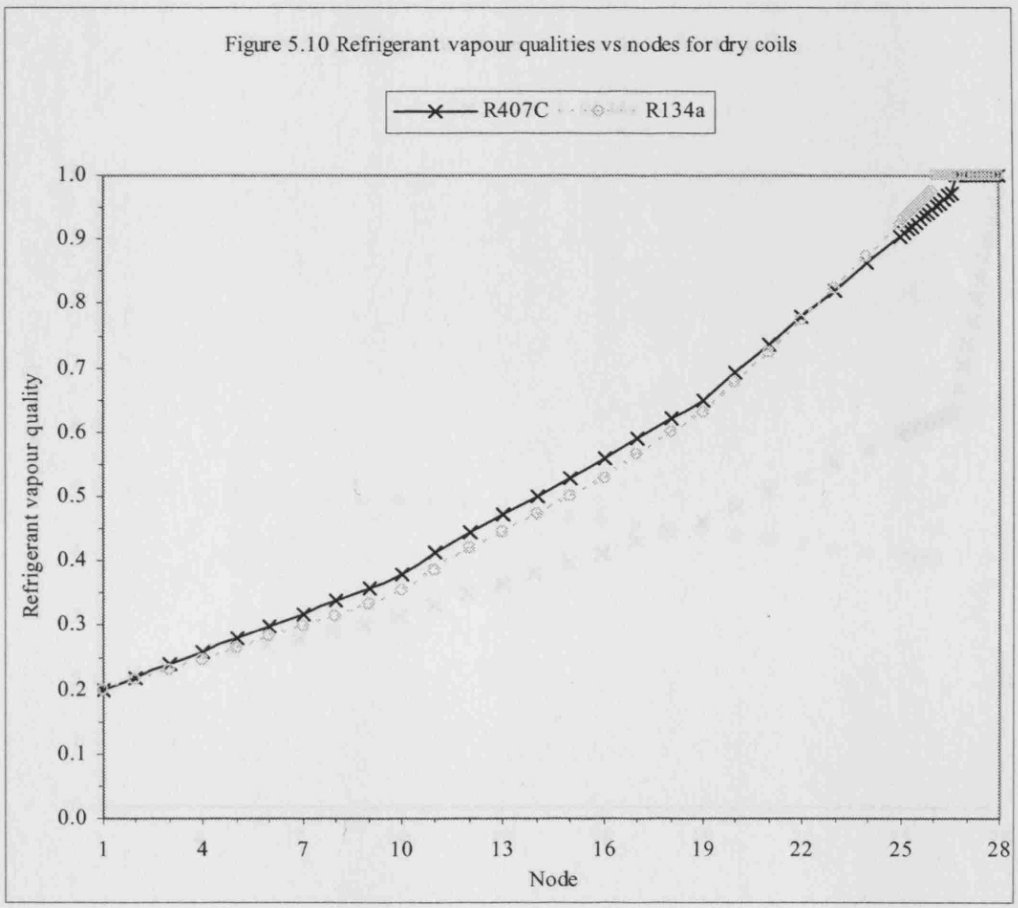

Figure 5.11 Refrigerant pressure drops per unit length vs nodes for dry coils

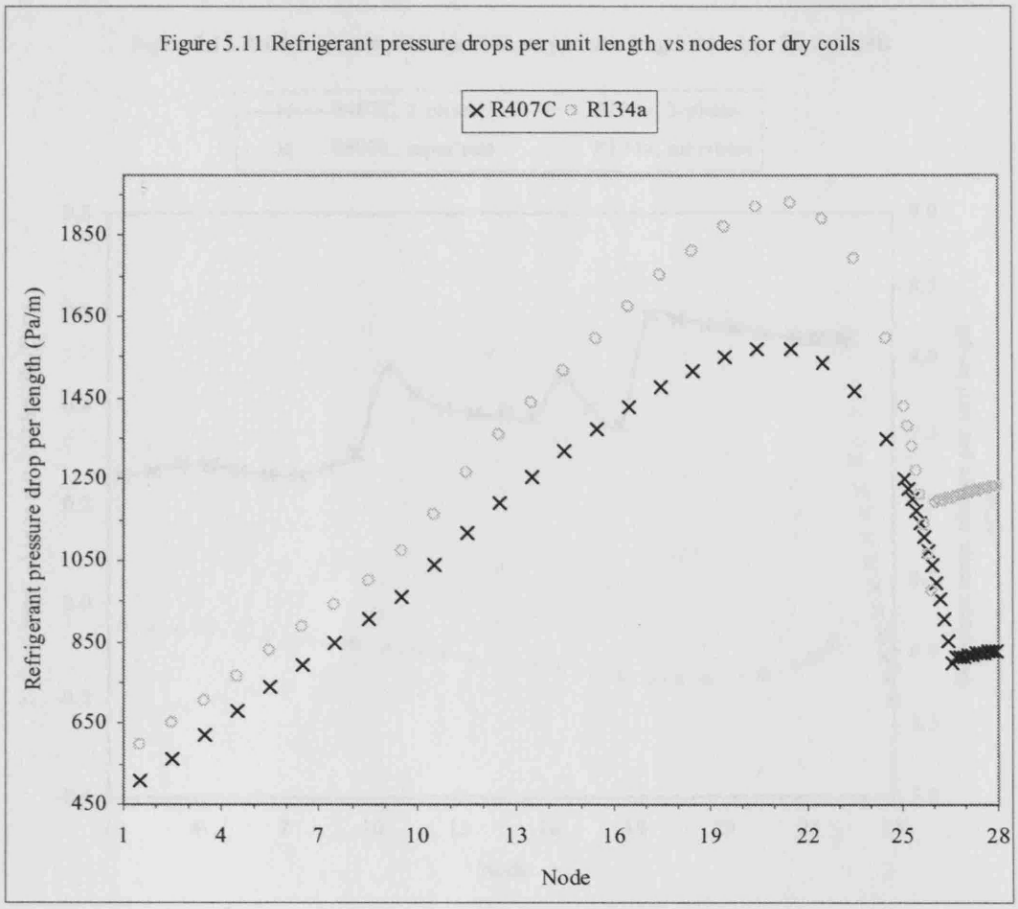

Figure 5.12 Refrigerant temperatures vs nodes for dry coils

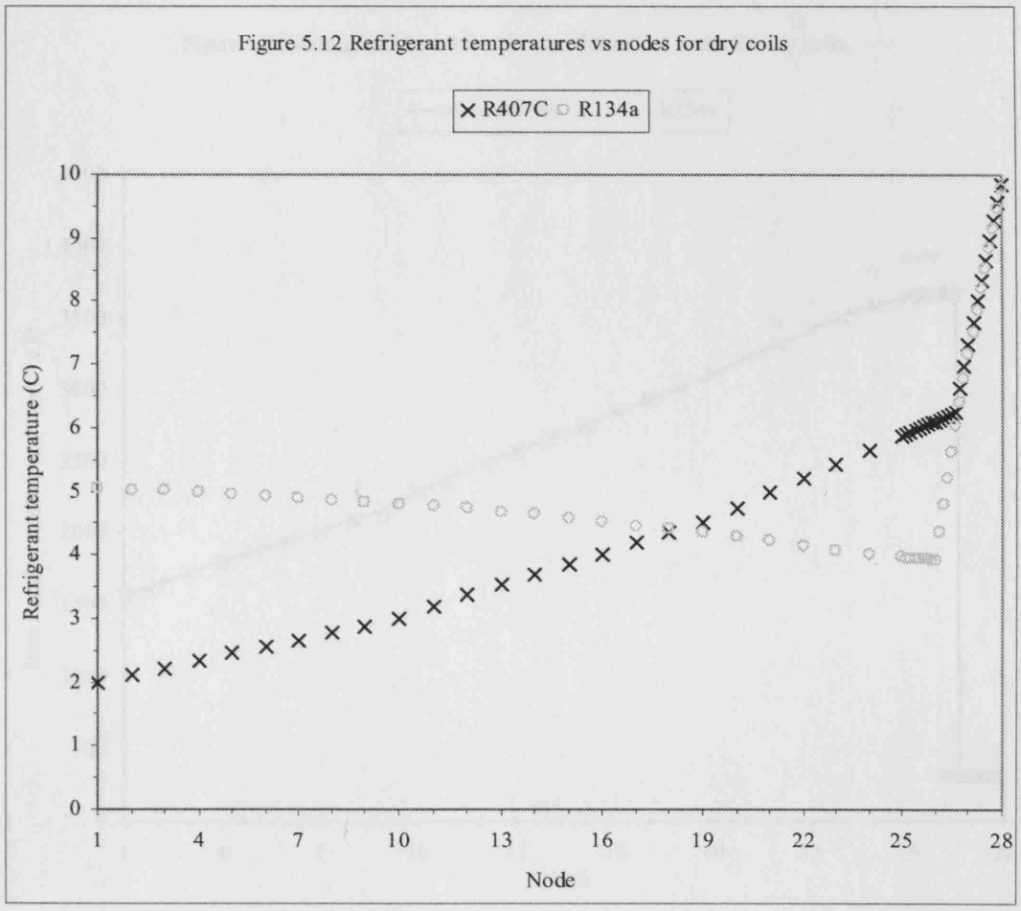

Figure 5.13 Refrigerant temperature changes per unit length vs nodes for dry coils

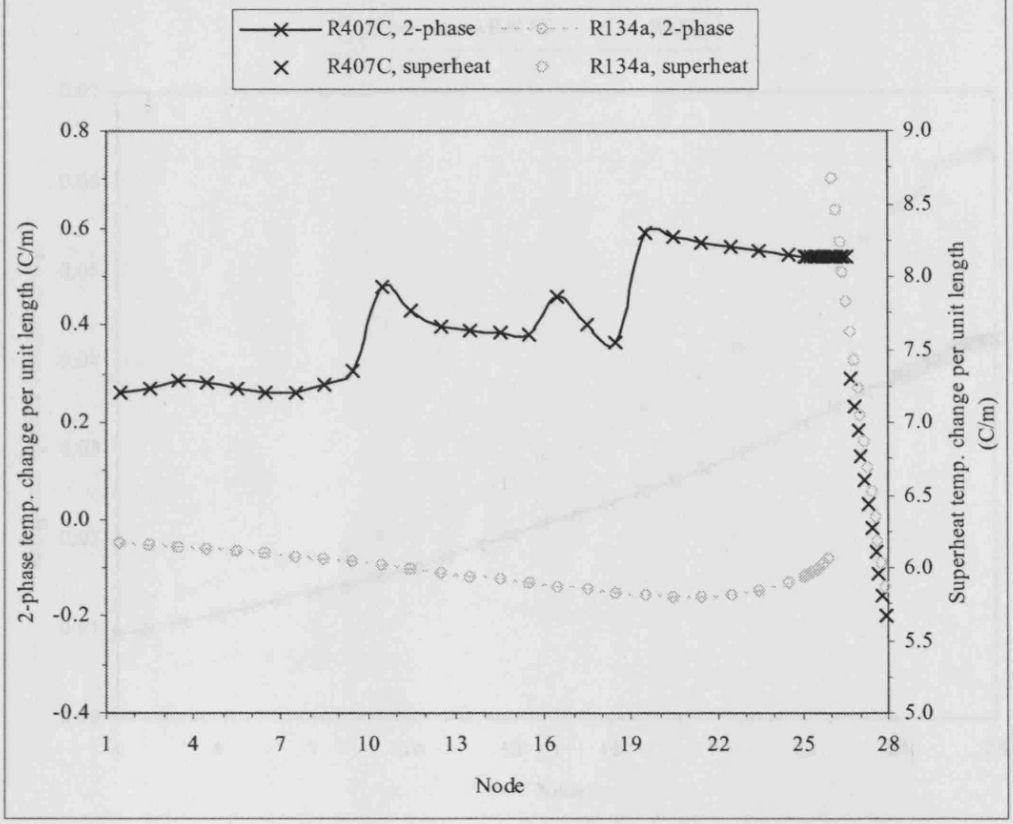

Figure 5.14 Refrigerant heat transfer coefficients vs nodes for dry coils

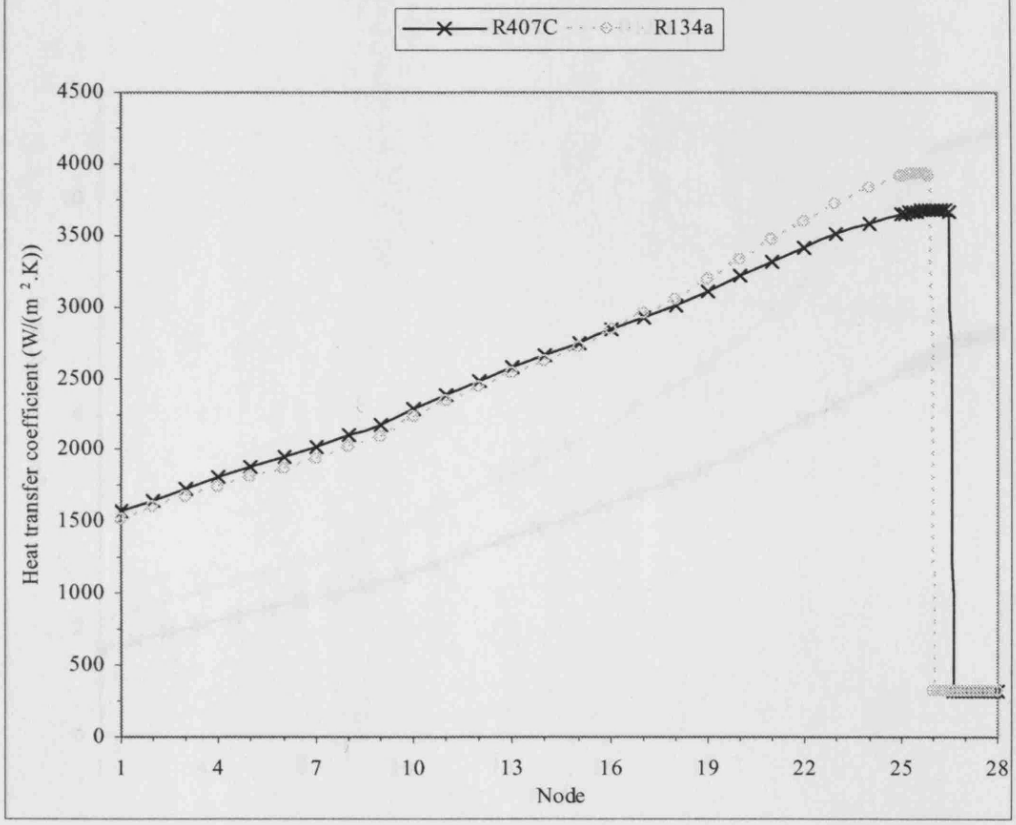

Figure 5.15 Refrigerant specific volumes vs nodes for dry coils

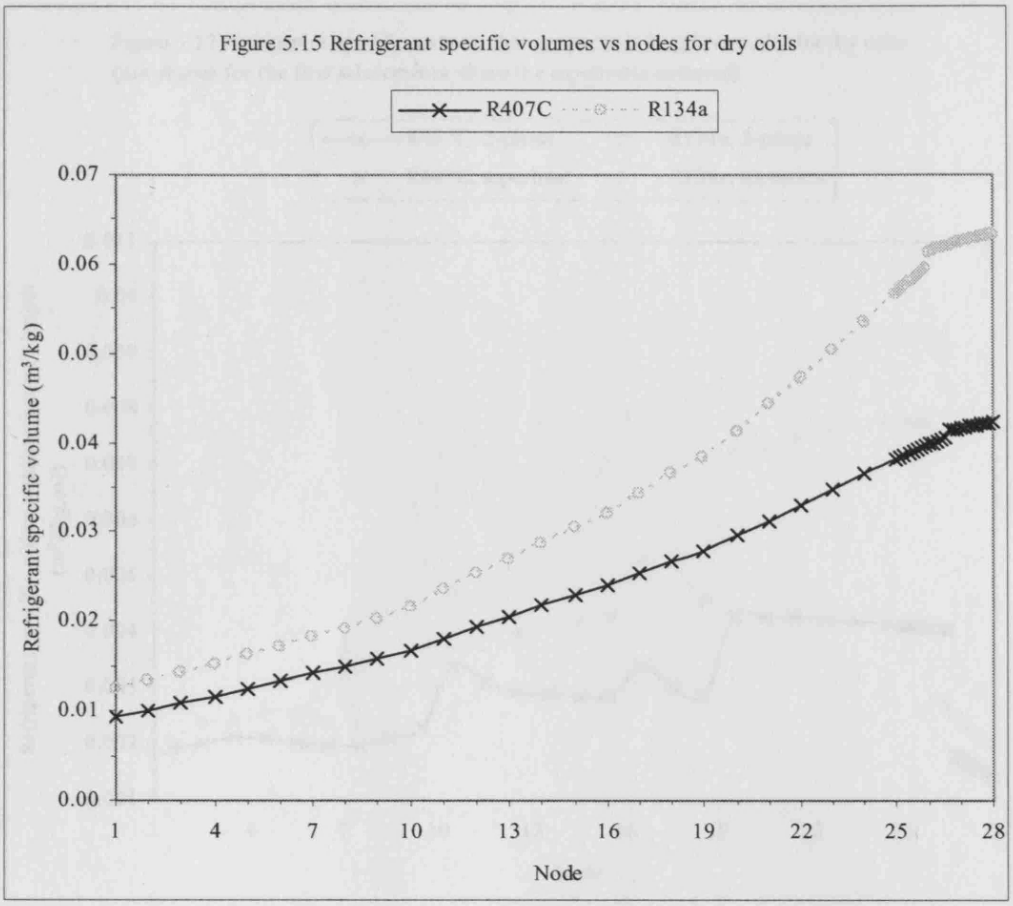

Figure 5.16 Refrigerant velocities vs nodes for dry coils

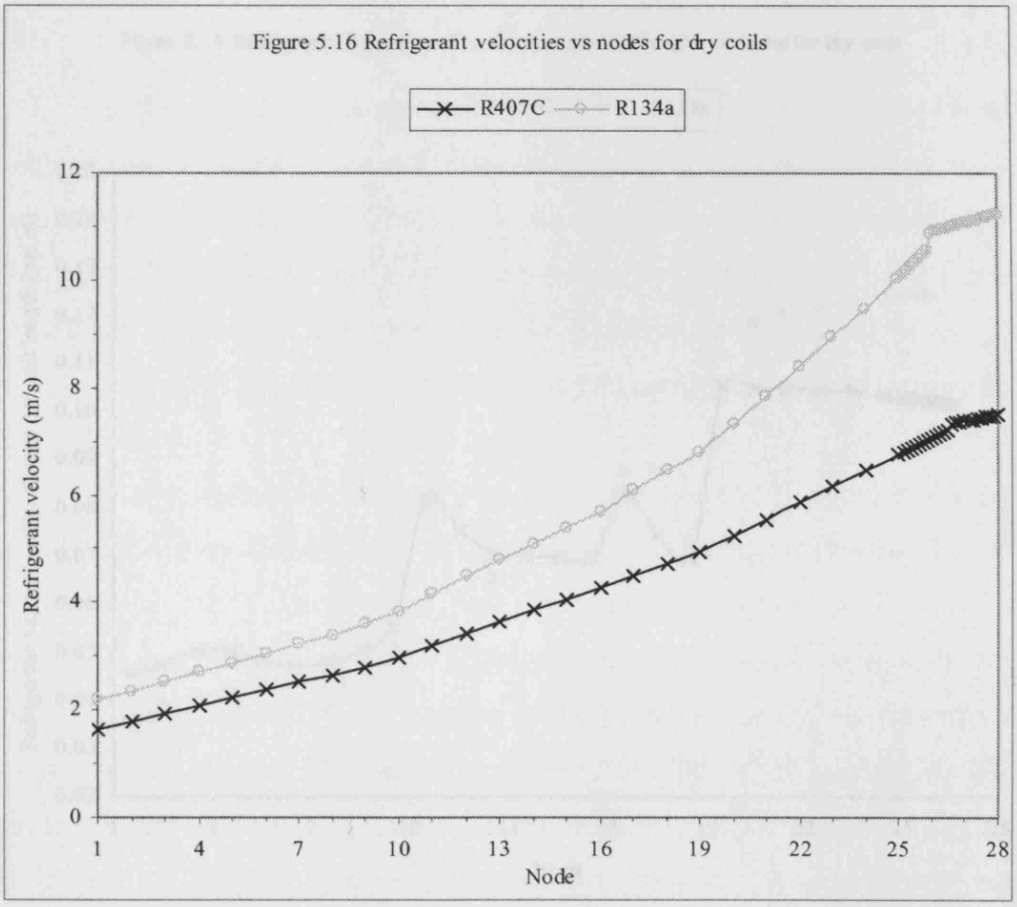

Figure 5.17 Refrigerant-specific-volume changes per unit length vs nodes for dry coils (not shown for the first subelements where the superheats occurred)

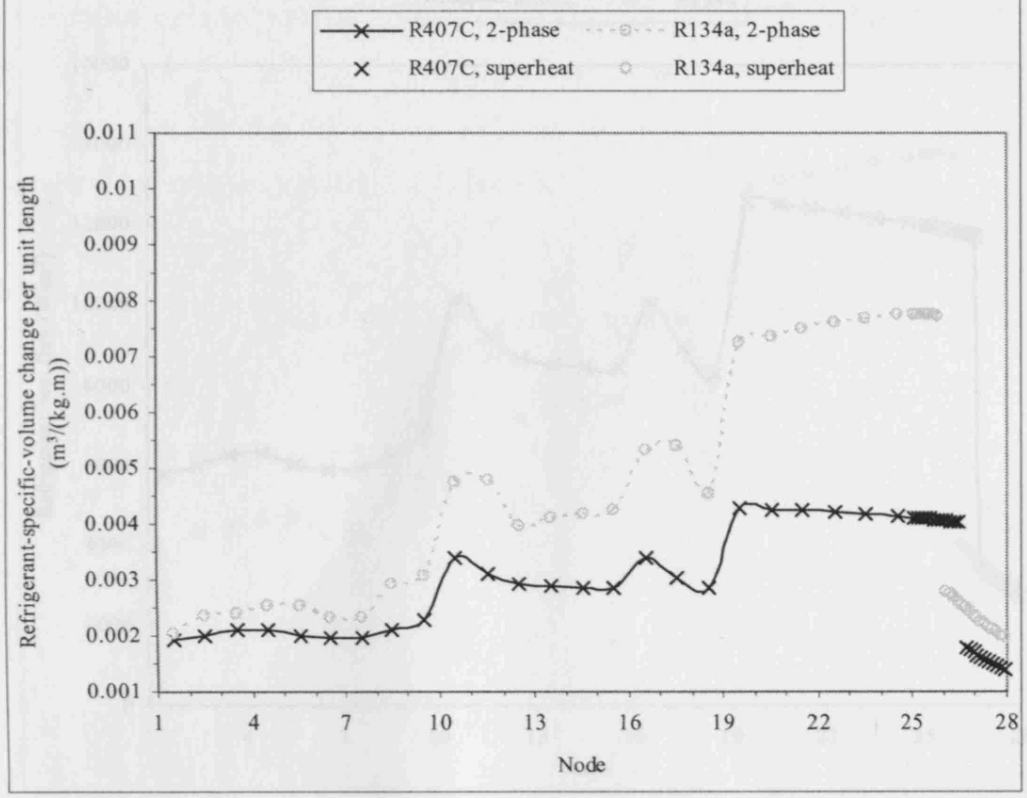

Figure 5.18 Refrigerant-vapour-quality changes per unit length vs nodes for dry coils

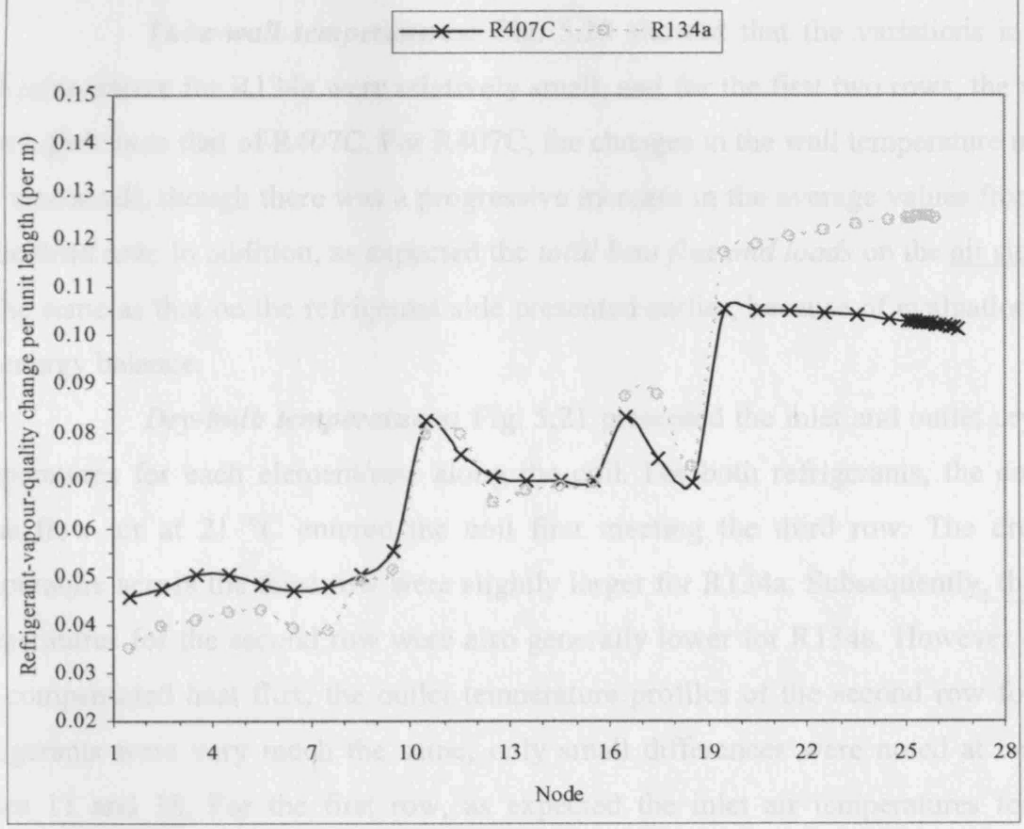

Figure 5.19 Refrigerant heat fluxes vs nodes for dry coils

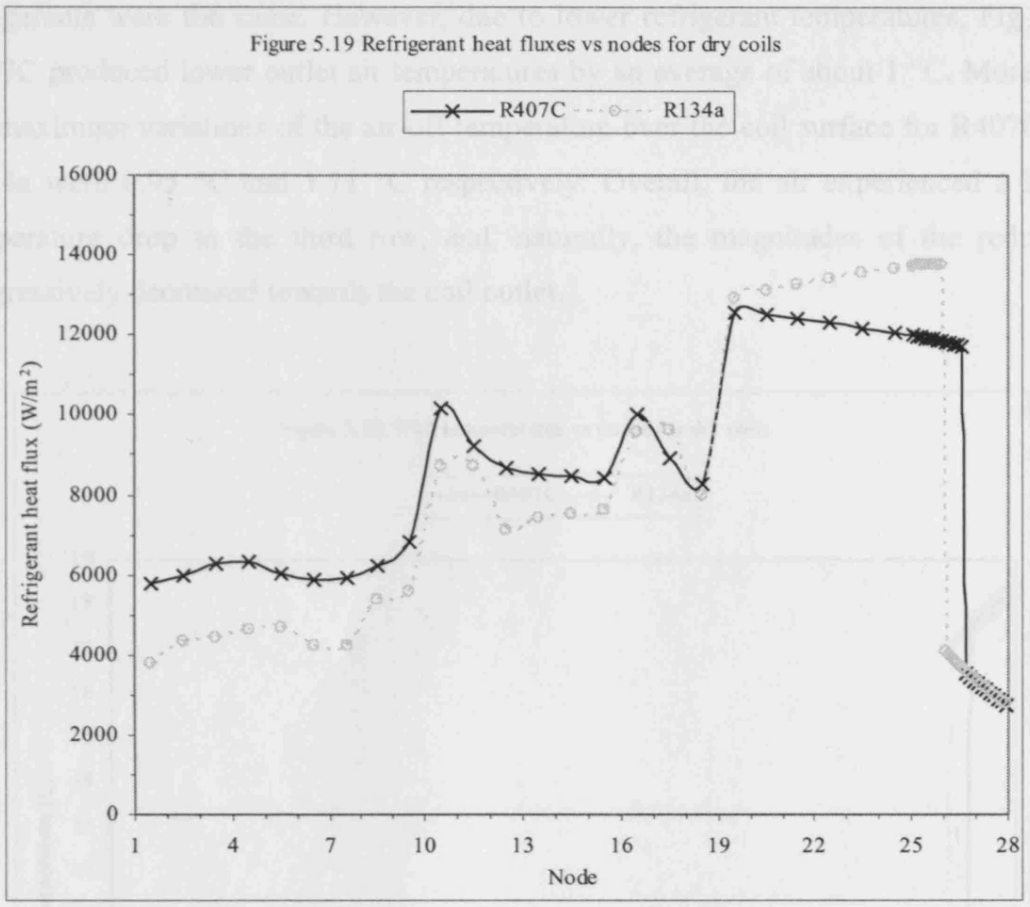

b) Air-side performance

Tube-wall temperatures: Fig. 5.20 showed that the variations in tube-wall temperature for R134a were relatively small, and for the first two rows, the values were higher than that of R407C. For R407C, the changes in the wall temperature in each row was small, though there was a progressive increase in the average values from first to the third row. In addition, as expected the *total heat flux and loads* on the air side will be the same as that on the refrigerant side presented earlier, because of evaluation from the energy balance.

Dry-bulb temperatures: Fig. 5.21 presented the inlet and outlet dry-bulb temperatures for each element/row along the coil. For both refrigerants, the counter-cross flow air at 21 °C entered the coil first meeting the third row. The drops in temperature across the third row were slightly larger for R134a. Subsequently, the inlet temperatures for the second row were also generally lower for R134a. However due to the compensated heat flux, the outlet temperature profiles of the second row for both refrigerants were very much the same; only small differences were noted at between nodes 11 and 18. For the first row, as expected the inlet air temperatures for both

refrigerants were the same. However, due to lower refrigerant temperatures, Fig 5.12, R407C produced lower outlet air temperatures by an average of about 1 °C. Moreover, the maximum variations of the air-off temperature over the coil surface for R407C and R134a were 0.95 °C and 1.11 °C respectively. Overall, the air experienced a larger temperature drop in the third row, and, naturally, the magnitudes of the reduction progressively decreased towards the coil outlet.

Figure 5.20 Wall temperatures vs nodes for dry coils

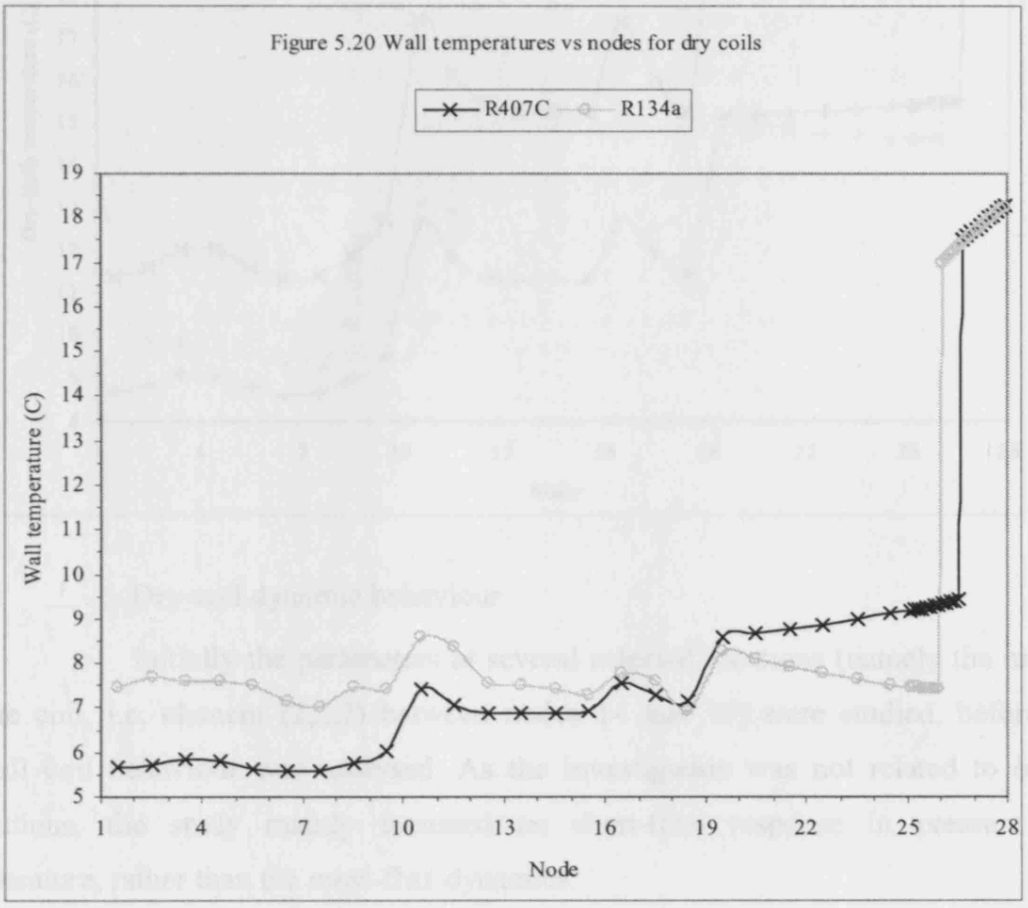

Figure 5.21 Dry-bulb temperatures vs nodes for dry coils

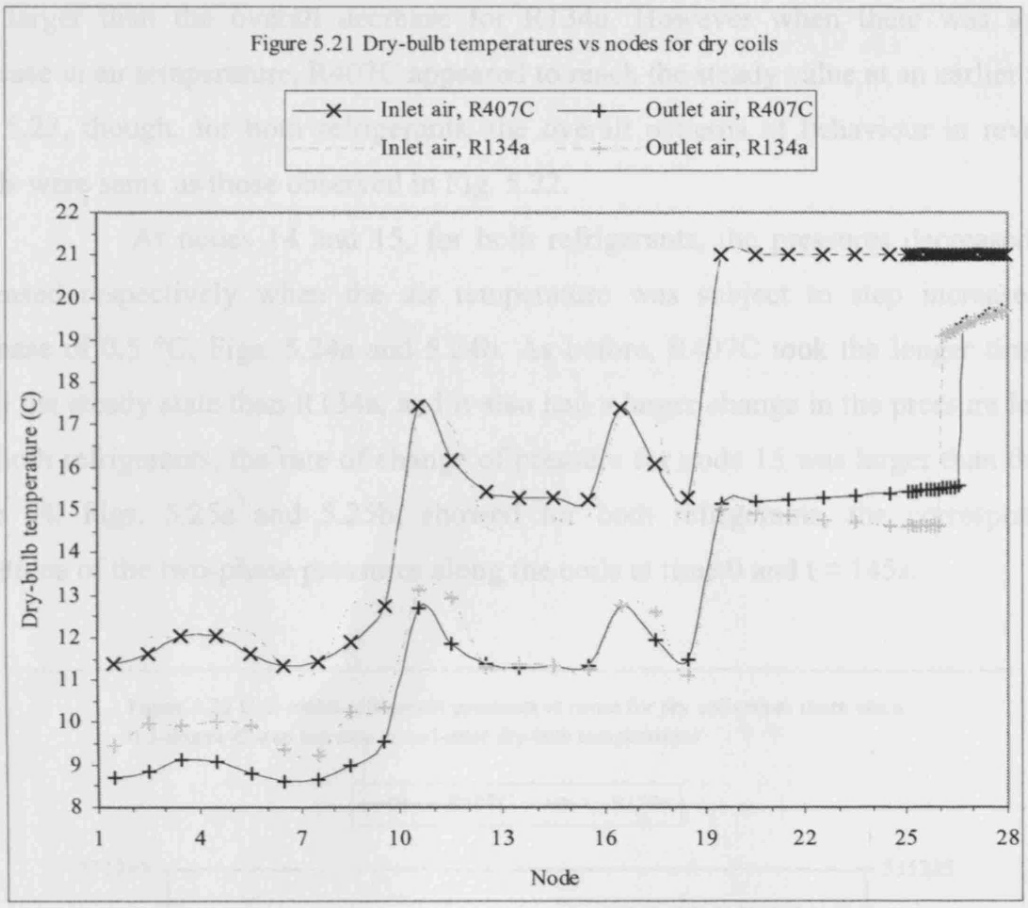

5.2.2 Dry-coil dynamic behaviour

Initially the parameters at several selected locations (namely the middle of the coil, i.e. element (2,2,2) between nodes 14 and 15) were studied, before the overall coil behaviour was analysed. As the investigation was not related to on-off operations, the study mainly focussed on short-time response in pressure and temperature, rather than the mass-flux dynamics.

a) Refrigerant-side performance

Refrigerant pressures and related parameters: For R407C, when subject to step increase of 0.5 °C in the coil-inlet dry-bulb temperature, Fig. 5.22, the coil-outlet pressure dropped slightly initially before increasing gradually reaching a steady state value at around 80 seconds. There were some minor fluctuations with time up to around 50s. On the other hand, for R134a, the outlet pressure dropped sharply to a minimum level within the first 20 seconds. The drop was accompanied by a relative large degree of fluctuations. The pressure then increased smoothly and reached a steady level earlier than that for R407C. The magnitude of the overall increase in the pressure for R407C

was larger than the overall decrease for R134a. However when there was a step decrease in air temperature, R407C appeared to reach the steady value at an earlier time, Fig. 5.23, though, for both refrigerants, the overall patterns of behaviour in reversed trends were same as those observed in Fig. 5.22.

At nodes 14 and 15, for both refrigerants, the pressures decreased and increased respectively when the air temperature was subject to step increase and decrease of 0.5 °C, Figs. 5.24a and 5.24b. As before, R407C took the longer times to reach the steady state than R134a, and it also had a larger change in the pressure levels. For both refrigerants, the rate of change of pressure for node 15 was larger than that of node 14. Figs. 5.25a and 5.25b, showed for both refrigerants, the corresponding variations of the two-phase pressures along the coils at time 0 and t = 145s.

Figure 5.22 Coil-outlet refrigerant pressures vs times for dry coils when there was a 0.5-degree-C step increase in coil-inlet dry-bulb temperatures

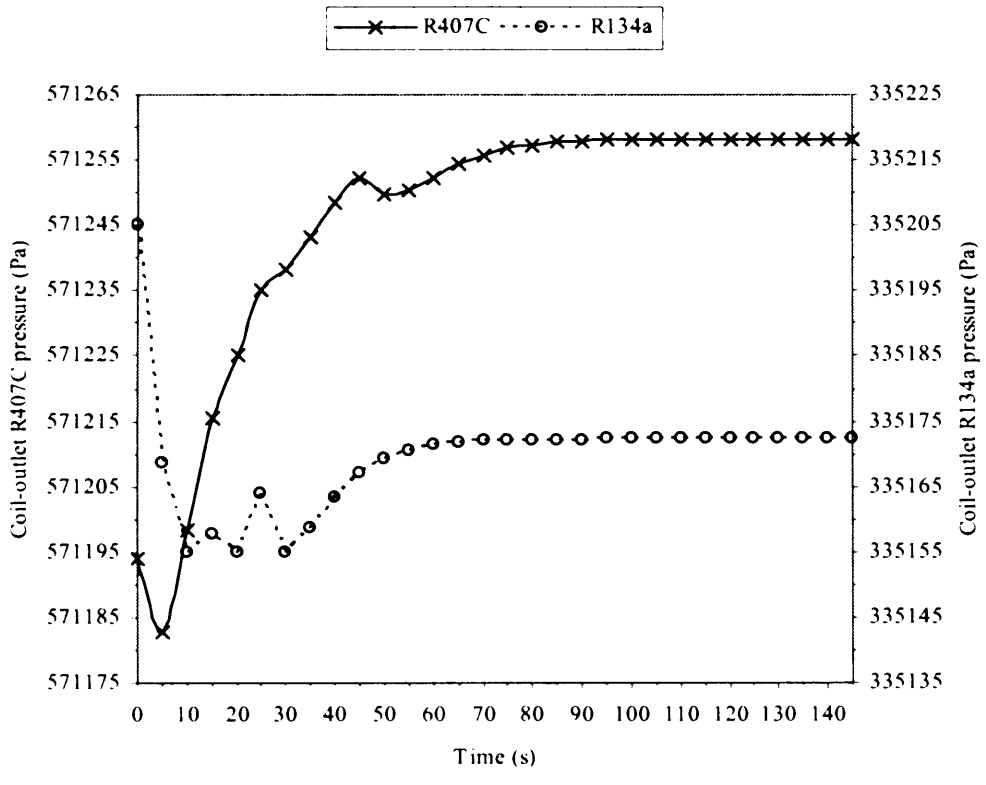

Figure 5.23 Coil-outlet refrigerant pressures vs times for dry coils when there was a 0.5-degree-C step decrease in coil-inlet dry-bulb temperatures

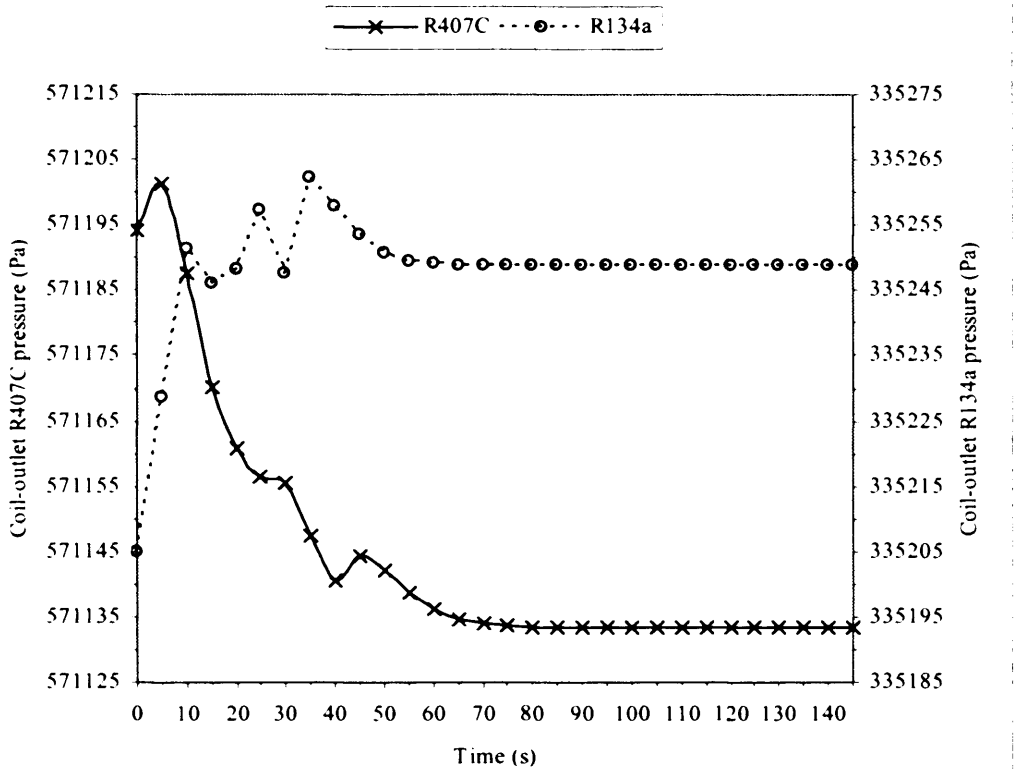

Figure 5.24a Refrigerant pressures at nodes 14 and 15 vs times for dry coils when there was a 0.5-degree-C step increase in coil-inlet dry-bulb temperatures

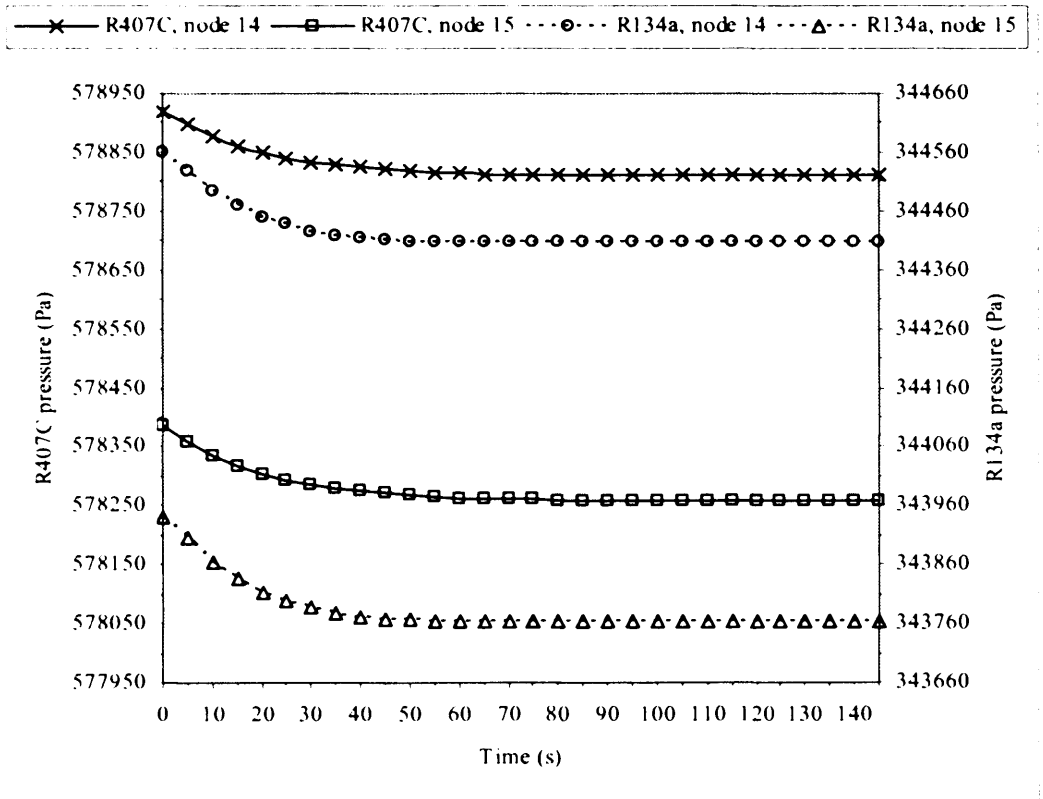

Figure 5.24b Refrigerant pressures at nodes 14 and 15 vs times for dry coils when there was a 0.5-degree-C step decrease in coil-inlet dry-bulb temperatures

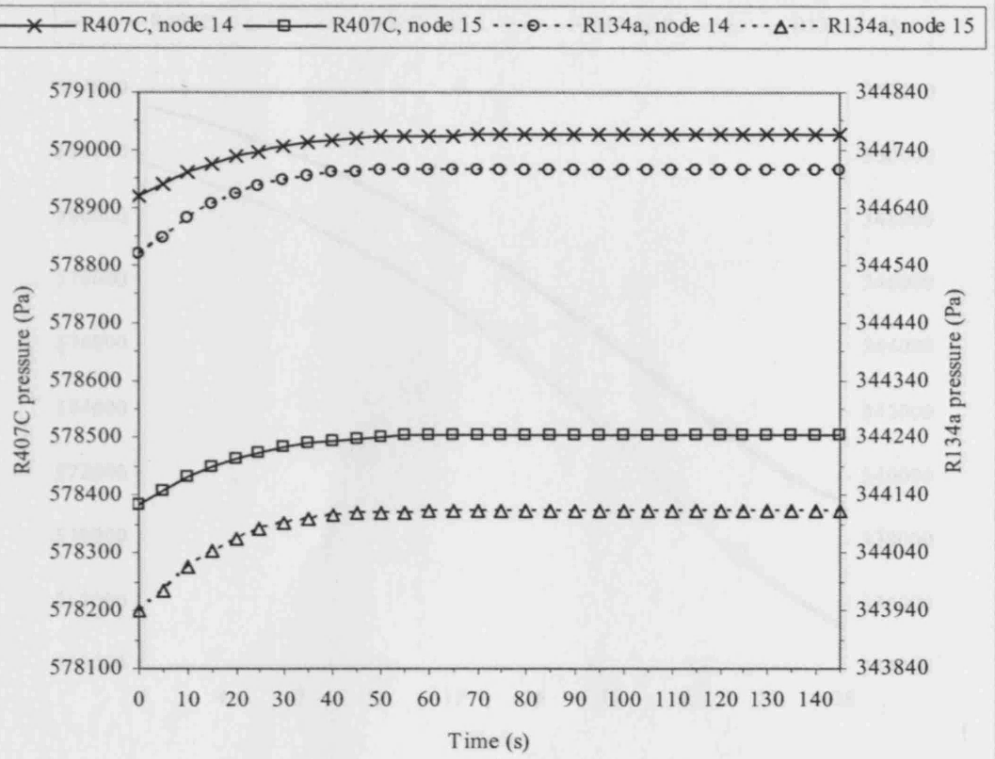

Figure 5.25a Refrigerant pressures vs nodes at 0 and 145 seconds for dry coils when there was a 0.5-degree-C step increase in coil-inlet dry-bulb temperatures

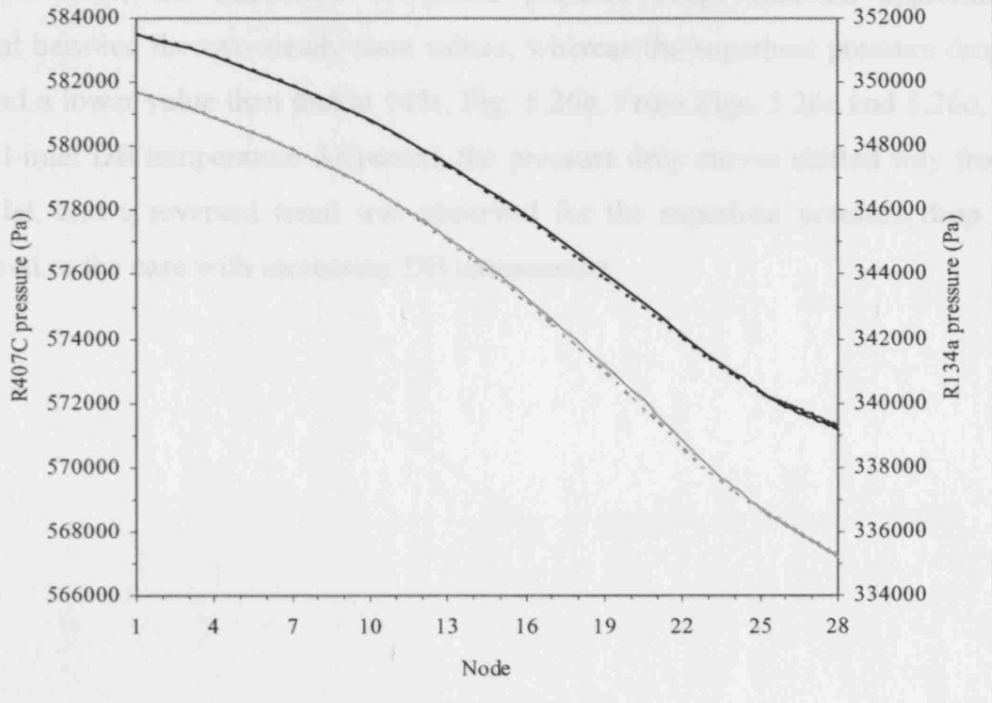

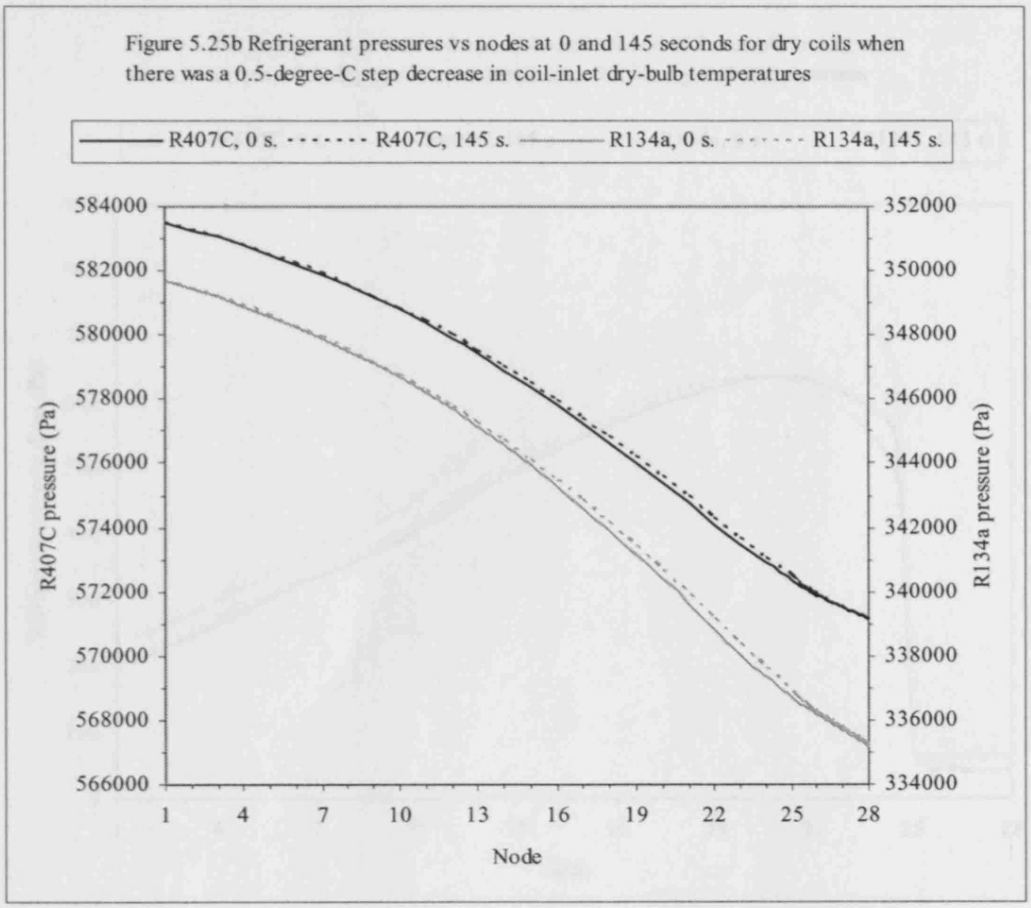

Figure 5.25b Refrigerant pressures vs nodes at 0 and 145 seconds for dry coils when there was a 0.5-degree-C step decrease in coil-inlet dry-bulb temperatures

From Fig. 5.26a, for both refrigerants, when the coil-inlet DB temperature increased, the pressure-drop curve shifted towards to the refrigerant coil inlet. However, the maximum two-phase pressure drop remained approximately constant between the two steady state values, whereas the superheat pressure drop at 0 time had a lower value than that at 145s, Fig. 5.26b. From Figs. 5.26c and 5.26d, when the coil-inlet DB temperature decreased, the pressure drop curves shifted way from the coil inlet, and a reversed trend was observed for the superheat pressure drop when compared to the case with increasing DB temperature.

Figure 5.26a Refrigerant pressure drops vs nodes at 0 and 145 seconds for dry coils when there was a 0.5-degree-C step increase in coil-inlet dry-bulb temperatures

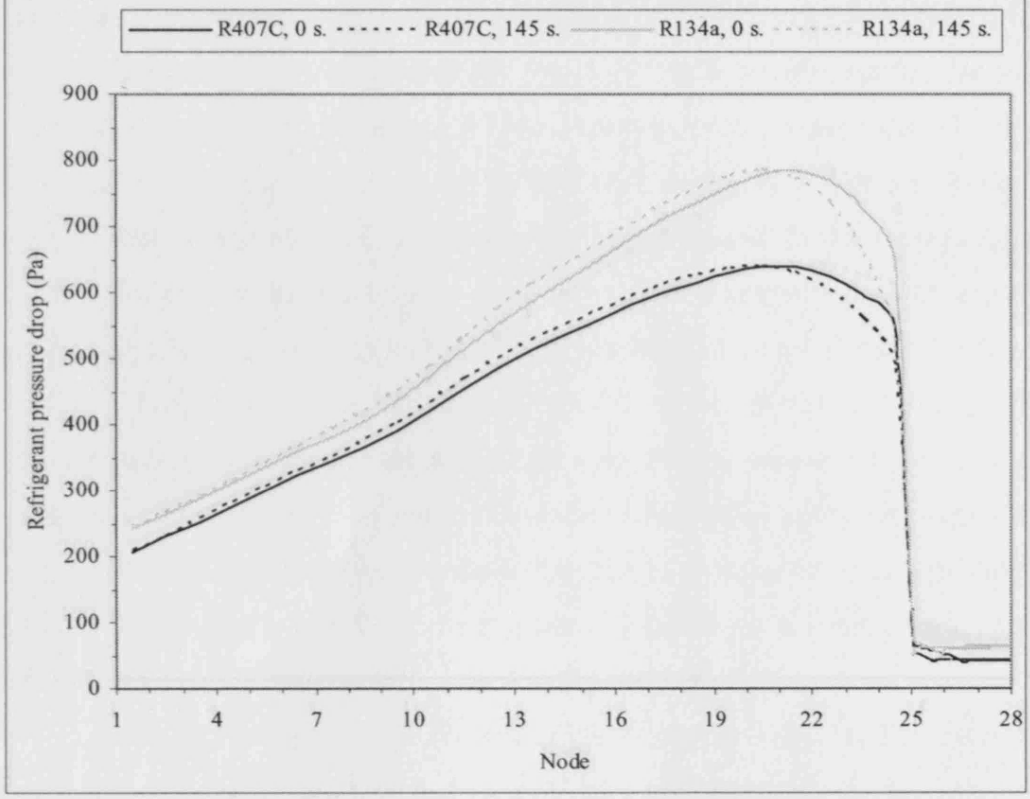

Figure 5.26b Refrigerant pressure drops vs nodes at seconds 0 and 145 for dry coils when there was a 0.5-degree-C step increase in coil-inlet dry-bulb temperatures

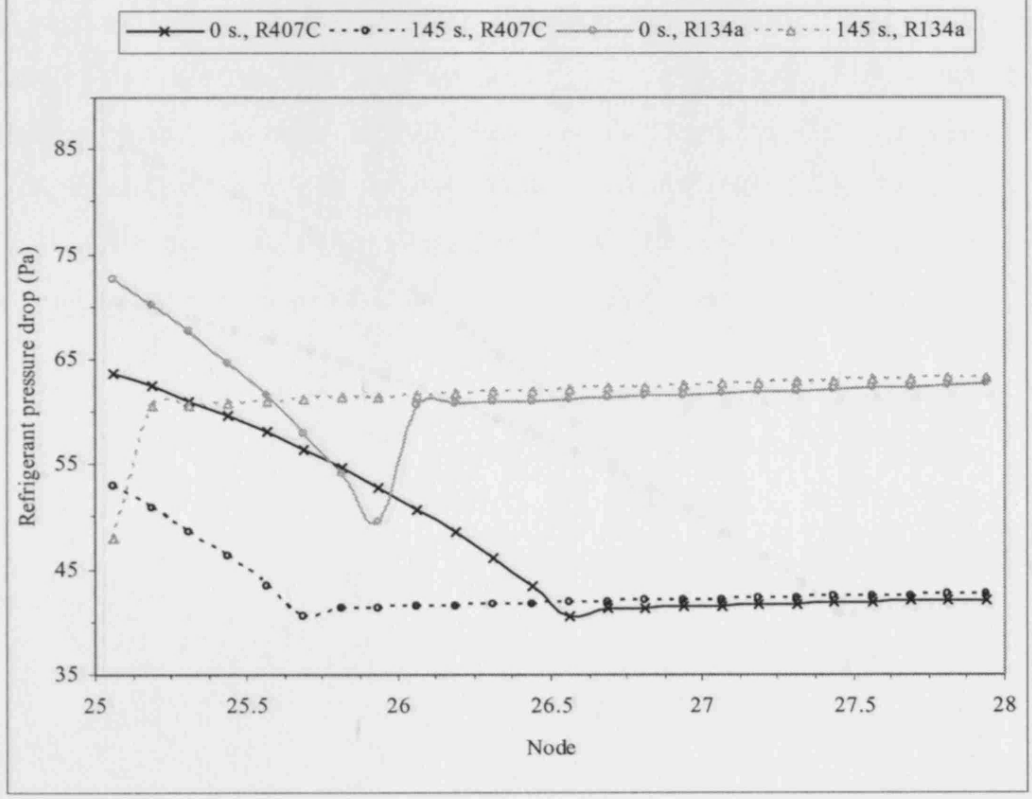

Figure 5.26c Refrigerant pressure drops vs nodes at 0 and 145 seconds for dry coils when there was a 0.5-degree-C step decrease in coil-inlet dry-bulb temperatures

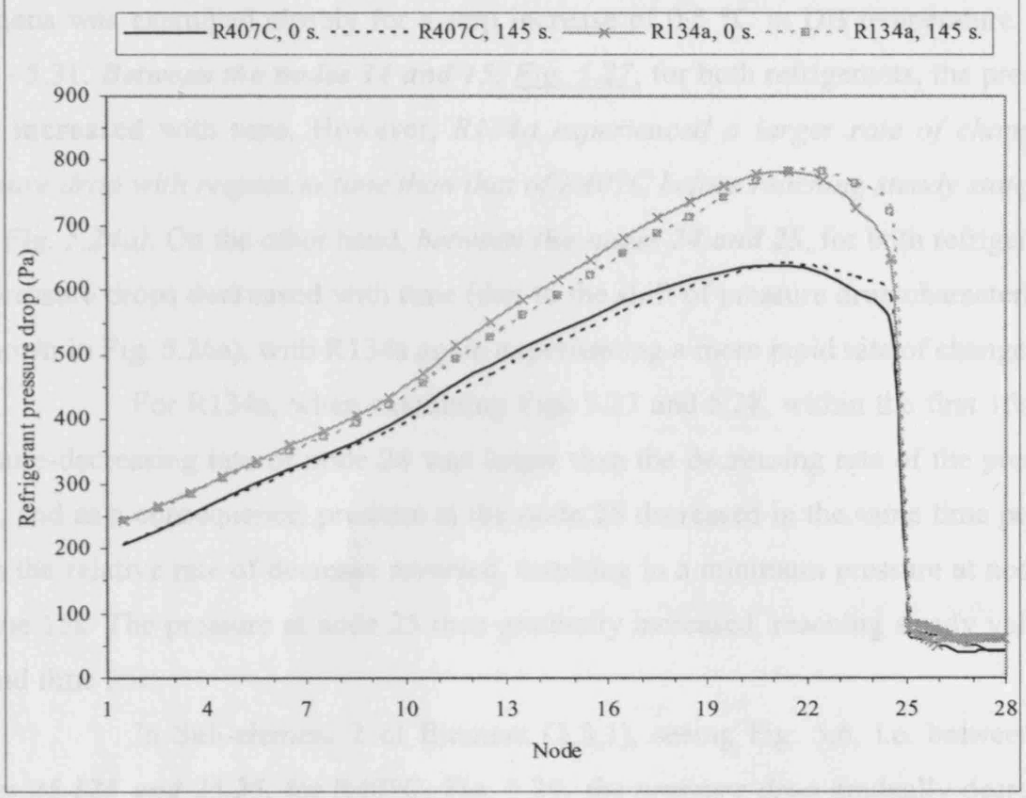

Figure 5.26d Refrigerant pressure drops vs nodes at seconds 0 and 145 for dry coils when there was a 0.5-degree-C step decrease in coil-inlet dry-bulb temperatures

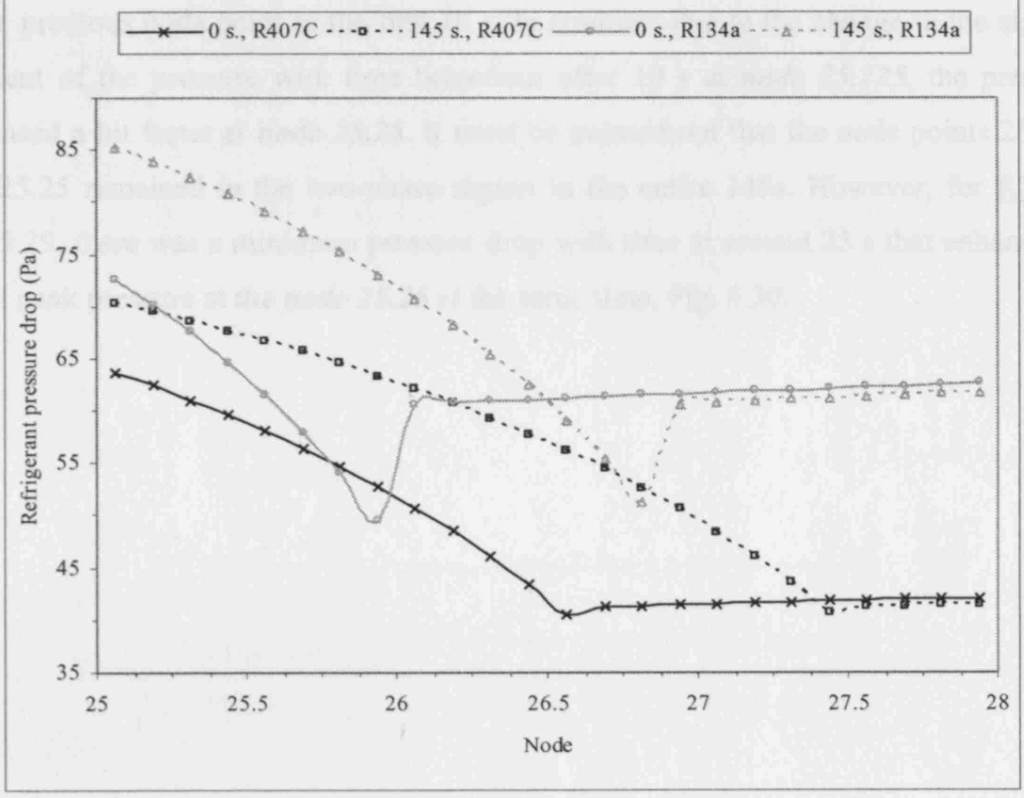

The dynamic development of pressure along the coil at several selected locations was examined closely for a step increase of 0.5 °C in DB temperature, Figs 5.27 - 5.31. ***Between the nodes 14 and 15***, *Fig. 5.27*, for both refrigerants, the pressure drop **increased** with time. However, *R134a experienced a larger rate of change of pressure drop with respect to time than that of R407C before reaching steady state (see also Fig. 5.24a)*. On the other hand, ***between the nodes 24 and 25***, for both refrigerants, the pressure drops **decreased** with time (due to the shift of pressure drop characteristics as shown in Fig. 5.26a), with R134a again experiencing a more rapid rate of change.

For R134a, when examining Figs 5.27 and 5.28, within the first 15s, the pressure-decreasing rate of node 24 was larger than the decreasing rate of the pressure drop, and as a consequence, pressure at the node 25 decreased in the same time period. Then the relative rate of decrease reversed, resulting in a minimum pressure at node 25 at time 15s. The pressure at node 25 then gradually increased, reaching steady value at around time 55s.

In Sub-element 2 of Element (3,3,1), seeing Fig. 5.6, i.e. between ***the nodes 25.125 and 25.25***, for R407C, Fig. 5.29, *the pressure drop* gradually decreased with time (see also Fig. 5.26b). When combining with the decreasing pressure with time at ***node 25.125***, Fig. 5.30, the rate of change of pressure at ***node 25.25*** was less than that at the previous node point in the first 10 s. In contrast, due to the change in the sign of gradient of the pressure with time behaviour after 10 s at ***node 25.125***, the pressure increased a bit faster at ***node 25.25***. It must be pointed out that the node points 25.125 and 25.25 remained in the two-phase region in the entire 145s. However, for R134a, Fig. 5.29, there was a minimum pressure drop with time at around 25 s that enhanced a small peak pressure at ***the node 25.25*** at the same time, Fig. 5.30.

Figure 5.27 Refrigerant pressure drops vs times at various elements for dry coils when there was a 0.5-degree-C increase in dry-bulb temperatures

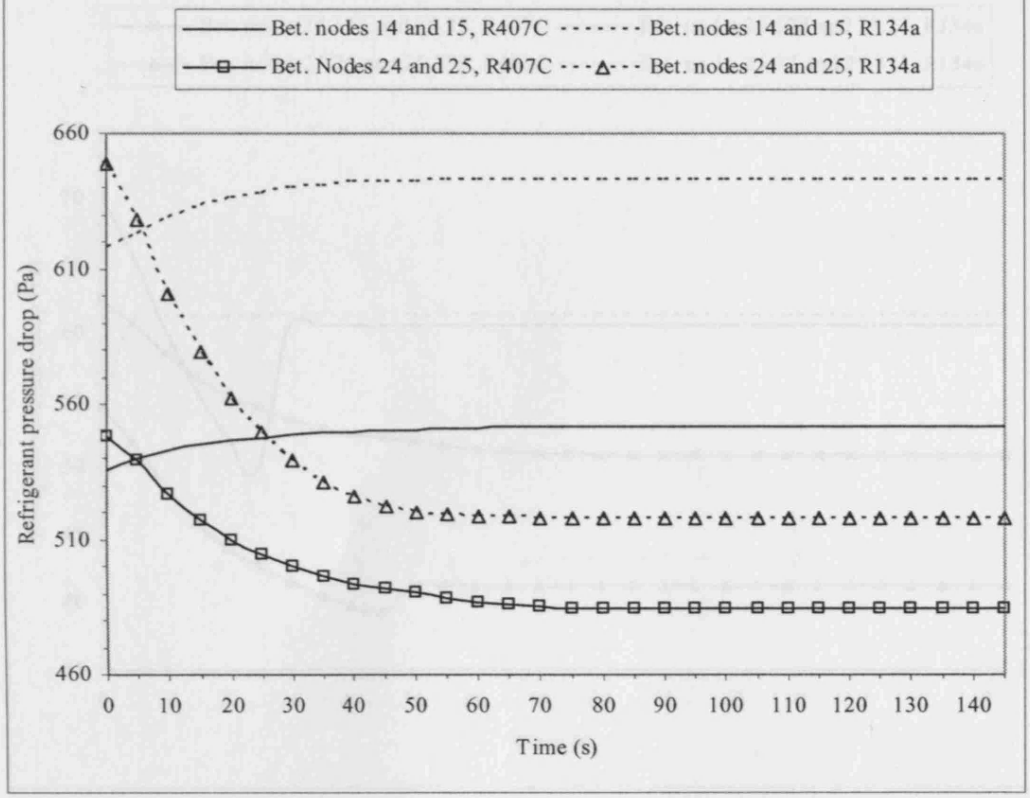

Figure 5.28 Refrigerant pressures vs times at nodes 24 and 25 for dry coils when there was a 0.5-degree-C step increase in coil-inlet dry-bulb temperature

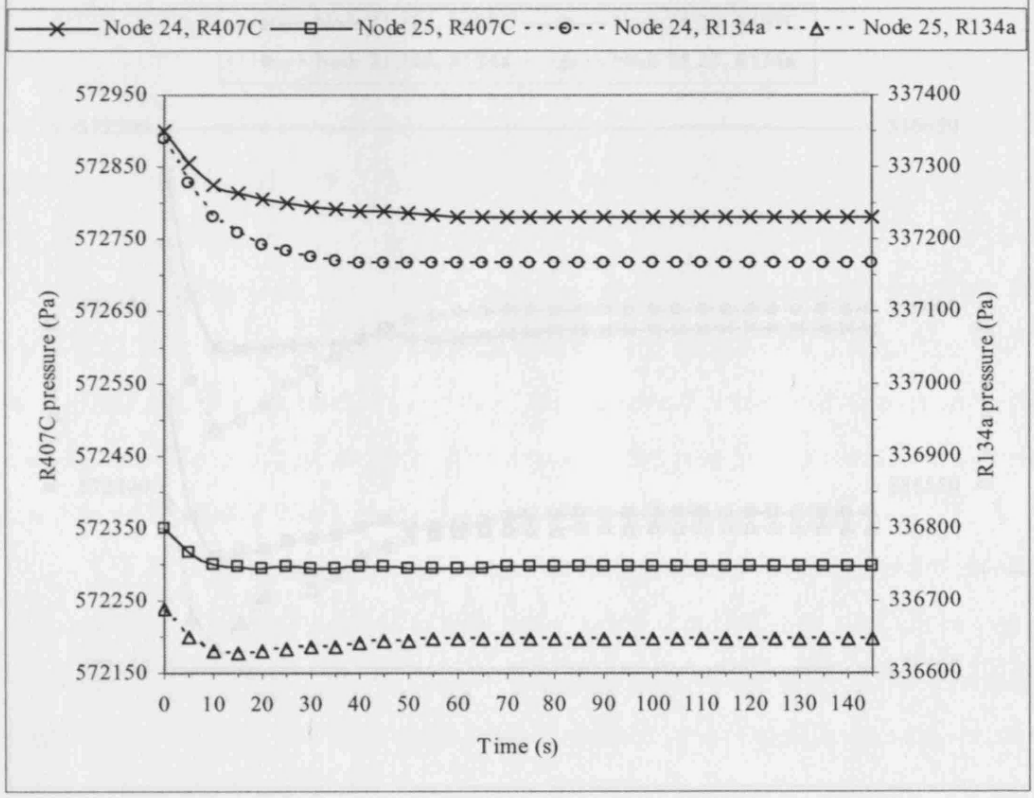

Figure 5.29 Refrigerant pressure drops vs times at various subelements for dry coils when there was a 0.5-degree-C increase in coil-inlet dry-bulb temperatures

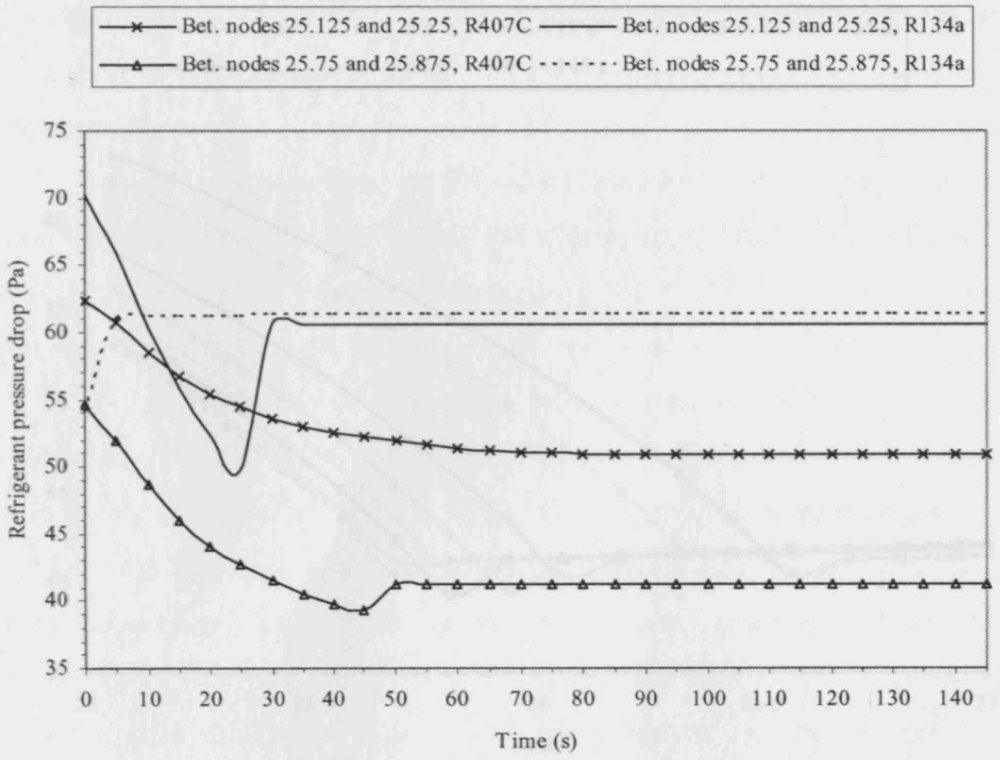

Figure 5.30 Refrigerant pressures vs times at nodes 25.125 and 25.25 for dry coils when there was a 0.5-degree-C step increase in coil-inlet dry-bulb temperatures

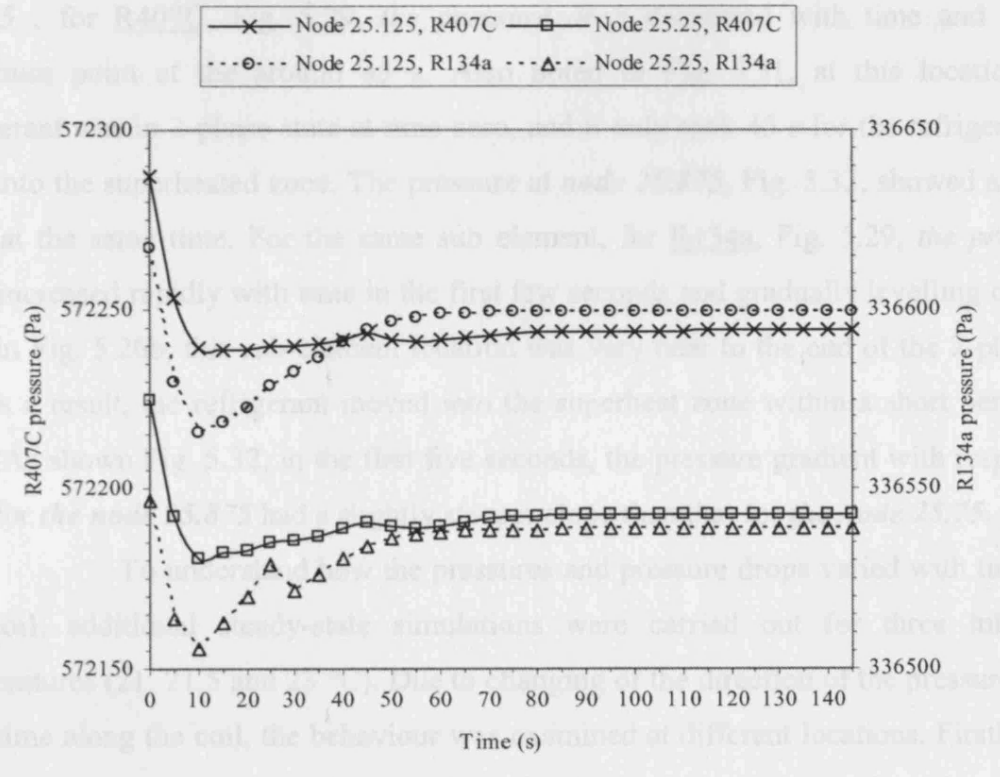

Figure 5.31 R407C pressure drops vs nodes at various times for dry coils when there was a 0.5-degree-C step increase in coil-inlet dry-bulb temperatures

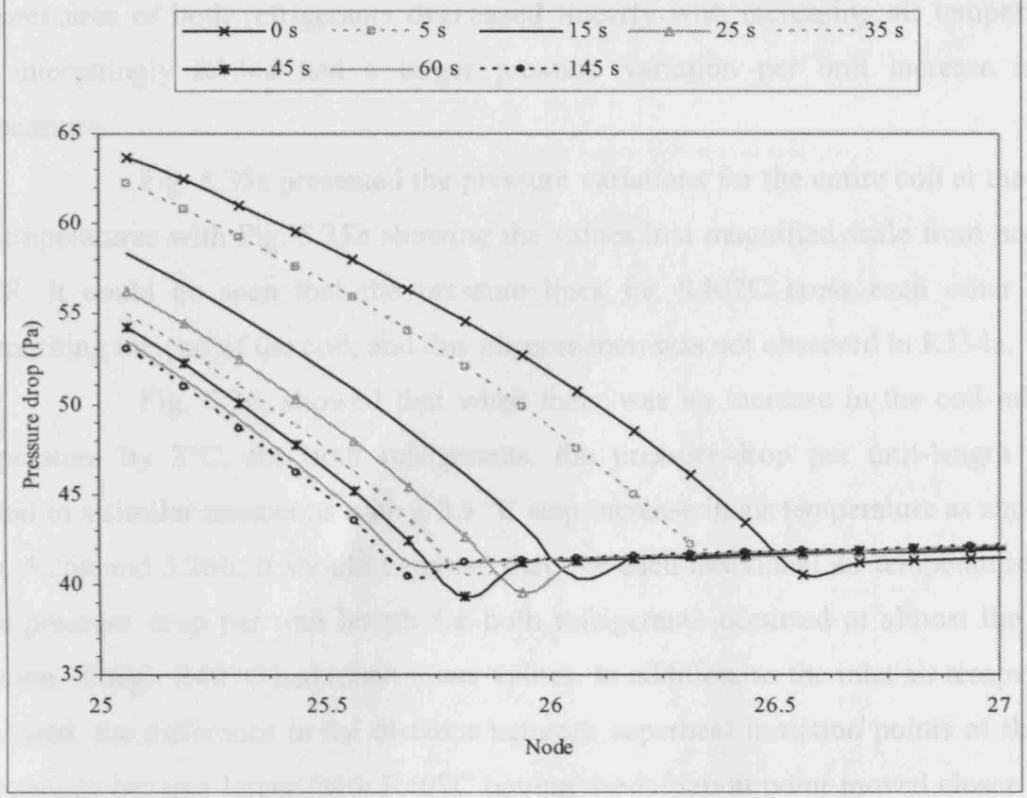

In Sub-element 7 of Element (3,3,1), being between ***the nodes 25.75 and 25.875*** , for R407C, Fig. 5.29, *the pressure drop* decreased with time and had a minimum point at the around 45 s. Also noted in Fig. 5.31, at this location the refrigerant was in 2-phase state at time zero, and it only took 45 s for the refrigerant to shift into the superheated zone. The pressure at ***node 25.875***, Fig. 5.32, showed a small peak at the same time. For the same sub element, for R134a, Fig. 5.29, *the pressure drop* increased rapidly with time in the first few seconds and gradually levelling off. As seen in Fig. 5.26b, this sub-element location was very near to the end of the 2-ph zone and as a result, the refrigerant moved into the superheat zone within a short period of time. As shown Fig. 5.32, in the first five seconds, the pressure gradient with respect to time for ***the node 25.875*** had a slightly steeper slope than that for ***the node 25.75.***

To understand how the pressures and pressure drops varied with times in the coil, additional steady-state simulations were carried out for three inlet air temperatures (21, 21.5 and 23 °C). Due to changing of the direction of the pressure drop with time along the coil, the behaviour was examined at different locations. Firstly, Fig 5.33 shows that the *coil-outlet* pressure of R407C increased linearly, whereas for

R134a, the pressure decreased linearly, and R407C had a larger change in the pressure with respect to the change in the air temperature. *However*, at the node 15 (Fig. 5.34), the pressures of both refrigerants **decreased** linearly with increasing air temperature, and interestingly R134a had a larger pressure variation per unit increase in the temperature.

Fig. 5.35a presented the pressure variations for the entire coil at the three air temperatures with Fig. 5.35b showing the values in a magnified scale from node 22 to 28. It could be seen that the pressure lines for R407C cross each other when approaching the end of the coil, and this phenomenon was not observed in R134a.

Fig. 5.36, showed that when there was an increase in the coil-inlet air temperature by 2°C, for both refrigerants, the pressure-drop per unit-length curve shifted in a similar manner as with a 0.5 °C step increase in air temperature as shown in Figs. 5.26a and 5.26b. It should be noted that, for each individual air temperatures, the peak pressure drop per unit length for both refrigerants occurred at almost the same location, though R407C had much lower values. In addition, as the inlet air temperature increased, the difference in the distance between superheat initiation points of the two refrigerants became larger, with R407C having the initiation point moved closer to the end of the coil. It was also noted that, in both the two-phase and superheat regions, at either an element or a sub-element level, R407C had a smaller sensitivity in the change of pressure drop per unit length to the change in the coil-inlet air temperatures when compared to that of R134a.

Figure 5.32 Refrigerant pressures vs times at nodes 25.75 and 25.875 for dry coils when there was a 0.5-degree-C increase in coil-inlet dry-bulb temperatures

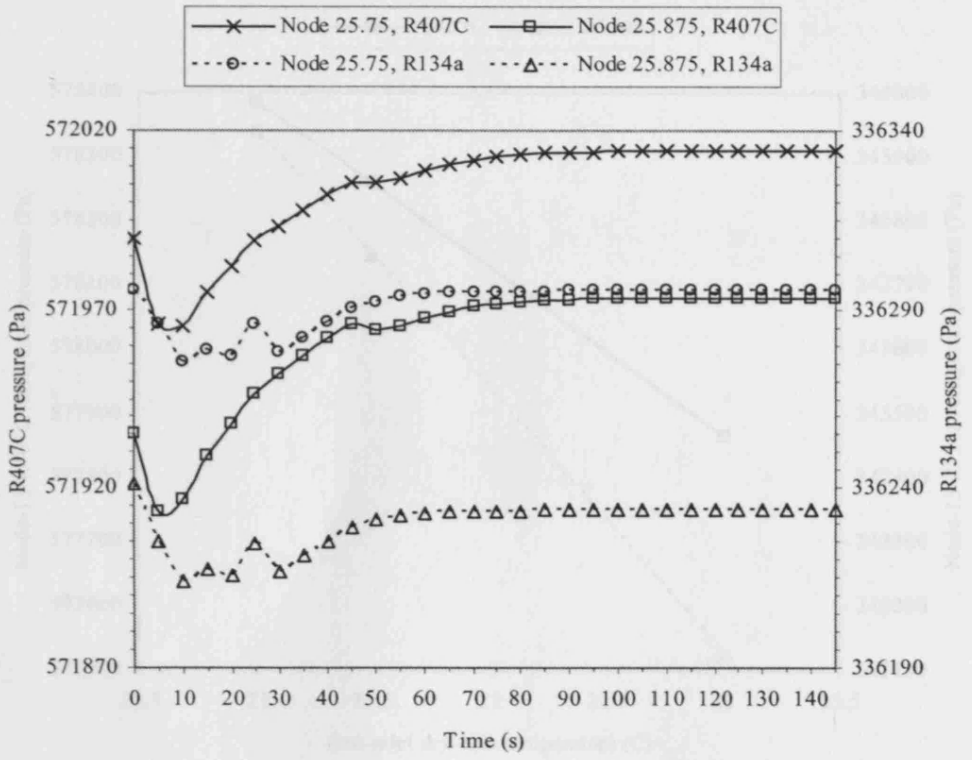

Figure 5.33 Coil-outlet refrigerant pressures vs various coil-inlet dry-bulb temperatures for dry coils

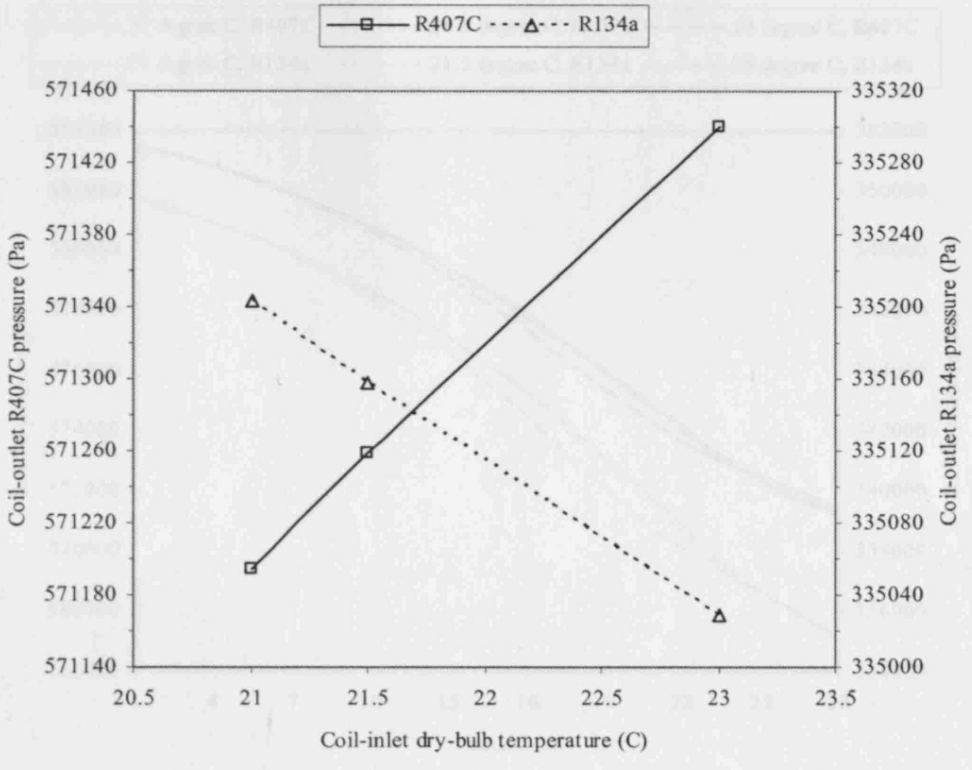

Figure 5.34 Node-15 refrigerant pressures vs various coil-inlet dry-bulb temperatures for dry coils

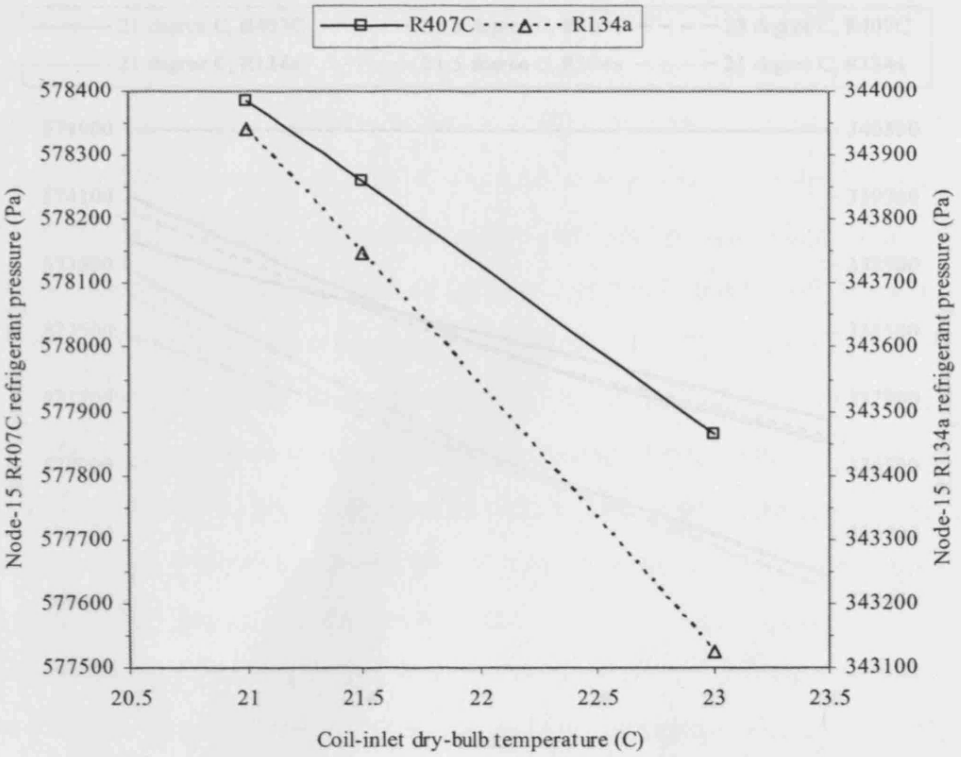

Figure 5.35a Refrigerant pressures vs node for various coil-inlet dry-bulb temperatures for dry coils

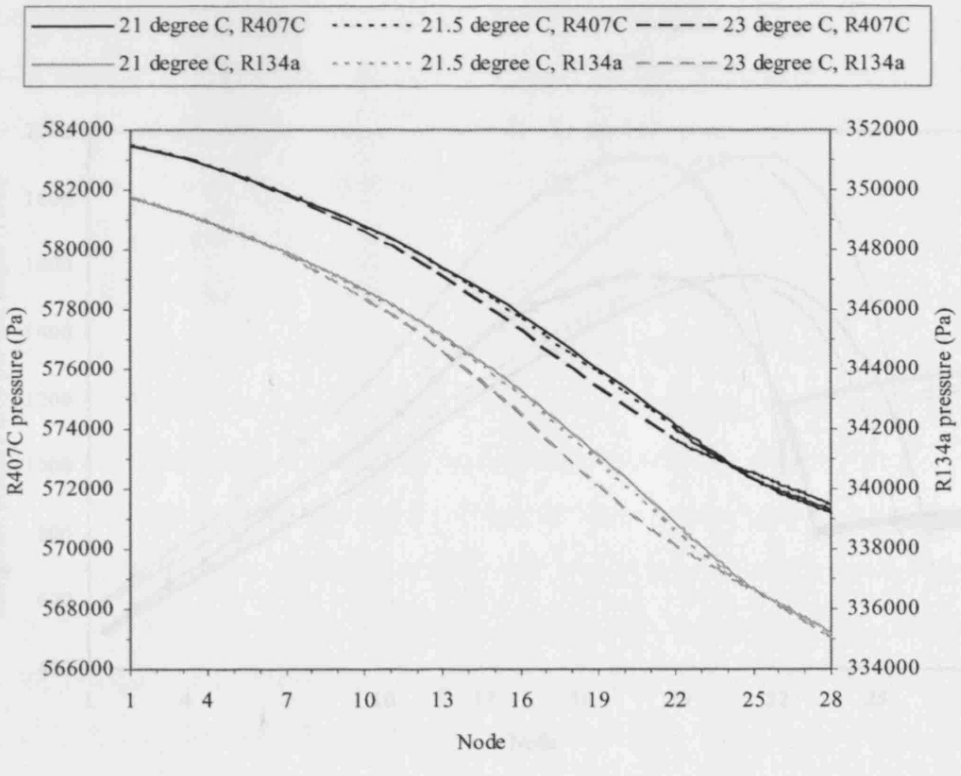

Figure 5.35b Refrigerant pressures vs nodes for various coil-inlet dry-bulb temperatures for dry coils

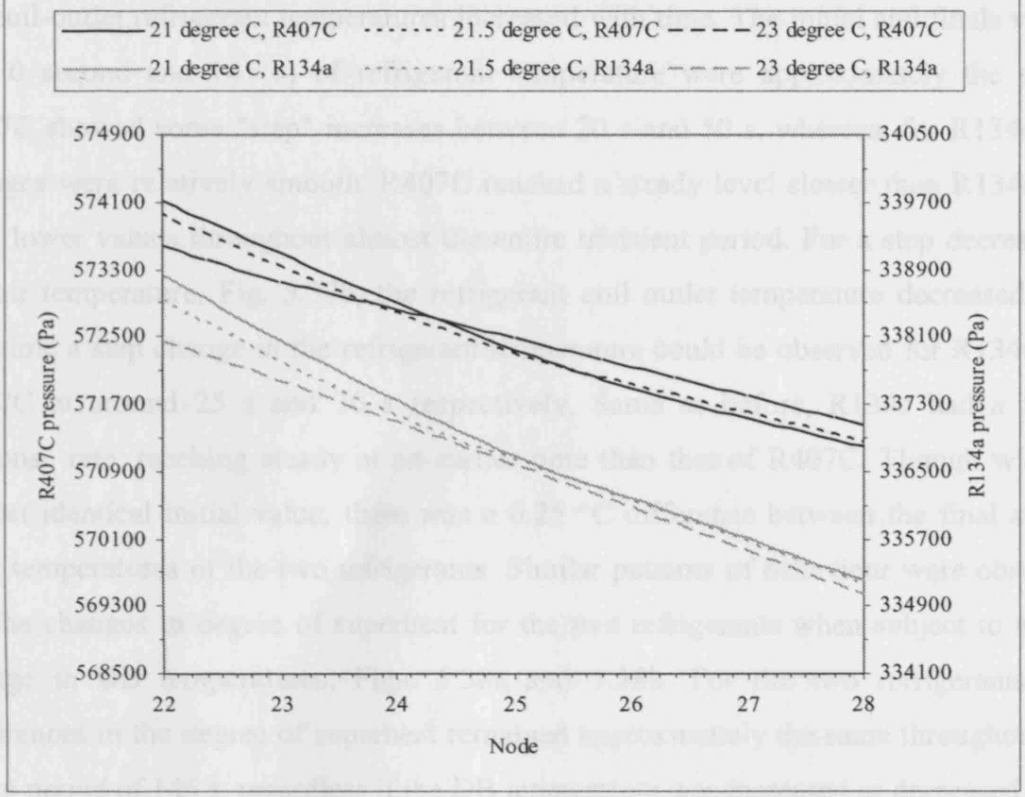

Figure 5.36 Refrigerant pressure drops per unit length vs nodes for various coil-inlet dry-out temperatures for dry coils

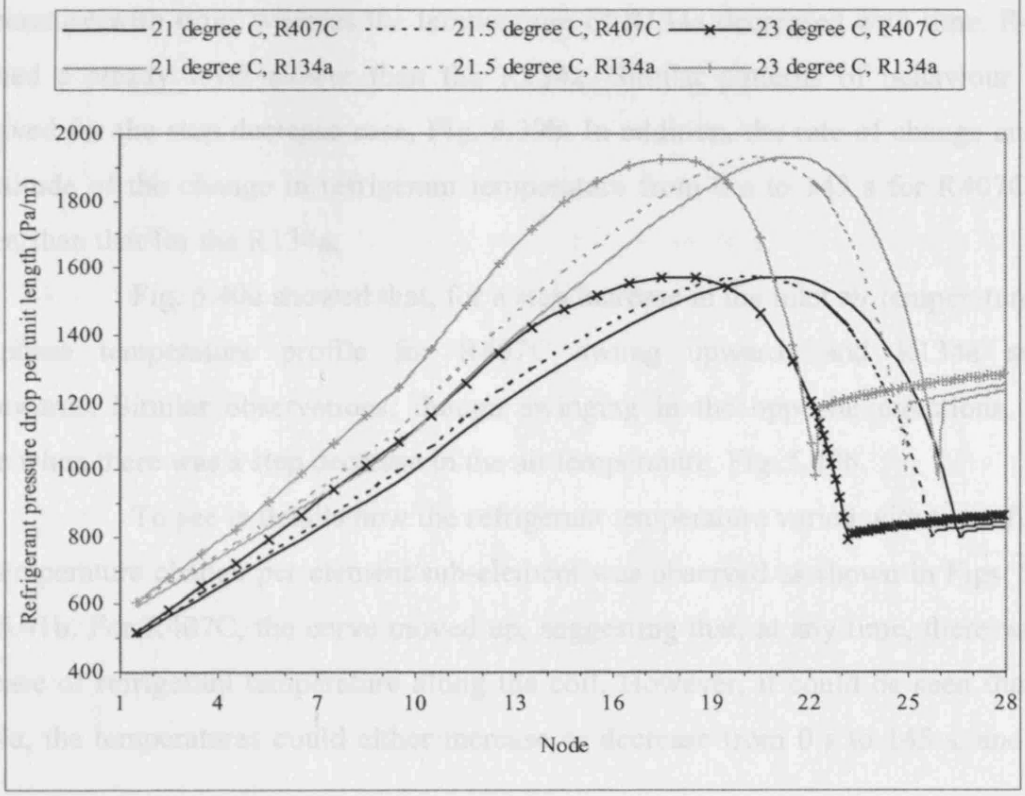

Refrigerant temperatures and related parameters: When there was a step increase in the inlet air temperature (by 0.5 °C), Fig. 5.37a, for both refrigerants, the coil-outlet refrigerant temperatures increased with time. The initial and finals values (i.e. 0 second and 145 s) of refrigerant temperature were approximately the same. R407C showed some "step" increases between 20 s and 50 s, whereas, for R134a, the changes were relatively smooth. R407C reached a steady level slower than R134a and with lower values throughout almost the entire transient period. For a step decrease in the air temperature, Fig. 5.37b, the refrigerant coil outlet temperature decreased, and this time a step change in the refrigerant temperature could be observed for R134a and R407C at around 25 s and 30 s respectively. Same as before, R134a had a faster response rate, reaching steady at an earlier time than that of R407C. Though with an almost identical initial value, there was a 0.25 °C difference between the final steady state temperatures of the two refrigerants. Similar patterns of behaviour were observed for the changes in degree of superheat for the two refrigerants when subject to a step change in DB temperatures, Figs. 5.38a and 5.38b. For the two refrigerants, the differences in the degree of superheat remained approximately the same throughout the entire period of 145 s, regardless if the DB temperature was increased or decreased.

For the two-phase region at the nodes 14 and 15, when there was a step increase in the air temperature, Fig. 5.39a, R407C showed a graduate increase in temperature with time, whereas the temperature of R134a decreased with time. R407C reached a steady level slower than the R134a. Similar patterns of behaviour were observed for the step decrease case, Fig. 5.39b. In addition, the rate of change and the magnitude of the change in refrigerant temperature from 0 s to 145 s for R407C was larger, than that for the R134a.

Fig. 5.40a showed that, for a step increase in the inlet air temperature, the two-phase temperature profile for R407C swung upwards and R134a swung downwards. Similar observations, though swinging in the opposite directions, were made when there was a step decrease in the air temperature, Fig. 5.40b.

To see in details how the refrigerant temperature varied with time, firstly, the temperature change per element/sub-element was observed as shown in Figs. 5.41a and 5.41b. For R407C, the curve moved up, suggesting that, at any time, there was an increase of refrigerant temperature along the coil. However, it could be seen that, for R134a, the temperatures could either increase or decrease from 0 s to 145 s, and they

were in the negative range, Fig. 5.41b. For 134a, for a large part of the coil, the 145 s curve was lower than that of 0 s curve

From Fig. 5.42, for the element (2,2,2), being between nodes 14 and 15, in the 2-phase region, the temperature change of R407C increased with time up to the steady-state at around 65 s, with a sharp rise in the first 15 s, resulting in the two temperature profiles with different gradients shown in Fig. 5.39a. On the other hand, there was a temperature change in opposite direction for R134a though with the *magnitude* of the changes increased with time, and it reached the steady value faster than that of R407C. The difference between the changes at 0 s and 145 s for R407C was two times more than that for R134a.

Between the nodes 24 and 25, still within the 2-phase region, Fig. 5.43, for both the refrigerants, the temperature change per element increased with time. However, for R407C, there was a rapid increase in the first 20 s, reaching the steady-state at around 70 s. However, for R134a, there was a sharp increase (though in opposition direction) within the first 40 s, reaching steady value at about 60 s; however the *magnitude* of the temperature change was decreasing with time. At this location, interestingly, the difference between the magnitudes at 0 s and 145 s for R407C was about a half of that for R134a. From Fig. 5.44, for R407C, the rate of change of temperature at node 25 for the first 20 s was clearly higher than that at node 24. The observations made in Fig. 5.43, for R134a, offered an explanation as why the temperature at node 24 decreased with time, whereas that at node 25 decreased slightly initially and remained fairly constant for the rest of the time.

The simulation showed that between nodes 25.125 and 25.25, i.e. at Sub-element 2 of Element (3,3,1), R407C remained as *two-phase* flow from 0 s to 145 s (Fig. 5.41a), and its behaviour was similar to that observed at other two-phase locations described previously (Fig. 5.39a and 5.42 to 5.44). When compared to R407C, the temperature change of R134a, Fig. 5.45, was in the opposite direction with decreasing of the magnitude of change in the first 25 seconds. The refrigerant (R134a) then became single phase and the magnitude of the temperature change increased rapidly before reaching steady value at around 60 s; the corresponding variations in temperature with time at that location were shown in Fig. 5.46, showing a substantial jump in temperature at 30 s.

Refrigerant heat transfer coefficients: For the 2-phase section, when subject to a step increase in the inlet air temperature, Fig. 5.47, for both the refrigerants,

at the nodes 14 and 15, being respectively the inlet and outlet of the Element (2,2,2), the HTCs increased gradually with time. However R407C had a slower rate of change than R134a, also reaching the steady-state level at a later time of around 70 s. For *almost* every node, except at some nodes in the first two tubes of the first row, the magnitude of the change in HTC from 0 s to 145 s for R407C was smaller than that for R134a, Fig. 5.48. Similar opposite trends were observed for a step decrease in the air temperature.

Refrigerant specific volumes: For the transient responses, the specific refrigerant volumes at the coil outlet (Figs. 5.49a and 5.49b) behaved similarly to that of the outlet refrigerant temperature (Figs. 5.37a and 5.37b). However, R407C had a smaller magnitude of change than R134a (Fig. 5.49a), whereas the changes in the outlet refrigerant temperatures were approximately the same when subject to an increase in air temperature (Fig. 5.37a). When examining Fig. 5.49b and Fig. 5.37b, however, for a step decrease in the air temperature, R407C had smaller magnitudes of change for both parameters.

As shown in Fig. 5.50, at nodes 14 and 15, the 2-phase specific volume of R407C changed slower than that of R134a when there was a step increase in the inlet air temperature; a similar observation was made at the coil outlet. However, it was contrary to the observations made for the transient behaviour of the refrigerant temperatures at the same locations (Fig. 5.39a), in which a faster response for R407C was noted. The overall magnitude of change at each node, from 0 s to 145 s, for R407C was about half of that for R134a.

Similar trends were noted for the time variations of the vapour quality, Fig. 5.51. For the vapour quality, the description was similar to that for the 2-phase specific volume, except for having slight differences between both refrigerants for the magnitude of change from 0 s to steady-state.

Figure 5.37a Coil-outlet refrigerant temperatures vs times for dry coils when there was a 0.5-degree-C increase in dry-bulb temperatures

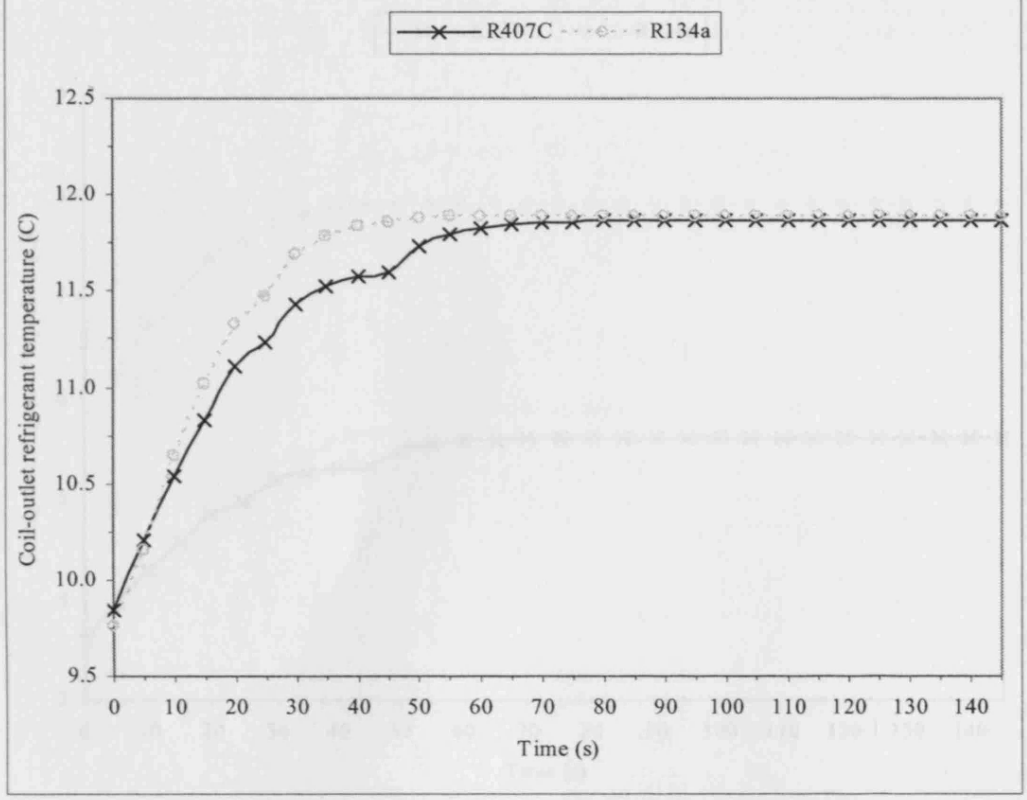

Figure 5.37b Coil-outlet refrigerant temperatures vs times for dry coils when there was a 0.5-degree-C decrease in dry-bulb temperatures

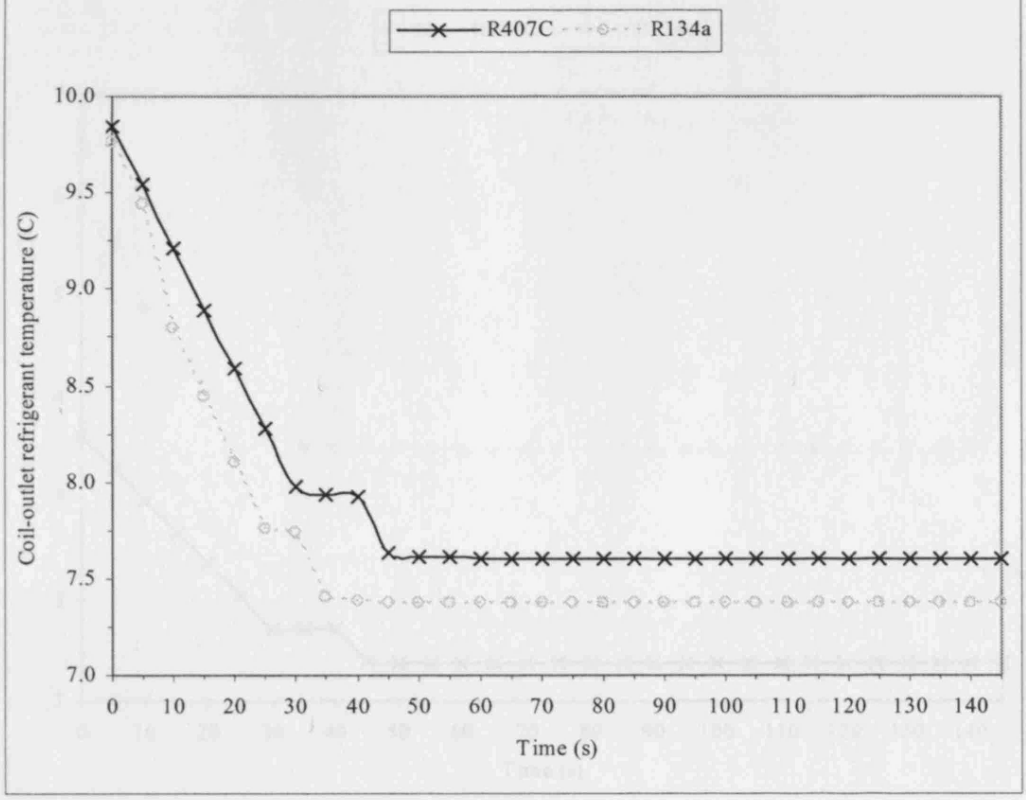

Figure 5.38a Refrigerant degrees of superheat vs times for dry coils when dry-bulb temperatures increased in dynamic modes

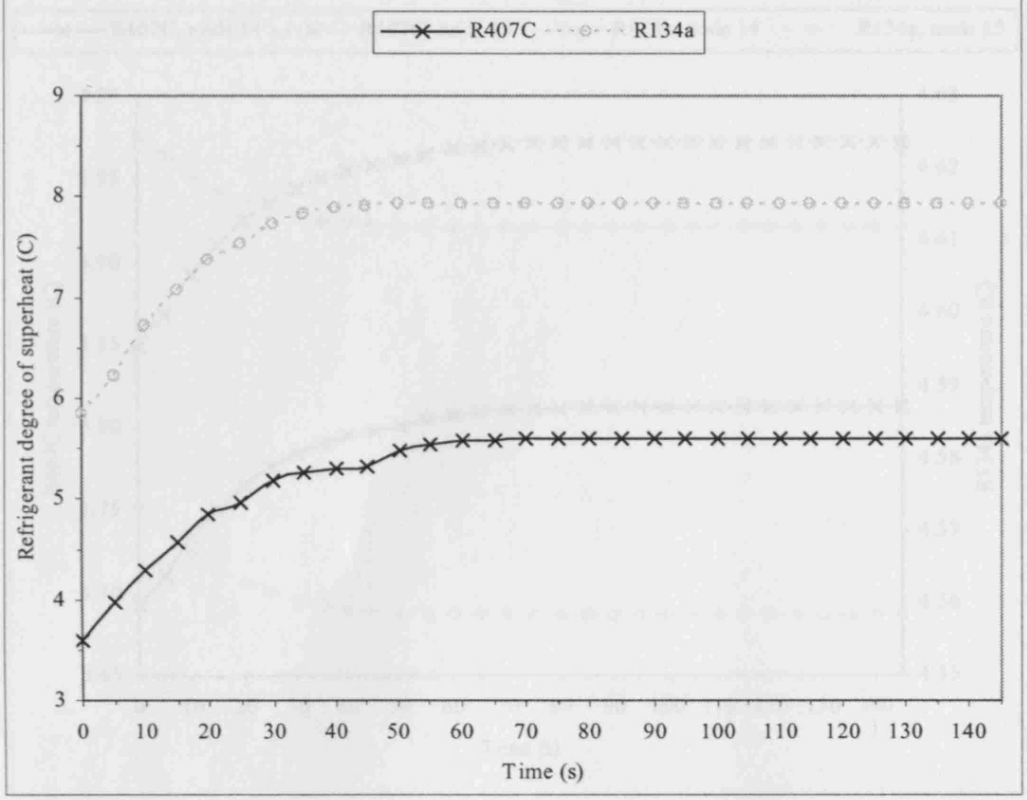

Figure 5.38b Refrigerant degrees of superheat vs times for dry coils when dry-bulb temperatures decreased in dynamic modes

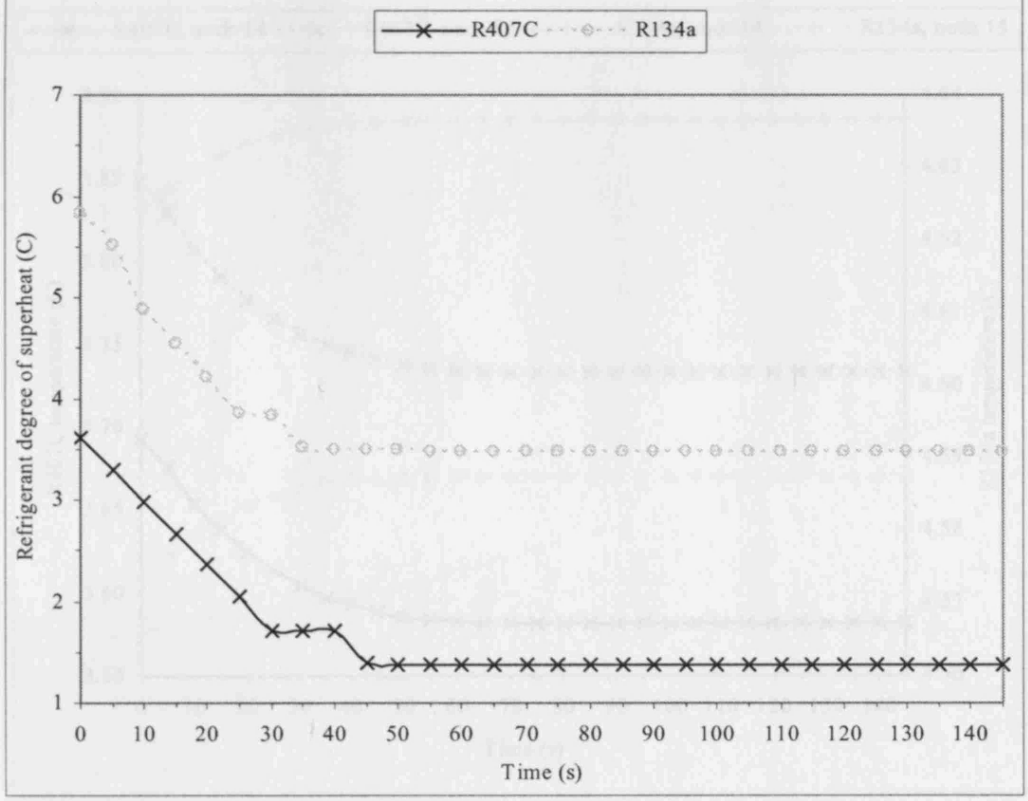

Figure 5.39a Refrigerant temperatures at nodes 14 and 15 vs times for dry coils when there was a 0.5-degree-C increase in dry-bulb temperatures

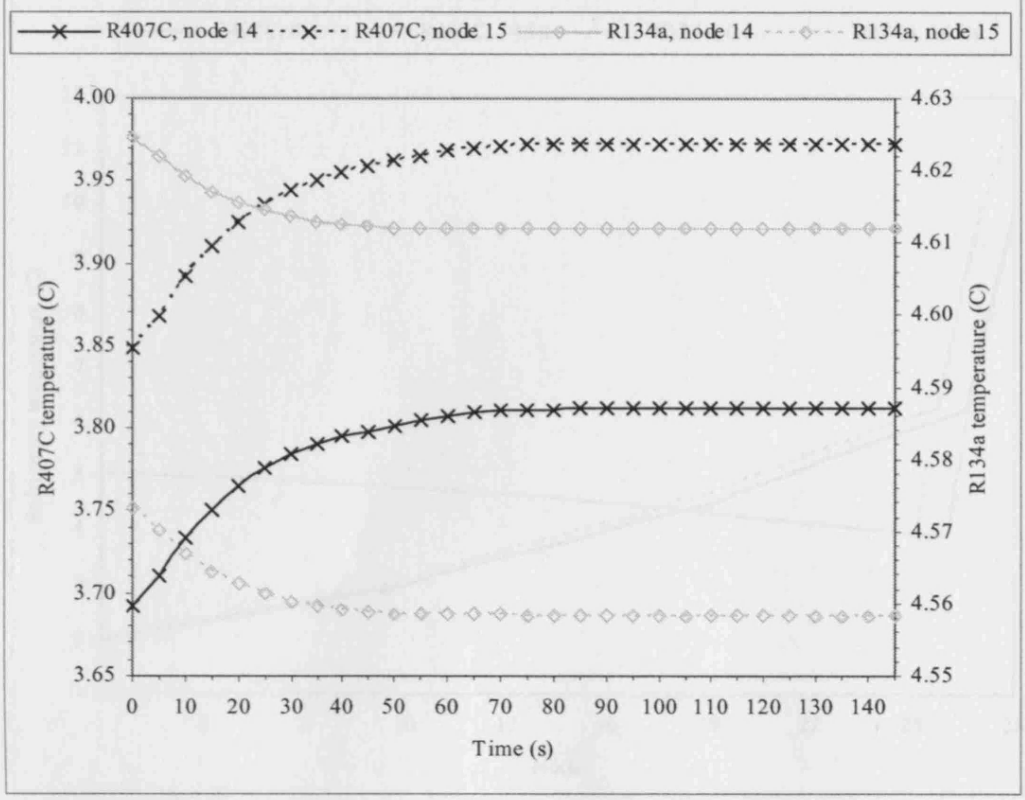

Figure 5.39b Refrigerant temperatures at nodes 14 and 15 vs times for dry coils when there was a 0.5-degree-C decrease in dry-bulb temperatures

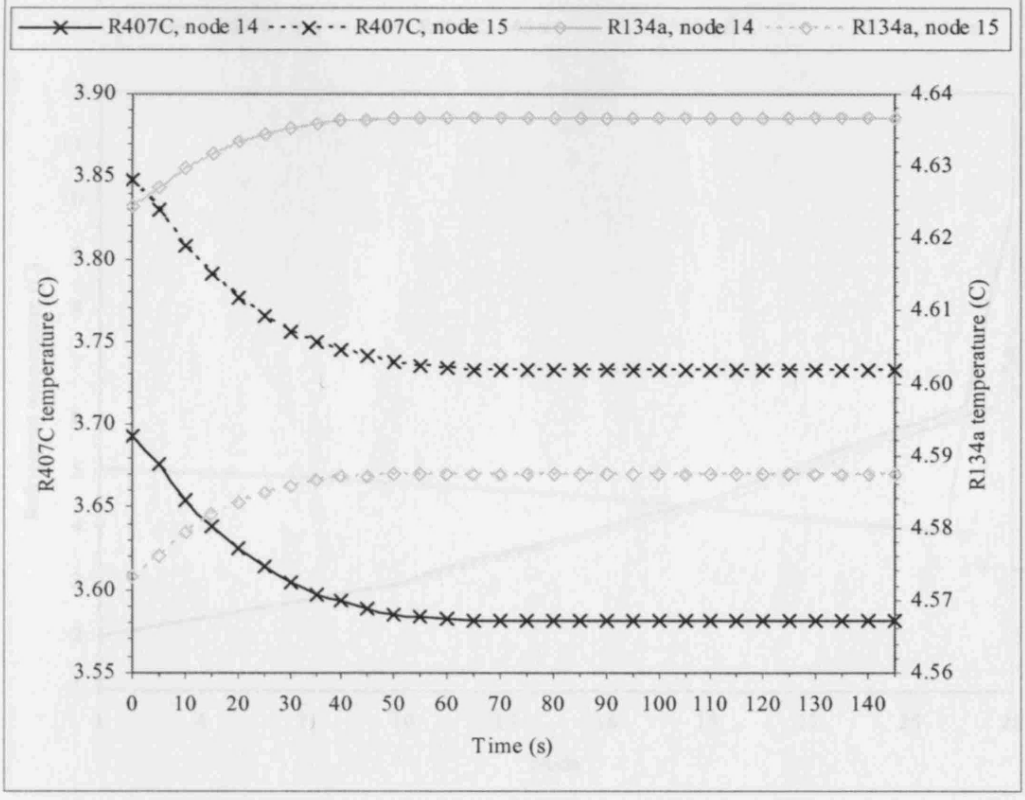

Figure 5.40a Refrigerant temperatures vs nodes at 0 and 145 seconds for dry coils when there was a 0.5-degree-C step increase in coil-inlet dry-bulb temperatures

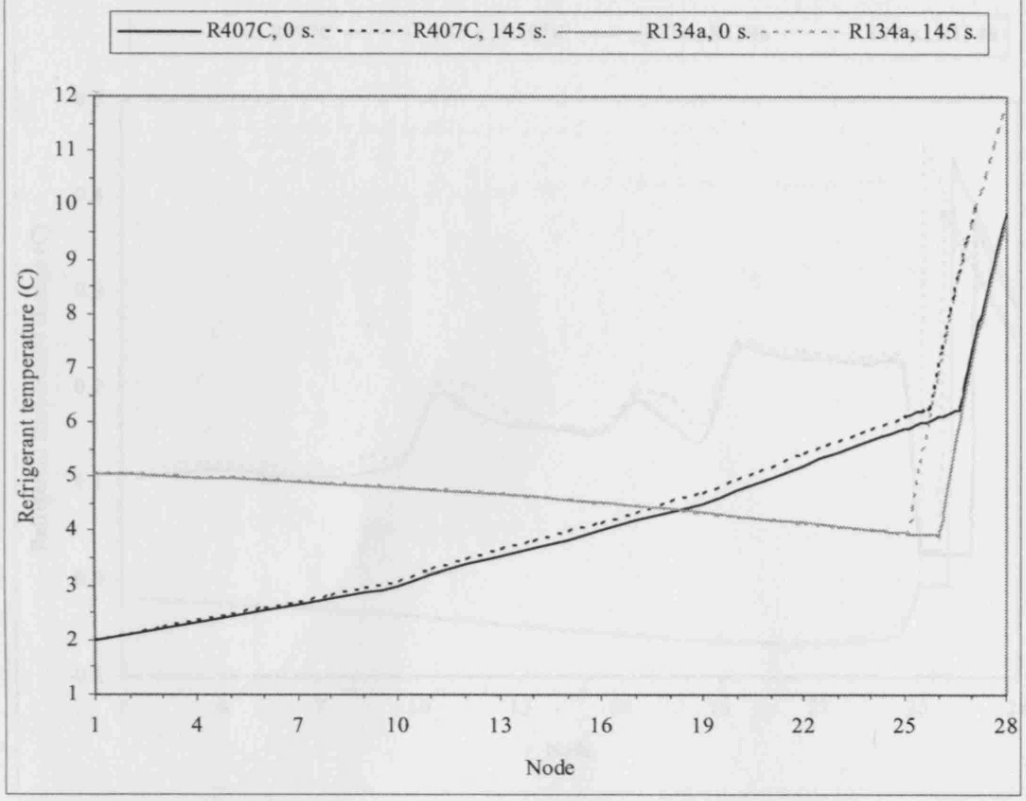

Figure 5.40b Refrigerant temperatures vs nodes at 0 and 145 seconds for dry coils when there was a 0.5-degree-C step decrease in coil-inlet dry-bulb temperatures

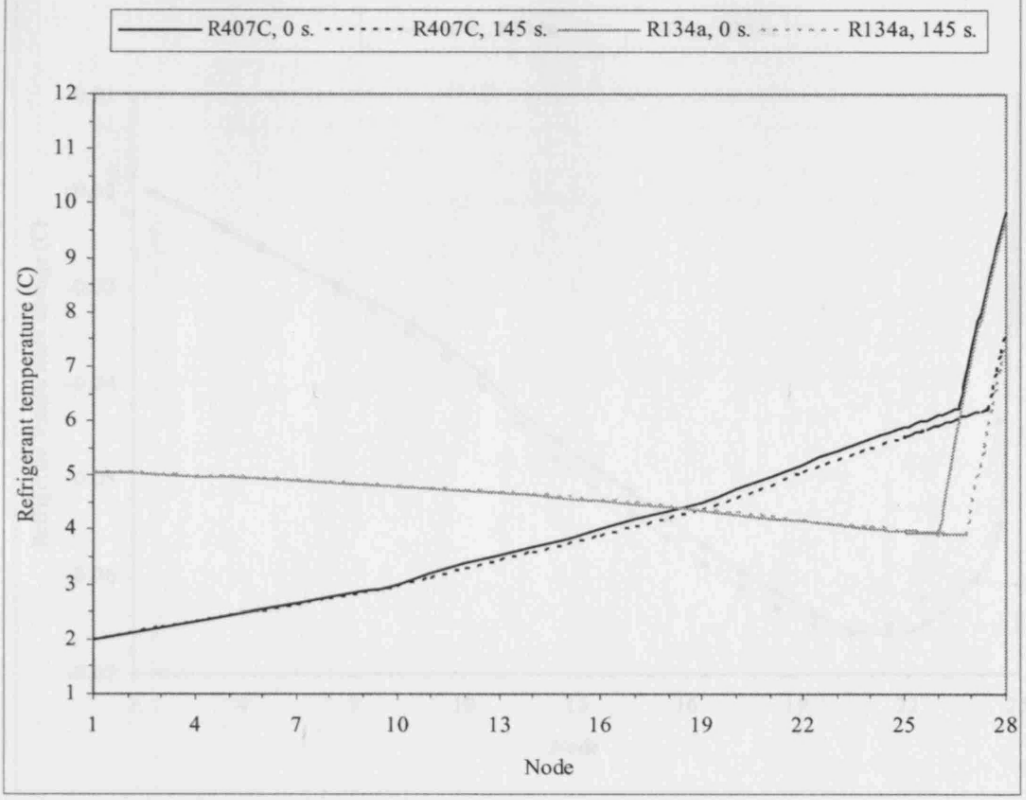

Figure 5.41a Refrigerant temperature changes vs nodes at seconds 0 and 145 for dry coils when there was a 0.5-degree-C step increase in coil-inlet dry-bulb temperatures

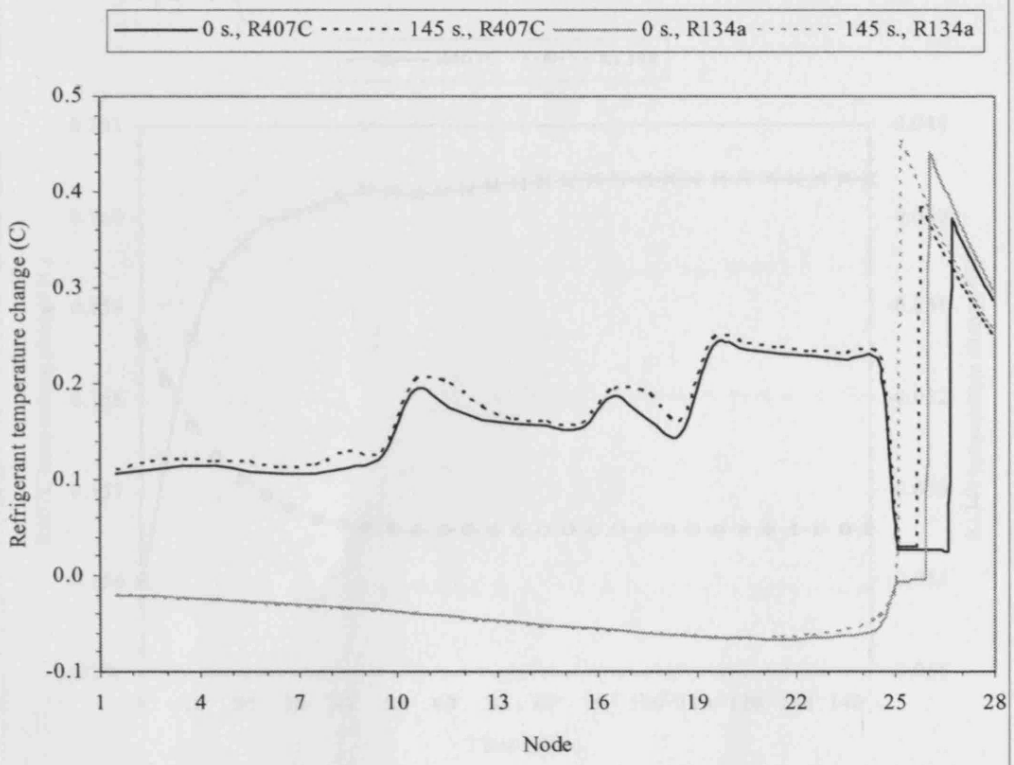

Figure 5.41b Refrigerant temperature changes vs nodes at seconds 0 and 145 for a dry coil when there was a 0.5-degree-C step increase in coil-inlet dry-bulb temperature

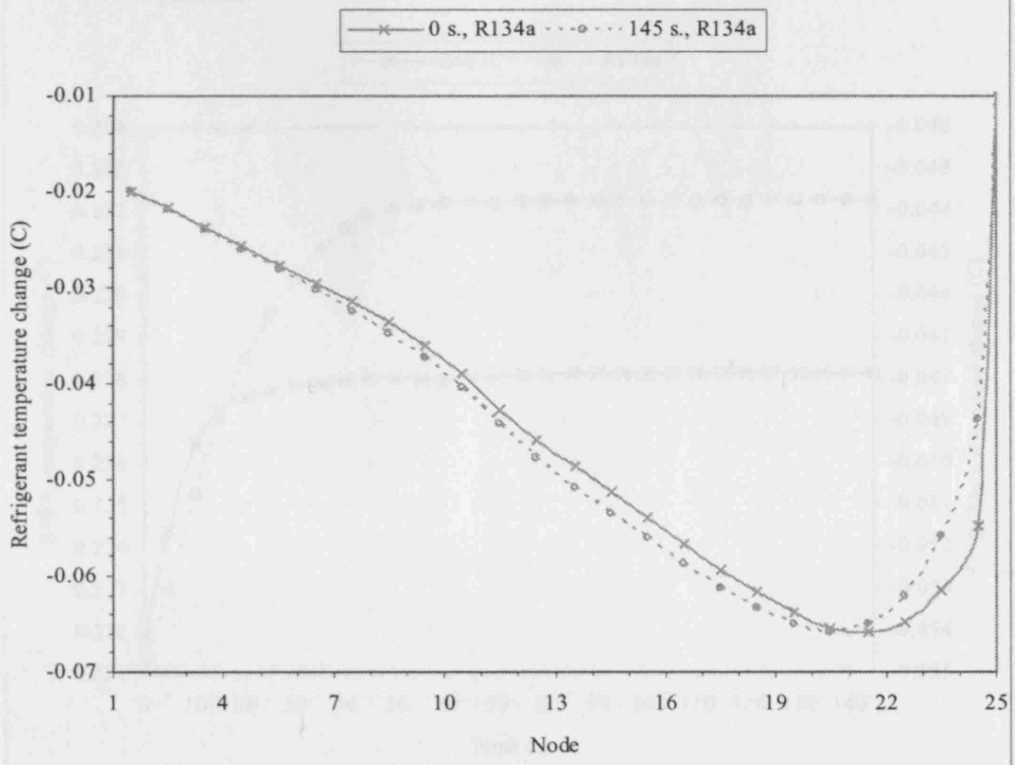

Figure 5.42 Refrigerant temperature changes vs times at the element between nodes 14 and 15 for dry coils when there was a 0.5-degree-C increase in dry-bulb temperatures

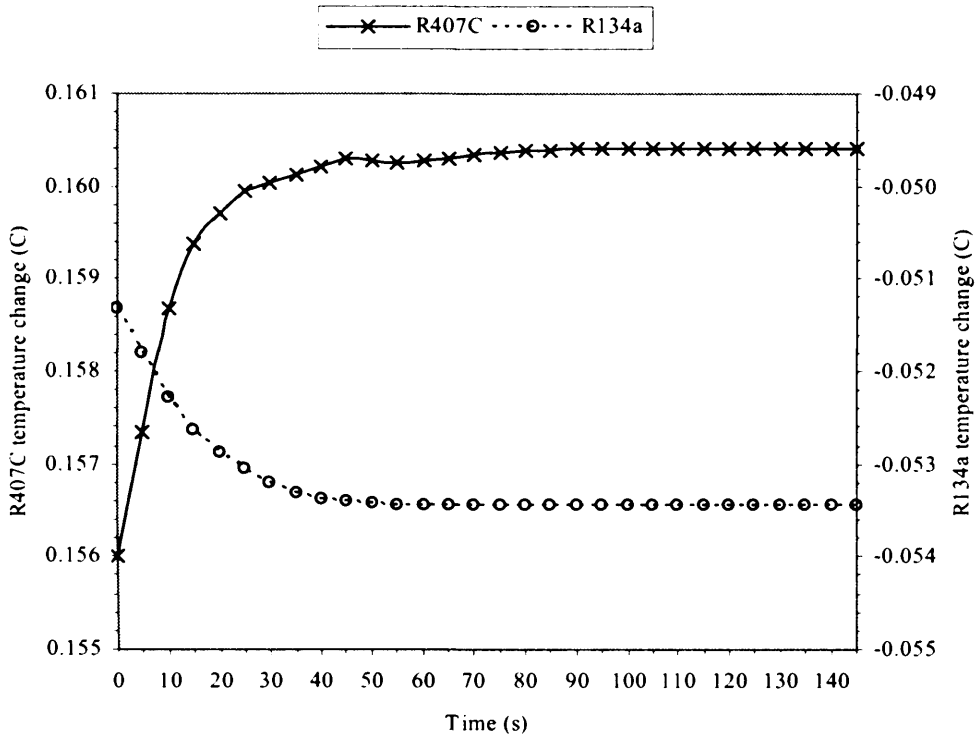

Figure 5.43 Refrigerant temperature changes vs times at the element between nodes 24 and 25 for dry coils when there was a 0.5-degree-C increase in dry-bulb temperatures

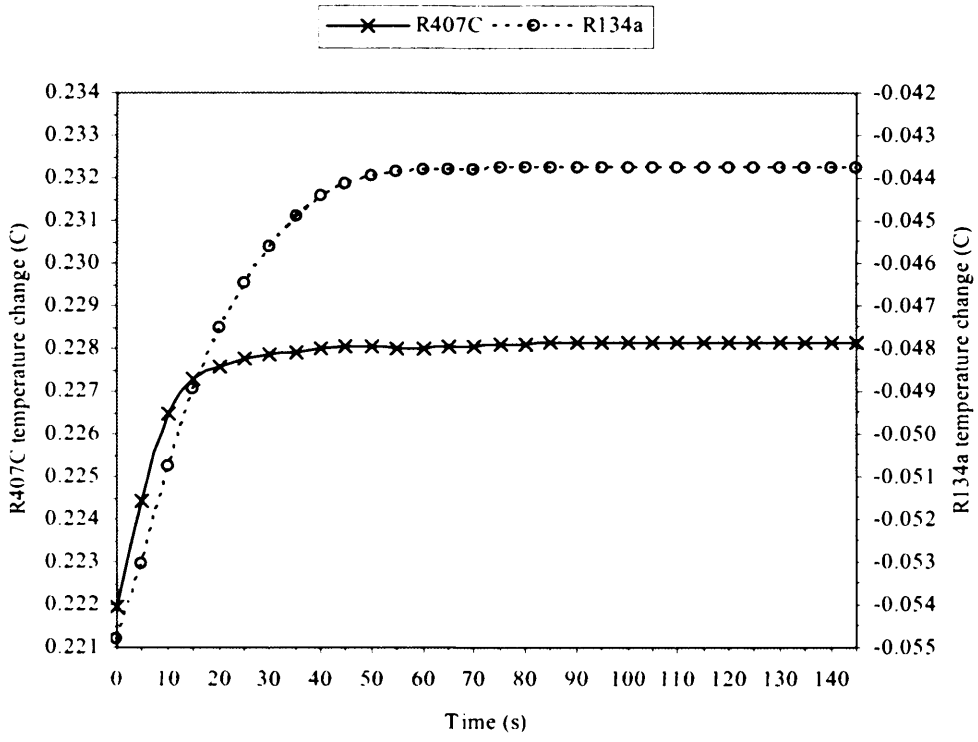

Figure 5.44 Refrigerant temperatures at nodes 24 and 25 vs times for dry coils when there was a 0.5-degree-C increase in dry-bulb temperatures

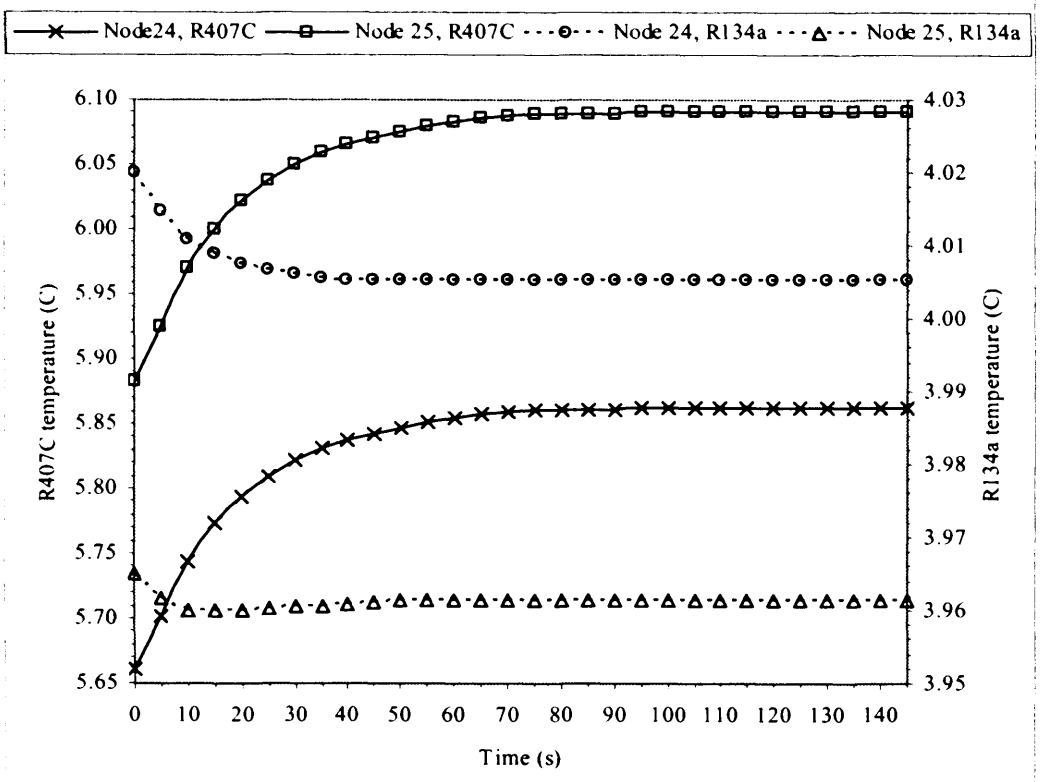

Figure 5.45 R134a temperature changes vs times at the sub-element between nodes 25.125 and 25.25 for dry coils when there was a 0.5-degree-C increase in dry-bulb temperatures

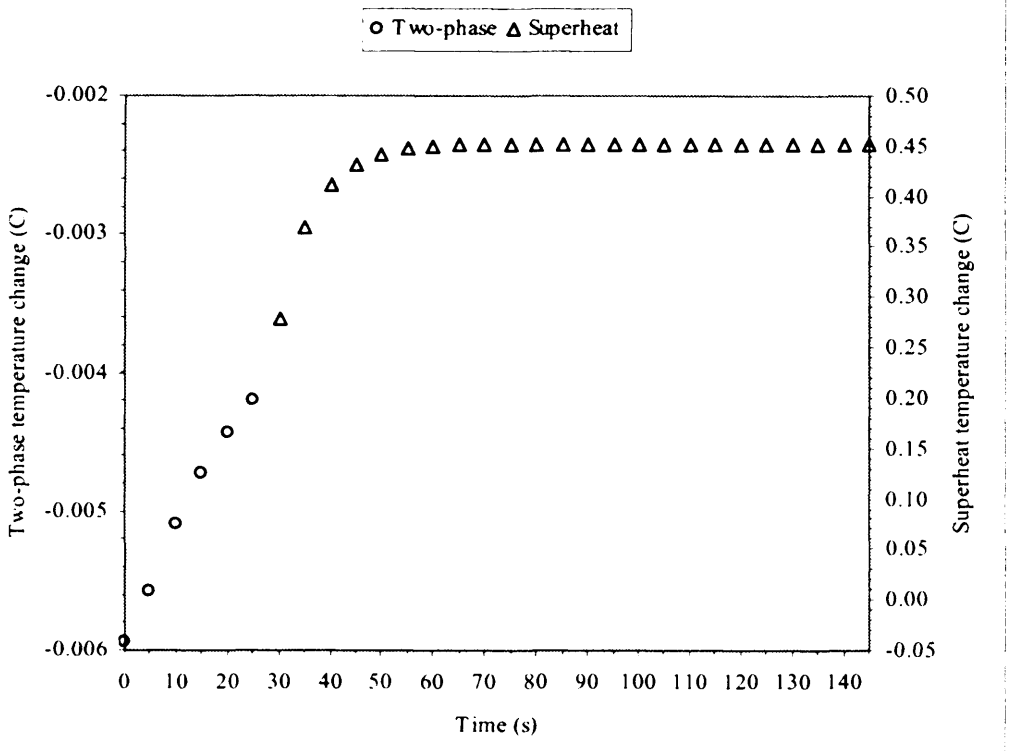

Figure 5.46 R134a temperatures at nodes 25.125 and 25.25 vs times for dry coils when there was a 0.5-degree-C increase in dry-bulb temperatures

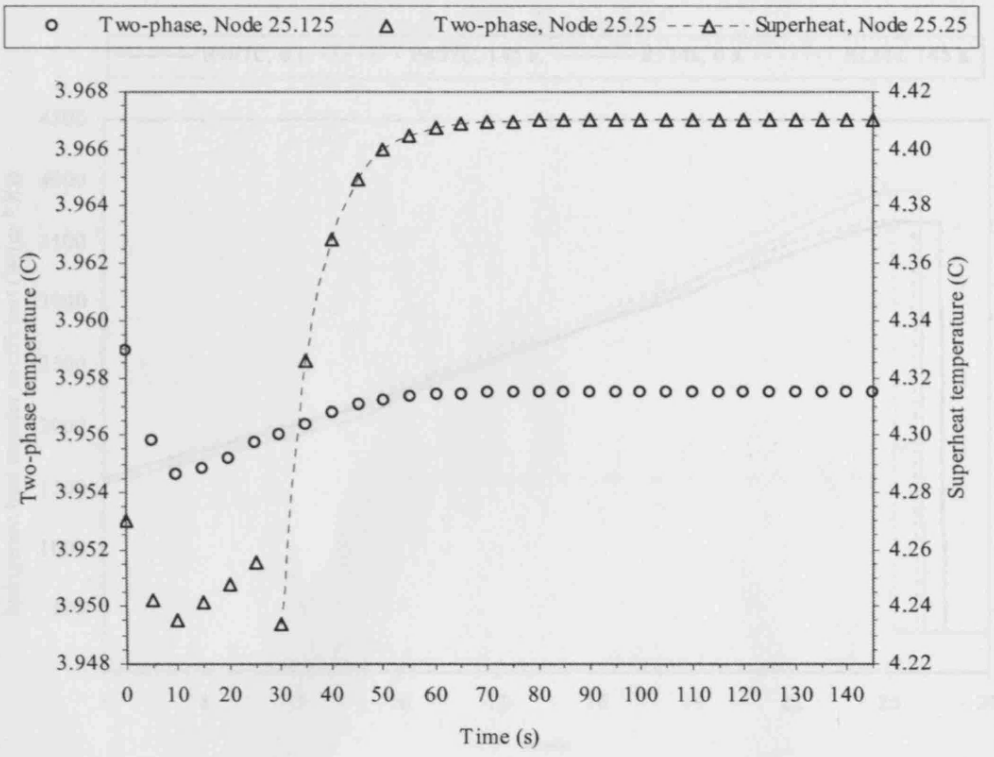

Figure 5.47 Refrigerant heat transfer coefficients at nodes 14 and 15 vs times for dry coils when there was a 0.5-degree-C step increase in coil-inlet dry-bulb temperatures

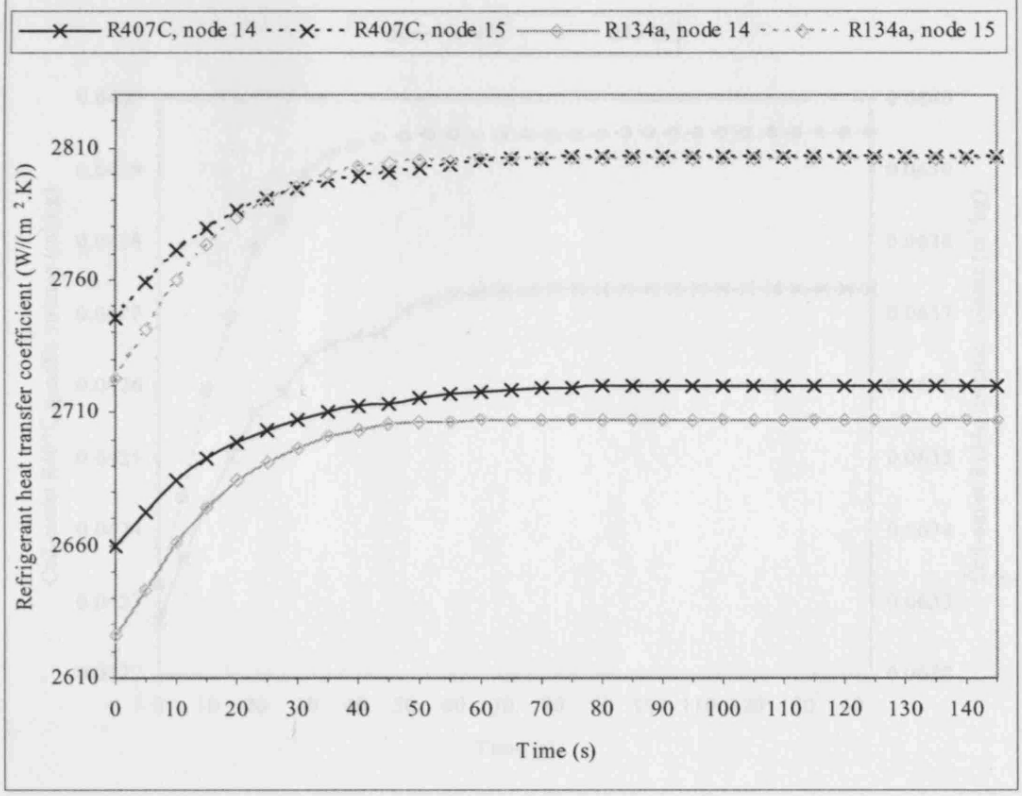

Figure 5.48 Refrigerant heat transfer coefficients vs nodes at 0 and 145 seconds for dry coils when there was a 0.5-degree-C step increase in coil-inlet dry-bulb temperatures

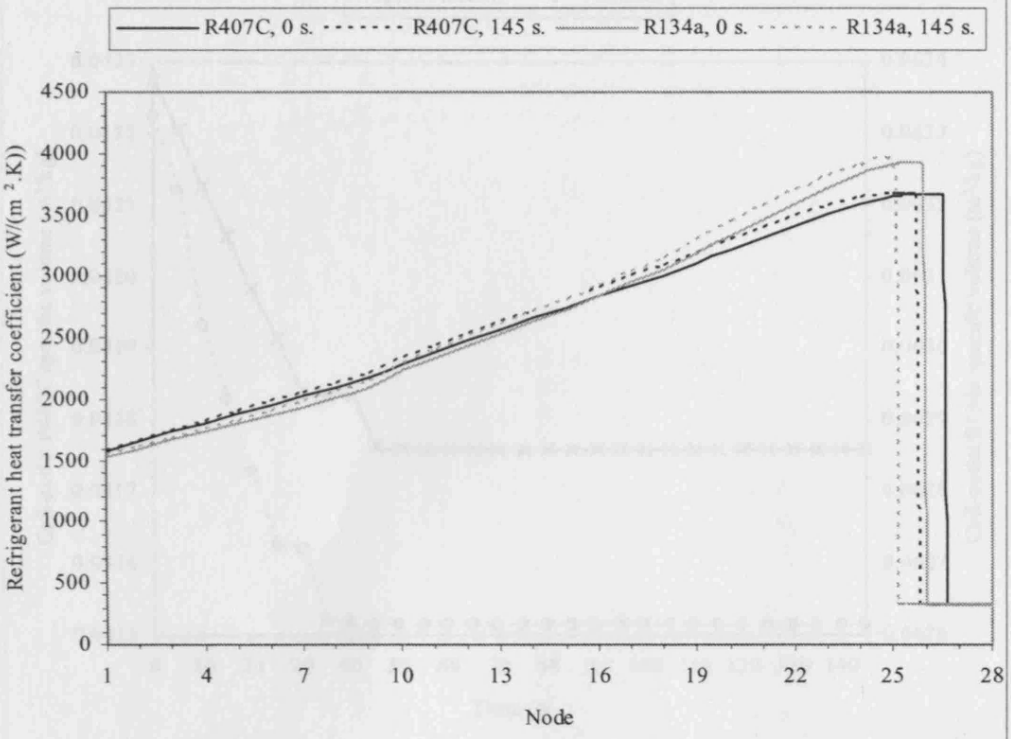

Figure 5.49a Coil-outlet refrigerant specific volumes vs times for dry coils when there was a 0.5-degree-C step increase in coil-inlet dry-bulb temperatures

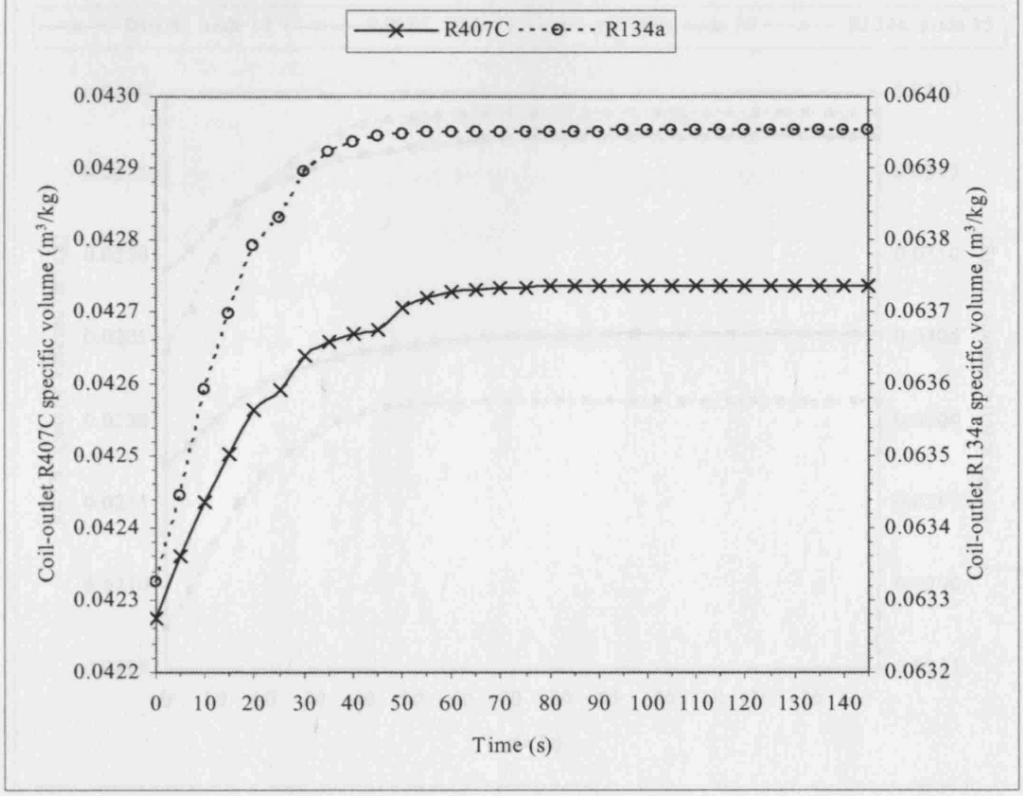

Figure 5.49b Coil-outlet refrigerant specific volumes vs times for dry coils when there was a 0.5-degree-C step decrease in coil-inlet dry-bulb temperatures

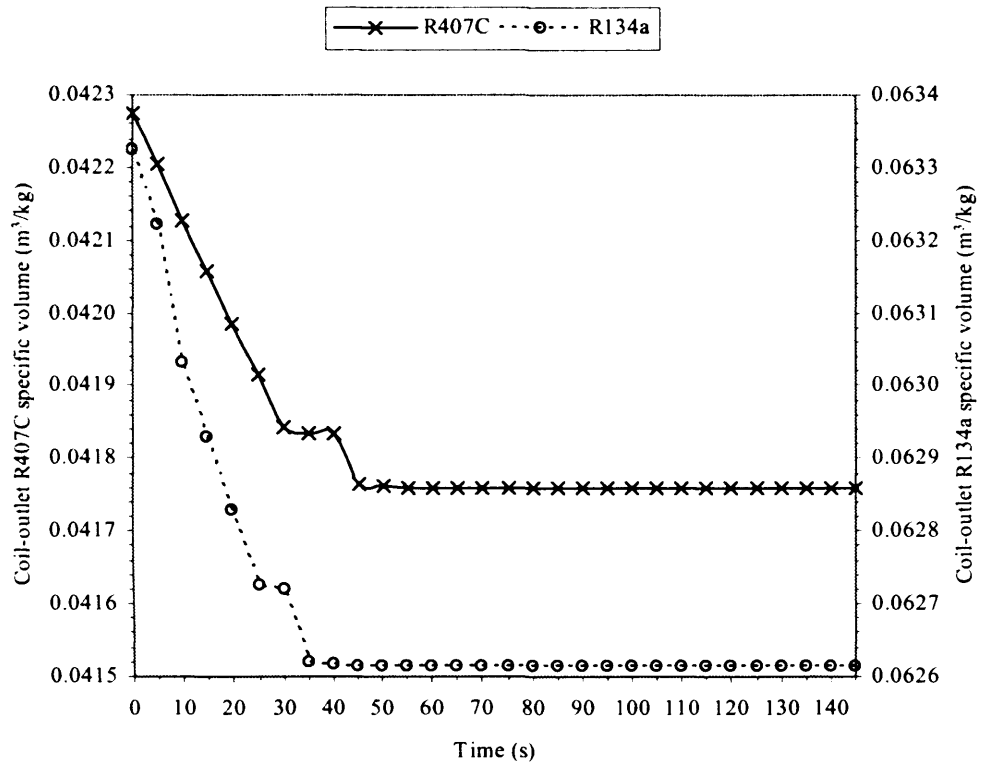

Figure 5.50 Refrigerant specific volumes at nodes 14 and 15 vs times for dry coils when there was a 0.5-degree-C step increase in coil-inlet dry-bulb temperatures

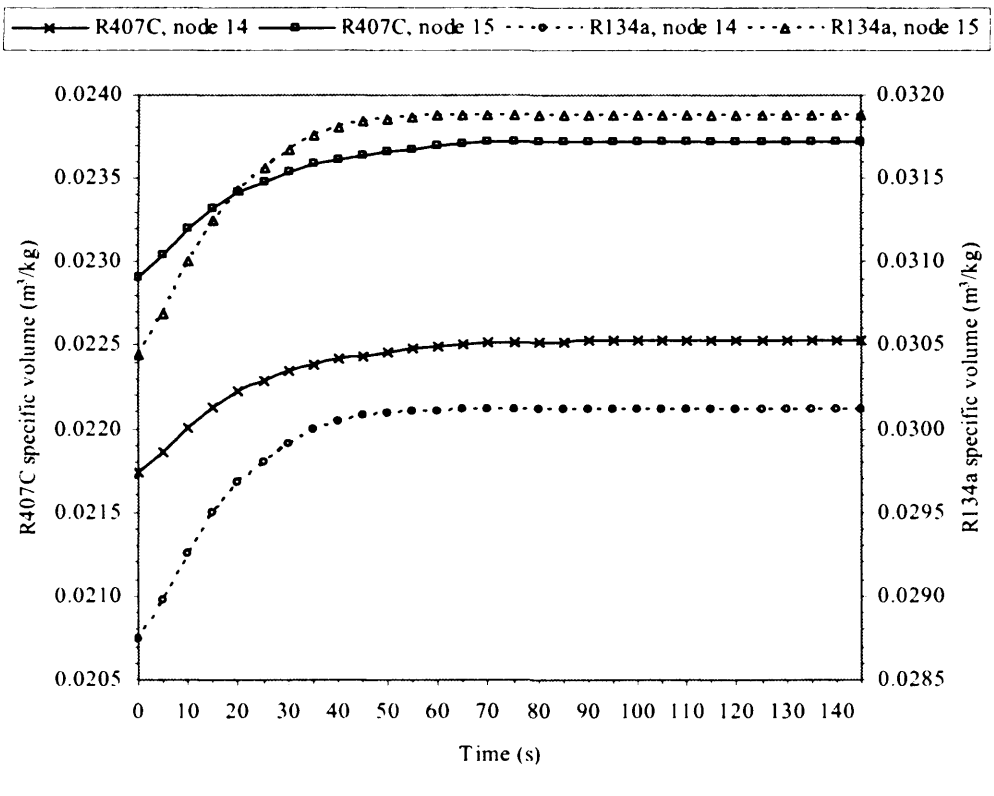

Figure 5.51 Refrigerant vapour qualities at nodes 14 and 15 vs times for dry coils when there was a 0.5-degree-C step increase in coil-inlet dry-bulb temperatures

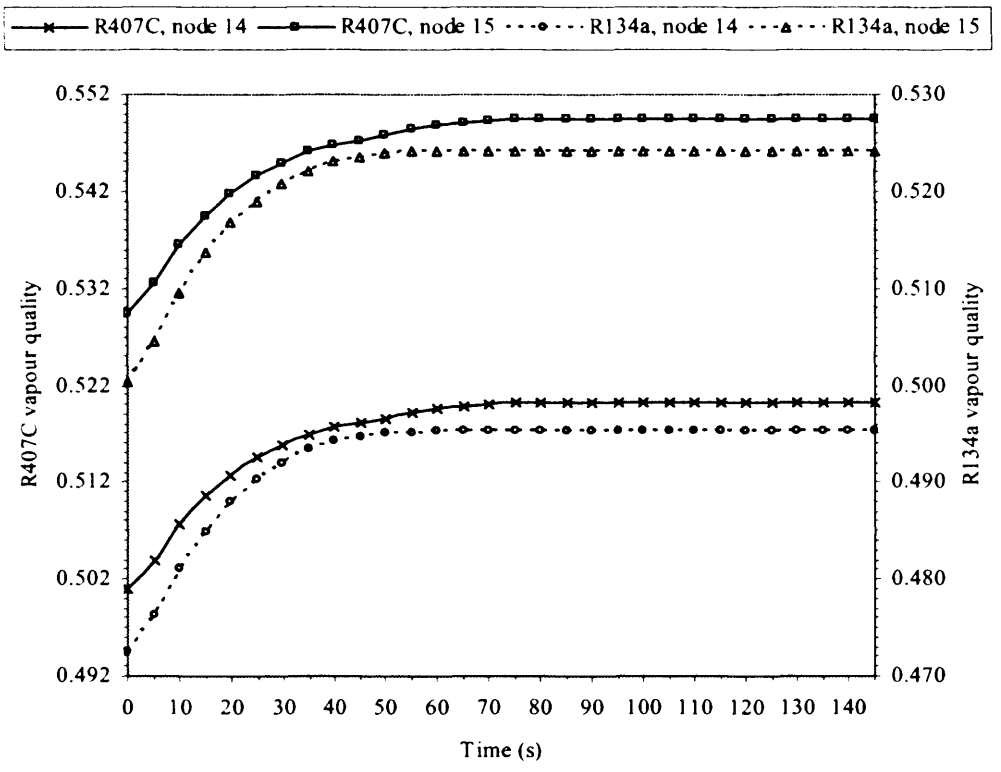

Refrigerant heat fluxes: It is important to note that for both refrigerants, Fig. 5.52, the heat flux values reached the steady state much faster than most of the other parameters discussed earlier. Between nodes 14 and 15, there was a sharp rise in the first 15 seconds, reaching steady values are around 30 s. Overall, R407C experienced a smaller magnitude of change between the steady states than that for R134a. As expected, for both refrigerants, the heat flux along the coil increased with time when subject to an increase in air temperature, Fig. 5.53. As a direct effect of the increase in superheat, there was a larger rise in heat flux, as a function of time, at around nodes 11 to 13, Fig. 5.54.

Figure 5.52 Refrigerant heat fluxes at element (2,2,2) between nodes 14 and 15 vs times for dry coils when there was a 0.5-degree-C step increase in coil-inlet dry-bulb temperatures

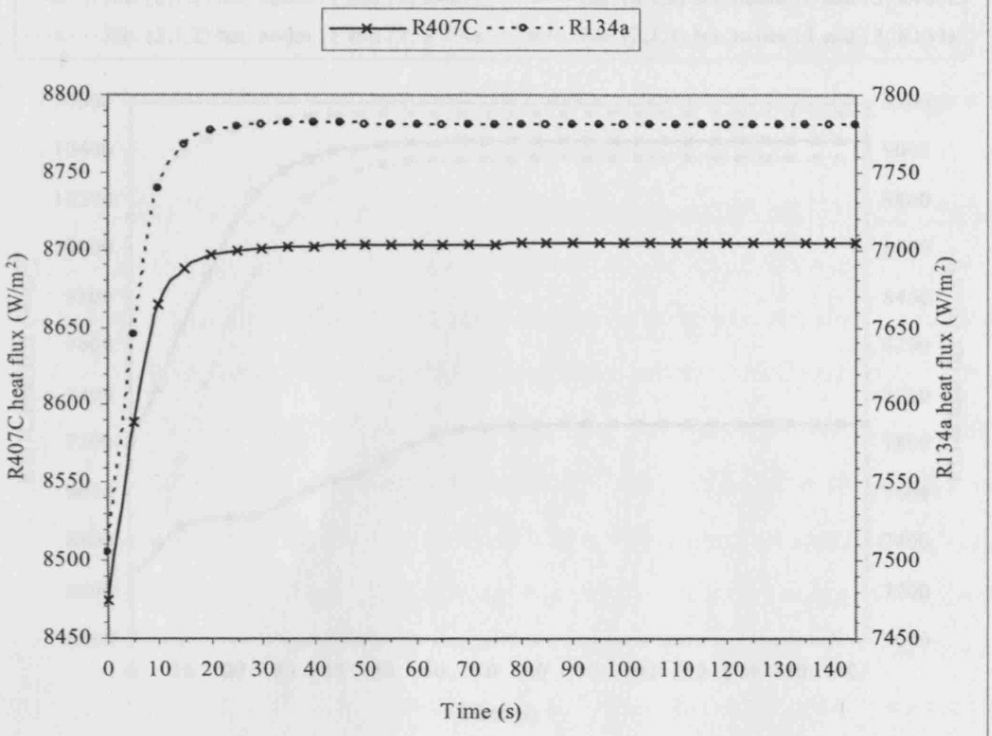

Figure 5.53 Refrigerant heat fluxes vs nodes at 0 and 145 seconds for dry coils when there was a 0.5-degree-C step increase in coil-inlet dry-bulb temperatures

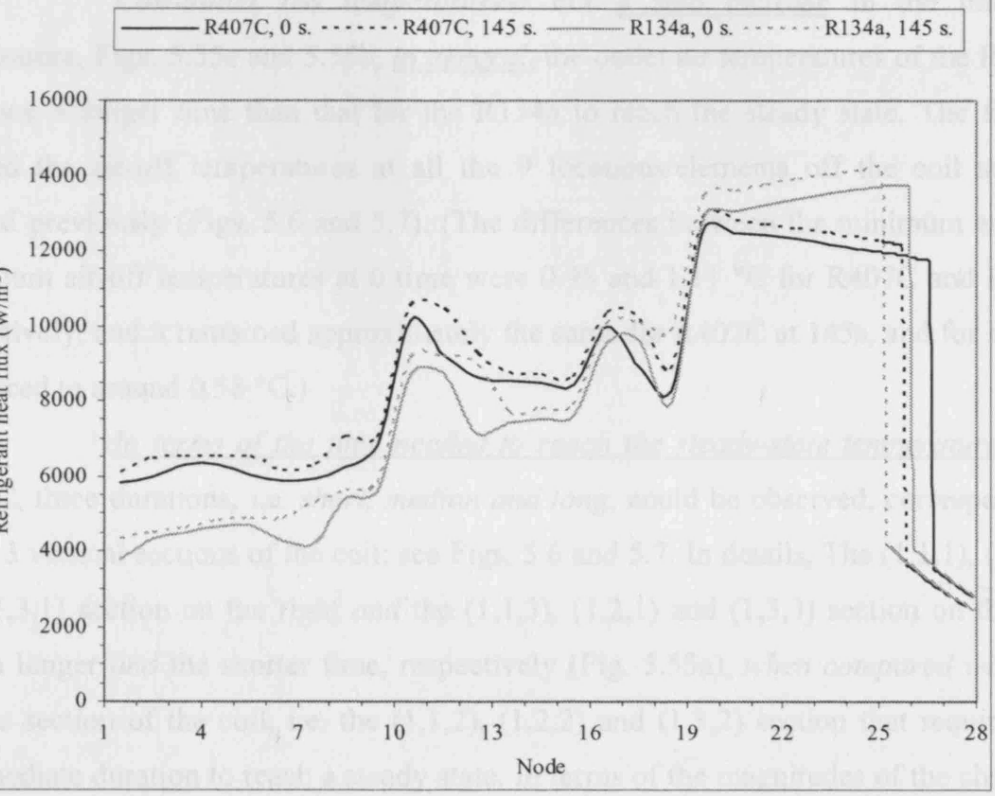

Figure 5.54 Refrigerant heat fluxes at elements (2,1,2) and (2,1,3) vs times for dry coils when there was a 0.5-degree-C increase in dry-bulb temperatures

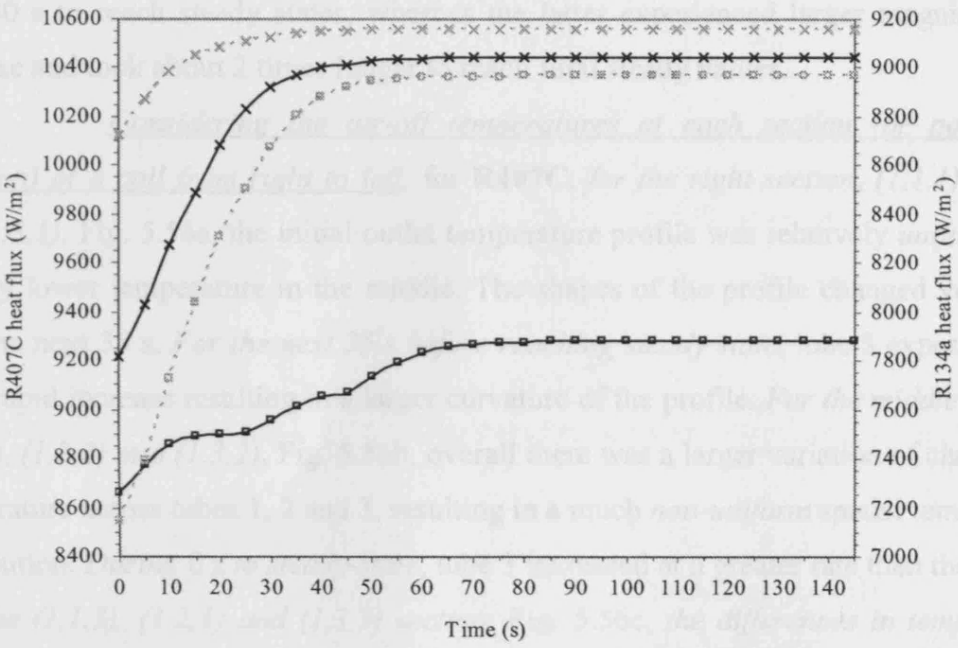

b) Air-side performance

Coil-outlet DB temperatures: For a step increase in the inlet air temperature, Figs. 5.55a and 5.55b, *in general*, the outlet air temperatures of the R407C coil took a longer time than that for the R134a to reach the steady state. The figures showed the air-off temperatures at all the 9 locations/elements off the coil surface defined previously (Figs. 5.6 and 5.7). (The differences between the minimum and the maximum air-off temperatures at 0 time were 0.95 and 1.11 °C for R407C and R134a respectively, and it remained approximately the same for R407C at 145s, and for R134a it reduced to around 0.58 °C.)

In terms of the time needed to reach the steady-state temperatures, for **R407C**, three durations, i.e. *short, median and long*, could be observed, corresponding to the 3 vertical sections of the coil; see Figs. 5.6 and 5.7. In details, The (1,1,1), (1,2,3) and (1,3,1) section on the right *and* the (1,1,3), (1,2,1) and (1,3,3) section on the left took a longer *and* the shorter time, respectively (Fig. 5.55a), *when compared with* the middle section of the coil, i.e. the (1,1,2), (1,2,2) and (1,3,2) section that required an intermediate duration to reach a steady state. In terms of the magnitudes of the changes,

the middle section had the largest values. For **R134a**, only two durations (*short and long*) could be identified (Fig. 5.55b) which could be mapped to the behaviour of the middle ((1,1,2), (1,2,2) and (1,3,2)) and left ((1,1,3), (1,2,1) and (1,3,3)) sections, *and* the right section ((1,1,1), (1,2,3) and (1,3,1)), respectively. The former took only less than 30 s to reach steady states, whereas the latter experienced larger magnitudes of increase and took about 2 times longer to reach final steady values.

Considering the air-off temperatures at each section (or pattern of duration) of a coil from right to left, for **R407C**, *for the right section, (1,1,1), (1,2,3) and (1,3,1),* Fig. 5.56a, the initial outlet temperature profile was relatively *uniform* with slightly lower temperature in the middle. The shapes of the profile changed very little over the next 35 s. *For the next 35 s before reaching steady state*, tube 3 experienced a more rapid increase resulting in a larger curvature of the profile. *For the middle section, (1,1,2), (1,2,2) and (1,3,2)*, Fig. 5.56b, overall there was a larger variation of changes of temperature across tubes 1, 2 and 3, resulting in a much *non-uniform* spatial temperature distribution. *During 0 s to steady-state*, tube 3 increased at a greater rate than the others. *For the (1,1,3), (1,2,1) and (1,3,3) section*, Fig. 5.56c, *the differences in temperature between tubes 2 and 3 were relatively large*, when compared to the other two sections. *Both the magnitudes and the profiles* of the air-off temperature changed relatively little with time in this section.

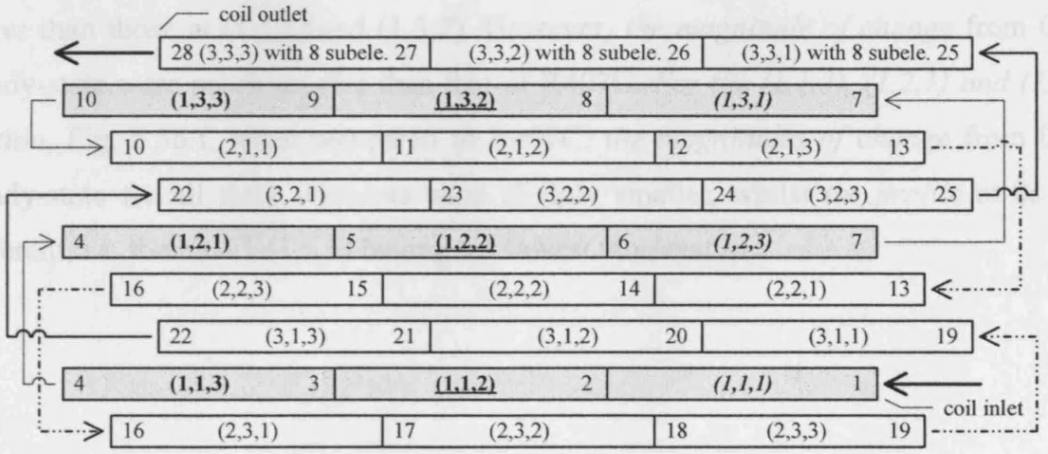

Figure 5.6 For Element and Sub-element arrangements in the refrigerant circuit following the flow of the refrigerant, an Element was labelled with either a ***node numbers*** or a ***bracketed code***. The former started from the coil-inlet to the coil-outlet, whilst the latter represented the row, tube, and element numbers, respectively. For instance, the Element 2 of the tube 1 in the row 1 had the inlet and outlet nodes 2 and 3, and was represented by a (1,1,2), i.e. (row 1, tube 1, element 2), respectively. For the last tube, each element was divided into 8 sub-elements and hence each sub-element took up $1/8^{th}$ (or 0.125) of the length of the element. Therefore, as an example, the second Sub-element of (3,3,1) was labelled as having its inlet and outlet nodes as 25.125 and 25.25, respectively. The highlighted tubes corresponded to the tubes in row 1 of Fig. 5.7.

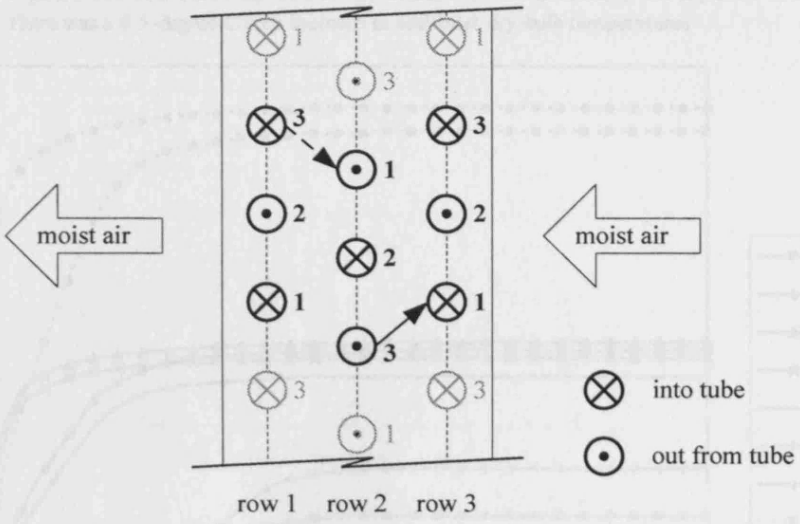

Figure 5.7 Side view of the coil by looking from the coil end with the refrigerant coil-inlet

For **R134a**, *for the right section, (1,1,1), (1,2,3) and (1,3,1),* Fig. 5.56d, at time 0 s the temperature profile was quite different to that of the R407C, i.e. being *non-uniform* but linear, having the temperature decreasing from tube 3 (1,3,1) to tube 1 (1,1,1). *After the first 10 s*, R134a behaved similarly to that of R407C. *For the middle section, (1,1,2), (1,2,2) and (1,3,2),* Fig. 5.56e, from 0s to steady-state, *the profiles* were generally similar to that of R407C, in a way that the air-off temperatures of tube 2 were lower than those at (1,1,2) and (1,3,2). However, *the magnitude of change* from 0s to steady-state were much smaller than that of R407C. *For the (1,1,3), (1,2,1) and (1,3,3) section*, Fig. 5.56.f, when compared to R407C, *the magnitudes of change* from 0s to steady-state for all three elements were slightly smaller, whilst *the profile* at 0s was different, i.e. the tube 1 (1,1,3) having the lowest temperature.

Figure 5.55a Coil-outlet dry-bulb temperatures for R407C vs times for dry coils when there was a 0.5-degree-C step increase in coil-inlet dry-bulb temperatures

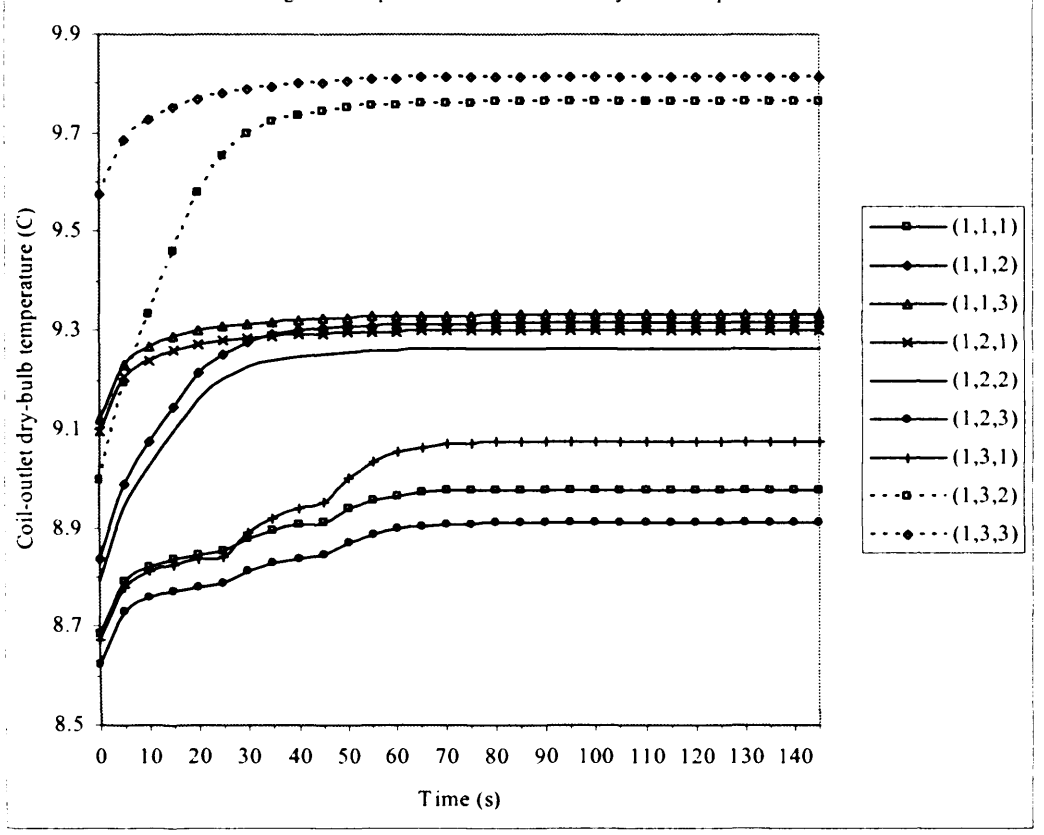

Figure 5.55b Coil-outlet dry-bulb temperatures for R134a vs times for dry coils when there was a 0.5-degree-C step increase in coil-inlet dry-bulb temperatures

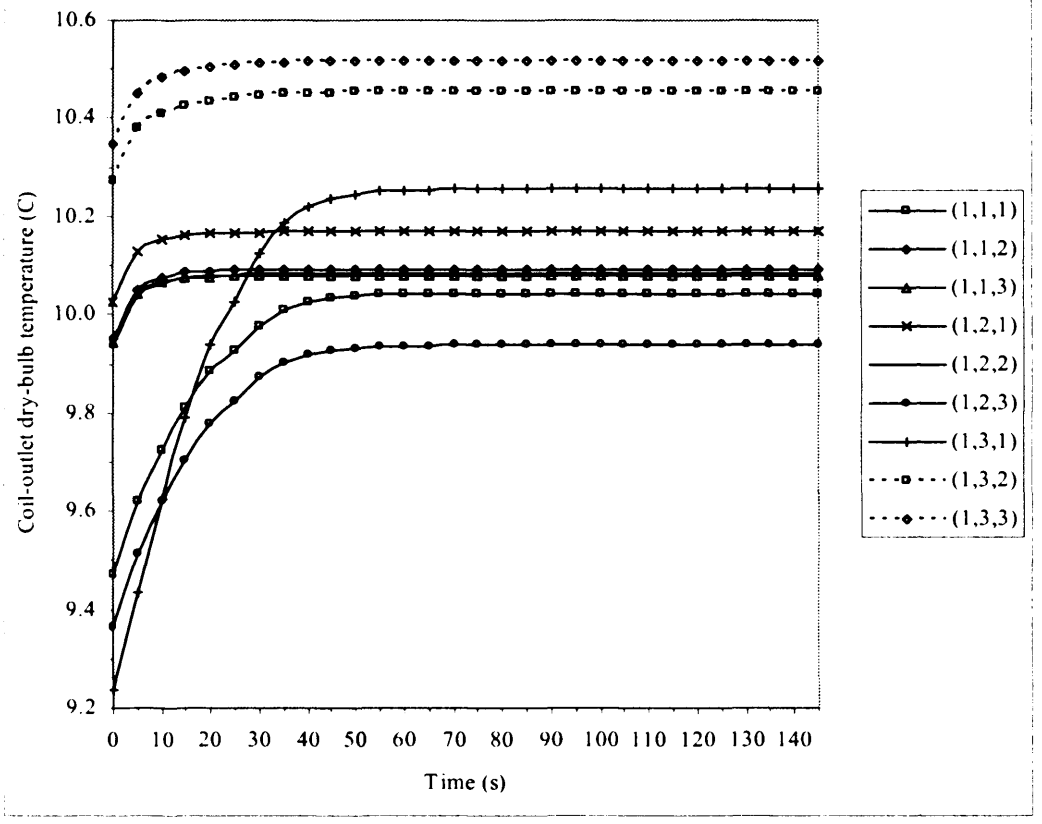

Figure 5.56a Coil-outlet dry-bulb temperatures for R407C at elements (1,1,1), (1,2,3) and (1,3,1) at various times for dry coils when there was a 0.5-degree-C step increase in coil-inlet dry-bulb temperatures

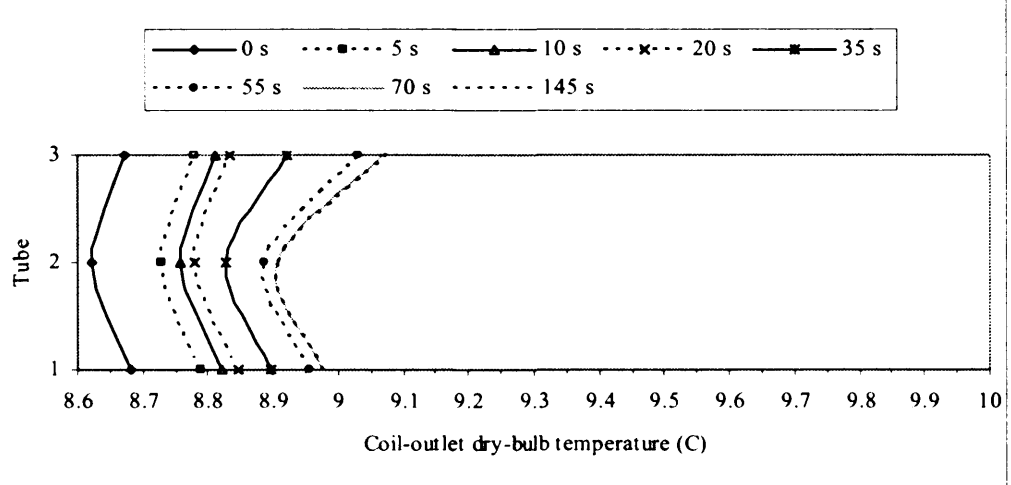

Figure 5.56b Coil-outlet dry-bulb temperatures for R407C at elements (1,1,2), (1,2,2) and (1,3,2) at various times for dry coils when there was a 0.5-degree-C step increase in coil-inlet dry-bulb temperatures

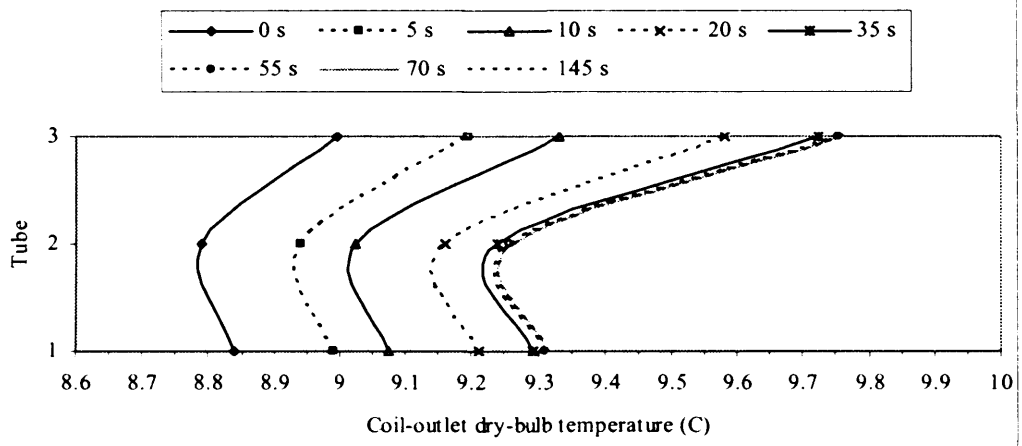

Figure 5.56c Coil-outlet dry-bulb temperatures for R407C at elements (1,1,3), (1,2,1) and (1,3,3) at various times for dry coils when there was a 0.5-degree-C step increase in coil-inlet dry-bulb temperatures

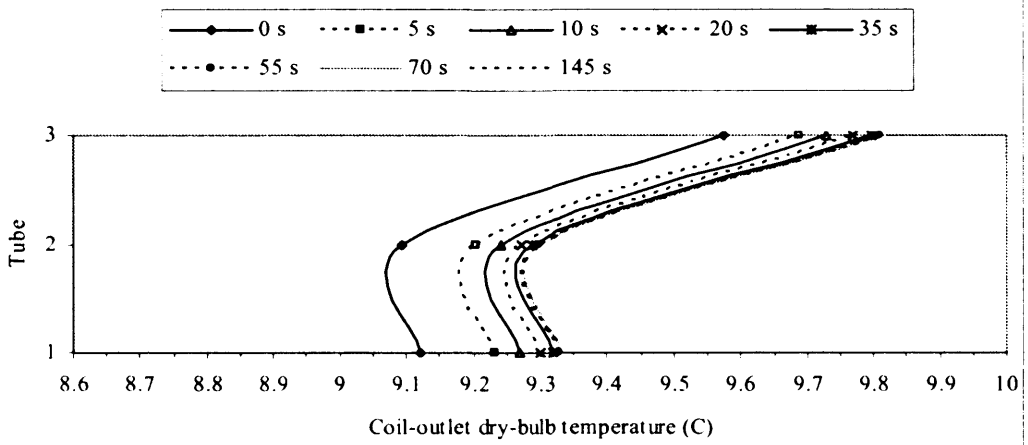

Figure 5.56d Coil-outlet dry-bulb temperatures for R134a at elements (1,1,1), (1,2,3) and (1,3,1) at various times for dry coils when there was a 0.5-degree-C step increase in coil-inlet dry-bulb temperatures

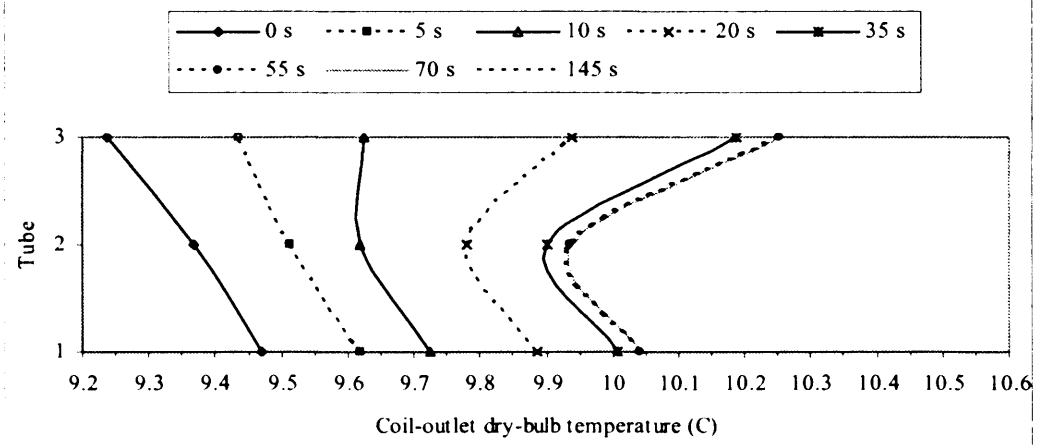

Figure 5.56e Coil-outlet dry-bulb temperatures for R134a at elements (1,1,2), (1,2,2) and (1,3,2) at various times for dry coils when there was a 0.5-degree-C step increase in coil-inlet dry-bulb temperatures

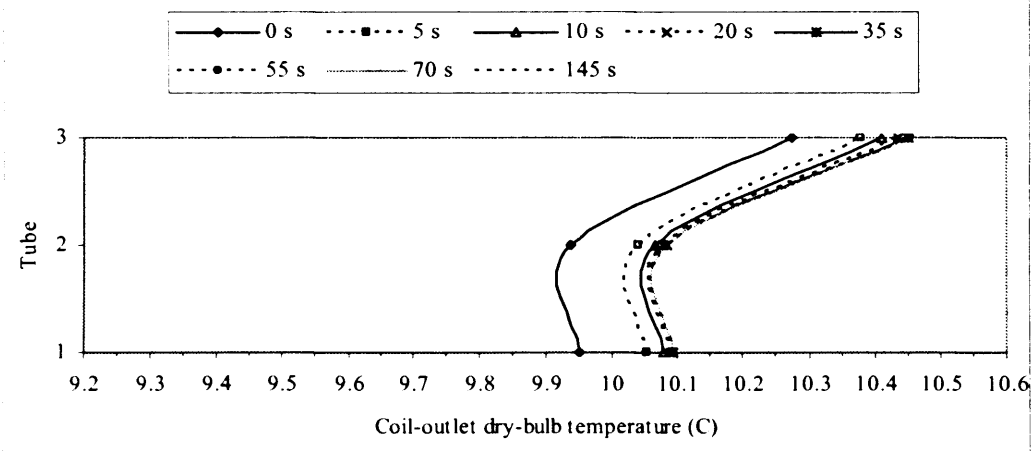

Figure 5.56f Coil-outlet dry-bulb temperatures for R134a at elements (1,1,3), (1,2,1) and (1,3,3) at various times for dry coils when there was a 0.5-degree-C step increase in coil-inlet dry-bulb temperatures

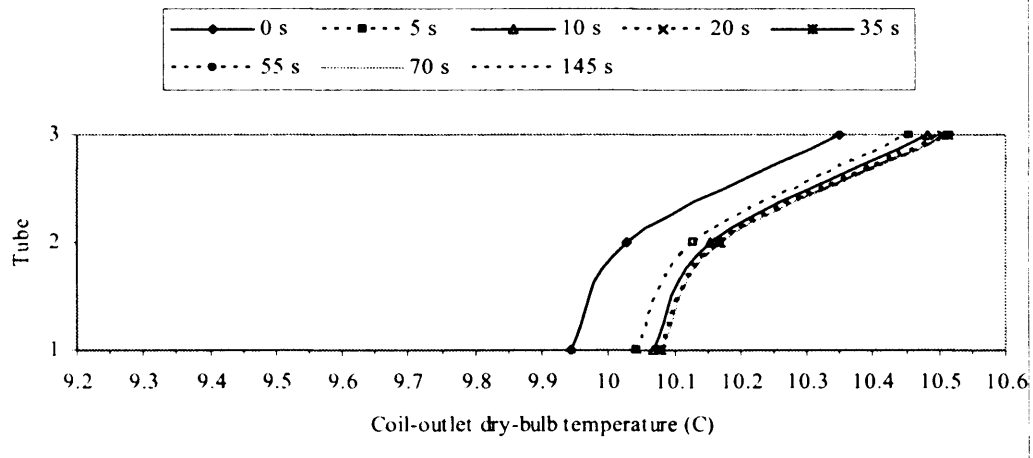

To gain a better understanding of both the spatial and temporal variations of the air-off DB temperature, the initiation positions of the refrigerant superheat were examined. Before going into details, one must bare in mind that, when referring to Fig. 5.7, the air-on temperature of tube 3 in the second row depended on *both* the air-off temperatures of tube 1 in the 3rd row *and* of the tube 3 in the 3rd row of the next refrigerant circuit below it. Also noted was that the superheat section was "confined" to the tube 3 of the 3rd row for the cases of 0.5 C increase in air-on temperature. Similarly, the air-on temperature of tube 3 of the 1st row was affected by the air-off temperature of tube 3 in the 2nd row from the next refrigerant circuit above it. *Fig. 5.57* showed the positions of the superheat initiation at 0, 30 and 50 seconds for **R407C** moved from the 6th sub-element of (3,3,2), 8th sub-element of (3,3,1) and 7th sub-element of (3,3,1), steadying at 50 s. For **R134a**, it occurred in the 1st sub-element of (3,3,2) at 0 s, and moved to the 8th sub-element of (3,3,1) in 5 s. Finally, it settled in the 2nd sub-element at 30 s.

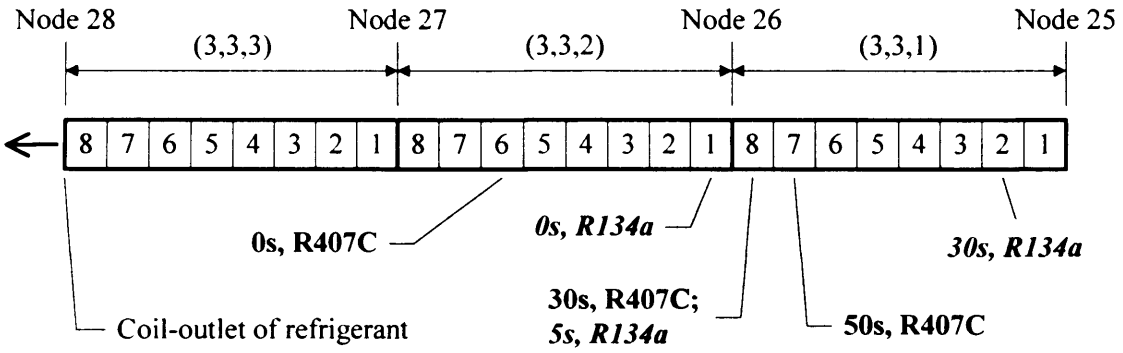

Figure 5.57 Initiation position of superheat with time when having a 0.5 °C increase in coil-inlet DB temperature (The numbers shown in tubes were Sub-element numbers.)

In conclusions, for either refrigerant, for a step increase of the coil-inlet DB temperature, the movement of the superheat-initiation location had an impact on the time to reaching steady-state of the air-off temperature. For example, for both refrigerants, in the element (3,3,1), the movements of the superheat-initiation location caused the long time duration for the (1,1,1), (1,2,3) and (1,3,1) section to settle.

In addition, when compared to the 2-phase refrigerant, the heat flux of the superheated refrigerant is much smaller, Fig. 5.53. Hence, the rate of change with time of the air-off temperature for a part of the tube containing the 2-phase refrigerant is

much smaller than that containing the superheated refrigerant. For instance, for R407C, with the element (3,3,2) involving the movement of the superheat-initiation location, the (1,1,2), (1,2,2) and (1,3,2) section have larger values of the rate of change with time (i.e. the magnitudes of change with time from 0s to steady-state) than that for the (1,1,3), (1,2,1) and (1,3,3) section, which corresponded to the element (3,3,3) that contained the superheat refrigerant all the times.

Tube-wall temperatures: For a step increase in the air inlet temperature, Fig. 5.58 showed the transient variation of the wall temperature at node 14 (2,2,2) for both refrigerants. For R407C, the tube-wall temperature increased with time, whereas for R134a the temperature increased, peaking at around 10 s, and then gradually decreased to the steady-state level that was only marginally higher than the initial steady state value. R407C took a longer time to reach the steady-value that was 0.14 °C higher than the initial value. For the air heat fluxes at the same element, Fig. 5.59, essentially the two refrigerants had the same behaviour, rising sharply initially and settling fast to steady values.

The transient behaviour of the wall temperature could be explained by examining collectively its independent parameters: the rates of changes of refrigerant heat fluxes, refrigerant HTCs and refrigerant temperatures. Firstly, based on the Newton's cooling Law by combining the first 2 parameters into a ratio, as shown in Fig. 5.60a, for both refrigerants, the ratios of the refrigerant heat flux ***to*** the refrigerant HTC increased sharply and peaked at around 10 s, and then, the ratios decreased gradually with time. The initial increase was due to the fact that the rates of changes with time for the heat flux were faster than that of the HTC, see Figs. 5.51 and 5.52. The latter then had a faster rate of change than the former resulting in a decrease of the ratio after the 10 s. At the same instant, Fig. 5.60b, for R407C, the refrigerant temperature increased with time. The relative rates of changes of the decreasing ratio and the increasing refrigerant temperature resulted in an increase of wall temperature from 10 s. However, for R134a, the refrigerant temperature decreased with time, Fig. 5.60b, and therefore, the transient profiles of the wall temperature and the ratio were essentially similar.

Figure 5.58 Wall temperatures at node 14 based on (2,2,2) vs times for dry coils when there was a 0.5-degree-C step increase in coil-inlet dry-bulb temperatures

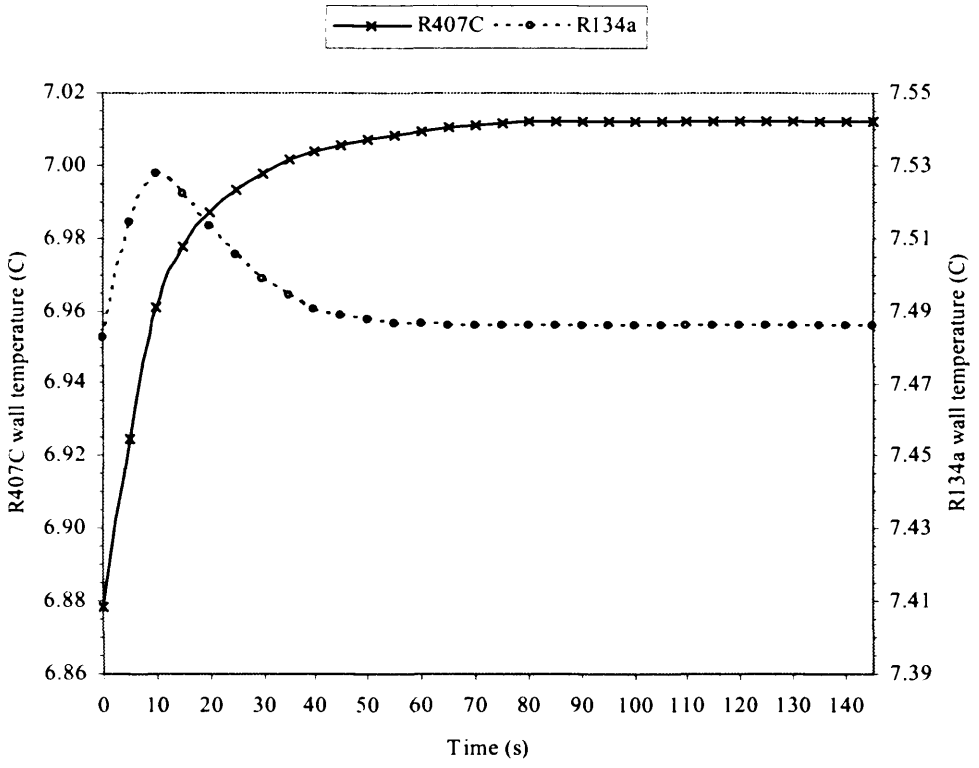

Figure 5.59 Air heat fluxes at (2,2,2) between nodes 14 and 15 vs times for dry coils when there was a 0.5-degree-C step increase in coil-inlet dry-bulb temperatures

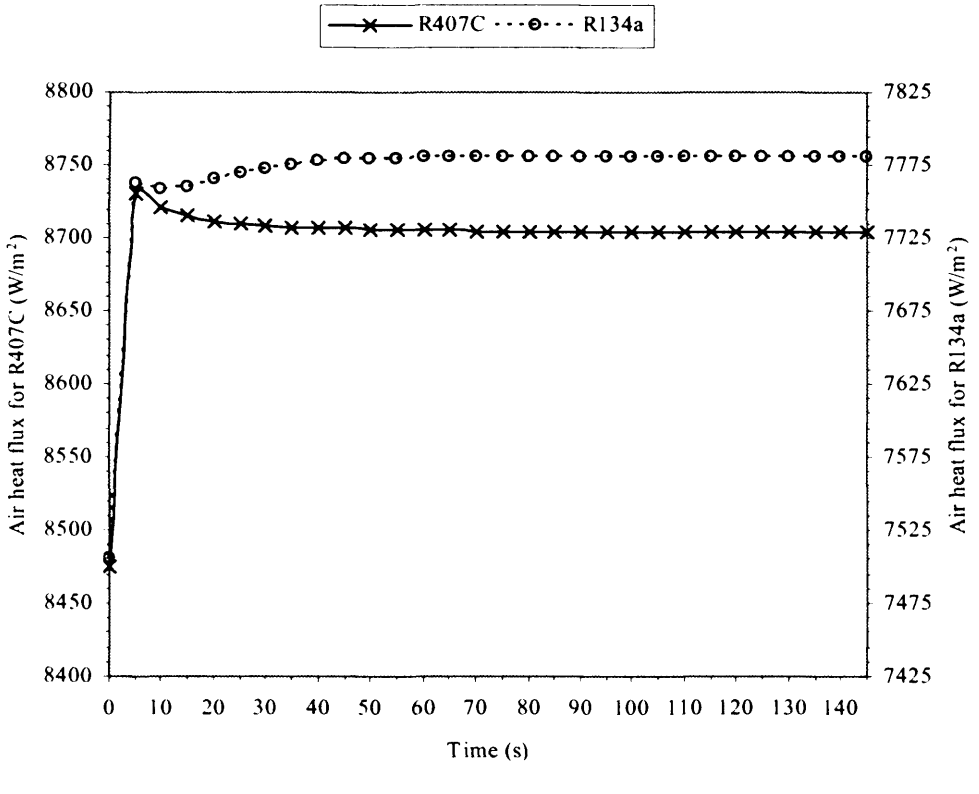

Figure 5.60a Ratios of refrigerant heat flux to refrigerant heat transfer coefficient at node 14 based on (2,2,2) vs times for dry coils when there was a 0.5-degree-C step increase in coil-inlet dry-bulb temperatures

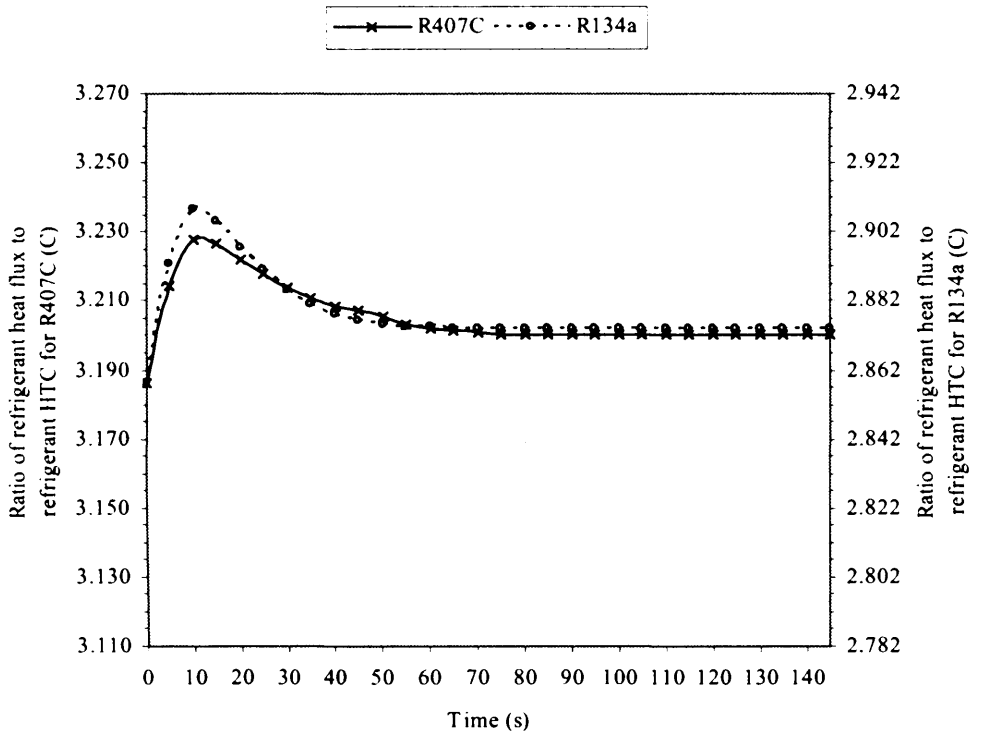

Figure 5.60b Refrigerant temperatures at node 14 vs times for dry coils when there was a 0.5-degree-C increase in dry-bulb temperatures

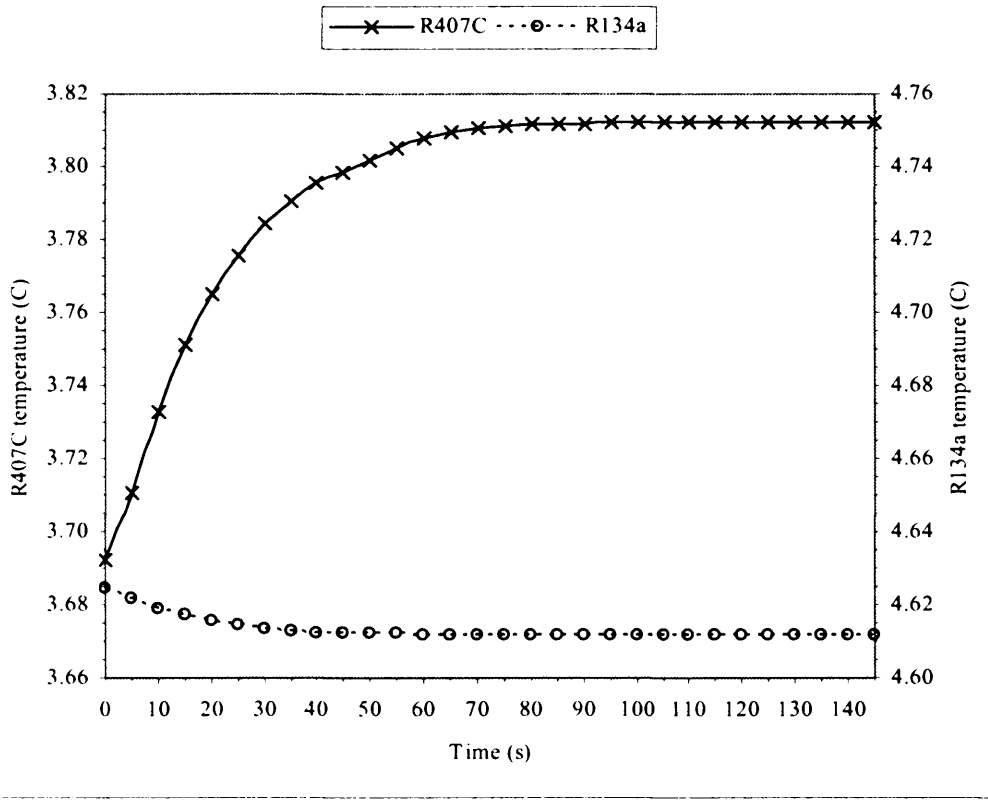

With both refrigerants, the transient profiles of the wall temperature could be different depending on location; for instance, the profile at node 12 was different to that at node 14. It should be pointed out here that for R134a the wall temperature could go up then come down as well as just going up, as shown in Figs. 5.58 and 5.61 respectively, but it was observed that for R407C the wall temperature only increased with time when subject to a step increase in air temperature.

Total heat loads: Fig 5.62a showed that, for both refrigerants, for the 3rd row, the air heat loads increased with a peak at 5s, and after that, it decreased to steady values that were lower than the initial load. For the 1st and the 2nd rows, the heat loads gradually increased to steady values. Fig 5.62b presented the time variations of the total air heat load and R407C reached a steady-state level later than R134a.

Figure 5.61 Wall temperatures at node 12 based on (2,1,3) vs times for dry coils when there was a 0.5-degree-C step increase in coil-inlet dry-bulb temperatures

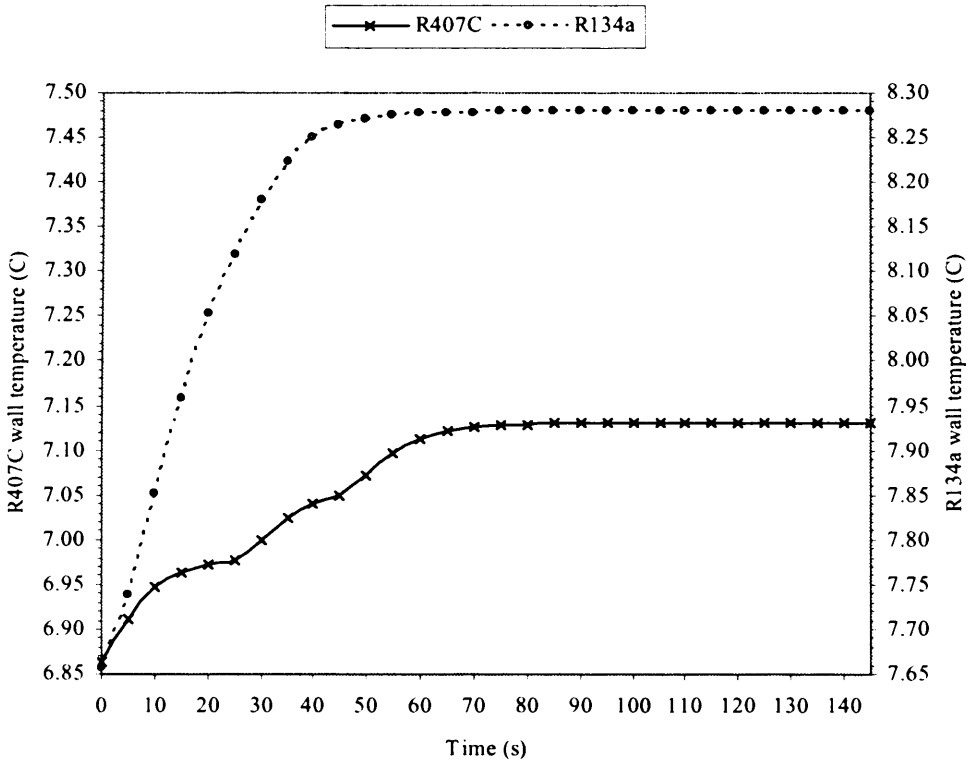

Figure 5.62a Row air heat loads vs times for dry coils when there was a 0.5-degree-C step increase in coil-inlet dry-bulb temperatures

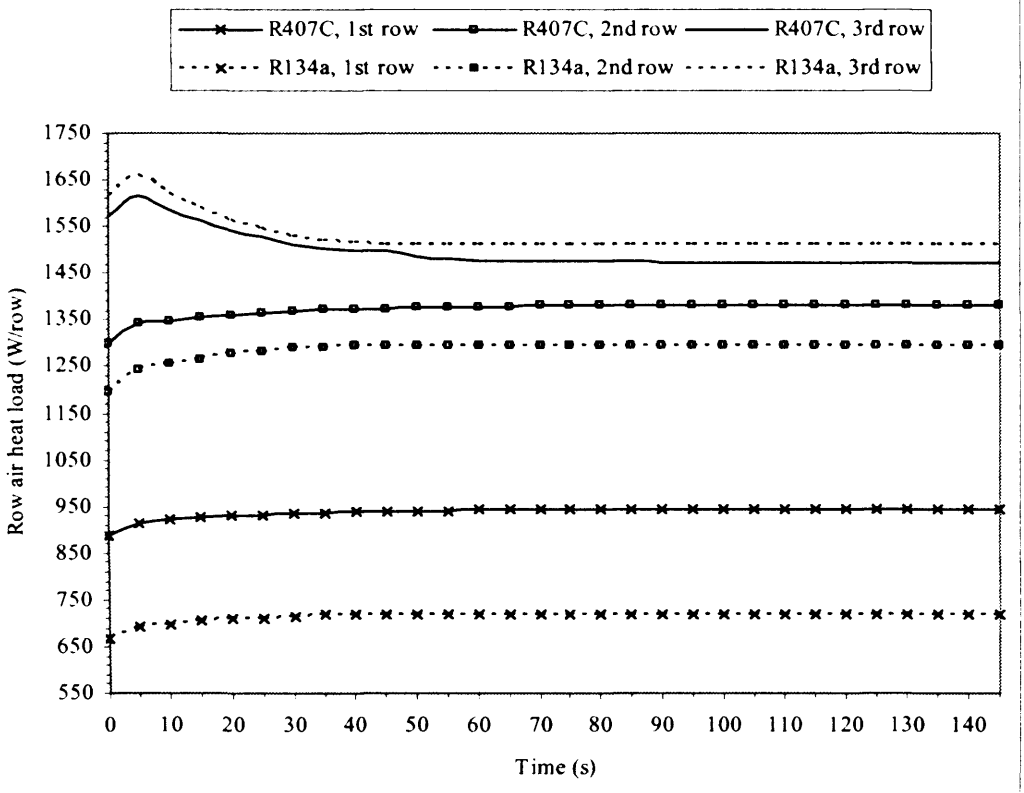

Figure 5.62b Air heat loads vs times for dry coils when there was a 0.5-degree-C step increase in coil-inlet dry-bulb temperatures

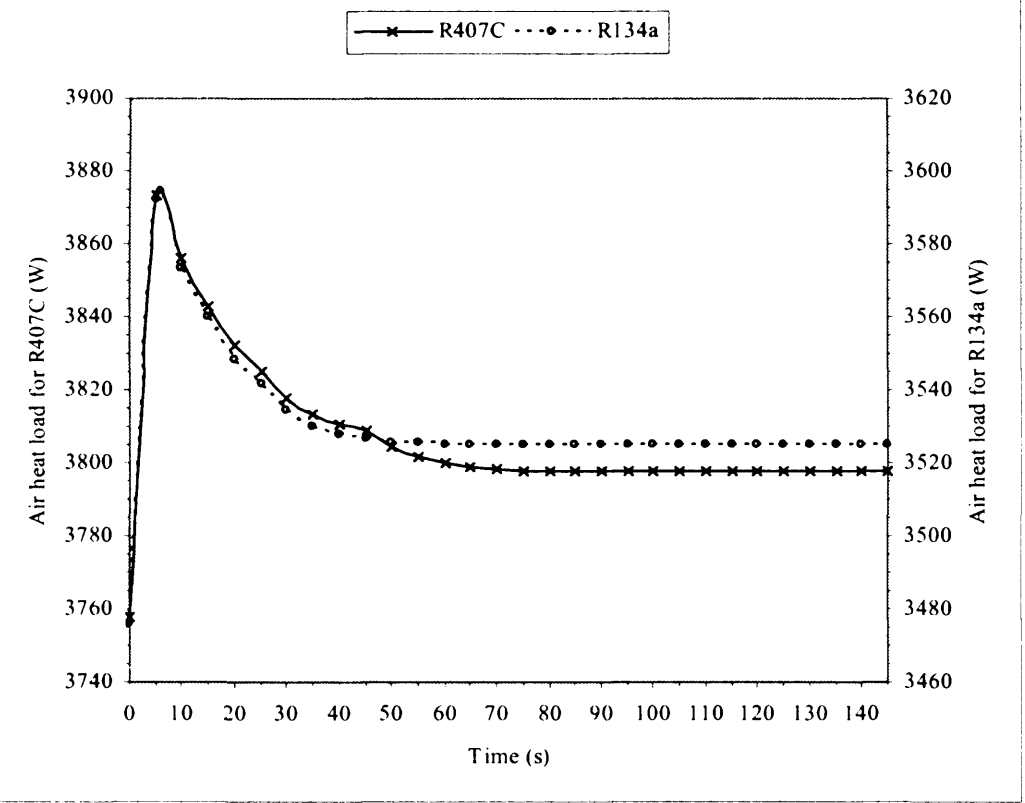

5.3 Result Discussion for Dry Coil

5.3.1 Dry-coil steady-state behaviour

The main findings in steady-state dry-coil behaviour *(under the previously established scheme for comparing the mixed and the pure refrigerants)* are discussed, and the implications of the results are addressed. Wherever appropriate, the results were compared with another researchers' work.

The working pressure of R407C was about 1.7 times larger than that of R134a. At the same time, the pressure drop of R407C was about 15% less than that of R134a. For both refrigerants, the patterns of the pressure-drop profile were similar together, and the maximum values occurred at about the same locations within the coils. The differences in operating pressure and the pressure drop for the two refrigerants are due the differences in refrigerant properties, whereas the similar pressure drop profiles results from the same flow patterns. Thus, R407C appears to offer benefits from refrigerant-side energy management point of view, since it has a lower pressure drop, equivalent to a lower energy loss in a system, in applications such as VRV systems.

The two-phase temperature gliding-up of R407C was about 4 times larger than the temperature drop of R134a. The first, second and third row temperature glide-ups were minimum, medium, and maximum, while the row temperature drops were minimum, maximum, and medium, respectively. The temperature variations are related to the two-phase degrees of freedom, being 3 and 1 for R407C and R134a respectively. *Based on the profiles of the temperature change per element/sub-element, it can be said that,* for R407C, the glide-up for an element exhibits explicitly a *close* link with the heat flux through its composition variations. The more the heat flux, the more evaporation of a more volatile component(s) is, causing the temperature glide up. *On the other hand,* for R134a, the temperature drop depended only on the refrigerant pressure drop. For a cross counter-flow coil, *when compared to R134a,* the matching of the air-R407C temperature profiles will be relatively easy to implement, because, for a high (or low) value of a row-inlet air temperature, the R407C temperature has a large (or small) gradient.

Moreover the superheat-initiation position of R407C was nearer to the refrigerant coil-outlet than that of R134a, implying that the R407C coil has a larger two-phase heat transfer, resulting in a better overall coil performance.

Based on the configurations of the coil and the refrigerant circuit in the study, for *the refrigerant heat flux along the coil* (Figs. 5.12 and 5.19), *in row 3*, for both refrigerants, the *profiles* of the superheat and 2-phase temperature significantly influenced *that* of the heat flux. *From row 2 to row 1*, because of the decreasing in the gliding of the temperatures, and due to the coil/refrigerant-circuit configuration, the difference between the average gradients per row of the heat flux between the two refrigerants was getting smaller. For both refrigerants, the variations of the refrigerant specific volume and the vapour quality, Figs. 5.17 and 5.18, can be discussed similarly as that done for the refrigerant heat flux.

For *the DB temperature at the outlet of a row*, the analysis is similar to that for the refrigerant heat flux. When comparing R407C with R134a, there are no significant differences between the variation of the coil-outlet dry-bulb temperatures caused by the temperature variations along the coil and the superheat temperature. This observation should be useful for improving the coil configuration and the refrigerant circuit arrangement. For instance, use more than 2 rows in a coil (reducing both temperature glide and superheat temperature effects) or a smaller number of refrigerant circuit if possible (reducing the superheat temperature effect).

The temperature of the tube wall can also use the discussion adopted for the refrigerant heat flux. In addition, due to the temperature gliding *and* the coil/refrigerant-circuit configuration the tube-wall temperature variation along the coil for R407C was thus larger than that for R134a.

Comparing with another research: Jia et al.'s work [1999] investigated the superheat-initiation-position effect upon the distribution of the dry-bulb temperature along the coil when using R134a. From the author's work, it demonstrated that, when comparing R407C with R134a, the dry-bulb temperature distributions are influenced by the refrigerant temperature glide in addition to the superheat effect.

Table 5.10 highlighted the difference between the two refrigerants, R407C and R134a, and summarised the superheat effect on the refrigerant heat flux, the wall temperature and the dry-bulb temperature along the coil.

Table 5.10 List of major findings in the steady-state behaviour based on under the refrigerant-comparison scheme, i.e. having the same: coil-inlet air condition, coil-inlet refrigerant mass flow rate and vapour quality, and coil-outlet refrigerant temperature

Refrigerant pressure and pressure drop	R407C has a higher operating pressure but a smaller overall pressure drop than R134a. The two refrigerants have different pressure drop per unit length (Pa/m) pattern along the two-phase region, but their peak values (Pa/m) occurred at about the same vapour qualities.
Refrigerant temperature	Due to composition shift, R407C experiences a larger two-phase temperature change (temperature gliding-up) than the R134a; for the latter, being a single-component refrigerant, the two-phase temperature change (decrease) was only caused by the pressure drop. The superheat-initiation position of R407C was nearer to the refrigerant coil-outlet than that of R134a. The two-phase temperature change per unit length of R407C was influenced mainly by the refrigerant heat flux, whereas that of R134a was only dependent on the refrigerant pressure drop.
Refrigerant HTC	Both R407C and R134a have similar magnitudes and patterns of variations of HTCs along the coil.
Refrigerant specific volume and vapour quality	The changes in the specific volume and the vapour quality of the refrigerants were influenced mainly by the heat fluxes along the coils that were in turn affected partly by their unique temperature profiles.
Refrigerant heat flux, tube-wall temperature, and row-outlet DB temperature	The influencing parameters were the 2-phase and the superheat temperature profiles, and the coil/refrigerant-circuit configurations. The variations of tube-wall temperature **along the coil** for a mixed refrigerant were larger than that for a pure refrigerant, whereas, when compared to a pure refrigerant, the variations of the ***coil-outlet*** DB temperature for a mixed refrigerant was not significantly different.

5.3.2 Dry-coil dynamic behaviour

The discussion for the time response of the coil variables was based on *a step change (increase or decrease) of 0.5 °C DB temperature at the coil inlet, unless otherwise mentioned.* The discussion focused on some of the main observations and the mechanism of the transient changes, and the understanding of the differences between the pure and mixture refrigerants.

What are main observations and what can be learnt from the results?

Regarding the coil-outlet refrigerant pressure, for either refrigerant (unless otherwise stated), 4 issues were discussed. **First,** *the profile of the pressure-drop vs. distance in the 2-phase region* can be divided in to 2 parts: *a positive-gradient profile (from the coil-inlet to the maximum-value location), and a negative-gradient profile (from the maximum-value location to the superheat-initiation location).* For *the profile in the superheat region,* only *a positive-gradient part* was observed.

Second, when having a step increase (Figs. 5.26a, 5.26b and 5.36), there is *a significant shifting of the profile in the 2-phase region*. The pressure drop within the positive-gradient part of the coil increased with time whereas the negative-gradient part had a negative rate of change with time. (In *the superheat region*, the change with time is insignificant.) ***Moreover***, when compared to R134a, the movement of the profile of the pressure drop vs. distance of R407C is less sensitive to the change of the coil-inlet DB temperature.

Third, generally, for an element, *based on a particular variation of the inlet pressure with time, the dynamic of the outlet pressure is then a function of the dynamic of the pressure drop* (Figs. 5.29 to 5.31). **Finally**, it can then be said that, due to the fact that R134a had a higher sensitivity of the pressure-drop-profile shifting to a step change of the coil-inlet DB temperature than R407C, the rate of change of the coil-outlet refrigerant pressure for R134a was on average smaller than and opposite to that for R407C. In addition, mostly, the local pressure of R134a responded faster than that of R407C.

For the two-phase section, the temperature of R134a generally responds slower than that of R407C. For a step increase of the coil-inlet air temperature, between 0 s to the steady-state, the magnitude of change of the temperature for R134a increased up to the location of the maximum pressure drop, and decreased afterwards. However, the corresponding value for R407C always increases and is about ten times larger than that of R134a. This difference between the two refrigerants can be explained based on the degrees of freedom; for R407C, its refrigerant temperature links directly to the refrigerant heat flux, whereas, for R134a, the temperature depends on the refrigerant pressure. For mixture refrigerants, the magnitudes of changes would be expected to magnify, for the rows with their inlet DB temperature influenced further by the superheat effect.

As expected, the refrigerant temperature gradient in the superheat region was much larger than that in the two-phase region for both refrigerants. In addition, the superheat-initiation of R134a occurs at an earlier position than that of R407C. As a result, the changes in the coil-outlet refrigerant-temperature with time for both refrigerants were in almost the same. However, the speed of R134a is slightly faster than that of R407C, implying for both refrigerants, there are little differences in temperature variations at the compressor inlets.

At the coil outlet, from the 0 second to the final steady state, the pressure and temperature of R407C changed in the same positive or negative direction, whereas, those of R134a changed in the opposite directions. This should be taken into consideration, when studying the TEV-controls. In addition, the specific volume of R407C was less sensitive (i.e. faster response and larger magnitude) to the change of the air temperature than that of R134a, giving it a more stable compressor operation.

For the 2-phase region, when compared to R407C, R134a is in the same direction, and has a higher speed and a larger magnitude of change with time. This implies that, at any time in the dynamic mode, for a given difference between the wall and the refrigerant temperatures, the percentage of increase in refrigerant heat transfer for R134a is more than that for R407C.

For both refrigerants, there were variations of the refrigerant heat flux along the coil and variations of the coil air-off temperature distributions in terms of the time response rate and the magnitude of change. As explained previously, the variations were mainly influenced by the initiation position of the superheat. To minimise these variations, the movement of the superheat initiation point should be kept small, the overall tube length should be proportionally much longer than the superheat region.

For the 2-phase region, the ratio of the refrigerant heat flux to the refrigerant HTC influenced the speed and magnitude of changes of the tube-wall temperature, and for R134a the direction of change could be positive and/or negative. However, due to the additional influence of the temperature glide, R407 only experienced an increase in the tube-wall temperature. Although this is unlikely to have a strong impact on the operation of dry coil, this would certainly affect the wet coil behaviour.

For **both refrigerants**, the total air heat load of the coil and the air heat load of the last row (i.e. row 3) changed sharply within short period of time, and then approached gradually to steady-state; whereas, for the other rows, the loads responded gradually to the step change. In other words, *both refrigerants had similar dynamics of the air heat loads.*

For both R407C and R134a, the (Fig. 5.62b), **within the first 5 s**, there was no difference in their total air heat **load** variations with time, suggesting that they had the same dynamics in the increase of the accumulated heat in the fin-and-tube-wall. **Between 5s and 50s**, R407C had slower decreasing rates of change with time of *the total heat load* than R134a. It was because that *R407C had slower rates of change of the*

superheat-initiation location (Fig. 5.63), i.e. having slower rates of decreasing of the length of the 2-phase region. **From 50s onwards**, reversing the trend, R134a had *the heat load* levelling at an earlier time of 75s as compared to 90s for R407C. This was due to *the combined dynamics of the superheat initiation location and the accumulated heat in the fin-and-tube-wall.* In addition, over the entire transient period, R407C needed to cope with a larger *total heat energy change* than R134a, as calculated by time-integration of the air heat load profiles (Fig. 5.62b) until steady state. It should also be noticed that, due to *the temperature gliding effect*, the difference between the 0 s and the steady-state values for R407C was less than that for R134a.

Figure 5.63 Superheat-initiation locations vs times for dry coils when there was a 0.5-degree-C step increase in coil-inlet dry-bulb temperatures

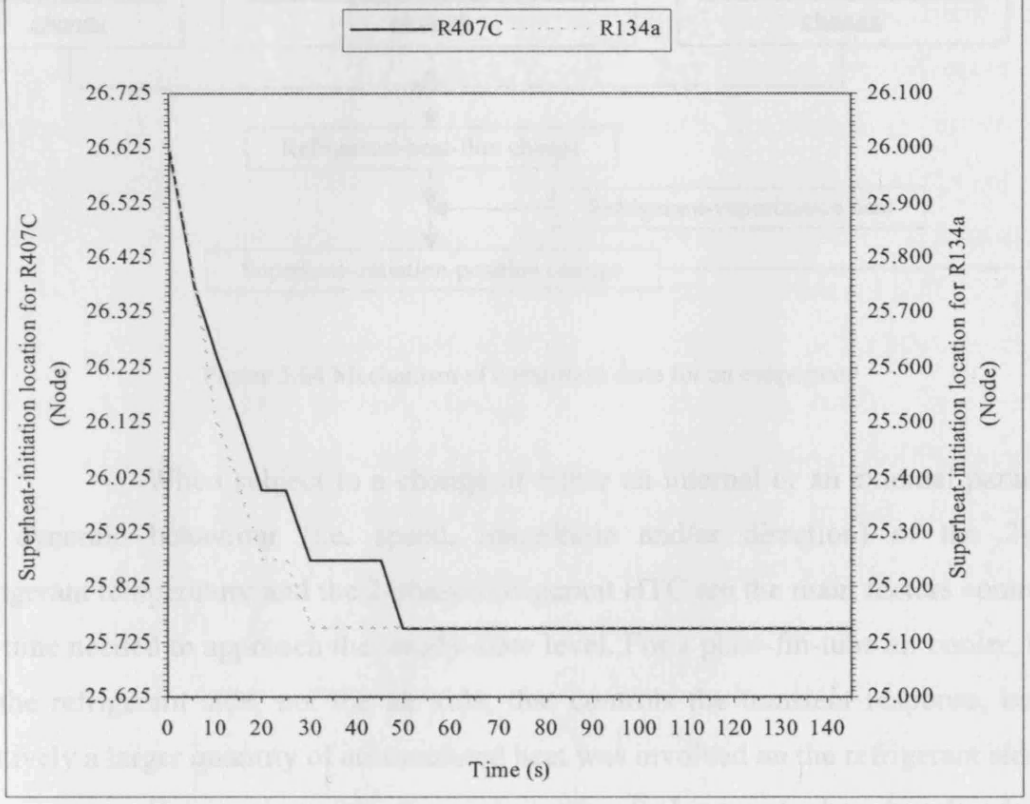

In analysing the dynamic behaviour, it is important to understand the cause and the associated end effects of **the transient process**. Fig. 5.64 demonstrates the sequence of the events, when there is either an air- or a refrigerant- side change, the accumulated heat in the fin and tube *induces* the occurrence of the transient process. In fact, any material in the coil can accumulate heat; however, its significance depends on the magnitude of its thermal diffusivity; the larger the value of the thermal diffusivity,

the less amount of accumulated heat. The air and refrigerant flows, though with *negligible* accumulated heat, can also influence the transient behaviour of the coil, via the superheat and the refrigerant-related effects.

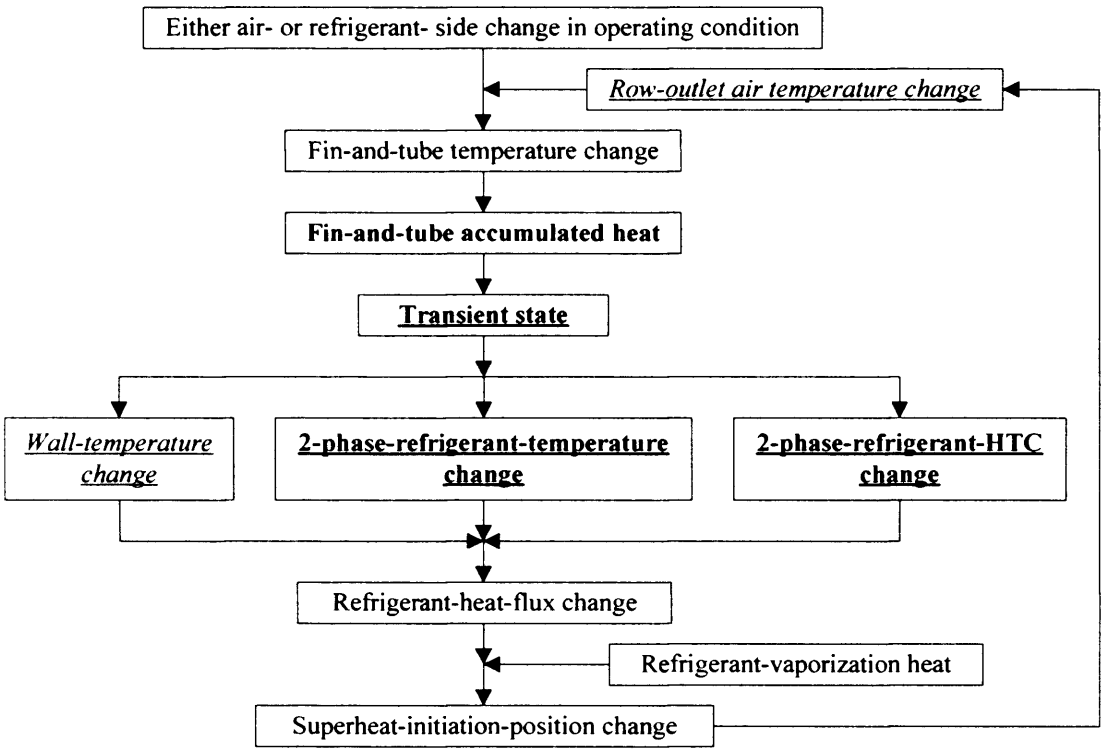

Figure 5.64 Mechanism of a transient state for an evaporator

When subject to a change of either an internal or an external parameter, the dynamic behaviour (i.e. speed, magnitude and/or direction) of the 2-phase refrigerant temperature and the 2-phase refrigerant HTC are the main factors controlling the time needed to approach the steady-state level. For a plate-fin-tube air cooler, it will be the refrigerant side, not the air side, that controls the transient response, because relatively a larger quantity of accumulated heat was involved on the refrigerant side.

Hence, there are three elements of changes to be considered: wall-temperature change, refrigerant-temperature change, and refrigerant-HTC change. For the wall-temperature dynamics, as discussed previously, it was a function of the dynamics of the refrigerant temperature, the refrigerant HTC and the refrigerant heat flux. Then, its involvement in the transient process was indirectly explained by the behaviour of the stated three parameters.

Considering the entire 2-phase region, for R407C, the directions of change of the air and the refrigerant temperatures were the same. For R134a, the directions of changes were mostly opposite. As a result, for R407C, at any point of time between 0 s to reaching steady-state, the difference between the air and the refrigerant temperatures varies relatively little. On the other hand, for R134a, at a location having the opposite directions of changes for air and refrigerant temperatures, as the time passes, for the step-increase case, the difference is getting larger.

For a refrigerant with a higher rate of change of the 2-phase refrigerant HTC, allowing a faster transfer of refrigerant heat flux. The results show that R134a has a higher rate than R407C.

Any of the three changes discussed above will result in a dynamic variation of the refrigerant-heat-flux, which in turn causes the superheat-initiation-position to move. In addition, with a difference in the values of the latent heat of vaporization between the two refrigerants, it will further enhance the difference in the movement of the initiation position. The movement results in a change in the row-outlet DB temperature and the coil temperature, affecting the overall transient of the coil.

As an example (referring to Fig. 5.64), when having a 0.5°C step increase of the inlet air temperature, the coil refrigerant temperature profile for R407C "rotate" counter-clockwise with a large magnitude of change, whilst that for R134a was reversed in direction with a much smaller change of magnitude, Fig. 5.40a. Based on this observation *alone*, one *may* deduce that, from the 0s to steady-state, R407C involved a smaller quantity of coil refrigerant heat energy (calculated by the time integration of the product of the heat load (W) and time (s)). Nevertheless, based on the dynamics of the "difference-from-0s" coil refrigerant heat load (i.e. subtracting from the current coil heat load, the value at the 0s), Fig. 5.65, R407C (3.264 kJ, i.e. an area under curve) had a larger value than that of R134a (2.886 kJ). In "managing" the coil heat-energy, since R407C had a smaller rate of change in the refrigerant HTC with time than R134a (Fig. 5.47a), the reaching-steady-state time of R407C for the movement of superheat initiation location should be longer than that of R134a. This is supported by Fig. 5.63.

Figure 5.65 For coil refrigerant heat loads, plotting difference values between at considered time and at 0 s vs times for dry coils when there was a 0.5-degree-C step increase in coil-inlet dry-bulb temperatures

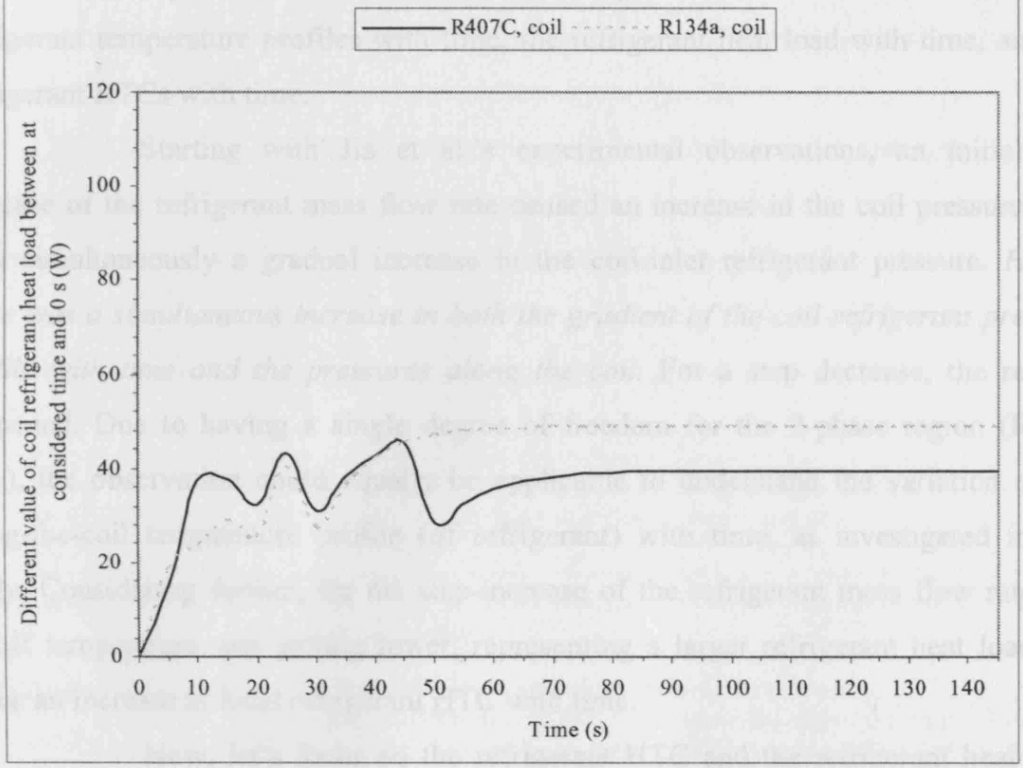

Comparing with another research: For R134a, Jia et al. [1995, 1999] did an experiment on a refrigeration cycle and performed a simulation for the evaporator under a wet-coil condition. At 0 s, a step increase of the refrigerant mass flow rate was introduced; having reached steady-state for a period of time, a step decrease of the flow rate with the same magnitude followed. The experimental results showed that, the magnitudes of change in the degrees of superheat were about the same in both cases, with naturally a smaller value of the degree of superheat and a lower value of air-off temperature at the increased flow rate. In addition, when having a step increase, the coil-inlet refrigerant pressure increased with time. However, it was observed that the time used to reach steady state for a step increase was longer than that for a step decrease. *It was suggested by Jia et al that the step-increase case had the accumulated heat of the coil in the superheat region (that must be removed), whereas the step-decrease had not; this caused the difference in the time used for reaching the steady state.*

For the present work, in relation to Jia et al's suggestion, the author put forward another explanation; it was thought that the difference in the time required to

reach steady state was caused by the difference in the paths of changes associated with the HTC and heat load of the refrigerant. Based on transient mechanism presented in Fig. 5.64, the explanation was as follow, involving 3 factors: the variation of the coil refrigerant temperature profiles with time, the refrigerant heat load with time, and the refrigerant HTCs with time.

Starting with Jia et al.'s experimental observations, an initial step increase of the refrigerant mass flow rate caused an increase in the coil pressure drop with simultaneously a gradual increase in the coil-inlet refrigerant pressure. *Hence, there was a simultaneous increase in both the gradient of the coil refrigerant pressure profile with time and the pressures along the coil.* For a step decrease, the reverse happened. Due to having a single degree of freedom for the 2-phase region (R134a only), the observation could equally be applicable to understand the variation of the along-the-coil temperature profile (of refrigerant) with time, as investigated in this study. Considering further, for the step-increase of the refrigerant mass flow rate, the air-off temperature was getting lower, representing a larger refrigerant heat load and hence an increase in local refrigerant HTC with time.

Now, let's focus on the refrigerant HTC and the refrigerant heat load. The refrigerant heat load in fact represented the difference between the temperatures of the refrigerant and the tube-wall (linked to the air inlet and air-off temperatures). For both parameters, *the paths of the changes of both step-change cases* were not the same. (It was not just the accumulated heat flux of the coil in the superheat region as suggested by Jia et al.) Hence, the interaction between the refrigerant and the tube-wall temperatures at any instance of the transient duration resulted in having a difference in the overall time for reaching the steady-state.

From the current study, new insights and detailed information (Summary in Table 5.11) was obtained as follows: **First**, it is found that R407C has a less sensitivity of the pressure-drop-profile shifting than R134a, enabling us to understand better the behaviour of the coil outlet pressure, which directly influence the TEV control. **Second**, the work provides details of the two-phase dynamics of the R407C and R134a temperature gliding profiles in terms of speed, direction and magnitude, as well as the dynamics of the refrigerant HTC for both refrigerants. These could help analysing different coil operations when using pure or mixed refrigerants.

Third, for a given refrigerant, there are variations in response speed and magnitude of the refrigerant heat flux along the coil, and of the coil-outlet DB

temperatures when subject to external disturbance. This will help understanding the relationship between coil configurations/refrigerant circuits and the ***control dynamics*** of the refrigerant heat load. **Fourth**, it was found that unlike R134a, the wall-temperature dynamics of R407C always responses with no drop/peak for a step increase/decrease, respectively; resulting in different coil operations under wet condition. **Finally**, it was shown that the speed and the direction of changes of the total air heat load for both refrigerants are the same. However, R134a has a larger magnitude of change of the total air heat load than R407C due to the associated temperature glide effect.

Table 5.11 A summary of the dynamic behaviour when subject to a change in the coil-inlet dry-bulb temperature

Fin-and-tube accumulated heat fluxes	Due to a significant amount of fin-and-tube heat capacitance, there was always a change in the accumulated heat flux in the fin and tube.
Superheat effect	The initiation position of the superheat influences dynamic response of the coil outlet DB temperature.
Refrigerant pressure drop	The pressure of R134a would response faster than that of R407C. Between two refrigerants, the difference in the sensitivity of the pressure-drop-profile shifting resulted in the different developed direction and magnitude of the pressure versus time along the coil and at the coil outlet.
Refrigerant temperature	The temperature of R134a responded slower than that of R407C. However, R134a reached a steady-state level quicker than R407C. Nevertheless, the changes in the coil-outlet refrigerant temperatures with time were almost the same in terms of direction and magnitude.
Refrigerant HTC, Refrigerant specific volume	The 2-phase HTC of R134a responded faster to the change in the inlet air temperature and reached a steady-state level quicker than that of R407C. Same observation applied to the refrigerant specific volume along the coil and at the coil outlet.
Refrigerant heat flux	Along the coil, for both refrigerants, there were variations of the refrigerant heat flux in terms of the time response and the magnitude of change.
Dry-bulb temperature	To reach a steady-state level, R134a used less time than R407C; the associated speed depends on the superheat effect.
Tube-wall temperature	For the 2-phase region, the ratio of the refrigerant heat flux to the refrigerant HTC influenced both speed and direction of the tube-wall temperature for R134a. It affected only the speed of the tube-wall temperature for R407C. For reaching a steady-state level, R134a used less time than R407C.

5.4 Totally-wet-coil Results and Discussion

Before presenting and discussing the results, it is useful/necessary to provide some details concerning the influence of the refrigerant type that was observed

from the dry-coil simulation and their relevance to the totally-wet coil study regarding the coil configuration, the refrigerant circuit and operating conditions, and the resolutions in simulation. From the dry-coil, when comparing the two refrigerants, for the steady-state, the along-the-coil 2-phase wall temperature profiles were different in the gradients. For the dynamics, when having a step increase of the coil-inlet air temperature, the local 2-phase wall temperature with time for R407C always increased with no peak, whereas that for R134a increased with either a peak or no peak. Because the condensation on the air-side of the coils was a function of the wall temperature, the raised observation can give an idea of the difference in coil behaviour between the 2 refrigerants.

For the coil configuration, as shown in Table 5.12, it is seen that, compared to the dry-coil, there were less rows per coil, but in each refrigerant circuit having more tube per row. The reasons for such an arrangement were previously explained in Section 4.6.2 of the wet-coil simulation. In addition, since the effective HTC of the wet coil was about two times larger than that of the dry coil, a larger value of the fin spacing to thickness ratio was used so that the refrigerant mass flow rate would not be too high, avoiding excessive coil refrigerant pressure drop.

Table 5.12 Coil configurations for totally-wet-coil conditions when using R407C and R134a (Referring to Table 5.6, being for only details that were different to the dry-coil conditions shown here)

Numbers of rows	2
Numbers of tubes in a row	16
Numbers of refrigerant circuits	4
Fin spacing to thickness ratio	17.2

For each refrigerant circuit, the flow directions of both air and refrigerant were shown in Figs. 5.66 and 5.67, which also show the numbering of the rows, tubes, elements and sub-elements. Table 5.13 showed the assigned operating conditions.

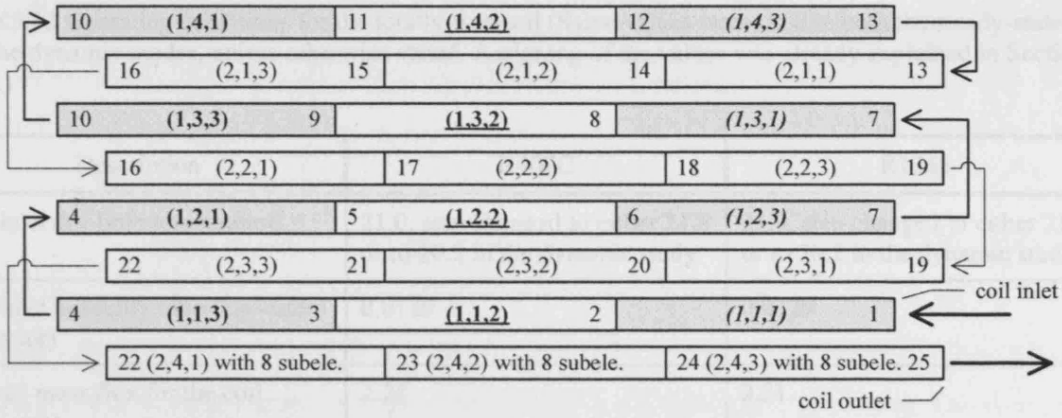

Figure 5.66 Element and Sub-element arrangements in the refrigerant circuit had the numbers in the brackets corresponded to the row, tube, and element numbers, respectively. The highlighted tubes corresponded to the tubes in row 1 of Fig. 5.67.

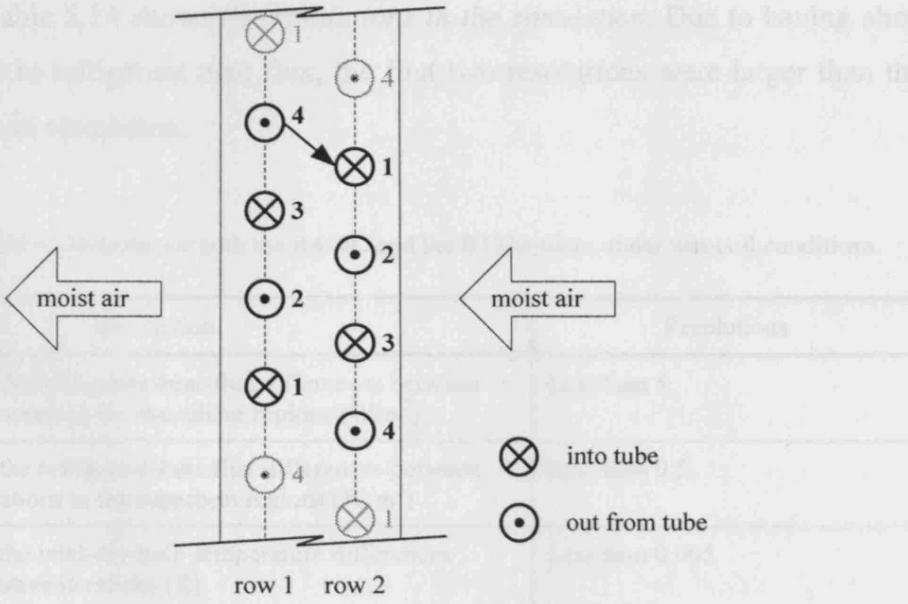

Figure 5.67 Side view of the coil by looking from the coil end with the refrigerant coil-inlet

Table 5.13 Operating conditions for the totally-wet-coil (Same values were used in both the steady-state and the dynamic modes, unless otherwise stated. Assigning of the values was already explained in Section 4.6.2.)

Description	R407C	R134a
Coil-inlet dry-bulb temperature (°C)	21.0, step changed to either 21.8 or to 20.2 in the dynamic study	21.0, step changed to either 21.8 or to 20.2 in the dynamic study
Coil-inlet humidity ratio (kg water / kg dry air)	0.0129	0.0129
Inlet air mass flux for the coil ($kg/(s.m^2)$)	2.21	2.21
Refrigerant-inlet conditions	2.0 °C and 583488 Pa Mass flow rate = 0.0541 kg/s	5.9 °C and vapour quality = 0.2 Mass flow rate = 0.0541 kg/s

Table 5.14 shows *the resolutions in the simulation.* Due to having about two times larger in refrigerant heat flux, the first two resolutions were larger than that used in the dry coil simulation.

Table 5.14 Simulation resolutions for both the R407C and the R134a cases under wet-coil conditions

Description	Resolutions
Absolute values of the refrigerant-heat-flux differences between the consecutive iterations in the two-phase regions (W/m^2)	Less than 5
Absolute values of the refrigerant-heat-flux differences between the consecutive iterations in the superheat regions (W/m^2)	Less than 0.5
Absolute values of the inlet-dry-bulb-temperature differences between the consecutive iterations (K)	Less than 0.005
Absolute values of the coil-outlet-dry-bulb-temperature differences between the consecutive iterations (K)	Less than 0.005
Absolute values of the inlet-dry-humidity-ratio differences between the consecutive iterations (kg of water/kg of dry air)	Less than 0.000005
Absolute values of the coil-outlet-humidity-ratio differences between the consecutive iterations (kg of water/kg of dry air)	Less than 0.000005

5.4.1 Totally-wet-coil steady-state behaviour

Tables 5.15 and 5.16 highlight the details of the main findings and the key observations, and the knowledge gain. In Table 5.15, the studied parameters, mainly refrigerant-side, were selected on 2 bases, i.e. to provide additional information on the coil behaviour (when compared to the dry-coil) and on parameters un-related to the

refrigerant mass flux. Table 5.16 mainly concerned with the air-side parameters for the wet coils; as expected, they are dependent on the air-on conditions. The work was compared with previous research too. To author's knowledge, all of observations and discussion given were original.

Main findings and key observations: On **the refrigerant side**, based on the same pressure and temperature of R407C and the same vapour quality of R134a at the coil-inlet for both wet and dry coils, ***the coil-inlet pressure*** of R134a for the wet coil would have a higher value than that for the dry coil. However, similar to the dry coil, R407C had a smaller ***overall pressure drop*** than R134a. Relatively to the dry coils, in the 2-phase region, the R407C temperature glide-up and the R134a temperature drop for the wet coils were smaller and larger, respectively. The two coil conditions showed opposite trends in ***the temperature gliding for the two refrigerants***, i.e. for the dry coils: gliding-up was larger than temperature drop, whereas for the wet coils: being smaller, correspondingly. For either R407C or R134a, the ratio of the maximum *HTC* to that at the coil-inlet were about the same for both wet and dry coils. For both refrigerants, the ratios of ***the refrigerant heat load*** for the wet coil to that for the dry coil were of the same values, so were the ratios of the latent-or-sensible heat load of the wet coil to the dry-coil refrigerant heat load.

On **the air-side**, ***the coil-outlet DB temperatures*** of R407C had a smaller variation than that of R134a. Comparing the two refrigerants, the spatial profiles of ***the DB temperatures*** and ***the humidity ratios*** were similar. As for ***the condensate rates***, for the first-row (i.e. coil outlet) and the coil as a whole, R407C had higher values than R134a, whereas, for the last-row (i.e. the coil air-inlet), the reverse happened.

Table 5.15 Steady state of the totally-wet coils - results and discussion

Totally-wet conditions (Comparing R407C with R134a)	**To discuss the dehumidification process (the totally-wet effect), as compared to dry coil, for individual refrigerants**	**Based on observations from dry coil operation, further comments are given for the totally-wet coils**
Refrigerant pressures: (Fig. 5.68) The average value for R407C (555 kPa) is about 1.7 times higher than that for R134a (327 kPa).	For R407C, the coil-inlet pressures are the same for both coil conditions. For R134a, the coil-inlet pressure of the wet coil (about 360 kPa) was higher than that of the dry coil (about 350 kPa).	Refrigerant-type effect: The ratio of the R407C ***average pressure*** to the R134a ***average pressure*** for the wet coil was about the same value as that for the dry coil. This observation was also noticed in the ***pressure drop.*** *(It*

Table 5.15 Steady state of the totally-wet coils - results and discussion

Totally-wet conditions (Comparing R407C with R134a)	**To discuss the dehumidification process (the totally-wet effect), as compared to dry coil, for individual refrigerants**	**Based on observations from dry coil operation, further comments are given for the totally-wet coils**
For the overall pressure drops, R407C (57 kPa) had 0.85 times of R134a (67 kPa).	For each refrigerant, the coil pressure drop of the wet-coil was about 4.5 times of that of the dry-coil.	*should be borne in mind that, with the scheme of refrigerant comparison, the coil-outlet temperatures were about the same.)*
Refrigerant temperatures: (Fig. 5.69) At the coil inlet, the temperature of R407C was 2.0 °C, whereas that of R134a was 5.9 °C. In the 2-phase section, the temperature glide-up of R407C (1.86 °C) was around 0.35 times less than the temperature drop of R134a (5.35 °C). The average coil temperature for R407C (2.93 °C) was less than that for R134a (3.23 °C).	For the 2-phase region, for R407C, the temperature glide-up of the wet coil was about 50% of that of the dry coil (Fig. 5.12), whereas, for R134a, the temperature drop of the wet coil was about 5 times of that of the dry coil. At the coil inlet, for R407C, the temperature of the wet coil was the same as that of the dry coil, whereas, for R134a, the temperature of the wet coil (5.9 °C) was higher than that of the dry coil (5.05 °C).	Totally-wet effect: When comparing the two refrigerants, the ratio of the temperature glides of R407C to R134a for the wet coil (0.35) was less than that for the dry coil (4). In the wet coil, for both refrigerants, the refrigerant mass flow rates were larger, due to larger heat loads, than that in the dry coil; this caused a substantial increase in pressure drop. As discussed, the pressure drop influenced indirectly and directly the temperatures of R407C and R134a, respectively.
Refrigerant heat transfer coefficients: (Fig. 5.70) In the first row, both refrigerants had about the same values of increase of HTCs. In the last row, HTCs of R407C increased at a slower rate than that of R134a; the former therefore had lower values of HTC in the last row.	For each refrigerant, the pattern of the HTC profile of the wet coil was similar to that of the dry coil (Fig.5.14). The ratio of the maximum HTC to the corresponding coil-inlet value of the wet coil was also about the same as the dry coil (2.3 for R407C and 2.6 for R134a).	Refrigerant-type effect: Similar observations as that of the pressure behaviour as influenced by the refrigerant can be made.
Refrigerant heat fluxes: (Fig. 5.71) For the first row, due to the superheat effect, R407C had a smoother heat-flux profile than R134a. For the second row (i.e. the last row), both refrigerants had equally smoothness (based on its variation along the row), though for both rows, due to the temperature-glide effect, R407C has a smaller gradient of the heat fluxes than R134a.	For R407C, for the first row, the wet coil had a smoother heat-flux profile than the dry coil (Fig. 5.19), whereas, for the last row (i.e. the 2nd row for the wet coil and the 3rd row for the dry coil), both coil conditions had about the same smoothness. For R134a, for each row (of the first and the last rows), both coil conditions had around the same smoothness. The gradient of the heat fluxes, for R407C, for the first row, with the wet coil, (180 W/(m^2·elemental length)) was	Temperature glide effect: In the last row, on the refrigerant side, when compared R407C with R134a, both wet and dry coils had the same smoothness between the heat flux profiles of the two refrigerants. However, both profiles for the wet coil swung counter clock-wise, different to that for the refrigerant temperatures that swung in the opposite direction.

Table 5.15 Steady state of the totally-wet coils - results and discussion

Totally-wet conditions (Comparing R407C with R134a)	**To discuss the dehumidification process (the totally-wet effect), as compared to dry coil, for individual refrigerants**	**Based on observations from dry coil operation, further comments are given for the totally-wet coils**
	larger than that of the dry coil (41 W/(m^2·elemental length)). For the last row, the reverse happened (96 and -107 W/(m^2·elemental length), respectively). The corresponding values for R134a were 457, 172, 899 and 139 W/(m^2·elemental length), respectively.	
Refrigerant heat loads: For the first row, the heat load for R407C and R134a were 3618 W and 2849 W respectively, whereas, for the last row, R407C (5449 W) had a slightly less heat load than R134a (5459 W).	For R407C, the total heat load of the wet coil (9068 W) was about 2.4 times of that of the dry coil (3758 W). R134a had about the same factor (2.4) as that for R407C (8308 W vs 3476 W).	Refrigerant-type effect: The ratio of R407C to R134a total heat loads for the wet coil (1.09) was about the same as that for the dry coil (1.08). The discussion can be said to be similar to that for the pressure behaviour.
Tube-wall temperatures: (Fig. 5.72) When compared R407C with R134a, similar observations to that of the heat fluxes could be made, but with opposite gradients. (The superheat influenced the smoothness in the first row, whereas, the temperature-glide affected the gradients in the both rows.) For the first row, the average tube-wall temperature for R407C was lower than that for R134a, whereas, for the last row, R407C had higher values than R134a.	For both the first and the last row, with both refrigerants, the smoothness of the profiles could be described in a similar way as that of the heat fluxes. For the gradients of the tube-wall temperature, for R407C, the first row of the wet coil (-0.071 °C/elemental length) had a larger value, but being negative, than the dry coil (0.005 °C/elemental length). For the last row, the wet coil (-0.037 °C/elemental length) had a smaller value than the dry coil (0.1 °C/elemental length). For R134a, for both rows under both coil conditions, all the gradients were negative. For the first and the last rows, the wet coil: -0.157 and -0.414 °C/elemental length; the dry coil: -0.003 and -0.15 °C/elemental length, respectively.	Temperature glide effect: For both refrigerants, for the last and the first rows, the description can be carried out the same way as that for the refrigerant heat fluxes, but the direction of the swinging was opposite.
Inlet dry-bulb temperatures: (Fig. 5.73) For the first row, due to the superheat effect, the profile for R407C was smoother than that for R134a. The gradient for R407C was slightly less than that for R134a. The average	For the first row with R407C, the profile for the wet coil was smoother than that for the dry coil Fig. 5.21. The gradient for the wet coil (0.007 °C/elemental length) was less than that for the dry coil (0.05 °C/elemental length).	Coil-arrangement effect: As observed, due to the coil arrangement, for both refrigerants, for the first row, the gradients for both wet and dry coils are almost level.

Table 5.15 Steady state of the totally-wet coils - results and discussion

Totally-wet conditions (Comparing R407C with R134a)	**To discuss the dehumidification process (the totally-wet effect), as compared to dry coil, for individual refrigerants**	**Based on observations from dry coil operation, further comments are given for the totally-wet coils**
temperature for R407C was approximately the same as that for R134a.	For R134a, the profiles for the wet and the dry coils were equally smooth. The gradient for the wet coil (0.06 °C/elemental length) was slightly larger than that of the dry coil (0.03 °C/elemental length). For both refrigerants, the wet coil had higher DB temperatures than those of the dry coil.	
Outlet dry-bulb temperatures: (Fig. 5.73) For the first row, the profiles can be described the way as that for the inlet DB temperatures (i.e. the superheat affecting the smoothness). The two refrigerants have about the same gradients (due to the effect of the temperature-glide). All the temperatures for R407C were less than that for R134a at the corresponding elements. For the last row, both refrigerants had the same smoothness of the profiles. The gradient of R407C was less than that of R134a (due to the temperature-glide effect). On average, the temperatures for R407C were higher than that for R134a.	From Figs. 5.73 and 5.21, for the first row, for R407C, the profile of wet coil had a smaller variation than the dry coil, whereas, R134a gave no difference between the two coil conditions. For the dry coil, both refrigerants had about the same smoothness. For the first row, for R407C, the gradients for the wet and the dry coils were in the opposite directions, but the absolute values of the gradient for both coils were equal (±0.03 °C/elemental length). For R134a, the absolute value of the gradient for the wet coil (-0.04 °C/elemental length) was slightly less than that for the dry coil (0.05 °C/elemental length). For both refrigerants, all temperatures for the wet coils were higher than that for the dry coils. For both refrigerants, for the first row, the wet coils had higher temperatures than the dry coils. For the last row, the wet coils had mostly lower temperatures than the dry coils; only two elements between nodes 13 and 15 for R134a that the wet coil had a higher temperature than the dry coil.	Temperature glide effect: For both the last and the first rows, the description was as for the tube-wall temperatures.

Table 5.16 Steady state air-side parameters (that were unique in the totally-wet coil and/or were constant in the dry coils) of the totally-wet coils: results and discussion

Totally-wet conditions (Comparing R407C with R134a)	**Based on observations from dry coil operation, further comments are made for the totally-wet coils**
Humidity ratios: (Fig. 5.74) Considering both R407C and R134a cases, for both inlet and outlet HRs of individual rows; the profile, the smoothness, the gradient and the average values of the HRs behave similarly to that of the DB temperatures (Fig. 5.73).	Coil-arrangement effect: For the coil-arrangement effect upon the inlet HRs, see the discussion for the inlet DB temperatures (Table 5.15). Temperature-glide effect: For both refrigerants, for both the last and the first rows, by observing the profile of the outlet HRs and the profile of the difference between the inlet HR and the saturated HR at a surface of condensate on a tube wall (Fig. 5.75), it was clear that the outlet HRs were influenced by the latter. For the temperature-glide effect, see the discussion on the saturated HRs at surfaces of condensate on tube walls.
Saturated humidity ratios at surfaces of condensate on tube walls: (Fig. 5.76) The description was the same as that for the tube-wall temperatures.	Temperature-glide effect: When examining the profiles of the tube wall temperature and the saturated humidity ratios, it was apparent that there was a direct link. Based on the discussion of the tube wall temperature, the effect of the temperature glide was upon the saturated humidity ratios.
Inlet relative humidities: (Fig. 5.77) The description was similar to the inlet DB temperatures. Almost all the inlet RHs for R407C were lower than that for R134a.	
Outlet relative humidities: (Fig. 5.77) For the first row, the smoothness and the gradients can be described the same as that for the outlet DB temperatures. However, the variation of the outlet RHs for R407C was less than that for R134a. Relatively, for both refrigerants, the variation of outlet RHs was much less than that of the outlet DB temperatures. For the last row, the smoothness and the gradients can be described the same as that for the outlet DB temperatures. On average, the outlet RHs for R407C were lower than that for R134a.	
Condensate fluxes: (Fig. 5.78) The variations (both smoothness and gradients) for the first and the last rows were the same as that of the tube-wall temperatures; however, the gradients were in the opposite direction.	Coil-arrangement and temperature-glide effects: For both refrigerants, when examining profiles of differences between the inlet HR and the saturated HR at the surface of the condensate on the tube wall, Fig. 5.75, it was clear that the differences had an influence on the condensate heat fluxes. As discussed previously, the inlet HRs and the saturated HRs at the surfaces of the condensate were affected by the coil arrangement, and by the

Table 5.16 Steady state air-side parameters (that were unique in the totally-wet coil and/or were constant in the dry coils) of the totally-wet coils: results and discussion

Totally-wet conditions (Comparing R407C with R134a)	**Based on observations from dry coil operation, further comments are made for the totally-wet coils**
	temperature glide, respectively, as were the condensate fluxes.
Condensate rates: For the first row, R407C had a higher condensate rate (1.25E-5 kg/s) than R134a (9.98E-6 kg/s), whereas, for the last row, the reverse happened (1.57E-5 and 1.64E-5 kg/s, respectively). Overall R407C (2.83E-5 kg/s) had a higher condensate rate than R134a (2.64E-5 kg/s).	Temperature-glide and refrigerant-HTC effects: There was the small difference between the last-row condensate rates, because, for both refrigerants, the refrigerant HTCs in the superheat regions were much smaller than that in the 2-phase regions.
Latent heat fluxes: (Fig. 5.79) The profiles were similar to that of the condensate fluxes.	Coil-arrangement, temperature-glide and refrigerant-HTC effects: After having studied the profiles of the condensate fluxes (Fig. 5.78) and the latent heat fluxes, as well as the behaviour of the latent heat of condensation (J/kg of condensate) (Fig. 5.80), it can be said that the above three effects strongly dominated the influence of the latent heat of condensation on the latent heat fluxes.
Latent heat loads: The description was the same as that for the condensate rate with respect to R407C and R134a (for the first row: 1920 and 1530 W; for the last row: 2922 and 2896 W, for the coil: 4842 and 4426 W, respectively).	Temperature-glide and refrigerant-HTC effects: The discussion is the same as that for the condensate rates.
Sensible heat fluxes: (Fig. 5.81) The profiles were similar to that of the latent heat fluxes.	Coil-arrangement and temperature-glide effects: These two effects can be discussed in the same manner as for the inlet DB temperatures and the tube-wall temperatures.
Sensible heat loads: The numbers in the bracket corresponded respectively to that of the latent heat loads for R407C and R134a (for the first row: 1698 and 1319 W; for the last row: 2527 and 2563 W, for the entire coil: 4226 and 3882 W).	Temperature-glide and refrigerant-HTC effects: The discussion is similar to that for the condensate rates.
Effective heat transfer coefficients: (Fig. 5.82) For the first row, both refrigerants had the same smoothness and with an almost-zero gradient. All HTCs for R407C were less than that for R134a. For the last row, both refrigerants had the same smoothness, whereas, the gradient for R407C (almost zero) is marginally less than that for R134a (-0.09 %/elemental length). On average, R407C had a higher HTC than R134a.	Temperature-glide effect: Having examined the profiles of the refrigerant heat fluxes and the effective air-side HTCs, for both the 2-phase and the superheat regions, it can seen that the temperature variations along the coil dominated the effective HTC effect on the refrigerant heat flux.
Effective mass transfer coefficients: (Fig. 5.83) For both rows and both refrigerants, the profiles	Coil-arrangement, temperature-glide and refrigerant-HTC effects: Having studied the

Table 5.16 Steady state air-side parameters (that were unique in the totally-wet coil and/or were constant in the dry coils) of the totally-wet coils: results and discussion

Totally-wet conditions (Comparing R407C with R134a)	**Based on observations from dry coil operation, further comments are made for the totally-wet coils**
were similar to, but in the reverse direction to that of the effective HTCs.	profiles of the condensate fluxes and the effective MTCs, for both the 2-phase and the superheat regions, it seems that the effective MTC had a much less influence upon the condensate fluxes than the mentioned three effects.
Fin efficiencies: (Fig. 5.84) For both rows and both refrigerants, the profiles were similar to that of the effective MTCs.	Temperature-glide effect: The discussion is similar to that of the effective HTCs.

Figure 5.68 Refrigerant pressures vs nodes for totally-wet coils

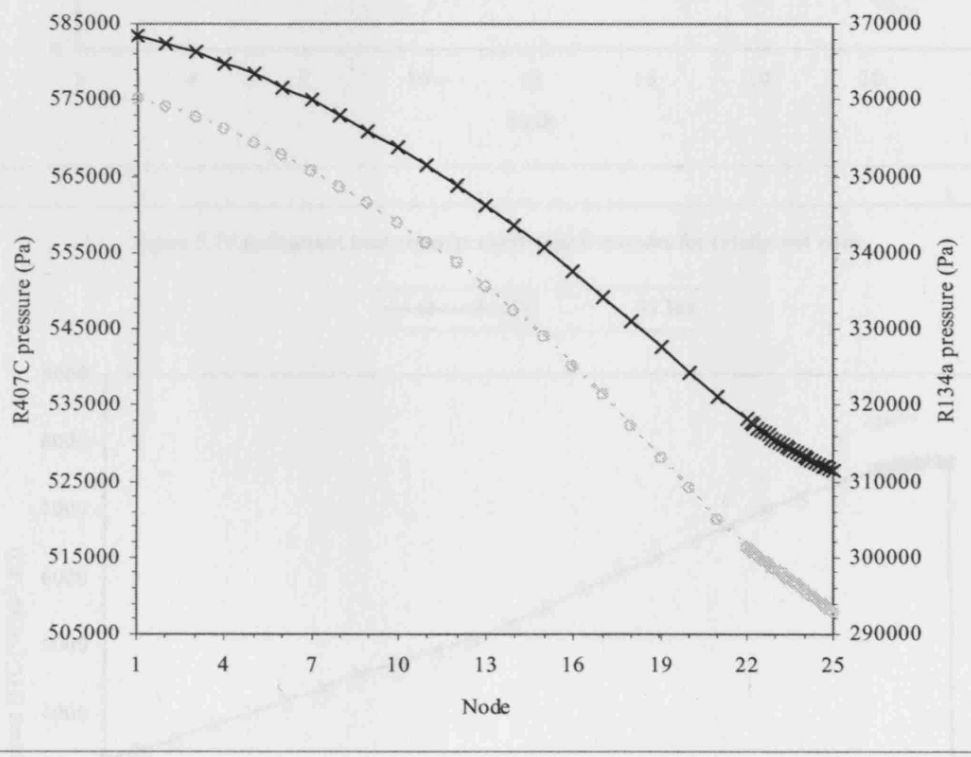

Figure 5.69 Refrigerant temperatures vs nodes for totally-wet coils

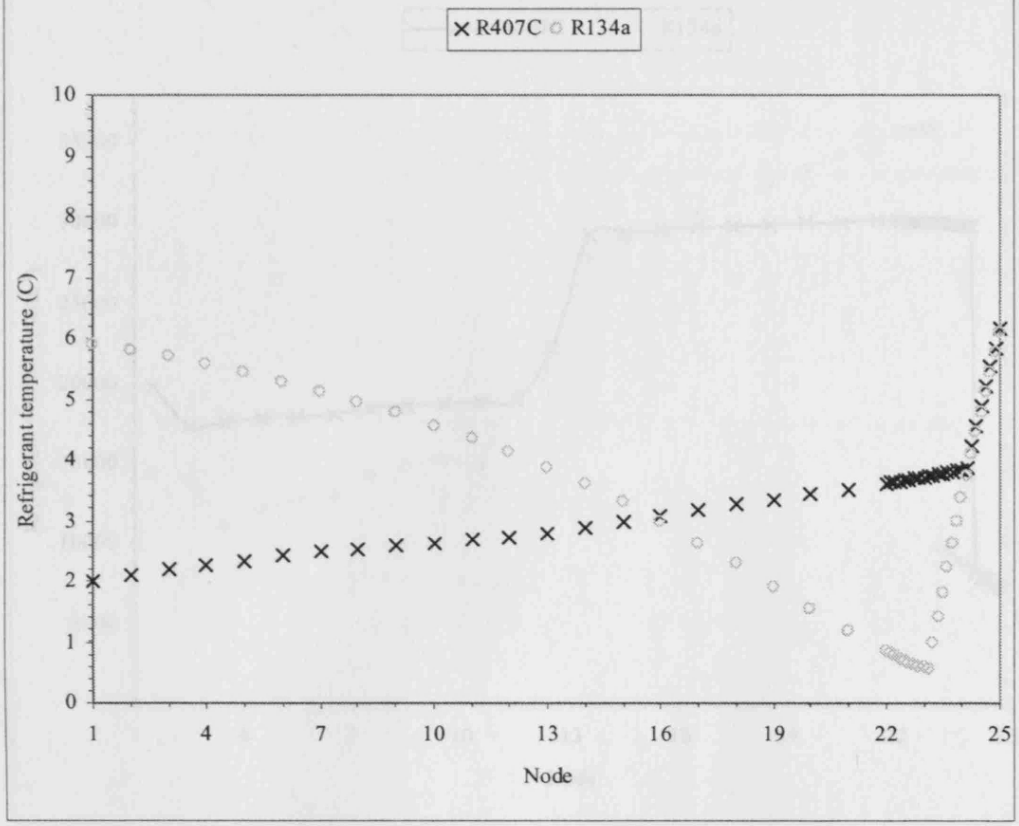

Figure 5.70 Refrigerant heat transfer coefficients vs nodes for totally-wet coils

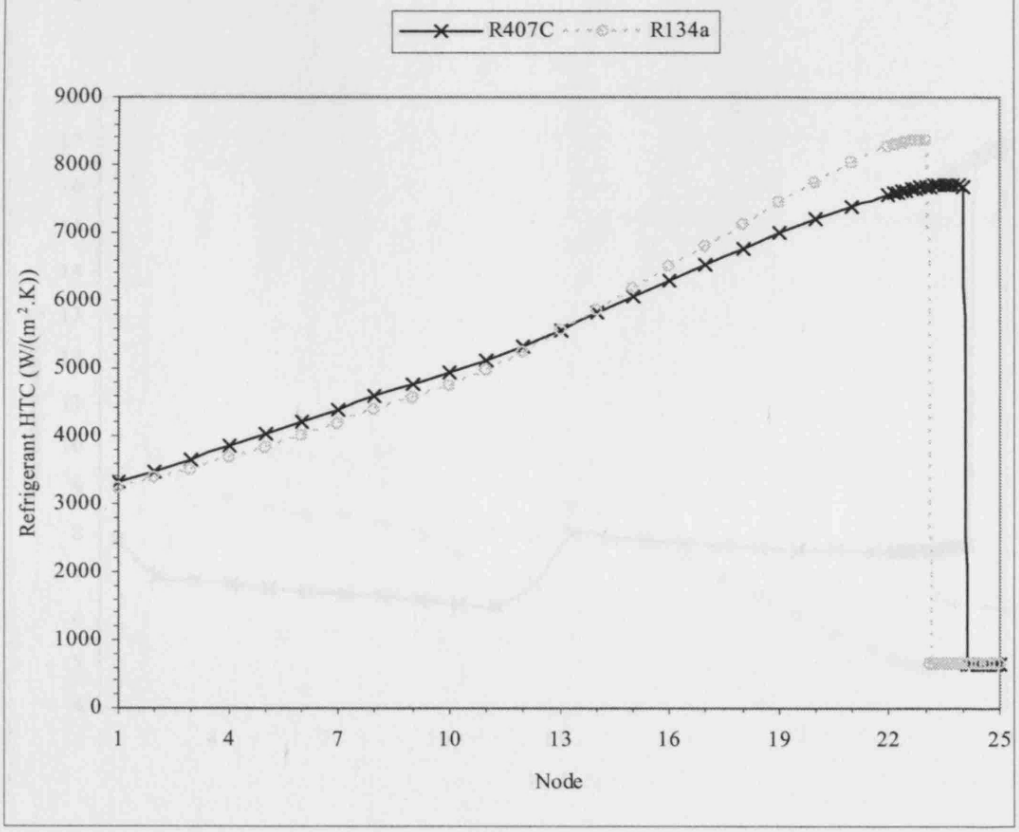

Figure 5.71 Refrigerant heat fluxes vs nodes for totally-wet coils

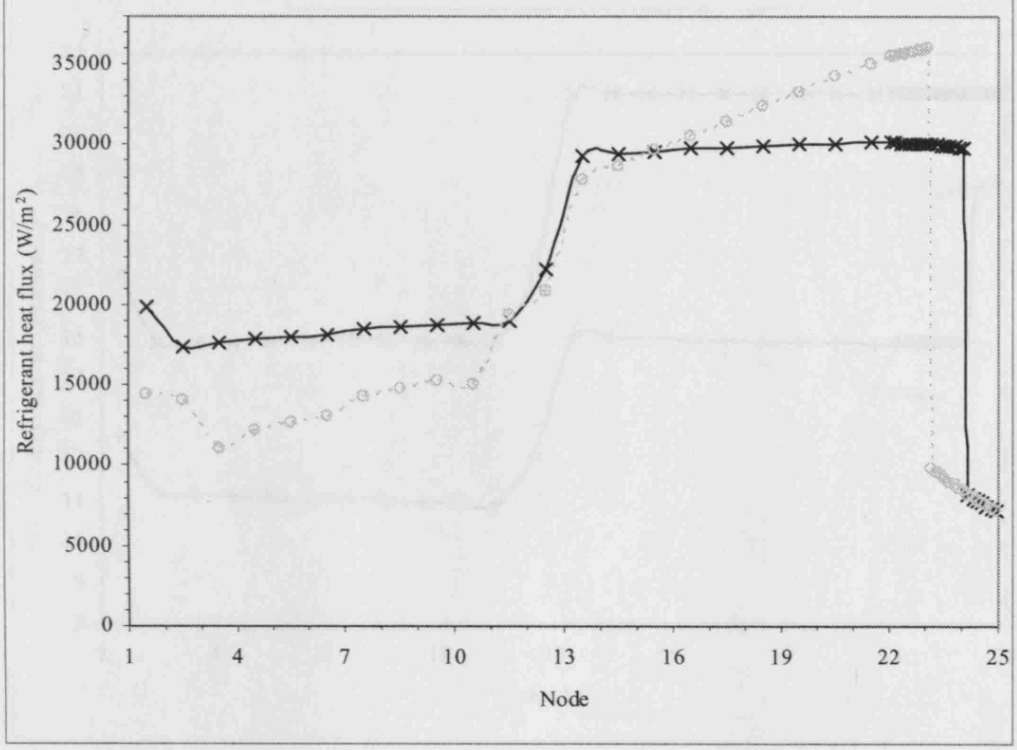

Figure 5.72 Wall temperatures vs nodes for totally-wet coils

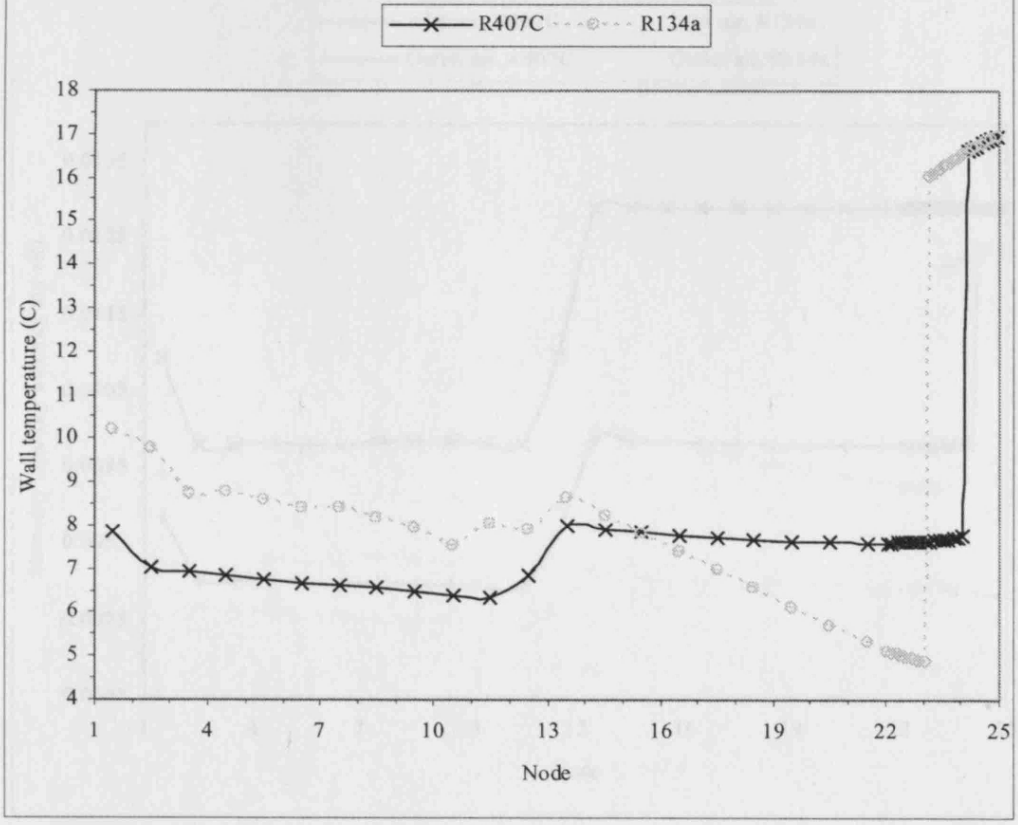

Figure 5.73 Dry-bulb temperatures vs nodes for totally-wet coils

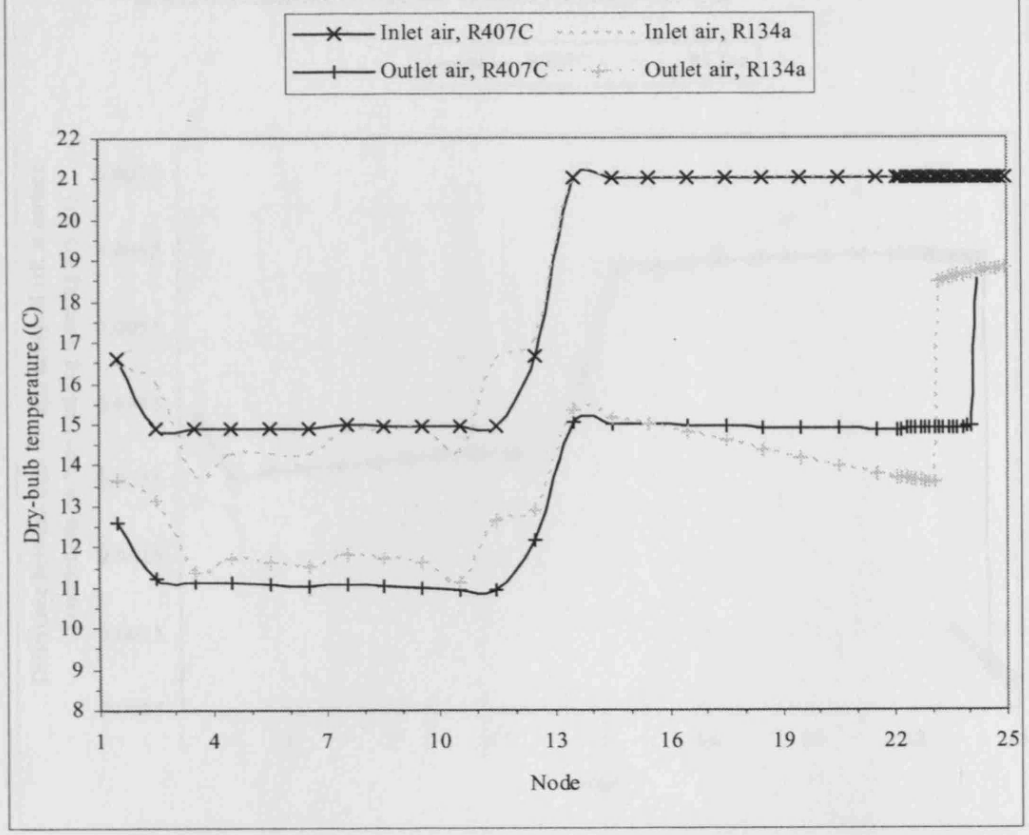

Figure 5.74 Humidity ratios vs nodes for totally-wet coils

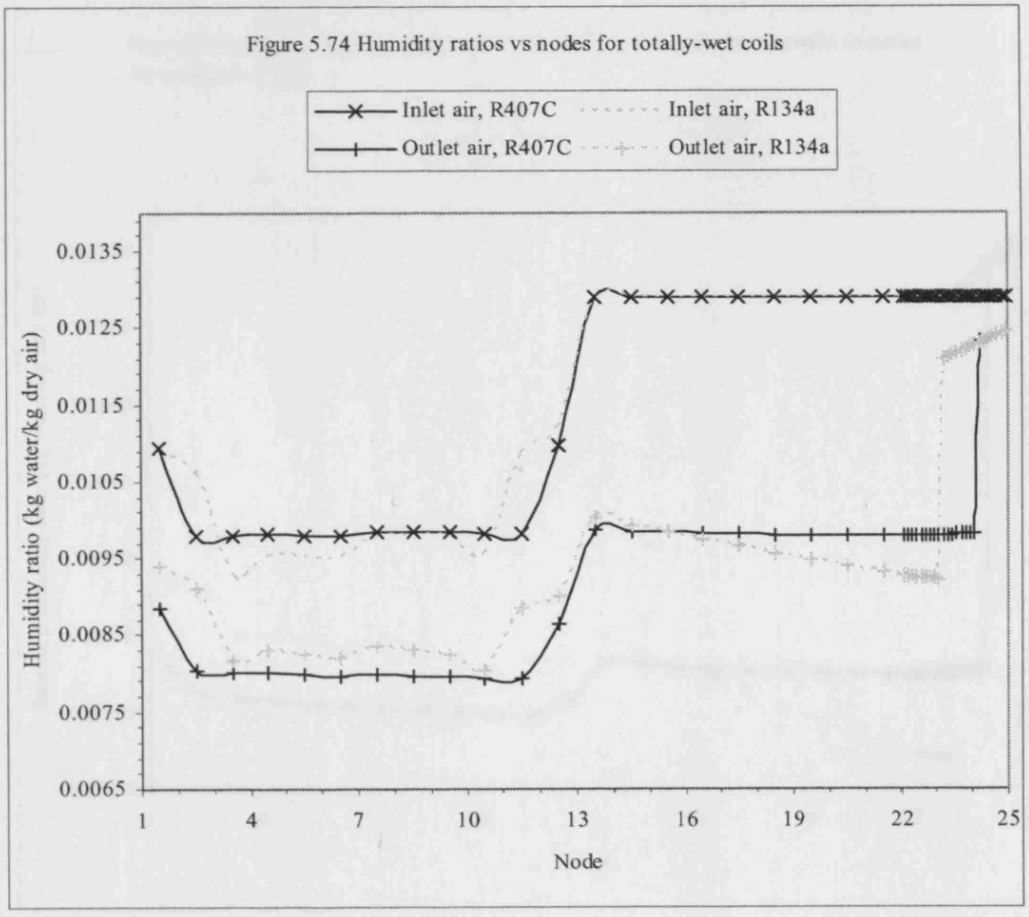

Figure 5.75 Differences between inlet humidity ratio and saturated humidity ratio at surface of condensate on tube wall vs nodes for totally-wet coils

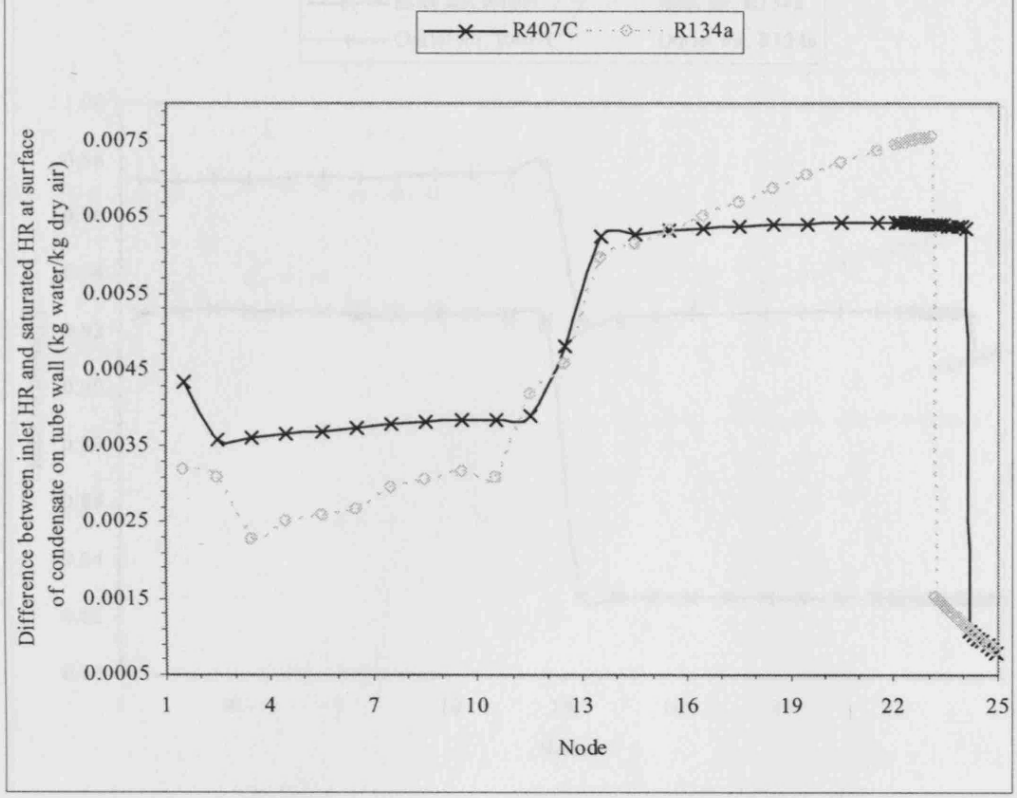

Figure 5.76 Saturated humidity ratios at surfaces of condensate on tube walls vs nodes for totally-wet coils

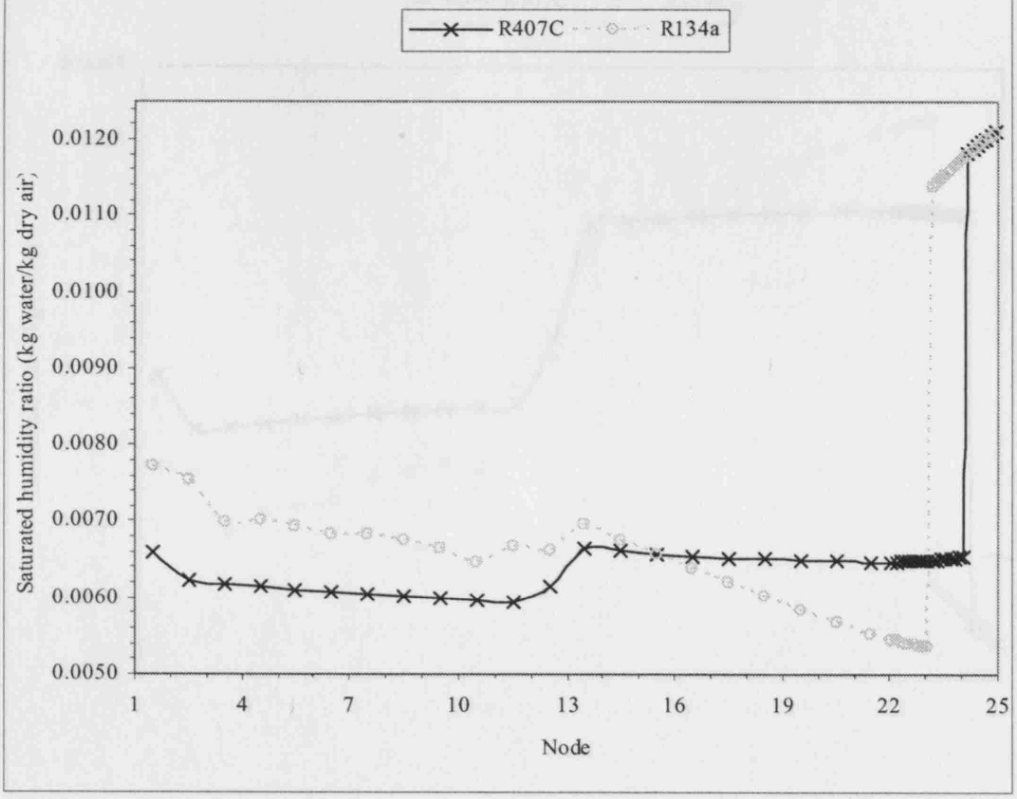

Figure 5.77 Relative humidities vs nodes for totally-wet coils

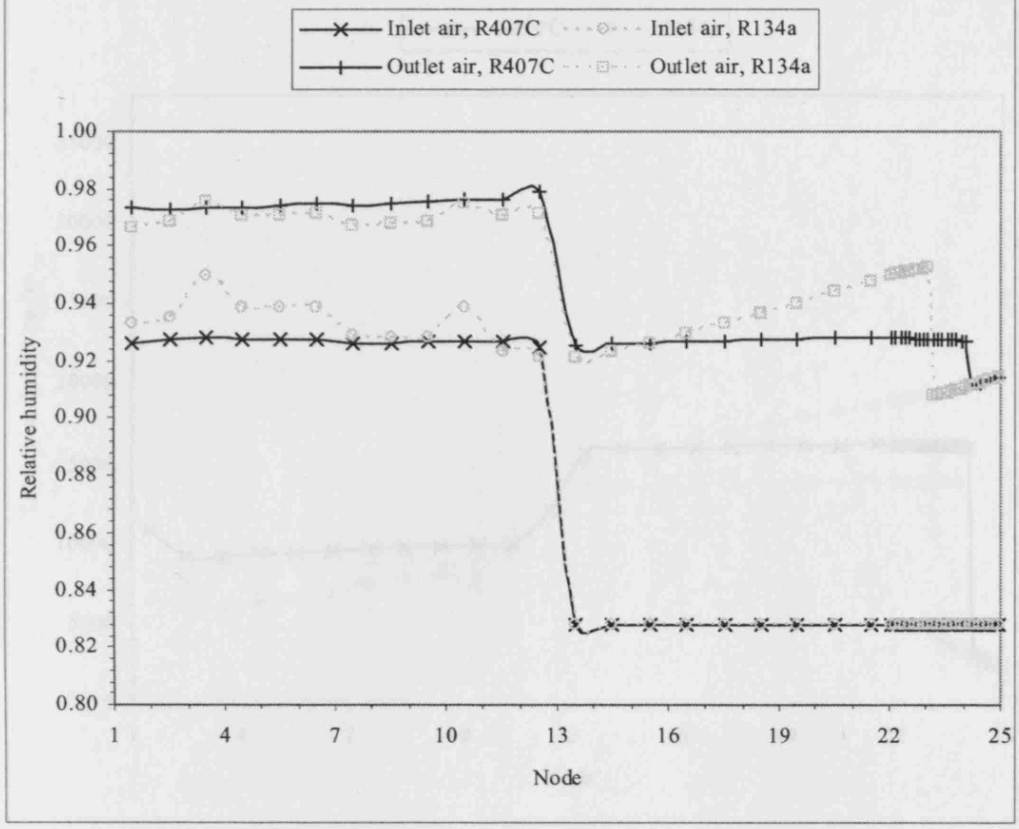

Figure 5.78 Condensate fluxes vs nodes for totally-wet coils

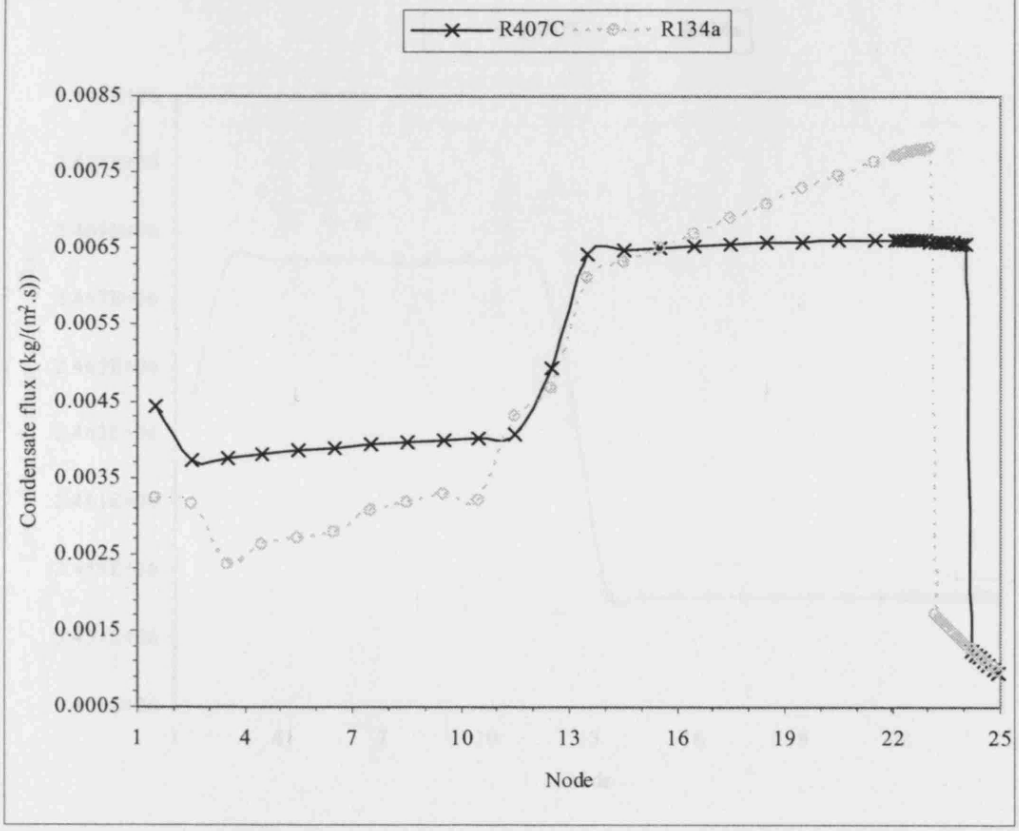

Figure 5.79 Latent heat fluxes vs nodes for totally-wet coils

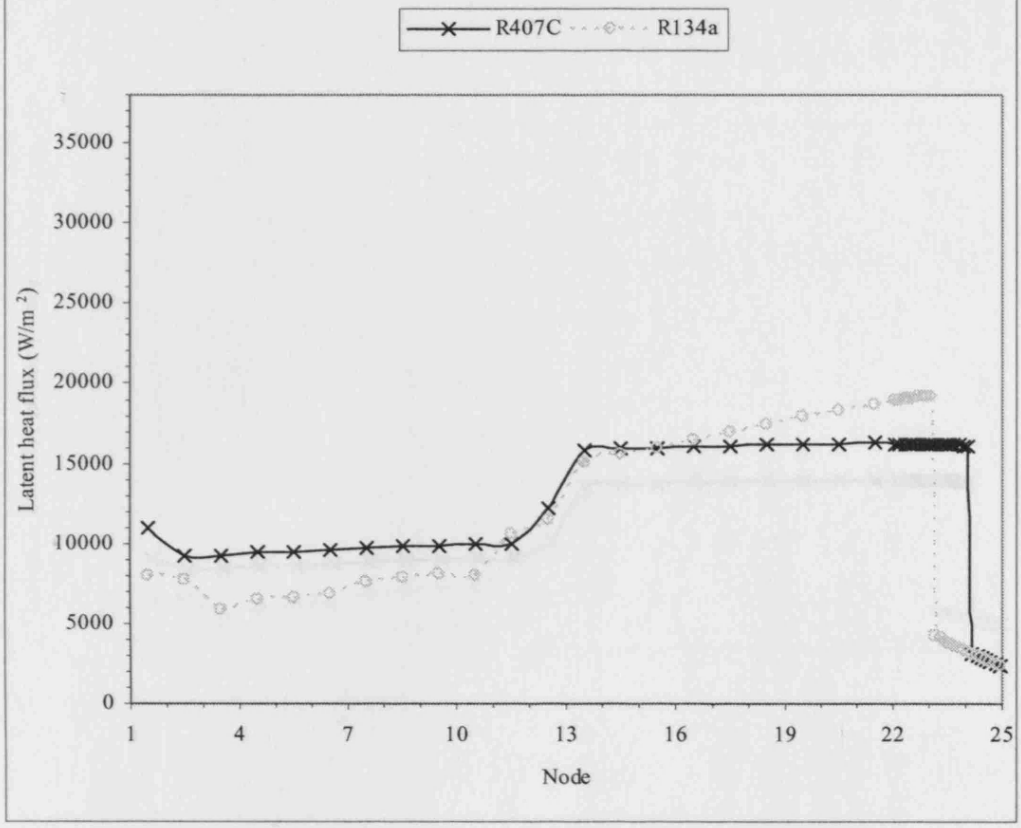

Figure 5.80 Latent heat of condensation vs nodes for totally-wet coils

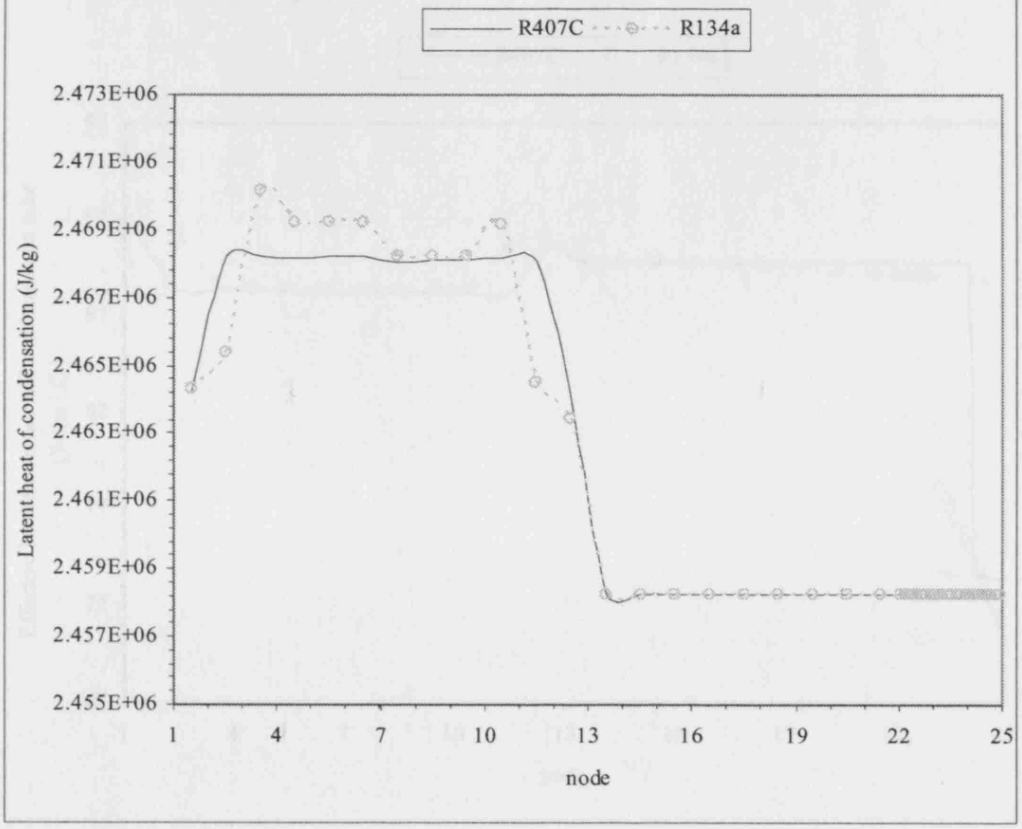

Figure 5.81 Sensible heat fluxes vs nodes for totally-wet coils

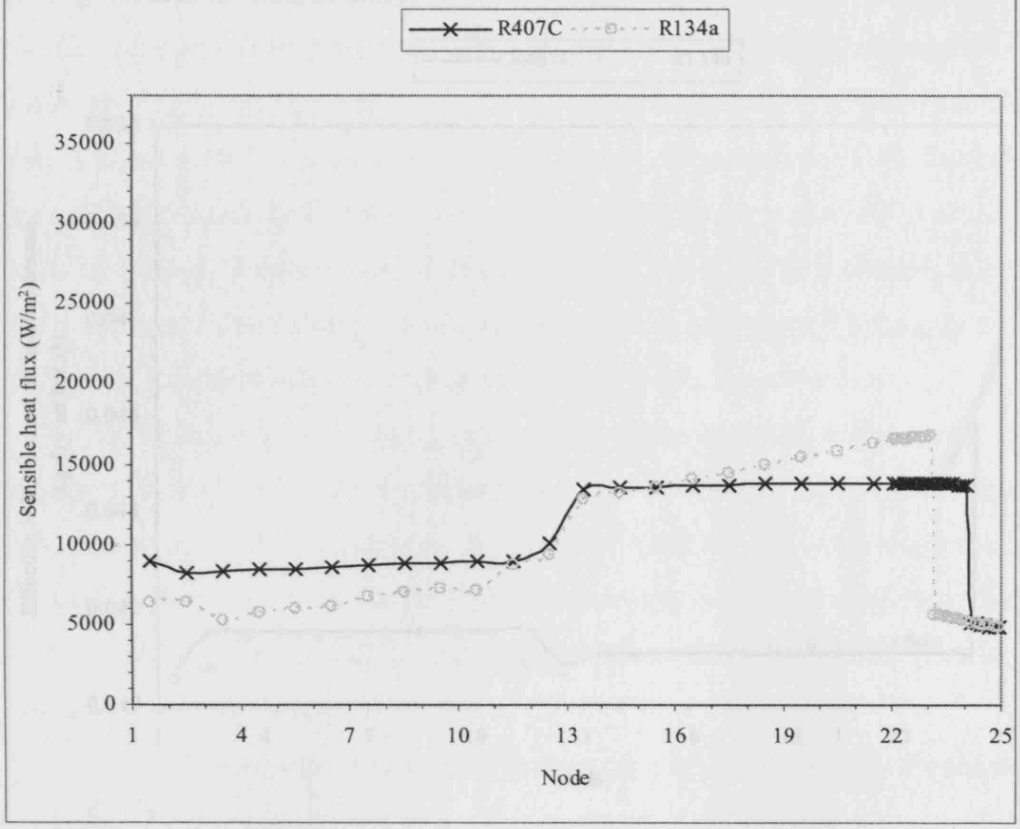

Figure 5.82 Effective heat transfer coefficients between air and condensate on tubes vs nodes for totally-wet coils

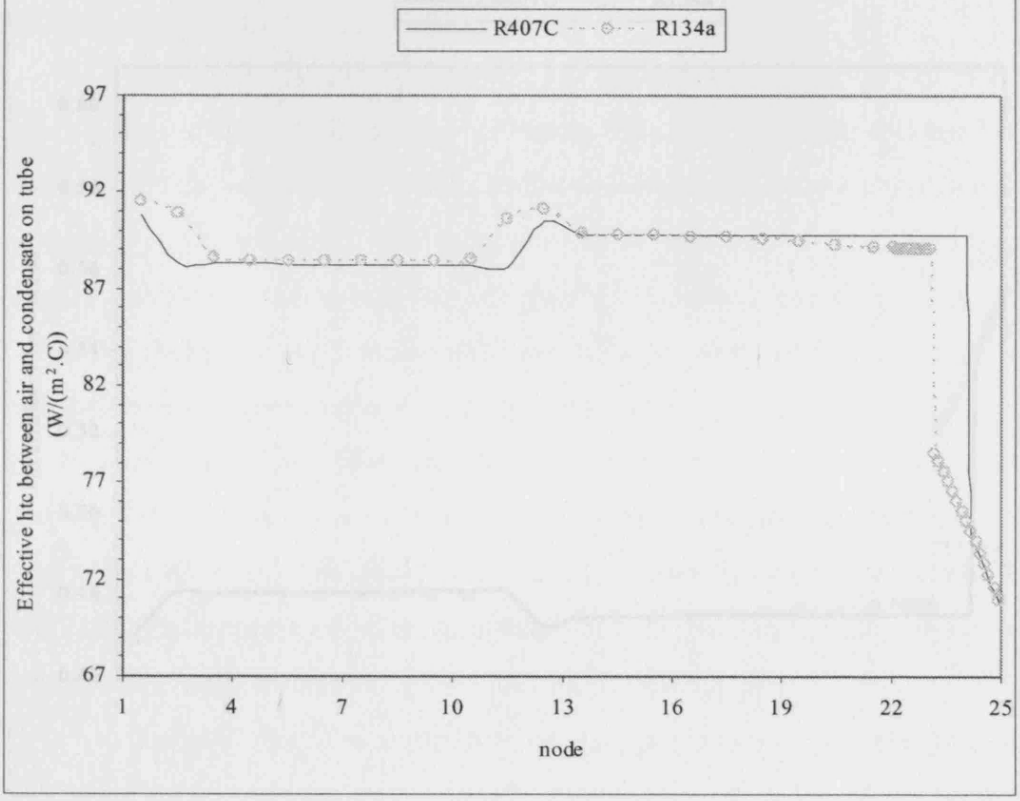

Figure 5.83 Effective mass transfer coefficients between air and condensate on tubes vs nodes for totally-wet coils

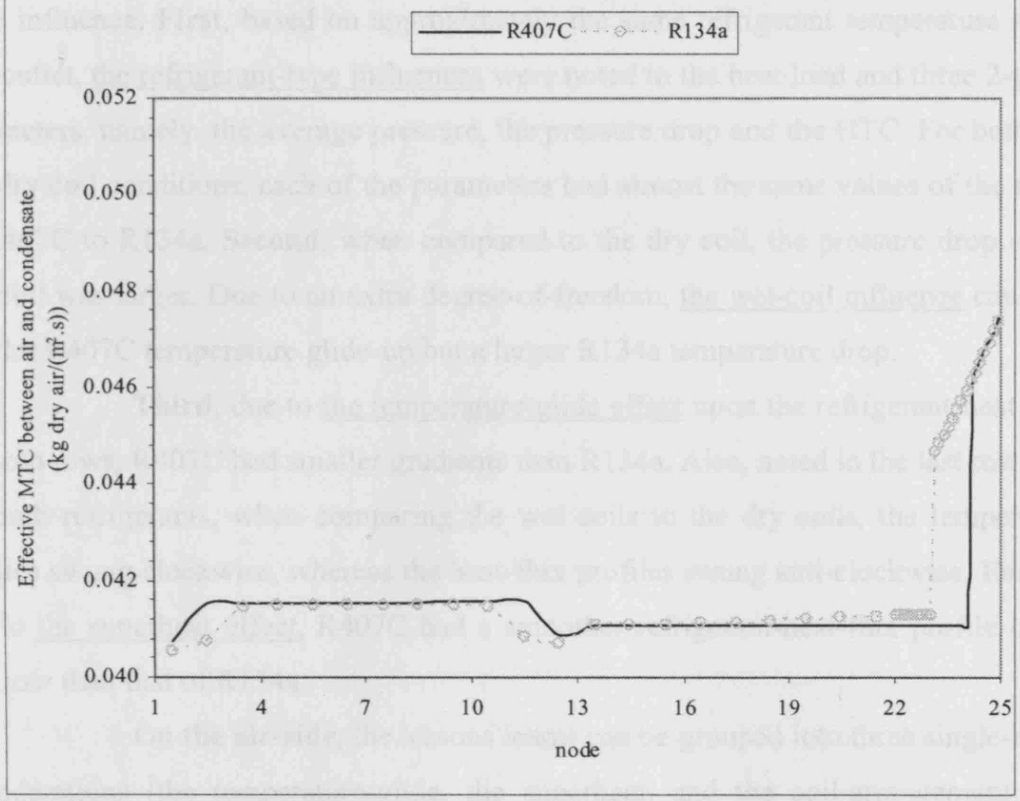

Figure 5.84 Fin efficiencies vs nodes for totally-wet coils

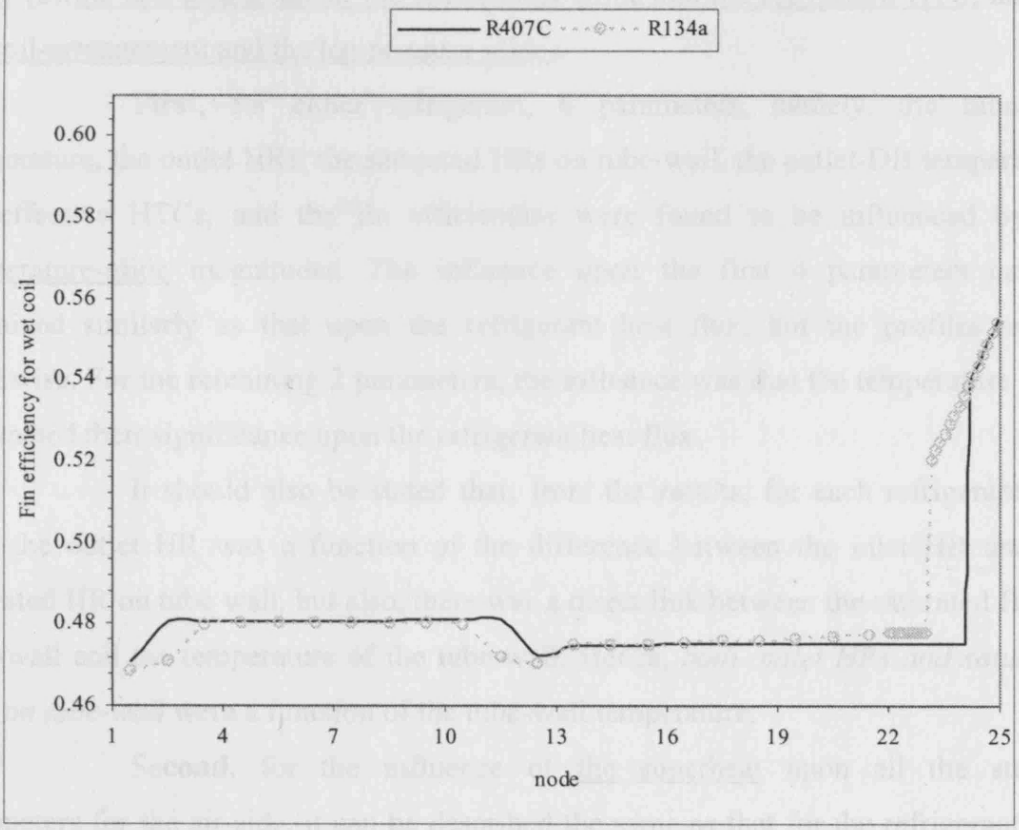

What can be learnt from the results? On **the refrigerant-side**, three effects were discussed: the refrigerant-type, the wet-coil conditions and the temperature-glide influence. **First**, based on approximately the same refrigerant temperature at the coil-outlet, the refrigerant-type influences were noted in the heat load and three 2-phase parameters, namely, the average pressure, the pressure drop and the HTC. For both wet and dry coil conditions, each of the parameters had almost the same values of the ratios of R407C to R134a. **Second**, when compared to the dry coil, the pressure drop of the wet coil was larger. Due to an extra degree-of-freedom, the wet-coil influence caused a smaller R407C temperature glide-up but a larger R134a temperature drop.

Third, due to the temperature-glide effect upon the refrigerant heat flux, for both rows, R407C had smaller gradients than R134a. Also, noted in the last row that, for both refrigerants, when comparing the wet coils to the dry coils, the temperature profiles swung clockwise, whereas the heat-flux profiles swung anti-clockwise. **Fourth**, due to the superheat effect, R407C had a smoother refrigerant-heat-flux profile in the first row than that of R134a.

On **the air-side**, the lessons learnt can be grouped into three single-effect considerations (the temperature-glide, the superheat, and the coil-arrangement) and three combined-effect considerations ((a) the temperature-glide and the refrigerant-HTC, (b) the coil-arrangement, the temperature-glide and the refrigerant-HTC, and (c) the coil-arrangement and the temperature-glide).

First, for either refrigerant, 6 parameters, namely, the tube-wall temperature, the outlet HRs, the saturated HRs on tube-wall, the outlet-DB temperature, the effective HTCs, and the fin efficiencies were found to be influenced by the temperature-glide magnitudes. The influence upon the first 4 parameters can be explained similarly as that upon the refrigerant heat flux, but the profiles swung clockwise. For the remaining 2 parameters, the influence was that the temperature glide dominated their significance upon the refrigerant heat flux.

It should also be stated that, from the results, for each refrigerant, not only the outlet HR was a function of the difference between the inlet HR and the saturated HR on tube wall, but also, there was a direct link between the saturated HR on tube-wall and the temperature of the tube-wall. Hence, *both outlet HRs and saturated HRs on tube-wall* were a function of the tube-wall temperature.

Second, for the influence of the superheat upon all the studied parameters for the air-side, it can be described the same as that for the refrigerant heat

flux. **Third**, for both coil conditions and for both refrigerants, due to the specific coil-arrangement, for all rows, the gradients of the DB temperatures and the humidity ratios against distance at the row-inlets were about zero.

Fourth, it was clear that the combined effect of the temperature-glide and the refrigerant-HTC effects influenced the condensate rates, and also the latent and sensible heat loads of the last row. As pointed previously, regarding the influence of the temperature glide and the refrigerant HTC upon the tube-wall temperature, the former affected on the average gradient of the profile, whereas the latter manipulated the local gradients.

When considering *the last row under the wet condition*, for either refrigerant, the refrigerant HTC in the superheat region was much smaller than that in the 2-phase region; meanwhile, the wall temperatures behaved oppositely. It should be borne in mind that the total length of the superheat region of R134a was longer than that of R407C.

In addition, in the 2-phase region, the temperature-glide effect caused R407C to have a larger average wall temperature than R134a. Hence, the difference between the average wall temperatures of the 2-phase and of the superheat regions for R407C was smaller than that for R134a.

Fifth, the coil-arrangement and the temperature-glide simultaneously influenced the condensate fluxes (via the difference between the inlet HR and the saturated HR on tube-wall) and the sensible heat flux. **Finally**, for both refrigerants, the coil-arrangement, the temperature-glide and the refrigerant-HTC effects suppressed the influences of the effective MTCs and the latent heat of condensation on the condensate fluxes and the latent heat fluxes, respectively.

(Before moving on, for a holistic view, it is useful to mention that R407C for the wet coil generally gave the smoother *heat-flux profile* than that for the dry coil, whereas, when using R134a, there was no difference for the smoothness between the two coil conditions. For the gradients of the profile, both refrigerants in the wet coils had larger gradients than that of the dry coils. However, for the change in the gradient of the wet coil from that of the dry coil, R407C had a smaller value than R134a. For *the coil-outlet DB temperature*, R407C in the wet coil had a smoother profile than that in the dry coil, whereas, R134a had the same smoothness for both coil conditions. Both refrigerants had about the same magnitudes of gradient for both coil conditions.)

Comparing with another research: Jia et al. [1999] dealt with R134a wet coils; however, the water vapour/condensate related parameters were not presented in their paper. For the author's work on wet coils, the emphasis was on comparing R407C with R134a, and therefore the superheat effect was not analysed in details, as performed on the dry coil. In addition, the effects of temperature-glide and the refrigerant-HTC on the DB temperatures and the HRs at the row-outlets were studied, as well as the influences of the coil-arrangement upon the DB temperatures and the HRs at the row-inlets.

5.4.2 Totally-wet-coil dynamic behaviour

The results were presented in a similar format as that of the steady state, Tables 5.17 and 5.18, The dynamic response, when subject to either a step increase or a step decrease of the coil-inlet DB temperature (±0.8 °C), was studied. However, the step increase was the default scenario for the discussion, unless otherwise stated.

Table 5.17 A summary of the transient study of the totally-wet coils: results and discussion (The step increase and decrease of the coil-inlet DB temperatures were ± 0.8 °C, respectively. The step increase is the default input, unless otherwise stated.)

Totally-wet conditions (Comparing R407C with R134a, unless otherwise mentioned)	**To discuss the dehumidification process (the totally-wet effect), as compared to dry coil, for individual refrigerants**	**Based on observations from dry coil operation, further comments are given for the totally-wet coils**
Coil-outlet refrigerant pressures: (Figs. 5.85 and 5.86) For each refrigerant, the profile of time variation of pressure can be described and discussed in a similar way as that of the dry coil, Fig. 5.22. R407C with a smooth profile had a larger rate of change than R134a; the latter had some fluctuations within the initial 35 seconds. (Referring to Section 5.22, the fluctuations were thought to come from the difference between the calculated values at the interface of changing from the 2-phase to the superheat states.) Moreover, R407C had a larger magnitude of change (276 Pa) than that of R134a (-209 Pa), both reaching steady-state in around 35 seconds.	When comparing to Fig. 5.22, the wet coils (R407C and R134a: 7.89 and -5.97 Pa/s) were on average about ten times faster than the dry coils (R407C and R134a: 0.84 and -0.51 Pa/s). In addition, for both refrigerants, the wet coils also had larger magnitudes of change with shorter transient response times than the dry coils. When there was a step decrease of the coil-inlet DB temperatures, Fig. 5.23, similar observation could be made with the corresponding figures for the rates of change: -10.37 and 6.07, and -0.85 and 0.73, respectively.	Refrigerant-type effect: For either wet- or dry- coil or for either step-increase or step-decrease of the coil-inlet DB temperature, when compared with R134a, R407C responded quicker to the changes in the DB temperature. Totally-wet effect: Due to the influence of coil condition, for the time rate of change of pressure, the ratio of R407C to R143a (-1.32) for the step increase case was smaller than that (-1.71) for the step decrease, whereas for the dry-coil, the reverse happened with the corresponding figures: -1.65 and -1.17.

Table 5.17 A summary of the transient study of the totally-wet coils: results and discussion (The step increase and decrease of the coil-inlet DB temperatures were ± 0.8 °C, respectively. The step increase is the default input, unless otherwise stated.)

Totally-wet conditions (Comparing R407C with R134a, unless otherwise mentioned)	**To discuss the dehumidification process (the totally-wet effect), as compared to dry coil, for individual refrigerants**	**Based on observations from dry coil operation, further comments are given for the totally-wet coils**
As expected, when there was a step decrease of the coil-inlet DB temperatures, the profiles reversed, but the trends were the same, but reaching the steady at a slightly earlier time of 30 seconds.		
Refrigerant pressure drops: (Fig. 5.87) For both refrigerants, the profiles can be described similarly as that of the dry coil, Fig. 5.26a	When comparing to Fig. 5.26a, both wet and dry coils had similar profiles though the wet coils experienced larger magnitudes of changes from 0s to steady-state than the dry coils.	Refrigerant-type effect: As previously discussed in the dry-coil that R134a had a higher sensitivity of the pressure-drop-profile shifting than R407C. This is also true for the wet coils.
Local 2-phase refrigerant temperatures: (Nodes 12 and 13) (Figs. 5.88 and 5.89) For both nodes 12 and 13, for both refrigerants, the amounts of time used in reaching steady-state were the same (25 seconds). However, the rates of change of R407C were higher than that of R134a. For **a step decrease** of the inlet air temperature, for the node13, for both refrigerants, the same description as the above can be applied. For the node 12, however, R407C had a **slower** rate of change than that for R134a. The discussion can be done similarly as in Sub-section 5.3.1 (for R407C: link between the temperature glide and the heat flux; for R134a; dependence of temperature on the pressure; seeing also Figs. 5.90 and 5.91), and Sub-section 5.3.2 (for either refrigerant: the relationship between the temperature change within an element, and its inlet and outlet temperatures).	(Figs. 5.39a and 5.39b) When comparing the temperatures of nodes 12 and 13 of the wet coil to the nodes 14 and 15 of the dry coil (both elements were in the middle of the coil) for either a step increase or a step decrease, three parameters were considered: time durations of reaching steady-state, magnitudes of change and rates of change. For time durations, for both refrigerants, the wet coils had smaller values than the dry coils. For magnitudes of change, for R407C, the wet coils had smaller values than the dry coils, whereas, for R134a, the reverse happened. For rates of change, for R134a, the wet coils had very higher values than the dry coils. For R407C, the wet coils normally had larger values than the dry coils. However, due the effect of the refrigerant heat flux, for a step decrease, the wet coil at Node 12 had a smaller rate of change than the dry coil at Node 14.	Refrigerant-type effect: Based on the results and observations on the dry-coil, the magnitudes of change were determined by the refrigerant properties (relating to: temperature, pressure and concentrations). Totally-wet effect: For the wet coils, both refrigerants had about the same time durations for reaching steady-state. For an element, when there was step increase or decrease, the difference in the magnitudes of change for R407C could be larger than, equal to or smaller than that for R134a. This resulted in that the difference in the speeds of change for R407C varied significantly, when comparing to that for R134a. For the dry coils, the time duration of reaching steady-state for R407C was about 60% longer than that for R134a, and the magnitude of change for R407C was around 9 times larger than that for R134a. In addition, it was found that, for both refrigerants, the variation in the difference of the magnitude of change had little influence upon the difference in the speeds of change.

Table 5.17 A summary of the transient study of the totally-wet coils: results and discussion (The step increase and decrease of the coil-inlet DB temperatures were ± 0.8 °C, respectively. The step increase is the default input, unless otherwise stated.)

Totally-wet conditions (Comparing R407C with R134a, unless otherwise mentioned)	**To discuss the dehumidification process (the totally-wet effect), as compared to dry coil, for individual refrigerants**	**Based on observations from dry coil operation, further comments are given for the totally-wet coils**
Refrigerant temperatures along the coil: (Figs. 5.92 and 5.93) The description can be given at the same for the dry coils.	Compared to Figs. 5.40a and 5.40b, for either a step-increase or a step-decrease case, the magnitudes of swinging for R407C for the wet coils were less than that for the dry coils, whereas the opposite happened for R134a. However, for both refrigerants, the change in the superheat-initiation position for the wet coils were less than that for the dry coils.	Refrigerant-type effect: Due to the difference in the degrees of freedom, the ratio of the magnitude of swinging for R407C to that for R134a of the wet coils was smaller than that of the dry coils; this observation also applied when subject to a step decrease in the coil-inlet DB temperature.
Degrees of superheat: (Figs. 5.94 and 5.95) The magnitude of change (1.5 °C) and the time duration used (30 seconds) for R407C to reach steady state were less than that (1.55 °C and 35 seconds) for R134a. The corresponding rates of change were 0.05 °C/s (R407C) and 0.044 °C/s (R134a). For a step decrease in the coil-inlet air temperature, the same description can be applied with the following corresponding figures: -1.61, 20, -1.69, 25, -0.081 and -0.068 °C/s.	Comparing to Figs. 5.38a and 5.38b, for a step increase or a decrease case, for both wet and dry coils, R407C had a slightly smaller magnitude of change than R134a. However, for the wet coils, R407C used less time duration than R134a, whereas, for the dry coils, the reverse happened. For the wet coils, R407C had a larger rate of change of superheat degrees than R134a, whereas, for the dry coils, it reversed.	
Coil-outlet refrigerant temperatures: (Figs. 5.96 and 5.97) For both refrigerants, the temperatures increased with time; R407C with a smooth profile had a marginally slower rate of change than R134a, both reaching steady-state in 30 seconds. R407C also had a slightly smaller magnitude of change (1.58 °C) than that of R134a (1.69 °C). For a step decrease of the coil-inlet DB temperatures, both refrigerants took about the same time to reach steady state. The	When comparing to Fig. 5.37a, for both refrigerants, the wet coils (R407C and R134a: 0.0527 and 0.0564 °C/s) had higher rates of change than the dry coils (0.0252 and 0.0354 °C/s, respectively). In addition, the wet coils had smaller magnitudes of change and had shorter transient times. The corresponding figures for the step decrease case were -0.068 and -0.0736, and -0.0345 and -0.0478, respectively.	Refrigerant-type effect: In all cases as mentioned in the coil-outlet refrigerant pressures, R407C had slower rates of response to change of the DB temperature than R134a. In addition, for the wet coils, the ratio of the rate of change of R407C to that of R134a w.r.t. a step-increase in the coil-inlet DB temperature (0.94) was a little higher than that corresponding to a step-decrease (0.92). For the dry coils, the same description applied, with the corresponding figures: 0.69 and 0.68, respectively.

Table 5.17 A summary of the transient study of the totally-wet coils: results and discussion (The step increase and decrease of the coil-inlet DB temperatures were ± 0.8 °C, respectively. The step increase is the default input, unless otherwise stated.)

Totally-wet conditions (Comparing R407C with R134a, unless otherwise mentioned)	**To discuss the dehumidification process (the totally-wet effect), as compared to dry coil, for individual refrigerants**	**Based on observations from dry coil operation, further comments are given for the totally-wet coils**
rate of change and the magnitude of change were both smaller for R407C. Superheat-region effect For both refrigerants, the magnitudes of change of the refrigerant temperature in the superheat region were much larger than that in the 2-phase region.		
Local 2-phase refrigerant heat transfer coefficients: (Nodes 12 and 13) (Figs. 5.98 and 5.99) For Nodes 12 and 13, R407C used less time (25 and 25 seconds respectively) in reaching steady-state, and had smaller magnitudes of change (84 and 89 W/(m^2.K)) than R134a (30 and 30 seconds; 119 and 127 W/(m^2.K)). The rates of change for R407C (3.36 and 3.56 W/(m^2.K.s) were about 0.84 times of that for R134a (3.97 and 4.23 W/(m^2.K.s). The corresponding figures for a step decrease were: 25, 25, -77, -87, 25, 25, -117, -125, -3.08, -3.48, 0.67, -4.68 and -5 W/(m^2.K.s). Refrigerant-type effect: The behaviour of magnitude of change and rate of change can be discussed the same way as that for dry coil in Sub-section 5.3.2.	When comparing to Nodes 14 and 15 in Figs. 47a and 47b, for both refrigerants, for both step change cases, the wet coils had larger rates of change than the dry coils.	
Tube-wall temperatures: (Fig. 5.100) (2-phase region only) For R407C, the tube-wall temperatures at 150 s were higher than that at 0 s, whereas, for R134a, that at 150 s were either higher or lower than that at 0 s. As examples, the changes with time at the Elements (1,2,2) and (2,2,2) were shown in Figs		

Table 5.17 A summary of the transient study of the totally-wet coils: results and discussion (The step increase and decrease of the coil-inlet DB temperatures were ± 0.8 °C, respectively. The step increase is the default input, unless otherwise stated.)

Totally-wet conditions (Comparing R407C with R134a, unless otherwise mentioned)	**To discuss the dehumidification process (the totally-wet effect), as compared to dry coil, for individual refrigerants**	**Based on observations from dry coil operation, further comments are given for the totally-wet coils**
5.101 and 5.102; the dynamic behaviour could be explained in the same way as that for dry coil being a function of three rates of changes, namely the refrigerant heat flux, refrigerant HTC and refrigerant temperature. In the 1st row, the largest increases of the tube-wall temperatures, for R407C, were in the Elements between the Nodes: 1 and 3, and 11 and 13, whereas, for R134a, they were in the Elements between the Nodes: 2 and 4, and 10 and 12. As explained previously (Sub-section 5.2.2), for R134a, the superheat effect via the refrigerant heat flux dominated the refrigerant-temperature influence.		

Table 5.18 Air-side parameters for dynamic mode of the totally-wet coils: results and comments. (The coil configurations were as shown in Figs. 5.66 and 5.67.)

Remark In this table four parameters related to refrigerant type are addressed: the effective MTC between the inlet air and the condensate on the tube wall, the difference between the inlet HR and the saturated HR on the tube-wall surface, the effective HTC between the inlet air and the condensate on the tube wall, and the difference between the inlet DB temperature and the wall temperature. The effective MTC ($U_{m,eff,wet}$), from the Eq. 3.25, is a function of the wet-coil humidity-ratio fin efficiency ($\eta_{W,fin,wet}$), which, from the Eq. 3.28, approximates to the wet-coil fin efficiency ($\eta_{fin,wet}$). The latter, from the Eq. 3.17, being a function of the HTC (U_{wet}) that, from the Eqs. 3.18 and 3.22, links to the wall temperature (being a function of a refrigerant type as discussed in the dry coils); in other words,. the effective MTC is a function of the refrigerant type.

$$U_{m,eff,wet} = \left(\frac{\eta_{W,fin,wet} A_{fin,wet} + A_{wall,o,wet}}{A_{o,total,wet}} \right) U_{m,wet} \tag{3.25}$$

$$\eta_{W,fin,wet} \equiv \eta_{fin,wet} \tag{3.28}$$

Table 5.18 Air-side parameters for dynamic mode of the totally-wet coils: results and comments. (The coil configurations were as shown in Figs. 5.66 and 5.67.)

$$\eta_{fin,wet} = \frac{\tanh\left(\left(\frac{2U_{wet}}{w_{fin}k_{fin}}\right)^{0.5}\psi\right)}{\left(\frac{2U_{wet}}{w_{fin}k_{fin}}\right)^{0.5}\psi} \quad (3.17)$$

$$U_{wet} = U_{wet,sen} + U_{wet,latent} \quad (3.18)$$

$$U_{wet,latent} = \frac{U_{m,wet}\, i_{fg,water}\left(W_{in} - W_{cond,wall}\right)}{\left(T_{db,in} - T_{wall,ave}\right)} \quad (3.22)$$

For the difference between the inlet HR and the saturated HR on the tube-wall surface, substituting the DB temperature in Eq. A.8 by the tube-wall temperature, the saturated HR in the Eq. A.9 then becomes a function of the tube-wall temperature. Then, as similar to the above argument, the difference between the HRs is also a function of the refrigerant type.

$$W_s = \frac{0.62198 p_{ws}}{\left(p_{wa} - p_{ws}\right)} \quad (A.9)$$

$$p_{ws} = 1000\left\{\mathrm{Exp}\left(\begin{array}{l}\left(\frac{-5.6745359E+3}{T_{db}}\right) - 5.1523058E-1 \\ -(9.677843E-3)T_{db} + (6.2215701E-7)T_{db}^2 \\ +(2.0747825E-9)T_{db}^3 - (9.484024E-13)T_{db}^4 \\ +4.1635019(\ln(T_{db}))\end{array}\right)\right\} \quad (A.8)$$

The effective HTC between the inlet air and the condensate on the tube wall, from the Eq. 3.12, is a function of the wet-coil fin efficiency ($\eta_{fin,wet}$) and the HTC (U_{wet}). As explained previously, the effective HTC is therefore a function of the refrigerant type.

$$U_{eff,wet} = \left(\frac{\eta_{fin,wet}A_{fin,wet} + A_{wall,o,wet}}{A_{o,total,wet}}\right)U_{wet} \quad (3.12)$$

Similarly it can be said that the difference between the inlet DB temperature and the wall temperature is a function of the refrigerant type.

Local condensate rates: (Fig. 5.103)

For both refrigerants, the Elements and Sub-elements can be divided into 3 groups: those affected directly and indirectly, and unaffected by the superheats, respectively.

For *the first group*, for both refrigerants, for all the Elements and Sub-elements within the superheat regions, the condensate rates at 150 s were smaller than that at 0 s.

For *the second group* in which the condensate rates at 150 s were larger than that at 0 s; this is for all Elements in the 1st and the 4th tubes of the 1st row for both refrigerants, except for the Elements (1,1,3 - between nodes 3 and 4) and (1,4,1 - between nodes 10 and 11) with the R407C case.

For *the third group*, referring to the rest of Elements, for R407C, the condensate rates at 150 s could be either larger or smaller than that at 0 s. For R134a, for the Elements in the 1st row, the condensate rates behaved the same as happened for R407C except for the Elements in the 2nd row, where higher values were observed.

Table 5.18 Air-side parameters for dynamic mode of the totally-wet coils: results and comments. (The coil configurations were as shown in Figs. 5.66 and 5.67.)

Effective-MTC effect:
For *the first group*, considering Elements (2,4,2 - between nodes 23 and 24) for R407C and (2,4,1 - between nodes 22 and 23) for R134a, respectively, R407C had a smaller negative rate of change of the condensate rate than R134a (Fig. 5.104). For both refrigerants, the profiles for the rates of change of the difference between the inlet HR and the saturated HR on the tube-wall surface (Fig. 5.105), were similar to that of the condensate rate. For both refrigerants, the effective MTC increased smoothly with time (Fig. 5.106), though in the opposite trend to the previous two parameters. Hence, it can be said that for the 1st group, for the influence upon the condensate rate, the difference between the HRs dominated that of the effective MTC.

For *the third group*, considering the Element (2,2,2 - between nodes 17 and 18), the condensate rate for both refrigerants increased with time; however, R407C had a peak at 5 s before dropping to its steady value, whereas R134a had a continuous increase from 0 s to 5 s (Fig. 5.107). For R407C, the difference between the inlet HR and the saturated HR on the tube-wall surface decreased gradually with time, whereas, for R134a, the final value increased slightly with a slight dip at 5 s (Fig. 5.108).

For the change of the effective MTC, both refrigerants had similar profiles and the MTC values increased with a deep gradient from 0 s to 5 s (Fig. 5.109). It can be seen that the dynamics of the condensate rate was influenced by the dynamics of both the effective MTC and the difference between the HRs. This was not the same as what happened in the 1st group.

For *the second group*, considering the Elements (1,1,2 - between nodes 2 and 3) and (1,1,3 - between nodes 3 and 4) for R407C and R134a, respectively, R407C had a smooth increase in the condensate rate, whereas R134a increased with a step between 10 s and 15 s (Fig. 5.110). The profiles of the change of the difference between the HRs with time, for both refrigerants, were similar to that for the condensate rates, though with a smaller gradient from 0 s to 5 s (Fig. 5.111). The effective MTC for R407C slightly decreased and R134a slightly increased, between 0 s and 25 s, and for each profile, there was a sharp peak at 5 s (Fig. 5.112). For each refrigerant, the effect of the effective MTC on the dynamic of the condensate rate was more prominent in this group than that observed in the first group.

In conclusion, it can be said that, for either refrigerant, the dynamics of the condensate rate were controlled mainly by the dynamics of the difference between the mentioned HRs, with additional influence from the dynamics of the effective MTC.

Coil-outlet humidity ratios:

a) General

For the coil-outlet humidity ratios, the elements can be arranged into 2 groups: those affected indirectly (Figs. 5.113 and 5.114) and those unaffected (Figs. 5.115 and 5.116) by the superheats.

Within *the first group*, for both refrigerants, the humidity ratios increased with time but at different rates.

For the second group, for each individual refrigerant, all profiles of the of change of the humidity ratio with time had the same pattern; however, for both refrigerants, the RHs had lower final steady state values (except for the Element (1,1,3 - between nodes 3 and 4) of R407C with a slight increase), and this behaviour was different to that of the first group. In addition, for R407C, the values dropped and then increased with a minimum point at 5 s, whereas, R134a decreased rapidly before reaching steady state.

Effective-MTC effect: For a given coil-inlet condition, the rate of change of the outlet humidity ratio with respect to time was a function of the rate of change of the condensate rate with time. Therefore the behaviour of both groups, under the influence of the MTC, can be discussed the same way as done for the corresponding groups in the local condensate rates.

Table 5.18 Air-side parameters for dynamic mode of the totally-wet coils: results and comments. (The coil configurations were as shown in Figs. 5.66 and 5.67.)

b) Variation over the coil-outlet for whole tubes that were unaffected by superheat

A reason for studying the coil-outlet-HR variation for the tubes that were unaffected by superheat in its entire length was explained in the "Coil-outlet DB temperatures".

For *the horizontal (e.g. a set of elements (1,4,1), (1,4,2) and (1,4,3)) and vertical (e.g. a set of elements: (1,1,1), (1,2,3), (1,3,1) and (1,4,3))* considerations, after analysing Figs. 5.117 to 5.122 the explanation can be similar to that provided for *the coil-outlet DB temperatures*. For the horizontal consideration, the corresponding figures were: 0.0004, -0.00003, 0.0001 and -0.0001 kg of water/kg of dry air, whereas, for the vertical consideration, the figures were: 0.00001, -0.00003, -0.00006, 0.00014, 0.00004 and -0.00006 kg of water/kg of dry air.

Coil-configuration and refrigerant-temperature-glide effects (for horizontal and vertical considerations): The discussion is similar to that given for the coil-outlet DB temperatures.

Local air heat fluxes:

The elements can be divided into the same 3 groups as done for the local condensate rates: affected directly and indirectly, and unaffected by the superheats. For the first group, for all the elements, the air heat fluxes at 150 s were smaller than that at 0 s, whereas, for the rest two groups, for all the elements, the reverse happened.

Effective-HTC effect:

For *the first group*, consider the Elements (2,4,2 - between nodes 23 and 24) for R407C and (2,4,1) (between nodes 22 and 23) for R134a, the former had a slightly slower rate of change (negative) of *the air heat flux* (Fig. 5.123). For both refrigerants, the variations of *the difference between inlet DB temperature and the wall temperature* with time (Fig. 5.124) had similar profiles to that of the air heat flux. For the rates of change (negative) of *the effective HTC between the inlet air and the condensate on the tube wall*, R407C had a larger gradient than R134a (Fig. 5.125). Overall it could be said that, for both refrigerants, the dynamics of the heat flux was influenced by the difference between the mentioned temperatures *a lot* more than by the effective HTC.

For *the third group*, considering Element (2,2,2 - between nodes 17 and 18), for each refrigerant, both the air heat flux and the temperature difference, having a similar profile, *increased* in a similar way. When compared to R134a, R407C had a *smaller* magnitude of change from 0s to steady-state. However, the ratio of the magnitudes of change between R407C and R134a for the air heat flux was smaller than that for the temperature difference (Figs. 5.126 and 5.127). However, the effective HTC behaved oppositely with *decreasing profiles*, and R407C had a *larger* magnitude of change from 0s to steady-state (Fig. 5.128). Therefore, it was seen that both the effective HTC and the temperature difference had an influence on the heat flux.

For *the second group*, let's consider Elements (1,1,2 - between nodes 2 and 3) and (1,1,3 - between nodes 3 and 4) for R407C and R134a, respectively. For *the air heat flux*, when compared to R134a, R407C had about the same positive rate of change, and had a smaller magnitude of change from 0s to steady-state (Fig. 5.129). For each refrigerant, the profile of *the temperature difference* (Fig. 5.130) was similar to that of the air heat flux; however, R407C had smaller gradient and the magnitude of change from 0s to steady-state. For the effective HTCs (Fig. 5.131), for both refrigerants, during the first 5s, they decreased; after that, they increased to reaching steady-state. Overall, between steady-states, the effective HTC of R407C increased, whereas that of R134a decreased, and R407C had a larger magnitude of change than R134a. For each refrigerant, when comparing to the third group, there appeared to have a larger influence of the dynamics of the effective HTC upon the dynamics of the air heat flux, relatively to the influenced by the dynamics of the temperature difference.

In conclusion, similar observations could be made as that for the local condensate rate.

Table 5.18 Air-side parameters for dynamic mode of the totally-wet coils: results and comments. (The coil configurations were as shown in Figs. 5.66 and 5.67.)

Coil-outlet DB temperatures:

a) General (Figs. 5.132 to 5.135)

The pattern of change of the coil-outlet DB temperatures with time for various elements were again divided into 2 groups (corresponding to that for the coil-outlet HRs), the first of which (Figs. 5.132 and 5.133), i.e. those affected indirectly by the superheat, could be described similarly to that for the coil-outlet HRs. For all elements of the second group (Figs. 5.134 and 5.135), i.e. those unaffected by the superheat, for change of the coil-outlet DB temperature, R407C had a smooth increase with a steep gradient within the first 5 s, and R134a also increased rather rapidly for the first 5 s and then decreased slightly from 5 s to 25 s before reaching steady state. For both refrigerants, the magnitudes of change from 0s to steady-state were positive.

Effective-HTC effect: Referring to the coil-outlet HRs, when considering the analogy between the HR and the DB temperature, the rate of change of the coil-outlet HR and that of the coil-outlet DB temperature, and the condensate rate and the air heat flux, similar discussions can be carried out as that done for the coil-outlet HRs.

b) Variation over the coil-outlet for whole tubes that were unaffected by superheat

In the results and discussion of the dry coils, it was already shown that for any superheat-affected elements and sub-elements, the superheat effect dominated the refrigerant-type effect. *Here, the focus is about the variation of the coil-outlet DB temperature from the Elements without any effect from the superheat.*

For *horizontal consideration*, **at any time (between 0 s to 150 s)**, for R407C (Figs. 5.136 to 5.138), for the 2nd tube, from Elements (1,2,3), (1,2,2) and (1,2,1), the temperatures insignificantly changed from low to high with a difference of about 0.1 °C. For the 3rd tube, naturally, from Elements (1,3,1), (1,3,2) and (1,3,3), the temperature variations were insignificantly (-0.07 °C) but in opposite direction. For R134a (Figs. 5.139 to 5.141), for the 2nd and the 3rd tubes, the behaviour is essentially the same , though with two and three times larger values: 0.19 °C and -0.23 °C, respectively.

For *vertical consideration*, **at any time**, for R407C (Figs. 5.136 to 5.138), in the vertical sections: (1,3,1) & (1,2,3), *(1,3,2) & (1,2,2)* and (1,3,3) & (1,2,1), the magnitudes of the temperature difference for each pair were from a small positive to a large negative value (0.02, *-0.06* and -0.15 °C, respectively). On the other hand, for R134a (Figs. 5.139 to 5.141), the corresponding magnitudes of the difference ranged from a large positive to small negative (0.32, *0.13* and -0.09 °C, respectively).

Coil-configuration effect (horizontal consideration): *When having an odd number row* (for instance, an one-row evaporator), for along the 2nd tube (from the Elements (1,2,3), (1,2,2) to (1,2,1)), the coil-outlet DB temperatures for R407C are from high to low, whereas, for along the 3rd tube (from Elements (1,3,1), (1,3,2) to (1,3,3)), the temperatures are from low to high. The changes were opposite to that of a 2-row evaporator. However, for R134a the pattern would remain the same as in a 2-row evaporator: namely from low to high in the 2nd tube and from high to low in the 3rd tube.

Refrigerant-temperature-glide effect (horizontal consideration): *When operating the coils with smaller increases in heat load* (e.g. a smaller step increase of the coil-inlet DB temperature), R407C would have a larger amount of the refrigerant temperature glide-up, whereas R134a would have a smaller refrigerant temperature drop. For along the 2nd tube (from (1,2,3), (1,2,2) to (1,2,1)) and the 3rd tube (from (1,3,1), (1,3,2) to (1,3,3)), the changes in temperatures for R407C would be larger than 0.1 °C and -0.07 °C, respectively), whereas, that for R134a would be smaller than 0.19 °C and < -0.23 °C, respectively.

Coil-configuration effect (for vertical consideration): *For an one-row evaporator*, the magnitudes of the changes of temperatures vertically downward, mentioned previously, for R407C are from a small positive to a large positive value. For R134a, the magnitudes are from small negative to large negative.

Table 5.18 Air-side parameters for dynamic mode of the totally-wet coils: results and comments. (The coil configurations were as shown in Figs. 5.66 and 5.67.)

Refrigerant-temperature-glide effect (for vertical consideration): *When the coils operate with smaller increases of heat load*, for both refrigerants, the directions of the changes in temperatures remained the same. However, R407C had a larger magnitude of the change, whereas, that for R134a had a smaller value.

Figure 5.85 Coil-outlet refrigerant pressures vs times for totally-wet coils when there was a 0.8-degree-C step increase in coil-inlet dry-bulb temperatures

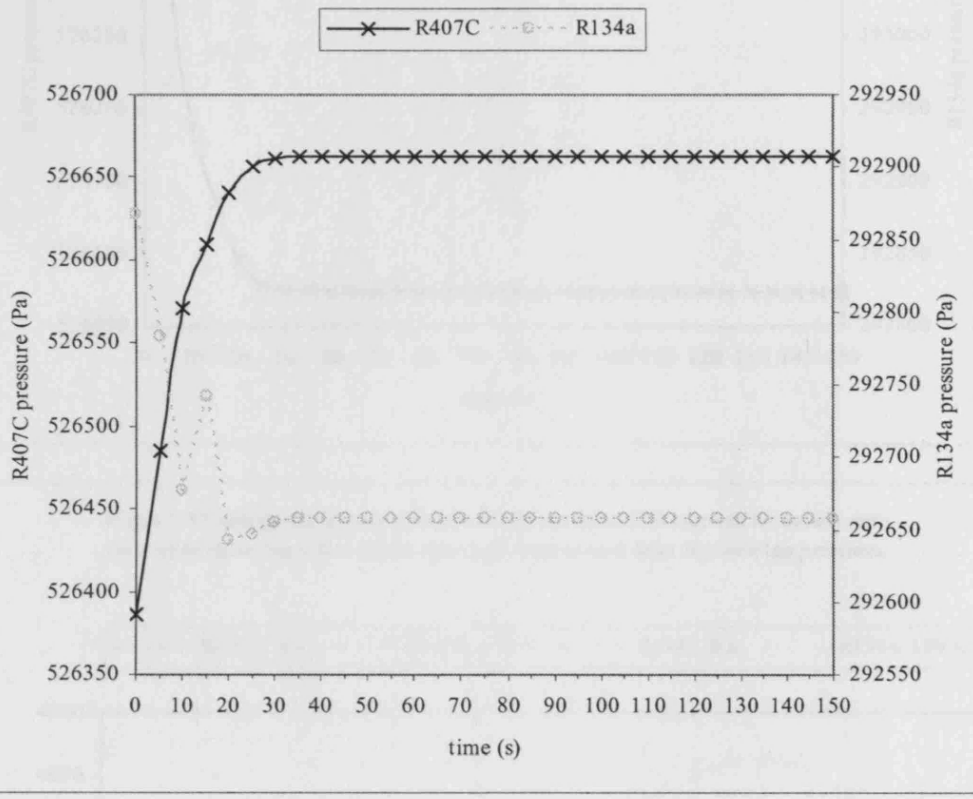

Figure 5.86 Coil-outlet refrigerant pressures vs times for totally-wet coils when there was a 0.8-degree-C step decrease in coil-inlet dry-bulb temperatures

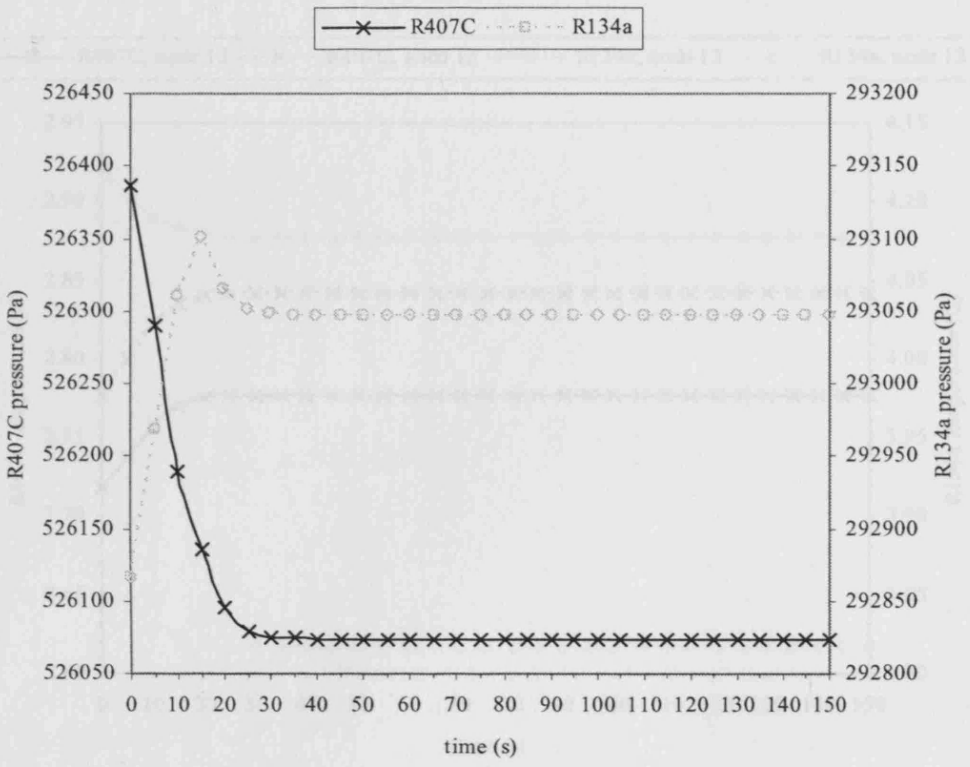

Figure 5.87 Refrigerant pressure drops vs nodes at 0 and 150 seconds for totally-wet coils when there was a 0.8-degree-C step increase in coil-inlet dry-bulb temperatures

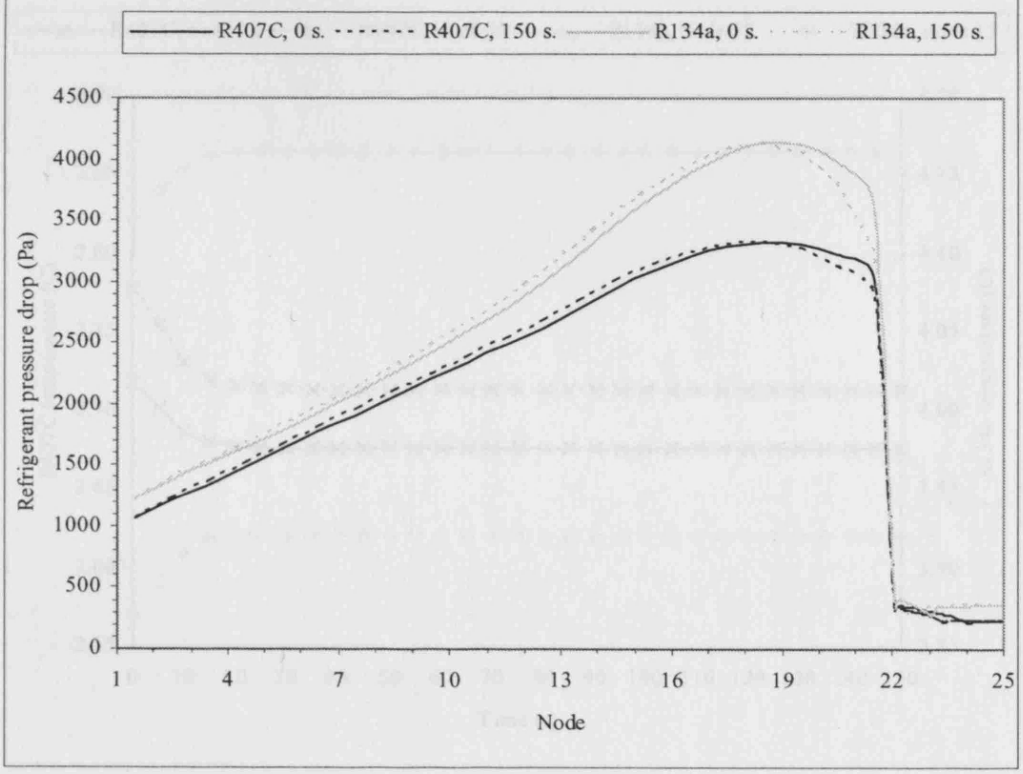

Figure 5.88 Refrigerant temperatures at nodes 12 and 13 vs times for totally-wet coils when there was a 0.8-degree-C step increase in coil-inlet dry-bulb temperatures

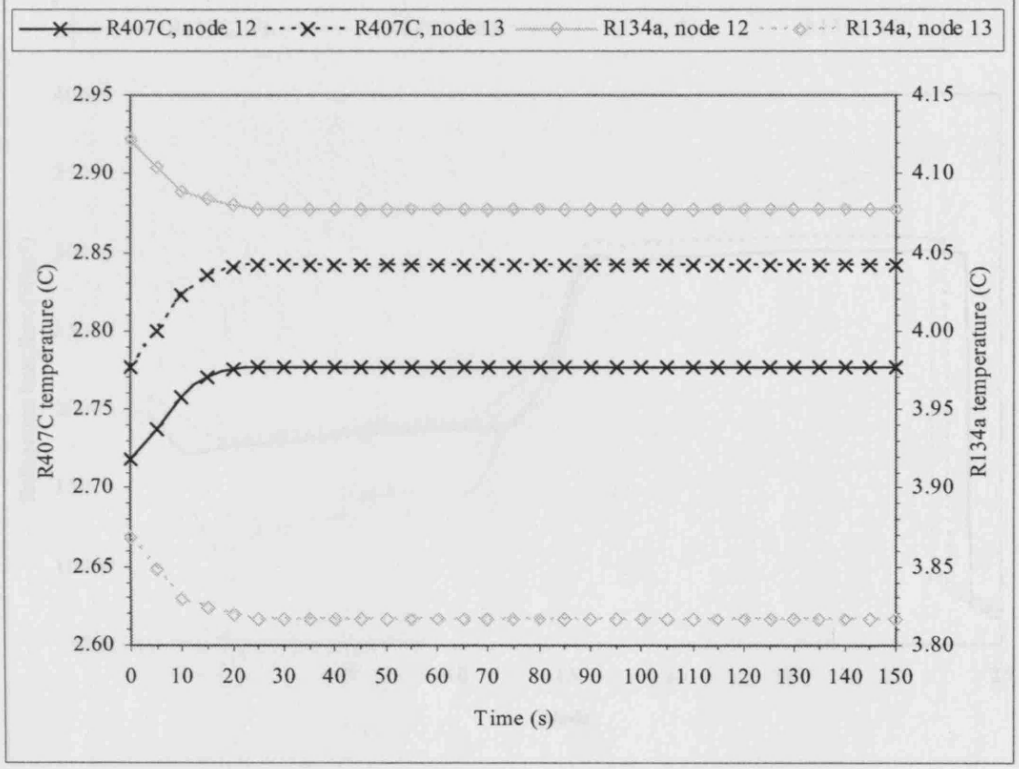

Figure 5.89 Refrigerant temperatures at nodes 12 and 13 vs times for totally-wet coils when there was a 0.8-degree-C step decrease in coil-inlet dry-bulb temperatures

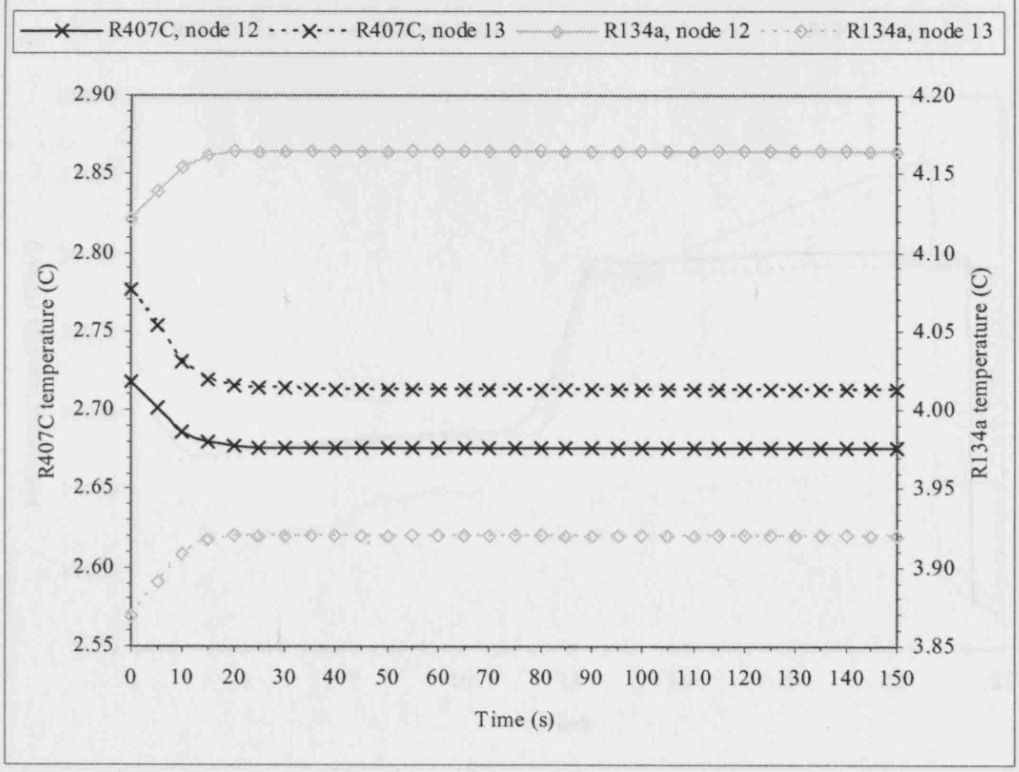

Figure 5.90 Refrigerant heat fluxes vs nodes at 0 and 150 seconds for totally-wet coils when there was a 0.8-degree-C step increase in coil-inlet dry-bulb temperatures

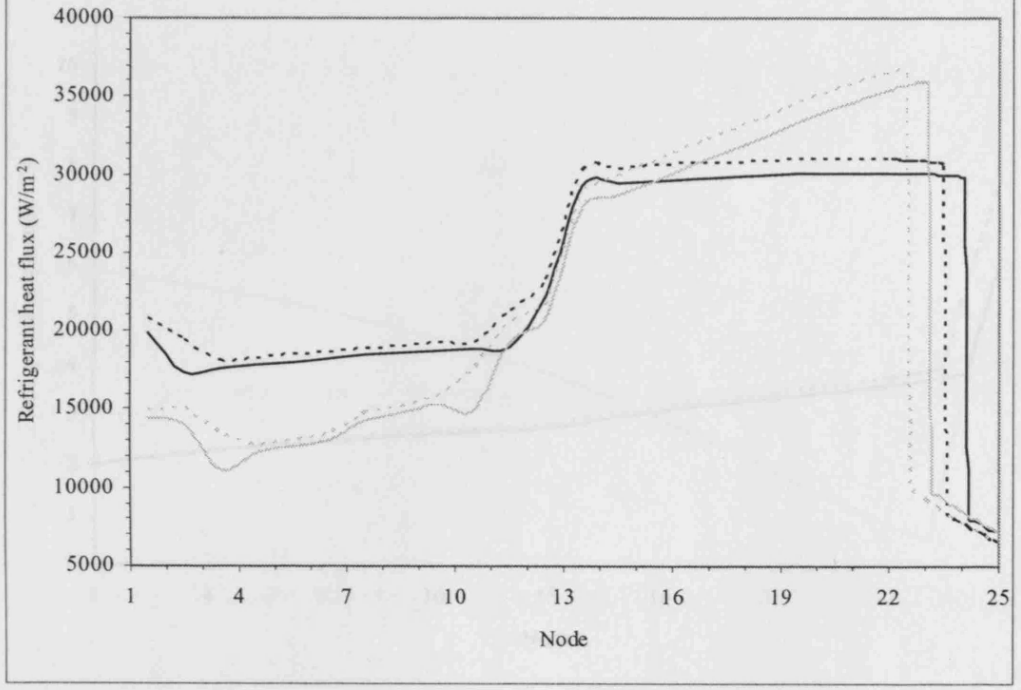

Figure 5.91 Refrigerant heat fluxes vs nodes at 0 and 150 seconds for totally-wet coils when there was a 0.8-degree-C step decrease in coil-inlet dry-bulb temperatures

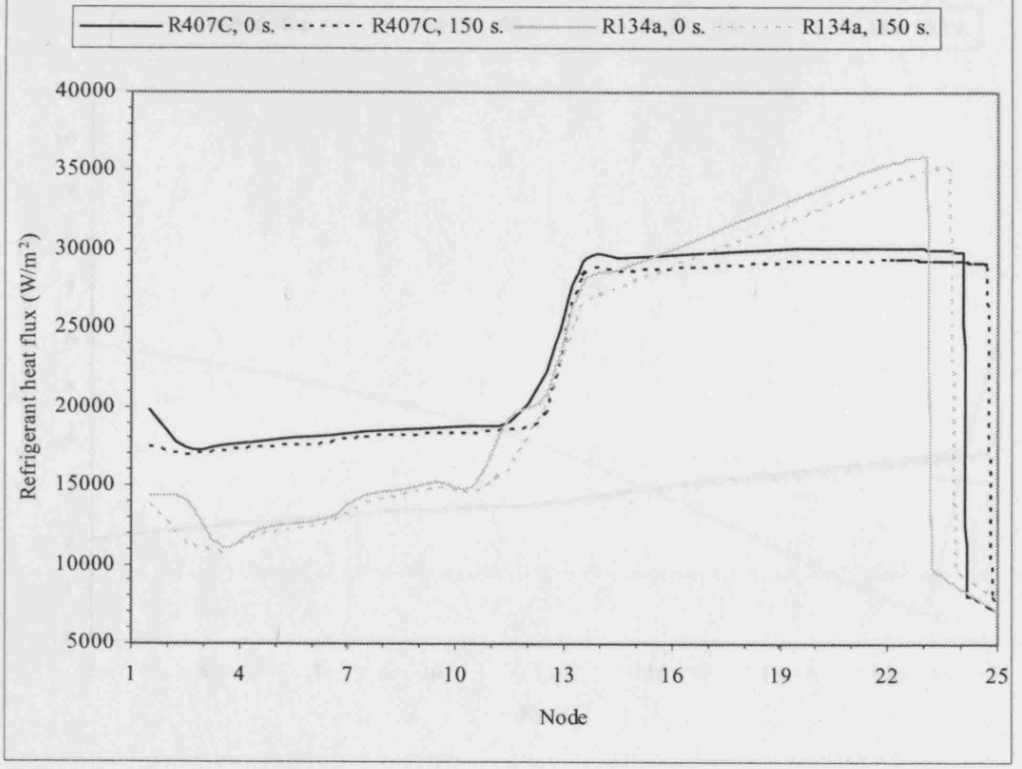

Figure 5.92 Refrigerant temperatures vs nodes at 0 and 150 seconds for totally-wet coils when there was a 0.8-degree-C step increase in coil-inlet dry-bulb temperatures

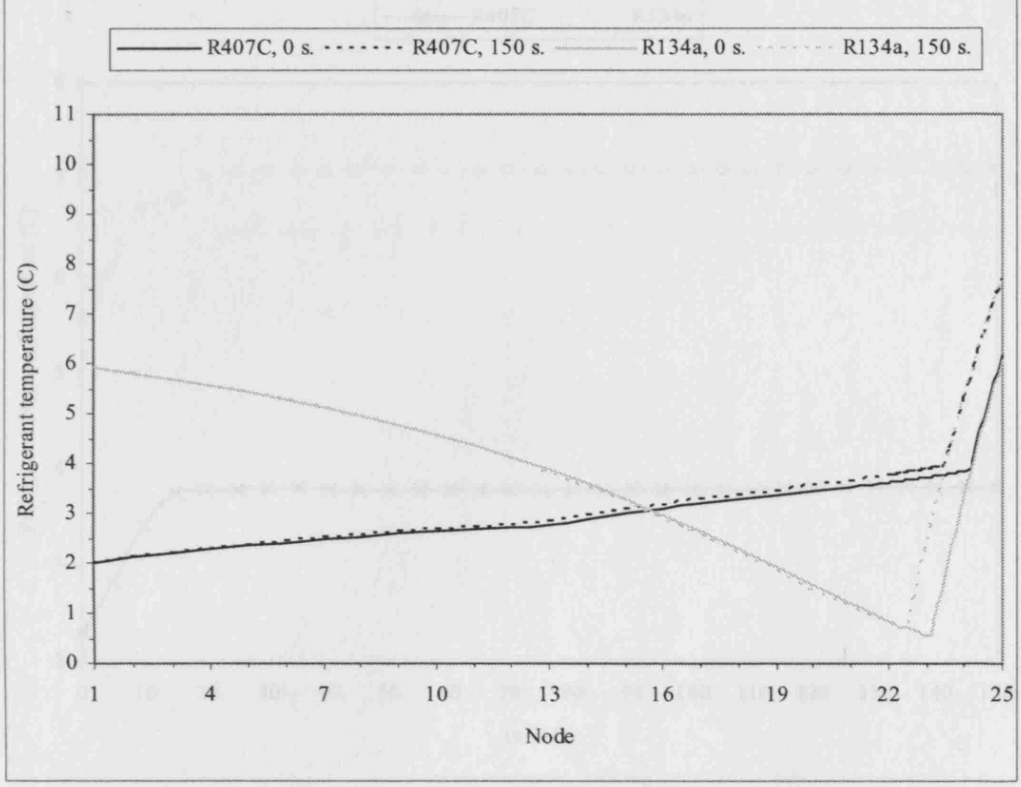

Figure 5.93 Refrigerant temperatures vs nodes at 0 and 150 seconds for totally-wet coils when there was a 0.8-degree-C step decrease in coil-inlet dry-bulb temperatures

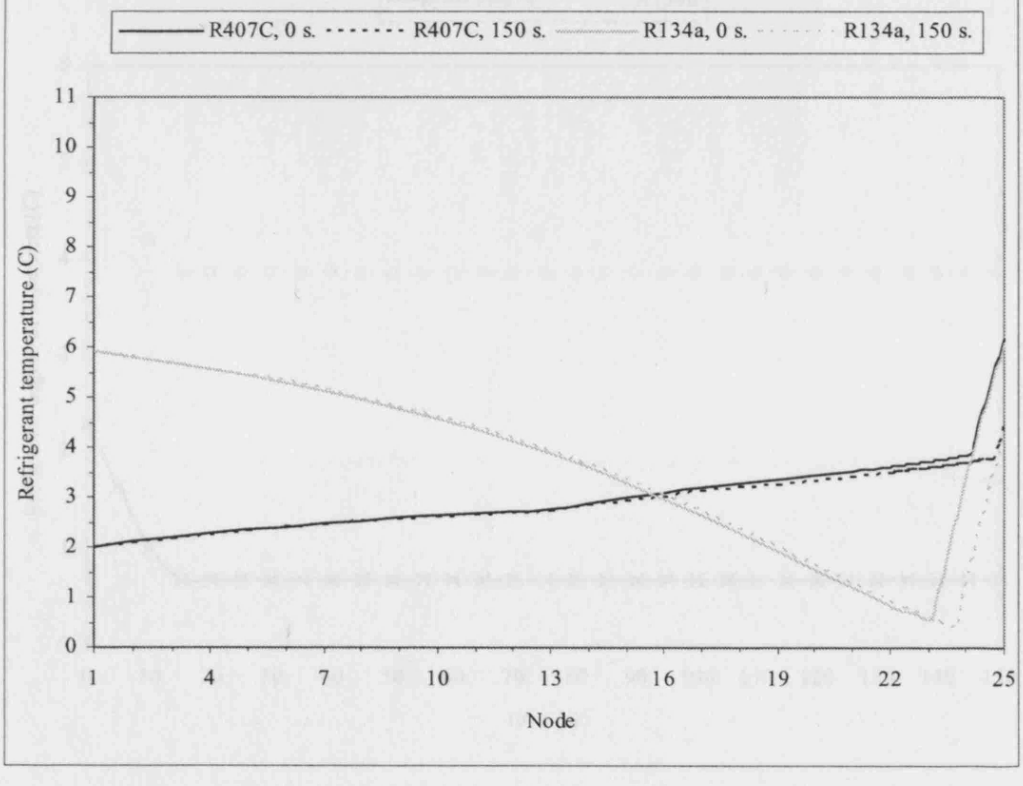

Figure 5.94 Refrigerant degrees of superheat vs times for totally-wet coils when there was a 0.8-degree-C step increase in coil-inlet dry-bulb temperatures

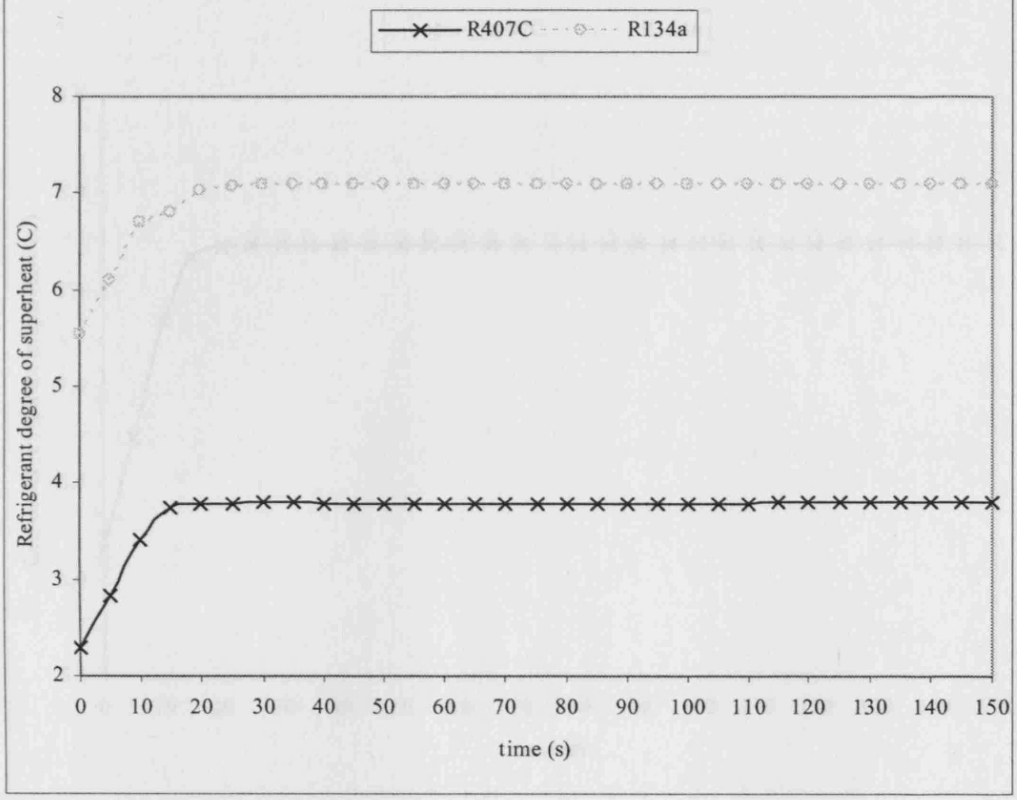

Figure 5.95 Refrigerant degrees of superheat vs times for totally-wet coils when there was a 0.8-degree-C step decrease in coil-inlet dry-bulb temperatures

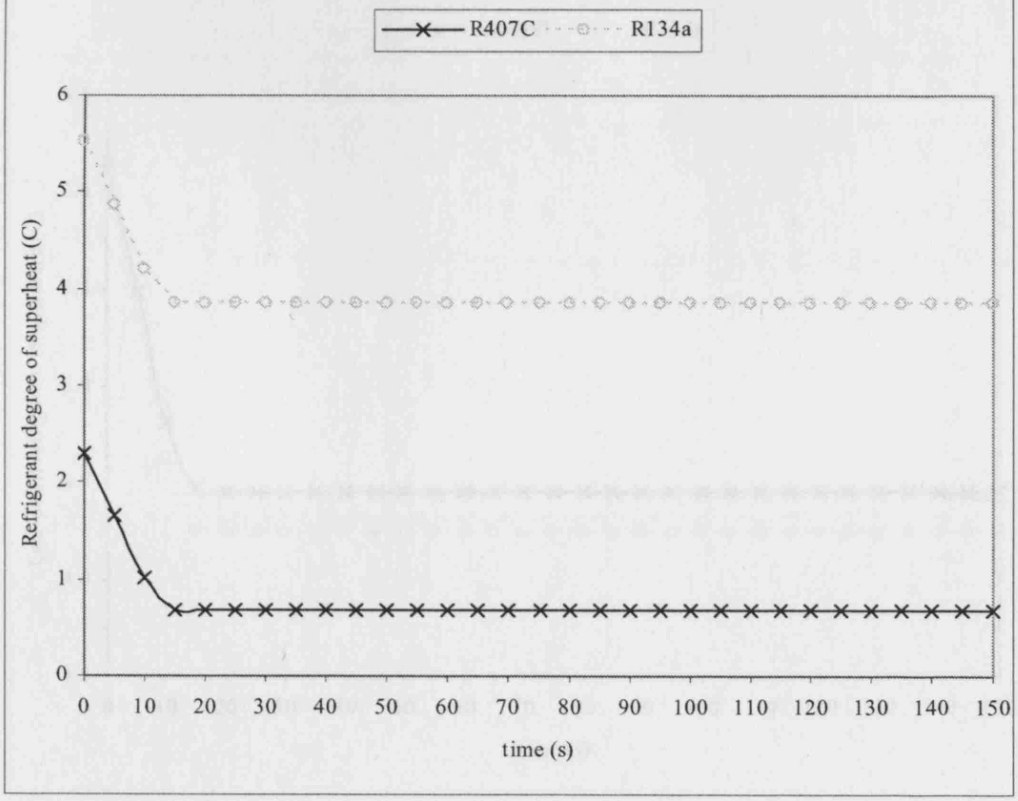

Figure 5.96 Coil-outlet refrigerant temperatures vs times for totally-wet coils when there was a 0.8-degree-C step increase in coil-inlet dry-bulb temperatures

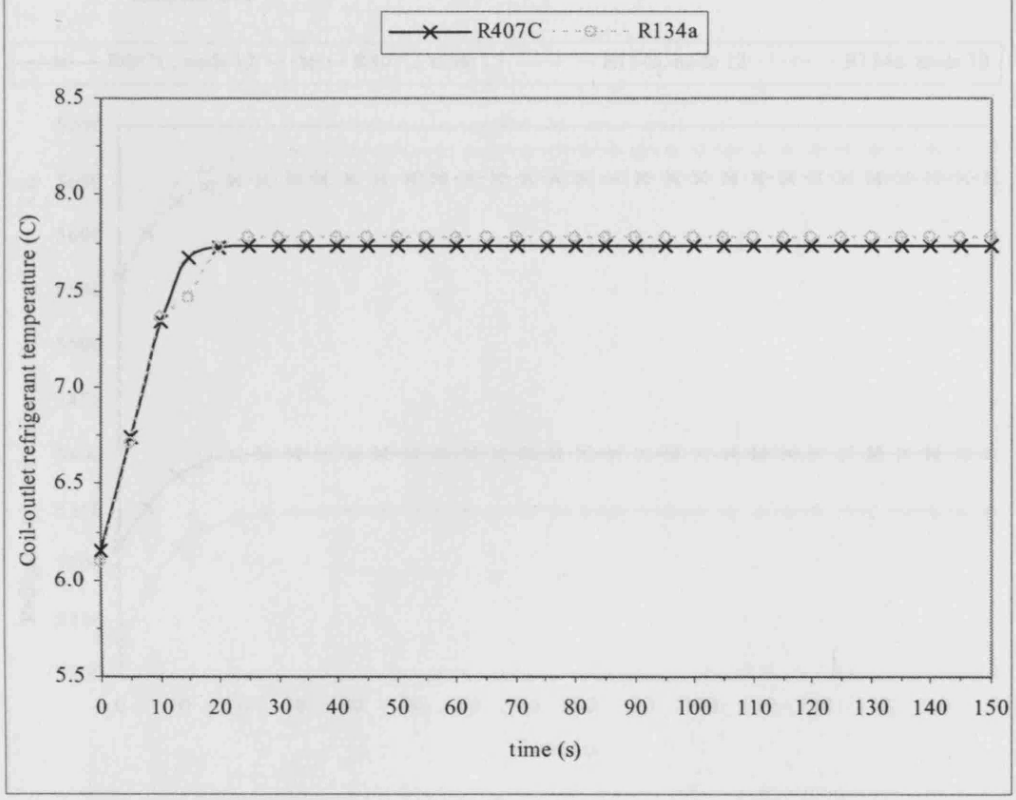

Figure 5.97 Coil-outlet refrigerant temperatures vs times for totally-wet coils when there was a 0.8-degree-C step decrease in coil-inlet dry-bulb temperatures

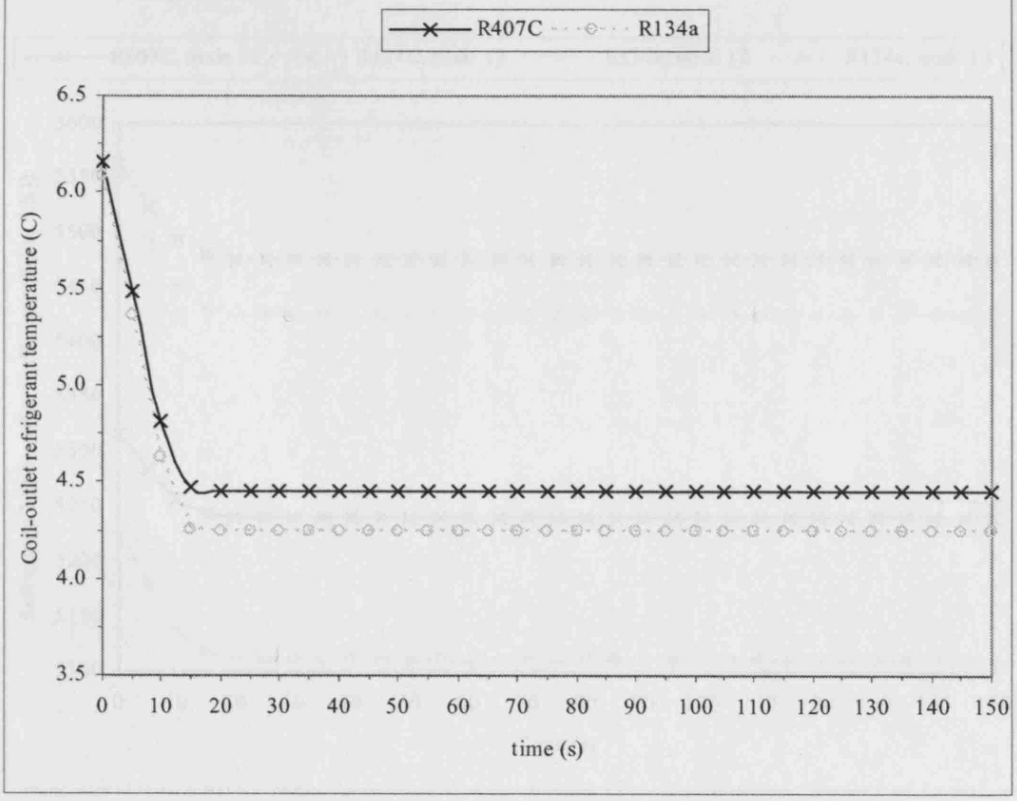

Figure 5.98 Refrigerant heat transfer coefficients at nodes 12 and 13 vs times for totally-wet coils when there was a 0.8-degree-C step increase in coil-inlet dry-bulb temperatures

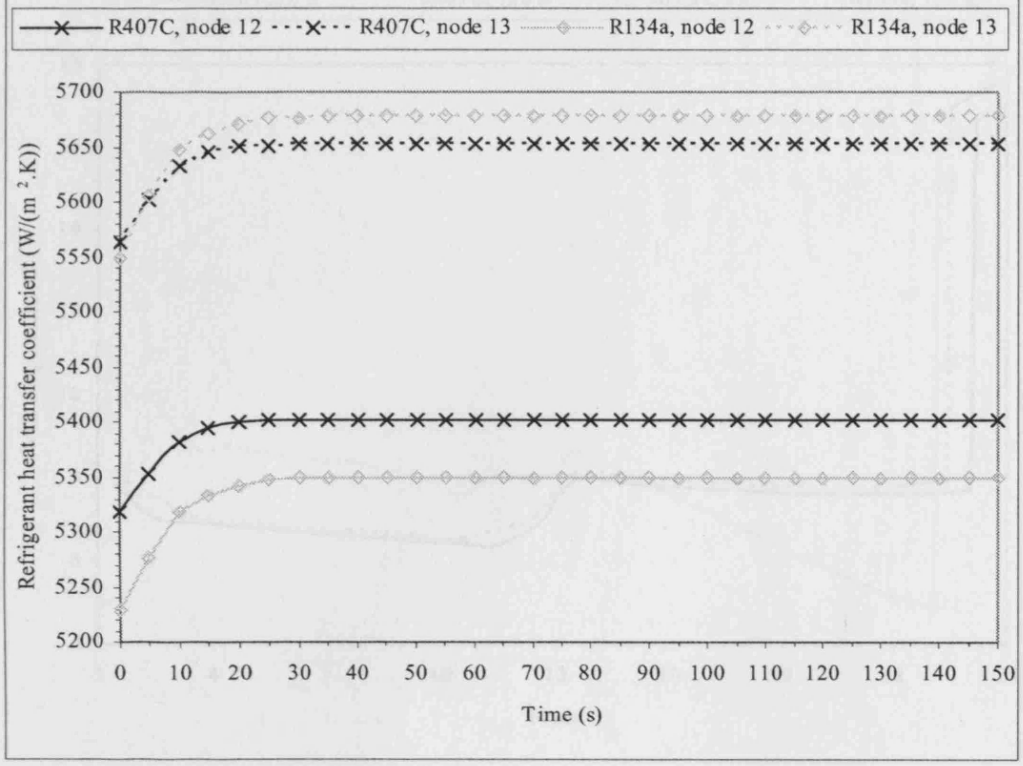

Figure 5.99 Refrigerant heat transfer coefficients at nodes 12 and 13 vs times for totally-wet coils when there was a 0.8-degree-C step decrease in coil-inlet dry-bulb temperatures

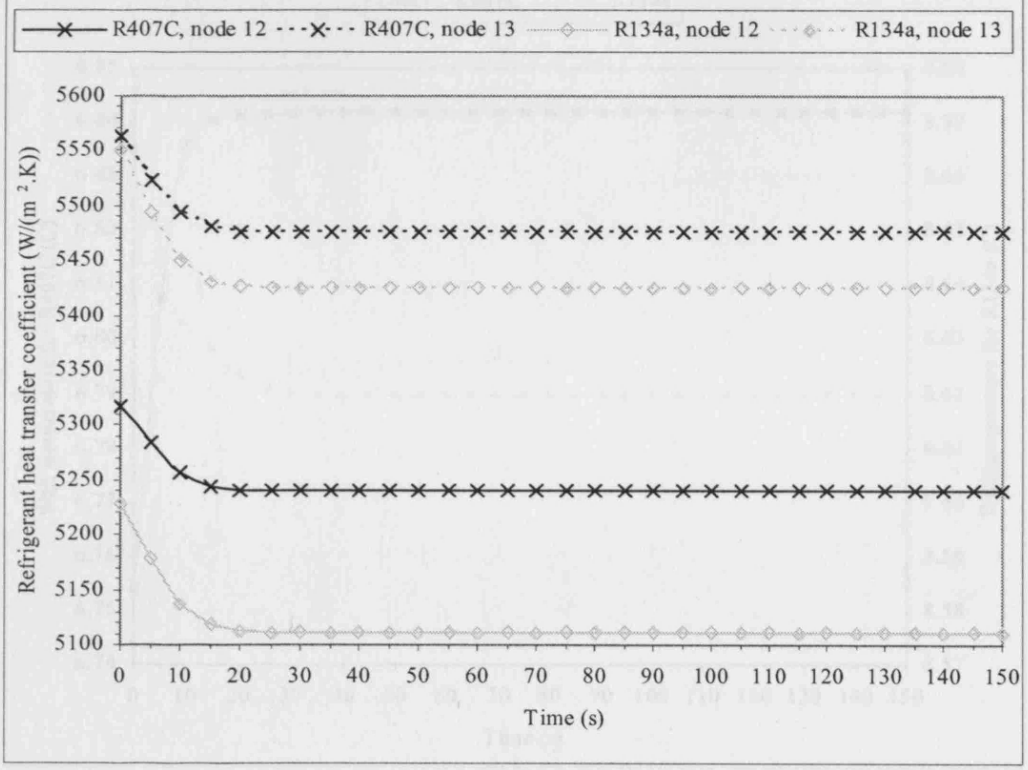

Figure 5.100 Wall temperatures vs nodes at 0 and 150 seconds for totally-wet coils when there was a 0.8-degree-C step increase in coil-inlet dry-bulb temperatures

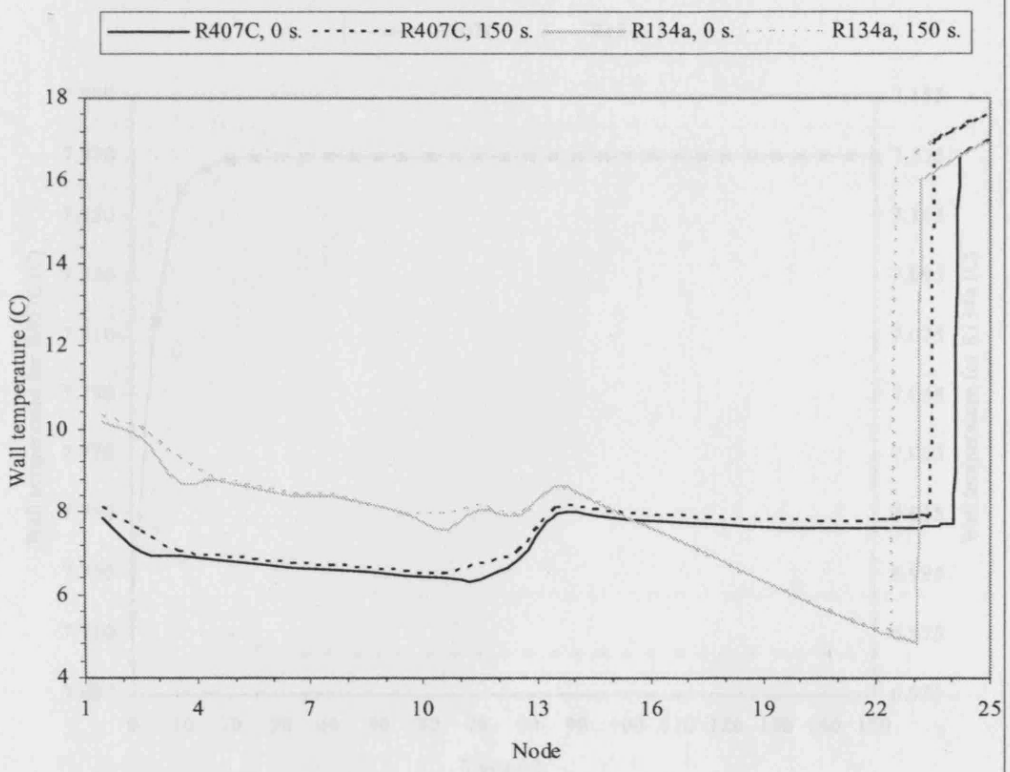

Figure 5.101 Wall temperatures vs time at Elements (1,2,2) for totally-wet coils when there was a 0.8-degree-C step increase in coil-inlet dry-bulb temperatures

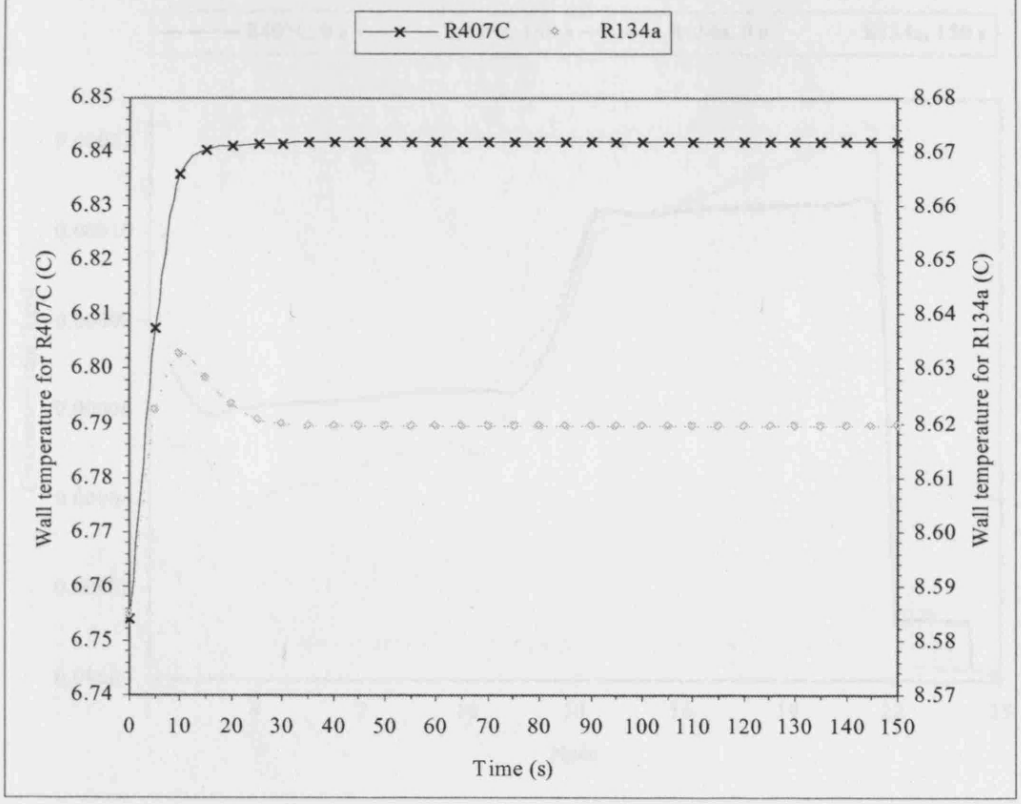

Figure 5.102 Wall temperatures vs time at Elements (2,2,2) for totally-wet coils when there was a 0.8-degree-C step increase in coil-inlet dry-bulb temperatures

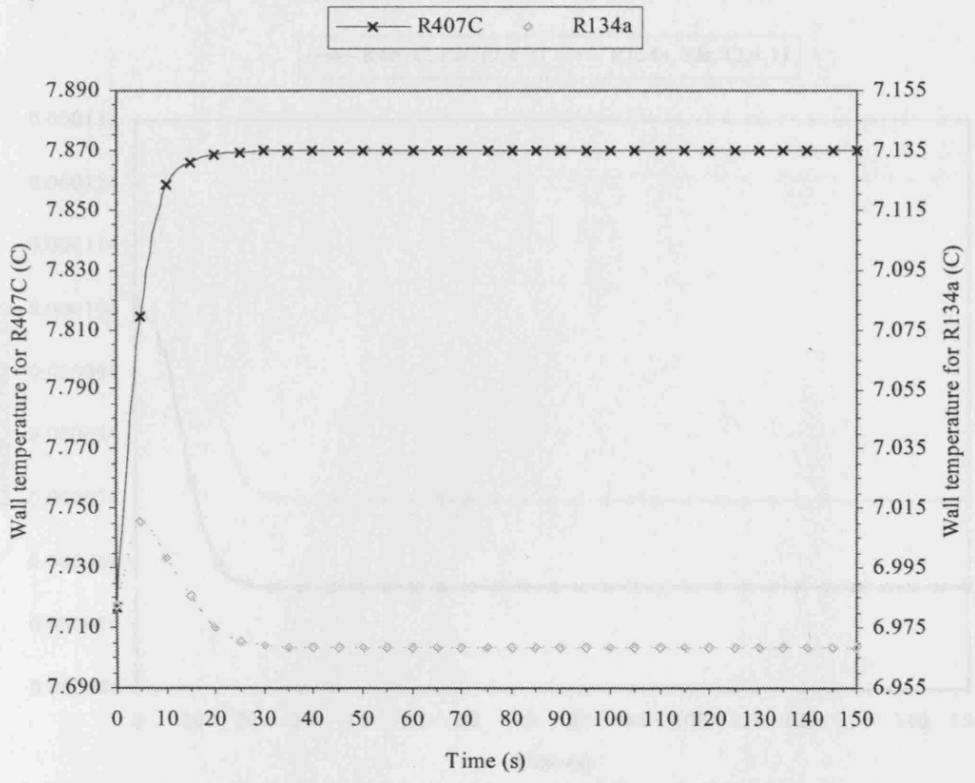

Figure 5.103 Condensate rates vs nodes for totally-wet coils when there was a step increase in coil-inlet dry-bulb temperatures

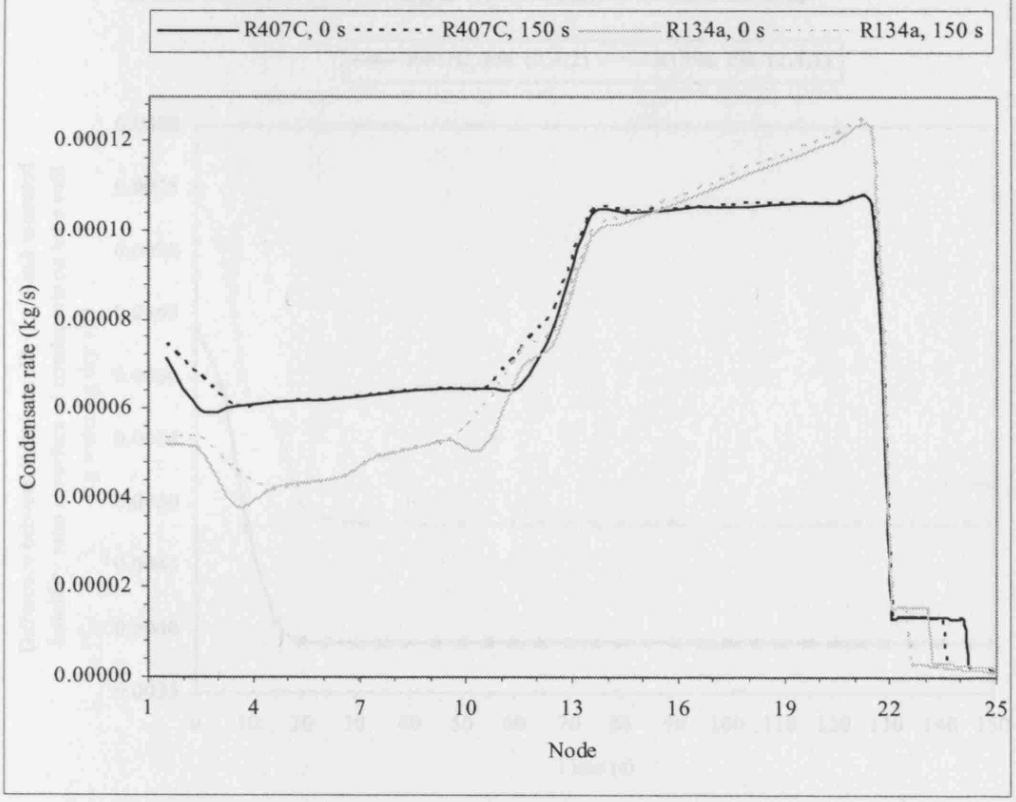

Figure 5.104 Condensate rates vs times at Elements (2,4,2) and (2,4,1) for R407C and R134a, respectively, for totally-wet coils when there was a 0.8-degree-C step increase in coil-inlet dry-bulb temperatures

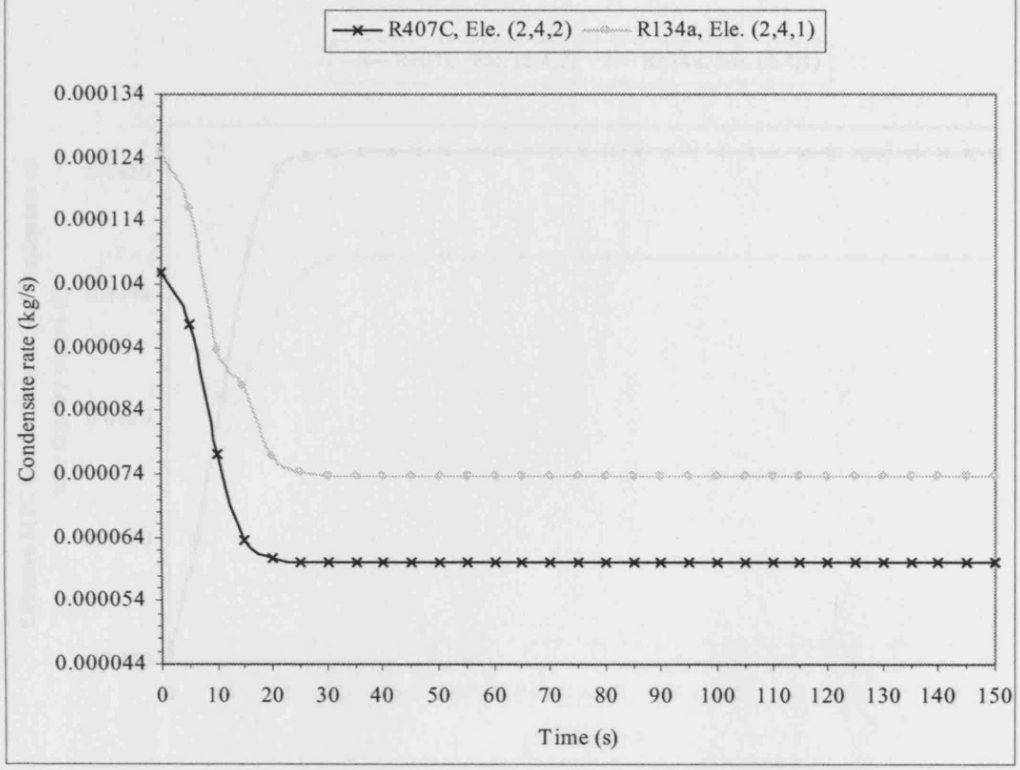

Figure 5.105 Diff. bet. inlet HR and sat. HR at surface of condensate on tube wall vs times at Elements (2,4,2) and (2,4,1) for R407C and R134a, respectively, for totally-wet coils when there was a 0.8-degree-C step increase in coil-inlet DB temp.

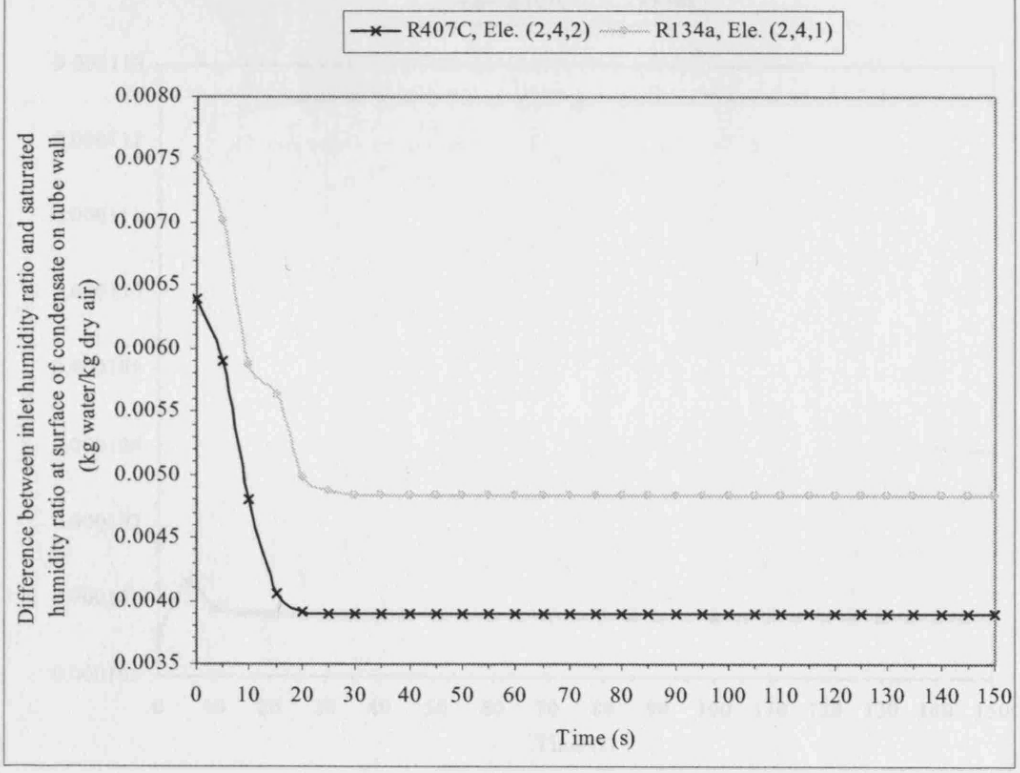

Figure 5.106 Effective MTCs between inlet air and condensate on tube vs times at Elements (2,4,2) and (2,4,1) for R407C and R134a, respectively, for totally-wet coils when there was a 0.8-degree-C step increase in coil-inlet DB temperatures

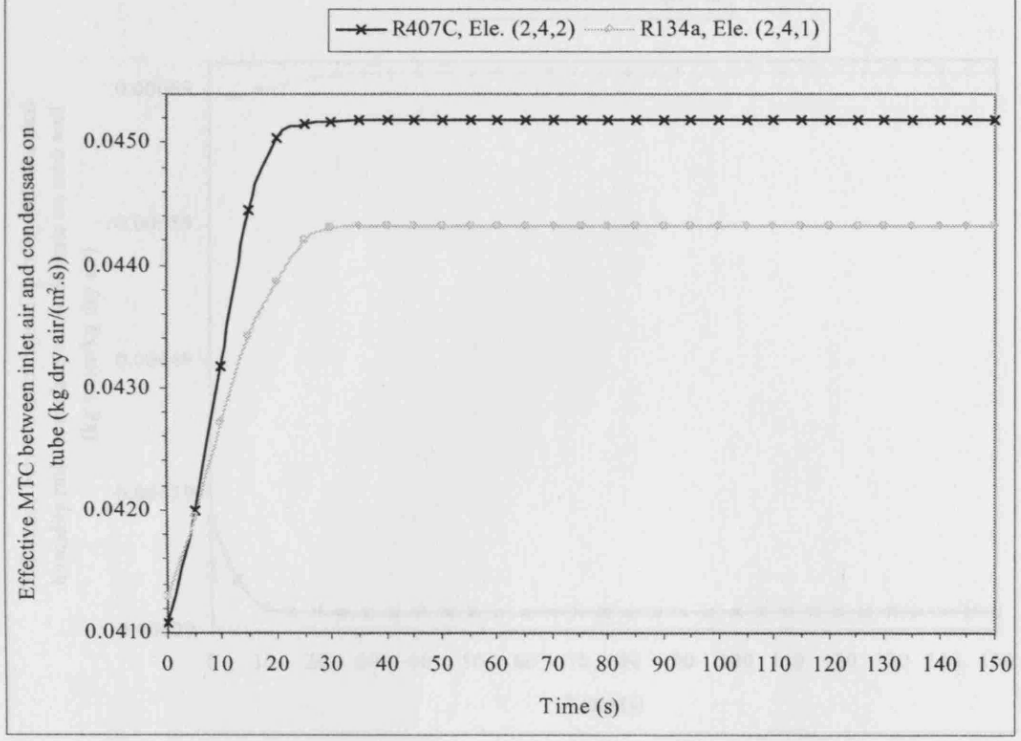

Figure 5.107 Condensate rates vs times at Elements (2,2,2) for totally-wet coils when there was a 0.8-degree-C step increase in coil-inlet dry-bulb temperatures

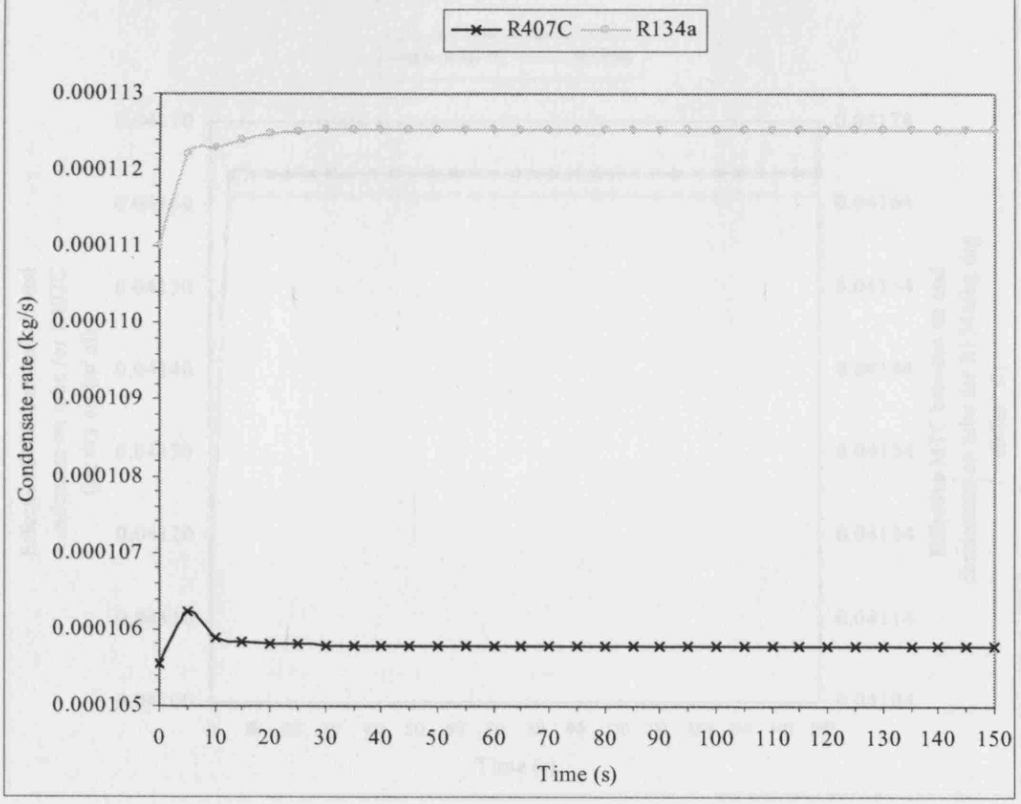

Figure 5.108 Differences between inlet humidity ratio and saturated humidity ratio at surface of condensate on tube wall vs times at Elements (2,2,2) for totally-wet coils when there was a 0.8-degree-C step increase in coil-inlet DB temperatures

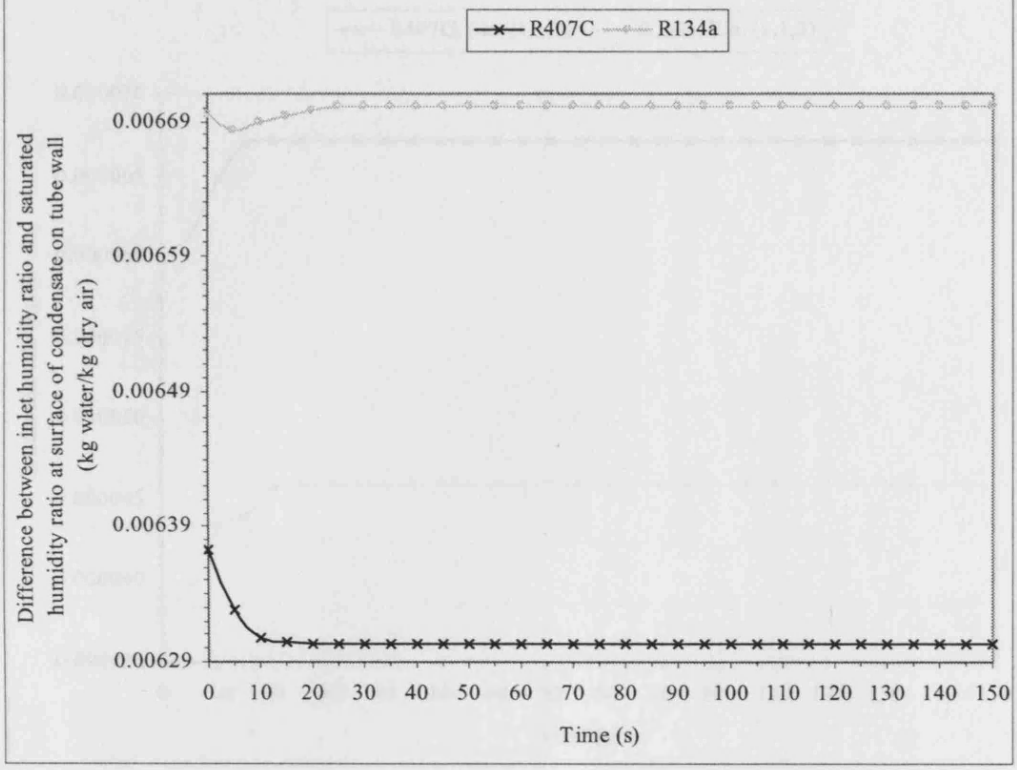

Figure 5.109 Effective mass transfer coefficients between inlet air and condensate on tube vs times at Elements (2,2,2) for totally-wet coils when there was a 0.8-degree-C step increase in coil-inlet dry-bulb temperatures

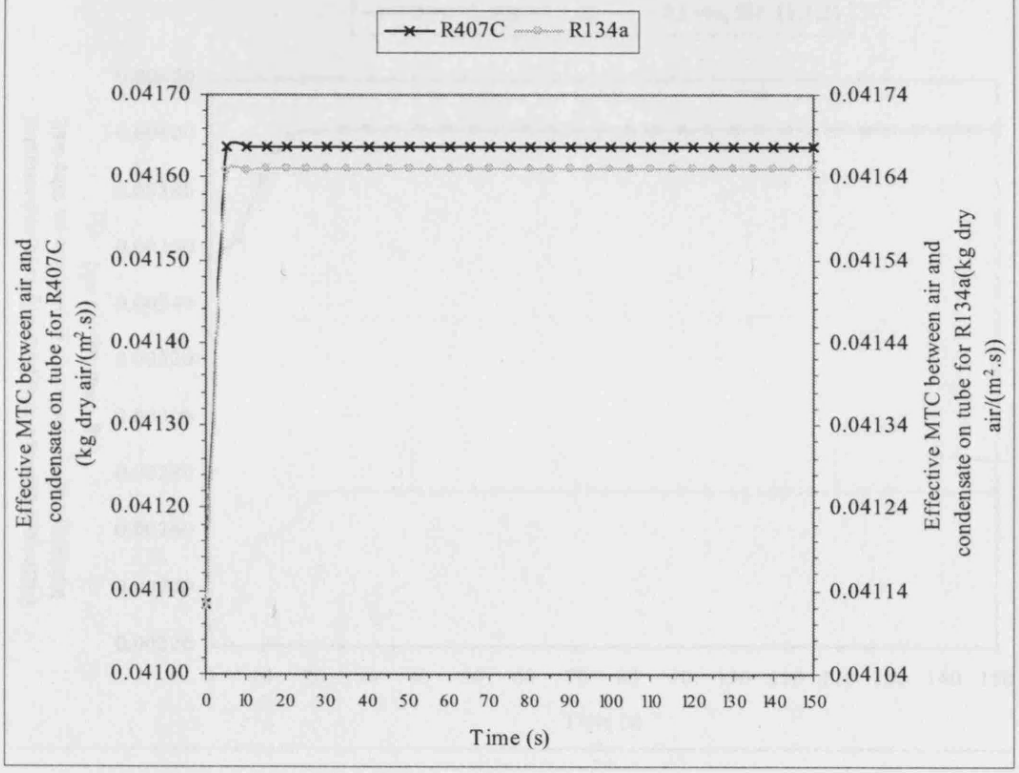

Figure 5.110 Condensate rates vs times at Elements (1,1,2) and (1,1,3) for R407C and R134a, respectively, for totally-wet coils when there was a 0.8-degree-C step increase in coil-inlet dry-bulb temperatures

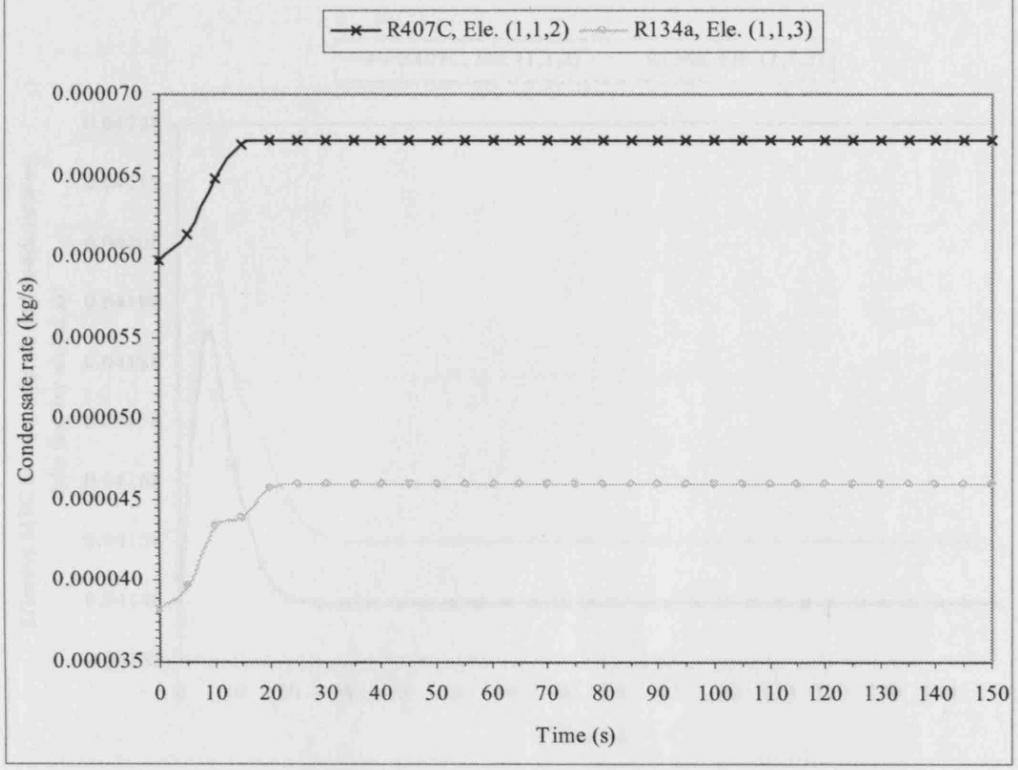

Figure 5.111 Diff. bet. inlet HR and sat. HR at surface of condensate on tube wall vs times at Elements (1,1,2) and (1,1,3) for R407C and R134a, respectively, for totally-wet coils when there was a 0.8-degree-C step increase in coil-inlet DB temp.

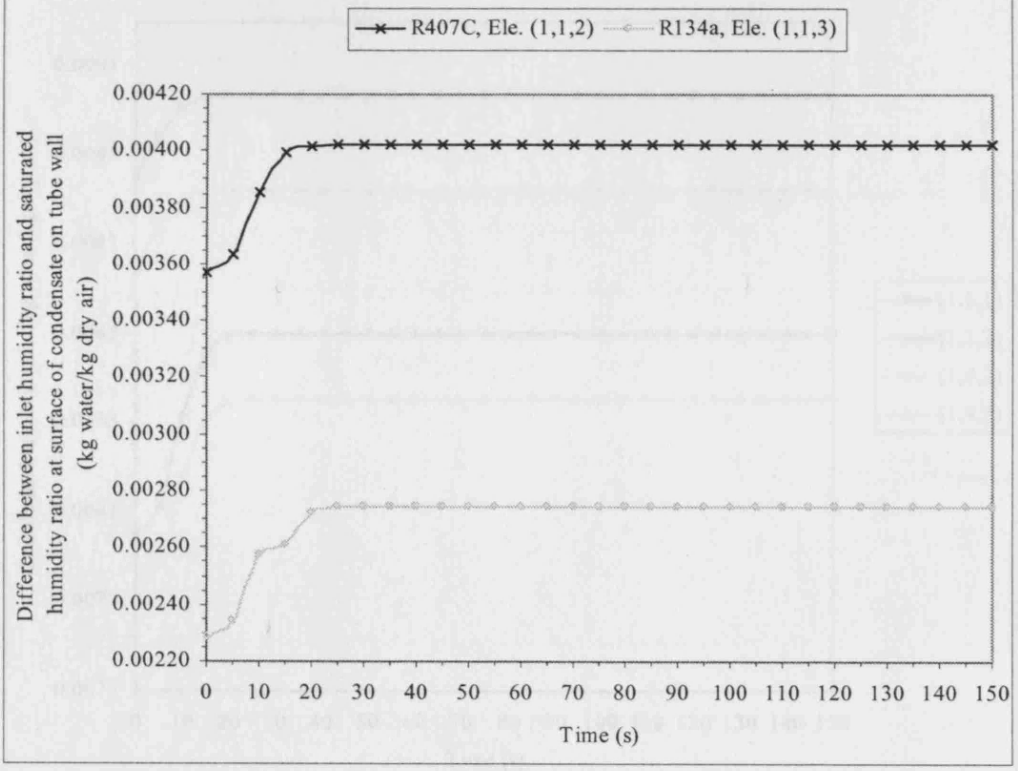

Figure 5.112 Effective MTCs between inlet air and condensate on tube vs times at Elements (1,1,2) and (1,1,3) for R407C and R134a, respectively, for totally-wet coils when there was a 0.8-degree-C step increase in coil-inlet DB temperatures

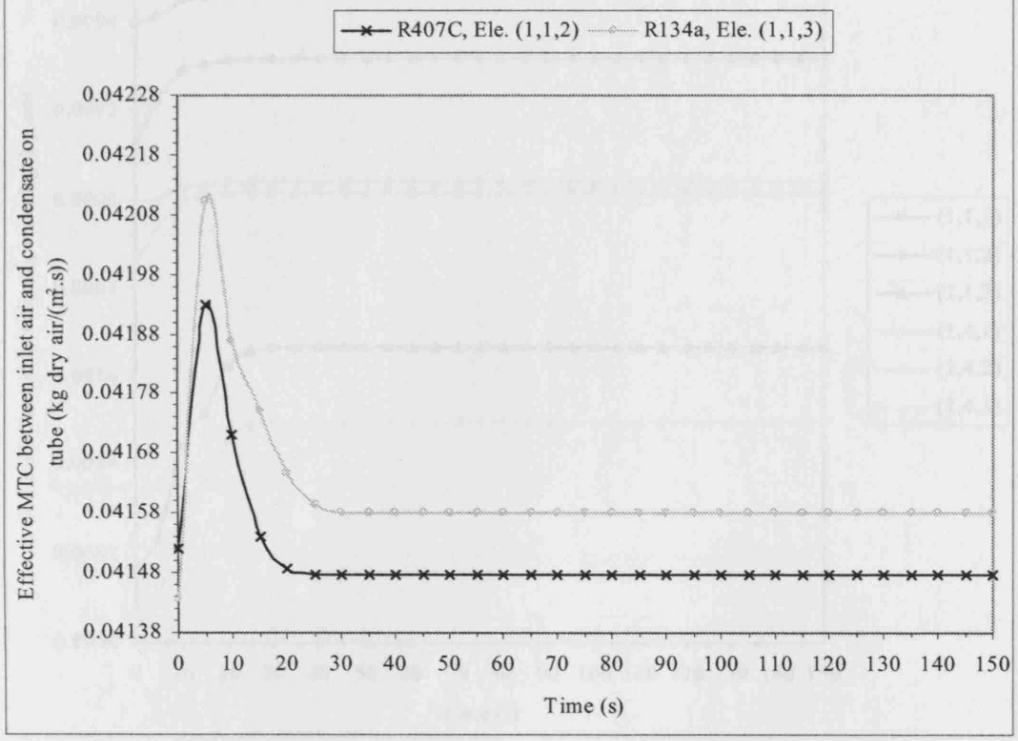

Figure 5.113 Coil-outlet humidity ratios (from Elements affected by superheat) for R407C vs times for totally-wet coils when there was a 0.8-degree-C step increase in coil-inlet dry-bulb temperatures

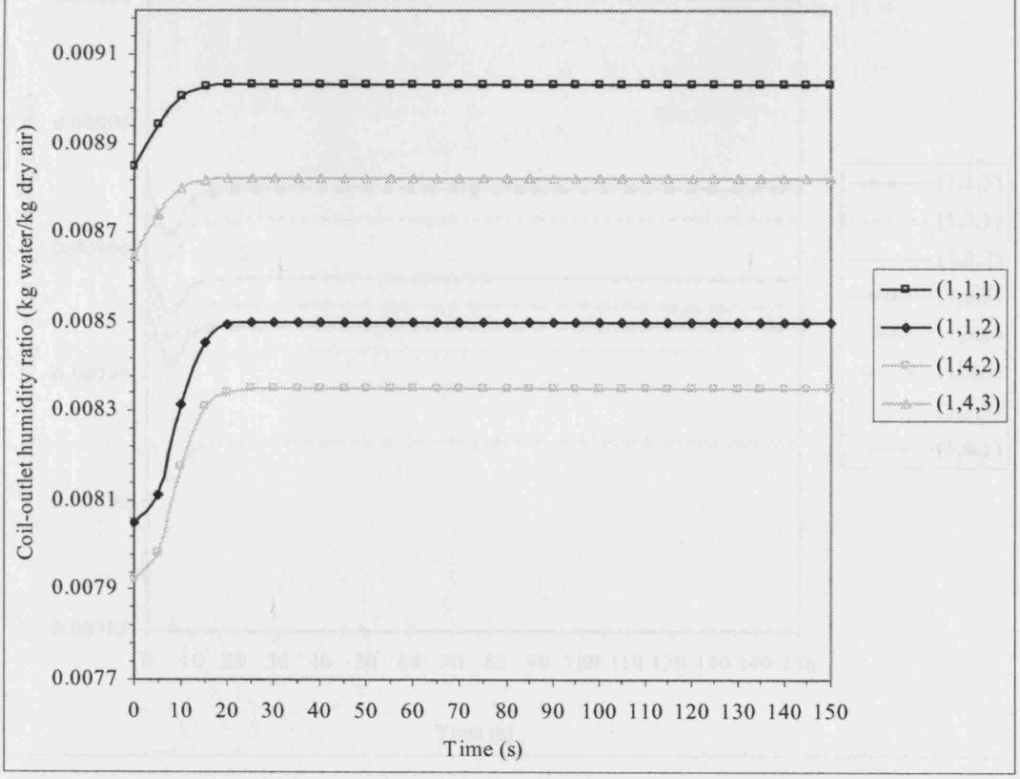

Figure 5.114 Coil-outlet humidity ratios (from Elements affected by superheat) for R134a vs times for totally-wet coils when there was a 0.8-degree-C step increase in coil-inlet dry-bulb temperatures

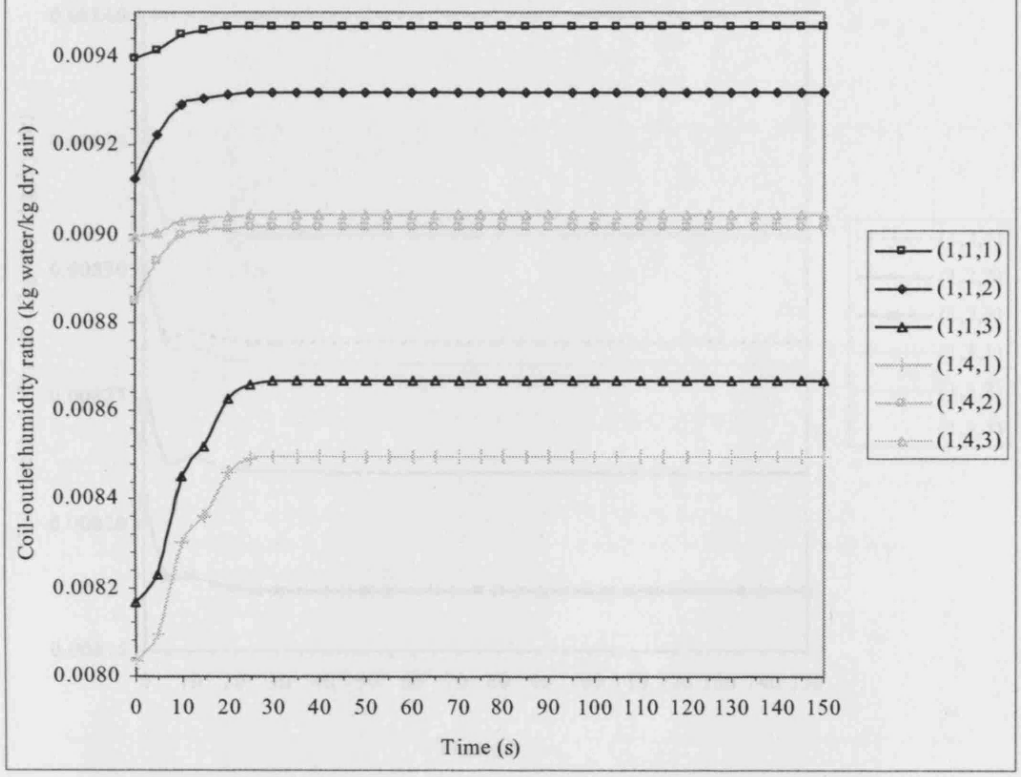

Figure 5.115 Coil-outlet humidity ratios (from Elements unaffected by superheat) for R407C vs times for totally-wet coils when there was a 0.8-degree-C step increase in coil-inlet dry-bulb temperatures

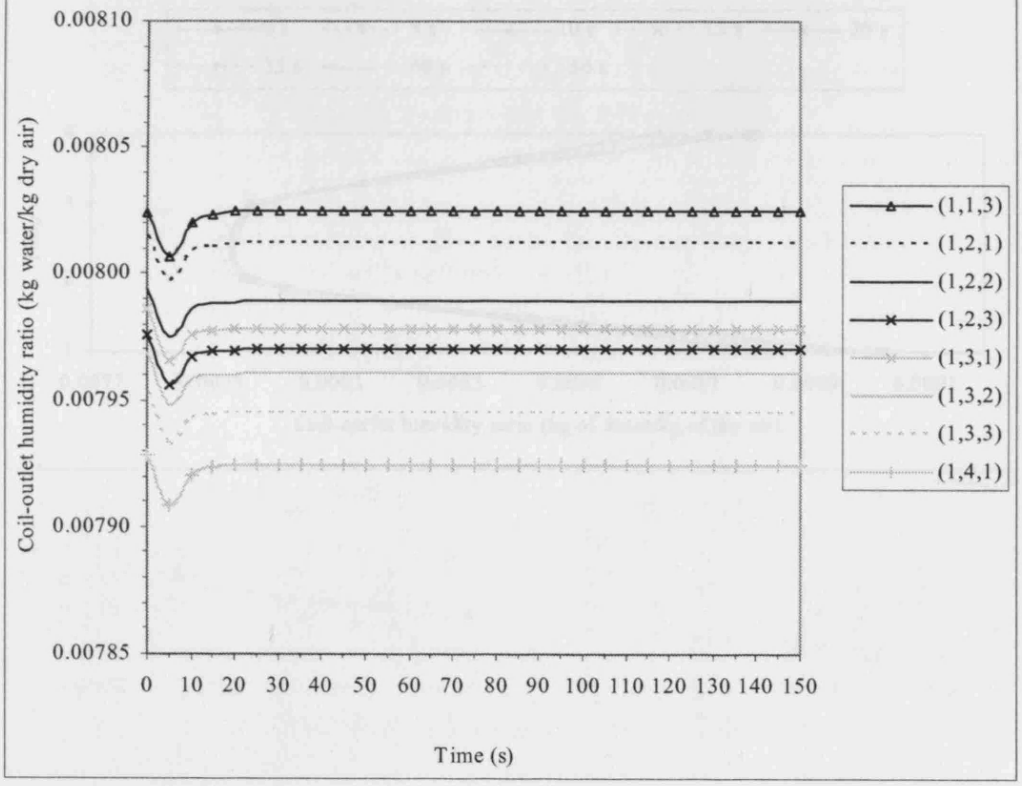

Figure 5.116 Coil-outlet humidity ratios (from Elements unaffected by superheat) for R134a vs times for totally-wet coils when there was a 0.8-degree-C step increase in coil-inlet dry-bulb temperatures

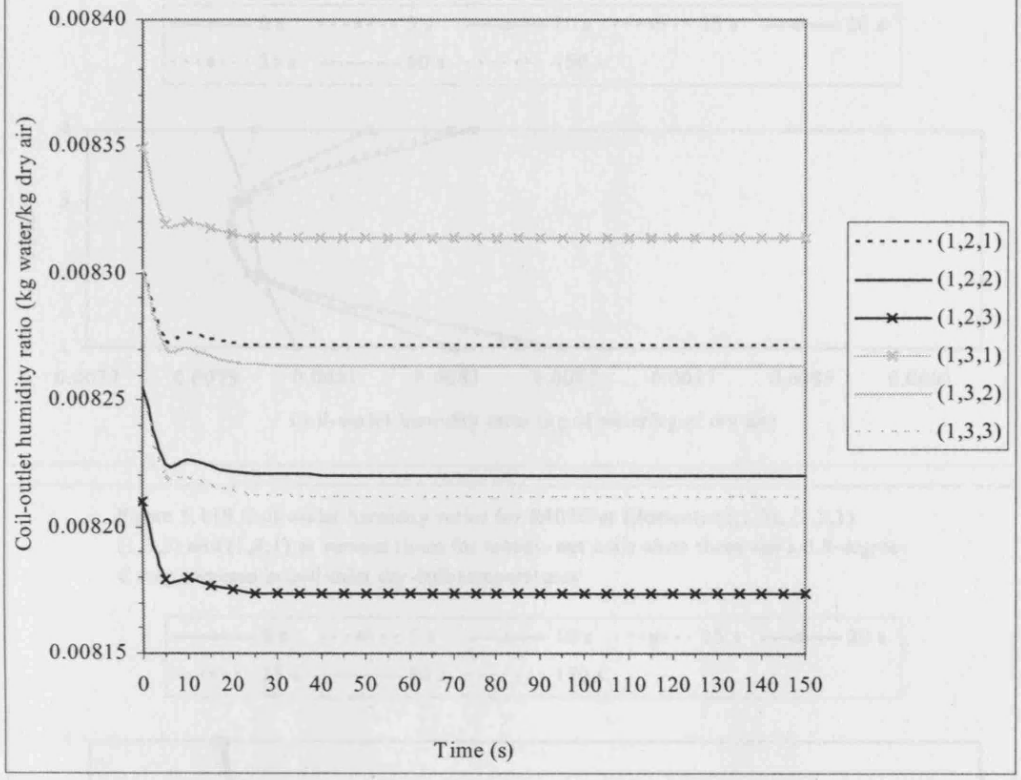

Figure 5.117 Coil-outlet humidity ratios for R407C at Elements (1,1,1), (1,2,3) (1,3,1) and (1,4,3) at various times for totally-wet coils when there was a 0.8-degree-C step increase in coil-inlet dry-bulb temperatures

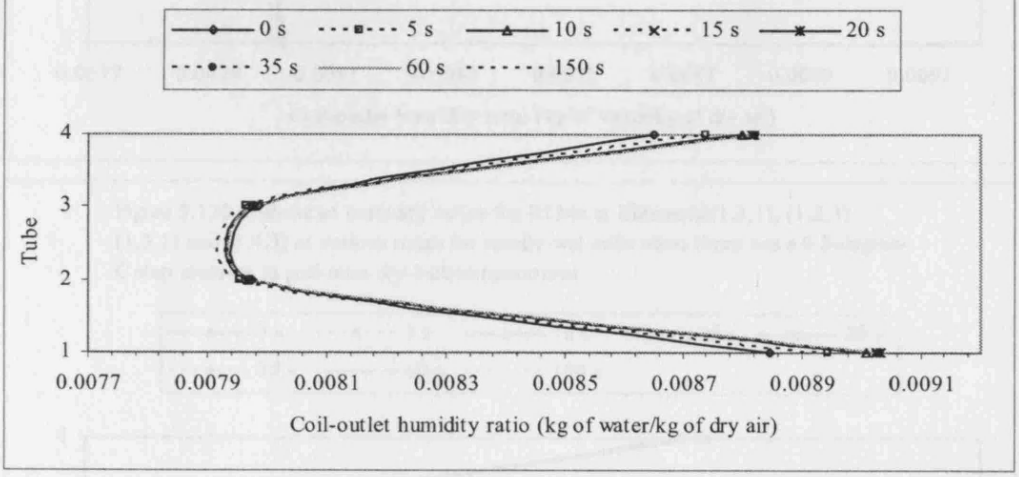

Figure 5.118 Coil-outlet humidity ratios for R407C at Elements (1,1,2), (1,2,2) (1,3,2) and (1,4,2) at various times for totally-wet coils when there was a 0.8-degree-C step increase in coil-inlet dry-bulb temperatures

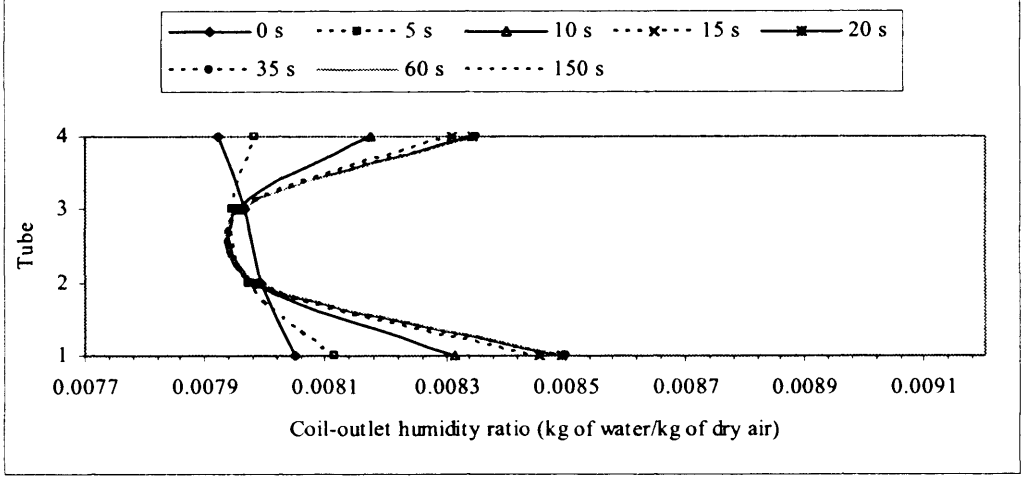

Figure 5.119 Coil-outlet humidity ratios for R407C at Elements (1,1,3), (1,2,1) (1,3,3) and (1,4,1) at various times for totally-wet coils when there was a 0.8-degree-C step increase in coil-inlet dry-bulb temperatures

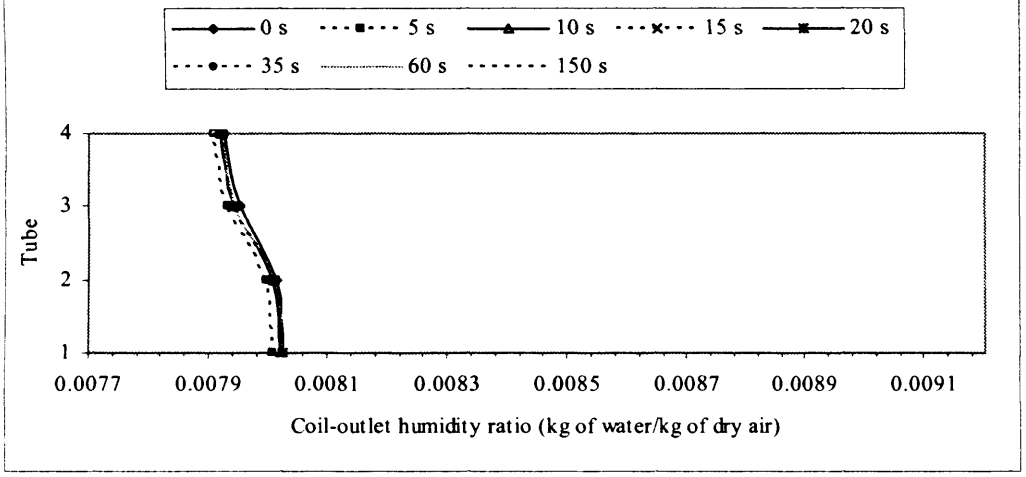

Figure 5.120 Coil-outlet humidity ratios for R134a at Elements (1,1,1), (1,2,3) (1,3,1) and (1,4,3) at various times for totally-wet coils when there was a 0.8-degree-C step increase in coil-inlet dry-bulb temperatures

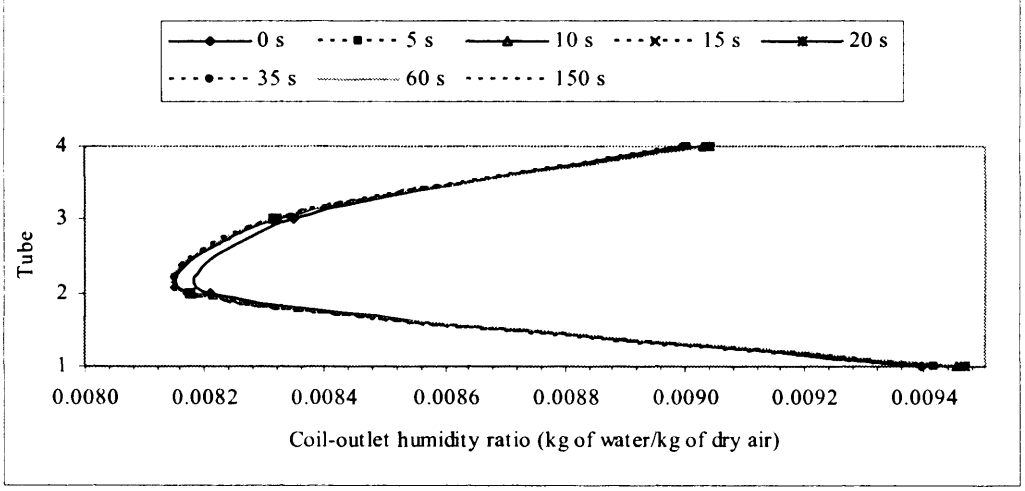

Figure 5.121 Coil-outlet humidity ratios for R134a at Elements (1,1,2), (1,2,2) (1,3,2) and (1,4,2) at various times for totally-wet coils when there was a 0.8-degree-C step increase in coil-inlet dry-bulb temperatures

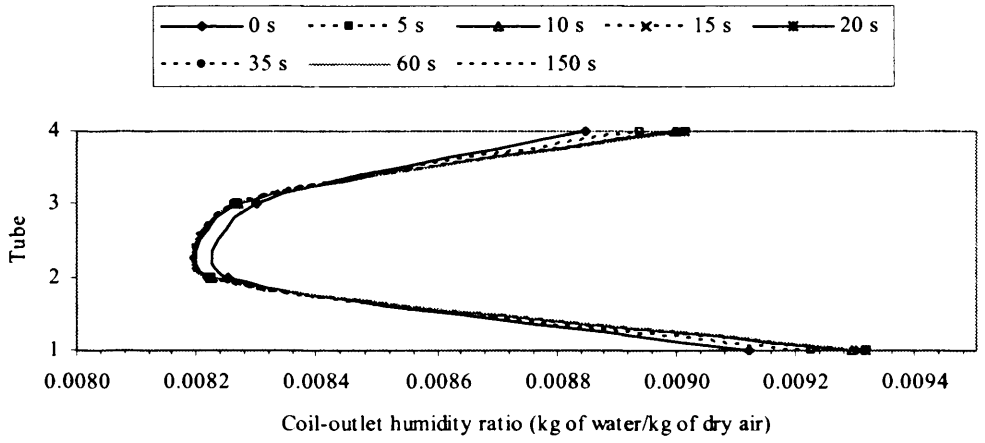

Figure 5.122 Coil-outlet humidity ratios for R134a at Elements (1,1,3), (1,2,1) (1,3,3) and (1,4,1) at various times for totally-wet coils when there was a 0.8-degree-C step increase in coil-inlet dry-bulb temperatures

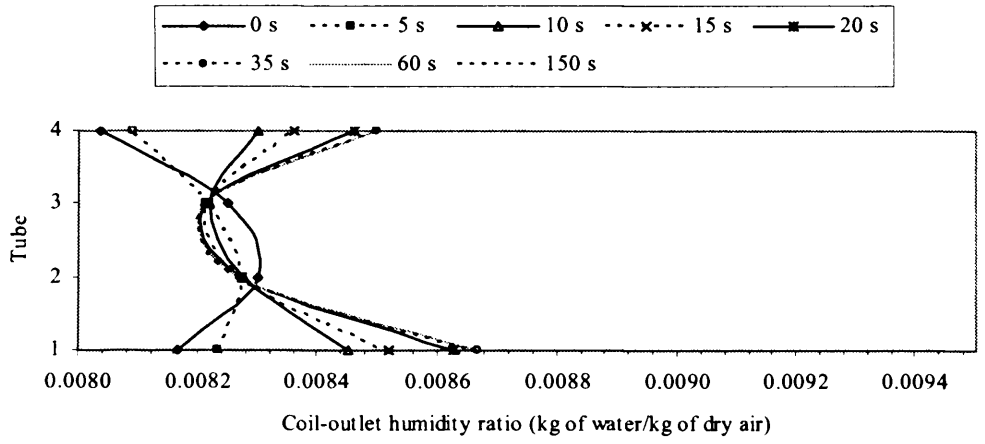

Figure 5.123 Air heat fluxes vs times at Elements (2,4,2) and (2,4,1) for R407C and R134a, respectively, for totally-wet coils when there was a 0.8-degree-C step increase in coil-inlet dry-bulb temperatures

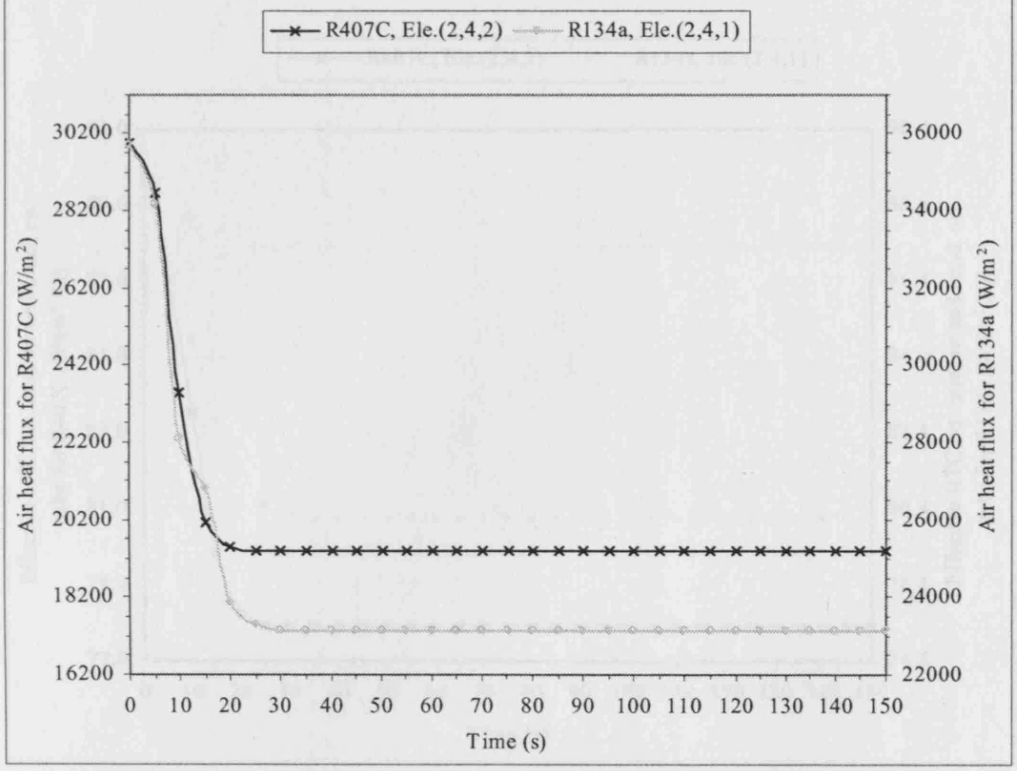

Figure 5.124 Differences between inlet DB temperature and wall temperature vs times at Elements (2,4,2) and (2,4,1) for R407C and R134a, respectively, for totally-wet coils when there was a 0.8-degree-C step increase in coil-inlet DB temperatures

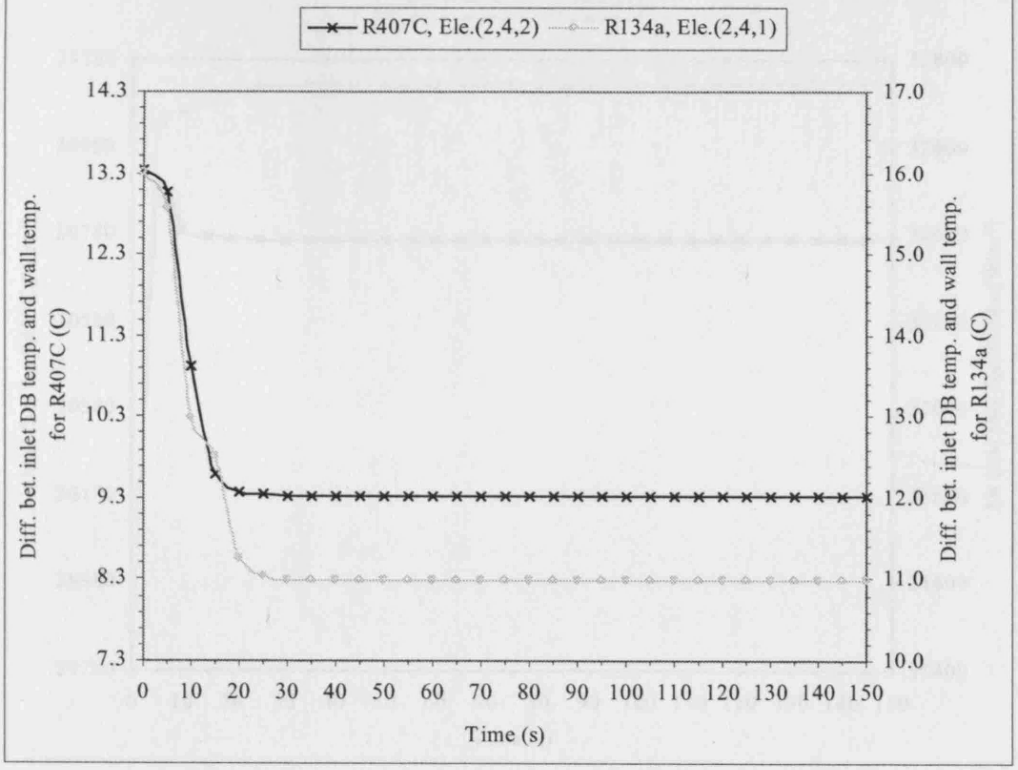

Figure 5.125 Effective HTCs between inlet air and condensate on tube vs times at Elements (2,4,2) and (2,4,1) for R407C and R134a, respectively, for totally-wet coils when there was a 0.8-degree-C step increase in coil-inlet DB temperatures

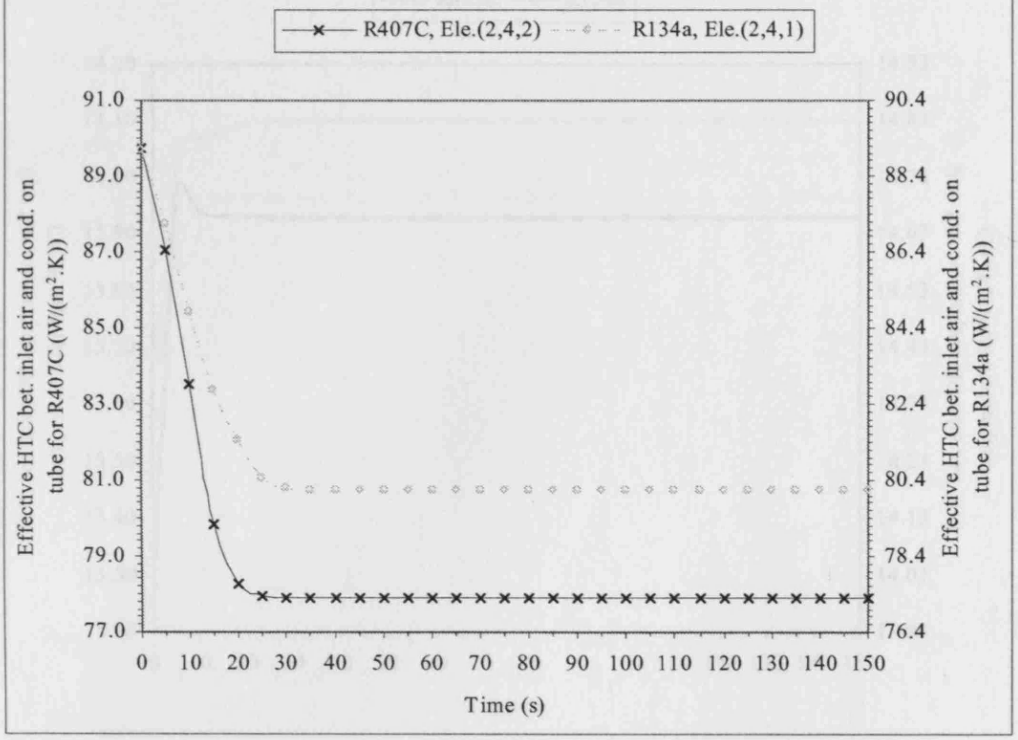

Figure 5.126 Air heat fluxes vs times at Elements (2,2,2) for totally-wet coils when there was a 0.8-degree-C step increase in coil-inlet dry-bulb temperatures

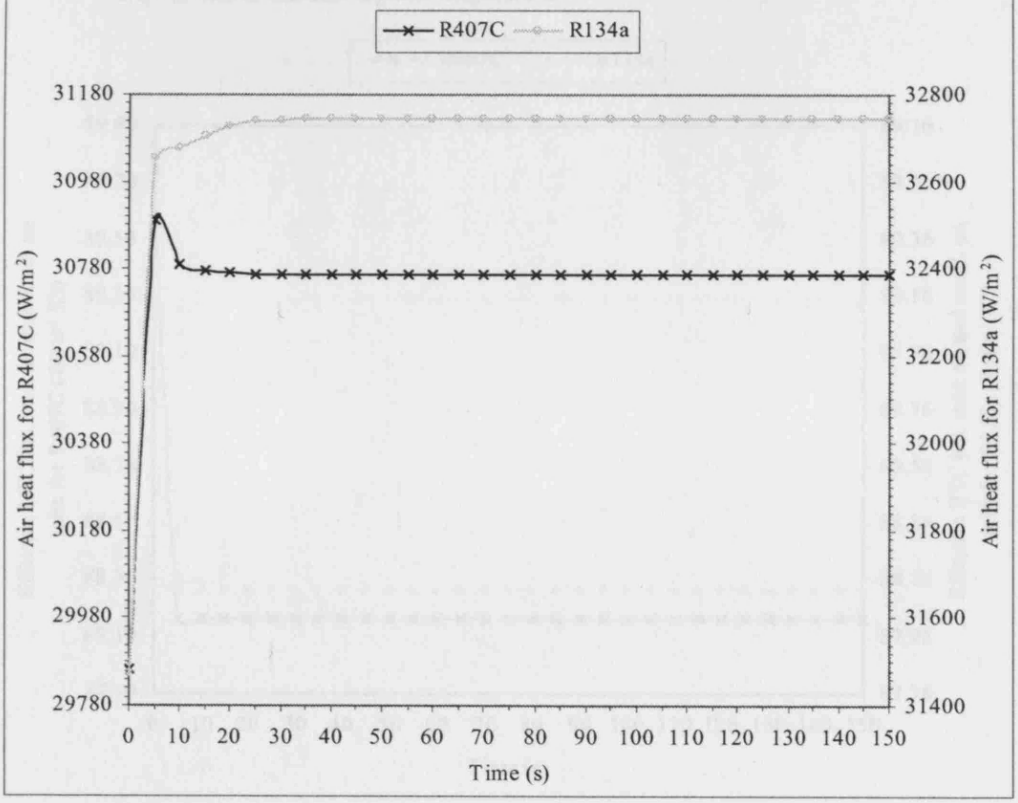

Figure 5.127 Differences between inlet dry-bulb temperature and wall temperature vs times at Elements (2,2,2) for totally-wet coils when there was a 0.8-degree-C step increase in coil-inlet DB temperatures

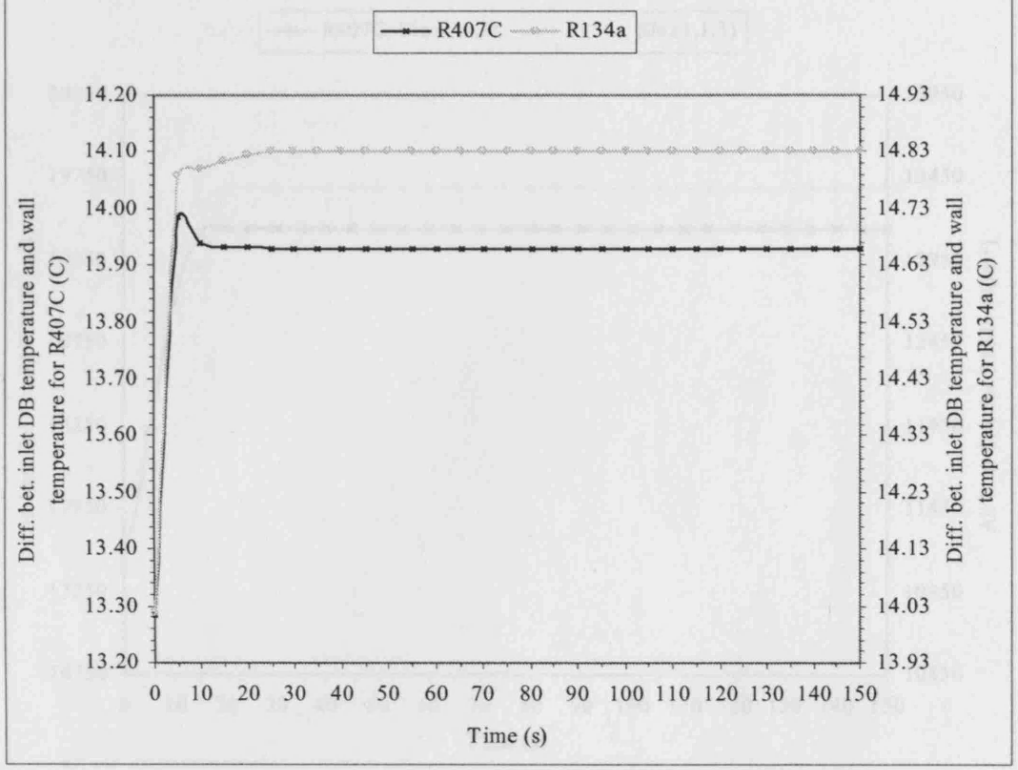

Figure 5.128 Effective heat transfer coefficients between inlet air and condensate on tube vs times at Elements (2,2,2) for totally-wet coils when there was a 0.8-degree-C step increase in coil-inlet dry-bulb temperatures

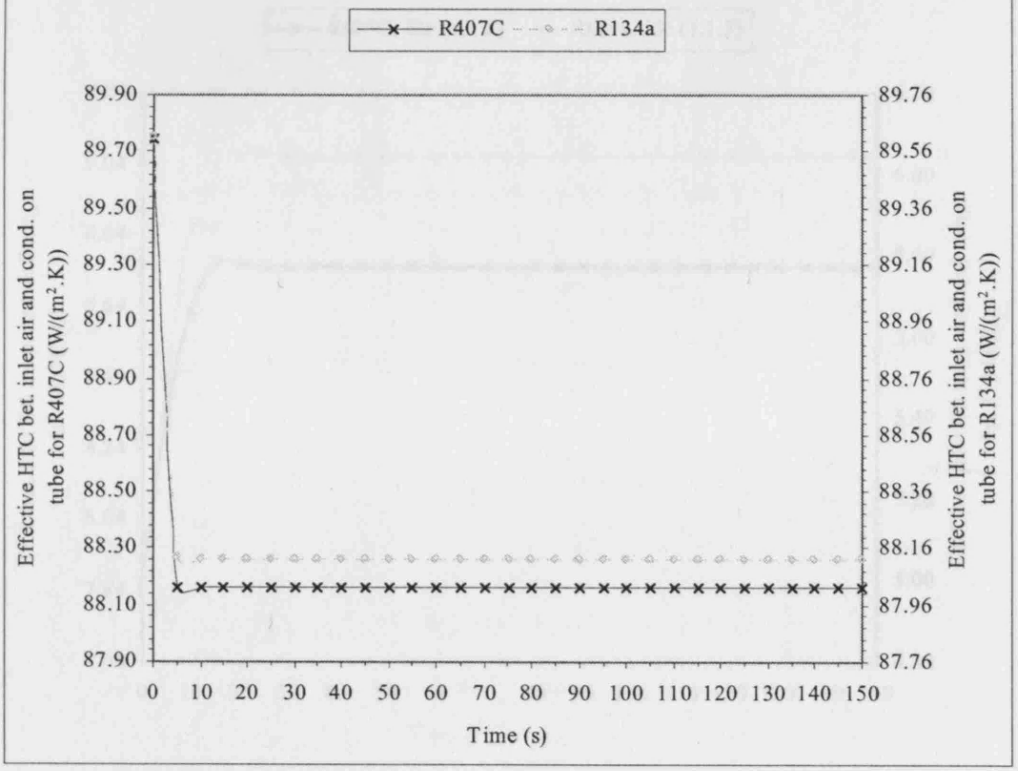

Figure 5.129 Air heat fluxes vs times at Elements (1,1,2) and (1,1,3) for R407C and R134a, respectively, for totally-wet coils when there was a 0.8-degree-C step increase in coil-inlet dry-bulb temperatures

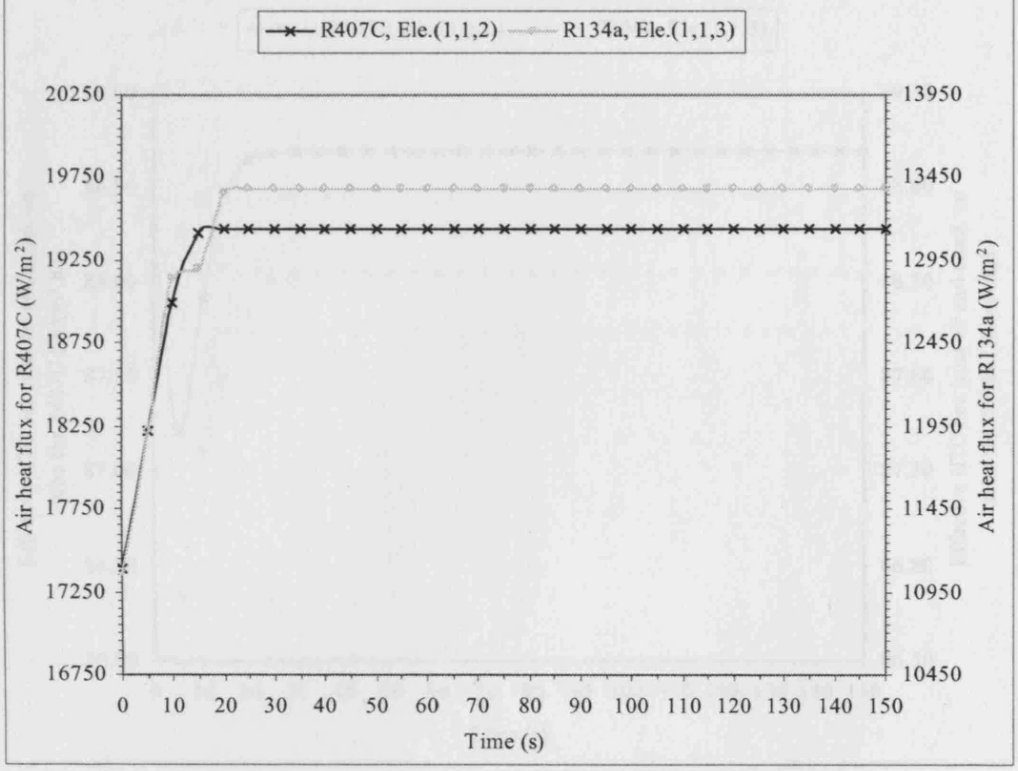

Figure 5.130 Differences between inlet DB temperature and wall temperature vs times at Elements (1,1,2) and (1,1,3) for R407C and R134a, respectively, for totally-wet coils when there was a 0.8-degree-C step increase in coil-inlet DB temperatures

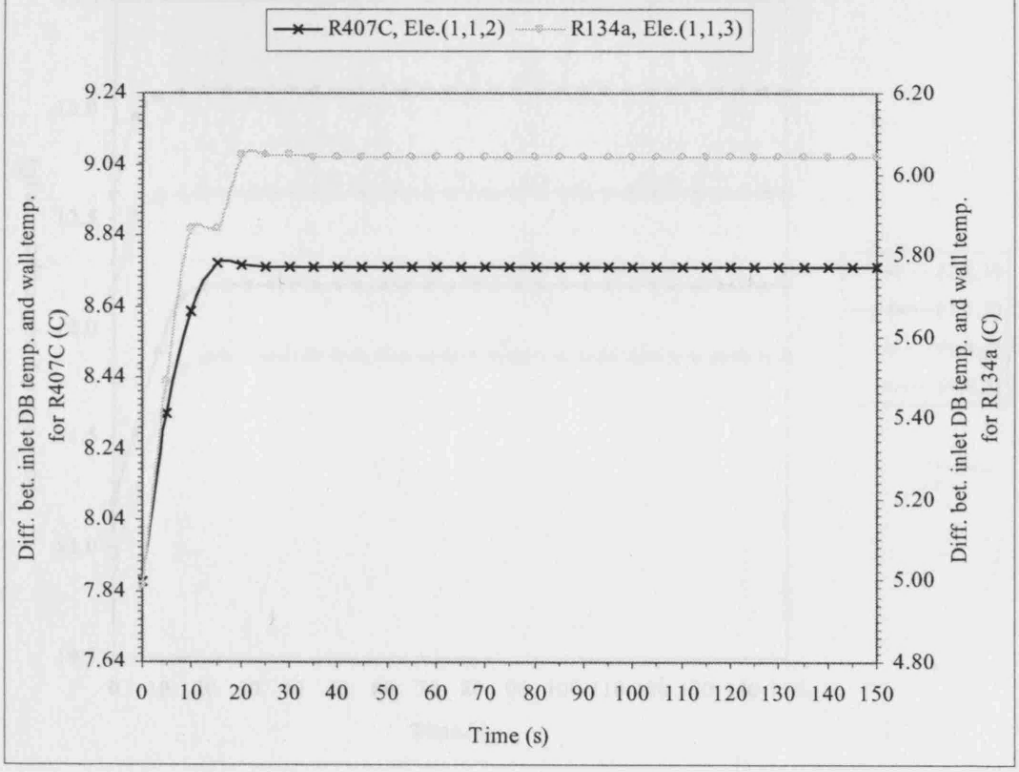

Figure 5.131 Effective HTCs between inlet air and condensate on tubes vs times at Elements (1,1,2) and (1,1,3) for R407C and R134a, respectively, for totally-wet coils when there was a 0.8-degree-C step increase in coil-inlet DB temperatures

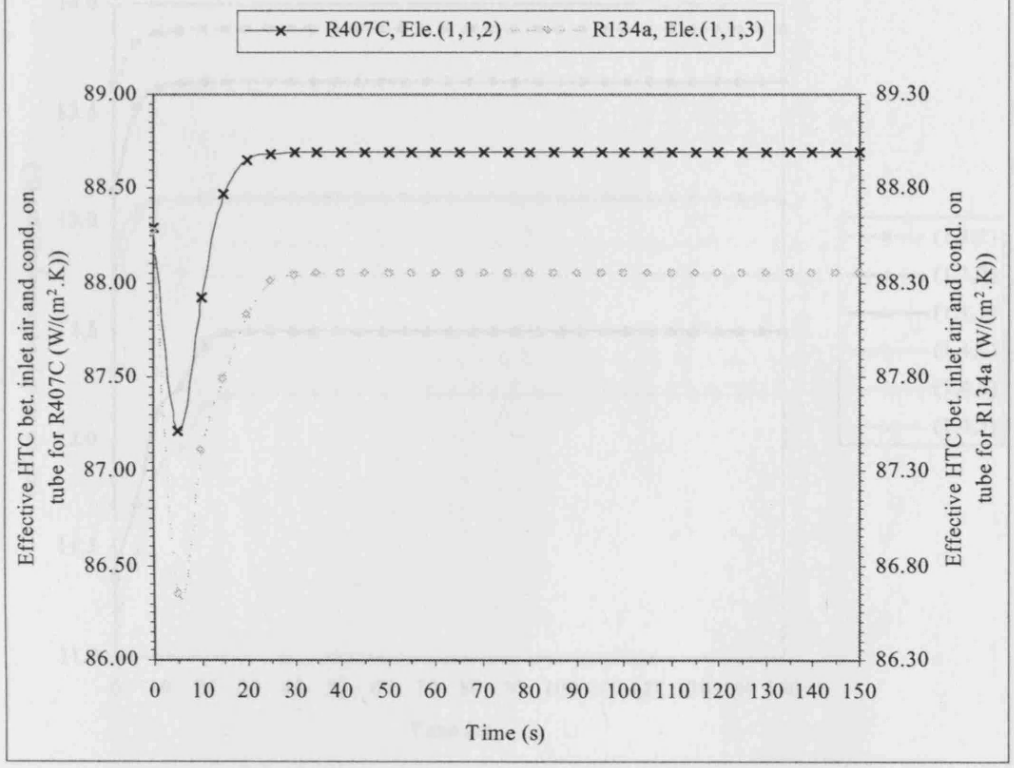

Figure 5.132 Coil-outlet dry-bulb temperatures (from Elements affected by superheat) for R407C vs times for totally-wet coils when there was a 0.8-degree-C step increase in coil-inlet dry-bulb temperatures

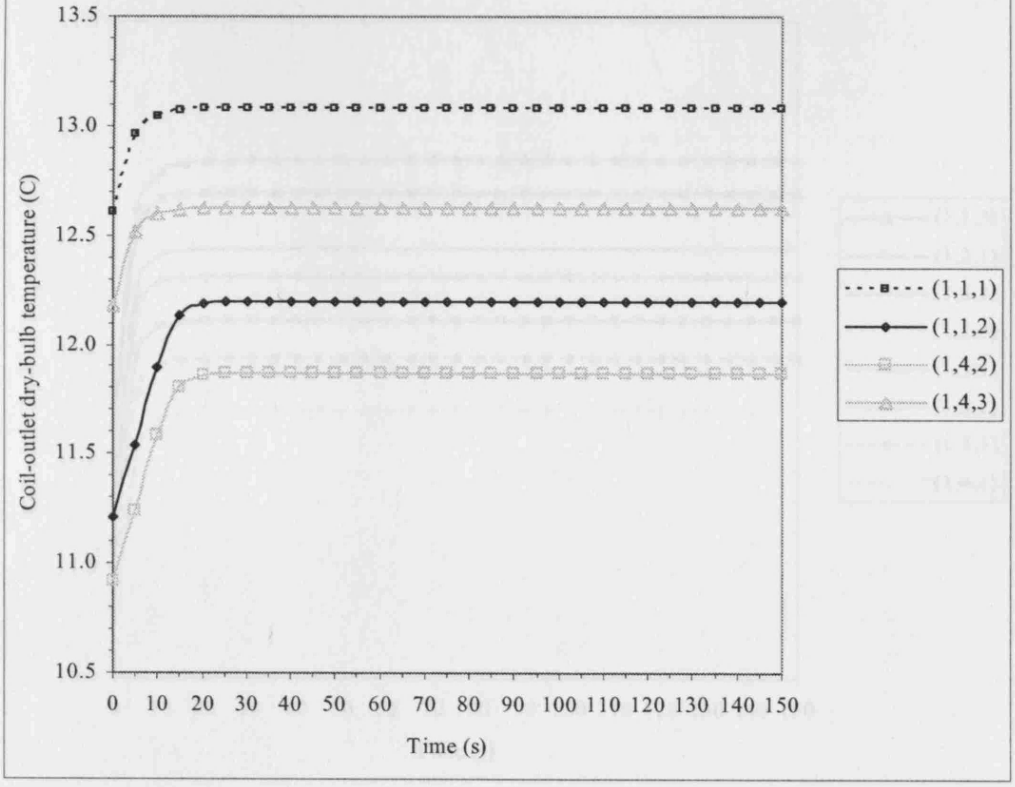

Figure 5.133 Coil-outlet dry-bulb temperatures (from Elements affected by superheat) for R134a vs times for totally-wet coils when there was a 0.8-degree-C step increase in coil-inlet dry-bulb temperatures

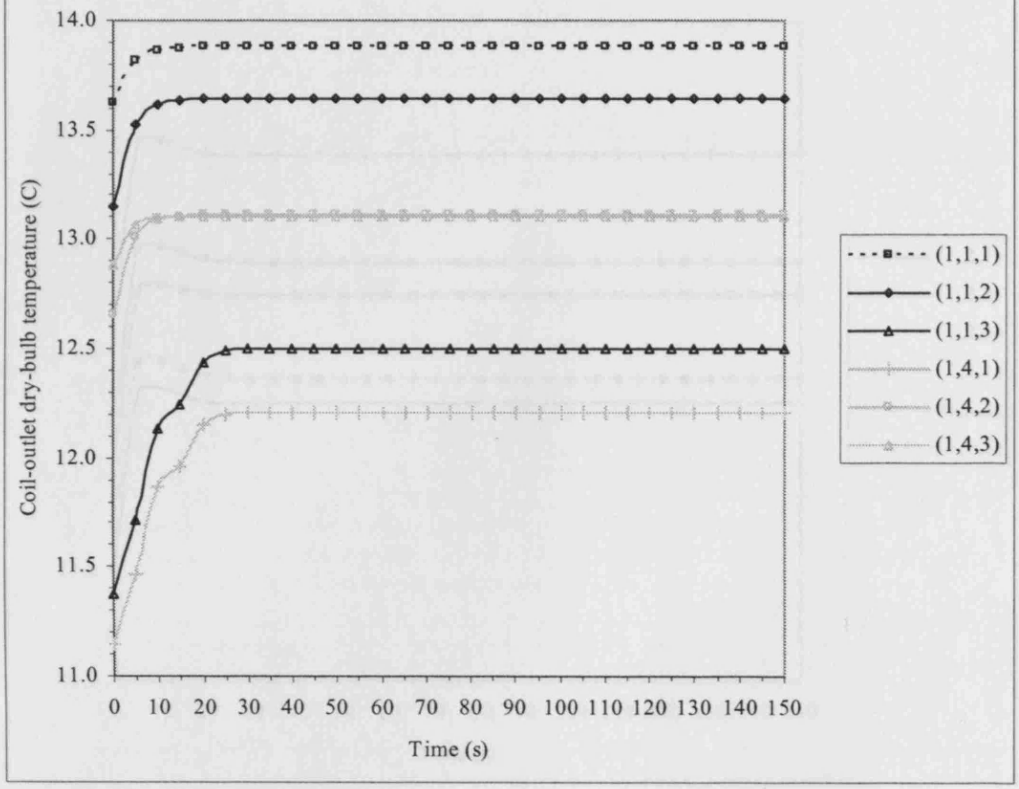

Figure 5.134 Coil-outlet dry-bulb temperatures (from Elements unaffected by superheat) for R407C vs times for totally-wet coils when there was a 0.8-degree-C step increase in coil-inlet dry-bulb temperatures

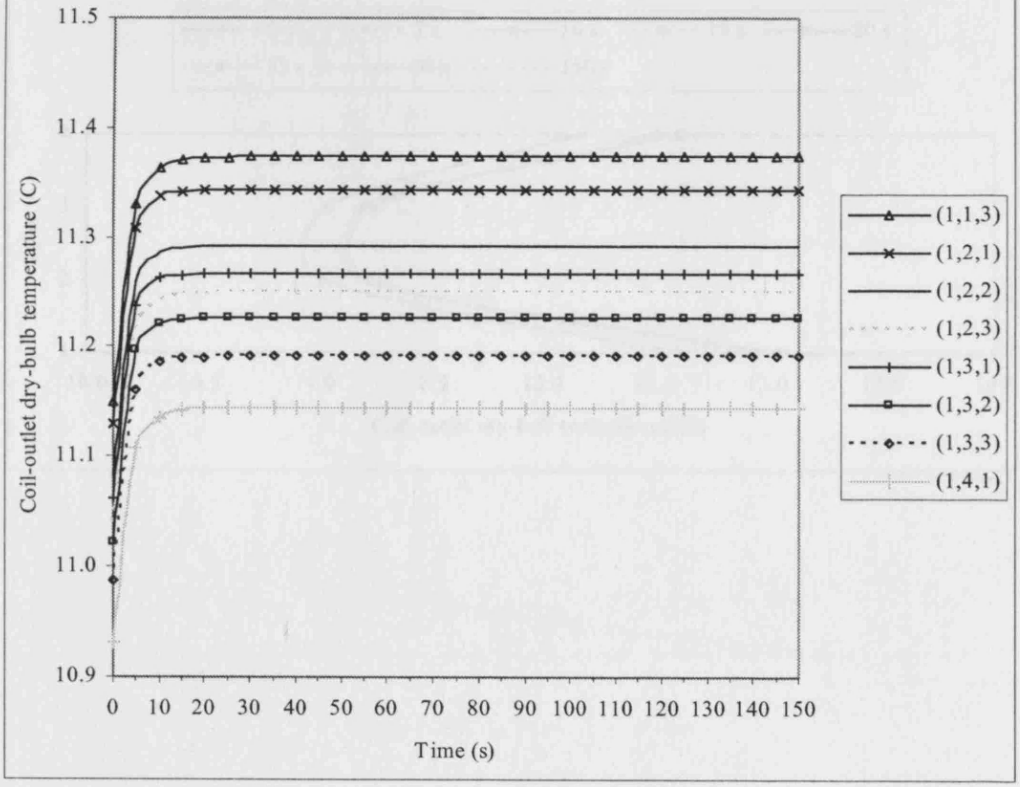

Figure 5.135 Coil-outlet dry-bulb temperatures (from Elements unaffected by superheat) for R134a vs times for totally-wet coils when there was a 0.8-degree-C step increase in coil-inlet dry-bulb temperatures

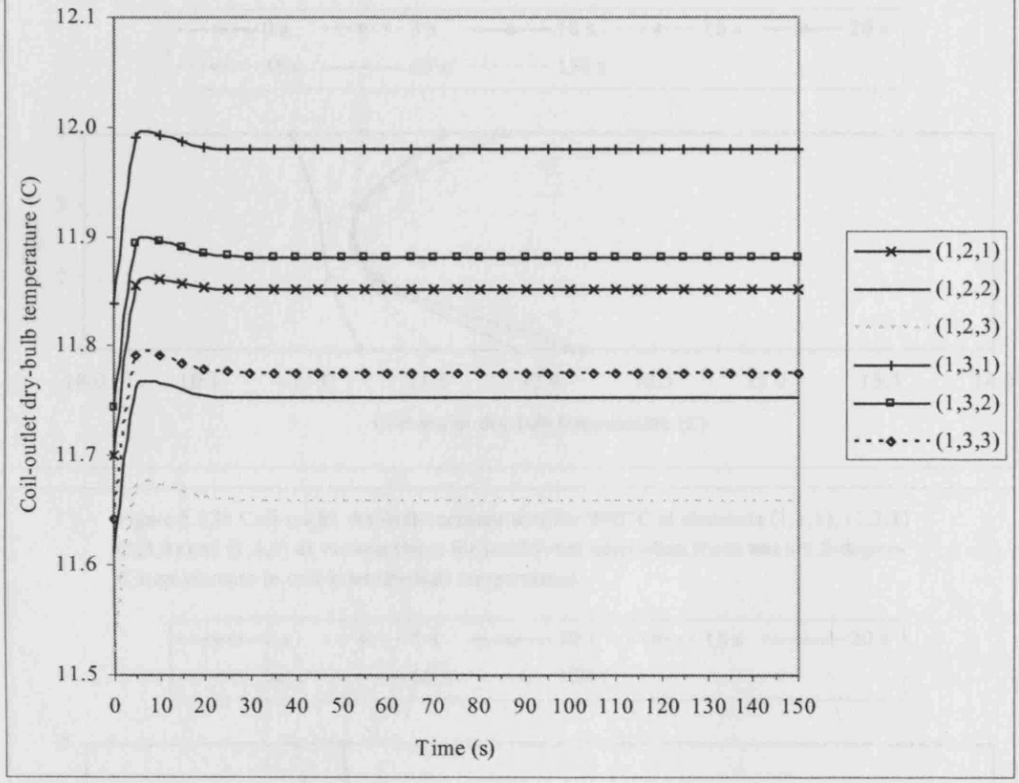

Figure 5.136 Coil-outlet dry-bulb temperatures for R407C at elements (1,1,1), (1,2,3) (1,3,1) and (1,4,3) at various times for totally-wet coils when there was a 0.8-degree-C step increase in coil-inlet dry-bulb temperatures

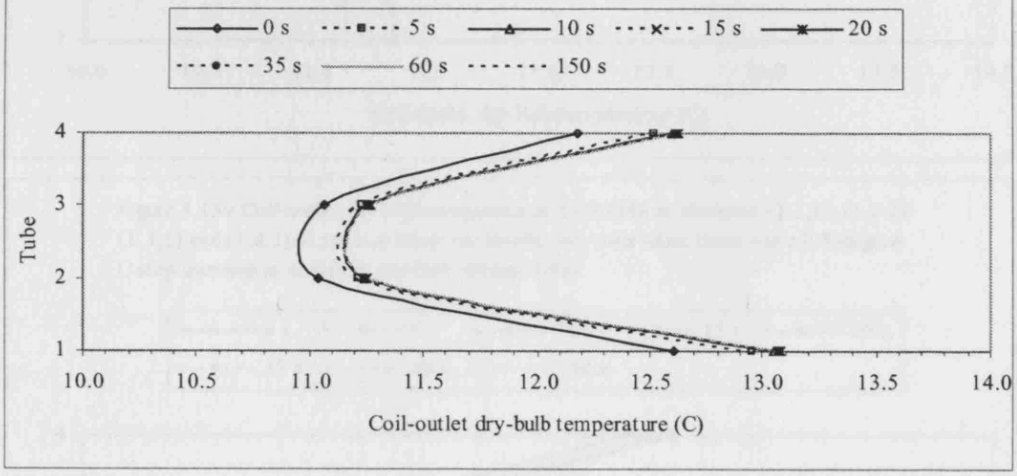

Figure 5.137 Coil-outlet dry-bulb temperatures for R407C at elements (1,1,2), (1,2,2) (1,3,2) and (1,4,2) at various times for totally-wet coils when there was a 0.8-degree-C step increase in coil-inlet dry-bulb temperatures

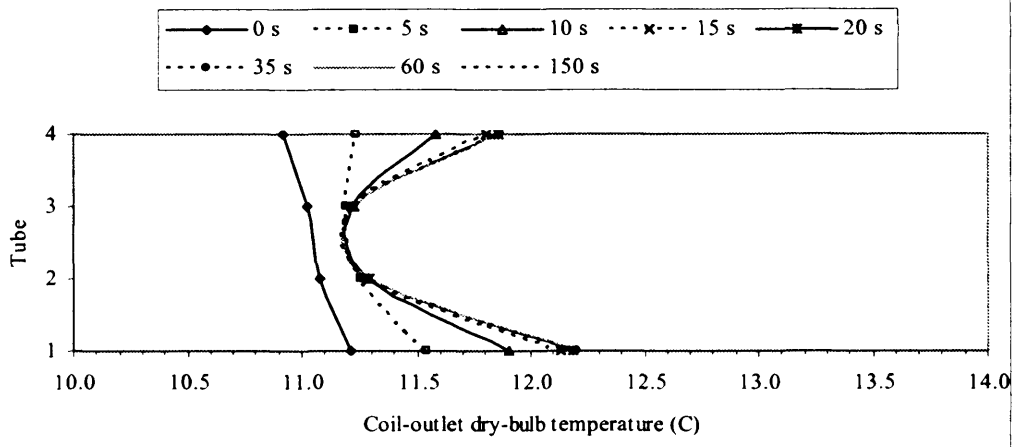

Figure 5.138 Coil-outlet dry-bulb temperatures for R407C at elements (1,1,3), (1,2,1) (1,3,3) and (1,4,1) at various times for totally-wet coils when there was a 0.8-degree-C step increase in coil-inlet dry-bulb temperatures

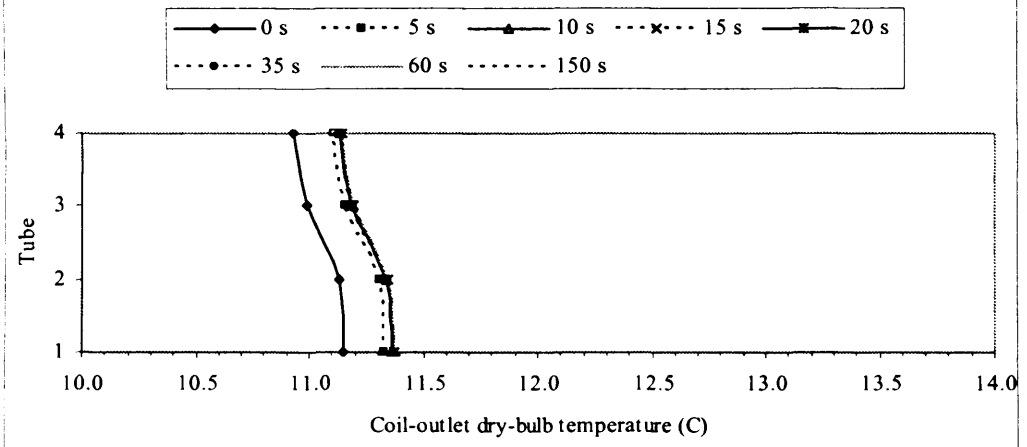

Figure 5.139 Coil-outlet dry-bulb temperatures for R134a at elements (1,1,1), (1,2,3) (1,3,1) and (1,4,3) at various times for totally-wet coils when there was a 0.8-degree-C step increase in coil-inlet dry-bulb temperatures

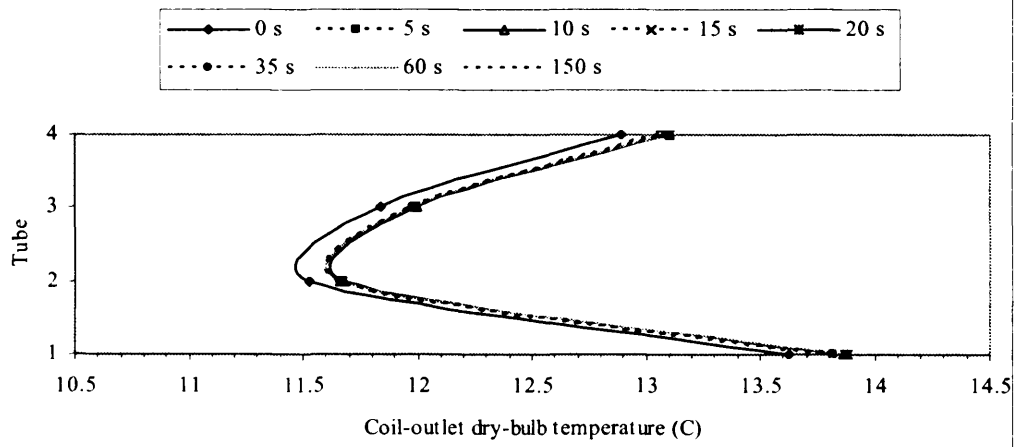

Figure 5.140 Coil-outlet dry-bulb temperatures for R134a at elements (1,1,2), (1,2,2) (1,3,2) and (1,4,2) at various times for totally-wet coils when there was a 0.8-degree-C step increase in coil-inlet dry-bulb temperatures

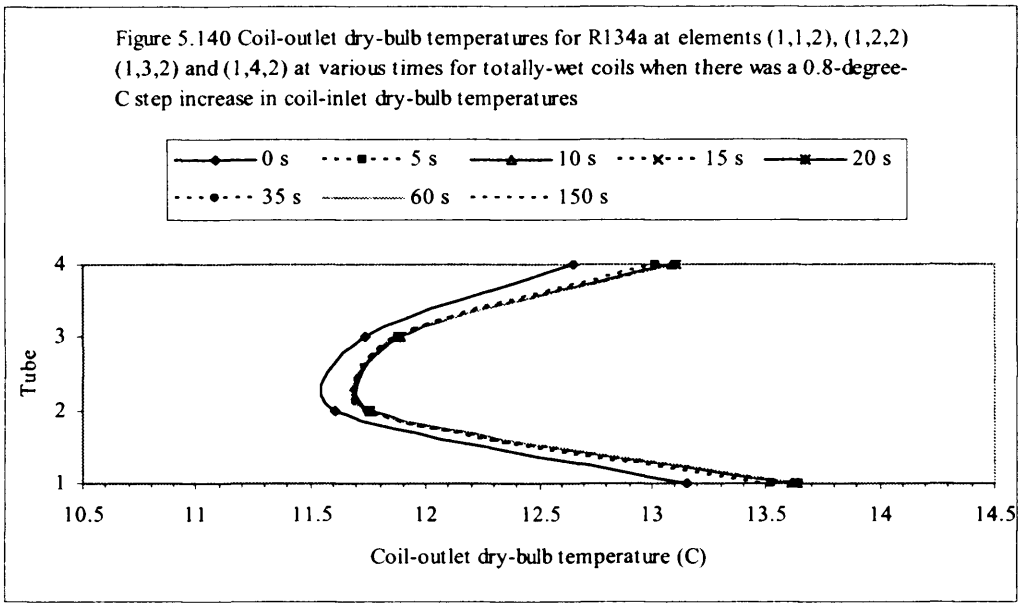

Figure 5.141 Coil-outlet dry-bulb temperatures for R134a at elements (1,1,3), (1,2,1) (1,3,3) and (1,4,1) at various times for totally-wet coils when there was a 0.8-degree-C step increase in coil-inlet dry-bulb temperatures

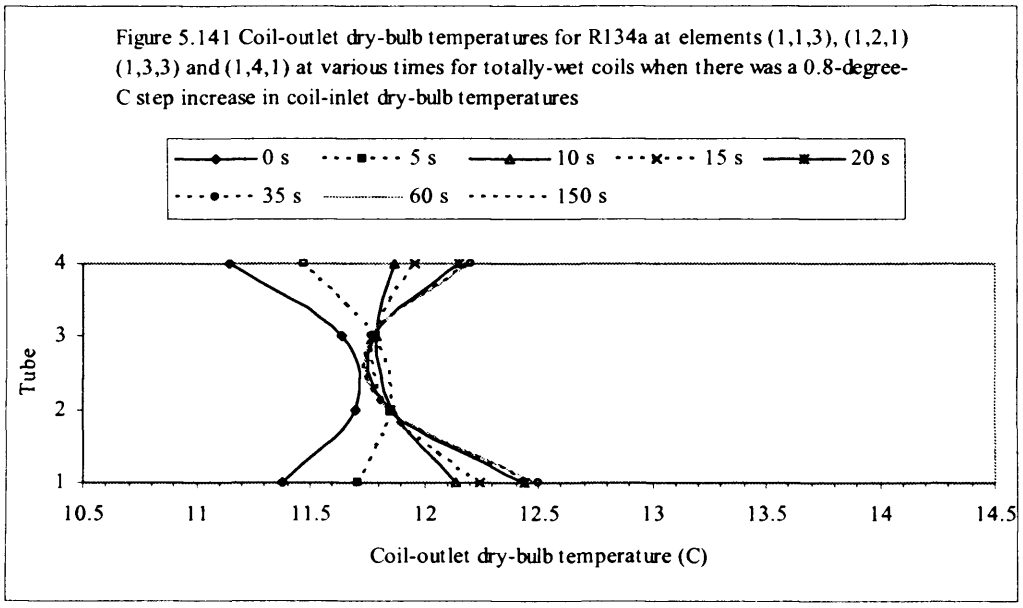

What are the key observations? For **the refrigerant side**, for both refrigerants, the time variations of ***coil-outlet pressures*** and ***local pressure drops*** were similar to that of the dry coils. However, the wet coils had a shorter transit time to reach steady state (because of a smaller number of rows than in the dry coil, thus with reduced superheat effect), with larger the rates of change (because of having larger total pressure drop in a shorter transit time) than for the dry coils.

For ***the local 2-phase refrigerant temperatures***, for either a step increase or decrease of the inlet air temperature, under the wet coil conditions, both refrigerants had about the same the transit times before reaching steady state, but they were shorter *when compared to the dry coils*. For R407C, the wet coils had smaller magnitudes of

change from 0 s to steady-state than the dry coils, whereas, for R134a, the reverse happened. When compared to the dry coils, for R407C, the rate of change for wet coils could be smaller or larger, whereas, for R134a, the wet coils always had much higher values. These were due to: for R407C, the close link between the R407C temperature glide and the refrigerant heat flux, and having 3 degrees of freedom; for R134a, that the temperature drop was only a function of the pressure drop (as discussed in Sub-section 5.3.1). In addition, for ***the refrigerant temperatures along the coil***, the magnitude of change for R407C was smaller than and opposite to that for R134a.

Concerning ***the superheat-initiation locations***, when compared to the dry coils (having a smaller step change), due to larger refrigerant mass flow rates encountered, both refrigerants had smaller movements in the superheat-initiation position from 0s to steady-state.

For ***the degrees of superheat***, based on the adopted refrigerant comparison scheme, for both coil conditions, between steady-states (initial and final), R407C had always shorter superheat regions than R134a. Moreover, R407C had slightly larger specific heat values (of the superheated vapour) than R134a, and hence, the degrees of superheat for R407C were always smaller than that for R134a. For the wet coils, the transit time for R407C was less than that for R134a, whereas, for the dry coils, the reverse happened (to be discussed later).

For ***the coil-outlet refrigerant temperatures***, both refrigerants had very much the same rate of change and the same transit time but with different magnitudes of change. When compared to the dry coils, for both refrigerants, the wet coils experienced larger rates of change of the temperature.

Concerning ***the local 2-phase refrigerant HTCs***, R407C had a shorter transit time and a slower rate of change than R134a. When compared to the dry coils, for both refrigerants, the wet coils had larger rates of change.

For ***the tube-wall temperatures***, a step increase of the coil-inlet DB temperature caused the tube-wall temperature of R407C to increase, whereas, the values for R134a could either increase or decrease. In addition, referring to that discussed in the dry coils, it can also be said that the dynamics of the temperature for the wet coils was a function of the rates of changes of the refrigerant heat flux, refrigerant HTC and refrigerant temperature.

For **the air-side**, for ***the local condensate rates***, for both refrigerants, the discussion concerned with 3 groups of elements: affected directly, affected indirectly

and unaffected by the superheats. The 1st group, which was in the superheat region, had decreases in the condensate rates, whereas, the 2nd group behaved oppositely. For the last group it could be either an increase or a decrease, except that the 2nd row of R134a always increased. Based on the same 3 groups, the 1st group had the rates of changes decreased, whereas, the other two groups behaved oppositely.

The results regarding ***the coil-outlet HRs*** could be divided into 2 groups: affected indirectly and unaffected by the superheats. The 1st group had increasing values with time at varied average gradients. For the 2nd group, both refrigerants had the negative magnitudes of change from 0s to steady-state. In addition, at any time (between 0 s to 150 s), the variation over the coil-outlet for all the tubes involved in this group could be described similarly as that done for the corresponding group regarding the coil-outlet DB temperatures.

For ***the coil-outlet DB temperatures***, also arranged into 2 groups (corresponding to that for ***the coil-outlet HRs***), the description of the 1st group was the same as that for the coil-outlet HRs. For the 2nd group (unaffected by the superheats), for both refrigerants, the magnitudes of change from 0s to steady-state were in the positive direction; this was opposite to that for the coil-outlet HR. Furthermore, for this group, at any time (between 0 s to 150 s), for the horizontal consideration, both refrigerants had similar profiles of the variations of the DB temperature, whereas, for the vertical consideration, each refrigerant behaved differently.

What can be learnt from the results? Three main areas to be addressed concerned with the refrigerant-side, the air-side and the transient process.

For **the refrigerant-side**, 4 main effects were examined: the sensitivity of pressure-drop-profile shifting to the step change of inlet DB temperature, the refrigerant-type, the totally-wet and the superheat-region. For the effect of sensitivity of pressure-drop-profile shifting upon the magnitudes and the rates of changes of the coil-outlet pressure, it behaved the same manner as that for the dry coils. In brief, for either refrigerant, the 2-phase pressure-drop vs. distance along the coil has a positive gradient until reaching a maximum where the gradient becomes zero. After that, the profile has a negative gradient. This steady-state behaviour results in a unique value of pressure at the coil-outlet. Under the transient state, the pressure drop profiles along the coils of both refrigerants move in the same manners, but with the different magnitudes (resulting from the difference in the sensitivity of the profile shifting to the change of the coil-inlet DB temperature).

The refrigerant-type mainly influenced two groups of parameters ((1) the pressure drops, and (2) the local 2-phase temperatures, the coil temperatures and the coil-outlet temperatures (these three parameters: influenced by or involved with the temperature glide), as well as the local 2-phase HTCs. For either a step increase or decrease input, for the pressure drops (the 1st group), under both dry and wet coil conditions, when compared to R134a, R407C had lower sensitivity of the pressure-drop-profile shifting, and smaller rates of change of the coil-outlet pressures. For the local 2-phase temperatures (a 2nd group parameter), for both coil conditions, the magnitudes of change were a function of the refrigerant-type (i.e. the degrees of freedom: temperature, pressure and concentrations). This resulted in that, for the coil temperatures, the ratio of the magnitude of swinging for R407C to that for R134a of the wet coils was smaller than that of the dry coils.

For the ratios of the rate of change of coil-outlet temperatures of R407C to that of R134a, the values for both coil conditions were less than 1, with the value for wet coil about 50% larger than that of the dry coils. In other words, *under either coil condition, R407C had a smaller outlet temperature than R134a.* However, when compared to the dry coil, R407C under the wet coil still had a smaller value though the difference between the two refrigerants reduced. For both coil conditions, the step-increase case had slightly larger ratios than the step decrease case. The dependence of local 2-phase HTCs on refrigerant type could be discussed the same way as done for the dry coils.

The totally-wet effect upon ***the coil-outlet pressures*** and ***the local 2-phase temperatures*** could be noted. For ***the former***, for both coil conditions, for the rates of change, the ratios of R407C to R134a were larger than 1. For the wet coils, the ratio for the case of the step-increase was smaller than that of the step-decrease, whereas, for the dry coils, the behaviour was opposite. *For both refrigerants, when compared to the dry coil, the coil-outlet pressures of the wet coil had much larger magnitudes of change from 0s to steady-state (due to larger refrigerant mass flow rates) with shorter time durations in reaching steady-state (due to using smaller number of row).* For ***the latter***, as discussed in Table 5.17, along the wet coils, the rates of change for R407C varied substantially, when compared to that for R134a. However, for the dry coils, the variations were insignificant.

For the superheat-region effect upon the coil-outlet refrigerant temperatures, as already discussed in the dry coils, for both refrigerants, the magnitudes

of change from 0 s to the final steady-state were controlled by the refrigerant temperature change per element/sub-element in the superheat regions, not the 2-phase regions.

For **the air-side**, there were 6 effects noted:

- the effective-MTC between the inlet air and the condensate on the tube wall,
- the difference between the inlet HR and the saturated HR on the tube-wall surface,
- the effective HTC between the inlet air and the condensate on the tube wall,
- the difference between the inlet DB temperature and the wall temperature,
- the coil-configuration, and
- the refrigerant-temperature-glide.

It should be borne in mind that each of the first four effects was in fact also a function of the refrigerant type.

The first two effects were noticed to influence *the local condensate rates* and *the coil-outlet HRs*. Regarding *the local condensate rates* at the locations (the 1st group) that were affected directly by the superheat, the rates of change for individual refrigerants were found to be almost solely dependent upon the HR's difference effect. However, for the 2nd group (affected indirectly by the superheat), the influence of the MTC was stronger than that for the 1st group. For the 3rd group (unaffected by the superheat), the both effects showed similar degree of influence upon the rate of change. It should be noticed that, for both refrigerants, both the magnitude of change of the MTC and of the HRs difference of the 3rd group were much smaller than that of the 1st group, but the *ratios* of the magnitude of change of the MTC *to* the magnitude of change of the HRs difference were larger for the 3rd group than for the 1st group.

For a given coil-inlet air condition, the rates of change of *the coil-outlet HRs* with time, for both refrigerants, were a function of the rates of change of the condensate rates with time. Therefore, the corresponding discussion was similar to that for the condensate rates.

Consider an analogy between the HTC and the MTC, and the inlet DB/wall temperature difference and the HRs difference. The discussion of the effects of

the HTC and the temperature difference upon the local air heat fluxes (the 1st, 2nd and 3rd groups) and the coil-outlet DB temperatures (the 1st and 2nd groups) would be similar to that of the MTC and HRs difference upon the local condensate rates (the 3rd, 2nd and 1st groups) and the coil-outlet HRs (the 2nd and 1st groups), respectively.

For the effect of the coil-configuration upon the DB temperatures and the HRs at the coil-outlet, for the 2nd group (unaffected by the superheat), the one-row evaporator was compared to the two-row evaporator. For along the tube, at any time, for R407C, the variation behaved oppositely (e.g. for along the 2nd tube, from the Elements (1,2,3), (1,2,2) to (1,2,1), the DB temperatures of the one-row coil being from high to low, instead of from low to hig in a two-row coil), whereas, for R134a, the direction of variation remained the same (e.g. for along the 2nd tube, the DB temperatures being from low to high in both one- and two- row coils). For the vertical, at any time, for R407C, the one-row evaporator behaved oppositely to the two-row evaporator. However, R134a behaved in a reversed manner.

For the refrigerant-temperature-glide effect upon *the DB temperatures and the HRs at the coil-outlet*, for the 2nd group (unaffected by the superheat), for both refrigerants, let's consider that the coils that experienced *a smaller step input (i.e. resulting in smaller refrigerant temperature gliding-up (R407C) and drop (R134a))*. For *the horizontal consideration*, at any time (between 0 s to 150 s), R407C was expected to have larger gradients of the DB temperature and outlet HRs, whereas, R134a should have much smaller gradients. For *the vertical consideration*, for both refrigerants, at any time, the behaviour could be described similarly as done for the horizontal consideration.

For **the transient process**, the two issues of particular interest were the underlying principles and the associated "validation" (i.e. "matching" the results with the relevant principles). For *the former*, for the totally-wet coils, each of the 2 main condensate-related parameters (the MTC and the HRs difference), as mentioned previously, was observed to be a function of *the refrigerant-type*. As discussed, Fig. 5.64 (for the dry coils), the transient process was based on the changes of 4 important parameters (the wall temperature, the 2-phase temperature and the 2-phase HTC of the refrigerant, and the superheat-initiation location), all of them linked directly to *the refrigerant-type*. In this respect, for both refrigerants, the dynamics of the totally-wet coils was considered quite similar to that of the dry coils. In other words, the associated

principles established for the dynamics of the dry coils in the Sub-section 5.3.2 is also applicable to that of the totally-wet coils.

The validation for the mechanism of the transient process (Fig. 5.64) was performed for both the step-increase and the step-decrease of the coil-inlet DB temperature for both coil conditions. The procedures were concerned respectively: *coil refrigerant temperature profiles*, *coil refrigerant heat energy* (calculated by the time integration of the product of the heat load (W) and time (s)), *rates of change of the refrigerant HTC* and *superheat initiation locations*. When there was *a step increase*, the coil refrigerant temperature profile of R407C swung counter-clockwise, whereas, R134a behaved oppositely with about the same magnitudes of change. For the coil refrigerant heat energy, let's consider firstly the dynamics of the different-from-0s coil refrigerant heat load (i.e. subtracting the present coil heat load with the 0s value) as shown in Fig. 5.142; R407C (2.290 kJ) had a smaller value (i.e. an area under curve) than that of R134a (2.482 kJ). Certainly, the two observations supported each other.

For the rates of change (positive) of the refrigerant HTC with time, R407C had a smaller value than R134a (Fig. 5.98). Therefore, one would anticipate that, *either* the transit time durations of the coil refrigerant-heat-load were the same for both refrigerants *or* that R407C had a smaller value than R134a. When examining the dynamic behaviour of the superheat-initiation locations (Fig. 5.143), R407C (15 s) reached steady-state earlier than R134a (20 s). This was supported by the fact that (Fig. 5.142) that R407C (25 s) had a smaller transit time of the coil refrigerant-heat-loads than that of R134a (30 s).

For *the step-decrease* case, for both refrigerants, the refrigerant temperature profiles swung oppositely to the step-increase case with about the same magnitude of change. However, from Fig. 5.144, R407C (2.105 kJ) had a slightly larger the different-from-0s coil refrigerant heat energy (i.e. magnitude of change of coil heat-energy) than R134a (2.100 kJ). Also based on the dynamics of the refrigerant HTCs (R407C had a smaller value of the negative rates of change than R134a (Fig. 5.99), it could be said that the transit time of the coil refrigerant-heat-load for R407C was *either* the same as *or* smaller than that for R134a. However, the superheat-initiation location of both refrigerants reached steady-state at the same time (15 s, Fig. 5.145). Therefore, the transit times of the coil refrigerant-heat-loads were about the same (25 s, Fig. 5.144) as illustrated in Fig. 5.64.

Figure 5.142 For coil refrigerant heat loads, plotting difference values between at considered time and at 0 s vs times for totally-wet coils when there was a 0.8-degree-C step increase in coil-inlet dry-bulb temperatures

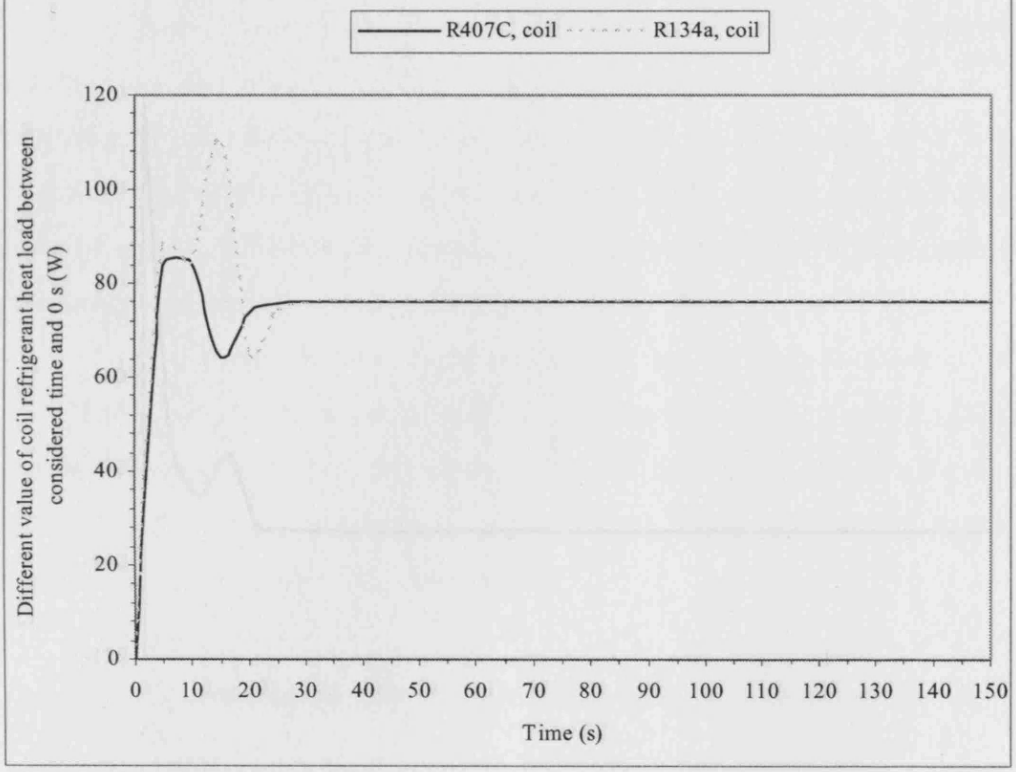

Figure 5.143 Superheat-initiation locations vs times for totally-wet coils when there was a 0.8-degree-C step increase in coil-inlet dry-bulb temperatures

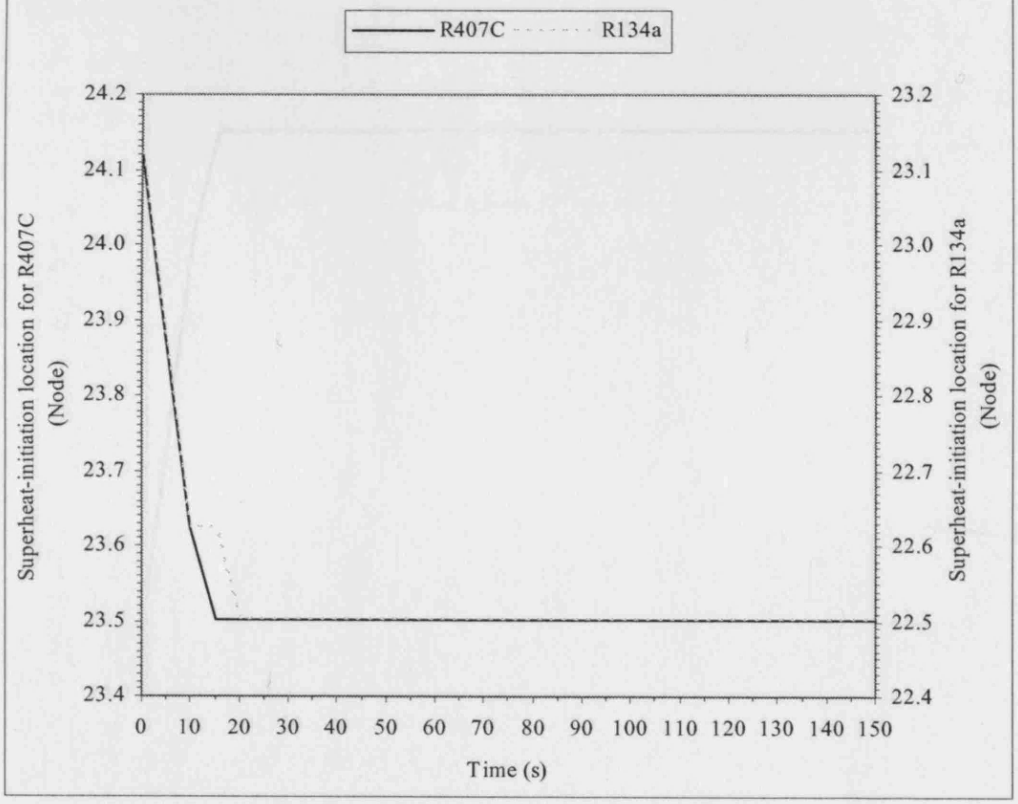

Figure 5.144 For coil refrigerant heat loads, plotting difference values between at considered time and at 0 s vs times for totally-wet coils when there was a 0.8-degree-C step decrease in coil-inlet dry-bulb temperatures

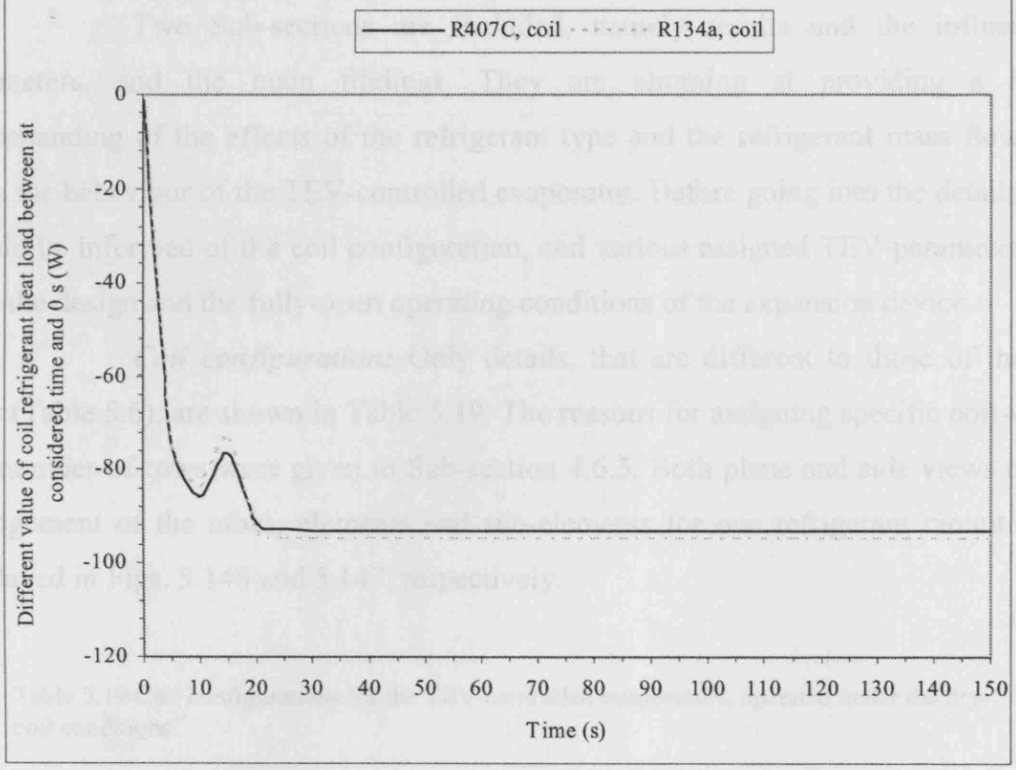

Figure 5.145 Superheat-initiation locations vs times for totally-wet coils when there was a 0.8-degree-C step decrease in coil-inlet dry-bulb temperatures

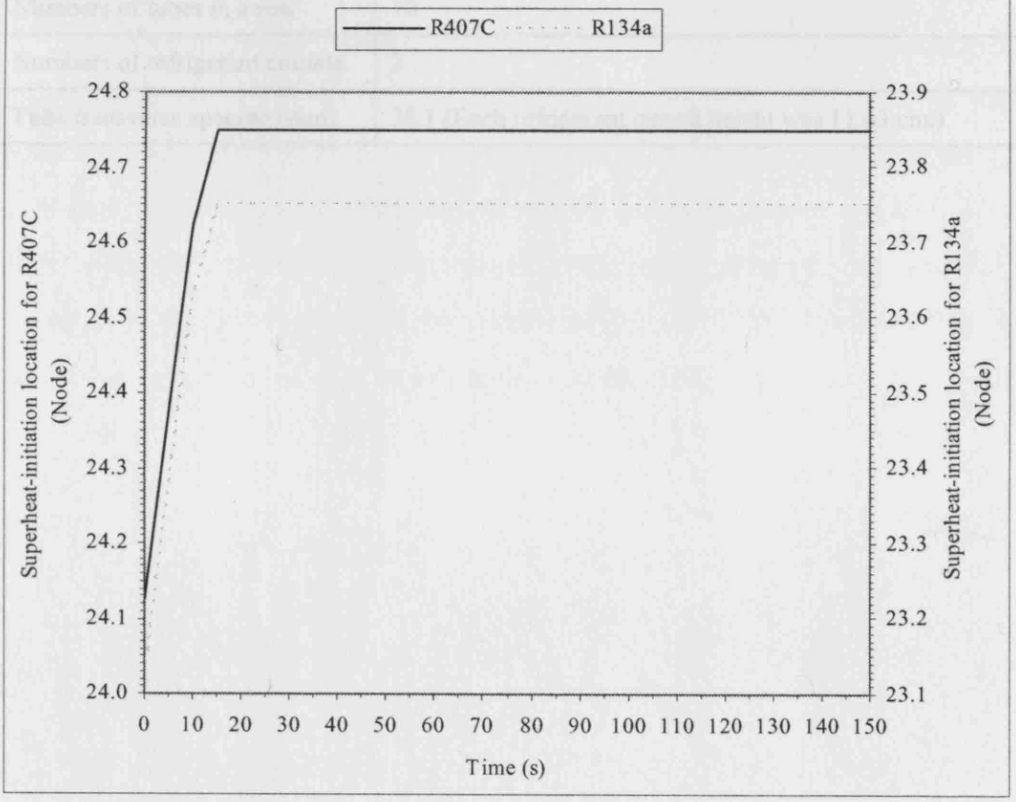

5.5 Results and discussion of a 1-row TEV-controlled evaporator

Two Sub-sections are included, namely results and the influencing parameters, and the main findings. They are aimming at providing a better understanding of the effects of the refrigerant type and the refrigerant mass flow rate upon the behaviour of the TEV-controlled evaporator. Before going into the details, one should be informed of the coil configuration, and various assigned TEV-parameters for both the design and the fully-open operating conditions of the expansion device.

Coil configuration: Only details, that are different to those of the dry coils (Table 5.6), are shown in Table 5.19. The reasons for assigning specific coil-width and number-of-rows were given in Sub-section 4.6.3. Both plane and side views of the arrangement of the tubes, elements and sub-elements for one refrigerant circuit were displayed in Figs. 5.146 and 5.147, respectively.

Table 5.19 Coil configurations for the TEV-controlled evaporators, operated under the dry-coil conditions

Coil width (cm)	170.7
Numbers of rows	1
Numbers of tubes in a row	10
Numbers of refrigerant circuits	2
Tube transverse spacing (mm)	38.1 (Each refrigerant circuit height was 11.43 cm.)

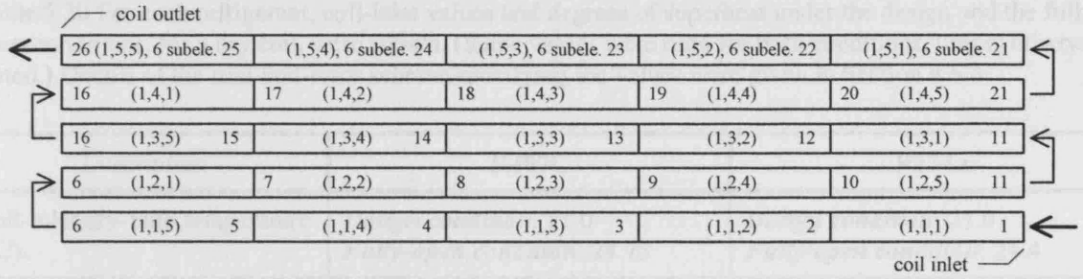

Figure 5.146 Arrangement of Elements and Sub-elements for the refrigerant circuit of the one-row evaporator had the numbers in the bracket represent the row, the tube and the element, correspondingly.

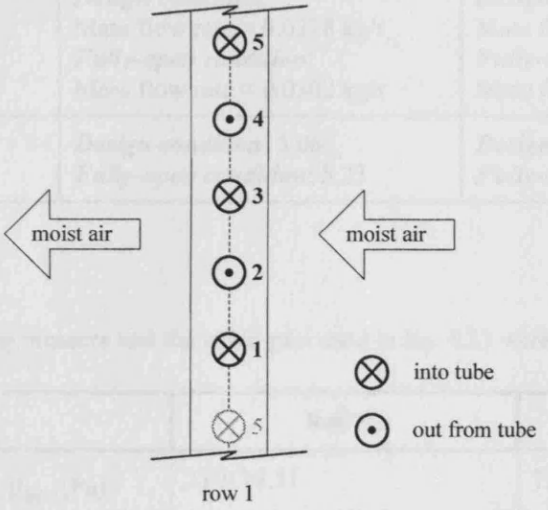

Figure 5.147 Tube arrangement viewing from the side of refrigerant coil-inlet

Inputs for the design and the fully-open operating conditions: Regard the refrigerant-circuit, the input values for the two refrigerants, resulted from the trial-and-error scheme (Sub-section 4.6.3), were shown in Table 5.20. For each refrigerant, as the investigation only concerned with the TEV-controlled evaporator, the refrigerant coil-inlet conditions as well as the valve gain remained unchanged, but the refrigerant mass flow rate remained as a variable regulated by the TEV. The superheat-setting pressure (p_{ss}) and the valve gain were shown in Table 5.21.

Table 5.20 For each refrigerant, coil-inlet values and degrees of superheat under the design and the fully open conditions, for a dry coil, were shown. (Same values were used for both conditions, unless otherwise stated.) Details of the trial-and-error scheme specifying the values were given in Section 4.6.3.

Description	**R407C**	**R134a**
Coil-inlet dry-bulb temperature (°C)	***Design condition***: 21.0 ***Fully-open condition***: 24.75	***Design condition***: 21.0 ***Fully-open condition***: 24.4
Inlet air mass flux for the coil ($kg/(s.m^2)$)	2.21	2.21
Refrigerant-inlet conditions	2.0 °C and 583488 Pa ***Design condition***: Mass flow rate = 0.0228 kg/s ***Fully-open condition***: Mass flow rate = 0.0302 kg/s	5.95 °C and vapour quality = 0.2 ***Design condition***: Mass flow rate = 0.0228 kg/s ***Fully-open condition***: Mass flow rate = 0.03065 kg/s
Degrees of superheat (°C)	***Design condition***: 5.06 ***Fully-open condition***: 5.23	***Design condition***: 6.20 ***Fully-open condition***: 6.39

Table 5.21 Superheat-setting pressure and the valve gain used in Eq. 4.33 were shown.

Description	**R407C**	**R134a**
Superheat-setting pressure, p_{ss}, (Pa)	210118.51	73675.90
Valve gain, K_v, (m·s)	1.04393573E-7	1.79980332E-7

5.5.1 Results and the influencing parameters

The study was to investigate the effect of the TEV-controlled refrigerant mass flow rate upon TG, HTC, pressure drop etc. under transient conditions. **Hence**, there were simulations of both without- and with- TEV cases, operated initially at the design condition followed by a 0.5 °C step change in the coil-inlet DB temperature (seeing also Sub-section 4.6.3). For the without- TEV case, for either refrigerant, the refrigerant mass flow rate was kept unchanged, whereas, for the other case, the flow rate was modulated by the TEV.

The simulated results for either case (Table 5.23) were shown for *two coil locations* (each involving two TEV input parameters - sensible bulb pressure and the external equaliser pressure) and 3 additional parameters (2 of which associated with the refrigerant and one related to the TEV output), detailed in Table 5.22, in which the terms "virtual" and "equivalent" would be explained later.

Table 5.22 The 2 coil locations and the 3 additional parameters that were involved in the TEV study, referring to Table 5.23 for the explanation for the terms "virtual" and "equivalent"

<table>
<tr><td colspan="4">The 1st location, i.e. at the outlet of the Sub-element just before the last Sub-element of 2-phase region.</td></tr>
<tr><td colspan="2">For the without-TEV coil, it was an assumed a virtual sensor-bulb and a virtual external-equalizer were installed.</td><td colspan="2">For the TEV-controlled coil, it was assumed a virtual sensor-bulb and a virtual external-equalizer were installed.</td></tr>
<tr><td>Equivalent External-Equalizer Pressure (EEEP) at the virtual external equalizer</td><td>Equivalent Sensor-Bulb Pressure (ESBP) at the virtual sensor bulb</td><td>EEEP at the virtual external equalizer</td><td>ESBP at the virtual sensor bulb</td></tr>
<tr><td colspan="4">The 2rd location, i.e. at the coil outlet.</td></tr>
<tr><td colspan="2">For the without-TEV coil, it was an assumed a virtual sensor-bulb and a virtual external-equalizer were installed.</td><td colspan="2">For the TEV-controlled coil</td></tr>
<tr><td>EEEP at the virtual external equalizer</td><td>ESBP at the virtual sensor bulb</td><td>External-Equalizer Pressure (EEP)</td><td>Sensor-Bulb Pressure (SBP)</td></tr>
<tr><td colspan="4">The 3 additional parameters, i.e. superheat-initiation location, degrees of superheat, and refrigerant mass flow rate at the TEV outlet.</td></tr>
</table>

Further details explaining the above are as follow. **First**, for the 2 observed locations, *the 1st one* was at the outlet of the Sub-element just before the last Sub-element of the *2-phase* region. It must be noted, though location-wise this is in fact the inlet of the last Sub-element of the two-phase region, it was not labelled as such because the authour wants to center his discussion on a sub-element which was enitrely within the two phase region. By referrring to the last sub-element, confusion may arise as its outlet was in fact in the superheat region. It must also be pointed out that for each case (i.e. with- or without- TEV) this was a unmoving location in the 2-phase region, and was unique for each individual refrigerant, Fig. 5.148. *The 2nd location* was at the refrigerant coil-outlet (i.e. the superheat measurement location, also known as the TEV sensor bulb location). There are 2 main reasons for selecting these two separate locations: (1) the 2-phase and the superheat regions are *generally* different in the magnitudes of the refrigerant HTC, the heat flux and the temperature sensitivity to heat flux. (2) The 2-phase mixture and pure refrigerants exhibit different behaviour in terms of temperature glide, whereas the two superheated refrigerants showed similar behaviour in terms of temperature changes.

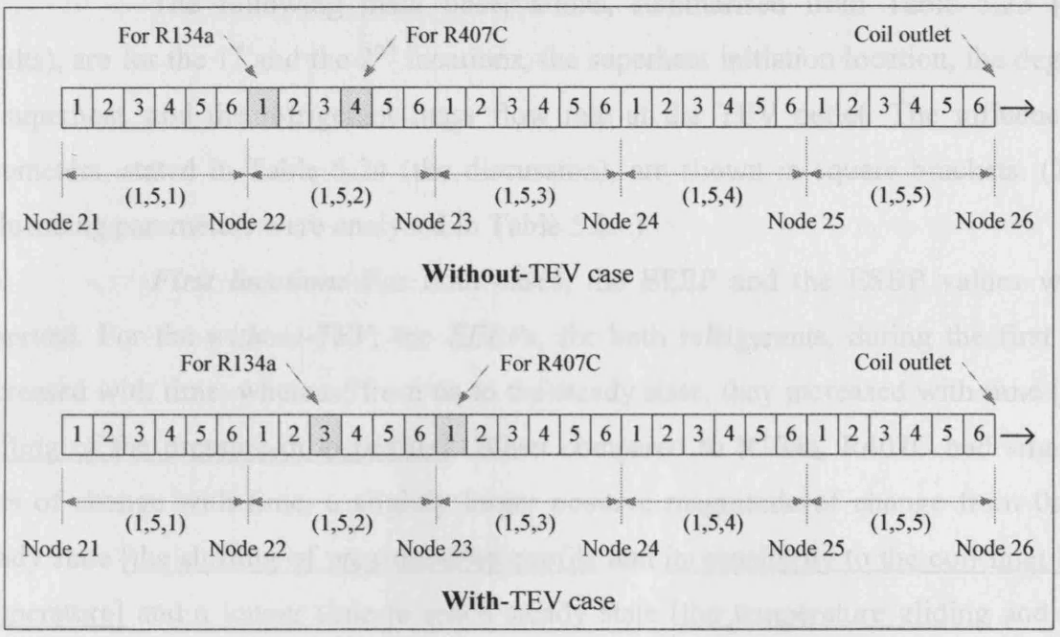

Figure 5.148 At the time 0s, for each case (without- and with- TEV), for each refrigerant, the Sub-element (just before the last Sub-element of the *2-phase* region, i.e. being in the 2-phase region) that its outlet is the 1st observed location in the coil was indicated.

Second, the control with a TEV is generally of feedback looping nature, i.e. the regulation of mass flow rate is a function of two TEV inputs (seeing also the Sub-section 4.4.3): the Sensor-Bulb Pressure (SBP) and the External Equalizer Pressure (EEP). *To understand the effect of the TEV-regulated mass flow rate*, one needs to look at each of the two pressures at each observed location. Therefore, for *the two 1st locations (one for the without-TEV case and one for the with-TEV case)* and *the 2nd location of the without-TEV case*, each was installed with a **virtual** sensor bulb (giving an **Equivalent** Sensor-Bulb Pressure, ESBP) and a **virtual** external equalizer (giving an **Equivalent** External Equalizer Pressure, EEEP). *The 2nd location of the with-TEV case*, which was physically fixed with both the sensor-bulb and the external equalizer, gives SBP and EEP, respectively.

Third, since *the transient variations of the degrees of superheat* has a direct link with *the superheat initiation location*, and for the with-TEV case, the degree of superheat is approximately constant and controlled by *the refrigerant mass flow rate*, the 3 related parameters: the superheat initiation location, the degree of superheat and the refrigerant mass flow rate were investigated. **Fourth**, for the with-TEV case, when the refrigerant mass flow rate experiences certain patterns of variation of the time rate of change, such as from small to large to small again, then ***an inflection point*** was defined when the largest rate of change took place, further explanations to follow.

The following main observations, summarised from Table 5.23 (the results), are for the 1st and the 2nd locations, the superheat initiation location, the degree of superheat, and the refrigerant mass flow rate at the TEV outlet. The influencing parameters, stated in Table 5.24 (the discussion), are shown in square brackets. (The influencing parameters were analysed in Table 5.25.)

First location: For both cases, the EEEP and the ESBP values were observed. For the *without-TEV*, the *EEEPs*, for both refrigerants, during the first 6s, decreased with time, whereas, from 6s to the steady state, they increased with time [the shifting of the pressure-drop profile]. When compared to R134a, R407C had smaller rates of change with time, a slightly larger positive magnitude of change from 0s to steady state [the shifting of pressure-drop-profile and its sensitivity to the coil-inlet DB temperature] and a longer time to reach steady state [the temperature gliding and the HTC].

With a TEV, the *EEEPs* from 0s to around 20s, for both refrigerants, decreased with time, and after that, R407C had some slight oscillations, whilst R134a increased slightly to reach steady state [the refrigerant mass flow rate]. When compared to R134a, R407C had a smaller negative magnitude of change from 0s to steady state.

Without a TEV, the *ESBP* is a function of the tube-wall temperature, and the influencing parameters are the temperature glide and the ratio of the refrigerant heat flux to the HTC. When compared to R134a, R407C had larger positive rates of change and a larger positive magnitude of change from 0s to steady state [the refrigerant temperature glide, the sensitivity of ESBP to Equivalent Sensor-Bulb Temperature (ESBT), and the observation location], and it took a longer time to reach steady state [the temperature gliding and HTC].

Regarding the values of the *ESBP with-TEV* [the refrigerant mass flow rate via its inflection points], for the rates of change between 0s and 7s, R407C had larger positive values than R134a. From 7s to around 21s, R407C had larger negative values than R134a. After that, the description is the same as that for the *EEEP with-TEV*. For the magnitudes of change between steady states, it can be described similarly to that of the *EEEP* in the *with-TEV case*.

Second location: For the *without-TEV case*, the investigated parameters were the *EEEP* and the *ESBP*, whereas, for the *with-TEV case*, they were the *EEP* and the *SBP*. For the *former case*, the description was not too similar to that of the 1st location. The 2 main differences [the sensitivity of the shifting of the pressure-drop

profile to the coil-inlet DB temperature] were: a) from 6s to steady state, both refrigerants had about the same rates of change with time, and b) R407C had two times larger the positive magnitude of change from 0s to steady state than R134a. Different to the dry-coil run in Sub-section 5.2.2 a), the coil-outlet pressure of R134a had the same direction (±) of the steady-to-steady change as that of R407C, reflecting that the pressure is affected by the pressure drop profile and its sensitivity to the change in coil-inlet DB temperature, both of which are also influenced by the coil configurations.

For the *with-TEV case, the EEP* [the mass flow rate], behaved similar to that of the *EEEP* of the 1st location. However, from 8s onwards, the difference between the refrigerants for the with-TEV EEPs at this location was larger than that for the *with-TEV EEEPs* at the 1st location [the sensitivity of the pressure-drop-profile to change in coil-inlet DB temperature].

For the *ESBP without-TEV*, comparing to that of the 1st location, the ratio of the magnitudes of change from 0s to steady state between R407C and R134a had halved [the superheated refrigerant temperature (linking to the superheat-initiation location) and the sensitivity of the ESBP to the ESBT]. The times in reaching steady state, for both refrigerants, had doubled [the superheat-initiation location].

For the *SBP with-TEV* [the refrigerant mass flow rate including its inflection points], each refrigerant had a peak, and R407C had small oscillations after the peak.

Superheat-initiation location: *With no TEV*, from 0s to steady state, the rates of change of the position were from small-to-large-to-small for R407C, and from large-to-small for R134a [the temperature gliding]. R407C had on average smaller rates than R134a [the HTC and the latent heat of vaporization]. R407C had a "1 sub-element" smaller magnitude of movement (but longer time in reaching steady state [the temperature glide and the HTC]) than R134a [the latent heat of vaporization and the total 2-phase refrigerant heat load].

When *with a TEV*, for *R407C* [the refrigerant mass flow rate via its inflection points], there was no movement until after 2s then the location moved away from the coil outlet and remained stationary between 4s and 10s. After that it started to move in the opposite direction, and stopped moving again between 12s until 16s, followed by oscillations afterwards. For *R134a* [the refrigerant mass flow rate via its inflection points], from 0s to 6s, the location moved away from the coil outlet; after that, the reverse happened and reached steady state at 14s. In addition, it was seen that the

rates of change for R407C were at any time smaller than that for R134a. In addition, as stated earlier in Section 5.2, concerning the small magnitudes of changes in the simulated results, any oscillations were considered or treated as genuine modulations of the parameters. It can be said that the modulation of the superheat-initiation location for R407C was associated with the operating characteristic of the TEV, and this could also occur for R134a depending on the conditions.

For the ***Degrees of superheat***, as expected, the results could be described similarly, though in the opposite direction, to that for the superheat initiation location [for the *without-TEV case*: the superheat-initiation location and its 2-phase temperature; for the *with-TEV case*: the same as that for the *without-TEV case*, and the refrigerant mass flow rate].

Refrigerant mass flow rate at the TEV outlet: As the mass flow rate was kept constant for the *without-TEV case*, the investigation concerned only the *with-TEV case* [the SBP and the EEP]. When compared to R134a, R407C had the same "small-large-small" pattern during 0s and the time having the peak value, but with smaller rates of change. After the peak, the mass flow rate of R407C decreased to having small oscillations, whereas R134a decrease to reach steady state.

Table 5.23 It was for when having a 0.5°C step **increase** of the coil-inlet DB temperature, for the interaction between the TEV control mechanism and the refrigerant type as based on the refrigerant pressure and the sensor-bulb pressure, for a **1-row evaporator**. The simulated **results** were presented for **2 locations** (2-phase and coil-outlet) and **3 parameters** (superheat-initiation location, degrees of superheat, and refrigerant mass flow rate at the TEV outlet). For all the 2 locations of **the coil without TEV** and for the 1st location of **the TEV-controlled evaporator**, ***each location*** was installed with a **virtual** external equalizer and a **virtual** sensor bulb; this resulted in the use of the term "**equivalent**" prefixed to external-equalizer pressure and sensor-bulb pressure.

The 1st location			
For the without-TEV coil, the mentioned outlet was at the Sub-elements (1,5,2,4) (R407C) and (1,5,2,1) (R134a) (Fig. 5.148). The main focus was on **the differences due to refrigerant type effect**.		**For the TEV-controlled coil**, the mentioned outlet was at the Sub-elements (1,5,3,1) (R407C) and (1,5,2,3) (R134a) (Fig. 5.148). The main observation was related to **the TEV control mechanism effect, particularly the refrigerant mass flow rate.**	
Equivalent External-Equalizer Pressure (**EEEP**) at the virtual external equalizer	Equivalent Sensor-Bulb Pressure (**ESBP**) at the virtual sensor bulb	**EEEP** at the virtual external equalizer	**ESBP** at the virtual sensor bulb
For the EEEP, Fig. 5.149, when compared to R134a, R407C had	For the ESBP, Fig. 5.150, when compared to R134a, R407C had	For the EEEP, Fig. 5.151, the description of the results (i.e. having a	For the ESBP, Fig. 5.152, for the rates of change, R407C (from

Table 5.23 It was for when having a 0.5°C step **increase** of the coil-inlet DB temperature, for the interaction between the TEV control mechanism and the refrigerant type as based on the refrigerant pressure and the sensor-bulb pressure, for a **1-row evaporator**. The simulated **results** were presented for **2 locations** (2-phase and coil-outlet) and **3 parameters** (superheat-initiation location, degrees of superheat, and refrigerant mass flow rate at the TEV outlet). For all the 2 locations of **the coil without TEV** and for the 1st location of **the TEV-controlled evaporator**, ***each location*** was installed with a **virtual** external equalizer and a **virtual** sensor bulb; this resulted in the use of the term "**equivalent**" prefixed to external-equalizer pressure and sensor-bulb pressure.

smaller rates of change and took more time to reach steady state. For both refrigerants, during the first 6s, the rates of change were negative from small to large, whereas, from 6s to the steady state, they were positive from large to small. From 0s to steady state, both refrigerants had an overall positive magnitude of change with R407C having a slightly larger value.	larger positive rates of change, an overall 3.5 times larger positive-magnitude of change and a longer time for reaching the steady state. In addition, for both refrigerants, the rates of change were from small-to-large-to-small.	longer time to reach steady state for R407C) was similar to that for the case of the without-TEV coil. However, both refrigerants had the negative rates of change (small-to-large-to-small) from 0s to 20s for R407C, and to 18s for R134a (where the minimum values of the EEEPs were). After that, the **EEEP** for R407C had a small increase followed by small amplitude oscillations, whereas **that** for R134a had a small increase to reach steady state. For the overall magnitude of change, R407C had a smaller negative value than R134a; it should be noticed that, when compared to the without-TEV case, for both refrigerants, the changes were in opposite direction.	0s to 8s) and R134a (from 0s to 6s) were positive (small-large-small, and small-large, respectively) but R407C had larger values. After that, the rates of change could be described similarly to the previous periods, but with negative gradients (small-large-small for both refrigerants). R407C had the lowest ESBP at 22s and oscillated slightly, whereas R134a had the lowest value at 20s (being earlier than that for R407C) and increased slightly to reach steady state at 44s. For the magnitude of change from 0s to steady state, the description was opposite to that for the without-TEV case
The 2nd location, i.e. at the coil outlet			
For the without-TEV coil, the main concern was **the refrigerant type influence**.		**For the TEV-controlled coil**, the main observation was again related to **the TEV control, particularly the change in refrigerant mass flow rate.**	
EEEP at the virtual external equalizer	**ESBP** at the virtual sensor bulb	External-Equalizer Pressure (**EEP**)	Sensor-Bulb Pressure (**SBP**)
As shown in Fig. 5.153, the description of the EEEP's variation was similar to that of the 1st location. However, there were 3 differences. *1)* For the	The description of the ESBP was similar to that of the 1st location, Fig. 5.154; however, for the positive magnitude of change from 0s to steady state, R407C had	When comparing the results, Fig. 5.155, with the without-TEV case, the description was similar to that given for the 1st position.	For the SBP (Fig. 5.156), the description was not too similar to that for the without-TEV case; there were 2 differences: *1)* having a peak (for R407C at 18s,

Table 5.23 It was for when having a 0.5°C step **increase** of the coil-inlet DB temperature, for the interaction between the TEV control mechanism and the refrigerant type as based on the refrigerant pressure and the sensor-bulb pressure, for a **1-row evaporator**. The simulated **results** were presented for **2 locations** (2-phase and coil-outlet) and **3 parameters** (superheat-initiation location, degrees of superheat, and refrigerant mass flow rate at the TEV outlet). For all the 2 locations of **the coil without TEV** and for the 1st location of **the TEV-controlled evaporator**, ***each location*** was installed with a **virtual** external equalizer and a **virtual** sensor bulb; this resulted in the use of the term "**equivalent**" prefixed to external-equalizer pressure and sensor-bulb pressure.

first 6s, for both refrigerants, the rates of change (negative gradients were from large to small. *2)* From 6s to the steady state, both refrigerants had about the similar positive rates of change. *3)* The positive magnitude of change from 0s to steady state for R407C was twice of that for R134a.	a 1.5 times larger than R134a. It should be noticed that, for both refrigerants, the time durations in reaching steady state were **more than 2 times** of that for the 1st location.	When compared this 2nd location to the 1st location, for each refrigerant, from 0s to 8s, the variations of EEP with time were similar. However, it should be noticed, from the 8s onwards, larger differences of EEPs between the two refrigerants were observed.	and for R134a at 14s), and *2)* having oscillations after the peak for R407C.
Superheat-initiation location			
Without-TEV coil		**TEV-controlled coil**	
From Fig. 5.157 (see also Fig. 5.146), using the refrigerant coil-outlet as the reference location, at the 0s, the superheat-initiation location for R407C (Sub-element (1,5,3,3)) was nearer to the reference location than that for R134a (Sub-element (1,5,3,1)). From 0s to steady state, the rates of change (negative gradients) for R407C (small-large-small) were on average smaller than that for R134a (large-small); also the negative magnitude (i.e. away from the reference location) of movement for R407C (-4 sub-elements) was smaller than that for R134a (-5 sub-elements). For the time in reaching steady state, R407C took longer than R134a.		For **R407C**, for the first 2s, there was no change in the location; from 2s to 4s, the location moved away from the refrigerant coil-outlet by one sub-element displacement, and remained there until the 10th s and then the location moved in the opposite direction by one sub-element length, Fig. 5.158. From 12s to 16s, there was no change, followed by some oscillations. For **R134a**, from 0s to 6s, the location moved away from the coil-outlet for one sub-element displacement per every 2 seconds; from 6s to 14s, it moved in the opposite direction towards the 0s Sub-element of the superheat-initiation location, reaching steady state, which was earlier than R407C. For the magnitude of change from 0s to steady state, R407C had about half sub-element displacement, whereas R134a had no displacement observed.	
Degrees of superheat			
Without-TEV coil		**TEV-controlled coil**	
, The degrees of superheat at 0s for R407C (5.06 °C) was smaller than that for R134a (6.2 °C), Fig. 5.159. The positive rates of change, the positive magnitude of change (small-large-small-large-small for R407C and small-large-small for R134a)		Generally, for both refrigerants, the curvatures of degree of superheat graphs behaved oppositely to that of the superheat-initiation location, Fig. 5.160, and the rates of change for R407C were smaller than that for R134a.	

Table 5.23 It was for when having a 0.5°C step **increase** of the coil-inlet DB temperature, for the interaction between the TEV control mechanism and the refrigerant type as based on the refrigerant pressure and the sensor-bulb pressure, for a **1-row evaporator**. The simulated **results** were presented for **2 locations** (2-phase and coil-outlet) and **3 parameters** (superheat-initiation location, degrees of superheat, and refrigerant mass flow rate at the TEV outlet). For all the 2 locations of **the coil without TEV** and for the 1st location of **the TEV-controlled evaporator**, ***each location*** was installed with a **virtual** external equalizer and a **virtual** sensor bulb; this resulted in the use of the term "**equivalent**" prefixed to external-equalizer pressure and sensor-bulb pressure.

and the reaching-steady-state time could be described in a manner similar to that for the superheat-initiation location for the without-TEV case.	For **R407C**, from 2s to 10s, the positive rates of change were from small-to-large-to-small, with a sharp decrease between 10s to 12s; and from that 12s to 16s, little positive rates of change were noticed. From 16s to 18s, there was a sharp decrease again; from 18s to 30s, slight negative rates of change occurred, followed by some oscillations For **R134a**, between 0s to 6s, the small-to-large positive rates of change were noted, followed by a levelling-off between 6s to 8s. From 8s to 14s, there were large negative rates of change (with a levelling-off during 10s and 12s) followed by a slight decrease until reaching steady state at 30s, which was earlier than that for R407C. The magnitude of change from 0s to steady state (being negative) for R407C was about the same value as that (being positive) for R134a.
Refrigerant mass flow rate at the TEV outlet	
Without-TEV coil	**TEV-controlled coil**
For both refrigerants, the refrigerant mass flow rates remained unchanged/constant at 0.0228 kg/s.	The positive rates of change (R407C had on average lower values than that for R134a) were from small-to-large-to-small between 0s and the time having the peakvalues (at 18s for R407C and 14s for R134a), Fig. 5.161. After that, R407C decreased smoothly until 32s when small oscillations started, whilst R134a decreased slightly to reach steady state at 36s. The positive magnitude of change between steady state for R407C was about 0.8 times smaller than that for R134a.

Table 5.24 The discussion of the results presented in Table 5.23

Superheat-initiation location	
Without-TEV coil	**TEV-controlled coil**
The results for the superheat-initiation location (Figs. 5.146 and 5.157) are analysed by addressing 4 issues as follows: (the discussion also concerned	The following 2 observations can show the interaction of the TEV control and the superheat-initiation location (Fig. 5.158).

Table 5.24 The discussion of the results presented in Table 5.23

<table>
<tr><td colspan="2">with Fig. 5.64 regarding the mechanism of a transient for a coil)
1) **The difference in the values** of the negative rate of change of the movement between the R407C (**small-large-small**) and R134a (**large-small**) are caused by the 2-phase temperature changes of individual refrigerants.
2) The smaller negative rates of change for R407C is resulted from the combined effects of both the refrigerant HTC and the latent heat of vaporization. Based on the same and constant refrigerant mass flow rate for both refrigerants, the smaller negative magnitude of movement for R407C is caused by the combined effects of both **the total 2-phase** refrigerant heat load (varied insignificantly with time) and the latent heat of vaporization.
3) A longer time to reach steady state for R407C is due to the effects of both the refrigerant temperature gliding-up/drop and refrigerant HTC.</td><td colspan="2">*1)* When compared to the without-TEV coils, the influence of the controlled refrigerant mass flow rate is noticed at 6s for both refrigerants, i.e. reversing the directions of the rates of change.

2) For both refrigerants, the inflection point of the positive rates of change of the mass flow rate (Fig. 5.161) corresponds to the "trough" of the superheat-initiation location, whereas that of the negative ones corresponds to the "peak".</td></tr>
<tr><td colspan="4">Degrees of superheat</td></tr>
<tr><td colspan="2">Without-TEV coil</td><td colspan="2">TEV-controlled coil</td></tr>
<tr><td colspan="2">As expected, for both refrigerants, the dynamics of the degrees of superheat (Fig. 5.159) conforms to (though oppositely) the movement of the superheat initiation location (Fig. 5.157). The dyanimcs is also *influenced by* the 2-phase temperature at the superheat initiation location (Fig. 5.162).</td><td colspan="2">(The **interaction** between the TEV control and the degrees of superheat can be described similarly to the observations made for the superheat-initiation location, except for using "peak" and "trough" instead of the reverse.)

Three main influencing parameters were identified, namely the **2-phase** temperature at the superheat-initiation location (Fig. 5.163), the superheat-initiation location (Fig. 5.158), and the refrigerant mass flow rate.</td></tr>
<tr><td colspan="4">Refrigerant mass flow rate at the TEV outlet</td></tr>
<tr><td colspan="2">Without-TEV coil</td><td colspan="2">TEV-controlled coil</td></tr>
<tr><td colspan="2">For both refrigerants, the refrigerant mass flow rate was kept constant at 0.0228 kg/s.</td><td colspan="2">Based on Eq. 4.33, both SBP and EEP were expected to affect the mass flow rate at the TEV outlet.</td></tr>
<tr><td colspan="4">The 1st location</td></tr>
<tr><td colspan="2">**For the without-TEV coil**, the mentioned outlet was at the Sub-elements (1,5,2,4) (R407C) and (1,5,2,1) (R134a) (Fig. 5.148). The main concern was **the refrigerant type effect**.</td><td colspan="2">**For the TEV-controlled coil**, the mentioned outlet was at the Sub-elements (1,5,3,1) (R407C) and (1,5,2,3) (R134a) (Fig. 5.148). The main observation was related to **the TEV control mechanism effect, particularly the refrigerant mass flow rate**.</td></tr>
<tr><td>**EEEP** at the virtual external equalizer</td><td>**ESBP** at the virtual sensor bulb</td><td>**EEEP** at the virtual external equalizer</td><td>**ESBP** at the virtual sensor bulb</td></tr>
<tr><td>Based on Section 5.2.2.a, it is suggested</td><td>As discussed in Section 5.3.2, in **the 2-phase**</td><td>By comparing to the without-TEV case, the</td><td>By **comparing to the without-TEV case**, the</td></tr>
</table>

Table 5.24 The discussion of the results presented in Table 5.23

that, **for each refrigerant**, due to the influence of the pressure-drop-profile shifting, the EEEP firstly decreases and then followed by an increase as the time passed, Fig. 5.149. From the discussion in Section 5.3.2, it can be said that, **between the 2 refrigerants**, because of the difference in sensitivity to the change in coil-inlet DB temperature of the pressure-drop-profile shifting, there are differences in the rates of change EEEP with time, and in the magnitudes of change from 0s to steady state. Based on the understanding of the mechanism of the transient of an evaporator (Section 5.3.2), **for each refrigerant**, for the 2-phase region of the **1-row coil**, the time for reaching steady state is considered a function of both the temperature gliding-up/drop and the HTC of the refrigerant.	region of either refrigerant, both the magnitude and direction of the rate of change of **the tube-wall temperature** (this corresponds to ESBT) with time are influenced by both the refrigerant temperature gliding-up/drop and the ratio of the refrigerant heat flux to the refrigerant HTC; however, due to the temperature gliding-up of R407C, the direction of the rate of change will not reverse (see also Sub-section 5.3.2). For ESBP, when comparing the two refrigerants, **the difference in** the rates of change and the magnitudes of change from 0s to steady-state are **mainly** caused by the influences of the refrigerant temperature gliding-up/drop, and the sensitivity of the ESBP to the change in Equivalent Sensor-Bulb Temperature (ESBT) as well as the observation location. For the time to reaching steady-state, the influencing parameters are the same as those stated for the EEEP of this location. In addition, the discussion for the 2nd location (to be given later) regarding both the temperature and pressure of the sensor-bulb, and the temperature of the tube-wall at the coil-outlet is equally applicable to this location.	effect of the TEV-controlled mass flow rate upon EEEP for both **rates of change** and **magnitudes of change from 0s to steady-state** can be seen. For **the former**, it is observed at the 6s upon the rates of change and from the 8s onwards upon also the directions of change. For **the latter**, both directions and magnitudes are affected. It is seen that the EEEP directions of both rates of change and magnitude of change from 0s to steady-state are opposite in direction to that for the refrigerant-mass-flow-rate.	effect of the TEV-controlled mass flow rate upon the rates of change of ESBP from 8s onwards can be noticed (R407C: for magnitude, whereas for both magnitude and **reversed** direction from 10s; R134a: for both magnitude changed and the direction reversed). For the effect on the magnitudes of change from 0s to steady-state, it can be discussed with same wordings as given for EEEP. For the present case, i.e. **the TEV-controlled coil**, for both refrigerants, the influence of the controlled refrigerant mass flow rates via their inflection points upon ESBPs can be described in a similar way (except using "peak" for "trough" and "trough" for "peak") as done for the superheat-initiation location.

Table 5.24 The discussion of the results presented in Table 5.23

The 2nd location, i.e. at the coil outlet			
For the without-TEV coil, the main concern was **the refrigerant type effect**.		**For the TEV-controlled coil**, the main observation made was related **the TEV control mechanism effect, particularly the refrigerant mass flow rate**	
EEEP at the virtual external equalizer	**ESBP** at the virtual sensor bulb	**EEP**	**SBP**
For all the 3 noted differences above (when compared to the 1st observed location), it is thought to be caused by the influence of the sensitivity of the pressure-drop-profile shifting to the change in coil-inlet DB temperature, i.e. the effect of the 2-phase pressure drop.	In general, for pure refrigerant such as R134a, **the sensor-bulb pressure is a function of the sensor-bulb temperature**. This is also applicable to R407C, since, as assumed in Sub-section 4.4.3, the mole fractions of the liquid phase in the sensor bulb remained unchanged at all times. It was also stated that, for either refrigerant, **the bulb temperature was approximately equal to the tube-wall temperatures at the coil-outlet**. For both the magnitude and the direction of the rate of change of the tube-wall temperature, the discussion given for the 1st location (**2-phase**) for R407C can also be applied to the **superheat** region of either refrigerant. For ESBP at the **virtual** sensor bulb, there are 3 main influencing parameters: the refrigerant temperature, the superheat-initiation location, and the sensitivity of the ESBP to the ESBT. For the time to reaching the steady-state, it is	Based on the comparison of the with- and without- TEV cases, the influence of the TEV-controlled mass flow rate upon EEP can be described in the same way as that for the 1st location. From the 8s onwards, the 2nd location had larger differences of EEPs between the 2 refrigerants than the 1st location; it is due to the effect of the sensitivity of the pressure-drop-profile shifting to the change in coil-inlet DB temperature.	By comparing to the without-TEV case, for both refrigerants, the influence of the controlled mass flow rates upon the slope of SBP with time can be seen from 6s onwards, whereas that is upon only the magnitudes (not the direction) of the change between 0s and the final steady-state. For the present case, for either refrigerant, the controlled refrigerant mass flow rate including its inflection point affects **directly** both the magnitude and direction of the rate of change of SBP.

Table 5.24 The discussion of the results presented in Table 5.23

	affected **mainly** by the location of the superheat-initiation point.		

Table 5.25 The ***analysis of the influencing parameters*** stated in the discussion (Table 5.24)

The influenced parameter: **the superheat-initiation location**	
Without-TEV coil	**TEV-controlled coil**
The 2-phase refrigerant temperature gliding-up/drop: From Fig. 5.164 (for Element (1,3,3)) and Sub-section 5.2.2.a, it can be **generally** said that the rates of change and the overall magnitude of change for R407C are much larger than and in the opposite direction (R407C: positive, R134a: negative) to that for R134a. Combined influence of refrigerant HTC and latent heat of vaporization: For **the former**, based on Fig. 5.165 (for Element (1,3,3)) and Sub-section 5.2.2.a, it can be said that, the positive rates of change for R407C are on average smaller than that for R134a. For **the latter**, the average value for R407C is about 1.1 times larger than that for R134a. The **total 2-phase** refrigerant heat load: Both refrigerants have insignificant variations during the transient time duration. Combined influence of the refrigerant temperature gliding-up/drop and refrigerant HTC: For **both parameters** (Figs. 5.164 and 5.165), the times in reaching steady state for R407C are slightly longer than that for R134a.	The controlled refrigerant mass flow rate: Based on the operation of the TEV in adjusting the degrees of superheat, the variation of the mass flow rate with time (Fig. 5.161) is calculated after the superheat-initiation location with time had been determined (Fig. 5.158). The inflection point of the controlled refrigerant mass flow rate with time: The analysis is in 3 steps: a general link, a proposed statement followed by a support statement. *1)* When having a step increase of the DB temperature, the accumulated heat flux of the fin-and-tube induces a transient state (Fig. 5.64), while the TEV-controlled mass flow rate *(influencing the refrigerant HTC to follow the corresponding dynamics, Figs. 5.166 to 5.169)* is moderated to cope with the refrigerant heat flux in order to maintain approximately the same degrees of superheat *(relating to the superheat initiation location)*. *2)* It is **proposed** that, for either refrigerant, the superheat initiation location seems to reflect the interaction between the fin-and-tube accumulated heat flux *(via the refrigerant heat flux)* and the TEV-controlled mass flow rate *(via the refrigerant HTC)*. *3)* Hence, in **the 2-phase region**, considering the ratio of the refrigerant heat flux (Fig. 5.170) to the HTC (Fig. 5.166), it is found that time-wise the troughs and the peaks of the ratio (Fig. 5.171) correspond (though oppositely) to that of the movement of the superheat initiation location with time, linking to the inflection point of the controlled mass flow rate with time.
The influenced parameter: **the degrees of superheat**	
Without-TEV coil	**TEV-controlled coil**

Table 5.25 The ***analysis of the influencing parameters*** stated in the discussion (Table 5.24)

Considering the **2-phase** temperature at the superheat-initiation location, for both refrigerants, the dynamic variations in the values of this parameter (from Fig. 5.162, R407C: 0.05 °C and R134a: 0.03 °C) are **much smaller than** that of the coil-outlet refrigerant temperature (from Fig. 5.172, R407C: 1.4 °C and R134a: 1.57 °C). Due to the degrees of superheat being equal to the difference between the coil-outlet refrigerant temperature and the **2-phase** temperature at the superheat-initiation location, it can then be concluded that the change in the degrees of superheat with time is mainly affected by the movement of the superheat initiation location but not so much by the change of the 2-phase temperature.	the **2-phase** temperature at the superheat-initiation location: For both refrigerants, the variations of the dynamic values (Fig. 5.163) are (about 5 to 10 times) smaller than that of the coil-outlet refrigerant temperature (Fig. 5.173). Accordingly, the dynamic of the degrees of superheat is then noted to be mainly influenced by the following 2 parameters. The superheat-initiation location: As analysed previously. The refrigerant mass flow rate: The analysis is as follow. *1)* For **either refrigerant**, the magnitude of the **HTC** in the **superheat region** is much smaller than (~10 times) that in the 2-phase region (for the heat flux: 5 times smaller), whereas the magnitude of the **difference between the outlet and inlet temperatures** behaves oppositely (i.e. larger) (R407C: 10 times and R134a: 30 times). **Hence**, the influence of the HTC (Fig. 5.168) on the heat flux (Fig. 5.174) could be noticed when the rates of change of the HTC at any particular times are **large**. **However**, correspondingly, **the rate of change of the heat flux** only had a **little** effect on the magnitudes of the temperature difference (Fig. 5.175). It can **then** be said that the heat flux (i.e. the HTC) has negligible effect on the rate of change of the refrigerant temperature in the superheated region. *2)* As explained previously for the superheat-initiation location, the **mass flow rate** influences the **HTC** and thus both have similar **dynamic behaviour** (Figs. 5.168 and 5.169). *3)* Generally, the **degrees of superheat** is equal to the difference between the **coil-outlet temperature** and the ending-2-phase temperature. *4)* In conclusion, in the **superheat region**, the effect of **the TEV-controlled mass flow rate** (via the variation of HTC with time) on **the dynamic variation of degrees of superheat** is **negligible**.
The influenced parameter: **the refrigerant mass flow rate at the TEV outlet**	
Without-TEV coil	**TEV-controlled coil**
For both refrigerants, the refrigerant mass flow rate remained unchanged at 0.0228 kg/s.	To compare the effects of both SBP and EEP, let's consider the following 4 issues focussing on the magnitude of the difference between the minimum and the maximum (MDMM) values occurred in the dynamics of the mass flow rate.

Table 5.25 The ***analysis of the influencing parameters*** stated in the discussion (Table 5.24)

<table>
<tr><td colspan="2"></td><td colspan="2">1) When assuming that the EEPs were constant, for the variations of mass flow rates with time (Fig. 5.176) both refrigerants had about the same MDMMs, and their curves are generally similar to that of SBPs of the 2nd location, i.e. at the coil outlet (Fig. 5.156).

2) When the SBPs were assumed to remain unchanged, for both refrigerants, the MDMM of the mass flow rates for R407C (Fig. 5.177) was about 40% of that for R134a. It is noticed that the directions of both curves are opposite to that of the EEPs of the 2nd location (Fig. 5.155).

3) When considering the above 2 issues together, the MDMMs of the dynamics of the mass flow rates with constant EEPs are larger than that with the constant SBPs.

4) In conclusion, the effects of SBPs on the mass flow rates are many times larger than that of the EEPs. (R407C: 11 times, R134a: 4 times), and EEPs only slightly enhance the SBP influences on the mass flow rates.</td></tr>
<tr><td colspan="4">The 1st location</td></tr>
<tr><td colspan="2">For the without-TEV coil, the mentioned outlet was at the Sub-elements (1,5,2,4) (R407C) and (1,5,2,1) (R134a) (Fig. 5.148). The main focus was on the differences due to refrigerant type effect.</td><td colspan="2">For the TEV-controlled coil, the mentioned outlet was at the Sub-elements (1,5,3,1) (R407C) and (1,5,2,3) (R134a) (Fig. 5.148). The main observation was related to the TEV control mechanism effect, particularly the refrigerant mass flow rate.</td></tr>
<tr><td>The influenced parameter: the EEEP at the virtual external equalizer</td><td>The influenced parameter: the ESBP at the virtual sensor bulb</td><td>The influenced parameter: the EEEP at the virtual external equalizer</td><td>The influenced parameter: the ESBP at the virtual sensor bulb</td></tr>
<tr><td><u>The pressure-drop-profile shifting</u>:
As explained in Section 5.2.2.a.

<u>The sensitivity of the pressure-drop-profile shifting to the change in coil-inlet DB temperature</u>:
As discussed in Section 5.3.2.

<u>Both the temperature gliding-up/drop and the HTC of the refrigerant</u>:
As described in Section 5.3.2.</td><td><u>The refrigerant temperature gliding-up/drop</u>:
As explained in Section 5.2.2.a.

<u>The sensitivity of the ESBP to the ESBT</u>:
The ESBP of R407C is more sensitive to the ESBT than that of R134a (Figs. 5.150 and 5.178).</td><td><u>TEV-controlled mass flow rate</u>:
As explained previously(referring to the issue 1 of the description about the effect of the inflection point of the mass flow rate upon the superheat-initiation location), concerning the influence of the mass flow rate upon the HTC, it is also applicable to the influence of mass flow rate upon EEEP here.</td><td><u>Both the TEV-controlled mass flow rate and its inflection point</u>:
Referring to the issues 2 and 3 of the analysis done for the influence of the inflection point of the mass flow rate on the superheat-initiation location with the TEV, it is also applicable here for explaining the influence on ESBT (Fig. 5.179), i.e. ESBP, by the inflection point (Fig. 5.152), at the virtual sensor bulb.</td></tr>
</table>

Table 5.25 The ***analysis of the influencing parameters*** stated in the discussion (Table 5.24)

The 2rd location, i.e. at the coil outlet			
For the without-TEV coil, the main concern was **the refrigerant type influence**.		**For the TEV-controlled coil**, the main observation was again related to **the TEV control, particularly the change in refrigerant mass flow rate**.	
The influenced parameter: the **EEEP** at the virtual external equalizer	The influenced parameter: the **ESBP** at the virtual sensor bulb	The influenced parameter: the **EEP**	The influenced parameter: the **SBP**
The sensitivity of the pressure-drop-profile shifting to the change in coil-inlet DB temperature: As discussed in Section 5.3.2.	The refrigerant temperature: As explained in Section 5.2.2.a. The superheat-initiation location: As previously analysed, the degree of superheat is a function of the superheat-initiation location. Hence, the superheat-initiation location influences the refrigerant temperature, i.e. the ESBP. The sensitivity of the ESBP to the ESBT: The explanation is similar to that of the 1st location and refers to Figs. 5.154 and 5.180. The superheat-initiation location: Based on the proposed mechanism of a transient state for an evaporator (Fig. 5.64), when applying it specifically for the superheat region of the 1-row coil, the superheat-initiation location is the main influencing parameter for the time in reaching steady-state of the ESBP.	The TEV-controlled mass flow rate: The explanation for the EEEP (with the TEV) of the 1st location is also applied to the EEP here. The sensitivity of the pressure-drop-profile shifting to the change in coil inlet air temperature: As discussed in Section 5.3.2.	The TEV-controlled mass flow rate: The explanation done for the influenced superheat-initiation location is also used here for the influenced SBP. The TEV-controlled mass flow rate including its inflection point: The description is arranged as follow. *1)* In the superheat region, **the refrigerant mass flow rate** influences the **HTC** by the way that was previously mentioned in the issue 1 of analysis for the influence upon **the superheat-initiation location with the TEV case** by **the inflection point of the mass flow rate**. *2)* For the comparison between the superheat and the 2-phase regions, for the **HTC**, the **heat flux**, and the **magnitude of the difference between the outlet and inlet temperatures**, the relevant discussions were already given in the issue 1 of analysis of the influence of **the mass flow rate** upon **the degrees of**

Table 5.25 The ***analysis of the influencing parameters*** stated in the discussion (Table 5.24)

			superheat with the TEV case. *3)* Hence, for either refrigerant, when comparing the superheat region to the 2-phase region, it can be said that, in the former, for influence upon the heat flux, the refrigerant temperature has a larger impact, whereas the HTC affects less. It can be seen that the inflection point of the HTC (Fig. 5.168) (i.e. the mass flow rate) cannot induce the occurrence of either a peak or a trough of the sensor-bulb temperature (Fig. 5.181) (i.e. the SBP).

Figure 5.149 At outlets of Sub-eles. (1,5,2,4; R407C) and (1,5,2,1; R134a) just before the last Sub-eles. of 2-phase, equiv. ext. equalizer press. at virtual TEVs vs times for dry coils for a 0.5-C step increase in coil-inlet DB temp.

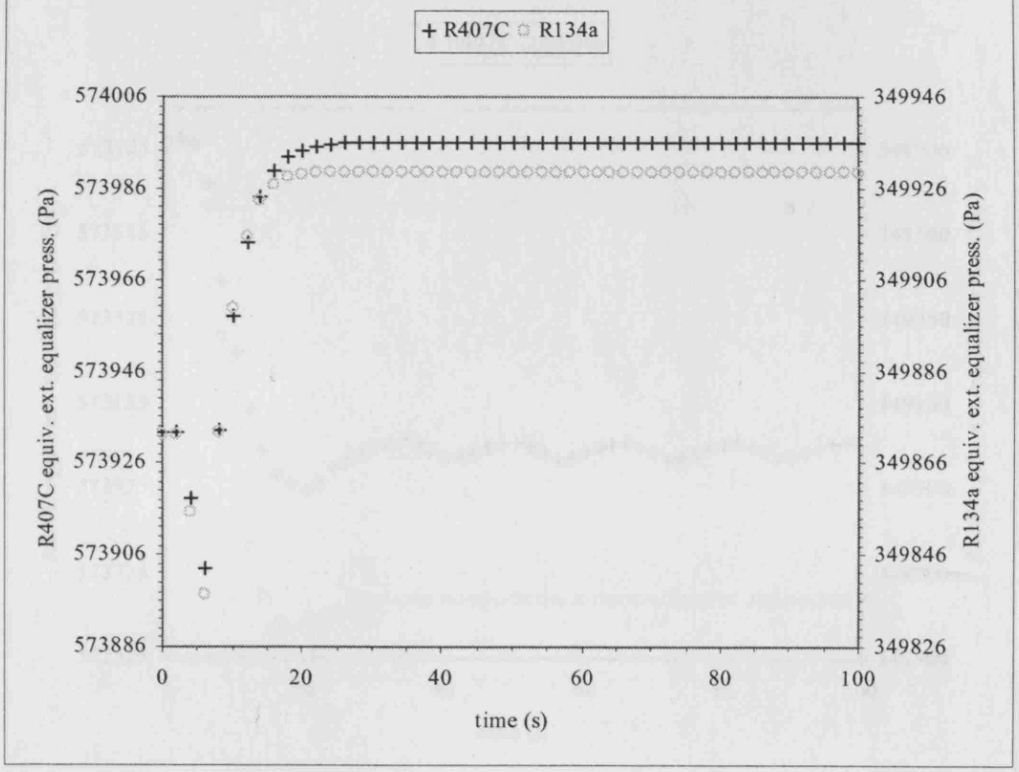

Figure 5.150 At outlets of Sub-eles. (1,5,2,4; R407C) and (1,5,2,1; R134a) just before the last Sub-eles. of 2-phase, equiv. bulb press. at virtual TEVs vs times for dry coils for a 0.5-C step increase in coil-inlet DB temp.

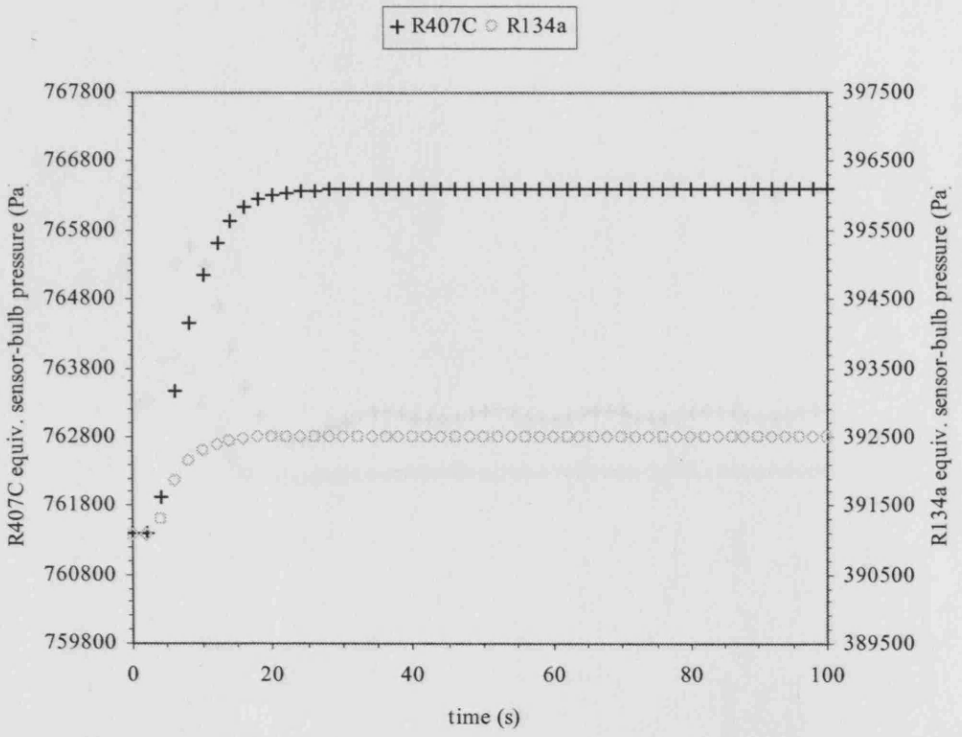

Figure 5.151 At outlets of Sub-eles. (1,5,3,1: R407C) and (1,5,2,3: R134a) just before the last Sub-eles. of 2-phase, equiv. ext. equalizer press. at virtual TEVs vs times for TEV-controlled dry coils for a 0.5-C step increase in coil-inlet DB temp.

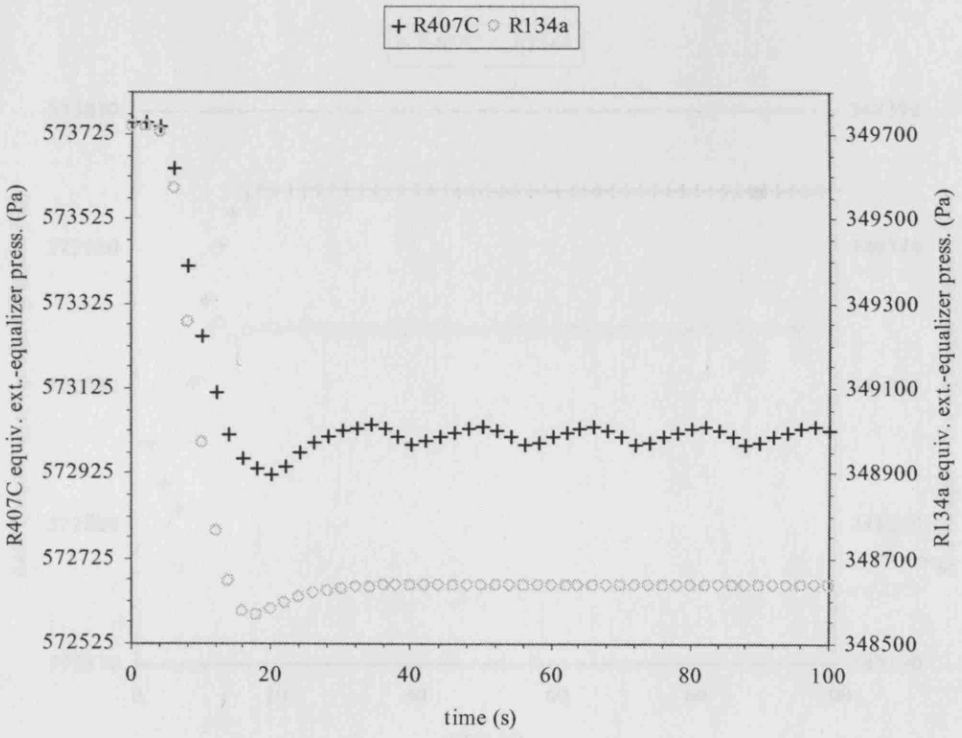

Figure 5.152 At outlets of Sub-eles. (1,5,3,1: R407C) and (1,5,2,3: R134a) just before the last Sub-eles. of 2-phase, equiv. bulb press. at virtual TEVs vs times for TEV-controlled dry coils for a 0.5-C step increase in coil-inlet DB temp.

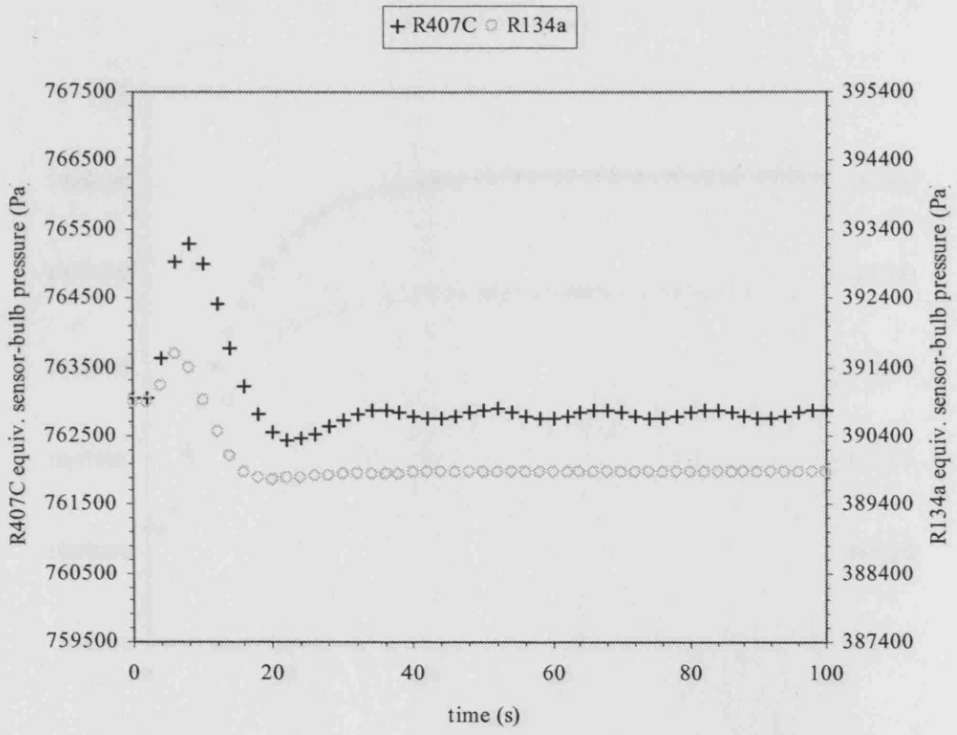

Figure 5.153 At the refrigerant coil-outlet, equivalent external-equalizer pressures at virtual TEVs vs times for dry coils, when there was a 0.5-degree-C step increase in coil-inlet dry-bulb temperatures

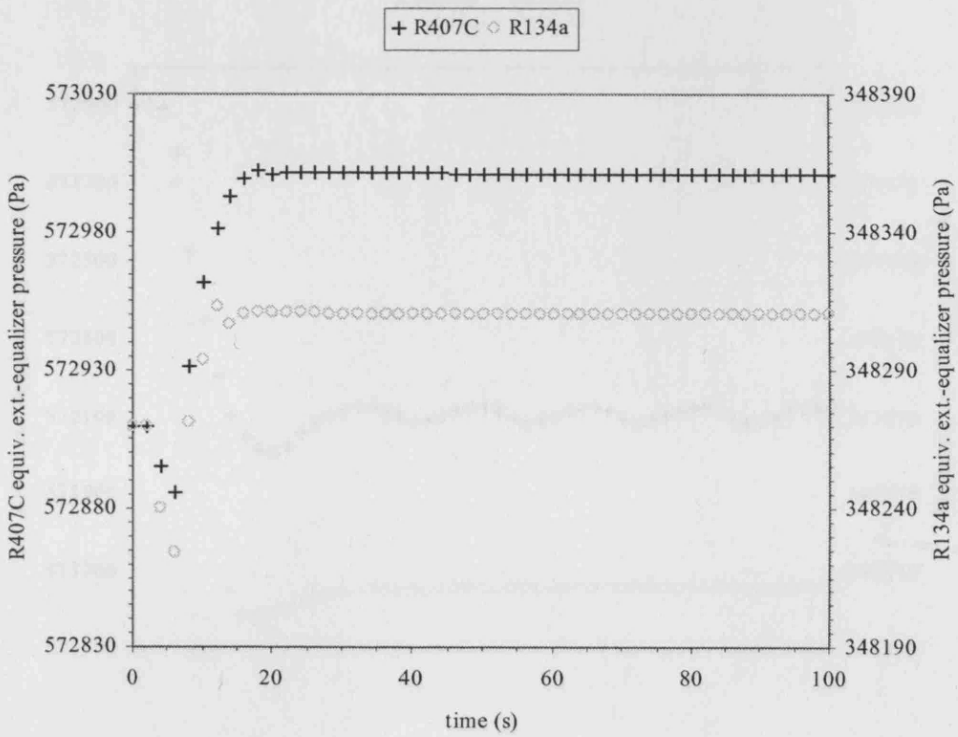

Figure 5.154 At the refrigerant coil-outlet, equivalent sensor-bulb pressures at virtual TEVs vs times for dry coils, when there was a 0.5-degree-C step increase in coil-inlet dry-bulb temperatures

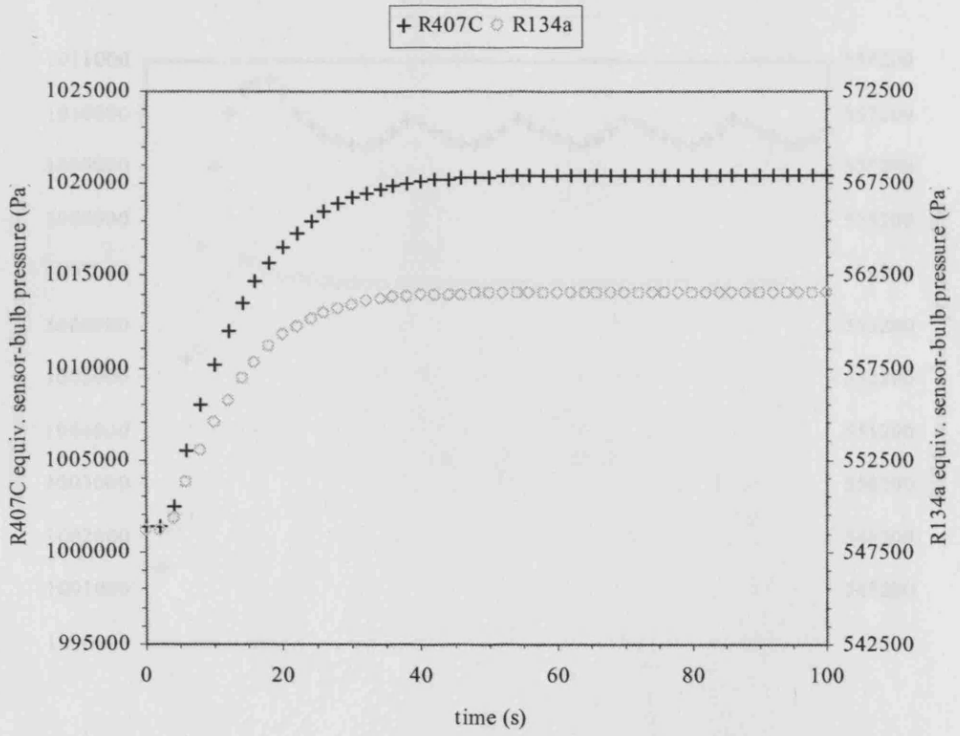

Figure 5.155 External-equalizer pressures vs times for TEV-controlled dry coils, when there was a 0.5-degree-C step increase in coil-inlet dry-bulb temperatures

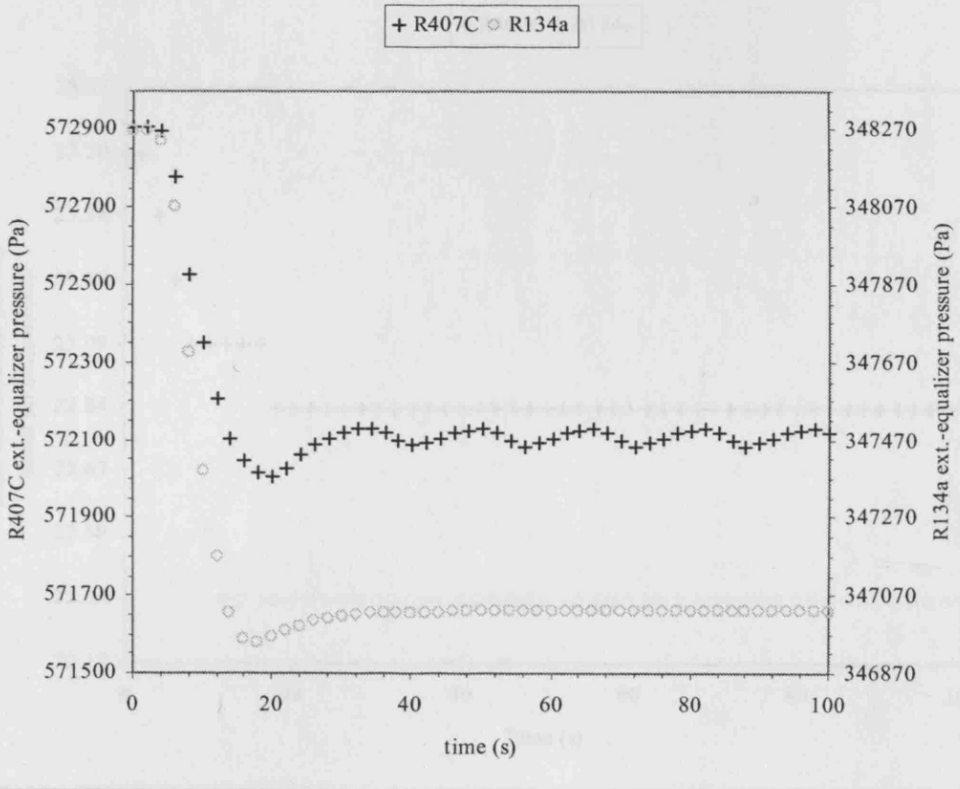

Figure 5.156 Sensor-bulb pressures vs times for TEV-controlled dry coils, when there was a 0.5-degree-C step increase in coil-inlet dry-bulb temperatures

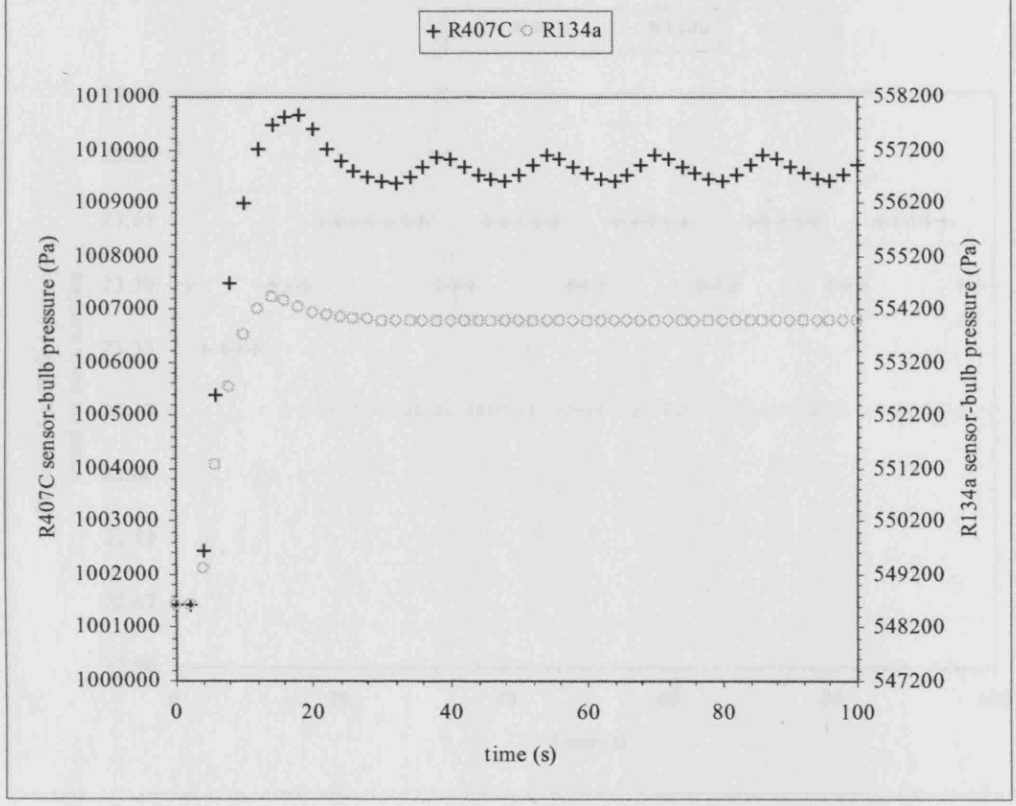

Figure 5.157 Superheat-initiation positions based on node numbers vs times for dry coils, when there was a 0.5-degree-C increase in dry-bulb temperatures

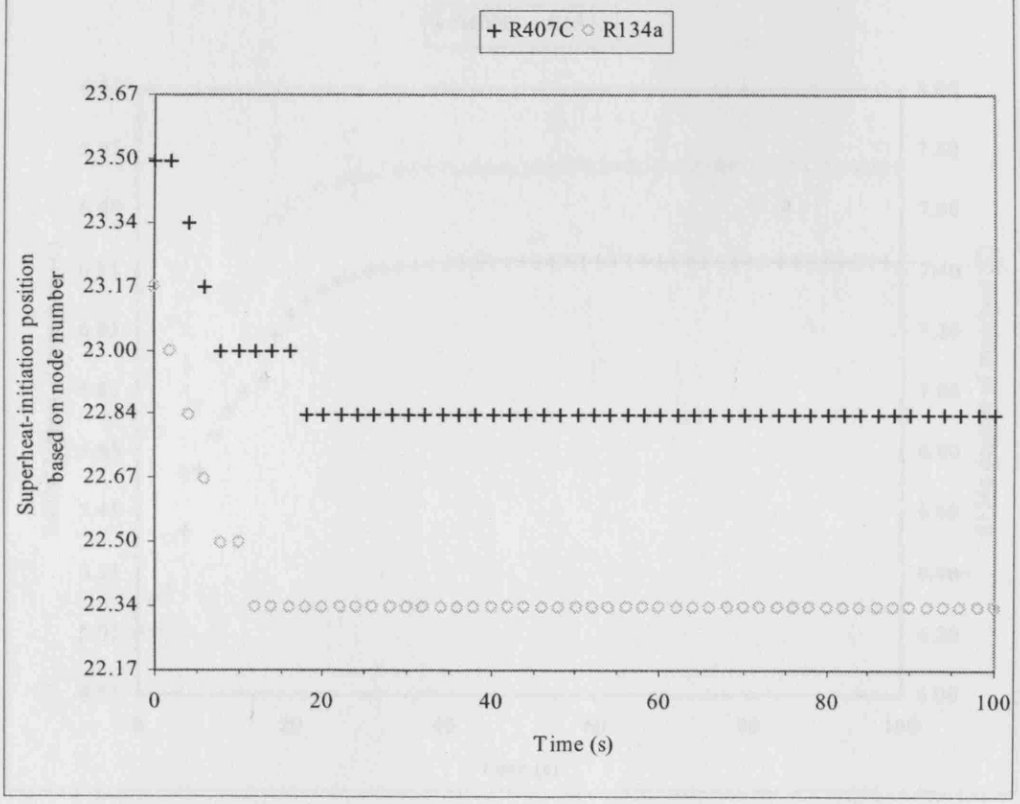

Figure 5.158 Superheat-initiation positions based on node numbers vs times for TEV-controlled dry coils, when there was a 0.5-degree-C increase in dry-bulb temperatures

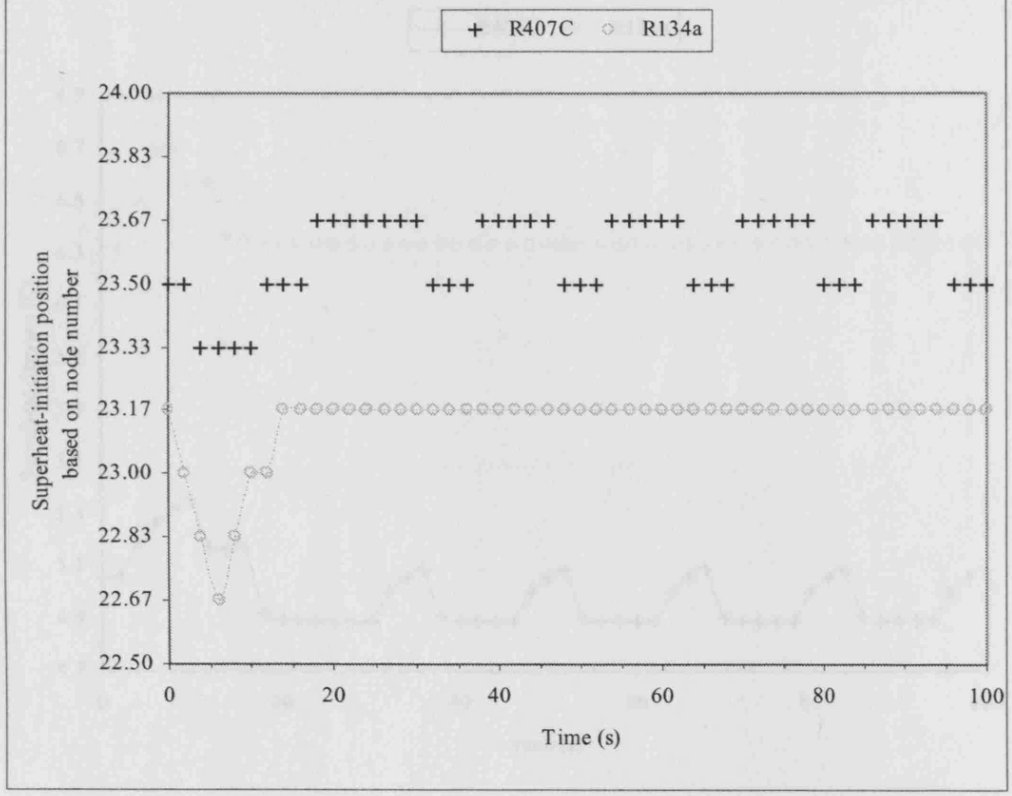

Figure 5.159 Refrigerant degrees of superheat vs times for dry coils, when there was a 0.5-degree-C increased in dry-bulb temperatures

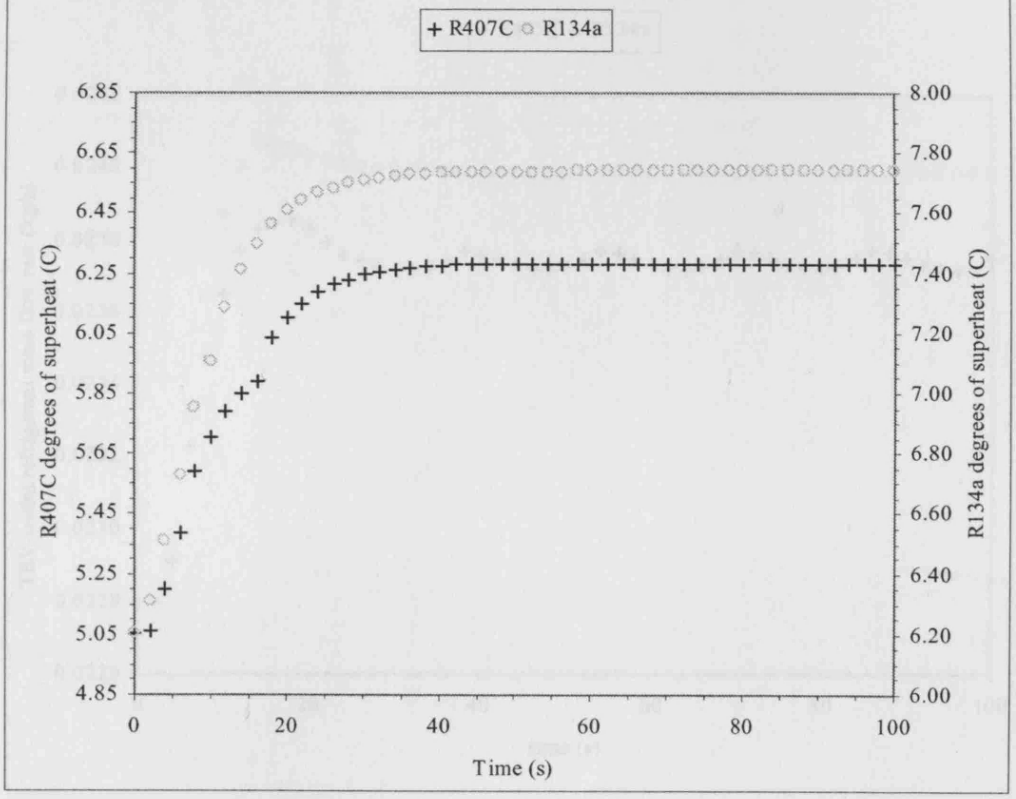

Figure 5.160 Superheat degrees vs times for TEV-controlled dry coils, when there was a 0.5-degree-C step increase in coil-inlet dry-bulb temperatures

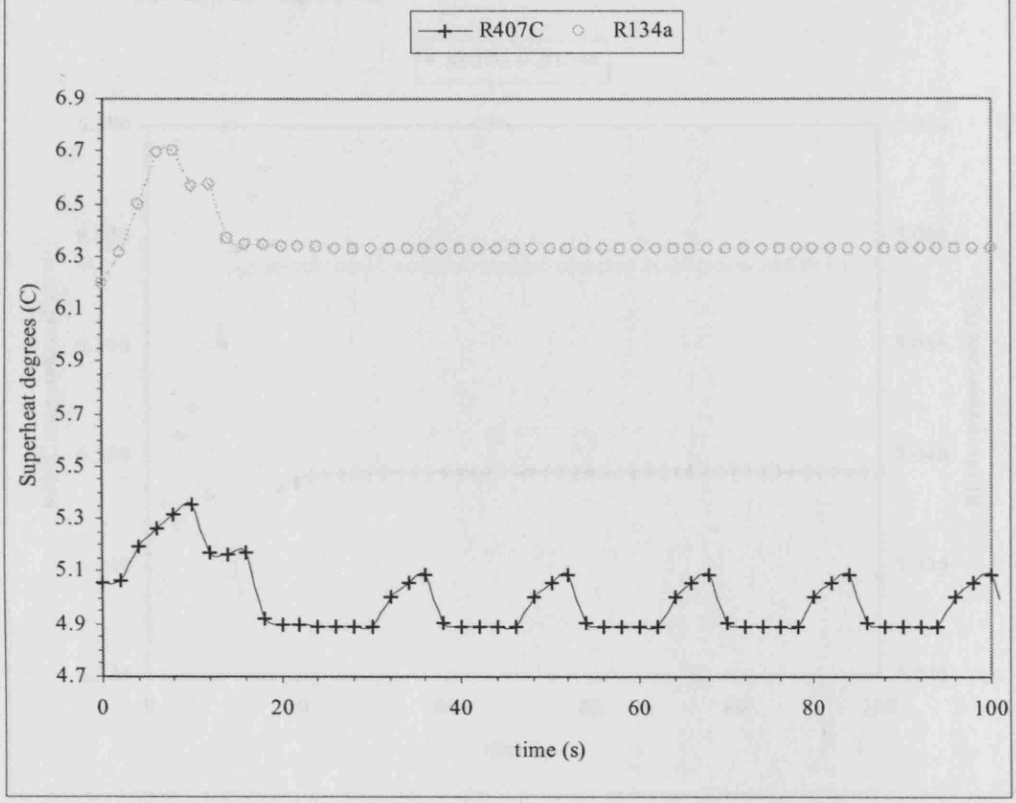

Figure 5.161 TEV-outlet refrigerant mass flow rates vs times for TEV-controlled dry coils, when there was a 0.5-degree-C step increase in coil-inlet dry-bulb temperatures

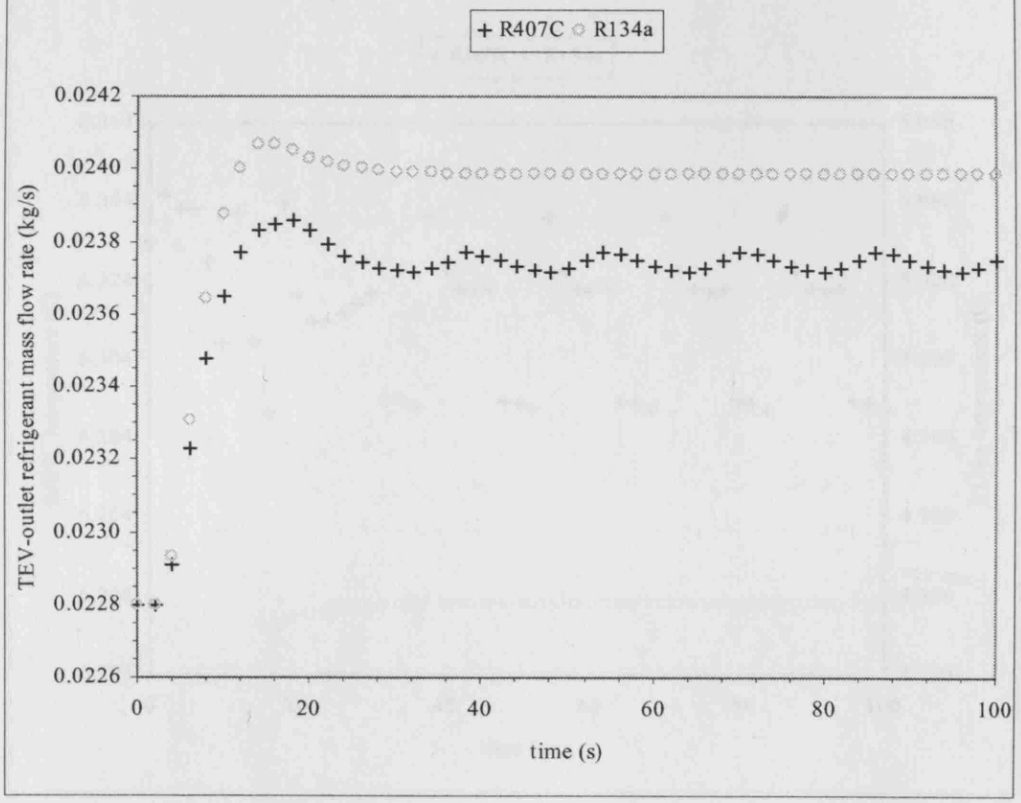

Figure 5.162 Two-phase refrigerant temperatures at the superheat-initiation locationvs times for dry coils, when there was a 0.5-degree-C step increase in coil-inlet dry-bulb temperatures

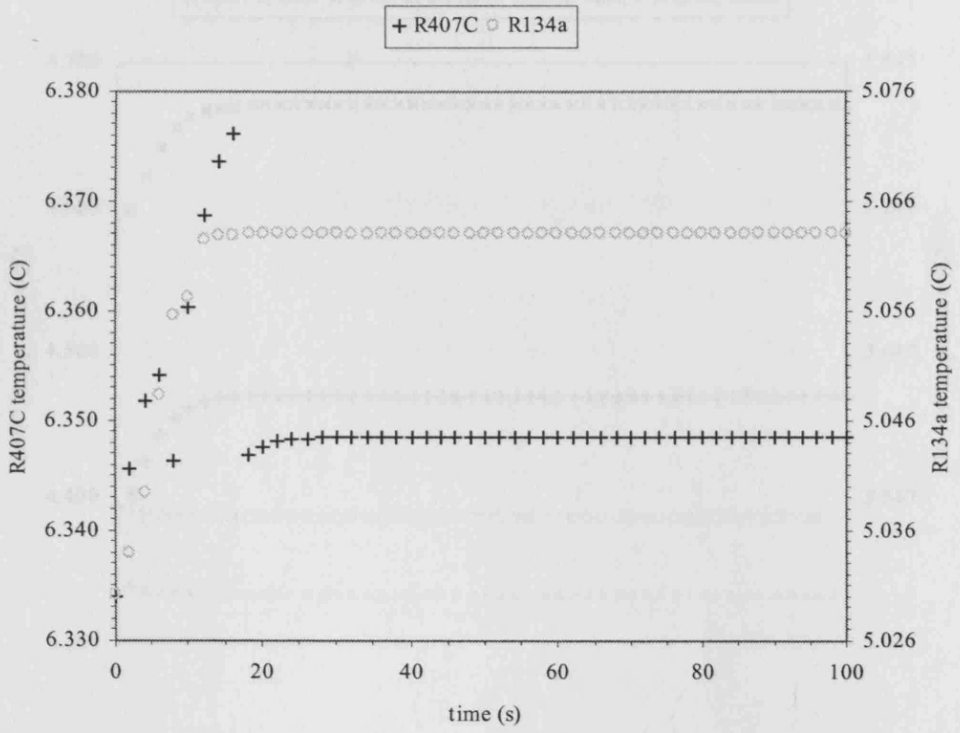

Figure 5.163 Two-phase refrigerant temperatures at the superheat-initiation location vs times for TEV-controlled dry coils, when there was a 0.5-degree-C step increase in coil-inlet dry-bulb temperatures

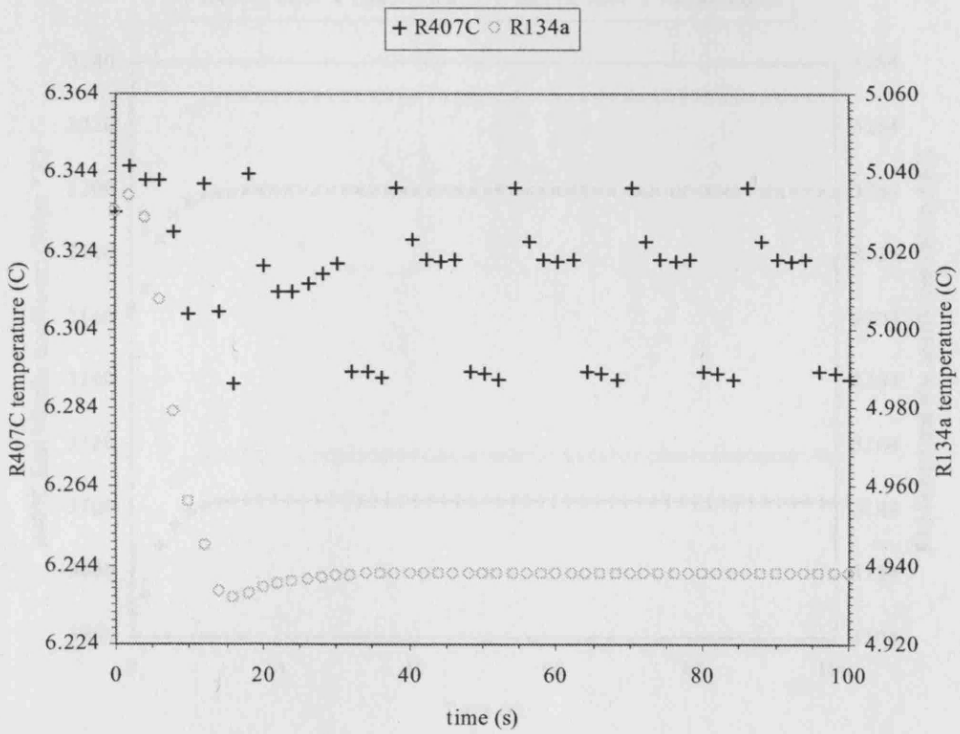

Figure 5.164 Refrigerant temperatures at Element (1,3,3) vs times for dry coils, when there was a 0.5-degree-C step increase in coil-inlet dry-bulb temperatures

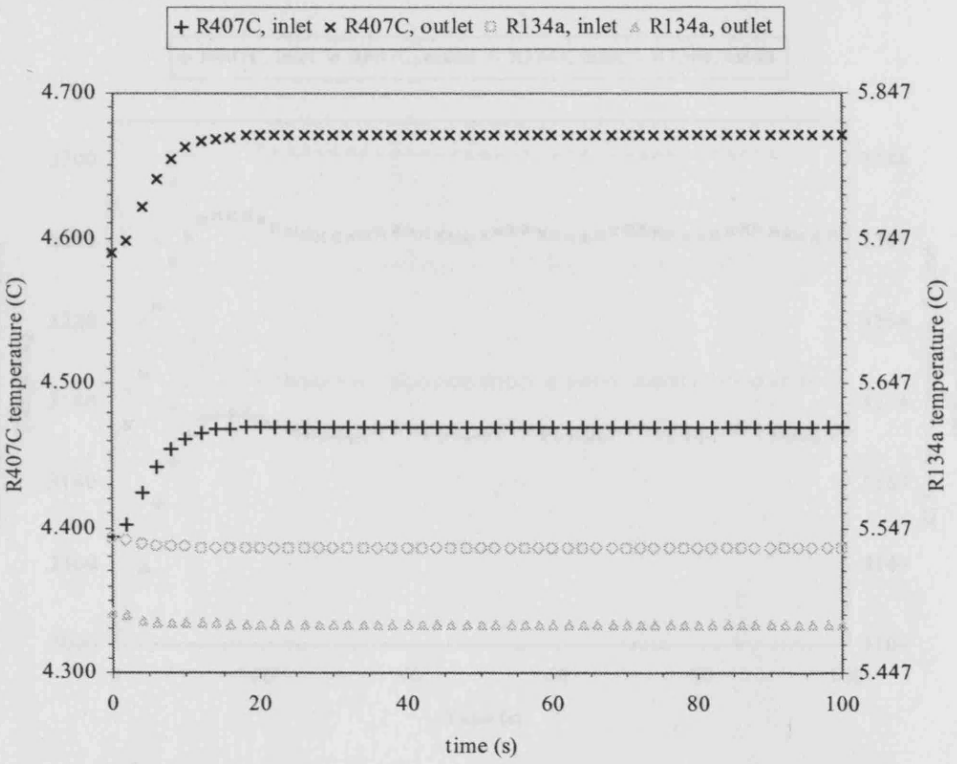

Figure 5.165 Two-phase heat transfer coefficients at Element (1,3,3) vs times for dry coils, when there was a 0.5-degree-C increase in dry-bulb temperatures

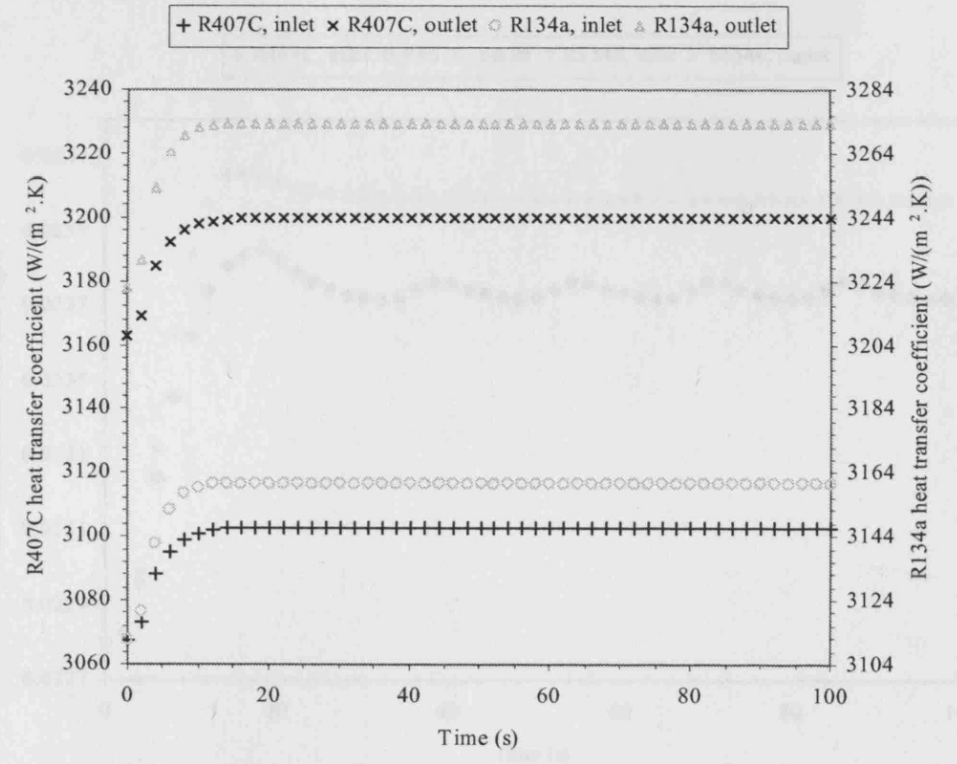

Figure 5.166 Two-phase heat transfer coefficients at Element (1,3,3) vs times for TEV-controlled dry coils, when there was a 0.5-degree-C increase in dry-bulb temperatures

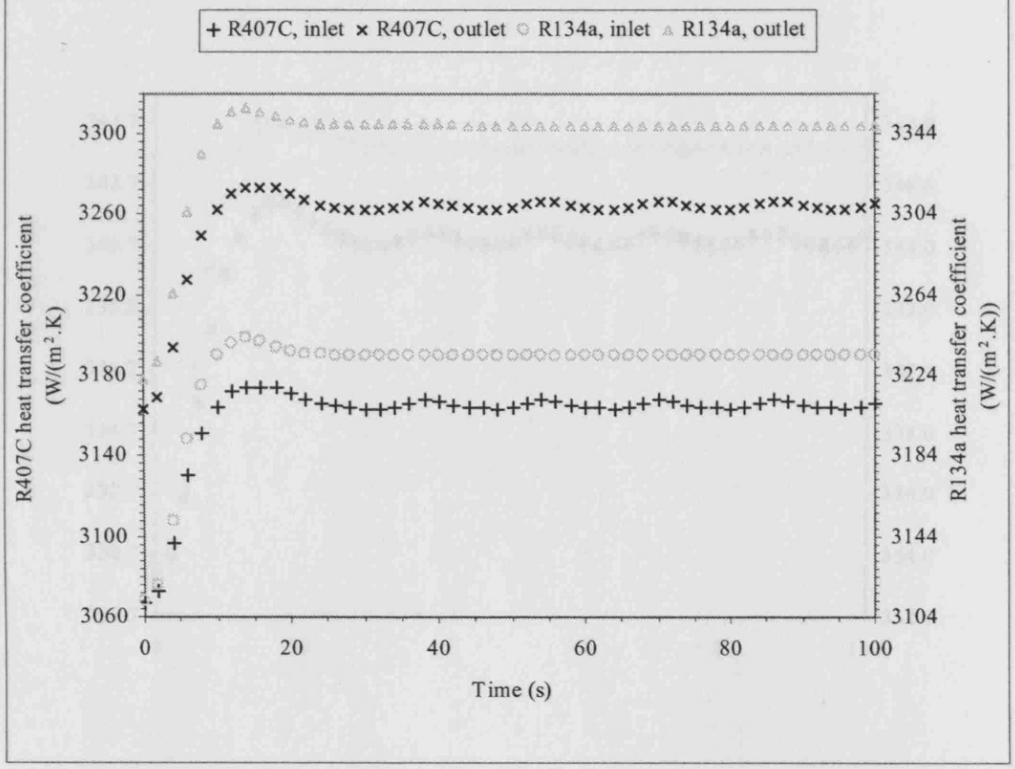

Figure 5.167 Refrigerant mass flow rates at Element (1,3,3) vs times for TEV-controlled dry coils, when there was a 0.5-degree-C step increase in coil-inlet dry-bulb temperatures

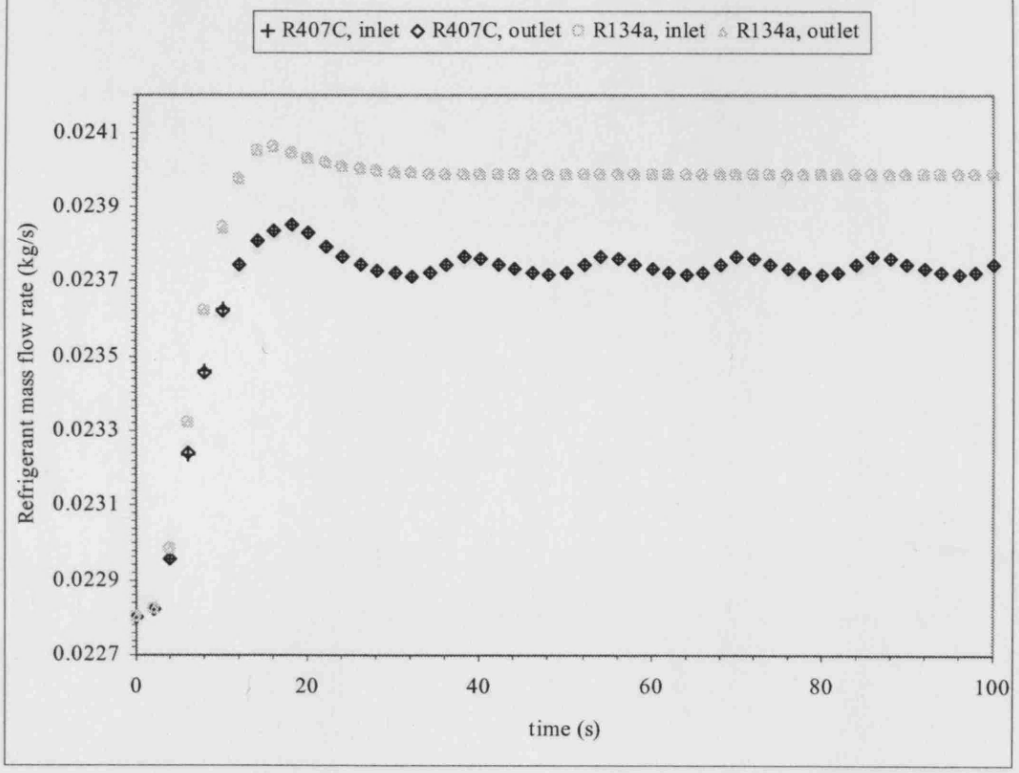

Figure 5.168 Superheat heat transfer coefficients at the last Sub-element of the coil vs times for TEV-controlled dry coils, when there was a 0.5-degree-C increase in dry-bulb temperatures

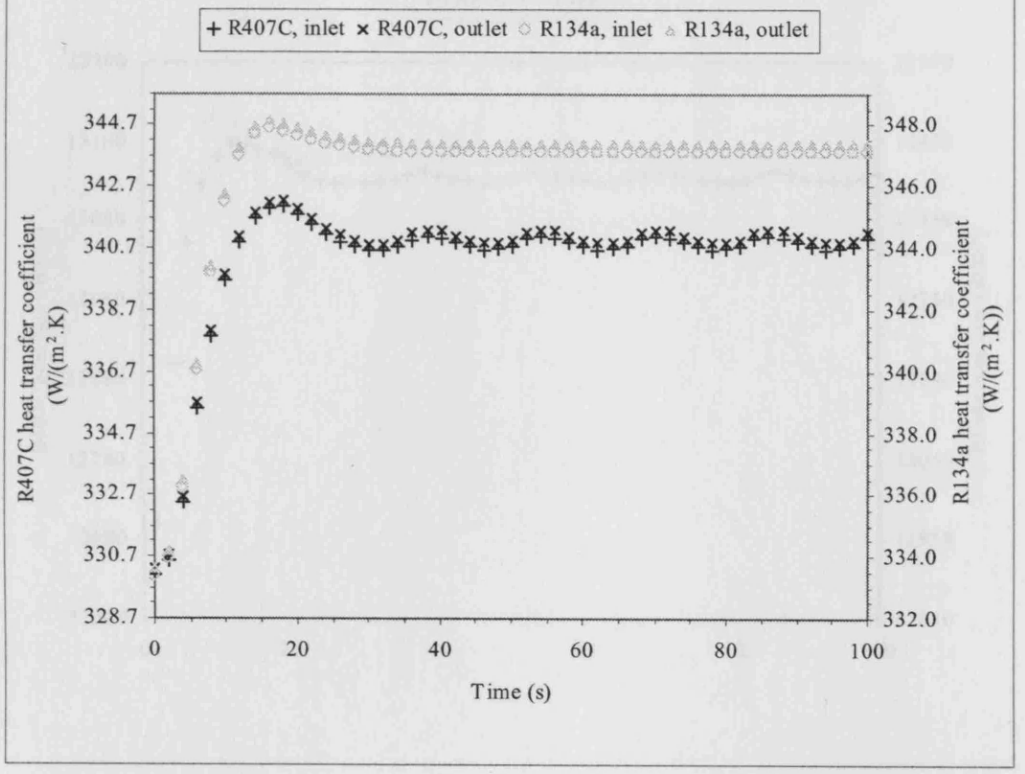

Figure 5.169 Superheat refrigerant mass flow rates at the last Sub-element of the coil vs times for TEV-controlled dry coils, when there was a 0.5-degree-C step increase in coil-inlet dry-bulb temperatures

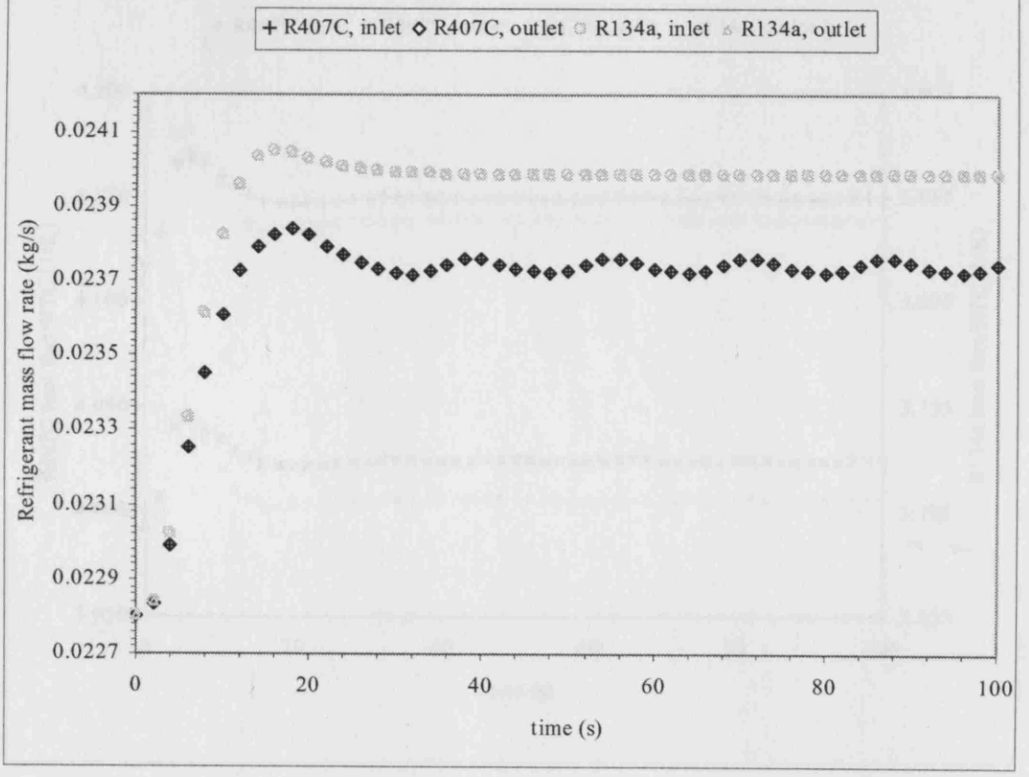

Figure 5.170 Refrigerant heat fluxs at Element (1,3,3) vs times for TEV-controlled dry coils, when there was a 0.5-degree-C increase in dry-bulb temperatures

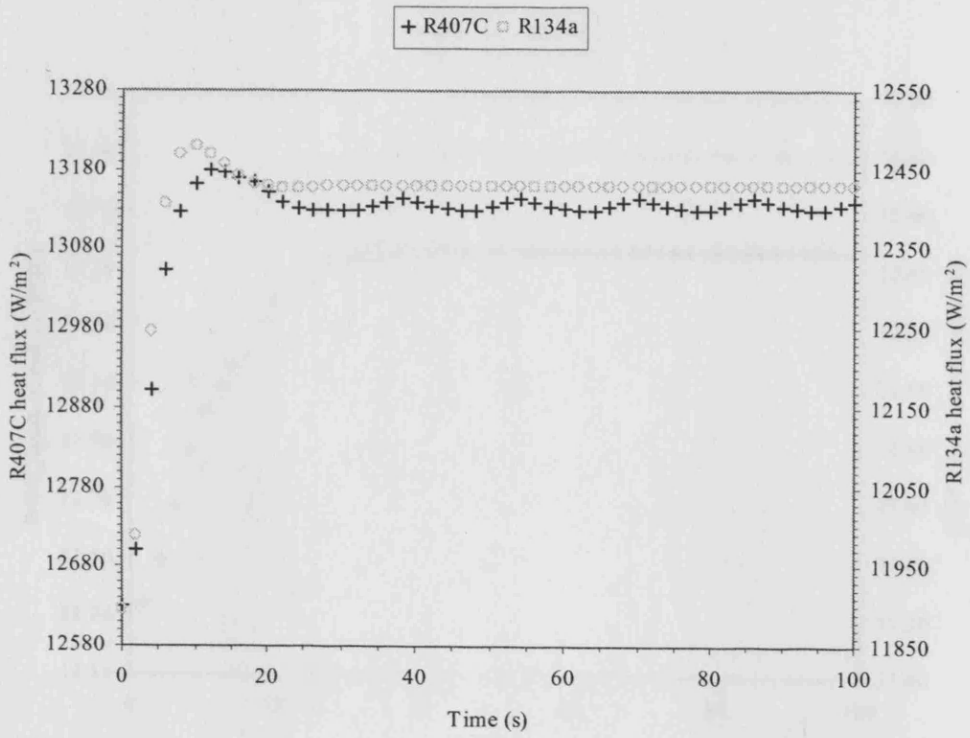

Figure 5.171 For 2-phase, ratios between refrigerant heat flux and HTC at Element (1,3,3) vs times for TEV-controlled dry coils, when there was a 0.5-degree-C increase in dry-bulb temperatures

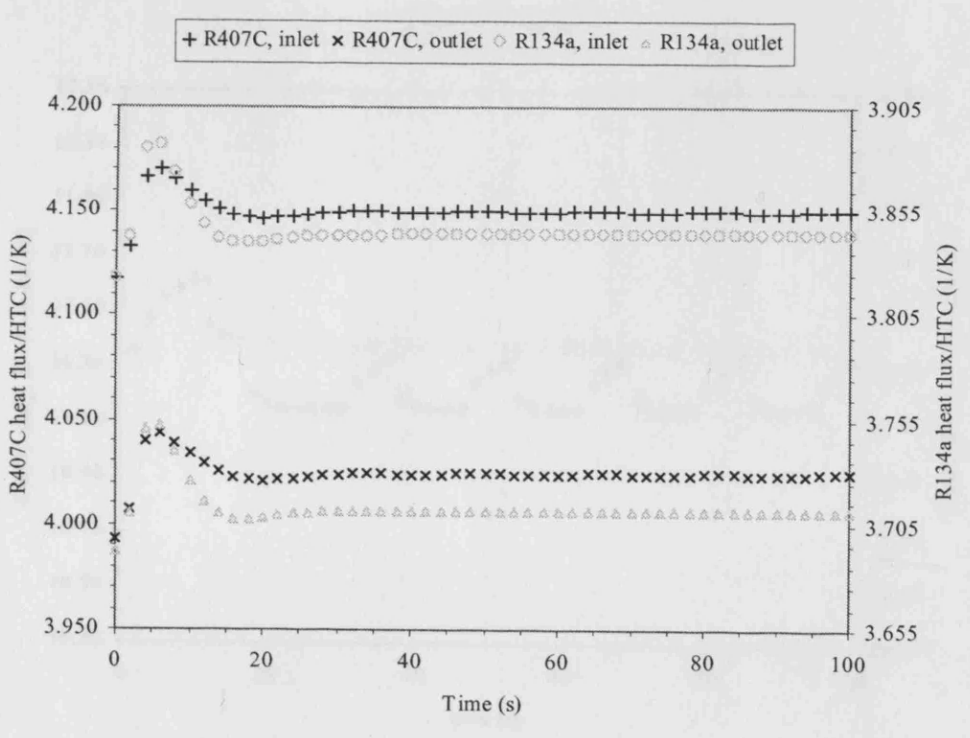

Figure 5.172 Refrigerant temperatures at the coil-outlet vs times for dry coils, when there was a 0.5-degree-C step increase in coil-inlet dry-bulb temperatures

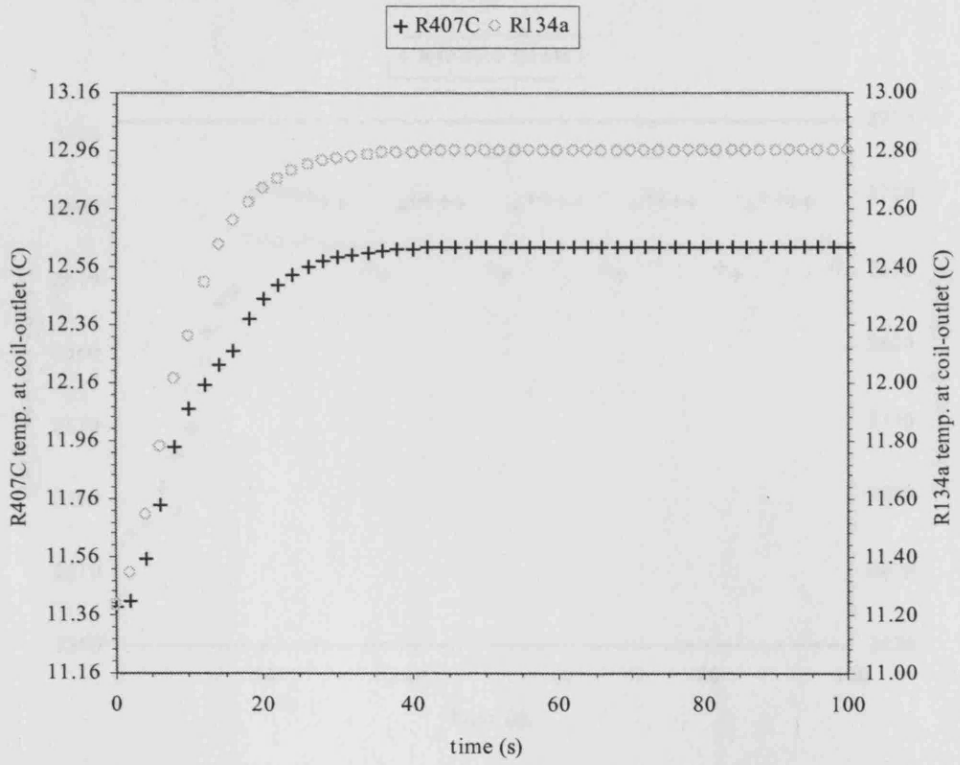

Figure 5.173 Refrigerant temperatures at the coil-outlet vs times for TEV-controlled dry coils, when there was a 0.5-degree-C step increase in coil-inlet dry-bulb temperatures

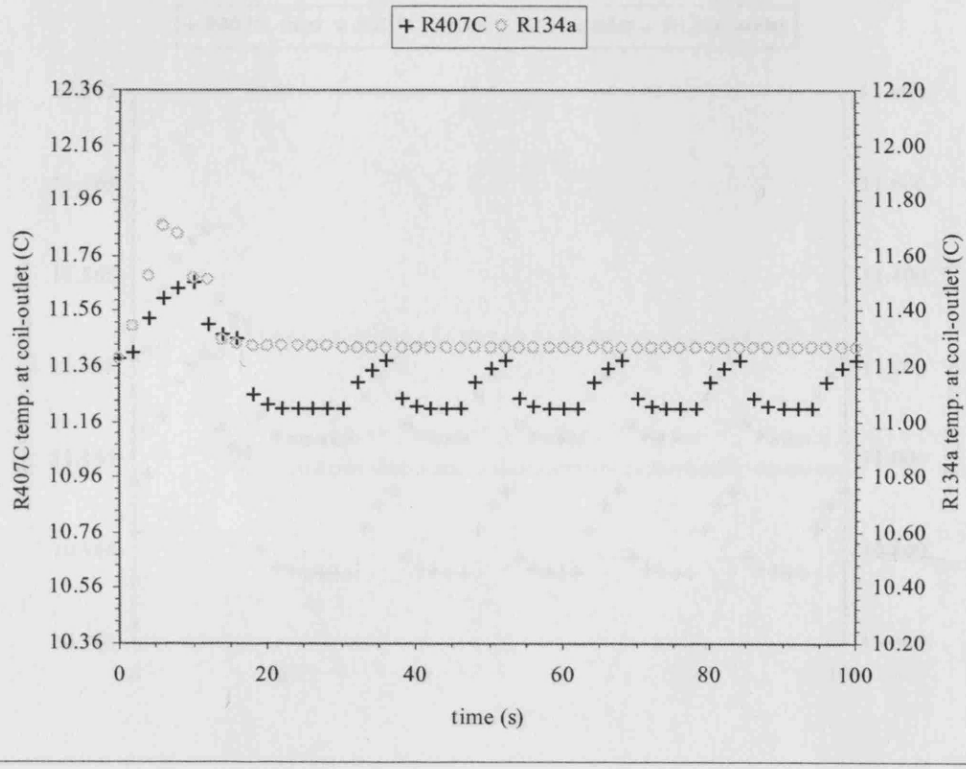

Figure 5.174 Superheat refrigerant heat fluxs at the last Sub-element of the coil vs times for TEV-controlled dry coils, when there was a 0.5-degree-C increase in dry-bulb temperatures

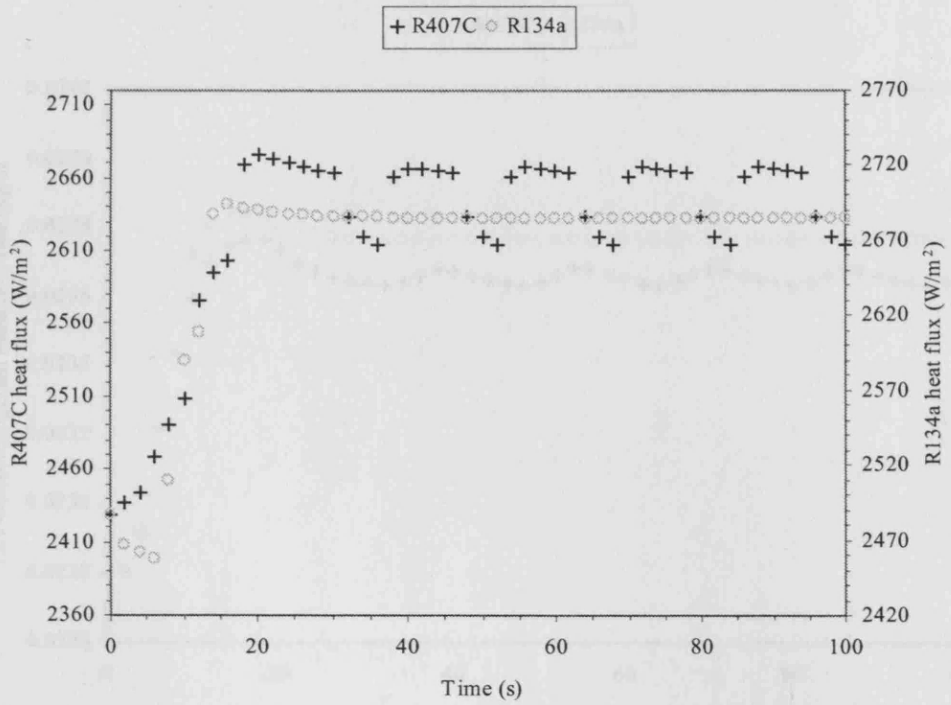

Figure 5.175 Superheat refrigerant temperatures at the last Sub-element of the coil vs times for TEV-controlled dry coils, when there was a 0.5-degree-C step increase in coil-inlet dry-bulb temperatures

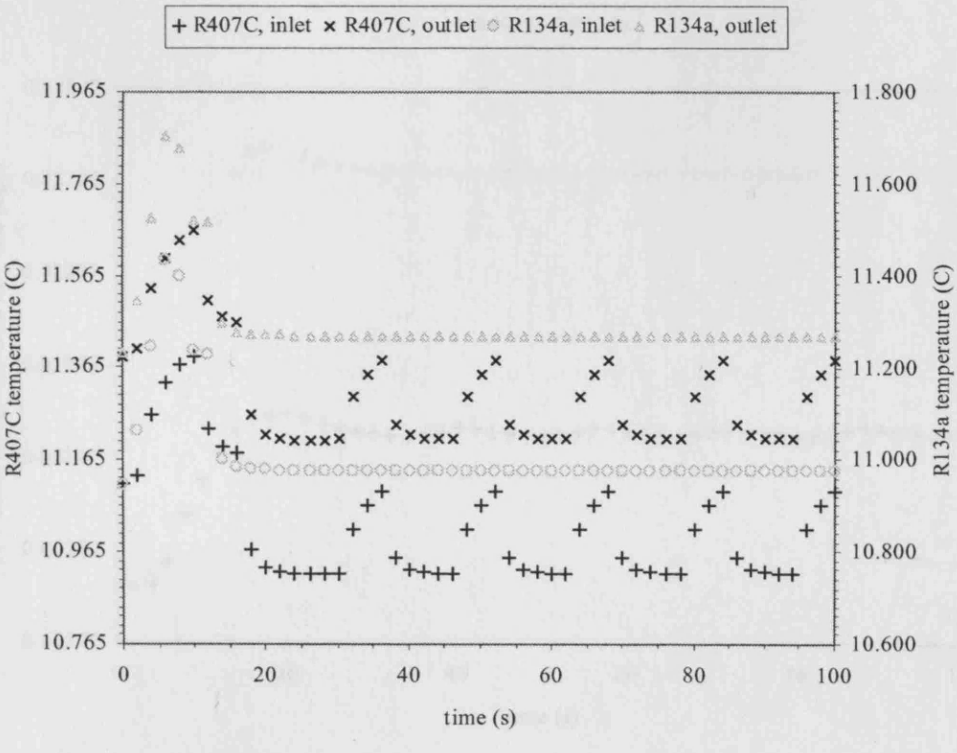

Figure 5.176 TEV-outlet refrigerant mass flow rates vs times for TEV-controlled dry coils, when having a 0.5-degree-C step increase in coil-inlet dry-bulb temperatures and assumed constant external equalizer pressure

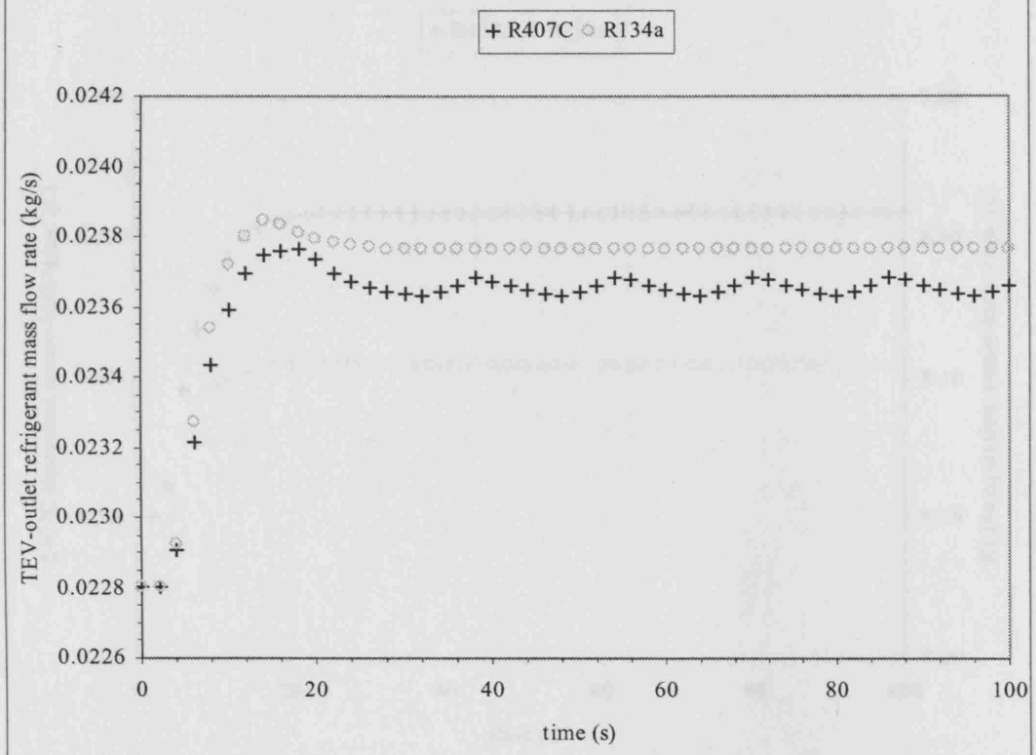

Figure 5.177 TEV-outlet refrigerant mass flow rates vs times for TEV-controlled dry coils, when having a 0.5-degree-C step increase in coil-inlet dry-bulb temperatures and assumed constant sensor-bulb pressure

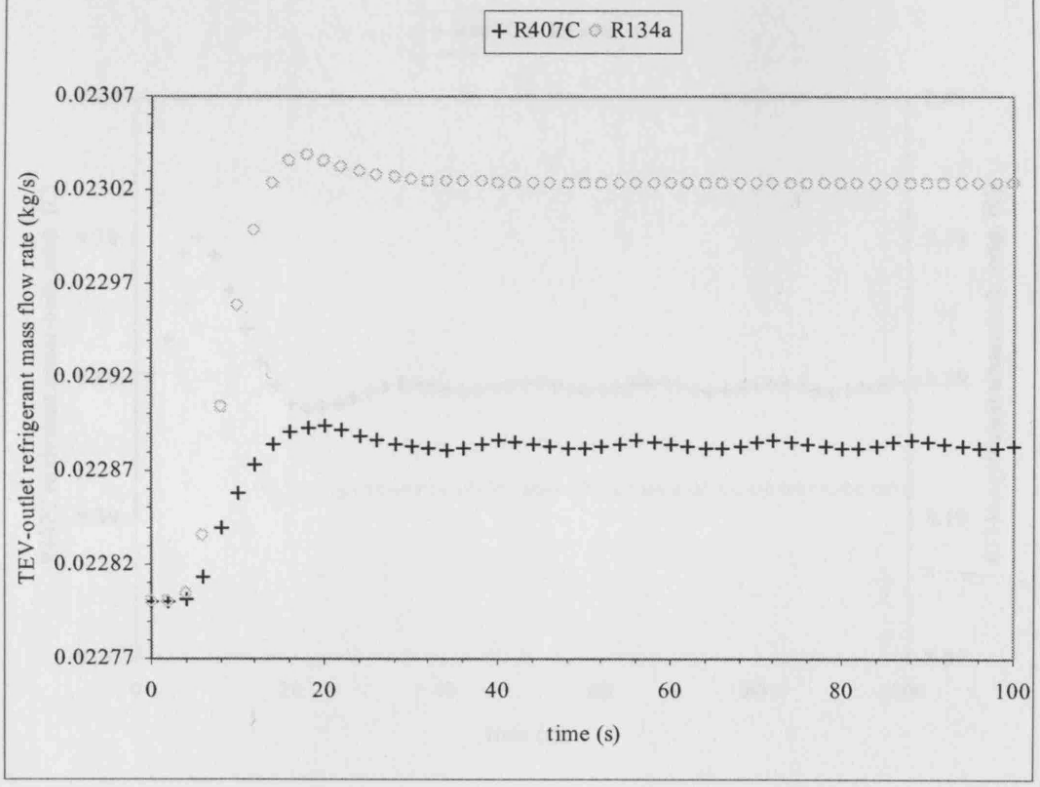

Figure 5.178 At outlets of Sub-eles. (1,5,2,4; R407C) and (1,5,2,1; R134a) just before the last Sub-eles. of 2-phase, equiv. bulb temp. at virtual TEVs vs times for dry coils for a 0.5-C step increase in coil-inlet DB temp.

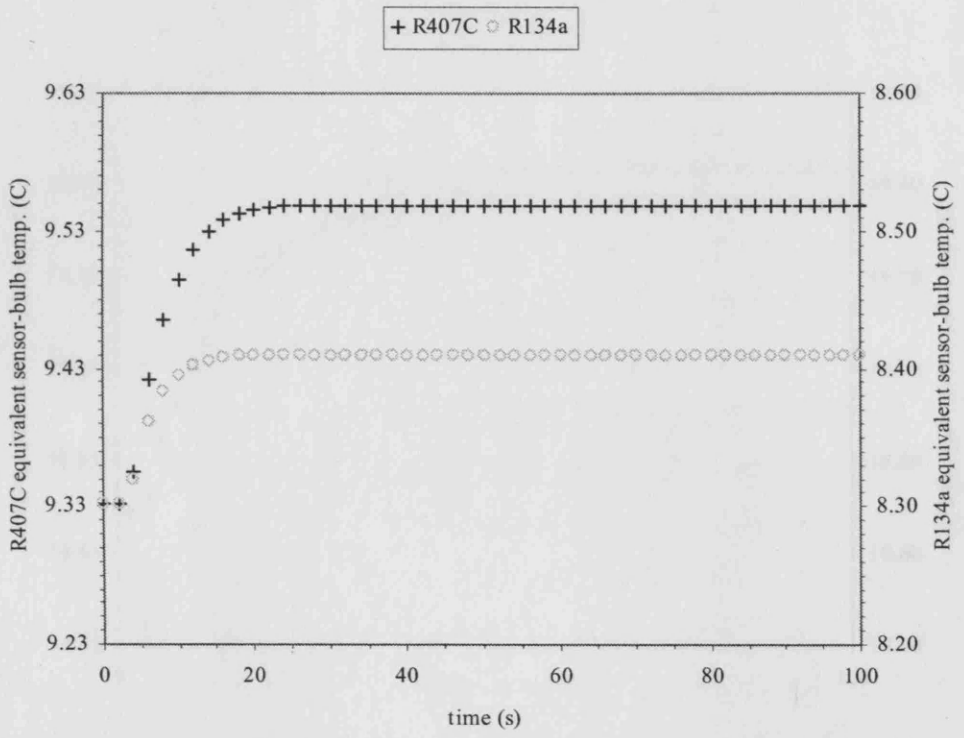

Figure 5.179 At outlets of Sub-eles. (1,5,3,1: R407C) and (1,5,2,3: R134a) just before the last Sub-eles. of 2-phase, equiv. bulb temp. at virtual TEVs vs times for TEV-controlled dry coils for a 0.5-C step increase in coil-inlet DB temp.

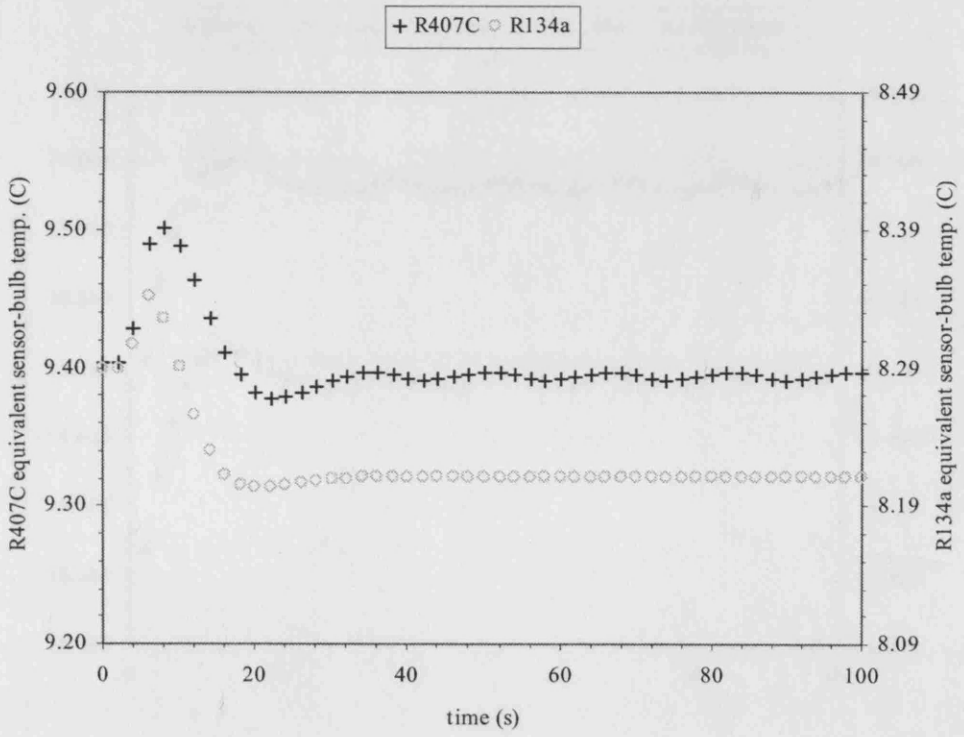

Figure 5.180 At the refrigerant coil-outlet, equivalent sensor-bulb temperatures at virtual TEVs vs times for dry coils, when there was a 0.5-degree-C step increase in coil-inlet dry-bulb temperatures

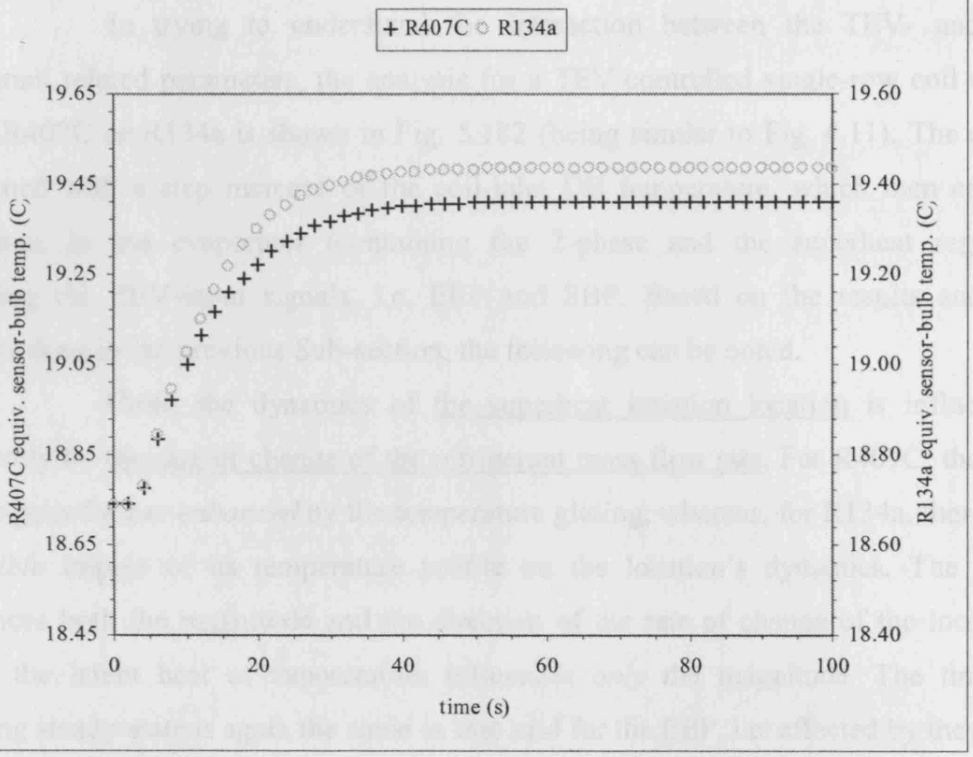

Figure 5.181 Superheat tube-wall temperatures at the last Sub-element of the coil vs times for TEV-controlled dry coils, when there was a 0.5-degree-C step increase in coil-inlet dry-bulb temperatures

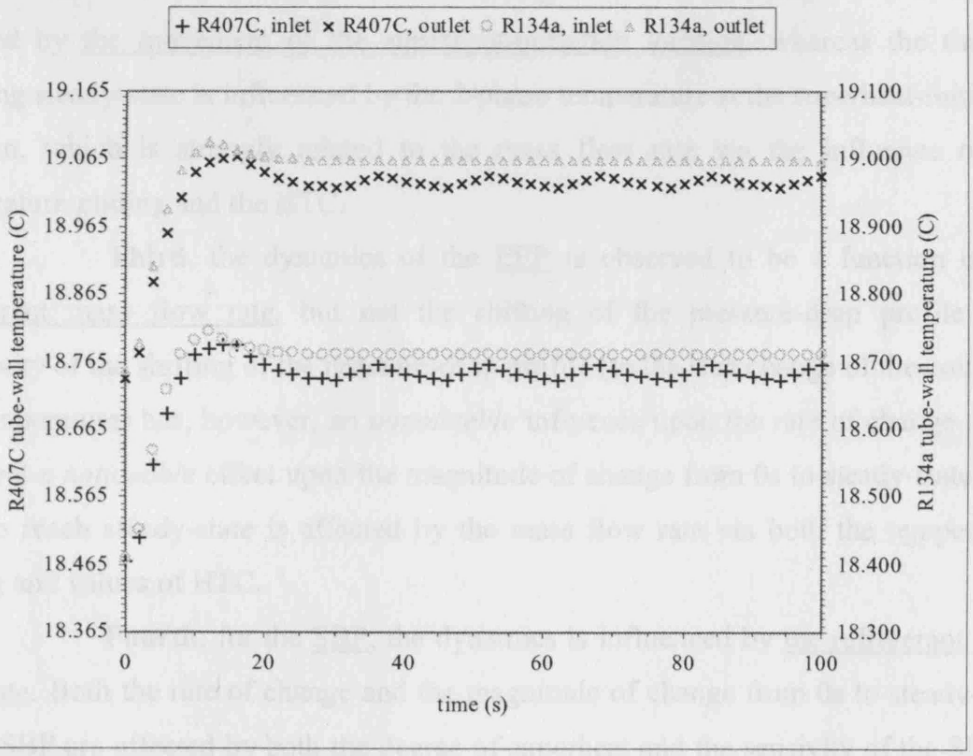

5.5.2 Main discoveries

In trying to understand the interaction between the TEV- and the refrigerant related parameters, the analysis for a TEV-controlled single-row coil using *either* R407C *or* R134a is shown in Fig. 5.182 (being similar to Fig. 4.11). The study concerned with a step increase of the coil-inlet DB temperature, which then caused transience in the evaporator (containing the 2-phase and the superheat regions) including the TEV-input signals, i.e. EEP and SBP. Based on the results and the analysis done in the previous Sub-section, the following can be noted.

First, the dynamics of the superheat intiation location is influenced sensitively by the rate of change of the refrigerant mass flow rate. For R407C, the rate of change is further *enhanced* by the temperature gliding, whereas, for R134a, there is a *negligible* impact of its temperature profile on the location's dynamics. The HTC influences both the magnitude and the direction of the rate of change of the location, whilst the latent heat of vaporization influences *only* the magnitude. The time to reaching steady-state is again the same as that said for the EEP, i.e. affected by the mass flow rate via both the temperature gliding and values of HTC.

Second, for the degree of superheat, the dynamics (including the rates of change with time and the magnitude of change from 0s to steady-state) is *mainly* affected by the movement of the superheat-initiation location, whereas the time to reaching steady-state is influenced by the 2-phase temperature at the superheat-initiation location, which is strongly related to the mass flow rate via the influence of the temperature gliding and the HTC.

Third, the dynamics of the EEP is observed to be a function of the refrigerant mass flow rate, but not the shifting of the pressure-drop profile. The sensitivity of the shifting of the pressure-drop profile (to the step change of the coil-inlet DB temperature) has, however, an *unnoticeble* influence upon the rate of change of the EEP, but a *noticeable* effect upon the magnitude of change from 0s to steady-state. The time to reach steady-state is affected by the mass flow rate via both the temperature gliding and values of HTC.

Fourth, for the SBP, the dynamics is influenced by the refrigerant mass flow rate. Both the rate of change and the magnitude of change from 0s to steady-state of the SBP are affected by both the degree of superheat and the sensivity of the SBP to

the SBT. The time to reaching steady-state is described the same way as that for the degree of superheat, i.e. influenced by the 2-phase temperature at the superheat-initiation location.

Fifth, for the dynamics of the refrigerant mass flow rate, the SBP is the main the influencing parameter, supplemented by the EEP.

Finally, in conclusion, in order to understand the function of the TEV in maintaining the degree of superheat, one needs to fullly appreciate both the influences of the *dynamics* of the superheat-initiation location (associated with the behaviour of the refrigerant in the coil), and the *time* for the temperature at the end of the 2-phase region to *reach steady-state*.

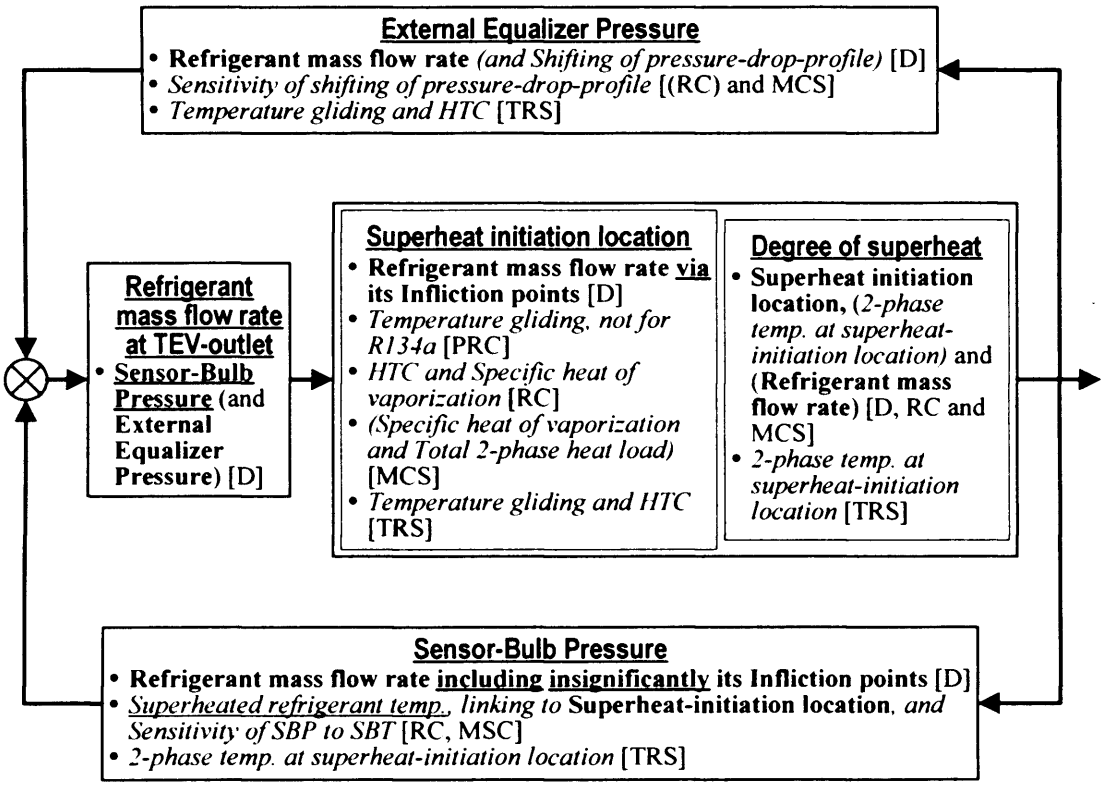

Figure 5.182 Based on the simulation of a single-row evaporator for both without- and with- TEV cases, the analysis of the TEV-controlled coil was proposed. **NB** "D"=Dynamics, "RC" =Rate of Change with time, "MCS" =Magnitude of change from 0s to steady-state, "TRS" =Time to Reaching Steady-state, "PRC" =Pattern of Rate of Change with time. The disturbance was a step increase of the coil-inlet DB temperature.

Chapter 6 Conclusion

6.1 Summary

The research concerned with a numerical investigation into steady and dynamic behaviour of direct-expansion air coolers. The main aim was to understand the influences of the unique characteristics of the ternary-mixture and pure (or single component) refrigerants on the cooler coil behaviour. R407C and R134a were chosen respectively for this study. The research programme was systematically started off with the dry coil simulations, and followed by the wet coils and the TEV-controlled coils (also run under dry conditions). Under the same air coil-inlet conditions, the performance of the two refrigerants were compared by setting the same steady-state values of mass flow rates and vapour qualities at the refrigerant coil inlets and of the temperature at the refrigerant coil outlets.

A distributive model, in which each of the tube was divided into elements, was constructed; this type of the model was particularly suitable for dynamic study. For developing the balancing/governing equations, for each element, the moist air contained the energy and condensate balances; the fin and tube-wall had energy balance and the refrigerant flow involved the continuity, momentum and energy balances. For the TEV, the energy equations were set up for the sensor bulb. At the diaphragm-and-needle valve linking the external equalizer, the equation for the regulated refrigerant mass flow rate involved the needle movement and the associated changes in the valve flow area. In the modelling and simulations, various problems were encountered and the solutions to them were fully discussed.

No experimental work was conducted in this study but the models were validated as far as practically possible based on published data. In addition, from

published works, the correlations and equations for the air-side HTC, the refrigerant HTC and pressure-drop, and the TEV mass flow rate were carefully reviewed for adoption. In all simulations, the refrigerant properties were obtained from REFPROP via a custom built software interface, run initially at steady state and later at dynamic state with either a step increase or decrease of the coil-inlet air DB temperature.

For the results and discussion, this is the first comprehensive set of dynamic data of evaporator run on mixtures and the author was not aware of any other published literatures on the dynamic study of this kind. It enabled us to enhance our understanding of the interactions of various properties and parameters, particularly the effects of the refrigerant type and the temperature gliding on the dynamic behaviour of the coil. The selection of the studied parameters, for both dry- and wet- coils, was governed by the refrigerant-and-air behaviour, the superheat effect, the pressure drop and the heat transfer potential. As for the TEV, the parameters were chosen in order to study the influence of the type and mass flow rate of the refrigerants upon operation of the TEV-controlled coils.

6.2 Main observations and findings

Based on the simulation on the chosen coil configurations and with the specific designed refrigerant comparison scheme, the following original findings were made.

6.2.1 Dry coils

Since the wet coils share many result details with the dry coils, these were mentioned later together in Section 6.2.2. Regarding the transient process of the dry coil, when having a disturbance, the accumulated heat in the fins and tubes, based on the governing equations, was observed to be the main parameter that induced the transient process.

The dynamic interactions of 5 main parameters, namely, the 2-phase refrigerant temperature, the 2-phase refrigerant HTC, the refrigerant heat flux, the latent heat of vaporization and the superheat-initiation location, via simulation, were found to govern the overall transient process, i.e. their magnitude, direction and rate of change. Each of these 5 parameters can be linked either directly or indirectly to the refrigerant properties.

6.2.2 Totally-wet coils

The findings were applicable to both refrigerants and both coil conditions (dry and wet), unless otherwise stated.

a) Steady-state

The combined effects of the temperature-glide and the refrigerant-HTC affect the latent and sensible heat loads in certain parts of the coil and the overall condensate rate. The condensate rates of the entire coil of R407C are larger than that of R134a, but the localised rates can follow different patterns/trends.

Through simulations, the temperature-glide was noticed to influence the outlet-DB temperature of the last row, the spatial variations of the refrigerant heat flux, the tube-wall temperature, the saturated HR on tube-wall, and the outlet HR. The magnitudes of temperature glide-up (a unique characteristic of zeotropic refrigerants) of R407C and the temperature drop of the R134a are of different values under dry or wet conditions, resulting in different spatial gradients of the above parameters. It was also observed that the influence of the effective air-side HTC and the fin efficiency on the refrigerant heat fluxes is suppressed by the more dominant effects of the temperature glide and the refrigerant HTC.

The coil arrangement was observed to affect the spatial distribution profiles of both the DB temperature and HR of the row inlets; and the combined influences of the temperature-glide and the coil-arrangement have an impact on the sensible heat flux (via the tube-wall temperature and the row-inlet DB temperature, respectively) and the condensate flux (via the difference between the saturated HR on tube-wall (affected by temperature glide) and the inlet HR (affected by coil arrangement)).

The combined effects of the temperature-glide, the refrigerant-HTC and the coil-arrangement were found to suppress the influences of the effective MTC and the latent heat of condensation on the mass and heat transfer, i.e. on the condensate flux and the latent heat flux, respectively.

Regarding the refrigerant-type effect, when R407C was compared to R134a, the followings were noticed. R407C has higher operating pressure, a smaller pressure drop, a higher sensitivity of the change of the 2-phase temperature to heat-flux (but, for R134a, being more dependent on pressure drop), a shorter superheat region, a similar spatial profile of HTC. In addition, both wet and dry coils have about the same

ratios of R407C to R134a for the operating pressure, the pressure drop, the HTC and the heat load. For the 2-phase region, both refrigerants have about the same values of the HTC for most length along the coil, except for the last 25% of the region that R407C has slightly smaller values than R134a.

Depending on the location, the superheat effect of individual refrigerant has an influence on the smoothness of profiles along the coil of the refrigerant heat flux and the air-side parameters, whereas the coil arrangement affects the spatial gradients too.

Based on the simulations, the wet coils suffer larger pressure drops than the dry coils. Furthermore, for the wet coils, the temperature gliding-up (for R407C) was smaller than the temperature drop (for R134a), whereas the reverse happened under the dry conditions.

b) Dynamic

It was found that, in the dynamics, the refrigerant temperature glide influences the magnitude and the direction of change of the gradients of the profiles of the DB temperature and HR at the coil-outlet tubes verses distance that are unaffected by the superheat. R407C and R134a therefore have opposite trends of changes.

As a result of the refrigerant-type effect, when compared to R134a, R407C has a slower response of refrigerant pressures, and a lower sensitivity of the pressure-drop-profile shifting when subjected to a step disturbance of inlet DB temperature. The observations also reveal that, for any refrigerant, the time variations of the coil-outlet pressure and the local pressure drop under the dry coil are similar to that under wet conditions. In addition, concerning the refrigerant temperature, R407C has a smaller rate of change of the coil-outlet refrigerant temperature than R134a. For the ratio of the magnitude of swinging of the coil refrigerant temperature for R407C to that for R134a, the wet coil had a smaller value than the dry coil. For the local 2-phase temperatures, R407C has mainly larger rates of change than R134a. As for the local tube-wall temperature, for the rate of change (±), for R407C, it behaves the same as that of the coil-inlet DB temperature, whereas, for R134a, it could be different. Furthermore, the HTCs of the two refrigerants have the same direction for the magnitude of change in response to a step change of the coil-inlet DB temperature. In the 2-phase region, the HTC of R407C has a smaller rate of change for the whole region, and for a large part of the coil, a smaller magnitude of change than R134a.

The shifting of the 2-phase pressure drop was noticed to be sensitive to the change of the coil-inlet DB temperature. The former obviously has a direct influence on the dynamics of the local pressure.

As the superheat region experiences a lot more the refrigerant temperature change per unit tube length than in the 2-phase, it thus controls the magnitude of change of the coil-outlet refrigerant temperature during the transient period of individual refrigerant. In addition, the superheat effect was found to influence the response of the outlet DB temperature.

Regarding the effect of running wet, when compared to the dry condition, a wet coil has a larger refrigerant mass flow rate, with correspondingly a larger pressure drop; hence, the magnitude of change of the coil-outlet pressure is larger. For the local 2-phase temperatures along the coil, the magnitudes of change for R407C had smaller values under wet coil than the dry coil, whereas, R134a had smaller values under dry conditions. Further, when compared to R134a, R407C had substantially more variations of the local 2-phase temperatures along the coil under wet condition, whereas, for dry coils, the variations of R407C were insignificant. This reflects the importance of understanding the interaction between refrigerant type and operating conditions on the rates of change of local 2-phase temperatures.

The rates of change of the local air heat fluxes (and the coil-outlet DB temperatures) were found to be dependent on the combined effects of the effective HTC of air and the inlet-DB-and-wall temperature difference, though the relative degree of dependence on the two effects was found to be a function of locations taking in account of superheat region. The same comment also applies to the understanding of the combined influences of the effective MTC and the HR difference upon the local condensate rates and the coil-outlet HRs.

6.2.3 TEV-controlled coils

The study revealed the influences of several TEV, refrigerant-type and temperature-glide related parameters upon the behaviour of the coils.

The TEV related parameters include (1) the refrigerant mass flow rate, (2) the SBP and (3) the EEP. The mass flow rate was found to affect the dynamics of the superheat initiation location, as well as the dynamics of the sensor bulb and external equaliser pressures. As in the TEV feedback loop, the SBP and EEP in turn regulate the mass flow rate, though it was found that the SBP has a lot more impact than the EEP.

Refrigerant-type related parameters include (1) the HTC, (2) the latent heat of vaporization, (3) the superheat-initiation location, (4) the sensitivity of the pressure-drop profile shifting to change of the coil-inlet DB temperature, and (5) both the degree of superheat and the sensitivity of the SBP to the change in SBT.

The study shows that, for the rate of change of the initiation location, the HTC influences both its magnitude and direction, whereas the latent heat of vaporization (R407C being slightly larger than R134a) affects only the magnitude. The initiation location itself influences the dynamics of the degree of superheat. It was noticed that the sensitivity of the shifting of the pressure drop profile has an influence on the magnitude of change of EEP between steady states, whereas both the rate of change and the magnitude of change of SBP was dependent on the combined effects of the degree of superheat, and the relation between SBP and SBT.

The temperature-glide involves three parameters, namely: (1) the temperature-glide, (2) the combined effect of the temperature gliding and the HTC, and (3) the 2-phase temperature at the superheat-initiation location (strongly linked to the second parameter). The temperature glide was shown to have am impact upon the rate of change of the superheat-initiation location for zeotropic mixtures, but not for the pure refrigerants. As for the transit time between steady states, the second parameter influences both the superheat-initiation location and the EEP, whereas the third parameter affects both the degree of superheat and the SBP.

6.3 Concluding remarks and future work

The work successfully provides a very comprehensive set of data through simulation and enables a deeper insight into the interactions of various refrigerant and coil configuration related parameters, and their influence on the dynamic process of many operation parameters of plate fin direct expansion evaporators. Further understanding was gained regarding the how refrigerant types influences the operation a TEV controlled evaporator. It is believed that the model developed can be coupled with models of other system components to form a complete system to study overall system dynamics.

The future simulation can be extended to cover a wider input range of inlet air condition and/or various types of disturbance. For the TEV, the future investigation should focus on the influence of refrigerant type on the occurrence of hunting. The effect of shift in circulation composition can be added, should the work be

extended to a full system simulation. The problem of partially-wet coil has not been fully resolved and still needs further efforts. The model can also be expanded to include frost dynamics.

Appendix A

Appendix A listed the standard equations employed for air property and psychrometry calculations and provided details of coil configurations considered in this study. It also gave the general equations for two- and single-phase calculations. A procedure used for calculating the two-phase heat transfer coefficient of a ternary zeotropic refrigerant mixture was explained in details.

A.1 Air

General properties: Based on Incropera and Witt's [1990] and Welty et al.'s [1984] documents, the specific heat capacity is estimated as Eq. A.1.

$$c_{p,a} = 1.005\text{E}3 \ \text{J}/\left(\text{kg}_{\text{dryair}} \cdot \text{K}\right) \tag{A.1}$$

The other properties for temperature range between 100 K to 400 K are shown as follows:

$$\mu_a = 10^{-7}\begin{pmatrix}(-0.000398571428571)\,T_{db}^2 \\ +(0.726928571428573)\,T_{db} \\ +2.80714285714267\end{pmatrix} \tag{A.2}$$

$$\text{Pr}_a = 0.0000008\,T_{db}^2 - 0.00071\,T_{db} + 0.847785714285715 \tag{A.3}$$

$$\nu_a = 10^{-6}\begin{pmatrix}(0.000123095238095)\,T_{db}^2 \\ +(0.020250952380952)\,T_{db} \\ -1.3191428571428\end{pmatrix} \tag{A.4}$$

$$D_{wa} = 10^{-7}\begin{pmatrix}(0.00232734400687)T_{db}^{2}\\+(0.236002581533186)T_{db}\\-18.7501563085351\end{pmatrix} \tag{A.5}$$

$$\rho_a = (376.412989079179)T_{db}^{(-1.01348380939561)} \tag{A.6}$$

Psychrometric: Psychrometry equations, taken from an ASHRAE handbook [1993], are as follows. The pure-water saturation vapour pressure over liquid water for the temperature range 273.15 K to 473.15 K is given by Eq. A.7.

$$p_{ws} = 1000\left(\mathrm{Exp}\begin{pmatrix}\left(\frac{-5.8002206E+3}{T_{db}}\right)-5.516256\\-(4.8640239E-2)T_{db}+(4.1764768E-5)T_{db}^{2}\\-(1.4452093E-8)T_{db}^{3}+6.5459673(\ln(T_{db}))\end{pmatrix}\right) \tag{A.7}$$

The pure-water saturation vapour pressure over ice for the temperature range 173.15 K to 273.15 K is given by Eq. A.8.

$$p_{ws} = 1000\left(\mathrm{Exp}\begin{pmatrix}\left(\frac{-5.6745359E+3}{T_{db}}\right)-5.1523058E-1\\-(9.677843E-3)T_{db}+(6.2215701E-7)T_{db}^{2}\\+(2.0747825E-9)T_{db}^{3}-(9.484024E-13)T_{db}^{4}\\+4.1635019(\ln(T_{db}))\end{pmatrix}\right) \tag{A.8}$$

The humidity ratio at saturation, the humidity ratio, the relative humidity and the water-vapour partial pressure are as in Eqs. A.9 to A.12.

$$W_s = \frac{0.62198p_{ws}}{(p_{wa}-p_{ws})} \tag{A.9}$$

$$W = \frac{\begin{pmatrix}(2501-2.38(T_{wb}-273.15))W_{s,T_{wb}}-\\((T_{db}-273.15)-(T_{wb}-273.15))\end{pmatrix}}{(2501-1.805(T_{db}-273.15)-4.186(T_{wb}-273.15))} \tag{A.10}$$

$$R_h = \frac{\left(\frac{W}{W_s}\right)}{\left(1-\left(1-\frac{W}{W_s}\right)\left(\frac{p_{ws}}{p_{wa}}\right)\right)} \tag{A.11}$$

$$p_w = \frac{p_{wa} W}{(0.62198 + W)} \tag{A.12}$$

The dew-point temperature for the range from 273.15 K to 366.15 K is calculated from Eq. A.13.

$$T_{dp} = \begin{pmatrix} 6.54 + 14.526\left(\ln\left(\frac{p_w}{1000}\right)\right) + 0.7389\left(\ln\left(\frac{p_w}{1000}\right)\right)^2 \\ + 0.09486\left(\ln\left(\frac{p_w}{1000}\right)\right)^3 + 0.4569\left(\frac{p_w}{1000}\right)^{0.1984} \end{pmatrix} + 273.15 \tag{A.13}$$

For the dew-point temperature below 273.15 K, it is determined from Eq. A.14.

$$T_{dp} = \left(6.09 + 12.608\left(\ln\left(\frac{p_w}{1000}\right)\right) + 0.4959\left(\ln\left(\frac{p_w}{1000}\right)\right)^2\right) + 273.15 \tag{A.14}$$

The moist-air specific enthalpy can be obtained from Eq. A.15.

$$i_{wa} = 1000\begin{pmatrix} 1.006(T_{db} - 273.15) + \\ W(2501 + 1.805(T_{db} - 273.15)) \end{pmatrix} \tag{A.15}$$

A.2 Coil

Turaga et al.'s evaporators: Its details [Turaga et al. 1988a, 1988b] shown in Table A.1 were used as a guideline for configuring evaporators in this thesis.

Table A.1 The parameters of Turaga et al.'s evaporators [1988a, 1988b] - fixed and variable

Fixed parameters			
Coil height	C_H	m	0.559
Coil width	C_W	m	1.219
Tube transverse spacing	S_T	m	0.0381

Tube longitudinal spacing	S_L	m	0.0381
Flat-plate aluminium fin thickness	w_{fin}	m	0.00016
Tube inside diameter	$D_{ID,tube}$	m	0.0126
Tube outside diameter	$D_{OD,tube}$	m	0.0134

Variable parameters

coil no.	N_R [N/A]	P_s [fin/m]	D_h [m]	A_{mf}/A_F [D/L]	N_{TR} [N/A]	L_d [m]	$A_{o,total}/A_p$ [D/L]	$A_{o,total}/A_{wall,t}$ [D/L]	s_{fin}/w_{fin} [D/L]
1	3	390	0.0032	0.58	15	0.114	26.5	27.0	17.2
2	3	470	0.0027	0.57	15	0.114	31.8	32.2	14.4
3	3	550	0.0022	0.56	15	0.114	37.2	37.4	12.3
4	4	550	0.0022	0.56	15	0.152	37.2	37.4	12.3
5	6	310	0.0040	0.60	15	0.229	21.2	21.8	21.6
6	6	390	0.0032	0.58	15	0.229	26.5	27.0	17.2
7	6	470	0.0027	0.57	15	0.229	31.8	32.2	14.4
8	8	310	0.0040	0.60	15	0.305	21.2	37.4	12.3
9	8	390	0.0032	0.58	15	0.305	26.5	27.0	17.2
10	8	550	0.0022	0.56	15	0.305	37.2	37.4	12.3

Coil configuration and coil-related variables: Details of a coil for the thesis consisted of three parts (Table A.2): physical properties, Turaga-based parameters and calculable parameters/variables.

Table A.2 The configurations and the related variables of coils

The physical-properties part [Incropera & Witt 1990]		
Aluminium density	kg/m^3	2702
Copper density	kg/m^3	8933

Aluminium specific heat capacity at constant pressure		J/(kg·K)	903
Copper specific heat capacity at constant pressure		J/(kg·K)	385
Aluminium thermal conductivity		W/(m·K)	237
Copper thermal conductivity		W/(m·K)	401
The Turaga-based-parameters part			
Coil width	C_w	m	1.219
Tube inside diameter	$D_{ID,tube}$	m	0.0126
Tube outside diameter	$D_{OD,tube}$	m	0.0134
Tube transverse spacing	S_T	m	0.0381
Tube longitudinal spacing	S_L	m	0.0381
Flat-plate aluminium fin thickness	w_{fin}	m	0.00016
Numbers of rows	N_R	N/A	3
Numbers of tubes per row	N_{TR}	N/A	15
Fin spacing to fin thickness ratio	s_{fin}/ w_{fin}	D/L	12.3

The calculable-parameters-or-variables part			
Coil height	m	$C_H = N_{TR} S_T$	(A.16.1)
Fin density	fin/m	$P_s = \frac{1}{\left(\frac{s_{fin}}{w_{fin}}\right) w_{fin}}$	(A.16.2)
Coil depth	m	$L_d = N_R S_L$	(A.16.3)
Coil-face area	m^2	$A_F = C_H C_W$	(A.16.4)
Equivalent fin diameter	m	$D_{fin,eq} = \left(\frac{4 S_T S_L}{\pi}\right)^{(1/2)}$	(A.16.5)
Tube diagonal spacing	m	$S_D = \left(\left(\frac{S_T}{2}\right)^2 + S_L{}^2\right)^{(1/2)}$	(A.17.1)
Fin obstruction factor (Sisamos 1994)	D/L	$F_{obs} = 1 - \left(\frac{w_{fin} P_s C_W}{C_W}\right)$	(A.17.2)
Ratio of minimum flow area to coil-face area (Sisamos 1994)	D/L	If $2(S_D - D_{OD,tube}) > (S_T - D_{OD,tube})$ then	

		$\left(\frac{A_{mf}}{A_F}\right)=\left(\frac{S_T}{S_T F_{obs}-D_{OD,tube}}\right)^{(-1)}$, otherwise	(A.17.3)
		$\left(\frac{A_{mf}}{A_F}\right)=\left(\frac{S_T}{2(S_D F_{obs}-D_{OD,tube})}\right)^{(-1)}$	(A.17.4)
Air mass flux at minimum flow area (Sisamos 1994)	kg/(s·m^2)	$G_{a,mf}=\frac{G_a}{\left(\frac{A_{mf}}{A_{cf}}\right)}$	(A.17.5)
Primary surface area of tube wall	m^2	$A_p=\pi D_{OD,tube} N_{TR} N_R C_W$	(A.18.1)
Outside tube-wall surface area between fins	m^2	$A_{wall,o}=\pi D_{OD,tube}\left(P_s^{-1}-w_{fin}\right)P_s N_{TR} N_R C_W$	(A.18.2)
Surface area of fins with negligence of surface area due to fin thickness	m^2	$A_{fin}=2\left(S_T S_L-\frac{\pi D_{OD,tube}^2}{4}\right)P_s N_{TR} N_R C_W$	(A.18.3)
Total air side surface area	m^2	$A_o=A_{fin}+A_{wall,o}$	(A.18.4)
Coil hydraulic diameter (Turaga 1988)	m	$D_h=4\left(\frac{A_{mf}}{A_F}A_F\right)\left(\frac{L_d}{A_o}\right)$	(A.18.5)
Mass of tube per unit length	kg/m	$m_{tube}=\frac{\pi\left(D_{OD,tube}^2-D_{ID,tube}^2\right)\rho_{tube}}{4}$	(A.19.1)
Mass of fin per unit length	kg/m	$m_{fin}=\left(S_T S_L-\frac{\pi D_{OD,tube}^2}{4}\right)w_{fin} P_s \rho_{fin}$	(A.19.2)

A.3 Refrigerant

Equations for general calculations of two- and single- phases, and equations, data and procedures for the two-phase HTC calculation of a zeotropic refrigerant mixture were given.

General equations for two-phase flow: The average velocity can be calculated from Eq. A.20:

$$\bar{u}_{ref}=\frac{G_{ref}}{\bar{\rho}_{ref}} \tag{A.20}$$

where the mass flux is shown in Eq. A.21:

$$G_{ref} = \frac{\dot{m}_{ref}}{A_{tube}} = \frac{\dot{m}_{ref}}{\left(\frac{\pi D_{ID,tube}^2}{4}\right)} \tag{A.21}$$

The mass flux can also be detailed as a function of liquid-and-vapour parameters as Eq. A.22.1:

$$\begin{aligned} G_{ref} &= G_{ref,v} + G_{ref,l} = G_{ref}x + G_{ref}(1-x) \\ &= \frac{\dot{m}_{ref,v}}{A_{tube}} + \frac{\dot{m}_{ref,l}}{A_{tube}} \\ &= \frac{\rho_{ref,v} u_{ref,v} A_{tube,v}}{A_{tube}} + \frac{\rho_{ref,l} u_{ref,l} A_{tube,l}}{A_{tube}} \\ &= \rho_{ref,v} u_{ref,v} \alpha + \rho_{ref,l} u_{ref,l} (1-\alpha) \end{aligned} \tag{A.22.1}$$

where

$$\alpha = \frac{A_{tube,v}}{A_{tube}} \tag{A.22.2}$$

$$(1-\alpha) = \frac{A_{tube,l}}{A_{tube}} \tag{A.22.3}$$

With Eqs. A.20 and A.22.1, the average density can be shown in Eq. A.23.1.

$$\begin{aligned} \bar{\rho}_{ref} &= \frac{G_{ref,v} + G_{ref,l}}{\bar{u}_{ref}} \\ &= \frac{\rho_{ref,v} u_{ref,v} \alpha}{\bar{u}_{ref}} + \frac{\rho_{ref,l} u_{ref,l} (1-\alpha)}{\bar{u}_{ref}} \end{aligned} \tag{A.23.1}$$

For the homogeneous flow model that the slip factor equals to one, i.e. the same value of the vapour and the liquid velocities, then the average density is as Eq. A.23.2.

$$\bar{\rho}_{ref} = \alpha \rho_{ref,v} + (1-\alpha)\rho_{ref,l} \tag{A.23.2}$$

In addition, Reynolds number for total-flow-assumed-liquid can be shown as Eq. A.23.3.

$$Re_{fo} = \frac{GD_{ID}}{\mu_l} \tag{A.23.3}$$

General equations for single-phase flow:

$$u_{ref} = \frac{G_{ref}}{\rho_{ref}} \tag{A.24}$$

$$Re_{ID,ref} = \frac{G_{ref} D_{ID,tube}}{\mu_{ref}} \tag{A.25}$$

$$Pr_{ref} = \frac{\mu_{ref} c_{p,ref}}{k_{ref}} \tag{A.26}$$

$$Nu_{ID,ref} = \frac{h_{ref} D_{ID,tube}}{k_{ref}} \tag{A.27}$$

General equations and variables for refrigerant mixture: For the critical pressure of a mixture, it can be obtained from Eq. A.28 (Perry & Chilton 1973):

$$p_{c,m} = p_{c,m,ideal}\left(9\left(\frac{\sum\left(X_i\left(\frac{T_{nbp,i}}{100}\right)^2\right)}{\left(\sum\left(X_i\left(\frac{T_{nbp,i}}{100}\right)\right)\right)^2} - 1\right) + 1\right) \tag{A.28}$$

where

$$p_{c,m,ideal} = \Sigma\left(X_i p_{c,i}\right) \tag{A.29}$$

In order to calculate the the surface tensions of R407C (R32/R125/R134a: 0.23/0.25/0.52 by weight), it is necessary to know the surface tensions of R32, R125 and R134a, being obtainable from Eqs. A30 to A.32, respectively. The equations were resulted from the curve fitting of the data in the range from 193.15 K to 313.15 K, given from Refprop (Huber 1996).

$$\begin{aligned}&\sigma_{R32} = \\ &0.000000000833333T_{R32}^3 - 0.00000032975T_{R32}^2 - \\ &0.000210843214583T_{R32} + 0.077931464523756\end{aligned} \tag{A.30}$$

$$\sigma_{R125} = 0.000000000703125T_{R125}^3 - 0.000000304300781T_{R125}^2 - 0.000121392897852T_{R125} + 0.048402963200945 \quad (A.31)$$

$$\sigma_{R134a} = 0.000000000585938T_{R134a}^3 - 0.000000271664342T_{R134a}^2 - 0.000130554282436T_{R134a} + 0.055827495809754 \quad (A.32)$$

The surface tension of R407C can be calculated from Eq. A.33 (Reid et al. 1987).

$$\sigma_m = \left(\rho_{l,m} \sum \left(\frac{X_i \sigma_i^{(1/4)}}{\rho_{l,i}} \right) \right)^4 \quad (A.33)$$

For other properties of each component in R407C, it was shown in Table A.3.

Table A.3 Some physical and thermodynamics properties of each component of R407C

Molecular weight of R32	M_{R32}	gm/gmole	52.02
Molecular weight of R125	M_{R125}	gm/gmole	120.02
Molecular weight of R134a	M_{R134a}	gm/gmole	102.03
Critical pressure of R32	$p_{c,R32}$	Pa	5795000
Critical pressure of R125	$p_{c,R125}$	Pa	3629000
Critical pressure of R134a	$p_{c,R134a}$	Pa	4067000
Normal boiling point temperature of R32	$T_{nbp,R32}$	K	221.4
Normal boiling point temperature of R125	$T_{nbp,R125}$	K	225.01
Normal boiling point temperature of R134a	$T_{nbp,R134a}$	K	247.08
Vapour pressure of R32 (at 298.15 K)	$p_{v,R32}$	Pa	1693000
Vapour pressure of R125 (at 298.15 K)	$p_{v,R125}$	Pa	1379000
Vapour pressure of R134a (at 298.15 K)	$p_{v,R134a}$	Pa	665500

Calculation procedure for HTC of 2-phase ternary zeotropic refrigerant mixture: The equation/correlation (Eq. 3.121) developed by Jung et al. [1989b] for binary zeotropic and near-azeotropic refrigerant mixtures was applied to calculate the HTC of R407C, which is a ternary mixture.

$$h_{tp} = \frac{N}{C_{UN}} h_{UN} + C_{me} F_p h_{lo} \tag{3.121}$$

It should be borne in mind that, at the charge condition, R407C is a liquid single-phase fluid with R32/R125/R134a 0.23/0.25/0.52 by weight. Mole fractions of each component in and molecular weight of the R407C are obtained by Eqs A.34, A.35, A.36 and A.37, respectively.

$$X_{R32,charge} = \frac{\left(\frac{\Theta_{R32,charge}}{M_{R32}}\right)}{\left(\frac{\Theta_{R32,charge}}{M_{R32}} + \frac{\Theta_{R125,charge}}{M_{R125}} + \frac{\Theta_{R134a,charge}}{M_{R134a}}\right)} \tag{A.34}$$

$$X_{R125,charge} = \frac{\left(\frac{\Theta_{R125,charge}}{M_{R125}}\right)}{\left(\frac{\Theta_{R32,charge}}{M_{R32}} + \frac{\Theta_{R125,charge}}{M_{R125}} + \frac{\Theta_{R134a,charge}}{M_{R134a}}\right)} \tag{A.35}$$

$$X_{R134a,charge} = 1 - X_{R32,charge} - X_{R125,charge} \tag{A.36}$$

$$M_{R407C,charge} = M_{R32} X_{R32,charge} + M_{R125} X_{R125,charge} + M_{R134a} X_{R134a,charge} \tag{A.37}$$

The nucleate-boiling N parameter is calculated from Eq. 3.99 or 3.100.

$$N = 4048 X_{tt}^{1.22} Bo^{1.13} \qquad \text{for } X_{tt} < 1 \tag{3.99}$$

$$N = 2.0 - 0.1 X_{tt}^{-0.28} Bo^{-0.33} \qquad \text{for } 1 \le X_{tt} \le 5 \tag{3.100}$$

The Martinelli parameter, X_{tt}, and the boiling number, Bo, in the above two equations are determined from Eqs. 3.79 and 3.98, respectively.

$$X_{tt} = \left(\frac{1-x}{x}\right)^{0.9} \left(\frac{\rho_v}{\rho_l}\right)^{0.5} \left(\frac{\mu_l}{\mu_v}\right)^{0.1} \tag{3.79}$$

$$Bo = \frac{q}{Gi_{fg}} \tag{3.98}$$

The molecular weights of R407C for the liquid- and vapour- phases are obtained by using Eqs. A38 and A.39, respectively.

$$M_{R407C,l} = M_{R32}X_{R32} + M_{R125}X_{R125} + M_{R134a}X_{R134a} \quad (A.38)$$

$$M_{R407C,v} = M_{R32}Y_{R32} + M_{R125}Y_{R125} + M_{R134a}Y_{R134a} \quad (A.39)$$

The F_p parameter is calculated by using Eq. 3.92.

$$F_p = 2.37\left(0.29 + \frac{1}{X_{tt}}\right)^{0.85} \quad (3.92)$$

The convective HTC for the liquid-alone flow, h_{lo}, is determined by using Eq. 3.67.

$$Nu_{lo} = 0.023Re_{lo}^{0.8}Pr_l^{0.4} \quad (3.67)$$

To obtain the C_{me} parameter, the C_{UN} parameter and the Unal HTC (h_{UN}), it should be reminded that, as explained in Section 4.4, this thesis adopted Judge & Radermacher's implementation [1997] in using Jung et al.'s correlation [1989b] for ternary mixtures. Then, R407C, being R32/R125/R134a, is "divided" into or "seen" as two groups. The first group is a pseudo R32/R125, and the second group is a pseudo R134a; the pseudo R32/R125 is more volatile than the pseudo R134a.

The C_{me} parameter, considering the mixture effect of the mass transfer resistance, is determined by using Eq. 3.103.A.a, which is for $0.9 < C_{me} < 1$. (The letter 'A.' represents Judge & Radermacher's implementation [1997] stated in this thesis in Appendix A, and the following alphabet refers to how many times the equation was used in the implementation.)

$$C_{me} = 1 - 0.35\left|Y_{pseudo(R32/R125)} - X_{pseudo(R32/R125)}\right|^{1.56} \quad (3.103.A.a)$$

The liquid- and vapour- phase mole fractions of the pseudo R32/R125 can be calculated from Eqs. A.40 and A.41, respectively.

$$X_{pseudo(R32/R125)} = X_{R32} + X_{R125} \quad (A.40)$$

$$Y_{pseudo(R32/R125)} = Y_{R32} + Y_{R125} \quad (A.41)$$

The C_{UN} parameter, accounting for the mixture effects in nucleate boiling region and being developed by Unal, can be calculated by using Eq. 3.110 and Eqs. 3.111.A.a to 3.115.A.a.

$$C_{UN} = (1.0 + (b_2 + b_3)(1.0 + b_4))(1.0 + b_5) \quad (3.110)$$

$$b_2 = (1.0 - X_{pseudo(R32/R125)}) \ln\left(\frac{1.01 - X_{pseudo(R32/R125)}}{1.01 - Y_{pseudo(R32/R125)}}\right) + X_{pseudo(R32/R125)} \ln\left(\frac{X_{pseudo(R32/R125)}}{Y_{pseudo(R32/R125)}}\right) + |Y_{pseudo(R32/R125)} - X_{pseudo(R32/R125)}|^{1.5} \quad (3.111.A.a)$$

$$b_3 = 0.0 \quad \text{for} \quad X_{pseudo(R32/R125)} \geq 0.01 \quad (3.112.A.a)$$

$$b_3 = \left(\frac{Y_{pseudo(R32/R125)}}{X_{pseudo(R32/R125)}}\right)^{0.1} - 1 \quad \text{for} \quad X_{pseudo(R32/R125)} \geq 0.01 \quad (3.113.A.a)$$

$$b_4 = 152\left(\frac{p}{p_{c,pseudo(R32/R125)}}\right)^{3.9} \quad (3.114.A.a)$$

$$b_5 = 0.92(|Y_{pseudo(R32/R125)} - X_{pseudo(R32/R125)}|)^{0.001} \left(\frac{p}{p_{c,pseudo(R32/R125)}}\right)^{0.66} \quad (3.115.A.a)$$

For the pseudo R32/R125, its mole fractions in the liquid and the vapour phases are determined by Eqs. A.40 and A.41, respectively. Its critical pressure is calculated by applying Eqs. A.28, A.29, A.42 and A.43.

$$X_{R32,charge,pseudo(R32/R125)} = \frac{X_{R32,charge}}{X_{R32,charge} + X_{R125,charge}} \quad (A.42)$$

$$X_{R125,feed,pseudo(R32/R125)} = \frac{X_{R125,feed}}{X_{R32,feed} + X_{R125,feed}} \quad (A.43)$$

The Unal HTC (h_{UN}) is determined by using Eq. 3.119:

$$\frac{h_{UN}}{h_i} = \frac{1}{C_{UN}} \quad (3.119)$$

where

$$h_i = \frac{1}{\frac{X_{pseudo(R32/R125)}}{h_{SA,pseudo(R32/R125)}} + \frac{X_{pseudoR134a}}{h_{SA,pseudoR134a}}} \qquad (3.120.A.a)$$

In Eq. 3.120.A.a, the liquid-phase mole fractions of the pseudo (R32/R125) and the pseudo R134a are obtained from Eqs. A.40 and A.44, respectively.

$$X_{pseudoR134a} = X_{R134a} \qquad (A.44)$$

The $h_{SA,pseudoR134a}$ is calculated from Eqs. 3.70.A.a, 3.94.A.a and 3.95.A.a.

$$h_{SA,pseudoR134a} = 207\frac{k_{l,pseudoR134a}}{(bd)_{pseudoR134a}}\left(\frac{(bd)_{pseudoR134a}\,q}{k_{l,pseudoR134a}\,T_{sat,pseudoR134a}}\right)^{0.745}\left(\frac{\rho_{v,pseudoR134a}}{\rho_{l,pseudoR134a}}\right)^{0.581} Pr_{l,pseudoR134a}^{0.533} \qquad (3.94.A.a)$$

$$Pr_{l,pseudoR134a} = \left(\frac{\mu_l c_{pl}}{k_l}\right)_{pseudoR134a} \qquad (3.70.A.a)$$

$$(bd)_{pseudoR134a} = 0.0146\beta\left(\frac{2\sigma_{pseudoR134a}}{(\rho_l - \rho_v)_{pseudoR134a}\,g}\right)^{0.5} \qquad (3.95.A.a)$$

The saturated liquid and vapour physical properties of the pseudo R134a are obtained on a basis of the R407C pressure and the molecular weight of the pseudo R134a, employing Eqs. A.44 and A.45.

$$M_{pseudoR134a,l} = M_{R134a} \qquad (A.44)$$

$$M_{pseudoR134a,v} = M_{R134a} \qquad (A.45)$$

Based on the R407C pressure, the surface tension of the pseudo R134a is calculated by using Eq. A.32. The h_{SA} of the pseudo (R32/R125) is calculated from Eqs. 3.70.A.b, 3.94.A.b, and 3.95.A.b.

$$h_{SA,pseudo(R32/R125)} = 207\frac{k_{l,pseudo(R32/R125)}}{(bd)_{pseudo(R32/R125)}}\left(\frac{(bd)_{pseudo(R32/R125)}q}{k_{l,pseudo(R32/R125)}T_{sat,pseudo(R32/R125)}}\right)^{0.745}\left(\frac{\rho_{v,pseudo(R32/R125)}}{\rho_{l,pseudo(R32/R125)}}\right)^{0.581}Pr_{l,pseudo(R32/R125)}^{0.533} \quad (3.94.A.b)$$

$$Pr_{l,pseudo(R32/R125)} = \left(\frac{\mu_l c_{pl}}{k_l}\right)_{pseudo(R32/R125)} \quad (3.70.A.b)$$

$$(bd)_{pseudo(R32/R125)} = 0.0146\beta\left(\frac{2\sigma_{pseudo(R32/R125)}}{(\rho_l-\rho_v)_{pseudo(R32/R125)}g}\right)^{0.5} \quad (3.95.A.b)$$

The saturated -liquid and -vapour physical properties of the pseudo R32/R125 are based on the R407C pressure and the mole fractions of the each component in the pseudo R32/R125, which relate to the molecular weights (see Eqs. A.46 to A.51).

$$X_{R32,pseudo(R32/R125)} = \frac{X_{R32}}{X_{R32}+X_{R125}} \quad (A.46)$$

$$X_{R125,pseudo(R32/R125)} = \frac{X_{R125}}{X_{R32}+X_{R125}} \quad (A.47)$$

$$M_{pseudo(R32/R125),l} = M_{R32}X_{R32,pseudo(R32/R125)} + M_{R125}X_{R125,pseudo(R32/R125)} \quad (A.48)$$

$$Y_{R32,pseudo(R32/R125)} = \frac{Y_{R32}}{Y_{R32}+Y_{R125}} \quad (A.49)$$

$$Y_{R125,pseudo(R32/R125)} = \frac{Y_{R125}}{Y_{R32}+Y_{R125}} \quad (A.50)$$

$$M_{pseudo(R32/R125),v} = M_{R32}Y_{R32,pseudo(R32/R125)} + M_{R125}Y_{R125,pseudo(R32/R125)} \quad (A.51)$$

The surface tension of the pseudo R32/R125 is calculated by using Eq. A.33 on a basis of the R407C pressure. The saturated temperature of the pseudo R32/R125 used in the surface-tension calculation is an average temperature between the bubble- and dew-point temperatures of the pseudo R32/R125. These bubble- and dew- point temperatures of the pseudo R32/R125 are based on the R407C pressure and the saturated-liquid and -vapour mole fractions of the each component in the pseudo R32/R125 (see Eqs. A.46, A.47, A.49 and A.50).

Appendix B

For simulation sequences presented in Chapter 4, more details were given as follows: Tables B.1 to B.3 for the dry-, the totally-wet- and the TEV-controlled-coils, respectively.

Table B.1 For the dry-coil, seeing also Fig. 4.12, the simulation and the iteration sequences are described for both steady-state and dynamic modes. The bold letters are for the steady-state, and the italic-underlined letters are for the dynamic, whereas the normal letters are for both modes. The number in the brackets refers to either the equation number or the subroutine number when using Refprop.

1	Assign the evaporator configuration, and set numbers of the elements per tube and the sub-elements per element. *Set the marching time step.*
2	Set the inlet air condition at the coil face: the DB temperature, the pressure and the humidity ratio. Set the inlet refrigerant condition at the coil inlet; for R134a, the temperature and the vapour quality are known, whereas, for R407C, the temperature and the pressure are known, and it should be recognized that the charging condition is under a liquid single-phase.
3	Set the inlet air mass flux, and the inlet refrigerant mass flow rate.
4	Calculate for a tube element/sub-element as follows:
4.1	Assume the DB temperature of the inlet air, if the tube element is not at the coil face.
4.2	Calculate the inlet-air properties (Eqs. A.1 to A.6).
4.3	Calculate the HTC between the air and the dry tube-wall surface area (Eq. 3.6), the dry-coil fin efficiency (Eq. 3.2), and then the effective HTC between the air and the dry tube-wall surface area (Eq. 3.1).
4.4	Calculate the length of the tube element/sub-element.
4.5	Check whether the refrigerant is superheated or not. Then, it is able to assume properly the initial guessed value of the DB temperature at the air-outlet of the element/sub-element.
4.6	Calculate the average value of the wall temperature (Eq. 4.1).

Table B.1 For the dry-coil, seeing also Fig. 4.12, the simulation and the iteration sequences are described for both steady-state and dynamic modes. The bold letters are for the steady-state, and the italic-underlined letters are for the dynamic, whereas the normal letters are for both modes. The number in the brackets refers to either the equation number or the subroutine number when using Refprop.

4.7	Calculate *the average refrigerant temperature (Eqs. 4.9 and 4.27)* and the tube-wall-to-refrigerant heat flux (Eq. 4.9).
4.8	If the refrigerant is superheated, go to Step 4.9; if not, go to Step 4.13.
4.9	At the refrigerant inlet of the element/sub-element, calculate: the properties (RefpPure3) (RefpMix4), the velocity, and the HTC (Eqs. 3.72 and 3.73) of the refrigerant, the wall temperature (Eq. 4.27).
4.10	Calculate the refrigerant pressure drop of the element/sub-element assuming the negligence of the accelerating and the potential pressure drops **(Eq. 3.91)** *(Eqs. 3.91 and 4.24) (For the initial iteration, assume there is no the rate of change of the accumulated momentum in the control volume.)*
4.11	At the refrigerant outlet of the element/sub-element, calculate: the pressure of the refrigerant, the state and the properties (RefpPure3) (RefpMix4) (Use the bisection method involving the continuity (Eq. 4.28) and energy (Eq. 4.32) equations to obtain the refrigerant velocity and temperature, respectively.) of the refrigerant, the refrigerant HTC (Eqs. 3.72 and 3.73), the wall temperature (Eq. 4.27).
4.12	Check the termination criterion of the iterative calculation by using the tube-wall-to-refrigerant heat flux. If satisfied, go to Step 4.16. If not yet satisfied, do as follows. **For the steady-state simulation, assign an iterative-based average wall temperature to calculate the outlet air enthalpy (Eq. 4.1). Calculate the outlet DB temperature (Eq. A.15), and then go back to Step 4.7.** *For the dynamic simulation, assign an iterative-based average refrigerant temperature. Apply the bisection method for two calculations: first, the average wall temperature (Eqs. 3.5 and 4.9); second, the outlet DB temperature (Eqs. 4.1 and A.15). Then go back to Step 4.6.*
4.13	At the refrigerant inlet of the element/sub-element, calculate: the properties (RefpPure1) (RefpMix1), the void fraction (Eq. 4.17), the velocity (Eq. A.21), and the HTC (see Appendices C and D) of the refrigerant, the wall temperature (Eq. 4.27).
4.14	At the refrigerant outlet of the element/sub-element, calculate as follows.
4.14.1	Use the bisection method to obtain the refrigerant state as follow: • Calculate the pressure drop **(see Appendix D)** *(Eqs. 3.91 and 4.24) (For the initial iteration, assume there is no rate of change of accumulated momentum in the control volume.)* Calculate the pressure at the refrigerant-outlet node of the element • Calculate the refrigerant properties (RefpPure2) (RefpMix1) (for R407C, including the vapour quality) and the void fraction (Eq. 4.17). Calculate the velocity by using the continuity equation (Eq. 4.16). Check convergence of the iterative calculation by using the energy equation (Eq. 4.26). If converged, go to Step 4.14.2; if not converged, go back to the first sub-step of this step, 4.14.1.

Table B.1 For the dry-coil, seeing also Fig. 4.12, the simulation and the iteration sequences are described for both steady-state and dynamic modes. The bold letters are for the steady-state, and the italic-underlined letters are for the dynamic, whereas the normal letters are for both modes. The number in the brackets refers to either the equation number or the subroutine number when using Refprop.

4.14.2	Calculate the refrigerant HTC and the wall temperature (Eq. 4.27).
4.15	This step can be explained the same as done in Step 4.12.
4.16	If the last sub-element has not yet been simulated, begin the calculation for the next tube element/sub-element by going to Step 4. If the last sub-element has been done, go to Step 4.17.
4.17	Check whether there are convergences of the difference between the inlet and the outlet DB temperatures, for each element inside the coil, and of the difference between the consecutive-loop values of the outlet DB temperatures, for each element at the coil outlet. If converged; the loop calculation for the steady-state or the present-time will terminate, go to Step 4.18. If not yet been converged, assign new values of the inlet air temperatures at each tube element in side the coil and go to Step 4.2.
4.18	Check whether the last time step has been done. If done, the simulation stops; if not yet been done, assign the next time step, and go to Step 4.

Table B.2 For the totally-wet-coil, with Fig. 4.13, the simulation and the iteration sequences are explained for both steady-state and dynamic modes. The bold letters are for the steady-state, and the italic-underlined letters are for the dynamic, whereas the normal letters are for both modes. The number in the brackets refers to either the equation number or the subroutine number when using Refprop.

1 to 3	Steps 1 to 3 can be explained the same as that of the Dry-Coil Simulation.
4	Calculate for a tube element/sub-element as follows.
4.1	Assume the DB temperature and the humidity ratio of the inlet air, if the tube element is not at the coil face.
4.2	Calculate the inlet-air properties (Eqs. A.1 to A.6).
4.3	**Assume that the element/sub-element is under a dry-coil condition. Calculate the HTC between the air and the dry tube-wall surface area (Eq. 3.6), the dry-coil fin efficiency (Eq. 3.2), and then the effective HTC between the air and the dry tube-wall surface area (Eq. 3.1).**
4.4	Calculate the length of the tube element/sub-element.
4.5	Check whether the refrigerant is superheated or not. Then, at the air-outlet of the element/sub-element, it is able to assume properly the initial guessed value*(s)* of the DB temperature *and/or the humidity ratio. In the dynamic mode, the scheme to obtain the initial guessed value(s) will also indicate whether the coil is wet or dry. If dry, calculate U_{dry} (Eq. 3.6), the dry-coil fin efficiency (Eq. 3.2) and $U_{eff,dry}$ (Eq. 3.1). If wet, calculate $U_{wet,sen}$ (Eq. 3.19), $U_{wet,latent}$ (Eq. 3.22), U_{wet} (Eq. 3.18), $U_{m,wet}$ (Eq. 3.26), the wet-coil fin efficiency (Eq. 3.17), $U_{eff,wet,sen}$ (Eq. 3.25), $U_{eff,wet,latent}$ (Eq. 3.24), $U_{eff,wet}$ (Eq. 3.12), and $U_{m,eff,wet}$ (Eq. 3.25).*
4.6	Calculate the average value of the wall temperature (Eq. 4.1 or 4.3) *and the average*

Table B.2 For the totally-wet-coil, with Fig. 4.13, the simulation and the iteration sequences are explained for both steady-state and dynamic modes. The bold letters are for the steady-state, and the italic-underlined letters are for the dynamic, whereas the normal letters are for both modes. The number in the brackets refers to either the equation number or the subroutine number when using Refprop.

	refrigerant temperature (Eqs. 4.9 and 4.27).
4.7	**Check whether the element/sub-element is under a wet-coil condition, for which the average wall temperature is less than the air dew-point temperature.** If wet-coil, go to Step 4.8; if not, go to Step 4.10.
4.8	**Calculate the heat and mass transfer coefficients: $U_{wet,sen}$ (Eq. 3.19), $U_{wet,latent}$ (Eq. 3.22), U_{wet} (Eq. 3.18) and $U_{m,wet}$ (Eq. 3.26). Calculate the wet-coil fin efficiency (Eq. 3.17) and the effective heat and mass transfer coefficients: $U_{eff,wet,sen}$ (Eq. 3.25), $U_{eff,wet,latent}$ (Eq. 3.24), $U_{eff,wet}$ (Eq. 3.12) and $U_{m,eff,wet}$ (Eq. 3.25). At the air outlet of the element/sub-element, calculate the DB temperature (Eq. A.15) and the humidity ratio (Eq. 4.8).**
4.9	Calculate the tube-wall-to-refrigerant heat flux for the wet-coil condition (Eq. 4.11), and then go to Step 4.11.
4.10	Calculate the tube-wall-to-refrigerant heat flux for the dry-coil condition (Eq. 4.9), and then go to Step 4.11.
4.11	If the refrigerant is superheated, go to Step 4.12; if not, go to Step 4.14.
4.12	Do the refrigerant-side calculation the same as done in Steps 4.9 to 4.11 of the Dry-Coil Simulation.
4.13	Check the termination criterion of the iterative calculation by using the tube-wall-to-refrigerant heat flux. If satisfied, go to Step 4.19. If not yet satisfied, do as the follows. **For the steady-state simulation, assign an iterative-based average wall temperature.** *For the dynamic simulation, assign an iterative-based average refrigerant temperature. Calculate the average wall temperature by using the bisection method with the energy balance of the finned tube (Eq. 4.11).* Go to Step 4.16.
4.14	Perform the calculations the same as explained in Steps 4.13 to 4.14.2 of the Dry-Coil Simulation.
4.15	Check the termination criterion of the iterative calculation by using the tube-wall-to-refrigerant heat flux. If satisfied, go to Step 4.19. If not yet satisfied, do as the follows. **For the steady-state simulation, assign an iterative-based average wall temperature.** *For the dynamic simulation, assign an iterative-based average refrigerant temperature. Calculate the average wall temperature by using the bisection method with the energy balance of the finned tube (Eq. 4.11).* Check whether there is a conflict between the wet-coil condition and the coil-checking condition (comparing the average wall temperature to the dew-point temperature). If having the conflict, assign the dry-coil HTC (U_{dry}) with the wet-coil HTC (U_{wet}); if not having, do nothing. Go to Step 4.16.
4.16	Check whether the element/sub-element is under a wet-coil condition, for which the average wall temperature is less than the air dew-point temperature. If wet-coil, go to Step 4.17; if not, go to Step 4.18.
4.17	Calculate the heat and mass transfer coefficients: $U_{wet,sen}$ (Eq. 3.19), $U_{wet,latent}$ (Eq. 3.22), U_{wet} (Eq. 3.18) and $U_{m,wet}$ (Eq. 3.26). Calculate the wet-coil fin efficiency (Eq. 3.17) and the effective heat and mass transfer coefficients: $U_{eff,wet,sen}$ (Eq. 3.25), $U_{eff,wet,latent}$ (Eq. 3.24), $U_{eff,wet}$ (Eq. 3.12) and $U_{m,eff,wet}$ (Eq. 3.25). At the air outlet of the element/sub-element, calculate the DB temperature (Eq. A.15) and the humidity ratio (Eq. 4.8). **For the steady-**

Table B.2 For the totally-wet-coil, with Fig. 4.13, the simulation and the iteration sequences are explained for both steady-state and dynamic modes. The bold letters are for the steady-state, and the italic-underlined letters are for the dynamic, whereas the normal letters are for both modes. The number in the brackets refers to either the equation number or the subroutine number when using Refprop.

	state mode, go back to Step 4.9, *whereas, for the dynamic mode, go back to Step 4.6.*
4.18	Calculate the DB temperature at the air outlet of the element/sub-element. **For the steady-state mode, go back to Step 4.10,** *whereas, for the dynamic mode, go back to Step 4.6.*
4.19	If the last sub-element has not yet been simulated, begin the calculation for the next tube element/sub-element by going to Step 4. If the last sub-element has been done, go to Step 4.20.
4.20	Check whether there are convergences of the difference between the inlet and the outlet values of both the DB temperatures and the humidity ratios (for each element inside the coil) and of the difference between the consecutive-loop values of the outlet DB temperatures and the humidity ratios (for each element at the coil outlet). If converged; the loop calculation for the steady-state or the present-time will terminate, and go to Step 4.21. If not yet been converged, assign new values of the inlet air temperatures and the humidity ratios at each tube element in side the coil and go to Step 4.2.
4.21	This Step is explained the same as that of the Dry-Coil Simulation.

Table B.3 For the TEV-controlled evaporator, seeing also Fig. 4.14, the simulation and the iteration sequences involving both steady-state and dynamic modes are described. The bold letters are for the steady-state, and the italic-underlined letters are for the dynamic, whereas the normal letters are for both modes. The number in the brackets refers to either the equation number or the subroutine number when using Refprop.

1	Details are the same as done in Step 1 of the Dry-Coil Simulation. In addition, set the valve-gain value, and the superheat-setting pressure.
2	It can be described the same as Step 2 of the Dry-Coil Simulation.
3	Set the inlet air mass flux, **and the inlet refrigerant mass flow rate.**
4	Do the same as details in Steps 4 to 17 of the Dry-Coil Simulation.
5	Check whether the last time step has been done. If done, the simulation stops; if not yet been done, assign the next time step.
6	*Calculate bulb pressure (Eq. 3.134 giving the bulb temperature and RefPure1 or RefMix1), and calculate coil-inlet refrigerant mass flow rate (Eq. 4.33), and go to Step 4.*

Appendix C

For obtaining refrigerant properties by calling Subroutines of Refprop (Huber 1996), written in FORTRAN 77 and run by Digital Visual Fortran (based on FORTRAN 90), Sub-procedures of the programs of this thesis, written with Visual Basic for Application (VBA), were explained here. Each Sub-procedure was programmed for setting the values needed by Refprop: PREFS Common Block and called Subroutines. It should be noticed that Sub-procedures were referred in Appendices B and C. All Subroutines in following Tables are the built-in routines of Refprop.

Table C.1 For R134a, Sub-procedure RefpPure1 is used to obtain physical and thermodynamics properties when knowing a temperature.

1	For the input argument, assign a temperature. The output arguments are a pressure, and liquid and vapour values of the following properties: densities, dynamic viscosities, thermal conductivities, enthalpies, and specific heat capacities.
2	Initialize coefficients of Refprop as the follows.
2.1	For PREFS, being a Common Block, first, assign NREFST = 2 in order to set the enthalpy and the entropy reference states, where the saturated liquids of both properties equal to 0 at -40 °F. Second, as a must of Refprop, assign INTACT = 1 so that the interaction parameters will be used properly. Finally, assign IEQN = 1, then, the CSD equation of state is selected in the involved calculations.
2.2	For Subroutine BCONST, set NC =1 for pure-component calculations. Assign an IR value to be 18, being the code of R134a.
3	For Subroutine BUBLT that is for computing saturation properties, its input arguments are the temperature, the logical variable (set LBUB = True for computing bubble-point properties) and the liquid mole fraction (set XL = 1). Its output arguments are the vapour mole fraction (XV), the saturation pressure, and the liquid and the vapour molar volumes.

Table C.1 For R134a, Sub-procedure RefpPure1 is used to obtain physical and thermodynamics properties when knowing a temperature.	
4	For additional liquid-phase properties, obtaining from Subroutine HCVCPS, the input arguments are: IQ code (IQ = 3), the temperature, the liquid molar volume (calculated from Step 3), and the liquid mole fraction (set XL = 1). The output arguments being for the liquid phase are: the enthalpy, the constant-volume and the constant-pressure specific heat capacities.
5	For additional vapour-phase properties, obtaining from Subroutine HCVCPS, the input and the output arguments are the same as that mentioned in Step 4, except that assign and receive, respectively, the vapour properties instead of the liquid properties.
6	To obtain transport properties in the liquid phase by calling Subroutine TRNSP, the input arguments are the temperature, the pressure (calculated from Step 3), the liquid mole fraction (set XL = 1), and NPH (set to equal to 1 for calculating liquid properties). The output arguments are the liquid-phase properties: the density, the dynamic viscosity and the thermal conductivity.
7	To use Subroutine TRNSP in calculating the vapour-phase properties, the input arguments are the same as that in Step 4, except setting the vapour mole fraction (XV = 1) and NPH = 2 instead of the liquid mole fraction and NPH = 1, respectively. The output arguments are the same as that in Step 6 but being the vapour-phase properties.

Table C.2 For R134a, Sub-procedure RefpPure2 gives physical and thermodynamics properties when knowing a pressure.	
1	The input argument is a pressure. The output arguments are: a temperature, and the rest as mentioned in Step 1 of RefpPure1.
2	Initialize coefficients of Refprop are the same as that in Steps 2.1 and 2.2 of RefpPure1.
3	To calculate saturation properties applying Subroutine BUBLP. The input and the output arguments are the same as that in Step 3 of RefpPure1, except that assign the pressure instead of the temperature and receive the temperature instead of the pressure, respectively.
4	To calculate additional properties of the liquid and vapour phases by using Subroutine HCVCPS, it can be explained as that done in Steps 4 and 5 of RefpPure1, respectively.
5	It is about Subroutine TRNSP, the detail can be explained as done in Step 6 of RefpPure1, except 'the pressure, the temperature (calculated from Step 3)'.
6	Use Subroutine TRNSP to obtain the vapour-phase properties. The description is the same as that in Step 7 of RefpPure1.

Table C.3 For R134a, Sub-procedure RefpPure3 is used to calculate physical and thermodynamics properties at a superheat state when knowing the temperature and the pressure.	
1	The input arguments are a temperature and a pressure. The output arguments are vapour properties: densities, dynamic viscosities, thermal conductivities, enthalpies, and specific heat capacities.
2	Initialize coefficients of Refprop, the explanation is as that done in Steps 2.1 and 2.2 of RefpPure1.
3	In applying the CSD equation of state, it is necessary to use Subroutine ESPAR before calling Subroutine VIT. The input arguments are the input qualifier (assign IQ = 0), for using with Subroutine VIT), the temperature, the mole fraction (X = 1). The output arguments, being for the CSD equation of state, are the attractive-term parameter (A) and the repulsive-term parameter (B).
4	For Subroutine VIT, the input arguments are the temperature, the pressure, the A and the B parameters, the initially-guessed superheat molar volume (VS = 8.3143*T/P, assigned in a corresponding Subroutine written in the Digital Visual Fortran language (DVF)), and the logical variable (set LLIQI = False for computing vapour-phase properties). The output argument is the converged superheat molar volume.
5	For Subroutine HCVCPS, applied to calculate the superheat properties, the input arguments are: IQ code (IQ = 3), the temperature, the superheat molar volume (calculated from Step 4), and the mole fraction (X = 1). The output arguments are the superheat values: the enthalpy, the constant-volume and the constant-pressure specific heat capacities.
6	For more superheat properties by using Subroutine TRNSP, the input arguments are the temperature, the pressure, the mole fraction (X = 1), and NPH (set to equal to 2 for calculating vapour properties). The output arguments are the density, the dynamic viscosity and the thermal conductivity.

Table C.4 For R407C, Sub-procedure RefpMix1 is used to obtain physical and thermodynamics properties when knowing a temperature, a pressure and the charge-condition mass fractions.	
1	The input arguments are a temperature, a pressure and the charge-condition mass fractions of each component. The output arguments are the liquid and the vapour mole fractions, the vapour quality, and the liquid and the vapour properties (densities, dynamic viscosities, thermal conductivities, enthalpies, and specific heat capacities).
2	Initialize coefficients of Refprop as the follows.
2.1	For PREFS, being a Common Block, first, since Subroutine RefpMix1 is for mixture calculations, assign NREFST = 4 in order to set the enthalpy and the entropy reference states, where the saturated liquids of both properties equal to 0 at -40 °F. The settings of INTACT and IEQN are the same as that done in Step 2.1 of RefpPure1.
2.2	For Subroutine BCONST, set NC =3 for R407C calculations. Assign IR values to be 9, 16 and 18, being the codes of R32, R125 and R134a, respectively.
3	Initialize the interaction parameters of R407C with Subroutine FSET. The input argument is the codes of IR, whereas the output arguments are the parameters that will be used internally and

Table C.4 For R407C, Sub-procedure RefpMix1 is used to obtain physical and thermodynamics properties when knowing a temperature, a pressure and the charge-condition mass fractions.

	further by Refprop.
4	For each component at the charging condition, convert the mass fraction into the mole fraction.
5	According to Refprop, for setting up the reference state of R407C, it is necessary to call Subroutine REFMIX after calling Subroutines BCONST and FSET. The input arguments are the charging-condition mole fractions and the value of the number of the components (NC =3).
6	For Subroutine FLASHN, its input arguments are the temperature and pressure values mentioned in Step 1, the charging-condition mole fractions, the initially-guessed values of the liquid and the vapour mole fractions (assigned in a corresponding Subroutine written in the DVF language), and the value of the number of the components (NC =3). The output arguments are the converged values of the liquid and the vapour mole fractions, the vapour quality, and the liquid and the vapour molar volumes.
7	Applying Subroutine BUBLT for computing bubble-point properties, the input arguments are the temperature mentioned in Step 1, the logical variable (set LBUB = True for computing bubble-point properties) and the liquid mole fractions. Its output arguments are the vapour mole fractions, the pressure, and the liquid and the vapour molar volumes.
8	Calculating dew-point properties by using Subroutine BUBLT, the input arguments are the temperature mentioned in Step 1, LBUB assigned with 'False', and the vapour mole fractions. The output arguments are the liquid mole fractions, the pressure, and the liquid and the vapour molar volumes.
9	Calculate the liquid-phase properties by using Subroutine HCVCPS. The input arguments are IQ code (IQ = 3), the temperature mentioned in Step 1, the liquid molar volume calculated in Step 7, and the liquid mole fractions being the converged values in Step 6. The output arguments are the enthalpy, the constant-volume and the constant-pressure specific heat capacities.
10	Calculate the vapour-phase properties by using Subroutine HCVCPS. The input arguments are IQ code (IQ = 3), the temperature mentioned in Step 1, the vapour molar volume calculated in Step 8, and the vapour mole fractions being the converged values in Step 6. The output arguments are the vapour-phase values of the same properties as in Step 9.
11	Calculate the liquid-phase properties by calling Subroutine TRNSP, when the input arguments are the temperature and pressure values mentioned in Step 1, the liquid mole fractions being the converged values in Step 6, and NPH (set to equal to 1 for calculating liquid properties). The output arguments are the density, the dynamic viscosity and the thermal conductivity.
12	Calculate the vapour-phase properties by calling Subroutine TRNSP, when the input arguments are the temperature and pressure values mentioned in Step 1, the vapour mole fractions being the converged values in Step 6, and NPH (set to equal to 2 for calculating vapour properties). The output arguments are the vapour-phase values of the same properties as in Step 11.

Table C.5 For the pseudo R32/R125 at its bubble point, Sub-procedure RefpMix1_gr12_bi_LB gives physical and thermodynamics properties when knowing the pressure and the liquid mole fractions.	
1	This Subroutine is for the pseudo R32/R125 at its bubble point. The input arguments are a pressure and liquid mole fractions of each component. The output arguments are the bubble-point temperature, the liquid properties (density, dynamic viscosity, thermal conductivity, enthalpy, and specific heat capacity).
2	Initialize coefficients of Refprop as the follows.
2.1	For PREFS, being a Common Block, the initialization can be explained the same as done in Step 2.1 of RefpMix1.
2.2	For Subroutine BCONST, set NC =2. Assign IR values to be 9 and 16, being the codes of R32 and R125, respectively.
3	For Subroutine FSET, used in initializing the interaction parameters, it can be explained the same as done in Step 3 of RefpMix1.
4	By using Subroutine REFMIX to set up the reference state of the pseudo R32/R125 at its bubble point, the input arguments are the liquid mole fractions of R32 and R125 mentioned in Step 1, and NC = 2.
5	For using Subroutine BUBLP to compute bubble-point properties, its input arguments are the pressure and the liquid mole fractions mentioned in Step 1, and the logical variable (set LBUB = True). Its output arguments are the vapour mole fractions, the temperature, and the liquid and the vapour molar volumes.
6	To obtain the liquid-phase properties by using Subroutine HCVCPS, its input arguments are IQ code (IQ = 3), the liquid mole fractions mentioned in Step 1, and the temperature and the liquid molar volume calculated in Step 5. The output arguments are the enthalpy, the constant-volume and the constant-pressure specific heat capacities.
7	Use Subroutine TRNSP to calculate more the liquid-phase properties, the input arguments are the pressure and the liquid mole fractions mentioned in Step 1, the temperature calculated in Step 5, and NPH (set to equal to 1 for calculating liquid properties). The output arguments are the density, the dynamic viscosity and the thermal conductivity.

Table C.6 For the pseudo R32/R125 at its dew point, Sub-procedure RefpMix1_gr12_bi_LB is used to obtain physical and thermodynamics properties when knowing the pressure and the vapour mole fractions.	
1	This Subroutine is for the pseudo R32/R125 at its dew point. The input arguments are a pressure and vapour mole fractions of each component. The output arguments are the dew-point temperature, the vapour properties (density, dynamic viscosity, thermal conductivity, enthalpy, and specific heat capacity).
2	The initializations of the coefficients (Common Block PREFS and Subroutine BCONST) and the interaction parameters (Subroutine FSET) can be described the same as done in Steps 2 and 3 of Subroutine RefpMix1_gr12_bi_LB.
3	By using Subroutine REFMIX to set up the reference state of the pseudo R32/R125 at its dew

Table C.6 For the pseudo R32/R125 at its dew point, Sub-procedure RefpMix1_gr12_bi_LB is used to obtain physical and thermodynamics properties when knowing the pressure and the vapour mole fractions.

	point, the input arguments are the vapour mole fractions of R32 and R125 mentioned in Step 1, and NC = 2.
4	For using Subroutine BUBLP to compute dew-point properties, its input arguments are the pressure and the vapour mole fractions mentioned in Step 1, and the logical variable (set LBUB = False). Its output arguments are the liquid mole fractions, the temperature, and the liquid and the vapour molar volumes.
5	To obtain the vapour-phase properties by using Subroutine HCVCPS, its input arguments are IQ code (IQ = 3), the vapour mole fractions mentioned in Step 1, and the temperature and the vapour molar volume calculated in Step 4. The output arguments are the enthalpy, the constant-volume and the constant-pressure specific heat capacities.
6	Use Subroutine TRNSP to calculate more the vapour-phase properties, the input arguments are the pressure and the vapour mole fractions mentioned in Step 1, the temperature calculated in Step 4, and NPH (set to equal to 1 for calculating liquid properties). The output arguments are the density, the dynamic viscosity and the thermal conductivity.

Table C.7 Sub-procedure RefpMix1_gr12_1 gives the liquid density of pure R32 when knowing a pressure based on the bubble point of the pseudo R32/R125.

1	This Subroutine is for determining liquid-phase density of R32 as a pure component. The input argument is a pressure, whereas the output argument is the liquid-phase density.
2	Initialize coefficients of Refprop as the follows.
2.1	Common Block PREFS is assigned as done for Step 2.1 of RefpPure1.
2.2	For Subroutine BCONST, set NC =1 for pure-component calculations. Assign an IR value to be 9, being the code of R32.
3	For Subroutine BUBLP that is for computing saturation properties, its input arguments are the pressure mentioned in Step 1, the logical variable (set LBUB = True for computing bubble-point properties) and the liquid mole fraction (set XL = 1). Its output arguments are the vapour mole fraction (XV), the saturation temperature, and the liquid and the vapour molar volumes.
4	To obtain the liquid density by calling Subroutine TRNSP, the input arguments are the pressure, the temperature (calculated from Step 3), the liquid mole fraction (set XL = 1), and NPH (set to equal to 1 for calculating liquid properties). The output arguments are the liquid-phase properties: the density, the dynamic viscosity and the thermal conductivity.

Table C.8 Sub-procedure RefpMix1_gr12_2 gives the liquid density of pure R125 when knowing a pressure based on the bubble point of the pseudo R32/R125.	
1	This Subroutine is for determining liquid-phase density of R125 as a pure component. The input argument is a pressure, whereas the output argument is the liquid-phase density.
2	All of the details are the same as that of Subroutine RefpMix1_gr12_1 from Steps 2 to 4, except that assign an IR value to be 16 instead of 9.

Table C.9 For the pseudo R134a, Sub-procedure RefpMix1_gr3 gives physical and thermodynamics properties when knowing a pressure.	
1	Subroutine RefpMix1_gr3 is for obtaining thermodynamics and physical properties of R134a as a pure component. The input argument is a pressure, whereas the output arguments are a temperature, and liquid and vapour properties: densities, dynamic viscosities, thermal conductivities, enthalpies, and specific heat capacities.
2	Initialize coefficients of Refprop as the follows.
2.1	Common Block PREFS is assigned as done for Step 2.1 of RefpPure1.
2.2	For Subroutine BCONST, set NC =1 for pure-component calculations. Assign an IR value to be 18, being the code of R134a.
3	For Subroutine BUBLP that is for computing saturation properties, its input arguments are the pressure, the logical variable (set LBUB = True for computing bubble-point properties) and the liquid mole fraction (set XL = 1). Its output arguments are the vapour mole fraction (XV), the saturation temperature, and the liquid and the vapour molar volumes.
4	For additional liquid-phase properties, obtaining from Subroutine HCVCPS, the input arguments are: IQ code (IQ = 3), the temperature, the liquid molar volume (calculated from Step 3), and the liquid mole fraction (set XL = 1). The output arguments being for the liquid phase are: the enthalpy, the constant-volume and the constant-pressure specific heat capacities.
5	For additional vapour-phase properties, obtaining from Subroutine HCVCPS, the input and the output arguments are the same as that mentioned in Step 4, except that assign and receive, respectively, the vapour properties instead of the liquid properties.
6	To obtain transport properties in the liquid phase by calling Subroutine TRNSP, the input arguments are the pressure, the temperature (calculated from Step 3), the liquid mole fraction (set XL = 1), and NPH (set to equal to 1 for calculating liquid properties). The output arguments are the liquid-phase properties: the density, the dynamic viscosity and the thermal conductivity.
7	To use Subroutine TRNSP in calculating the vapour-phase properties, the input arguments are the same as that in Step 6, except setting the vapour mole fraction (XV = 1) and NPH = 2 instead of the liquid mole fraction (XL = 1) and NPH = 1, respectively. The output arguments are the same as that in Step 6 but being the vapour-phase properties.

Table C.10 For R407C, Sub-procedure RefpMix4 is used to obtain physical and thermodynamics properties at a superheat state when knowing the temperature and the pressure and the charge-condition mass fractions.

1	The input arguments are a temperature, a pressure, and the charge-condition mass fractions. The output arguments are superheat properties: densities, dynamic viscosities, thermal conductivities, enthalpies, and specific heat capacities.
2	Do the same as done in Steps 2 to 5 of RefpMix1 for the follows: initializing coefficients of Refprop and the interaction parameters of R407C, converting the mass fraction into the mole fraction, and calling Subroutine REFMIX
3	For Subroutine ESPAR, the description is the same as done in Step 3 of RefpPure3, except that use 'the charging-condition mole fractions' instead of 'the mole fraction (X = 1)'.
4	For Subroutine VIT, the explanation is the same as done in Step 4 of RefpPure3.
5	Subroutines HCVCPS and TRNSP can be described the same as done in Steps 5 and 6 of RefpPure3, respectively, except that use 'the charging-condition mole fractions' instead of 'the mole fraction (X = 1)'.

Appendix D

Sample calculations of pressure drop and HTCs in a 2-phase region were given. The conditions of the calculations for a tube element were as shown in Table D.1. It should be noticed that, for each refrigerant, the same value of the refrigerant heat flux was used for the calculations. In addition, all calculated variables/parameters were 'Double' data type of VBA language.

Table D.1 Some information and calculated results were given here to be used in following Sections. (Details and values of coil were the same as described in 'Coil configurations and coil-related variables' of Section A.2 of Appendix A.)

Inner tube diameter	D_{ID}	m	Assigned	0.0126
Condition of inner surface of tube	N/A	N/A	Assigned	smooth
Length of tube element	L	m	$\frac{C_W}{\text{Elements per tube}}$ where (Elements per tube = 3)	0.4063
Refrigerant mass flow rate	$\dot{m}$	kg/s	Assigned	0.0221
Refrigerant mass flux	G	$kg/(s \cdot m^2)$	Eq. A.21	177.1685
Refrigerant heat flux: For R134a For R407C	q_{wf}	W/m^2	Eq. 4.9	2451.0676 5578.2917

D.1 Two-phase pressure drop of R407C

As discussed in Sub-section 2.7.4, there is no mixture-composition dependence on the pressure drops, and Jung & Radermacher's correlation [1989] was

selected for this thesis, therefore only the calculation of the pressure drop for R407C was presented in Table D.2. The considered element was at the coil-inlet element (1,1,1).

Table D.2 Pressure-drop calculation of R407C at the coil-inlet element

At the inlet of the element				
Temperature	T	°C	Known value	2.0000
Pressure	p	Pa	Known value	583,488.0000
Vapour quality	x	Dimensionless	RefpMix1	0.2000
Liquid dynamic viscosity	μ_l	kg/(m·s)	RefpMix1	2.1983 E-4
Vapour dynamic viscosity	μ_v	kg/(m·s)	RefpMix1	1.1609 E-5
Liquid density	ρ_l	kg/m^3	RefpMix1	1249.8065
Vapour density	ρ_v	kg/m^3	RefpMix1	23.2187
At the outlet of the element				
Vapour quality	x	Dimensionless	numerical cal.	0.2080
Parameters and terms calculated by using the physical values at the inlet of the element.				
Martinelli parameter	X_{tt}	Dimensionless	Eq. 3.79	0.6369
Integration term in Eq. 3.90	$\int_{x_1}^{x_2} \Phi_{fo}^2 dx$	Dimensionless	Eq. 3.85 and numerical cal.	0.1363
Reynolds number for total-flow-assumed-liquid	Re_{fo}	Dimensionless	Eq. A.23.3	10154.8709
Fanning friction factor for total-flow-assumed-liquid	$f_{Fan,fo}$	Dimensionless	Eq. 3.77	7.2681 E-3
Desired calculated result				
Pressure drop for the element	Δp	Pa	Eq. 3.90	200.7678

D.2 Two-phase heat transfer coefficient of R134a

For the calculation of the 2-phase HTC of R134a, the example shown in Table D.3 was done at the inlet of the coil-inlet element. Most of the relevant equations were given in Chapter 3.

Table D.3 Two-phase HTC calculation of R134a at the inlet of the coil-inlet element

Temperature	T	°C	Known value	5.0500
Vapour quality	x	Dimensionless	Known value	0.2000
Pressure	p	Pa	RefpPure1	349,710.1801
Liquid thermal conductivity	k_l	J/(s·m·K)	RefpPure1	9.1316 E-2
Liquid specific heat capacity	$c_{p,l}$	J/(kg·K)	RefpPure1	1336.0309
Liquid dynamic viscosity	μ_l	kg/(m·s)	RefpPure1	2.6963 E-4
Vapour dynamic viscosity	μ_v	kg/(m·s)	RefpPure1	1.1144 E-5
Liquid density	ρ_l	kg/m^3	RefpPure1	1277.0018
Vapour density	ρ_v	kg/m^3	RefpPure1	16.9162
Reynolds number when liquid-alone-flow	Re_{lo}	Dimensionless	Eq. 3.69	6623.4231
Liquid Prandtl number	Pr_l	Dimensionless	Eq. 3.70	3.9449
Convective HTC of modified Dittus-Boelter	h_{lo}	$W/(m^2 \cdot K)$	Eqs. 3.67 and 3.68	328.9908
Surface tension	σ	J/m^2	Eq. A.32	1.1098 E-2
Equilibrium break-off-diameter	bd	m	Eq. 3.95	6.8484 E-4
Nucleate-pool-boiling HTC of Stephan & Abdelsalam	h_{SA}	$W/(m^2 \cdot K)$	Eq. 3.94	614.4579
Specific latent enthalpy	i_{fg}	J/(kg·K)	Based on RefpPure1	197,613.2717
Boiling number	Bo	Dimensionless	Eq. 3.98	7.0009 E-5
Martinelli parameter	X_{tt}	Dimensionless	Eq. 3.79	0.5512
N parameter	N	Dimensionless	Eqs. 3.99 and 3.100	3.9503 E-2
F_p parameter	F_p	Dimensionless	Eq. 3.92	4.4606

Two-phase HTC	h_{tp}	W/(m^2·K)	Eq. 3.101	1491.7801

D.3 Two-phase heat transfer coefficient of R407C

As explained in Section A.3 of Appendix A for the calculation procedure of HTC for 2-phase ternary zeotropic refrigerant mixture, an calculation example was shown in Table D.4. It should be noted that the considered element was also the first element of the coil. The calculation also illustrated the use of Refprop's Flash Subroutine, which utilizes the liquid charge-concentrations.

Table D.4 Two-phase HTC calculation of R407C (For any equation number with 'A.', its equation detail is shown in Appendix A.)

At the charge-condition for R407C				
Mole fraction of R32	$x_{R32,charge}$	Dimensionless	Eq. A.34	0.3811
Mole fraction of R125	$x_{R125,charge}$	Dimensionless	Eq. A.35	0.1796
Mole fraction of R134a	$x_{R134a,charge}$	Dimensionless	Eq. A.36	0.4393
Molecular weight of R407C	$M_{R407C,charge}$	g/mol	Eq. A.37	86.2002
At the element inlet for R407C				
Temperature	T	°C	Known value	2.0000
Pressure	p	Pa	Known value	583,488.0000
Vapour quality	x	Dimensionless	RefpMix1	0.2000
Liquid Mole fraction of R32	x_{R32}	Dimensionless	RefpMix1	0.3491
Liquid Mole fraction of R125	x_{R125}	Dimensionless	RefpMix1	0.1691
Liquid Mole fraction of R134a	x_{R134a}	Dimensionless	RefpMix1	0.4818
Liquid molecular weight	$M_{R407C,l}$	g/mol	Eq. A.38	87.6129
Vapour Mole fraction of R32	y_{R32}	Dimensionless	RefpMix1	0.4994

Vapour Mole fraction of R125	Y_{R125}	Dimensionless	RefpMix1	0.2183
Vapour Mole fraction of R134a	Y_{R134a}	Dimensionless	RefpMix1	0.2823
Vapour molecular weight	$M_{R407C,v}$	g/mol	Eq. A.39	80.9817
Liquid thermal conductivity	$k_{R407C,l}$	J/(s·m·K)	RefpMix1	0.1010
Liquid specific heat capacity	$c_{p,R407C,l}$	J/(kg·K)	RefpMix1	1393.9860
Liquid dynamic viscosity	$\mu_{R407C,l}$	kg/(m·s)	RefpMix1	2.1983 E-4
Vapour dynamic viscosity	$\mu_{R407C,v}$	kg/(m·s)	RefpMix1	1.1609 E-5
Liquid density	$\rho_{R407C,l}$	kg/m^3	RefpMix1	1249.8065
Vapour density	$\rho_{R407C,v}$	kg/m^3	RefpMix1	23.2187
Reynolds number when assumed liquid-alone-flow	$Re_{R407C,lo}$	Dimensionless	Eq. 3.69	8123.8559
Liquid Prandtl number	$Pr_{R407C,l}$	Dimensionless	Eq. 3.70	3.0347
Convective HTC of modified Dittus-Boelter	$h_{lo,R407C}$	$W/(m^2 \cdot K)$	Eqs. 3.67 and 3.68	385.6871
Specific latent enthalpy	$i_{fg,R407C}$	J/(kg·K)	Based on RefpMix1	222,565.1837
Boiling number	Bo_{R407C}	Dimensionless	Eq. 3.98	1.4147 E-4
Martinelli parameter	$X_{tt,R407C}$	Dimensionless	Eq. 3.79	0.6369
N parameter	N	Dimensionless	Eqs. 3.99 and 3.100	0.1043
F_p parameter	F_p	Dimensionless	Eq. 3.92	4.0166
At the charge-condition for the R32-and-R125 group of the pseudo binary mixture (the R32-and-R125 group and the R134a group)				
Liquid mole fraction of R32	$X_{R32,charge,pseudo(R32/R125)}$	Dimensionless	Eq. A.42	0.6798
Liquid mole fraction of R125	$X_{R125,charge,pseudo(R32/R125)}$	Dimensionless	Eq. A.43	0.3202

Critical pressure	$p_{c,pseudo(R32/R125)}$	Pa	Eqs. A.28 and A.29	5,103,980.1163
At the element inlet for the R32-and-R125 group of the pseudo binary mixture (the R32-and-R125 group and the R134a group), unless otherwise specified				
Liquid mole fraction	$x_{pseudo(R32/R125)}$	Dimensionless	Eq. A.40	0.5182
Vapour mole fraction	$y_{pseudo(R32/R125)}$	Dimensionless	Eq. A.41	0.7177
C_{me} parameter	C_{me}	Dimensionless	Eq. 3.103.A.a	0.9717
b_2 parameter	$b_{2,pseudo(R32/R125)}$	Dimensionless	Eq. 3.111.A.a	0.1711
b_3 parameter	$b_{3,pseudo(R32/R125)}$	Dimensionless	Eqs. 3.112.A.a and 3.113.A.a	0.0000
b_4 parameter	$b_{4,pseudo(R32/R125)}$	Dimensionless	Eq. 3.114.A.a	0.0322
b_5 parameter	$b_{5,pseudo(R32/R125)}$	Dimensionless	Eq. 3.115.A.a	0.2195
C_{UN} parameter	C_{UN}	Dimensionless	Eq. 3.110	1.4349
Liquid mole fraction of R32	$x_{R32,pseudo(R32/R125)}$	Dimensionless	Eq. A.46	0.6737
Liquid mole fraction of R125	$x_{R125,pseudo(R32/R125)}$	Dimensionless	Eq. A.47	0.3263
Liquid molecular weight	$M_{pseudo(R32/R125),l}$	g/mol	Eq. A.48	74.2076
Vapour mole fraction of R32	$y_{R32,pseudo(R32/R125)}$	Dimensionless	Eq. A.49	0.6958
Vapour mole fraction of R125	$y_{R125,pseudo(R32/R125)}$	Dimensionless	Eq. A.50	0.3042
Vapour molecular weight	$M_{pseudo(R32/R125),v}$	g/mol	Eq. A.51	52.0200
Liquid thermal conductivity	$k_{l,pseudo(R32/R125)}$	J/(s·m·K)	RefpMix1_gr12_bi_LB	0.1186
Liquid specific heat capacity	$c_{p,l,pseudo(R32/R125)}$	J/(kg·K)	RefpMix1_gr12_bi_LB	1460.2947
Liquid dynamic viscosity	$\mu_{l,pseudo(R32/R125)}$	kg/(m·s)	RefpMix1_gr12_bi_LB	1.9503 E-4
Liquid density	$\rho_{l,pseudo(R32/R125)}$	kg/m^3	RefpMix1_gr12_bi_LB	1239.9663
Bubble-point temperature	$T_{bubble,pseudo(R32/R125)}$	°C	RefpMix1_gr12_bi_LB	-9.3731

Vapour density	$\rho_{v,pseudo(R32/R125)}$	kg/m^3	RefpMix1_gr12_bi _VD	21.702
Dew-point temperature	$T_{dew,pseudo(R32/R125)}$	°C	RefpMix1_gr12_bi _VD	-9.3726
Liquid density	$\rho_{l,pseudo(R32/R125),R32}$	kg/m^3	RefpMix1_gr12_1	1085.1654
Liquid density	$\rho_{l,pseudo(R32/R125),R125}$	kg/m^3	RefpMix1_gr12_2	1340.4089
Saturation temperature	$T_{sat,pseudo(R32/R125)}$	°C	Arithmetic mean between the bubble-point and the dew-point temperatures calculated above	-9.3728
Liquid Prandtl number	$Pr_{pseudo(R32/R125),l}$	Dimensionless	Eq. 3.70	2.4022
Surface tension	$\sigma_{pseudo(R32/R125)}$	N/m	Eq. A.33	1.6516 E-2
Equilibrium break-off-diameter	$bd_{pseudo(R32/R125)}$	m	Eq. 3.95	8.4967 E-4
Nucleate-pool-boiling HTC of Stephan & Abdelsalam	$h_{SA,pseudo(R32/R125)}$	W/(m^2·K)	Eq. 3.94.A.b	1077.1786
At the element inlet for the R134a group of the pseudo binary mixture (the R32-and-R125 group and the R134a group)				
Liquid thermal conductivity	$k_{l,pseudoR134a}$	J/(s·m·K)	RefpMix1_gr3	8.3349 E-2
Liquid specific heat capacity	$c_{p,l,pseudoR134a}$	J/(kg·K)	RefpMix1_gr3	1392.6997
Liquid dynamic viscosity	$\mu_{l,pseudoR134a}$	kg/(m·s)	RefpMix1_gr3	2.2032 E-4
Liquid density	$\rho_{l,pseudoR134a}$	kg/m^3	RefpMix1_gr3	1221.4542
Vapour density	$\rho_{v,pseudoR134a}$	kg/m^3	RefpMix1_gr3	27.9059
Saturation temperature	$T_{sat,pseudoR134a}$	°C	RefpMix1_gr3	20.6694
Liquid Prandtl number	$Pr_{pseudoR134a,l}$	Dimensionless	Eq. 3.70	3.6813
Surface tension	$\sigma_{pseudoR134a}$	N/m	Eq. A.32	8.8779 E-3
Equilibrium break-off-diameter	$bd_{pseudoR134a}$	m	Eq. 3.95	6.2937 E-4

Nucleate-pool-boiling HTC of Stephan & Abdelsalam	$h_{SA,pseudoR134a}$	W/(m^2·K)	Eq. 3.94.A.a	1437.6712
At the element inlet for R407C (continued)				
C_{me} parameter	C_{me}	Dimensionless	Eq. 3.103.A.a	0.9717
Nucleate-pool-boiling HTC of h_{in}	h_{in}	W/(m^2·K)	Eq. 3.120.A.a	1225.2009
C_{UN} parameter	C_{UN}	Dimensionless	Eq. 3.110	1.4349
Nucleate-pool-boiling HTC of Unal	$h_{UN,R407C}$	W/(m^2·K)	Eq. 3.119	853.8707
Two-phase HTC	$h_{tp,R407C}$	W/(m^2·K)	Eq. 3.121	1567.3593

References

Admiraal, D. M. & Bullard, C. W. 1993, *Heat transfer in refrigerator condensers and evaporators*, Air Conditioning and Refrigeration Center, University of Illinois at Urbana-Champaign, USA, ACRC TR-48.

Admiraal, D. M. & Bullard, C. W. 1995, "Experimental validation of heat exchanger models for refrigerator/freezers", *ASHRAE Trans.*, vol. 101, part 1, pp. 34-42.

Altman, M., Norries, R. H., & Staub, F. W. 1960, "Local and average heat transfer and pressure drop of refrigerants", *J.Heat Transfer*, vol. 82, no. C, pp. 189-198.

Anderson, S. W., Rich, D. G., & Geary, D. F. 1961, "Evaporation of refrigerant 22 in a horizontal 3/4-in. OD tube", *ASHRAE Trans.* pp. 28-42.

ASHRAE 1993, *ASHRAE handbook: Fundamentals*, SI edn, ASHRAE, Georgia, USA.

Atwood, T. 1990, "Refrigerants and energy efficiency", *Int.J.Refrig.*, vol. 13, no. 4, pp. 270-273.

Baker, O. 1954, "Simultaneous flow of oil and gas", *The Oil and Gas Journal*, vol. 53, pp. 185-195.

Bennett, D. L. & Chen, J. C. 1980, "Forced convective boiling in vertical tubes for saturated pure components and binary mixtures", *AIChE J.*, vol. 26, pp. 454-461.

Bensafi, A., Borg, S., & Parent, D. 1997, "CYRANO: a computational model for the detailed design of plate-fin-and-tube heat exchangers using pure and mixed refrigerants", *Int.J.Refrig.*, vol. 20, no. 3, pp. 218-228.

Biven, D., Shiflett, M., Wells, W., Shealy, G., Yokozeki, A., Patron, D., Kolliopoulos, K., Allgood, C., & Chisolm, T. 1995, "HCFC-22 alternatives for air conditions and heat pumps", *ASHRAE Trans.*, vol. 101, part 2, pp. 1065-1071.

Bjorge, R. W., Hall, G. R., & Rohsenow, W. M. 1982, "Correlation of forced convection boiling heat transfer data", *Int.J.Heat Mass Transfer*, vol. 25, pp. 753-757.

Braven, K. R. D. & Troxel, S. O. 1990, "Method for predicting the performance of nonazeotropic mixtures in heat pumps", *ASHRAE Trans.*, vol. 96, part 1, pp. 305-311.

British Standard. BS 5720:1979 Code of practice for mechanical ventilation and air conditioning buildings. 1979.
Ref Type: Serial (Book,Monograph)

Broersen, P. M. T. & van der Jagt, M. F. G. 1980, "Hunting of evaporators controlled by a thermostatic expansion valve", *Trans.of the ASME*, vol. 102, pp. 130-135.

Calm, J. M. & Didion, D. A. 1998, "Trade-offs in refrigerant selections: past, present, and future", *Int.J.Refrig.*, vol. 21, no. 4, pp. 308-321.

Calus, W. F. & Leonidopoulos, D. J. 1974, "Pool boiling - binary liquid mixtures", *Int.J.Heat Mass Transfer*, vol. 17, pp. 249-256.

Carey, V. P. 1992, *Liquid-vapour phase-change phenomena* Hemisphere Publishing Corporation, London.

Chen, J. C. 1963, "A correlation for boiling heat transfer to saturated fluids in convective flow", *ASME Paper* no. 63-HT-34, pp. 1-11.

Chen, J. C. 1966, "Correlation for boiling heat transfer to saturated fluids in convective flow", *Ind.Engng.Chem.Proc.Design Dev.*, vol. 5, no. 3, pp. 322-339.

Chen, J. F. 1992, *Optimization of vapour compression air conditioner/heat pumps using refrigerant mixtures,* Dept. of Chem. Eng., The Univ. of Leeds.

Chilton, T. H. & Colburn, A. P. 1934, "Mass transfer (absorption) coefficients - Prediction from data on heat transfer and fluid friction", *Ind.Engng.Chem.* no. November, 1934.

Chisholm, D. 1973, "Void fraction during two-phase flow", *J.Mech.Engng.Sci.*, vol. 15, pp. 235-236.

Chisholm, D. 1967, "Theoretical basic for the Lockhart-Martinelli Correlation for two-phase flow", *Int.J.Heat Mass Transfer*, vol. 10, pp. 1767-1778.

Chuah, Y. K., Hung, C. C., & Tseng, P. C. 1998, "Experiments on the dehumidification performance of a finned tube heat exchanger", *HVAC&R Research*, vol. 4, no. 2, pp. 167-178.

Collier, J. G., Lacey, P. M. C., & Pulling, D. J. 1964, "Heat transfer to two-phase gas liquid mixtures in the liquid dispersed region in the annulus", *AERE*, vol. R-3809.

Collier, J. G. & Thome, J. R. 1996, *Convective boiling and condensation* Oxford Univ. Press Inc., New York, USA.

Cooper, M. G. 1984, "Saturation nucleate pool boiling: A simple correlation", First U.K. National Conference on Heat Transfer, vol.2 (I.Chem.E.Symposium Series, no.86), United Kingdom, pp. 785-793.

Davis, E. J. & Anderson, G. H. 1996, "The incipience of nucleate boiling in forced convection flow", *AIChE J.*, vol. 12, pp. 774-780.

Domanski, P. 1991, "Simulation of an evaporator with non-uniform one-dimensional air distribution", *ASHRAE Trans.*, vol. 97, part 1, pp. 793-802.

Domanski, P. & McLinden, M. 1992, "A simplified cycle simulation model for the performance rating of refrigerants and refrigerant mixtures", *Int.J.Refrig.*, vol. 15, no. 2, pp. 81-88.

Domanski, P. A., Yashar, D., & Kim, M. 2005, "Performance of a finned-tube evaporator optimized for different refrigerants and its effect on system efficiency", *Int.J.of Refrig.*, vol. 28, no. No.6, pp. 820-827.

E.I.du Pont de Nemours and Company. Physical property data for Suva 134a, Suva 409A, Suva MP39, Suva MP66, Freon 12, and Freon 500. http://www.dupont.com/suva/emea/index.html . 2002. E.I.du Pont de Nemours and Company.
Ref Type: Electronic Citation

E.I.du Pont de Nemours and Company. Physical property data for Suva 407C, Suva 410A, and Freon 22. http://www.dupont.com/suva/emea/index.html . 2002. E.I.du Pont de Nemours and Company.
Ref Type: Electronic Citation

Ebisu, T. & Torikoshi, K. 1995, "Experimental studies on crossflow heat exchanger performance using non-azeotropic refrigerant mixture", International Institute of Refrigeration, 19th Congress of Refrigeration, Proceedings IVa, Theme 4, Energy, working substances and environment, August 20 - 25, 1995, The Hague, The Netherlands, pp. 163-170.

Eckels, S. J. & Pate, M. B. 1991, "Evaporation and condensation of HFC-134a and CFC-12 in a smooth tube and a micro-fin tube", *ASHRAE Trans.*, vol. 97, part 2, pp. 71-81.

Elmahdy, A. H. & Biggs, B. C. 1979, "Finned tube heat exchanger: Correlation of dry surface heat transfer data", *ASHRAE Trans.*, vol. 85, part 2, pp. 262-273.

Forster, H. K. & Zuber, N. 1955, "Dynamics of vapor bubbles and boiling heat transfer", *AIChE J.*, vol. 1, no. 4, pp. 531-535.

Gosney, W. B. 1982, *Principles of refrigeration*, First edn, Cambridge University Press.

Granryd, E. 1991, "Heat transfer in flow evaporation of non-azeotropic refrigerant mixtures: A theory approach", Proc. of the 18th Int. Congr. of Refrig., pp. 1330-1334.

Gray, D. L. & Webb, R. L. 1986, "Heat transfer and friction correlations for plate-finned-tube heat exchangers having plain fins", Proc. of the 8th Int. Heat Transfer Conf., San Francisco.

Greco, A. & Vanoli, G. P. 2005, "Flow-boiling of R22, R134a, R507, R404A and R410A inside a smooth horizontal tube", *Int.J.of Refrig.*, vol. 28, no. 6, pp. 872-880.

Grimm, N. R. & Rosaler, R. C. 1990, *Handbook of HVAC design* Mc Graw-Hill, USA.

Gungor, K. E. & Winterton, R. H. S. 1986, "A general correlation for flow boiling in tubes and annuli", *Int.J.Heat Mass Transfer*, vol. 29, no. 3, pp. 351-358.

Haselden, G. G. & Chen, J. C. 1994, "A computer simulation program for mixed refrigerant air conditioning", *Int.J.Refrig.*, vol. 17, no. 5, pp. 343-350.

Hewitt, G. F. 1990, *Hemisphere handbook of heat exchanger design, chapter 2.3.2* Hemisphere Publishing Corporation, New York.

Hewitt, G. F., Shires, G. L., & Bott, T. R. 1994, *Process heat transfer* CRC Press Inc., USA.

Hihara, E. & Saito, T. 1990, "Forced convective boiling heat transfer of binary mixtures in a horizontal tube", Proc. of the 9th Heat Transfer Conf., Jerusalem, pp. 123-128.

Hsu, Y. Y. 1962, "On the size of range of active nucleation cavities on a heating surface", *J.Heat Transfer*, vol. 84, pp. 207-216.

Hsu, Y. Y. & Graham, R. W. 1976, "Transport processes in boiling and two phase systems," McGraw-Hill, New York, pp. 3-49.

Huber, M., Gallagher, J., McLinden, M., & Morrison, G. NIST thermodynamic properties of refrigerants and refrigerant mixtures database (REFPROP) version 5.0. 1996. USA., U.S. Department of Commerce.
Ref Type: Computer Program

Hwang, Y., Judge, J., & Radermacher, R. 1997, "Experience with refrigerant mixtures", *ASHRAE Trans.*, vol. 103, part 1, pp. 765-776.

Incropera, F. P. & De Witt, D. P. 2002, *Fundamentals of heat and mass transfer*, Fifth edn, John Wiley & Sons, USA.

Incropera, F. P. & Witt, D. P. D. 1990, *Fundamentals of heat and mass transfer* John Wiley & Sons, Inc., Singapore.

Inoue, T. & Monde, M. 1994, "Nucleate pool boiling heat transfer in binary mixtures", *Warme-und-Stoffubertragung*, vol. 29, pp. 171-180.

James, K. A. & James, R. W. 1987, "Transient analysis of thermostatic expansion valves for refrigeration system evaporators using mathematical models", *Trans.of Inst.of M.C.*, vol. 9, no. 4, pp. 198-205.

Jia, X., Tso, C. P., Chia, P. K., & Jolly, P. 1995, "A distributed model for prediction of the transient response of an evaporator", *Int.J.Refrig.*, vol. 18, no. 5, pp. 336-342.

Jia, X., Tso, C. P., Jolly, P., & Wong, Y. W. 1999, "Distributed steady and dynamic modelling of dry-expansion evaporators", *Int.J.Refrig.*, vol. 22, no. 2, pp. 126-136.

Judge, J., Hwang, Y., & Radermacher, R. 1996, *A transient and steady-state study of pure and mixed refrigerants in a residential heat pump*, Center for Environmental

Energy Engineering, University of Maryland, Maryland, USA, EPA Cooperative Agreement CR 822356.

Judge, J. & Radermacher, R. 1997, "A heat exchanger model for mixtures and pure refrigerant cycle simulations", *Int.J.Refrig.*, vol. 20, no. 4, pp. 244-255.

Jung, D. S., McLinden, M., Radermacher, R., & Didion, D. 1989b, "A study of flow boiling heat transfer with refrigerant mixtures", *Int.J.Heat Mass Transfer*, vol. 32, no. 9, pp. 1751-1764.

Jung, D. S., McLinden, M., Radermacher, R., & Didion, D. 1989a, "Horizontal flow boiling heat transfer experiments with a mixture of R22/R114", *Int.J.Heat Mass Transfer*, vol. 32, no. 1, pp. 131-145.

Jung, D. S. & Radermacher, R. 1989, "Prediction of pressure drop during horizontal annular flow boiling of pure and mixed refrigerants", *Int.J.Heat Mass Transfer*, vol. 32, no. 12, pp. 2435-2446.

Jung, D. S. & Radermacher, R. 1991, "Prediction of heat transfer coefficients of various refrigerants during evaporation", *ASHRAE Trans.*, vol. 97, part 2, pp. 48-53.

Jung, D. S. & Radermacher, R. 1993, "Prediction of evaporation heat transfer coefficient and pressure drop of refrigerant mixtures in horizontal tubes", *Int.J.Refrig.*, vol. 16, no. 3, pp. 201-209.

Kandlikar, S. G. 1991, "Correlating heat transfer data in binary systems", *ASME HTD*, vol. 159, pp. 163-170.

Klimenko, V. V. 1984, "Heat transfer in forced convection boiling in a channel", Proc. 7th All-Union Heat and Mass Transfer Conf., Minsk, pp. 99-103.

Klimenko, V. V. 1988, "A general correlation for two-phase forced flow heat transfer", *Int.J.Heat Mass Transfer*, vol. 31, pp. 541-552.

Klimenko, V. V. 1990, "A general correlation for two-phase forced flow heat transfer: Second assessment", *Int.J.Heat Mass Transfer*, vol. 33, pp. 2073-2088.

Kondepudi, S. N. 1992, "The need to adapt heat pump simulation tools to incorporate environmentally safe refrigerants and their mixtures", ASME, Fluids Engineering Division (Publication) FED, Vol.145, Industrial and Environmental Applications of Fluid Mechanics, Winter Annual Meeting of ASME, Nov 8-13 1992, Anaheim, CA, USA, pp. 173-179.

Kutateladze, S. S. 1961, "Boiling heat transfer", *Int.J.Heat Mass Transfer*, vol. 4, pp. 31-45.

Lee, J., Kwon, Y. C., & Kim, M. H. 2003, "An improved method for analyzing a fin and tube evaporator containing a zeotropic mixture refrigerant with air mal-distribution", *Int.J.of Refrig.*, vol. 26, no. 6, pp. 707-720.

Liu, Z. & Winterton, R. H. S. 1991, "A general correlation for saturated and subcooled flow boiling in tubes and annuli based on a nucleate pool boiling", *Int.J.Heat Mass Transfer*, vol. 34, pp. 2759-2765.

Lockhart, R. W. & Martinelli, R. C. 1949, "Proposed correlation of data for isothermal two-phase two-component flow in pipes", *Chem.Eng.Prog.*, vol. 45, pp. 39-48.

MacArthur, J. W. 1984, "Transient heat pump behaviour: A theoretical investigation", *Int.J.Refrig.*, vol. 7, no. 2, pp. 123-132.

Martinelli, R. C., Boelter, L. M. K., Taylor, T. H. M., Thomsen, E. G., & Morrin, E. H. 1944, "Isothermal pressure drop for two-phase two-component flow in a horizontal pipe", *Trans.ASME*, vol. 66, pp. 139-151.

Martinelli, R. C. & Nelson, D. B. 1948, "Prediction of pressure drop during forced-circulation boiling of water", *ASME*, vol. 70, pp. 695-702.

Martinelli, R. C., Putnam, J. A., & Lockhart, R. W. 1946, "Two-phase two-component flow in the viscous region", *Trans.AIChE*, vol. 42, p. 681.

McQuiston, F. C. 1975, "Fin efficiency with combined heat and mass transfer", *ASHRAE Trans.*, vol. 81, part 1, pp. 350-354.

McQuiston, F. C. 1978, "Correlation of heat, mass and momentum transport coefficients for plate-fin-tube heat transfer surfaces with staggered tubes", *ASHRAE Trans.*, vol. 84, part 1, pp. 294-309.

McQuiston, F. C. 1978, "Heat, mass and momentum transfer data for five plate-fin-tube heat transfer surfaces", *ASHRAE Trans.*, vol. 84, part 1, pp. 266-293.

McQuiston, F. C. & Parker, J. D. 1994, *Heating, Ventilating, and Air Conditioning: Analysis and Design*, Fourth edn, John Wiley & Sons, Inc..

Microsoft Company. Mixed-language programming. http://www.microsoft.co...ers/mixedlang/fbtoc.htm . 1998. Microsoft Company.
Ref Type: Electronic Citation

Mithraratne, P. 1992, *Dynamic analysis of thermostatic expansion valve and evaporator,* MSc Thesis, The King's College, University of London.

Mithraratne, P., Wijeysundera, N. E., & Bong, T. Y. 2000, "Dynamic simulation of a thermostatically controlled counter-flow evaporator", *Int.J.Refrig.*, vol. 23, pp. 174-189.

Moran, M. J. 1993, *Fundamentals of thermodynamics*, Second edn, John Wiley & Sons Inc.

Morrison, G. & McLinden, M. 1985, "Two refrigerant mixtures and the hard sphere fluid", *ASHRAE Trans.*, vol. 91, part 2B, pp. 929-943.

Murata, K. & Hashizume, K. 1993, "Force convective boiling of non-azeotropic refrigerant mixtures inside tubes", *Trans.of the ASME*, vol. 115, pp. 680-689.

Najork, H. 1971, "Investigations on the dynamical behaviour of evaporators with thermostatic expansion valve", Proc. of the XIII Int.Congr. of Refrig., Washington D.C., pp. 759-769.

NAS Systems Division Office. Ozone Depletion, History and politics. http://www.nas.nasa.gov/About/Education/Ozone/history.html . 2001. 2007.
Ref Type: Electronic Citation

Nishikawa, K., Fujita, Y., Ohata, H., & Hidaka, S. 1982, "Effect of the surface roughness on the nucleate boiling heat transfer over the wide range of pressure", Proc. 7th Int. Heat Transfer Conf., vol.4, pp. 61-66.

Omag, B. 1999, *A study on the operation of thermostatic expansion valve,* MSc. Thesis, Mech. Eng. Dept., University College London.

Oskarsson, S. P., Krakow, K. I., & Lin, S. 1990a, "Evaporator models for operation with dry, wet, and frosted finned surfaces, Part I: Heat transfer and fluid flow theory", *ASHRAE Trans.*, vol. 96, part 1, pp. 373-380.

Oskarsson, S. P., Krakow, K. I., & Lin, S. 1990b, "Evaporator models for operation with dry, wet, and frosted finned surfaces, Part II: Evaporator models and verification", *ASHRAE Trans.*, vol. 96, part 1, pp. 381-392.

Perry, R. H. & Chilton, T. H. 1973, *Chemical engineers' handbook*, Fifth edn, McGraw-Hill, New York.

Pierre, B. 1957, "Stromningsmotstand vid Kokande Koldmedier", *Kylteknisk Tidskrift*, vol. 6.

Premoli, A., Francesco, D., & Prina, A. A. 1971, "Dimensionless correlation for determining the density of two-phase mixtures", *Lo Thermotecnica*, vol. 25, pp. 17-26.

Radermacher, R. 1984, "Heat pump cycles with nonazeotropic refrigerant mixtures in thermodynamic diagrams", *ASHRAE Trans.*, vol. 90, part 2A, pp. 166-174.

Reid, R. C., Prausnitz, J. M., & Poling, B. E. 1987, *The properties of gases &.liquids*, 4th Edition edn, McGraw-Hill, Inc., USA.

Rich, D. G. 1973, "The effect of fin spacing on the heat transfer and friction performance of multi-row, smooth plate fin-and-tube heat exchangers", *ASHRAE Trans.*, vol. 79, part 2, pp. 137-145.

Roetzel, W. & Xuan, Y. 1999, *Dynamic behaviour of heat exchangers* WIT Press/Computational Mechanics Publications, Great Britain.

Rohsenow, W. M. & Hartnett, J. P. 1998, *Handbook of heat transfer*, Third edn, McGraw-Hill, USA.

Ross, H., Jung, D., & Radermacher, R. 1987, "Horizontal flow boiling of pure and mixed refrigerants", *Int.J.Heat Mass Transfer*, vol. 30, no. 5, pp. 979-992.

Scriven, L. E. 1959, "On the dynamics of phase growth", *Chem.Eng.Sci.*, vol. 10, pp. 1-13.

Shah, M. M. 1976, "A new correlations for heat transfer during boiling flow through pipes", *ASHRAE Trans.*, vol. 82, part 2, pp. 66-86.

Shah, M. M. 1982, "Chart correlations for saturated boiling heat transfer: Equations and further study", *ASHRAE Trans.*, vol. 88, part 1, pp. 185-196.

Singal, L. C., Sharma, C. P., & Varma, H. K. 1983, "Pressure drop during forced convection boiling of binary refrigerant mixtures", *Int.J.Multiphase Flow*, vol. 9, no. 3, pp. 309-323.

Sisamos, C. 1994, *Simulation model of finned tube evaporator coils operating under frosting conditions*, M.Sc., University College London.

Smith, J. M. & Ness, H. C. V. 1987, *Introduciton to chemical engineering thermodynamics*, International edn, McGraw-Hill, Singapore.

Smith, S. L. 1970, "Void fraction in two-phase flow: a correlation based upon an equal velocity heat model", *Proc.Inst.Mech.Engrs.*, vol. 184, pp. 647-664.

Soumerai, H. 1987, *Practical thermodynamic tools for heat exchanger design engineers* John Wiley, New York.

Stephan, K. & Abdelsalam, M. 1980, "Heat transfer correlations for natural convection boiling", *Int.J.Heat Mass Transfer*, vol. 23, pp. 73-87.

Stephan, K. & Korner, M. 1969, "Calculation of heat transfer in evaporating binary mixtures", *Chemie Ingr.Tech.*, vol. 41, pp. 409-417.

Thome, J. R. 1983, "Prediciton of binary mixture boiling heat transfer coefficients using only phase equilibrium data", *Int.J.Heat Mass Transfer*, vol. 26, no. 7, pp. 965-974.

Touber, S. 1984, "Priciples and methods for mathematical modelling the steady-state and dynamic behaviour of refrigeration components and installations", Int. Inst. of Refrig., Proceedings of meetings of: Commission B2 (Advances in refrigeration and heat pump technology achieved by the application of micro-electronics and the control of systems by micro-electronic devices), pp. 163-175.

Turaga, M., Lin, S., & Fazio, P. P. 1988b, "Correlations for heat transfer and pressure drop factors for direct expansion air cooling and dehumidifying coils", *ASHRAE Trans.*, vol. 94, part 2, pp. 616-630.

Turaga, M., Lin, S., & Fazio, P. P. 1988a, "Performance of direct expansion plate finned tube coils for air cooling and dehumidification", *Int.J.Refrig.*, vol. 11, no. 2, pp. 78-86.

Unal, H. C. 1986, "Prediction of nucleate pool boiling heat transfer coefficients for boiling mixtures", *Int.J.Heat Mass Transfer*, vol. 29, no. 4, pp. 637-640.

Wallis, G. B. 1969, *One dimension two-phase flow* McGraw-Hill, New York.

Wang, F. Q., Maidment, G. C., & Tozer, R. M. 2007, "A novel special distributed method for dynamic refrigeration system simulation", *Int.J.of Refrig.*, vol. 30, no. No.5, pp. 887-903.

Wang, H. & Touber, S. 1991, "Distributed and non-steady-state modelling of an air cooler", *Int.J.Refrig.*, vol. 14, no. 2, pp. 98-111.

Welty, J. R., Wicks, C. E., & Wilson, R. E. 1984, *Fundamentals of momentum, heat, and mass transfer* John Wiley & Sons, USA.

Whalley, P. B. 1990, *Boiling condensation and gas-liquid flow* Oxford Univ. Press, New York, USA.

Zhang, L., Hihara, E., & Saito, T. 1997, "Boiling heat transfer of a ternary refrigerant mixture inside a horizontal smooth tube", *Int.J.Heat Mass Transfer*, vol. 40, no. 9, pp. 2009-2017.